/N-39
33/85

Coupled Structural, Thermal, Phase-Change and Electromagnetic Analysis for Superconductors Volume I

C.A. Felippa, C. Farhat, K.C. Park, C. Militello, and J.J. Schuler
University of Colorado
Boulder, Colorado

January 1996

National Aeronautics and
Space Administration

TABLE OF CONTENTS

INTRODUCTION

VOLUME I

Page

i

VOLUME II

SUMMARY

Described are the theoretical development and computer implementation of reliable and efficient methods for the analysis of coupled mechanical problems that involve the interaction of mechanical, thermal, phase-change and electromagnetic subproblems. The focus application has been the modeling of superconductivity and associated quantum-state phase-change phenomena. In support of this objective the work has addressed the following issues: (1) development of variational principles for finite elements, (2) finite element modeling of the electromagnetic problem, (3) coupling of thermal and mechanical effects, and (4) computer implementation and solution of the superconductivity transition problem. The main accomplishments have been: (1) the development of the theory of parametrized and gauged variational principles, (2) the application of those principled to the construction of electromagnetic, thermal and mechanical finite elements, and (3) the coupling of electromagnetic finite elements with thermal and superconducting effects, and (4) the first detailed finite element simulations of bulk superconductors, in particular the Meissner effect and the nature of the normal conducting boundary layer. The theoretical development is described in two volumes. Volume I describes mostly formulations for specific problems. Volume II describes generalization of those formulations.

1. INTRODUCTION

Many engineering applications of interest to NASA require the solution of coupled mechanical problems. A coupled problem consists of two or more subproblems that can be separately characterized by virtue of their physical nature. Simulation of coupled problems is complicated by the two-way nature of the interaction between the subproblems. This interaction has to be considered when seeking steady-state or transient solutions. The treatment of subproblems as a coupled problem, as opposed to considering them as a single, indivisible problem, arises from the different physical nature of each subproblem. Such differences encourages customized treatment, from modeling through computer implementation. Examples of coupled problems in aerospace are: design of propulsion systems (coupling structures, flow, thermomechanics and combustion), active vibration control of space structures (coupling structures and control), prediction of flutter in turbomachinery (coupling structures, combustion, and gasdynamics) and airplane wings (coupling structures and aerodynamics).

The work reported here deals with coupled problems that contain an electromagnetic field as one of their subproblems. The research has addressed both theoretical and application components. The theoretical component deals generally with methods for finite element modeling of electromagnetic, thermal, mechanical and phase-change effects individually and then considering their interaction in coupled problems. Because the domain of applications that lead to such problems is extremely wide and as yet remains largely unexplored, the application component of the research was focused on the particular problem of superconductivity.

Superconductivity involves primarily the interaction of electromagnetic and thermal fields. It may secondarily interact with mechanical effects such as motion or couling fluid flow. Transition from normal to superconducting state is a phase change phenomenon that involves quantum-mechanics effects. For conventional Type I and II bulk superconductors transition is largely controlled by magnetic field intensity and temperature. Consequently the transition problem displays three of the four effects addressed in the theoretical component of this work.

The following narrative outlines the main developments and accomplishment of this research project. Details are provided in the attached publication material.

2. DEVELOPMENT OF THERMOMECHANICAL ELEMENTS

Initial effort over the period September 1988 through February 1989 was focused on the variational basis for constructing high-performance mechanical and thermal elements. This primarily theoretical effort was carried out by one of the P.I.s (CAF) with the assistance of Carmelo Militello (a doctoral graduate student mainly supported by a research fellowship). The point of departure was previous research, funded by ONR and NRL, on the free-formulation variational principles reported in References [1–3].

A more general variational formulation for the mechanical elements, which includes the assumed natural strain (ANS) formulation, was established and reported in References [5–7,9]. One key

byproduct of this work was the Assumed Natural Deviatoric Strain (ANDES) formulation, which is as a modification of the ANS that satisfies *a priori* the patch test. The ANDES formulation was reported in References [5,10,18]. It became eventually a focus of Militello's thesis [15], and the basis for constructing several high-performance mechanical plate and membrane elements [14,20–22].

New representations of thermal fields were not addressed as standard formulations were considered adequate for the coupled-field phases of this research. The framework of parametrized variational principles was extended, however, to encompass incompressibility [16,17], micropolar elasticity [23,24] and electromagnetodynamics [25].

3. DEVELOPMENT OF ELECTROMAGNETIC ELEMENTS

3.1 Theoretical Developments

Early in this research phase it was decided to base the development of electromagnetic (EM) finite elements on variational principles that utilize electric and magnetic potentials as primary fields rather than on the EM field intensity and/or fluxes (as done in most of the existing EM finite element technology). It was felt that this choice provides for a generality of application that encompasses both normal and superconducting materials as well as taking care automatically of boundary and interior interfaces. These advantages more than compensate two difficulties: no general variational formulation of this finite element class existed, and potential fields are less physically meaningful than intensity and flux fields. The first obstacle was effectively removed by the developments outlined below. The difficulty with physical meaning of potentials impacts primarily *a priori* understanding on how to specify boundary conditions, and can be overcome by solving a range of practical problems.

Early work on this subject, carried out by one of the P.I.s (CAF) from September 1988 through August 1989, was exploratory in nature. The scalar potential formulation of acoustoelastic fluid fields, which satisfy the same governing equations as the electric-potential field, was investigated in collaboration with R. Ohayon of ONERA (France). This research, reported in References [4,8], did clarify the way to obtain general potential-based variational principles than can be procedurally translated to the far more complex EM case, which involves vector potentials.

3.2 Normal-Conducting One-Dimensional EM Elements

On January 1989 James J. Schuler, a first-year graduate student, started his Ph. D. research in electromagnetic finite elements with full support from this grant. By late 1989 a new class of electromagnetic finite elements based on a four-potential variational principle had been formulated and tested. The development steps are summarized below, and described more fully in a journal article [11].

A variational statement for the electromagnetic equations (Maxwell equations) in an arbitrary material was obtained. The primary variable of this principle is the four-potential, which integrates the scalar electric potential with the vector magnetic potential. The principle derived here generalizes those previously published in the literature, which are restricted to free space. Because of

its generality, it can serve as a basis to model ferromagnetic, semiconductor and superconducting materials. The principle was initially constructed using the canonical decomposition method formerly validated for the acoustoelastic-fluid potential by Felippa and Ohayon [4,8]. A simplified formulation for non-polarizable materials was found later "working backwards" from the general principle and is the one presented in Reference [11].

The variational principle is applicable for one, two and three space dimensions. It is applicable to both static and dynamic analysis under harmonic or transient loading. To quickly validate the application to finite elements, the principle was specialized to normal conductors with one-dimensional axisymmetric geometry. A finite element model with linear variation of the radial potential component in space was developed and implemented in straightforward fashion. The development of the forcing function, however, was more involved. The resulting implementation was tested on the static problem of the field associated with a cylindrical conductor and excellent agreement with the analytical solution was obtained [11].

3.3 Normal-Conducting Two-Dimensional EM Elements

Extension of the methodology outlined in 3.2 to multiple space dimensions brought surprises. In two and three dimensions it was found that the Lorentz gauge constraint was not automatically enforced by the finite element shape functions. The constraint was added through a Lagrangian multiplier, thus producing the so-called "gauged potential variational principle" presented by Schuler and Felippa [13]. The modification delayed the development of multidimensional EM elements for several months while several ways of discretizing the gauged potential were tried and evaluated. Eventually it was decided to treat the multiplier as an element-level degree of freedom that enforces gauge interaction in a mean sense over each element.

The multidimensional EM elements were incorporated into a program that can solve problems with arbitrary axisymmetric geometry. The program is restricted to treat static (time-independent) problems with a known current density distribution. Excellent results, reported in Reference [13], were obtained for two problems of simple geometry.

3.4 Current Predicting EM Elements

For the envisioned extension to superconductivity it was realized that the problems described in Sections 3.2 and 3.3 were overly restricted in that the distribution of the electric current is assumed known *a priori* and is uniform throughout a conductor. In general, temperature gradients within a conductor and a conductor's geometry cause the current distribution within a conductor to be non-uniform and therefore unknown. To accurately capture the effects of thermal-electromagnetic coupling it was therefore necessary to construct an electromagnetic finite element that could predict electric current densities given the total electric current. This task was started on June 1991 by Schuler and Felippa and required further modifications of the four-potential variational principle. A one-dimensional time-independent axisymmetric geometry element was tested on a variable current problem with known analytical solution. Values for the current density as computed by the finite element method agreed well with analytical predictions. These developments are reported in References [19,25,26].

3

3.5 Superconducting EM Elements

This task also started in 1991. The generality of the previously outlined four-potential variational formulation allowed for the straightforward extension of this method to Type I and II bulk super-conductors treated by the Ginzburg-Landau model. Only the time-independent one-dimensional case was explored because of the extremely nonlinear nature of the problem and the presence of extremely high gradients that necessitates highly graded meshes to treat boundary layers. The nonlinearities are in part due to the boundary type behavior of the current density stream that occurs within a bulk superconductor.

Initial attempts using the potential based variational approach predicted desired EM quantities but numerical problems surfaced that caused the investigators to suspect the validity of the numerical solutions. These problems and the original formulation of the problem are described in a preliminary report [18]. These numerical difficulties were eventually overcome through the use of a highly graded finite element mesh, a reformulation of the quantum mechanical wavefunction ψ, and a four-part scaling scheme. The resulting finite element was eventually thermally coupled through temperature dependent material parameters as discussed in Section 4 below.

4. THE COUPLED PROBLEM

4.1 Thermomechanical Interaction

One of the P.I.s (KCP) contributed his expertise in partitioned analysis methods to the development and testing of an unconditionally-stable, second-order accurate, staggered time integration procedure for treating thermomechanical coupling. This research was led by Professor C. Farhat, who was supported by other sources, and is reported in Reference [12]. The method described in this article is the basis for ongoing work in thermomechanical coupling for supersonic atmospheric and reentry vehicle structures.

4.2 Thermoelectromagnetic Interaction

On May 1992, work on a suitable finite element model for thermal conduction in a normal conductor was started. A conventional heat conduction finite element was used and heat convection boundary conditions were assumed. The main difference with respect to usual heat conduction analysis is that material properties of the normal conducting finite element were allowed to be temperature dependent. the temperature of the conductor, and that the internal heat source is coupled to the EM current intensity via by Ohm's law. The conducting wire problem was used as test for the computer implementation. Insertion of actual values for material properties gave a highly ill-conditioned system of equations for the independent variables. The ill-conditioning was overcome by use of a specialized finite element mesh and matrix scaling techniques. These techniques as well as results for the thermal elements are discussed in Reference [25].

4

4.3 Modeling of Quantum-State Phase Changes

After developing EM finite elements for the normal and superconducting phases of a conductor and adding thermal effects to each element separately, they were used to form a comprehensive program that could choose the correct quantum-state (QS). The correct state is determined by checking whether the critical temperature of the conductor and the critical magnetic field have been exceeded. If they are, the program uses the current-predicting element discussed in Section 3.3, coupled with the thermal element of Section 4.2. Otherwise the the program uses the Ginsburg-Landau superconducting finite element discussed in Section 3.5. In the most general case these conditions hold over different regions of a partly-superconducting system.

4.4 Analysis of Fully Coupled Problem

The coupled EM-thermal-QS finite element models were first tested on a one-dimensional time-independent Type I superconductor cylindrical wire carrying a specified total current. Even for this highly idealized situation there is no available analytical solution. The finite element performed extremely well in that several important physical phenomena were predicted. First and foremost was the identification of the Meissner effect, which is the almost total expulsion of the magnetic field from the superconducting interior of the conductor. The phenomenon is caused by the current density stream traveling in a thin (skin) boundary layer at the conductor's surface, an expected physical behavior that was also clearly displayed by the finite element solution. The value of the magnetic field at the conductor's surface can be determined by analytical means and the finite element model correctly predicted that condition.

Finally, the finite element model of the foregoing problem was tested using a variety of temperature and current loads. These tests also followed expected physical behavior – as either the current load or the temperature of the system was increased, the depth of the boundary layer increased to accommodate the increasing energy of the system. The complete program performed well and determined the correct equilibrium state, as expected, for a varity of thermal and current loadings. These results, as well as the tracing of the nonlinear equilibrium path using incremental-iterative solution procedures with arclength control are are discussed in detail in Schuler's thesis [26].

The main shortcoming of the one-dimensional model is that it cannot determine the actual distribution of EM quantities at the transition point when the partly-superconducting wire suddenly transitions to being a normal conductor. At such a branching point, the system effectively becomes two-dimensional thus transcending the modeling capabilities of the one-dimensional finite elements. Time constraint on the reported research activity did not allow for the extension of the one-dimensional elements to include this case. Such an extension is to proceed under separate (NSF) funding as part of a Grand Challenge Applications project.

5. CONCLUSIONS

The main accomplishment of this research can be summarized as follows.

1. A general variational framework to construct finite elements for a wide range of application problems (mechanical, thermal, fluid and electromagnetic) was developed.

2. A comprehensive set of electromagnetic finite elements for normal and superconducting media was developed and validated. This set includes thermal coupling and current-prediction effects.

3. The first detailed simulation of partly superconducting bulk superconductors by finite element methods. Key physical effects, notably the Meissner effect and the changes in the depth and distribution of the normal-conducting boundary layer were clearly identified.

These accomplishments open the door to the application of the finite element method to more complex coupled EM problems. In particular: more spatial dimensions, time dependency, frequency-state-dependent material properties, high-temperature superconductivity, and EM interaction with mechanical effects.

PARAMETRIZED MULTIFIELD VARIATIONAL PRINCIPLES IN ELASTICITY: I. MIXED FUNCTIONALS

SUMMARY

A one-parameter family of mixed variational principles for linear elasticity is constructed. This family includes the generalized Hellinger-Reissner and total potential energy principles as special cases. The presence of the free parameter offers an opportunity for the systematic derivation of energy-balanced finite elements that combine displacement and stress assumptions. It is shown that Fraeijs de Veubeke's stress-assumption limitation principle takes a particularly elegant expression in terms of the parametrized discrete form. Other possible parametrizations are briefly discussed.

GOVERNING EQUATIONS

Consider a *linearly elastic body* under static loading that occupies the volume V. The body is bounded by the surface S, which is decomposed into $S : S_d \cup S_t$. Displacements are prescribed on S_d while surface tractions are prescribed on S_t. The outward unit normal on S is denoted by $\mathbf{n} \equiv n_i$. The presence of internal natural or artificial interfaces is not treated in this paper.

The three unknown volume fields are displacements $\mathbf{u} \equiv u_i$, infinitesimal strains $\mathbf{e} \equiv e_{ij}$, and stresses $\sigma \equiv \sigma_{ij}$. The problem data include: the body force field $\mathbf{b} \equiv b_i$ in V, prescribed displacements $\hat{\mathbf{d}} \equiv \hat{d}_i$ on S_d, and prescribed surface tractions $\hat{\mathbf{t}} \equiv \hat{t}_i$ on S_t.

The relations between the volume fields are the strain-displacement equations

$$\mathbf{e} = \tfrac{1}{2}(\nabla \mathbf{u} + \nabla^T \mathbf{u}) = \mathbf{Du} \qquad \text{or} \qquad e_{ij} = \tfrac{1}{2}(u_{i,j} + u_{j,i}) \quad \text{in } V, \tag{1}$$

the constitutive equations

$$\sigma = \mathbf{E}\mathbf{e} \qquad \text{or} \qquad \sigma_{ij} = E_{ijkl}e_{kl} \quad \text{in } V, \tag{2}$$

and the equilibrium (balance) equations

$$-\text{div}\,\sigma = \mathbf{D}^*\sigma = \mathbf{b} \qquad \text{or} \qquad \sigma_{ij,j} + b_i = 0 \quad \text{in } V, \tag{3}$$

in which $\mathbf{D}^* = -\text{div}$ denotes the adjoint operator of $\mathbf{D} = \tfrac{1}{2}(\nabla + \nabla^T)$.

The stress vector with respect to a direction defined by the unit vector $\mathbf{v}$ is denoted as $\sigma_v = \sigma.\mathbf{v}$, or $\sigma_{vi} = \sigma_{ij}v_j$. On S the surface-traction stress vector is defined as

$$\sigma_n = \sigma.\mathbf{n}, \qquad \text{or} \qquad \sigma_{ni} = \sigma_{ij}n_j. \tag{4}$$

With this definition the traction boundary conditions may be stated as

$$\sigma_n = \hat{\mathbf{t}} \quad \text{or} \quad \sigma_{ij}n_j = \hat{t}_i \quad \text{on } S_t, \tag{5}$$

and the displacement boundary conditions as

$$\mathbf{u} = \hat{\mathbf{d}} \quad \text{or} \quad u_i = \hat{d}_i \quad \text{on } S_d. \tag{6}$$

NOTATION

Field Dependency. In variational methods of approximation we do not work of course with the exact fields that satisfy the governing equations (1-3,5-6), but with *independent* (primary) fields, which are subject to variations, and *dependent* (secondary, associated, derived) fields, which are not. The approximation is determined by taking variations with respect to the independent fields.

An *independently varied* field will be identified by a superposed tilde, for example $\tilde{\mathbf{u}}$. A dependent field is identified by writing the independent field symbol as superscript. For example, if the displacements are independently varied, the derived strain and stress fields are

$$\mathbf{e}^u = \tfrac{1}{2}(\nabla + \nabla^T)\tilde{\mathbf{u}} = \mathbf{D}\tilde{\mathbf{u}}, \qquad \sigma^u = \mathbf{E}\mathbf{e}^u = \mathbf{E}\mathbf{D}\tilde{\mathbf{u}}. \tag{7}$$

An advantage of this convention is that $\mathbf{u}$, $\mathbf{e}$ and σ may be reserved for the *exact* fields.

Integral Abbreviations. Volume and surface integrals will be abbreviated by placing domain-subscripted parentheses and square brackets, respectively, around the integrand. For example:

$$(f)_V \stackrel{\text{def}}{=} \int_V f\, dV, \quad [f]_S \stackrel{\text{def}}{=} \int_S f\, dS, \quad [f]_{S_d} \stackrel{\text{def}}{=} \int_{S_d} f\, dS, \quad [f]_{S_t} \stackrel{\text{def}}{=} \int_{S_t} f\, dS. \tag{8}$$

If $\mathbf{f}$ and $\mathbf{g}$ are vector functions, and $\mathbf{p}$ and $\mathbf{q}$ tensor functions, their inner product over V is denoted in the usual manner

$$(\mathbf{f}, \mathbf{g})_V \stackrel{\text{def}}{=} \int_V \mathbf{f}.\mathbf{g}\, dV = \int_V f_i g_i\, dV, \qquad (\mathbf{p}, \mathbf{q})_V \stackrel{\text{def}}{=} \int_V \mathbf{p}.\mathbf{q}\, dV = \int_V p_{ij} q_{ij}\, dV, \tag{9}$$

and similarly for surface integrals, in which case square brackets are used.

Domain Assertions. Finally, the notation

$$(a = b)_V, \qquad [a = b]_S, \qquad [a = b]_{S_d}, \qquad [a = b]_{S_t}, \tag{10}$$

is used to assert that the relation $a = b$ is valid at each point of V, S, S_d and S_t, respectively.

In addition, Oden and Reddy[3] list an "unnamed" functional whose t-generalized version is

$$\Pi_U^t(\bar{\mathbf{u}}, \bar{\sigma}, \bar{\mathbf{t}}) = (\sigma^u, \mathbf{e}^u)_V - \tfrac{1}{2}(\bar{\sigma}, \mathbf{e}^\sigma)_V - (\bar{\sigma}, \mathbf{e}^u)_V - P^t. \tag{19}$$

These three functionals are special cases of the following parametrized form

$$\Pi_\gamma^t(\bar{\mathbf{u}}, \bar{\sigma}, \bar{\mathbf{t}}) = \tfrac{1}{2}(1-\gamma)(\sigma^u, \mathbf{e}^u)_V - \tfrac{1}{2}\gamma(\bar{\sigma}, \mathbf{e}^\sigma)_V + \gamma(\bar{\sigma}, \mathbf{e}^u)_V - P^t, \tag{20}$$

where γ is a scalar. If $\gamma = 1, 0, -1$ we obtain the functionals Π_R^t, Π_P^t and Π_U^t, respectively. The first variation of (20) is

$$\begin{aligned}
\delta\Pi_\gamma^t = \gamma\left(\mathbf{e}^u - \mathbf{e}^\sigma, \delta\bar{\sigma}\right)_V - (\text{div}\,\sigma^\gamma + \mathbf{b}, \delta\bar{\mathbf{u}})_V \\
- \left[\hat{\mathbf{t}} - \sigma_n^\gamma, \delta\bar{\mathbf{u}}\right]_{S_t} - \left[\hat{\mathbf{t}} - \sigma_n^\gamma, \delta\bar{\mathbf{u}})\right]_{S_d} - \left[\mathbf{u} - \hat{\mathbf{d}}, \delta\bar{\mathbf{t}}\right]_{S_d},
\end{aligned} \tag{21}$$

in which σ^γ and σ_n^γ denote the γ-weighted stresses

$$\sigma^\gamma \overset{\text{def}}{=} \gamma\bar{\sigma} + (1-\gamma)\sigma^u, \qquad \sigma_n^\gamma \overset{\text{def}}{=} \gamma\bar{\sigma}_n + (1-\gamma)\sigma_n^u. \tag{22}$$

If $\gamma \neq 0$, the Euler equations and natural boundary conditions are

$$(\mathbf{e}^u = \mathbf{e}^\sigma)_V, \quad (\text{div}\,\sigma^\gamma + \mathbf{b} = 0)_V, \quad [\sigma_n^\gamma = \hat{\mathbf{t}}]_{S_t}, \quad [\sigma_n^\gamma = \bar{\mathbf{t}}]_{S_d}, \quad [\mathbf{u} = \hat{\mathbf{d}}]_{S_d}. \tag{23}$$

The constitutive equations do not appear since they are enforced *a priori* in Π_γ^t. If $\gamma = 0$, the first Euler equation drops out.

ENERGY BALANCING

Distances. Let $U(\epsilon) = \tfrac{1}{2}(\mathbf{E}\epsilon, \epsilon)_V$ denote the strain energy associated with field ϵ. We may rewrite (20) as a potential-energy deviator

$$\Pi_\gamma^t = \Pi_P^t - \gamma\,U(\mathbf{e}^u - \mathbf{e}^\sigma), \tag{24}$$

because

$$\begin{aligned}
\frac{\Pi_\gamma^t - \Pi_P^t}{\gamma/2} = (\bar{\sigma}, \mathbf{e}^\sigma - \mathbf{e}^u) - (\bar{\sigma} - \sigma^u, \mathbf{e}^u)_V = \\
(\sigma^u - \bar{\sigma}, \mathbf{e}^u - \mathbf{e}^\sigma)_V = (\mathbf{E}\mathbf{e}^u - \mathbf{E}\mathbf{e}^\sigma, \mathbf{e}^u - \mathbf{e}^\sigma)_V.
\end{aligned} \tag{25}$$

If $\mathbf{E}$ is positive definite, $U(\mathbf{e}^u - \mathbf{e}^\sigma) \geq 0$ and consequently

$$\Pi_\gamma^t \leq \Pi_P^t \quad \text{if} \quad \gamma > 0. \tag{26}$$

If $\bar{\mathbf{u}}$ is kinematically admissible, Π_P^t exceeds the exact potential energy as shown below. It follows that to improve solutions in energy we expect to take $\gamma \geq 0$. Thus principles associated with $\gamma < 0$ have limited practical interest.

Let $\Pi(u)$ denote the exact potential energy

$$\Pi(u) = \tfrac{1}{2}(\sigma, e)_V - (b, u)_V - [\hat{t}, u]_{S_t} \tag{27}$$

where σ and e denotes the exact stress and strain field, respectively. If $\tilde{u}$ is kinematically admissible and thus satisfies $[\tilde{u} = \hat{d}]_{S_d}$, then the energy distance from $\Pi'_P(\tilde{u})$ to the exact functional (27) is (see *e.g.* §34 of Gurtin[4])

$$\Pi'_P - \Pi = \tfrac{1}{2}(\sigma^u - \sigma, e^u - e)_V = U(e^u - e) \tag{28}$$

Optimal Approximation. To derive an "energy balanced" approximation we impose the condition $\Pi'_\gamma = \Pi$, which yields

$$\gamma_{opt} = \frac{U(e^u - e)}{U(e^u - e^\sigma)} = \frac{(\sigma^u - \sigma, e^u - e)}{(\sigma^u - \tilde{\sigma}, e^u - e^\sigma)}. \tag{29}$$

For example, if we assume that the exact stresses and strains lie halfway between the approximate fields,

$$\sigma = \tfrac{1}{2}(\sigma^u + \tilde{\sigma}), \qquad e = \tfrac{1}{2}(e^\sigma + e^u), \tag{30}$$

then $\gamma_{opt} = \tfrac{1}{4}$.

THREE-FIELD DISCRETIZATION

To construct a 3-field finite element approximation based on Π'_γ, globally assume*

$$(\tilde{u} = Nq)_V, \qquad (\tilde{\sigma} = Aa)_V, \qquad [\tilde{t} = Ss]_{S_d} \tag{31}$$

Here matrices N, A and S collect generalized displacement shape functions, internal stress modes and boundary traction modes, respectively, whereas column vectors q, a and s collect generalized displacements†, stress mode amplitudes, and surface traction amplitudes, respectively. The derived fields are

$$(e^u = DNq = Bq)_V, \qquad (\sigma^u = EBq)_V, \qquad (e^\sigma = E^{-1}\tilde{\sigma} = E^{-1}Aa)_V. \tag{32}$$

Inserting these expressions into Π'_γ we obtain the algebraic form

$$\Pi'_\gamma(a, q, s) = \tfrac{1}{2}(1 - \gamma)q^T K_u q - \tfrac{1}{2}\gamma a^T Ca + \gamma q^T Qa - q^T f_d - s^T Rq - s^T f_s. \tag{33}$$

The matrices K_u, C, Q and R that appear in (31) are called displacement-stiffness, compliance, leverage and boundary-dislocation matrices, respectively, and are given by

$$K_u = (B^T EB)_V, \quad C = (A^T E^{-1}A)_V, \quad Q = (B^T A)_V, \quad R = [S^T N]_{S_d} \tag{34}$$

---

* Following usual practice in finite element work, the components of σ and e will be arranged as column vectors whereas the moduli in E will be arranged as a square symmetric matrix.

† If q are nodal displacements, N contains conventional shape functions. But for the present study we need not specialize to that level.

Both K_u and C are symmetric. The forcing vectors are

$$\mathbf{f}_q = (\mathbf{N}^T\mathbf{b})_V + [\mathbf{N}^T\hat{\mathbf{t}}]_{S_t}, \qquad \mathbf{f}_s = -[\mathbf{S}^T\hat{\mathbf{d}}]_{S_d} \tag{35}$$

Vector $\mathbf{f}_q$ contains generalized forces (conjugate to $\mathbf{q}$) whereas $\mathbf{f}_s$ contains generalized displacements. Making (33) stationary yields the linear system

$$\begin{bmatrix} -\gamma\mathbf{C} & \gamma\mathbf{Q}^T & 0 \\ \gamma\mathbf{Q} & (1-\gamma)\mathbf{K}_u & -\mathbf{R}^T \\ 0 & -\mathbf{R} & 0 \end{bmatrix} \begin{Bmatrix} \mathbf{a} \\ \mathbf{q} \\ \mathbf{s} \end{Bmatrix} = \begin{Bmatrix} 0 \\ \mathbf{f}_q \\ \mathbf{f}_s \end{Bmatrix} \tag{36}$$

The first matrix equation is the discrete analog of $(\mathbf{e}^u = \mathbf{e}^\sigma)_V$ in (23) and expresses internal compatibility. The second one is the discrete analog of the next three relations, and expresses equilibrium. The last relation is the discrete analog of $[\mathbf{u} = \bar{\mathbf{u}}]_{S_d}$ and enforces boundary compatibility.

Since there is no force term on the first matrix equation, the stress amplitude vector $\mathbf{a}$ can be readily condensed out if C is nonsingular, and we get

$$\begin{bmatrix} \mathbf{K} & -\mathbf{R}^T \\ -\mathbf{R} & 0 \end{bmatrix} \begin{Bmatrix} \mathbf{q} \\ \mathbf{s} \end{Bmatrix} = \begin{Bmatrix} \mathbf{f}_q \\ \mathbf{f}_s \end{Bmatrix} \tag{37}$$

where

$$\mathbf{K} = (1-\gamma)\mathbf{K}_u + \gamma\mathbf{Q}\mathbf{C}^{-1}\mathbf{Q}^T = (1-\gamma)\mathbf{K}_u + \gamma\mathbf{K}_\sigma \tag{38}$$

is the *effective stiffness matrix*. This is a γ-weighted combination of the displacement-assumed stiffness matrix $\mathbf{K}_u$ and the stress-assumed stiffness matrix $\mathbf{K}_\sigma = \mathbf{Q}\mathbf{C}^{-1}\mathbf{Q}^T$. If the assumed displacements satisfy $[\bar{\mathbf{u}} = \hat{\mathbf{d}}]_{S_d}$, the contribution from $[\bar{\mathbf{t}}, \bar{\mathbf{u}} - \hat{\mathbf{d}}]_{S_d}$ drops out and we are left with the conventional stiffness equations

$$\mathbf{K}\mathbf{q} = \mathbf{f}_q \tag{39}$$

LIMITATION PRINCIPLE

The famous limitation principle of Fraeijs de Veubeke[5] takes on a particularly striking algebraic representation in terms of the parametrized matrix system (36). This principle applies when the derived stress field σ^u is contained in the assumed stress field $\tilde{\sigma}$:

$$\tilde{\sigma} \ni \sigma^u = \mathbf{E}\mathbf{D}\bar{\mathbf{u}} \tag{40}$$

This inclusion can be expressed in matrix form as

$$\tilde{\sigma} = \mathbf{A}\mathbf{a} = \mathbf{E}\mathbf{B}\mathbf{a}_q + \mathbf{A}_x\mathbf{a}_x = [\mathbf{E}\mathbf{B} \quad \mathbf{A}_x] \begin{Bmatrix} \mathbf{a}_q \\ \mathbf{a}_x \end{Bmatrix} \tag{41}$$

Here $\mathbf{a}_q$ contains the same number of entries as $\mathbf{q}$ whereas $\mathbf{A}_x$ contains "excess" stress modes. Inserting (41) into (36) and calling $\mathbf{Q}_x = (\mathbf{B}^T\mathbf{A}_x)_V$ and $\mathbf{C}_{xx} = (\mathbf{A}_x^T\mathbf{E}^{-1}\mathbf{A}_x)_V$ we get

$$\begin{bmatrix} -\gamma\mathbf{K}_u & -\gamma\mathbf{Q}_x & \gamma\mathbf{K}_u & 0 \\ -\gamma\mathbf{Q}_x^T & -\gamma\mathbf{C}_{xx} & \gamma\mathbf{Q}_x^T & 0 \\ \gamma\mathbf{K}_u & \gamma\mathbf{Q}_x & (1-\gamma)\mathbf{K}_u & -\mathbf{R}^T \\ 0 & 0 & -\mathbf{R} & 0 \end{bmatrix} \begin{Bmatrix} \mathbf{a}_q \\ \mathbf{a}_x \\ \mathbf{q} \\ \mathbf{s} \end{Bmatrix} = \begin{Bmatrix} 0 \\ 0 \\ \mathbf{f}_q \\ \mathbf{f}_s \end{Bmatrix} \tag{42}$$

The first two matrix equations give $a_q = q$ and $a_x = 0$. Dropping the equations associated with the extra stress modes reduces (42) to

$$\begin{bmatrix} -\gamma K_u & \gamma K_u & 0 \\ \gamma K_u & (1-\gamma)K_u & -R^T \\ 0 & -R & 0 \end{bmatrix} \begin{Bmatrix} q \\ q \\ s \end{Bmatrix} = \begin{Bmatrix} 0 \\ f_q \\ f_s \end{Bmatrix} \tag{43}$$

which obviously condenses to (37) with $K = K_u$ for any γ. The solution (q, a, s) becomes independent of γ. In other words, it is useless to inject additional degrees of freedom in the stresses beyond σ^μ if the three-field variational principle is used. Furthermore, if $\sigma^\mu \equiv \bar{\sigma}$ there is no point in using anything else than the potential energy principle $\gamma = 0$.

In fact the limitation principle expresses nothing more than the algebraic identity, valid for any γ,

$$\begin{bmatrix} -\gamma X & -\gamma Y & \gamma X \\ -\gamma Y^T & -\gamma Z & \gamma Y^T \\ \gamma X & \gamma Y & (1-\gamma)X \end{bmatrix} \begin{Bmatrix} x \\ 0 \\ x \end{Bmatrix} = \begin{Bmatrix} 0 \\ 0 \\ Xx \end{Bmatrix} \tag{44}$$

where X is symmetric and Y, Z arbitrary.

Constant Stress Assumption. If the derived field σ^μ varies over V, assuming a constant stress field $\bar{\sigma}$ for $\bar{\sigma}$ is a safe way to get around the limitation principle. In this case it is convenient to take $a \equiv \bar{\sigma}$ and $A = I$ (the identity matrix) in (31) so that $(\bar{\sigma} = \bar{\sigma})_V$. Then the stress-assumed stiffness matrix is

$$\overline{K}_\sigma = \upsilon \overline{B}^T \overline{E} \overline{B} \tag{45}$$

where υ denotes the total volume $\upsilon = (1)_V$, and $\overline{B}$ and $\overline{E}$ are the over-the-volume averages

$$\overline{B} = (B)_V/\upsilon, \qquad \overline{E}^{-1} = (E^{-1})_V/\upsilon \tag{46}$$

The effective stiffness matrix (38) is a weighted average of K_u and $\overline{K}_\sigma$. Since $\overline{K}_\sigma$ is typically rank deficient, $\gamma = 1$ is excluded.

TWO-FIELD DISCRETIZATION

If the relation $[t = \sigma_n]_S$ is imposed *a priori* as an essential boundary condition, t is no longer an independently varied field, and Π'_γ becomes a two-field functional. The last finite element assumption of (31) is replaced by

$$[t^\sigma = \sigma_n = A_n a]_{S_d}, \tag{47}$$

where A_n denotes the normal projection of A on S_d, and the finite element equations become

$$\begin{bmatrix} -\gamma C & \gamma(Q+P)^T \\ \gamma(Q+P) & (1-\gamma)K_u \end{bmatrix} \begin{Bmatrix} a \\ q \end{Bmatrix} = \begin{Bmatrix} f_a \\ f_q \end{Bmatrix}, \tag{48}$$

with

$$P = [N^T A_n]_{S_d} \qquad f_a = [N^T \hat{d}]_{S_d}. \tag{49}$$

12

A range analysis such as performed in the previous subsection reveals that the limitation principle does not generally apply if $[u \neq \hat{d}]_{S_d}$. The effect of the additional stress modes is to improve the satisfaction of boundary compatibility. But if the assumed displacements satisfy $[u = \hat{d}]_{S_d}$, P and f_a drop out and the limitation principle again holds.

RELATED FINITE ELEMENT MODELS

The parametrized functional Π'_γ may be used to construct finite element models by treating each element as a body of volume V and the element boundary as S. These elements differ from conventional ones in the appearance of the parameter γ. The element type will depend on the number of independent fields and the interelement continuity imposed on them. The most useful combinations are listed in Table 1.

Table 1 Some Finite Element Models Derivable From Π'_γ

No of independent fields	Interelement continuity on* $\bar{u}$	$\bar{\sigma}$	$\bar{t}$	Connected freedoms	Condensed freedoms	Resulting FE model	Limitation principle applies?
2	c	d	x	q	a	"stress relaxed" displacement	yes
2	d	c	l	s	q	continuous-stress traction-connected hybrid	no
3	d	d	c	s	q, a	discontinuous-stress traction-connected hybrid	yes

* c=continuous, d=discontinuous, x=not needed, l=linked to $\bar{\sigma}$ via (47)

NUMERICAL EXAMPLE

The application of the preceding theory to finite element development is illustrated with a simple 2D element that belongs to the first class listed in Table 1. Consider a rectangular 4-node plane-stress element referred to the $x \equiv x_1$ and $y \equiv x_2$ axes located along the rectangle sides. The element has constant thickness h, x-dimension L, y-dimension $H = \rho L$, and is made of isotropic elastic material with elastic modulus E and Poisson's ratio v. The internal displacement field ($u \equiv u_1$, $v \equiv u_2$) is constructed by the usual bilinear assumption, which satisfies interelement continuity. The internal stress field ($\sigma_{xx} \equiv \sigma_{11}$, $\sigma_{yy} \equiv \sigma_{22}$, $\tau_{xy} \equiv \sigma_{12}$, others zero) is constant. An independent surface traction field is not needed. The question investigated here is the value of γ that optimizes the behavior of the element in pure in-plane bending along the x axis.

The element freedom arrangement is

$$q^T = \langle\, u_1 \quad u_2 \quad u_3 \quad u_4 \quad v_1 \quad v_2 \quad v_3 \quad v_4 \,\rangle, \qquad a^T = \langle\, \sigma_{xx} \quad \sigma_{yy} \quad \tau_{xy} \,\rangle. \qquad (50)$$

The exactly-integrated conventional displacement stiffness is given by

$$
\mathbf{K}_u =
\begin{bmatrix}
k_1 & k_2 & k_3 & k_4 & k_5 & k_6 & k_7 & k_8 \\
 & k_1 & k_4 & k_3 & k_8 & k_7 & k_6 & k_5 \\
 & & k_1 & k_2 & k_7 & k_8 & k_5 & k_6 \\
 & & & k_1 & k_6 & k_5 & k_8 & k_7 \\
 & & & & k_9 & k_{10} & k_{11} & k_{12} \\
 & & & & & k_9 & k_{12} & k_{11} \\
 & symm & & & & & k_9 & k_{10} \\
 & & & & & & & k_9
\end{bmatrix},
\tag{51}
$$

where

$$k_1 = \tfrac{Eh}{6\rho}(1 - v + 2\rho^2), \qquad k_2 = \tfrac{Eh}{12\rho}(1 - v - 4\rho^2), \qquad k_3 = -\tfrac{Eh}{12\rho}(1 - v + 2\rho^2),$$

$$k_4 = -\tfrac{Eh}{6\rho}(1 - v - \rho^2), \qquad k_5 = -\tfrac{Eh}{8}(1 + v), \qquad k_6 = -\tfrac{Eh}{8}(1 - 3v),$$

$$k_7 = -\tfrac{Eh}{8}(1 + v), \qquad k_8 = -\tfrac{Eh}{8}(1 + 3v), \qquad k_9 = -\tfrac{Eh}{6\rho}(2 + (1 - v)\rho^2),$$

$$k_{10} = -\tfrac{Eh}{6\rho}(1 - (1 - v)\rho^2), \quad k_{11} = -\tfrac{Eh}{12\rho}(2 + (1 - v)\rho^2), \quad k_{12} = -\tfrac{Eh}{12\rho}(2 - (1 - v)\rho^2).$$
$$\tag{52}$$

The stress-assumed stiffness $\mathbf{K}_\sigma$ is given by (45), in which

$$
\bar{\mathbf{B}} = \frac{1}{2L}
\begin{bmatrix}
-1 & 1 & 1 & -1 & 0 & 0 & 0 & 0 \\
0 & 0 & 0 & 0 & -1/\rho & -1/\rho & 1/\rho & 1/\rho \\
-1/\rho & -1/\rho & 1/\rho & 1/\rho & -1 & 1 & 1 & -1
\end{bmatrix},
\tag{53}
$$

$$
\bar{\mathbf{E}} = \mathbf{E} = \frac{E}{1 - v^2}
\begin{bmatrix}
1 & v & 0 \\
v & 1 & 0 \\
0 & 0 & \tfrac{1-v}{2}
\end{bmatrix}, \qquad
\upsilon = hHL = \rho h L^2.
$$

$\mathbf{K}$ is the weighted combination (38). The test displacement field is that of pure bending about x:

$$u = -\kappa x y \quad , \quad v = \tfrac{1}{2}\kappa x^2 \tag{54}$$

where κ is the deformed beam curvature under the displacement field. Calculation of the energy ratio (29) over the element through MACSYMA yields

$$\gamma_{opt} = \frac{1 - v}{1 - v + 2\rho^2}. \tag{55}$$

For a square element, $\rho = 1$ and γ_{opt} varies from 1/3 to 2/10 as v changes from 0 to 1/2. This result was checked by solving the classical 4:1 cantilever beam problem (see Ref. 6, p. 49) for $v = 0$ with meshes of square elements. The values listed in Table 2 pertain to the two load cases of pure bending moment and parabolically-varying end shear, and are reported as the ratio of the computed to the exact tip displacement.

It is seen that this "stress relaxed" displacement model verifies (55) in that $\gamma = 1/3$ yields significantly better accuracy. However, the fact that the optimal γ depends strongly on the element aspect

14

Table 2 Computed/Exact Tip-Displacement Ratios for Cantilever Problem ($v = 0$)

Mesh	γ	Constant moment	End shear
1×4	0.0	0.6666	0.6631
	1/3	1.0000	0.9794
	2/3	2.0000	1.9291
	1.0	∞^*	∞^*
2×8	0.0	0.8889	0.8841
	1/3	1.0000	0.9911
	2/3	1.1142	1.1280
	1.0	1.3333	1.3118

* Rank deficient

ratio makes this "weighted stiffness" approach of dubious practical value for elements of arbitrary shape. The formulation discussed in Part II[2] attacks the optimal-element problem in a more general way through field decomposition and energy orthogonality arguments.

OTHER PARAMETRIZATIONS

A one-parameter family of strain-displacement mixed variational principles derived from the Hu-Washizu functional (11) by eliminating the stress field can be represented as

$$\Pi'_\beta(\bar{u}, \bar{e}, \bar{t}) = \tfrac{1}{2}(1 - \beta)(\sigma^u, e^u) - \tfrac{1}{2}\beta(\sigma^e, \bar{e})_V + \beta(\sigma^e, e^u)_V - P', \tag{56}$$

where β is a scalar. For $\beta = 0$ we recover again Π'_P whereas if $\beta = 1$ we obtain the Reissner-type strain-displacement principle listed in Oden and Reddy[3] generalized with an independent $\bar{t}$:

$$\Pi'_S(\bar{u}, \bar{e}, \bar{t}) = -\tfrac{1}{2}(\sigma^e, \bar{e})_V + (\sigma^e, e^u)_V - P'. \tag{57}$$

Continuing along this path, a two-parameter, four-field family that embeds both Π'_γ and Π'_β is easily constructed as

$$\Pi'_{\beta\gamma}(\bar{u}, \bar{e}, \bar{\sigma}, \bar{t}) = \tfrac{1}{2}(1 - \beta - \gamma)(\sigma^u, e^u)_V + (1 - \beta)\gamma\{(\bar{\sigma}, e^u)_V - \tfrac{1}{2}(\bar{\sigma}, e^\sigma)_V\} \\ + (1 - \gamma)\beta\{(\sigma^e, e^u)_V - \tfrac{1}{2}(\sigma^e, \bar{e})_V\} - P'. \tag{58}$$

This functional yields stress-displacement principles for $\beta = 0$ and strain-displacement principles for $\gamma = 0$. Finally, the Hu-Washizu principle itself may be embedded in a three-parameter form

$$\Pi'_{\alpha\beta\gamma} = (1 - \alpha)\Pi'_W + \alpha\Pi'_{\beta\gamma} \tag{59}$$

which obviously reduces to Π'_W for $\alpha = 1$ and to $\Pi'_{\beta\gamma}$ for $\alpha = 0$.

The superiority of one parametrized form variational principle over another as regards the construction of energy-balanced finite elements is not clear at this time.

CONCLUDING REMARKS

The parametrization (20) of the stress-displacement variational principles provide a unifying framework for the development of finite elements. This framework embodies the potential energy and Hellinger-Reissner principles, and encompasses displacement-assumed elements, conventional mixed elements and traction-connected hybrid elements. But it does not cover developments such as displacement-connected hybrid finite elements, incompatible elements and the free formulation.[7] To accomplish that one has to continue the process by introducing a d-generalized version of (20), internal boundaries, internal-field energy-orthogonal splitting, and selective kinematic constraints. These extensions are covered in a sequel paper.[2]

ACKNOWLEDGEMENTS

REFERENCES

1. K. Washizu, *Variational Methods in Elasticity and Plasticity*, Pergamon Press, Oxford, 1968

2. C. A. Felippa, 'Parametrized Multifield Variational Principles in Elasticity: II. Hybrid Functionals and the Free Formulation,' submitted to *Communications in Applied Numerical Methods*

3. J. T. Oden and J. N. Reddy, *Variational Methods in Theoretical Mechanics*, 2nd ed., Springer-Verlag, Berlin, 1983

4. M. Gurtin, 'The Linear Theory of Elasticity,' in Volume VIa/2 of *Encyclopedia of Physics*, ed. by C. Truesdell, Springer-Verlag, Berlin, 1972

5. B. M. Fraeijs de Veubeke, 'Displacement and Equilibrium Models in the Finite Element Method,' Ch. 9 in *Stress Analysis*, ed. by O. C. Zienkiewicz and G. Hollister, Wiley, London, 1965

6. P. G. Bergan and C. A. Felippa, 'A Triangular Membrane Element with Rotational Degrees of Freedom,' *Computer Methods in Applied Mechanics & Engineering*, 50, 1985, pp. 25–69

7. P. G. Bergan and M. K. Nygård, 'Finite elements with increased freedom in choosing shape functions,' *Int. J. Num. Meth. Engrg.*, 20, 1984, pp. 643–664

PARAMETRIZED MULTIFIELD VARIATIONAL PRINCIPLES IN ELASTICITY: II. HYBRID FUNCTIONALS AND THE FREE FORMULATION

SUMMARY

A one-parameter family of d-generalized hybrid/mixed variational principles for linear elasticity is constructed following a domain subdivision. The family includes the d-generalized Hellinger-Reissner and potential energy as special cases. The parametrized principle is discretized by independently varied internal displacements, stresses, and boundary displacements. The resulting finite element equations are studied following a physically motivated decomposition of the stress and internal displacement fields. The free formulation of Bergan and Nygård is shown to be a special case of this element type, and is obtained by assuming a constant internal stress field. The parameter appears as a scale factor of the higher order stiffness.

INTRODUCTION

This paper continues a study, initiated in Part I[1], of parametrized stress-displacement variational principles in linear elastostatics. The boundary value problem is as follows. We consider an elastic body of volume V and surface $S : S_t \cup S_d$. Surface tractions $\hat{t}$ are prescribed on S_t whereas displacements $\hat{d}$ are prescribed on S_d. The internal (volume) fields are displacements u, stresses σ, strains e and given body forces b. The internal field equations are $e = Du$, $\sigma = Ee$ and $D^*\sigma = b$ in V, where $D = \frac{1}{2}(\nabla + \nabla^T)$, $D^* = -\text{div}$, and E is the elastic modulus operator. The boundary conditions are $u = \hat{d}$ on S_d and $\sigma_n = \hat{t}$ on S_t.

The reader is referred to Part I[1] for additional notational conventions. Therein the following parametrized functional was introduced:

$$\Pi_\gamma^t(\bar{u}, \bar{\sigma}, \tilde{t}) = \tfrac{1}{2}(1 - \gamma)(\sigma^u, e^u)_V - \tfrac{1}{2}\gamma(\bar{\sigma}, e^\sigma)_V + \gamma(\bar{\sigma}, e^u)_V - P^t, \tag{1}$$

where γ is a scalar, and P^t is the forcing potential

$$P^t(\bar{u}, \tilde{t}) = (b, \bar{u})_V + [\tilde{t}, \bar{u} - \hat{u}]_{S_d} + [\hat{t}, \bar{u}]_{S_t}. \tag{2}$$

In this functional the volume fields $\bar{u}$, $\bar{e}$, $\bar{\sigma}$, and the surface field $\tilde{t}$ are subject to independent variations.

This functional "interpolates" the t-generalized Hellinger-Reissner and total potential energy functionals Π_R^t and Π_P^t, which are obtained for $\gamma = 1$ and $\gamma = 0$, respectively. The qualifier "t-generalized" means that the surface traction field $\tilde{t}$ is varied independently whereas in the conventional form of those principles, the constraint $[t = \sigma_n]_S$ is enforced *a priori*.
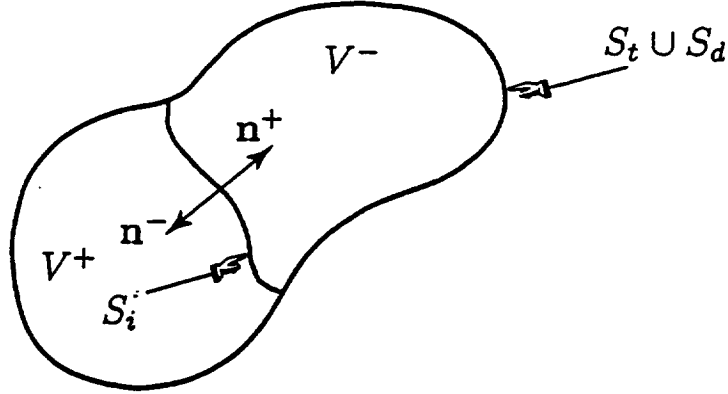
Figure 1. Internal interface example.

INTERNAL INTERFACES

In the following subsection an alternative version of (1) is constructed, in which boundary displacements d can be varied independently rather than boundary tractions t. These displacement play the role of Lagrange multipliers that relax internal displacement continuity. Variational principles of this form will be called d-generalized.

The choice of d as independent field is *not* variationally admissible on S_d or S_t. We must therefore extend the definition of boundary to include *internal interfaces* collectively designated as S_i. Thus

$$S : S_d \cup S_t \cup S_i \tag{3}$$

On S_i neither displacements nor tractions are prescribed. A simple case is illustrated in Figure 1, in which the interface S_i divides V into two subvolumes: V^+ and V^-.

An interface such as S_i on Figure 1 has two "sides" called S_i^+ and S_i^-, which identify S_i viewed as boundary of V^+ and V^-, respectively. At smooth points of S_i the unit normals n^+ and n^- point in opposite directions.

The integral abbreviations of Part I generalize as follows, using Figure 1 for definiteness. A volume integral is the sum of integrals over the subvolumes:

$$(f)_V \overset{\text{def}}{=} \int_{V^+} f \, dV + \int_{V^-} f \, dV. \tag{4}$$

An integral over S_i includes two contributions:

$$[g]_{S_i} \overset{\text{def}}{=} \int_{S_i^+} g^+ \, dS + \int_{S_i^-} g^- \, dS, \tag{5}$$

where g^+ and g^- denotes the value of the integrand g on S_i^+ and S_i^-, respectively. These two values may be different if g is discontinuous or involves a projection on the normals.

18

PARAMETRIZED d-GENERALIZED MIXED PRINCIPLE

Variational Principle. The d-generalized counterpart of Π_γ^t is

$$\Pi_\gamma^d(\bar{\mathbf{u}}, \bar{\sigma}, \bar{\mathbf{d}}) = \tfrac{1}{2}(1 - \gamma)(\sigma^u, \mathbf{e}^u)_V - \tfrac{1}{2}\gamma(\bar{\sigma}, \mathbf{e}^\sigma)_V + \gamma(\bar{\sigma}, \mathbf{e}^u)_V - P^d. \tag{6}$$

This agrees with (1) except for the forcing potential, which is

$$P^d(\bar{\mathbf{u}}, \bar{\sigma}, \bar{\mathbf{d}}) = (\mathbf{b}, \bar{\mathbf{u}})_V + [\bar{\sigma}_n, \bar{\mathbf{u}} - \hat{\mathbf{d}}]_{S_d} + [\hat{\mathbf{t}}, \bar{\mathbf{u}}]_{S_t} + [\bar{\sigma}_n, \bar{\mathbf{u}} - \bar{\mathbf{d}}]_{S_i}. \tag{7}$$

Defining the γ-weighted stresses

$$\sigma^\gamma \overset{\text{def}}{=} \gamma\bar{\sigma} + (1 - \gamma)\sigma^u \quad \text{in } V, \qquad \sigma_n^\gamma \overset{\text{def}}{=} \gamma\bar{\sigma}_n + (1 - \gamma)\sigma_n^u \quad \text{on } S. \tag{8}$$

the first variation can be written

$$\begin{aligned}
\delta\Pi_\gamma^d = \gamma\left(\mathbf{e}^u - \mathbf{e}^\sigma, \delta\bar{\sigma}\right)_V - (\operatorname{div}\sigma^\gamma + \mathbf{b}, \delta\bar{\mathbf{u}})_V - \left[\hat{\mathbf{t}} - \sigma_n^\gamma, \delta\bar{\mathbf{u}}\right]_{S_t} \\
- \left[\bar{\sigma}_n - \bar{\sigma}_n^\gamma, \delta\bar{\mathbf{u}}\right]_{S_d} - \left[\mathbf{u} - \hat{\mathbf{d}}, \delta\bar{\sigma}_n\right]_{S_d} \\
- \left[\bar{\sigma}_n - \bar{\sigma}_n^\gamma, \delta\bar{\mathbf{u}}\right]_{S_i} - \left[\bar{\mathbf{u}} - \bar{\mathbf{d}}, \delta\bar{\sigma}_n\right]_{S_i} - \left[\bar{\sigma}_n, \delta\bar{\mathbf{d}}\right]_{S_i}
\end{aligned} \tag{9}$$

Since $\mathbf{d}$ is unique on S_i whereas $\bar{\mathbf{u}}$ and $\bar{\sigma}$ are generally discontinuous on it, the interface integrals in (9) split as follows:

$$\begin{aligned}
\left[\bar{\sigma}_n - \bar{\sigma}_n^\gamma, \delta\bar{\mathbf{u}}\right]_{S_i} &= \left[\bar{\sigma}_n^+ - \bar{\sigma}_n^{\gamma+}, \delta\bar{\mathbf{u}}^+\right]_{S_i^+} + \left[\bar{\sigma}_n^- - \bar{\sigma}_n^{\gamma-}, \delta\bar{\mathbf{u}}^-\right]_{S_i^-} \\
\left[\bar{\mathbf{u}} - \bar{\mathbf{d}}, \delta\bar{\sigma}\right]_{S_i} &= \left[\bar{\mathbf{u}}^+ - \bar{\mathbf{d}}, \delta\bar{\sigma}_n^+\right]_{S_i^+} + \left[\bar{\mathbf{u}}^- - \bar{\mathbf{d}}, \delta\bar{\sigma}_n^-\right]_{S_i^-} \\
\left[\bar{\sigma}_n, \delta\bar{\mathbf{d}}\right]_{S_i} &= \left[\bar{\sigma}_n^+, \delta\bar{\mathbf{d}}\right]_{S_i^+} + \left[\bar{\sigma}_n^-, \delta\bar{\mathbf{d}}\right]_{S_i^-} = \left[\bar{\sigma}_n^+ - \bar{\sigma}_n^-, \delta\bar{\mathbf{d}}\right]_{S_i}
\end{aligned} \tag{10}$$

Setting the first variation to zero and taking (10) into account, the Euler equations and natural boundary conditions for $\gamma \neq 0$ are found to be

$$\begin{gathered}
(\mathbf{e}^u = \mathbf{e}^\sigma)_V, \quad (\operatorname{div}\sigma^\gamma + \mathbf{b} = 0)_V, \quad [\sigma_n^\gamma = \hat{\mathbf{t}}]_{S_t}, \quad [\sigma_n = \sigma_n^\gamma]_{S_d}, \quad [\mathbf{u} = \hat{\mathbf{d}}]_{S_d}, \\
[\sigma_n^{\gamma+} + \sigma_n^+ = 0]_{S_i}, \quad [\sigma_n^{\gamma-} + \sigma_n^- = 0]_{S_i}, \quad [\mathbf{u}^+ = \mathbf{u}^- = \mathbf{d}]_{S_i}, \quad [\sigma_n^+ + \sigma_n^- = 0]_{S_i}.
\end{gathered} \tag{11}$$

If $\gamma = 0$ the first equation, $(\mathbf{e}^u = \mathbf{e}^\sigma)_V$, drops out.

Modified Forcing Potential. Substituting $\mathbf{d}$ in lieu of $\mathbf{u}$ in the potential (7)

$$P^d(\bar{\mathbf{u}}, \bar{\sigma}, \bar{\mathbf{d}}) = (\mathbf{b}, \bar{\mathbf{u}})_V + [\bar{\sigma}_n, \bar{\mathbf{d}} - \hat{\mathbf{d}}]_{S_d} + [\hat{\mathbf{t}}, \bar{\mathbf{d}}]_{S_t} + [\bar{\sigma}_n, \bar{\mathbf{u}} - \bar{\mathbf{d}}]_{S_i}. \tag{12}$$

is *not* variationally admissible because incorrect Euler equations result. This form has appeared, however, in publications dealing with mixed-hybrid methods. A correct potential that resembles

(12) can be obtained in two stages. First, surface terms $[\tilde{\sigma}_n, \tilde{u} - \tilde{d}]_{S_t}$ and $[\tilde{\sigma}_n, \tilde{u} - \tilde{d}]_{S_d}$ are added and subtracted to produce

$$P^d(\tilde{u}, \tilde{\sigma}, \tilde{d}) = (b, \tilde{u})_V + [\tilde{\sigma}_n, \tilde{d} - \hat{d}]_{S_d} + [\tilde{\sigma}_n - \hat{t}, \tilde{u}]_{S_t} + [\hat{t}, \tilde{d}]_{S_t} + [\tilde{\sigma}_n, \tilde{u} - \tilde{d}]_S. \qquad (13)$$

Second, $\hat{t}$ is assumed to be in the range of $\tilde{\sigma}_n$ and the condition $[\tilde{\sigma}_n = \hat{t}]_{S_t}$ satisfied *a priori*, reducing (13) to

$$P^d(\tilde{u}, \tilde{\sigma}, \tilde{d}) = (b, \tilde{u})_V + [\tilde{\sigma}_n, \tilde{d} - \hat{d}]_{S_d} + [\hat{t}, \tilde{d}]_{S_t} + [\tilde{\sigma}_n, \tilde{u} - \tilde{d}]_S. \qquad (14)$$

This expression differs from (12) in that the all-important surface dislocation integral is taken over S rather than S_i. Further simplification results if the displacement boundary conditions $[\tilde{d} = \hat{d}]_{S_d}$ are exactly satisfied:

$$P^d(\tilde{u}, \tilde{\sigma}, \tilde{d}) = (b, \tilde{u})_V + [\hat{t}, \tilde{d}]_{S_t} + [\tilde{\sigma}_n, \tilde{u} - \tilde{d}]_S. \qquad (15)$$

This expression of P^d is used in the sequel, as modifications required to account for the case $[\tilde{d} \neq \hat{d}]_{S_d}$ are of minor importance.

FINITE ELEMENT APPROXIMATIONS

In this section the finite element discretization of Π_γ^d is studied. Assume formally

$$(\tilde{u} = Nq)_V, \qquad (\tilde{\sigma} = Aa)_V, \qquad [\tilde{d} = Vv]_S. \qquad (16)$$

Here matrices N, A and V collect generalized-displacement shape functions, internal stress modes and interface displacement modes, respectively, whereas column vectors q, a and v collect generalized internal displacements, stress mode amplitudes, and generalized interface displacements, respectively. The assumed volume fields need not be continuous across S. The derived fields are

$$(e^u = DNq = Bq)_V, \quad (\sigma^u = EBq)_V, \quad (e^\sigma = E^{-1}\tilde{\sigma} = E^{-1}Aa)_V. \qquad (17)$$

Inserting these expressions into Π_γ^d with the forcing potential (15), we obtain the algebraic form

$$\Pi_\gamma^d(a, q, s) = \tfrac{1}{2}(1 - \gamma)q^T K_u q - \tfrac{1}{2}\gamma a^T Ca + \gamma q^T Qa - q^T Pa + v^T La - q^T f_q - v^T f_v. \qquad (18)$$

where

$$K_u = (B^T EB)_V = K_u^T, \qquad C = (A^T E^{-1}A)_V = C^T, \qquad Q = (B^T A)_V,$$
$$L = [V^T A_n]_S, \qquad P = [N^T A_n]_S, \qquad f_q = (N^T b)_V, \qquad f_v = [N^T \hat{t}]_{S_t}. \qquad (19)$$

The matrices K_u, C, Q, L and P are called internal-displacement-stiffness, compliance, leverage, force-lumping, and boundary dislocation matrices, respectively. Making (18) stationary yields the linear system

$$\begin{bmatrix} -\gamma C & \gamma Q^T - P^T & L^T \\ \gamma Q - P & (1 - \gamma)K_u & 0 \\ L & 0 & 0 \end{bmatrix} \begin{Bmatrix} a \\ q \\ v \end{Bmatrix} = \begin{Bmatrix} 0 \\ f_q \\ f_v \end{Bmatrix} \qquad (20)$$

20

The first matrix equation is the discrete analog of the first, fifth and eight relations in (11), and expresses internal and boundary compatibility. The third equation is the discrete analog of the last relation, and expresses equilibrium across S_i. The second one is the discrete analog of the remaining relations, and expresses internal and boundary equilibrium.

Stress Condensation. If C is nonsingular, the stress amplitude vector a can be statically condensed from (20), giving

$$\begin{bmatrix} \mathbf{K}_q & \mathbf{K}_{qv}^T \\ \mathbf{K}_{qv} & \gamma^{-1}\mathbf{K}_v \end{bmatrix} \begin{Bmatrix} \mathbf{q} \\ \mathbf{v} \end{Bmatrix} = \begin{Bmatrix} \mathbf{f}_q \\ \mathbf{f}_v \end{Bmatrix} \tag{21}$$

in which

$$\mathbf{K}_q = (1-\gamma)\mathbf{K}_u + \gamma\mathbf{Q}\mathbf{C}^{-1}\mathbf{Q}^T - (\mathbf{P}\mathbf{C}^{-1}\mathbf{Q}^T + \mathbf{Q}\mathbf{C}^{-1}\mathbf{P}^T) + \gamma^{-1}\mathbf{P}\mathbf{C}^{-1}\mathbf{P}^T,$$
$$\mathbf{K}_{qv} = \mathbf{L}\mathbf{C}^{-1}\left(\mathbf{Q}^T - \gamma^{-1}\mathbf{P}^T\right), \qquad \mathbf{K}_v = \mathbf{L}\mathbf{C}^{-1}\mathbf{L}^T. \tag{22}$$

The coefficient submatrices will be identified as follows: $\mathbf{K}_q$ is the internal stiffness matrix, $\mathbf{K}_v$ is the boundary stiffness matrix, and $\mathbf{K}_{qv}$ is a internal-to-boundary coupling stiffness. The internal stiffness is similar but not identical to the effective stiffness matrix of t-generalized mixed principles[1]. We now proceed to reinterpret these results in terms of hybrid elements.

HYBRID ELEMENTS

Approach. The preceding treatment is relevant to the construction of *displacement-connected hybrid elements.* Hybrid elements based on more restricted assumptions were originally constructed by Pian and coworkers[2-4]. The principal features of the hybrid approach are:

(I)   The domain is subdivided into elements *before* the variational principle is established.

(II) Continuity requirements across element boundaries are relaxed by introducing boundary tractions or boundary displacements as Lagrange multiplier fields.

(III) All stress and internal-displacement degrees of freedom are eliminated (by either static condensation or kinematic constraints) at the *element level.*

Feature (I) says that hybrid functionals are effectively *mesh-dependent*, since the domain subdivision process introduces element boundaries which must be treated as *internal interfaces*, and therefore become part of the boundary portion S_i. Previous developments remain valid if we reinterpret "body" as "individual element," "volume" as "element volume," and "surface" as "interelement boundary."

Continuity and Connectors. The internal fields $\bar{\sigma}$ and $\bar{u}$ may be discontinuous across elements. The boundary displacement field $\bar{d}$, however, must be continuous on S_i, *i.e.* it must have the same value on adjacent elements. This conditions may be satisfied if $\bar{d}$ on an interface separating two elements *is uniquely interpolated by nodal values on that interface.* It is natural to take such nodal values as entries of v, which automatically becomes the vector of *connected node displacements* or *connectors.*

FIELD DECOMPOSITION

In this and subsequent sections we work with an *individual element* unless otherwise noted. The element volume is V and the element surface is $S : S_d \cup S_t \cup S_i$. The v subvector contains the

element-connector degrees of freedom, whereas $\mathbf{q}$ and $\mathbf{a}$ contain internal freedoms. To gain further insight into the structure of the element equations and to link up eventually with the free formulation, we proceed to decompose both internal element fields as follows.

Stress Decomposition. The assumed stress field, $\tilde{\sigma}$, is decomposed into a mean value, $\bar{\sigma}$, and a deviator:

$$\tilde{\sigma} = \bar{\sigma} + \sigma_h = \bar{\sigma} + \mathbf{A}_h \mathbf{a}_h, \tag{23}$$

in which

$$\bar{\sigma} = (\tilde{\sigma})_V / \upsilon, \qquad (\mathbf{A}_h)_V = \mathbf{0}, \tag{24}$$

where $\upsilon = (1)_V$ denotes the element volume. The second relation in (24) is obtained by integrating (23) over V and noting that $\mathbf{a}_h$ is arbitrary.

Internal Displacement Decomposition. Next, the $\bar{\mathbf{u}}$ assumption is decomposed into rigid body, constant strain, and higher order displacements:

$$\bar{\mathbf{u}} = \mathbf{N}_r \mathbf{q}_r + \mathbf{N}_c \mathbf{q}_c + \mathbf{N}_h \mathbf{q}_h. \tag{25}$$

Applying the strain operator $\mathbf{D} = \frac{1}{2}(\nabla + \nabla^T)$ to $\bar{\mathbf{u}}$ we get the associated strain field:

$$\mathbf{e}^u = \mathbf{D}\mathbf{N}_r \mathbf{q}_r + \mathbf{D}\mathbf{N}_c \mathbf{q}_c + \mathbf{D}\mathbf{N}_h \mathbf{q}_h = \mathbf{B}_r \mathbf{q}_r + \mathbf{B}_c \mathbf{q}_c + \mathbf{B}_h \mathbf{q}_h. \tag{26}$$

But $\mathbf{B}_r = \mathbf{D}\mathbf{N}_r$ vanishes because $\mathbf{N}_r$ contains only rigid-body modes. We are also free to select $\mathbf{B}_c = \mathbf{D}\mathbf{N}_c$ to be the identity matrix $\mathbf{I}$ if the generalized coordinates $\mathbf{q}_c$ are identified with the mean (volume-averaged) strain values $\bar{\mathbf{e}}^u$. Then (26) simplifies to

$$\mathbf{e}^u = \bar{\mathbf{e}}^u + \mathbf{e}_h^u = \bar{\mathbf{e}}^u + \mathbf{B}_h \mathbf{q}_h, \tag{27}$$

in which

$$\mathbf{q}_c = \bar{\mathbf{e}}^u = (\mathbf{e}^u)_V / \upsilon, \qquad (\mathbf{B}_h)_V = \mathbf{0}. \tag{28}$$

Equation Partitioning. Assume that all elastic moduli in $\mathbf{E}$ are *constant* over the element. The degree of freedom partition

$$\mathbf{a} = \left\{ \begin{array}{c} \bar{\sigma} \\ \mathbf{a}_h \end{array} \right\}, \qquad \mathbf{q} = \left\{ \begin{array}{c} \mathbf{q}_r \\ \bar{\mathbf{e}}^u \\ \mathbf{q}_h \end{array} \right\}, \tag{29}$$

induces the following partition of the element equations

$$\begin{bmatrix} -\gamma\upsilon\mathbf{E}^{-1} & \mathbf{0} & -\bar{\mathbf{P}}_r^T & \gamma\upsilon\mathbf{I} - \bar{\mathbf{P}}_c^T & -\bar{\mathbf{P}}_h^T & \bar{\mathbf{L}}^T \\ \mathbf{0} & -\gamma\mathbf{C}_h & -\mathbf{P}_{hr}^T & -\mathbf{P}_{hc}^T & \gamma\mathbf{Q}_h^T - \mathbf{P}_{hh}^T & \mathbf{L}_h^T \\ -\bar{\mathbf{P}}_r & \mathbf{P}_{hr} & \mathbf{0} & \mathbf{0} & \mathbf{0} & \mathbf{0} \\ \gamma\upsilon\mathbf{I} - \bar{\mathbf{P}}_c & \mathbf{P}_{hc} & \mathbf{0} & (1-\gamma)\upsilon\mathbf{E} & \mathbf{0} & \mathbf{0} \\ -\bar{\mathbf{P}}_h & \gamma\mathbf{Q}_h - \mathbf{P}_{hh} & \mathbf{0} & \mathbf{0} & (1-\gamma)\mathbf{K}_{qh} & \mathbf{0} \\ -\bar{\mathbf{L}} & -\mathbf{L}_h & \mathbf{0} & \mathbf{0} & \mathbf{0} & \mathbf{0} \end{bmatrix} \left\{ \begin{array}{c} \bar{\sigma} \\ \mathbf{a}_h \\ \mathbf{q}_r \\ \bar{\mathbf{e}}^u \\ \mathbf{q}_h \\ \mathbf{v} \end{array} \right\} = \left\{ \begin{array}{c} \mathbf{0} \\ \mathbf{0} \\ \mathbf{f}_{qr} \\ \mathbf{f}_{qc} \\ \mathbf{f}_{qh} \\ \mathbf{f}_v \end{array} \right\} \tag{30}$$

where

$$C_h = (A_h^T E^{-1} A_h) v, \qquad Q_h = (B_h^T A_h) v, \qquad K_{qh} = (B_h^T E B_h) v,$$

$$\bar{P}_x = [N_{xn}^T]_S, \quad x = r, c, h, \qquad P_{hx} = [N_x^T A_{hn}]_S, \quad x = r, c, h \tag{31}$$

$$\bar{L} = [V_n^T]_S, \qquad L_h = [V^T A_{hn}]_S, \qquad f_{qx} = (N_x^T b) v, \quad x = r, c, h$$

Integral transformations. Application of the divergence theorem to the work of the mean stress on e^u yields

$$(\bar{\sigma}, e^u)_V = (\bar{\sigma}, \bar{e}^u + B_h q_h)_V = v\bar{\sigma}^T \bar{e}^u + \bar{\sigma}^T (B_h) v q_h = v\bar{\sigma}^T \bar{e}^u$$

$$= [\bar{\sigma}_n, \bar{u}]_S = [\bar{\sigma}_n, N_r q_r + N_c \bar{e}^u + N_h q_h]_S = \bar{\sigma}^T (\bar{P}_r q_r + \bar{P}_c \bar{e}^u + \bar{P}_h q_h). \tag{32}$$

Hence,

$$\bar{P}_r = 0, \qquad \bar{P}_c = vI, \qquad \bar{P}_h = 0. \tag{33}$$

A similar analysis of the stress-deviator work $(\sigma_h, e^u)_V$ does not yield simple forms for the P_{hx} matrices unless σ_h is *divergence-free*, in which case

$$P_{hr} = 0, \qquad P_{hc} = 0, \qquad P_{hh} = Q_h. \tag{34}$$

Assuming (34) to hold, the element equations (30) simplify to

$$\begin{bmatrix} -\gamma v E^{-1} & 0 & 0 & -(1-\gamma)vI & 0 & \bar{L}^T \\ 0 & -\gamma C_h & 0 & 0 & -(1-\gamma)Q_h^T & L_h^T \\ 0 & 0 & 0 & 0 & 0 & 0 \\ -(1-\gamma)vI & 0 & 0 & (1-\gamma)vE & 0 & 0 \\ 0 & -(1-\gamma)Q_h & 0 & 0 & (1-\gamma)K_{qh} & 0 \\ -\bar{L} & -L_h & 0 & 0 & 0 & 0 \end{bmatrix} \begin{Bmatrix} \bar{\sigma} \\ a_h \\ q_r \\ \bar{e}^u \\ q_h \\ v \end{Bmatrix} = \begin{Bmatrix} 0 \\ 0 \\ f_{qr} \\ f_{qc} \\ f_{qh} \\ f_v \end{Bmatrix} \tag{35}$$

The stress freedoms $\bar{\sigma}$ and a_h may be eliminated by static condensation as before. To eliminate q_r, a kinematic transformation that uniquely determines the rigid body motion from the element interface motion is constructed:

$$q_r = H_r v \tag{36}$$

where H_r is a rectangular matrix derived in Appendix 1. Elimination of $\bar{\sigma}$, a_h and q_r gives

$$\begin{bmatrix} \frac{1-\gamma}{\gamma} vE & 0 & -\frac{1-\gamma}{\gamma} E\bar{L}^T \\ 0 & (1-\gamma)K_{qh} + \gamma K_{\sigma h} & K_{qvh}^T \\ -\frac{1-\gamma}{\gamma} \bar{L}E & K_{qvh} & \gamma^{-1} K_v \end{bmatrix} \begin{Bmatrix} \bar{e}^u \\ q_h \\ v \end{Bmatrix} = \begin{Bmatrix} f_{qc} \\ f_{qh} \\ f_v + H_r^T f_{qr} \end{Bmatrix} \tag{37}$$

where

$$K_{\sigma h} = Q_h C_h^{-1} Q_h^T, \qquad K_{qvh} = L_h C_h^{-1} Q_h^T, \qquad K_v = \bar{K}_v + K_{vh},$$

$$\bar{K}_v = v^{-1} \bar{L} E \bar{L}^T, \qquad K_{vh} = L_h C_h^{-1} L_h^T \tag{38}$$

Mean Strain Elimination. Subvector $\bar{\mathbf{e}}^u$ may be eliminated in two ways. Static condensation gives

$$\begin{bmatrix} (1-\gamma)\mathbf{K}_{qh} + \gamma\mathbf{K}_{\sigma h} & \mathbf{K}_{qvh}^T \\ \mathbf{K}_{qvh} & \overline{\mathbf{K}}_v + \gamma^{-1}\mathbf{K}_{vh} \end{bmatrix} \begin{Bmatrix} \mathbf{q}_h \\ \mathbf{v} \end{Bmatrix} = \begin{Bmatrix} \mathbf{f}_{qh} \\ \mathbf{f}_v + \mathbf{H}_r^T\mathbf{f}_{qr} + \upsilon^{-1}\overline{\mathbf{L}}\mathbf{f}_{qc} \end{Bmatrix} \tag{39}$$

On the other hand, if $\bar{\mathbf{e}}^u$ is eliminated through the kinematic constraint $\bar{\mathbf{e}}^u = \mathbf{H}_c\mathbf{v}$ derived in Appendix 1,

$$\begin{bmatrix} (1-\gamma)\mathbf{K}_{qh} + \gamma\mathbf{K}_{\sigma h} & \mathbf{K}_{qvh}^T \\ \mathbf{K}_{qvh} & \mathbf{K}_v' + \gamma^{-1}\mathbf{K}_{vh} \end{bmatrix} \begin{Bmatrix} \mathbf{q}_h \\ \mathbf{v} \end{Bmatrix} = \begin{Bmatrix} \mathbf{f}_{qh} \\ \mathbf{f}_v + \mathbf{H}_r^T\mathbf{f}_{qr} + \mathbf{H}_c^T\mathbf{f}_{qc} \end{Bmatrix} \tag{40}$$

where

$$\mathbf{K}_v' = \gamma^{-1}\overline{\mathbf{K}}_v + \frac{1-\gamma}{\gamma}\left(\upsilon\mathbf{H}_c^T\mathbf{E}\mathbf{H}_c - \mathbf{H}_c^T\mathbf{E}\overline{\mathbf{L}}^T - \overline{\mathbf{L}}\mathbf{E}\mathbf{H}_c\right) \tag{41}$$

The two methods furnish identical results if

$$\mathbf{H}_c = \upsilon^{-1}\overline{\mathbf{L}}^T \tag{42}$$

As discussed in Appendix 1, this relation may be obtained from the first matrix equation in (35) if either $\gamma = 0$, or $\mathbf{e}^u = \bar{\mathbf{e}}^\sigma = \mathbf{E}^{-1}\bar{\sigma}$. The last condition is obtained in the limit of a converged solution as the patch test analysis of Appendix 2 shows. In practice any difference between (39) and (40) for $\gamma \neq 0$ is not significant, and (39) is preferable on grounds of simplicity.

THE FREE FORMULATION

The free formulation of Bergan and Nygård[5] was originally constructed as an incompatible displacement model that passes a cancelling-tractions version of the patch test which Bergan and Hanssen called the individual patch test[6]. Here the formulation is reinterpreted in the context of a displacement-connected hybrid variational principle.

First, assume that the internal stress field is *constant*, so there are no $\mathbf{a}_h$ parameters. Then (39) reduces to

$$\begin{bmatrix} (1-\gamma)\mathbf{K}_{qh} & \mathbf{0} \\ \mathbf{0} & \overline{\mathbf{K}}_v \end{bmatrix} \begin{Bmatrix} \mathbf{q}_h \\ \mathbf{v} \end{Bmatrix} = \begin{Bmatrix} \mathbf{f}_{qh} \\ \mathbf{f}_v + \mathbf{H}_r^T\mathbf{f}_{qr} + \upsilon^{-1}\overline{\mathbf{L}}\mathbf{f}_{qc} \end{Bmatrix} \tag{43}$$

The equations for $\mathbf{q}_h$ uncouple. Consequently static condensation of $\mathbf{q}_h$ will not change the solution. We have run into a displacement limitation principle. This leads to the second assumption: the higher order internal displacement modes are eliminated by kinematic constraints that link $\mathbf{q}_h$ to the boundary displacements:

$$\mathbf{q}_h = \mathbf{H}_h\mathbf{v} \tag{44}$$

Matrix $\mathbf{H}_h$ is derived in Appendix 1. Application of this constraint to (43) furnishes the final stiffness equations

$$\mathbf{K}\mathbf{v} = [\mathbf{K}_b + (1-\gamma)\mathbf{K}_h]\,\mathbf{v} = \mathbf{f} \tag{45}$$

where

$$\mathbf{K}_b = \overline{\mathbf{K}}_v, \qquad \mathbf{K}_h = \mathbf{H}_h^T\mathbf{K}_{qh}\mathbf{H}_h, \qquad \mathbf{f} = \mathbf{f}_v + \mathbf{H}_r^T\mathbf{f}_{qr} + \upsilon^{-1}\overline{\mathbf{L}}\mathbf{f}_{qc} + \mathbf{H}_h\mathbf{f}_{qh}. \tag{46}$$

In the free formulation, K_b and K_h receive the name *basic* and *higher order* stiffness matrices, respectively. A $\frac{1}{2}$ scaling of K_h derived from energy-balancing studies was recommended by Bergan and Felippa[7] for a plane stress element. This corresponds to taking $\gamma = \frac{1}{2}$.

CONCLUDING REMARKS

It has been known[7] that the *basic-stiffness* part of the free formulation can be interpreted as a constant-stress hybrid element. But the interpretation of the higher order stiffness within a variational framework has been difficult. A key result of this paper is that this can be accomplished by a *parametrized* mixed-hybrid variational principle. Note that the free formulation cannot be obtained within the conventional Hellinger-Reissner principle ($\gamma = 1$), since then the higher-order stiffness vanishes and $K = \overline{K}_v$ is generally rank-deficient. And choosing $\gamma = 0$ does not account for the fact that the higher order stiffness can be scaled by a nonzero coefficient.

The variational framework is important because it allows consistent extensions of the free formulation that are not obvious from a physical standpoint. For example: allowing more internal displacement degrees of freedom than boundary freedoms, i.e. $m = \dim(q) - \dim(v) > 0$. A glance at (39) shows that m additional higher-order divergence-free stress fields have to be retained so that the coupling stiffness K_{qvh} does not vanish. The reduction of q_h can be then performed by a combination of static condensation and kinematic constraints.

ACKNOWLEDGEMENTS

REFERENCES

1. C. A. Felippa, 'Parametrized Multifield Variational Principles in Elasticity: I. Mixed Functionals,' submitted to *Communications in Applied Numerical Methods*

2. T. H. H. Pian, 'Derivation of element stiffness matrices by assumed stress distributions,' *AIAA Journal*, 2, pp. 1333–1336, 1964

3. T. H. H. Pian and P. Tong, 'Basis of finite element methods for solid continua,' *Int. J. Numer. Meth. Engrg.*, 1, pp. 3–29, 1969

4. T. H. H. Pian, 'Finite element methods by variational principles with relaxed continuity requirements,' in *Variational Methods in Engineering*, Vol. 1, ed. by C. A. Brebbia and H. Tottenham, Southampton University Press, 1973

5. P. G. Bergan and M. K. Nygård, 'Finite elements with increased freedom in choosing shape functions,' *Int. J. Num. Meth. Engrg.*, 20, 1984, pp. 643–664

6. P. G. Bergan and L. Hanssen, A new approach for deriving "good" finite elements, MAFELAP II Conference, Brunel University, 1975, in *The Mathematics of Finite Elements and Applications – Volume II*, ed. by J. R. Whiteman, Academic Press, London, 1976

7. P. G. Bergan and C. A. Felippa, 'A Triangular Membrane Element with Rotational Degrees of Freedom,' *Computer Methods in Applied Mechanics & Engineering*, 50, 1985, pp. 25–69

8. P. G. Bergan, 'Finite Elements Based on Energy Orthogonal Functions,' *Int. J. Num. Meth. Engrg.*, 15, 1980, pp. 1141–1555

9. B. M. Fraeijs de Veubeke, 'Variational Formulation and the Patch Test,' *Int. J. Num. Meth. Engrg*, 8, pp. 783–801, 1974

APPENDIX 1: KINEMATIC CONSTRAINTS

One of the principal assumptions invoked in the free formulation is that the dimension of q is the same as that of v and that the latter are physical node displacements. If so, evaluation of the expansion $\bar{u} = Nq$ on the element boundary S establishes the transformation

$$v = Gq \tag{47}$$

where matrix G is square. Furthermore, suppose that G is *nonsingular* and can be inverted:

$$q = G^{-1}v = Hv, \tag{48}$$

or, in partitioned form

$$q = \begin{Bmatrix} q_r \\ q_c \\ q_h \end{Bmatrix} = \begin{bmatrix} H_r \\ H_c \\ H_h \end{bmatrix} v. \tag{49}$$

The first matrix equation (the discrete compatibility equation) in (20) can be presented as

$$\gamma(e^u - e^\sigma, A)_V = L^T v - Q^T q = (L^T - Q^T H)v = (L^T G - Q^T)q. \tag{50}$$

Setting $\gamma = 0$ forces the constraint

$$L^T = Q^T H \quad \text{or} \quad L^T G = Q^T \tag{51}$$

to be satisfied. The same constraint emerges if $\gamma \neq 0$ and the finite element solution has converged in the sense that $e^u = e^\sigma$ is constant over the element. Now carrying out the freedom partition (29) and assuming divergence-free higher order stresses so that (34) holds, the constraint (51) partitions as

$$\begin{bmatrix} \bar{L}^T \\ L_h^T \end{bmatrix} = \begin{bmatrix} 0 & vI & 0 \\ 0 & 0 & Q_h^T \end{bmatrix} \begin{bmatrix} H_r \\ H_c \\ H_h \end{bmatrix} \quad \text{or} \quad \begin{bmatrix} \bar{L}^T \\ L_h^T \end{bmatrix} [G_r \quad G_c \quad G_h] = \begin{bmatrix} 0 & vI & 0 \\ 0 & 0 & Q_h^T \end{bmatrix}. \tag{52}$$

from which follow the relations

$$\begin{array}{llll} \bar{L}^T G_r = 0, & \bar{L}^T G_c = vI, & \bar{L}^T = vH_c, & \bar{L}^T G_h = 0, \\ L_h^T G_r = 0, & L_h^T G_c = 0, & L_h^T = vH_h, & L_h^T G_h = I. \end{array} \tag{53}$$

The first four were obtained through other means by Bergan[8] and Bergan and Nygård[5], who called them the *force orthogonality* conditions on account of the physical interpretation of $\bar{L}$ as a "boundary nodal force lumping" matrix.

APPENDIX 2: THE CANCELLING-TRACTIONS PATCH TEST

It is not apparent whether this element class passes the patch test for an arbitrary γ. To investigate this question we use the sketch of Figure 1 and view the subvolumes V^+ and V^- as *two elements* connected along S_i with

an external traction boundary S_t. Both elements are in a state of *constant stress* σ_0. The prescribed surface tractions are $[\hat{t} = \sigma_{0n}]_{S_t}$ and the body forces b vanish. We take (35) to be the governing equations for the two-element assembly. The only nonzero forces are $f_v = [V^T \hat{t}]_{S_t}$. The key observation is that

$$\bar{L} = [V_n^T]_S = [V_n^T]_{S_t},\qquad(54)$$

because the integral over S_i vanishes because V is identical for both elements on account of interface compatibility conditions, and $n^+ = -n^-$. Similarly for L_h. One may verify that for any γ the solution of (35) is

$$\bar{\sigma} = \sigma_0 = \bar{\sigma}^u,\qquad a_h = 0,\qquad \bar{e}^u = v^{-1}\bar{L}^T v,\qquad q_h = 0.\qquad(55)$$

The connector node displacement vector v satisfies

$$v\bar{L}E\bar{L}^T v = f_v \qquad(56)$$

and consistency with the third of (55) is easily verified from (54). If the rigid body modes are eliminated, $v = G_c \bar{e}^u$. Since the constant stress solution is recovered, the patch test is passed for any value of γ.

The physical meaning of this form of the patch test is that the *interface virtual work is zero* when the element patch is in a constant stress state[9].

THE EXTENDED FREE FORMULATION OF FINITE ELEMENTS IN LINEAR ELASTICITY

SUMMARY

The free formulation of Bergan and Nygård (1984) has been successfully used in the construction of high-performance finite elements for linear and nonlinear structural analysis. In its original form the formulation combines nonconforming internal displacement assumptions with a specialized version of the patch test. The original formulation is limited, however, by strict invertibility conditions linking the assumed displacement field to the nodal displacements. The present paper lifts those restrictions by recasting the free formulation within the framework of a mixed-hybrid functional that allows internal stresses, internal displacements and boundary displacements to vary independently. This functional contains a free parameter and includes the potential energy and the Hellinger-Reissner principles as special cases. The parameter appears in the higher order stiffness of the free formulation element equations.

1 Introduction

Bergan and Nygård (1984) have developed the so-called free formulation (FF) for the construction of displacement-based, incompatible finite elements. This work consolidated a decade of research of Bergan and coworkers at Trondheim, milestones of which may be found in Bergan and Hanssen (1976), Hanssen *et.al.* (1979) and Bergan (1980). The products of this research have been finite elements of high performance, especially for plates and shells. Linear applications are reported in the aforementioned papers as well as in Bergan and Wang (1984), Bergan and Felippa (1985) and Felippa and Bergan (1987); whereas nonlinear applications are presented in Bergan and Nygård (1985) and Nygård (1986). By "high performance" it is meant that solution of engineering accuracy can be obtained with coarse meshes of simple elements, and that those elements exhibit low distortion sensitivity.

The original FF was based on nonconforming displacement assumptions, the principle of virtual work and a specialized form of Irons' patch test that Bergan and Hanssen (1976) called the individual element test. A key ingredient of the FF is the separation of the element stiffness matrix into the sum of two parts, called *basic* and *higher order* stiffness, respectively. The basic part is constructed for convergence and the higher order part for numerical stability and (in recent work) accuracy.

An intriguing question has been: does the FF fit in a variational framework? This was partly answered by Bergan and Felippa (1985), who showed that the basic stiffness part was equivalent to a constant-stress hybrid element. But persistent efforts by the present author to encompass the higher order stiffness within a hybrid variational principle were unsuccessful until the development of parametrized mixed-hybrid functionals in Felippa (1989a,1989b). With the help of these more general functionals it is possible to show that the FF is a very special type of mixed-hybrid element which does not fit within the classical Hellinger-Reissner principle. In retrospect the classification of FF elements as hybrids is not surprising. Under mild conditions studied in the Appendix, hybrid elements satisfy Irons' patch test *a priori*, and the FF development has been founded on that premise.

To encompass the FF within the hybrid framework, the following assumptions must be invoked.

(I) A specific hybrid functional, identified as Π_γ^d in the sequel, is constructed. This functional depends linearly on a parameter γ.

(II) Three fields are assumed over each element:

  (a) a constant stress field,

  (b) an internal displacement field u defined by n_q generalized coordinates collected in vector q, and

  (c) a boundary displacement field d defined by n_v nodal displacements collected in vector v.

  Both d and u must represent rigid body motions and constant strain states exactly.

(III) The number of generalized coordinates, n_q, equals the number of nodal displacements, n_v,

and the square transformation matrix **G** relating $\mathbf{v} = \mathbf{Gq}$ is nonsingular.

In Felippa (1989b) it is shown that substituting the finite element expansions into Π_γ^d, rendering the functional stationary with respect to the degrees of freedom, and eliminating both internal fields by a combination of static condensation and kinematic constraints, leads to the FF stiffness equations in terms of the nodal displacements **v**. The parameter γ appears as a coefficient of the higher order stiffness. These stiffness equations can be readily implemented into any displacement-based finite element code.

This variational pathway to FF is of interest for two reasons. First, it explains the behavior of FF elements as regards convergence, stability and accuracy. Second, it opens up the door to extensions that are not obvious from a physical standpoint. Two such extensions involve: retaining higher order stress fields, and allowing more internal displacement modes that nodal displacements, that is, $n_q > n_v$. The main purpose of this paper is to study these two extensions, which are shown to be closely related. The resulting framework for deriving finite elements in elasticity is called the extended free formulation (EFF).

2 Governing Equations

Consider a *linearly elastic body* under static loading that occupies the volume V. The body is bounded by the surface S, which is decomposed into $S : S_d \cup S_t$. Displacements are prescribed on S_d whereas surface tractions are prescribed on S_t. The outward unit normal on S is denoted by $\mathbf{n} \equiv n_i$.

The three unknown volume fields are displacements $\mathbf{u} \equiv u_i$, infinitesimal strains $\mathbf{e} \equiv e_{ij}$, and stresses $\boldsymbol{\sigma} \equiv \sigma_{ij}$. The problem data include: the body force field $\mathbf{b} \equiv b_i$ in V, prescribed displacements $\hat{\mathbf{d}}$ on S_d, and prescribed surface tractions $\hat{\mathbf{t}} \equiv \hat{t}_i$ on S_t.

The relations between the volume fields are the strain-displacement equations

$$\mathbf{e} = \tfrac{1}{2}(\nabla \mathbf{u} + \nabla^T \mathbf{u}) = \mathbf{Du} \qquad \text{or} \qquad e_{ij} = \tfrac{1}{2}(u_{i,j} + u_{j,i}) \quad \text{in } V, \tag{1}$$

the constitutive equations

$$\boldsymbol{\sigma} = \mathbf{Ee} \qquad \text{or} \qquad \sigma_{ij} = E_{ijkl}e_{kl} \quad \text{in } V, \tag{2}$$

and the equilibrium (balance) equations

$$-\text{div}\,\boldsymbol{\sigma} = \mathbf{D}^*\boldsymbol{\sigma} = \mathbf{b} \qquad \text{or} \qquad \sigma_{ij,j} + b_i = 0 \quad \text{in } V, \tag{3}$$

in which $\mathbf{D}^* = -\text{div}$ denotes the adjoint operator of $\mathbf{D} = \tfrac{1}{2}(\nabla + \nabla^T)$.

The stress vector with respect to a direction defined by the unit vector **v** is denoted as $\sigma_v = \boldsymbol{\sigma}.\mathbf{v}$, or $\sigma_{vi} = \sigma_{ij}v_j$. On S the surface-traction stress vector is defined as

$$\sigma_n = \boldsymbol{\sigma}.\mathbf{n}, \qquad \text{or} \qquad \sigma_{ni} = \sigma_{ij}n_j. \tag{4}$$

With this definition the traction boundary conditions may be stated as

$$\sigma_n = \hat{\mathbf{t}} \qquad \text{or} \qquad \sigma_{ij}n_j = \hat{t}_i \qquad \text{on } S_t, \tag{5}$$

and the displacement boundary conditions as

$$\mathbf{u} = \hat{\mathbf{d}} \qquad \text{or} \qquad u_i = \hat{d}_i \qquad \text{on } S_d. \tag{6}$$

3 Notation

Field Dependency. In variational methods of approximation we do not work of course with the exact fields that satisfy the governing equations (1-3,5-6), but with *independent* (primary) fields, which are subject to variations, and *dependent* (secondary, associated, derived) fields, which are not. The approximation is determined by taking variations with respect to the independent fields.

An *independently varied* field will be identified by a superposed tilde, for example $\tilde{u}$. A dependent field is identified by writing the independent field symbol as superscript. For example, if the displacements are independently varied, the derived strain and stress fields are

$$\mathbf{e}^u = \tfrac{1}{2}(\nabla + \nabla^T)\tilde{u} = \mathbf{D}\tilde{u}, \qquad \sigma^u = \mathbf{E}\mathbf{e}^u = \mathbf{E}\mathbf{D}\tilde{u}. \tag{7}$$

An advantage of this convention is that $\mathbf{u}$, $\mathbf{e}$ and σ may be reserved for the *exact* fields.

Integral Abbreviations. Volume and surface integrals will be abbreviated by placing domain-subscripted parentheses and square brackets, respectively, around the integrand. For example:

$$(f)_V \stackrel{\text{def}}{=} \int_V f \, dV, \quad [f]_S \stackrel{\text{def}}{=} \int_S f \, dS, \quad [f]_{S_d} \stackrel{\text{def}}{=} \int_{S_d} f \, dS, \quad [f]_{S_t} \stackrel{\text{def}}{=} \int_{S_t} f \, dS. \tag{8}$$

If $\mathbf{f}$ and $\mathbf{g}$ are vector functions, and $\mathbf{p}$ and $\mathbf{q}$ tensor functions, their inner product over V is denoted in the usual manner

$$(\mathbf{f}, \mathbf{g})_V \stackrel{\text{def}}{=} \int_V \mathbf{f}.\mathbf{g} \, dV = \int_V f_i g_i \, dV, \qquad (\mathbf{p}, \mathbf{q})_V \stackrel{\text{def}}{=} \int_V \mathbf{p}.\mathbf{q} \, dV = \int_V p_{ij} q_{ij} \, dV, \tag{9}$$

and similarly for surface integrals, in which case square brackets are used.

Domain Assertions. The notation

$$(a = b)_V, \qquad [a = b]_S, \qquad [a = b]_{S_d}, \qquad [a = b]_{S_t}, \tag{10}$$

is used to assert that the relation $a = b$ is valid at each point of V, S, S_d and S_t, respectively.

Internal Interfaces. In the following subsections a variational principle is constructed, in which boundary displacements $\mathbf{d}$ can be varied independently from the internal displacements $\mathbf{u}$. These displacement play the role of Lagrange multipliers that relax internal displacement continuity. Variational principles of this form will be called *displacement-generalized,* or *d*-generalized for short.

The choice of $\mathbf{d}$ as independent field is *not* variationally admissible on S_d or S_t. We must therefore extend the definition of boundary to include *internal interfaces* collectively designated as S_i. Thus

$$S : S_d \cup S_t \cup S_i. \tag{11}$$
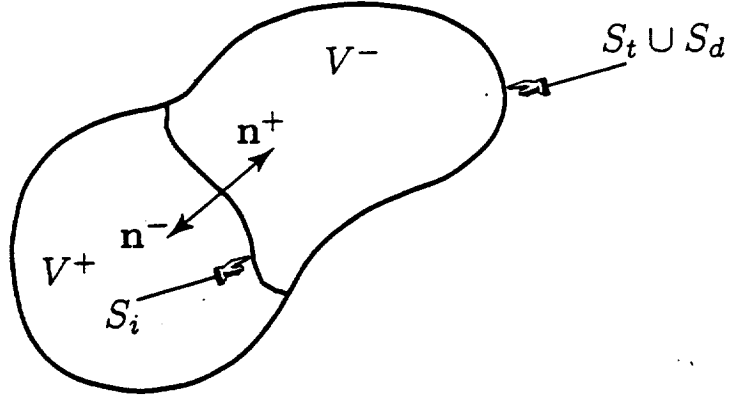
Figure 1. Internal interface example.

On S_i neither displacements nor tractions are prescribed. A simple case is illustrated in Figure 1, in which the interface S_i divides V into two subvolumes: V^+ and V^-.

An interface such as S_i on Figure 1 has two "sides" called S_i^+ and S_i^-, which identify S_i viewed as boundary of V^+ and V^-, respectively. At smooth points of S_i the unit normals $\mathbf{n}^+$ and $\mathbf{n}^-$ point in opposite directions.

The integral abbreviations (8)-(9) generalize as follows, using Figure 1 for definiteness. A volume integral is the sum of integrals over the subvolumes:

$$(f)_V \stackrel{\text{def}}{=} \int_{V^+} f\, dV + \int_{V^-} f\, dV. \tag{12}$$

An integral over S_i includes two contributions:

$$[g]_{S_i} \stackrel{\text{def}}{=} \int_{S_i^+} g^+\, dS + \int_{S_i^-} g^-\, dS, \tag{13}$$

where g^+ and g^- denotes the value of the integrand g on S_i^+ and S_i^-, respectively. These two values may be different if g is discontinuous or involves a projection on the normals.

4 The Hu-Washizu Principle

There are several essentially equivalent statements of the Hu-Washizu functional of linear elasticity. The starting form used here is the four-field functional

$$\Pi^d_W(\tilde{\mathbf{u}}, \tilde{\mathbf{e}}, \tilde{\sigma}, \tilde{\mathbf{d}}) = \tfrac{1}{2}(\sigma^e, \tilde{\mathbf{e}})_V + (\tilde{\sigma}, \mathbf{e}^u - \tilde{\mathbf{e}})_V - P^d, \tag{14}$$

where P^d is the "forcing" potential

$$P^d(\bar{u}, \bar{\sigma}, \bar{d}) = (b, \bar{u})_V + [\bar{\sigma}_n, \bar{u} - \hat{d}]_{S_d} + [\hat{t}, \bar{u}]_{S_t} + [\bar{\sigma}_n, \bar{u} - \bar{d}]_{S_i}. \tag{15}$$

The functional Π_W^d is called d-generalized in the sense that the volume fields $\bar{u}, \bar{e}, \bar{\sigma}$ *and* the surface displacement field $\bar{d}$ are subject to independent variations, whereas in the conventional form of the principle the relation $[d = \bar{u}]_{S_d \cup S_i}$ is enforced *a priori*. The superscript d is used to distinguish it from the t-generalized variant

$$\Pi_W^t(\bar{u}, \bar{e}, \bar{\sigma}, \bar{t}) = \tfrac{1}{2}(\sigma^e, \bar{e})_V + (\bar{\sigma}, e^u - \bar{e})_V - P^t, \tag{16}$$

in which the surface tractions $\bar{t}$ are varied independently from the internal stress field $\bar{\sigma}$. This is the starting form in the classical textbook of Washizu (1968). Parametrized versions of (16) are studied in further detail in Felippa (1989a).

Functionals that are not d- or t-generalized will be called *conventional*. The three versions differ only in the forcing potential term.

5 Parametrization

Constraining the Hu-Washizu functional (14) by selectively enforcing field equations and boundary conditions *a priori* yields six functionals listed (in their conventional form) in Ch. 4 of the monograph of Oden and Reddy (1983). Of particular interest for the present study are the d-generalized Hellinger-Reissner functional

$$\Pi_R^d(\bar{u}, \bar{\sigma}, \bar{d}) = -\tfrac{1}{2}(\bar{\sigma}, e^\sigma)_V + (\bar{\sigma}, e^u)_V - P^d, \tag{17}$$

as well as the d-generalized potential energy functional

$$\Pi_P^d(\bar{u}, \bar{d}) = \tfrac{1}{2}(\sigma^u, e^u)_V - P^d. \tag{18}$$

These two functionals are special cases of the following parametrized form

$$\Pi_\gamma^d(\bar{u}, \bar{\sigma}, \bar{d}) = \tfrac{1}{2}(1 - \gamma)(\sigma^u, e^u)_V - \tfrac{1}{2}\gamma(\bar{\sigma}, e^\sigma)_V + \gamma(\bar{\sigma}, e^u)_V - P^d, \tag{19}$$

where γ is a scalar. If $\gamma = 1$ and 0 we obtain the functionals Π_R^d and Π_P^d, respectively. Parametrized forms, such as (19), of the elasticity variational principles were studied by Chien (1983).

First Variation. Defining the γ-weighted stresses

$$\sigma^\gamma \stackrel{\text{def}}{=} \gamma\bar{\sigma} + (1 - \gamma)\sigma^u \quad \text{in } V, \qquad \sigma_n^\gamma \stackrel{\text{def}}{=} \gamma\bar{\sigma}_n + (1 - \gamma)\sigma_n^u \quad \text{on } S \tag{20}$$

the first variation of (19) can be written

$$\begin{aligned}
\delta\Pi_\gamma^d = {} & \gamma\left(e^u - e^\sigma, \delta\bar{\sigma}\right)_V - (\text{div } \sigma^\gamma + b, \delta\bar{u})_V - \left[\hat{t} - \sigma_n^\gamma, \delta\bar{u}\right]_{S_t} \\
& - \left[\bar{\sigma}_n - \bar{\sigma}_n^\gamma, \delta\bar{u}\right]_{S_d} - \left[u - \hat{d}, \delta\bar{\sigma}_n\right]_{S_d} \\
& - \left[\bar{\sigma}_n - \bar{\sigma}_n^\gamma, \delta\bar{u}\right]_{S_i} - \left[\bar{u} - \bar{d}, \delta\bar{\sigma}_n\right]_{S_i} - \left[\bar{\sigma}_n, \delta\bar{d}\right]_{S_i}
\end{aligned} \tag{21}$$

33

Since **d** is unique on S_i whereas $\tilde{\mathbf{u}}$ and $\tilde{\sigma}$ are generally discontinuous on it, the interface integrals in (22) split as follows:

$$\left[\tilde{\sigma}_n - \tilde{\sigma}_n^\gamma, \delta\tilde{\mathbf{u}}\right]_{S_i} = \left[\tilde{\sigma}_n^+ - \tilde{\sigma}_n^{\gamma+}, \delta\tilde{\mathbf{u}}^+\right]_{S_i^+} + \left[\tilde{\sigma}_n^- - \tilde{\sigma}_n^{\gamma-}, \delta\tilde{\mathbf{u}}^-\right]_{S_i^-},$$

$$\left[\tilde{\mathbf{u}} - \tilde{\mathbf{d}}, \delta\tilde{\sigma}\right]_{S_i} = \left[\tilde{\mathbf{u}}^+ - \tilde{\mathbf{d}}, \delta\tilde{\sigma}_n^+\right]_{S_i^+} + \left[\tilde{\mathbf{u}}^- - \tilde{\mathbf{d}}, \delta\tilde{\sigma}_n^-\right]_{S_i^-}, \tag{22}$$

$$\left[\tilde{\sigma}_n, \delta\tilde{\mathbf{d}}\right]_{S_i} = \left[\tilde{\sigma}_n^+, \delta\tilde{\mathbf{d}}\right]_{S_i^+} + \left[\tilde{\sigma}_n^-, \delta\tilde{\mathbf{d}}\right]_{S_i^-} = \left[\tilde{\sigma}_n^+ - \tilde{\sigma}_n^-, \delta\tilde{\mathbf{d}}\right]_{S_i}.$$

Setting the first variation to zero and taking (22) into account, the Euler equations and natural boundary conditions for $\gamma \neq 0$ are found to be

$$(\mathbf{e}^u = \mathbf{e}^\sigma)_V, \quad (\text{div}\,\sigma^\gamma + \mathbf{b} = 0)_V, \quad [\sigma_n^\gamma = \hat{\mathbf{t}}]_{S_t}, \quad [\sigma_n = \sigma_n^\gamma]_{S_d}, \quad [\mathbf{u} = \hat{\mathbf{d}}]_{S_d},$$
$$[\sigma_n^{\gamma+} + \sigma_n^+ = 0]_{S_i}, \quad [\sigma_n^{\gamma-} + \sigma_n^- = 0]_{S_i}, \quad [\mathbf{u}^+ = \mathbf{u}^- = \mathbf{d}]_{S_i}, \quad [\sigma_n^+ + \sigma_n^- = 0]_{S_i}. \tag{23}$$

The constitutive equations do not appear since they are enforced *a priori* in Π_γ^d. If $\gamma = 0$ the first equation, $(\mathbf{e}^u = \mathbf{e}^\sigma)_V$, drops out.

Modified Forcing Potential. Substituting **d** in lieu of **u** in the forcing potential (15)

$$P^d(\tilde{\mathbf{u}}, \tilde{\sigma}, \tilde{\mathbf{d}}) = (\mathbf{b}, \tilde{\mathbf{u}})_V + [\tilde{\sigma}_n, \tilde{\mathbf{d}} - \hat{\mathbf{d}}]_{S_d} + [\hat{\mathbf{t}}, \tilde{\mathbf{d}}]_{S_t} + [\tilde{\sigma}_n, \tilde{\mathbf{u}} - \tilde{\mathbf{d}}]_{S_i} \tag{24}$$

is *not* variationally admissible because incorrect Euler equations result. This form has appeared, however, in publications dealing with mixed-hybrid methods. A correct potential that resembles (24) can be obtained in two stages. First, surface terms $[\tilde{\sigma}_n, \tilde{\mathbf{u}} - \tilde{\mathbf{d}}]_{S_t}$ and $[\tilde{\sigma}_n, \tilde{\mathbf{u}} - \tilde{\mathbf{d}}]_{S_d}$ are added and subtracted to produce

$$P^d(\tilde{\mathbf{u}}, \tilde{\sigma}, \tilde{\mathbf{d}}) = (\mathbf{b}, \tilde{\mathbf{u}})_V + [\tilde{\sigma}_n, \tilde{\mathbf{d}} - \hat{\mathbf{d}}]_{S_d} - [\tilde{\sigma}_n - \hat{\mathbf{t}}, \tilde{\mathbf{u}}]_{S_t} + [\hat{\mathbf{t}}, \tilde{\mathbf{d}}]_{S_t} + [\tilde{\sigma}_n, \tilde{\mathbf{u}} - \tilde{\mathbf{d}}]_S. \tag{25}$$

Second, $\hat{\mathbf{t}}$ is assumed to be in the range of $\tilde{\sigma}_n$ and the condition $[\tilde{\sigma}_n = \hat{\mathbf{t}}]_{S_t}$ satisfied *a priori*, reducing (25) to

$$P^d(\tilde{\mathbf{u}}, \tilde{\sigma}, \tilde{\mathbf{d}}) = (\mathbf{b}, \tilde{\mathbf{u}})_V + [\tilde{\sigma}_n, \tilde{\mathbf{d}} - \hat{\mathbf{d}}]_{S_d} + [\hat{\mathbf{t}}, \tilde{\mathbf{d}}]_{S_t} + [\tilde{\sigma}_n, \tilde{\mathbf{u}} - \tilde{\mathbf{d}}]_S. \tag{26}$$

This expression differs from (24) in that the all-important surface dislocation integral is taken over S rather than S_i. Further simplification results if the displacement boundary conditions $[\tilde{\mathbf{d}} = \hat{\mathbf{d}}]_{S_d}$ are exactly satisfied:

$$P^d(\tilde{\mathbf{u}}, \tilde{\sigma}, \tilde{\mathbf{d}}) = (\mathbf{b}, \tilde{\mathbf{u}})_V + [\hat{\mathbf{t}}, \tilde{\mathbf{d}}]_{S_t} + [\tilde{\sigma}_n, \tilde{\mathbf{u}} - \tilde{\mathbf{d}}]_S. \tag{27}$$

This expression of P^d is used in the sequel, as modifications required to account for the case $[\tilde{\mathbf{d}} \neq \hat{\mathbf{d}}]_{S_d}$ are of minor importance.

6 Energy Balancing

Distances. Let $U(\epsilon) = \frac{1}{2}(E\epsilon, \epsilon)_V$ denote the strain energy associated with field ϵ. We may rewrite (19) as a potential-energy deviator

$$\Pi_\gamma^d = \Pi_P^d - \gamma\, U(e^u - e^\sigma), \tag{28}$$

because

$$\frac{\Pi_\gamma^d - \Pi_P^d}{\gamma/2} = (\bar{\sigma}, e^\sigma - e^u)_V - (\bar{\sigma} - \sigma^u, e^u)_V = \tag{29}$$

$$(\sigma^u - \bar{\sigma}, e^u - e^\sigma)_V = (Ee^u - Ee^\sigma, e^u - e^\sigma)_V.$$

If E is positive definite, $U(e^u - e^\sigma) \geq 0$ and consequently

$$\Pi_\gamma^d \leq \Pi_P^d \quad \text{if} \quad \gamma > 0. \tag{30}$$

If $\bar{u}$ is kinematically admissible, Π_P^d exceeds the exact potential energy as shown below. It follows that to improve solutions in energy we expect to take $\gamma \geq 0$. Thus principles associated with $\gamma < 0$ have limited practical interest.

Let $\Pi(u)$ denote the exact potential energy

$$\Pi(u) = \frac{1}{2}(\sigma, e)_V - (b, u)_V - [\hat{t}, u]_{S_t}, \tag{31}$$

where σ and e denotes the exact stress and strain field, respectively. If $\bar{u}$ is kinematically admissible and thus satisfies $[\bar{u} = \hat{d}]_{S_d}$, then the energy distance from $\Pi_P^d(\bar{u})$ to the exact functional (31) is [see *e.g.* §34 of Gurtin (1972)]

$$\Pi_P^d - \Pi = \frac{1}{2}(\sigma^u - \sigma, e^u - e)_V = U(e^u - e). \tag{32}$$

Adjusting γ. To derive an "energy balanced" approximation we impose the condition $\Pi_\gamma^d = \Pi$, which yields

$$\gamma_b = \frac{U(e^u - e)}{U(e^u - e^\sigma)} = \frac{(\sigma^u - \sigma, e^u - e)}{(\sigma^u - \bar{\sigma}, e^u - e^\sigma)}. \tag{33}$$

For example, if we assume that the exact stresses and strains lie halfway between the approximate fields,

$$\sigma = \frac{1}{2}(\sigma^u + \bar{\sigma}), \qquad e = \frac{1}{2}(e^\sigma + e^u), \tag{34}$$

then $\gamma_b = \frac{1}{4}$. But as the exact stresses and strains for the elasticity problem are not generally known in advance, the practical determination of γ_b has been based on application of (33) to element "patches" under simple load systems, as discussed in Bergan and Felippa (1985) and Felippa and Bergan (1987).

Error Estimates. The strain difference $e^u - e^\sigma$ may be used as a pointwise measure of solution accuracy, and the associated "dislocation work" $U(e^u - e^\sigma)$ as an energy error measure for applications such as adaptive mesh refinement.

7 Finite Element Discretization

In this section the finite element discretization of Π_γ^d is studied. Following usual practice in finite element work, the components of stresses and strains are arranged as one-dimensional arrays whereas the elastic moduli in E are arranged as a square symmetric matrix. The FE assumption is globally written

$$(\tilde{u} = Nq)_V, \qquad (\tilde{\sigma} = Aa)_V, \qquad [\tilde{d} = Vv]_S. \tag{35}$$

Here matrices N, A and V collect generalized-displacement shape functions, internal stress modes and interface displacement modes, respectively, whereas column vectors q, a and v collect generalized internal displacements, stress mode amplitudes, and generalized interface displacements, respectively. The assumed volume fields $\tilde{\sigma}$ and $\tilde{u}$ need not be continuous across S_i. The derived fields are

$$(e^u = DNq = Bq)_V, \qquad (\sigma^u = EBq)_V, \qquad (e^\sigma = E^{-1}\tilde{\sigma} = E^{-1}Aa)_V. \tag{36}$$

Inserting these expressions into Π_γ^d with the forcing potential (27), we obtain the algebraic form

$$\Pi_\gamma^d(a, q, s) = \tfrac{1}{2}(1 - \gamma)q^T K_u q - \tfrac{1}{2}\gamma a^T C a + \gamma q^T Q a - q^T P a + v^T L a - q^T f_q - v^T f_v \tag{37}$$

where

$$
\begin{aligned}
K_u &= (B^T E B)_V = K_u^T, & C &= (A^T E^{-1} A)_V = C^T, & Q &= (B^T A)_V, \\
L &= [V^T A_n]_S, & P &= [N^T A_n]_S, & f_q &= (N^T b)_V, & f_v &= [N^T \hat{t}]_{S_t}.
\end{aligned}
\tag{38}
$$

The matrices K_u, C, Q, L and P are called internal-displacement stiffness, compliance, leverage, nodal-force lumping, and boundary dislocation matrices, respectively. Making (37) stationary yields the linear system

$$
\begin{bmatrix}
-\gamma C & \gamma Q^T - P^T & L^T \\
\gamma Q - P & (1 - \gamma)K_u & 0 \\
L & 0 & 0
\end{bmatrix}
\begin{Bmatrix} a \\ q \\ v \end{Bmatrix}
=
\begin{Bmatrix} 0 \\ f_q \\ f_v \end{Bmatrix}.
\tag{39}
$$

The first matrix equation is the discrete analog of the first, fifth and eighth relations in (24), and expresses internal and boundary compatibility. The third matrix equation is the discrete analog of the last relation, and expresses equilibrium across S_i. The second matrix equation is the discrete analog of the remaining relations, and expresses internal and boundary equilibrium.

It is shown later (in Section 9) that if the assumed stress modes in A are *divergence free* (self-equilibrating), then $P \equiv Q$, and (39) simplifies to

$$
\begin{bmatrix}
-\gamma C & -(1 - \gamma)Q^T & L^T \\
-(1 - \gamma)Q & (1 - \gamma)K_u & 0 \\
L & 0 & 0
\end{bmatrix}
\begin{Bmatrix} a \\ q \\ v \end{Bmatrix}
=
\begin{Bmatrix} 0 \\ f_q \\ f_v \end{Bmatrix}.
\tag{40}
$$

These results are now re-interpreted in terms of hybrid elements.

8 Hybrid Elements

Approach. The preceding treatment is relevant to the construction of *displacement-connected hybrid elements*. Hybrid elements based on more restricted assumptions were originally constructed by Pian and coworkers; see Pian (1964), Pian and Tong (1969) and Pian (1973). From a modern perspective, the principal features of the hybrid formulation are:

(A) The domain is subdivided into elements *before* the variational principle is established.

(B) Continuity requirements across element boundaries are relaxed by introducing boundary tractions or boundary displacements as Lagrange multiplier fields.

(C) All stress and internal-displacement degrees of freedom are eliminated (by either static condensation or kinematic constraints) at the *element level*.

(A) says that hybrid functionals are effectively *mesh-dependent*, because the domain subdivision process introduces element boundaries which must be treated as *internal interfaces*, and therefore become part of S_i. Previous developments remain valid if one re-interprets "body" as "individual element," "volume" as "element volume," and "surface" as "interelement boundary."

Continuity and Connectors. The internal fields $\tilde{\sigma}$ and $\tilde{u}$ may be discontinuous across elements. The boundary displacement field $\tilde{d}$, however, must be continuous on S_i, *i.e.* it must have the same value on adjacent elements. This conditions may be satisfied if $\tilde{d}$ on an interface separating two elements *is uniquely interpolated by nodal values on that interface*. It is natural to take such nodal values as entries of v, which automatically becomes the vector of *connected node displacements* or *connectors*.

9 Kinematic Relations

In this and subsequent sections we work with an *individual element* unless otherwise noted. The element volume is V and the element surface is $S : S_d \cup S_t \cup S_i$. The v subvector contains n_v element-connector degrees of freedom, whereas q and a contain n_q and n_a internal freedoms, respectively. We shall assume that $n_q \geq n_v$.

The first matrix equation (the discrete compatibility equation) in (39) can be interpreted as the dislocation-energy balance statement

$$\tfrac{1}{2}\gamma(\tilde{\sigma}, e^u - e^\sigma)_V - a^T(P^T q - L^T v)_V = 0. \tag{41}$$

Setting $\gamma = 0$ and observing that a is arbitrary, (41) forces the kinematic constraint

$$P^T q = L^T v \tag{42}$$

to be satisfied. The same relation emerges if $\gamma \neq 0$ but the element displacements are forced to obey

$$(\tilde{\sigma}, e^u - e^\sigma)_V = 0 \tag{43}$$

as an *optimality* condition which says that the work of the strain error over the assumed stress field vanishes for arbitrary element motions. The constraint (42) plays a key role in subsequent derivations. An immediate consequence is that the first matrix equation in (39) reduces to the equivalent of (43), namely $\gamma \mathbf{a}^T(-\mathbf{Ca} + \mathbf{Q}^T \mathbf{q}) = 0$, thus, if $\gamma \neq 0$,

$$\mathbf{a} = \mathbf{C}^{-1}\mathbf{Q}^T\mathbf{q}, \qquad \text{or} \qquad \mathbf{a} = \mathbf{C}^{-1}\mathbf{L}^T\mathbf{v} \quad \text{if} \quad \mathbf{P} \equiv \mathbf{Q}. \tag{44}$$

Next, suppose that $\mathbf{q}$ and $\mathbf{v}$ are connected by the linear algebraic relations

$$\mathbf{v} = \mathbf{Gq}, \tag{45}$$

$$\mathbf{q} = \mathbf{Hv}, \tag{46}$$

where $\mathbf{G}$ is a $n_v \times n_q$ transformation matrix and $\mathbf{H}$ is a $n_q \times n_v$ transformation matrix. The determination of these matrices and their connecting relationships is discussed later. Using (45-46) the constraint (42) may be stated in two ways:

$$\mathbf{P}^T = \mathbf{L}^T\mathbf{G}, \qquad \mathbf{P}^T\mathbf{H} = \mathbf{L}^T. \tag{47}$$

Elimination of $\mathbf{a}$ and $\mathbf{q}$ in (39) through (44)-(46), with account taken of the second of (47), yields the external stiffness equations

$$\mathbf{Kv} = \mathbf{f}, \tag{48}$$

in which

$$\mathbf{K} = \gamma\left[\mathbf{LC}^{-1}\mathbf{Q}^T\mathbf{H} + \mathbf{H}^T\mathbf{QC}^{-1}\mathbf{L}^T - \mathbf{LC}^{-1}\mathbf{L}^T\right] + (1 - \gamma)\mathbf{H}^T\mathbf{K}_u\mathbf{H}, \quad \mathbf{f} = \mathbf{f}_v + \mathbf{H}^T\mathbf{f}_q. \tag{49}$$

If $\mathbf{P} \equiv \mathbf{Q}$, system (40) reduces to (48) but with

$$\mathbf{K} = \gamma\mathbf{LC}^{-1}\mathbf{L}^T + (1 - \gamma)\mathbf{H}^T\mathbf{K}_u\mathbf{H}. \tag{50}$$

10 Internal Field Decomposition

To gain further insight into the structure of the element stiffness equations (48) and eventually link up with the free formulation, we proceed to decompose both internal element fields as follows.

Stress Decomposition. The assumed stress field, $\tilde{\sigma}$, is decomposed into a mean value, $\bar{\sigma}$, and a deviator:

$$\tilde{\sigma} = \bar{\sigma} + \tilde{\sigma}_h = \bar{\sigma} + \mathbf{A}_h\mathbf{a}_h, \tag{51}$$

in which

$$\bar{\sigma} = (\tilde{\sigma})_V / \upsilon, \qquad (\mathbf{A}_h)_V = 0, \tag{52}$$

where $\upsilon = (1)_V$ denotes the element volume measure. The second relation in (52) is obtained by integrating (51) over V and noting that $\mathbf{a}_h$ is arbitrary.

Internal Displacement Decomposition. Next, the $\tilde{u}$ assumption is decomposed into rigid body, constant strain, and higher order displacements:

$$\tilde{u} = N_r q_r + N_c q_c + N_h q_h. \tag{53}$$

Applying the strain operator $D = \frac{1}{2}(\nabla + \nabla^T)$ to $\tilde{u}$ we get the associated strain field:

$$e^u = DN_r q_r + DN_c q_c + DN_h q_h = B_r q_r + B_c q_c + B_h q_h. \tag{54}$$

But $B_r = DN_r$ vanishes because N_r contains only rigid-body modes. We are also free to select $B_c = DN_c$ to be the identity matrix I if the generalized coordinates q_c are identified with the mean (volume-averaged) strain values $\bar{e}^u$. Consequently (54) simplifies to

$$e^u = \bar{e}^u + e_h^u = \bar{e}^u + B_h q_h, \tag{55}$$

in which

$$q_c = \bar{e}^u = (e^u)_V / \upsilon, \qquad (B_h)_V = 0. \tag{56}$$

Equation Partitioning. Assume that all elastic moduli in E are *constant* over the element. The degree of freedom partition

$$a = \left\{ \begin{array}{c} \bar{\sigma} \\ a_h \end{array} \right\}, \qquad q = \left\{ \begin{array}{c} q_r \\ \bar{e}^u \\ q_h \end{array} \right\}, \tag{57}$$

induces the following partition of the general element equations (39)

$$\begin{bmatrix} -\gamma \upsilon E^{-1} & 0 & -\bar{P}_r^T & \gamma \upsilon I - \bar{P}_c^T & -\bar{P}_h^T & \bar{L}^T \\ 0 & -\gamma C_h & -P_{hr}^T & -P_{hc}^T & \gamma Q_h^T - P_{hh}^T & L_h^T \\ -\bar{P}_r & P_{hr} & 0 & 0 & 0 & 0 \\ \gamma \upsilon I - \bar{P}_c & P_{hc} & 0 & (1-\gamma)\upsilon E & 0 & 0 \\ -\bar{P}_h & \gamma Q_h - P_{hh} & 0 & 0 & (1-\gamma)K_{qh} & 0 \\ \bar{L} & L_h & 0 & 0 & 0 & 0 \end{bmatrix} \left\{ \begin{array}{c} \bar{\sigma} \\ a_h \\ q_r \\ \bar{e}^u \\ q_h \\ v \end{array} \right\} = \left\{ \begin{array}{c} 0 \\ 0 \\ f_{qr} \\ f_{qc} \\ f_{qh} \\ f_v \end{array} \right\} \tag{58}$$

where

$$C_h = (A_h^T E^{-1} A_h)_V, \qquad Q_h = (B_h^T A_h)_V, \qquad K_{qh} = (B_h^T E B_h)_V,$$

$$\bar{P}_x = [N_{xn}^T]_S, \quad x = r, c, h, \qquad P_{hx} = [N_x^T A_{hn}]_S, \quad x = r, c, h, \tag{59}$$

$$\bar{L} = [V_n^T]_S, \qquad L_h = [V^T A_{hn}]_S, \qquad f_{qx} = (N_x^T b)_V, \quad x = r, c, h.$$

Integral Transformations. Application of the divergence theorem to the work of the mean stress on $\mathbf{e}^u$ yields

$$
\begin{aligned}
(\bar{\sigma}, \mathbf{e}^u)_V &= (\bar{\sigma}, \bar{\mathbf{e}}^u + \mathbf{B}_h \mathbf{q}_h)_V = v \bar{\sigma}^T \bar{\mathbf{e}}^u + \bar{\sigma}^T (\mathbf{B}_h)_V \mathbf{q}_h = v \bar{\sigma}^T \bar{\mathbf{e}}^u \\
&= [\bar{\sigma}_n, \bar{\mathbf{u}}]_S = [\bar{\sigma}_n, \mathbf{N}_r \mathbf{q}_r + \mathbf{N}_c \bar{\mathbf{e}}^u + \mathbf{N}_h \mathbf{q}_h]_S = \bar{\sigma}^T (\bar{\mathbf{P}}_r \mathbf{q}_r + \bar{\mathbf{P}}_c \bar{\mathbf{e}}^u + \bar{\mathbf{P}}_h \mathbf{q}_h).
\end{aligned}
\tag{60}
$$

Hence,

$$
\bar{\mathbf{P}}_r = 0, \qquad \bar{\mathbf{P}}_c = v\mathbf{I}, \qquad \bar{\mathbf{P}}_h = 0.
\tag{61}
$$

A similar analysis of the stress-deviator work $(\bar{\sigma}_h, \mathbf{e}^u)_V$ does not yield simple forms for the $\mathbf{P}_{hx}$ matrices unless $\bar{\sigma}_h$ is *divergence-free*, in which case

$$
\mathbf{P}_{hr} = 0, \qquad \mathbf{P}_{hc} = 0, \qquad \mathbf{P}_{hh} = \mathbf{Q}_h.
\tag{62}
$$

Hence $\mathbf{P} \equiv \mathbf{Q}$ as claimed in Section 7. Inserting (61-62) into (58) yields the partitioned form of (40):

$$
\begin{bmatrix}
-\gamma v \mathbf{E}^{-1} & 0 & 0 & -(1-\gamma)v\mathbf{I} & 0 & \bar{\mathbf{L}}^T \\
0 & -\gamma \mathbf{C}_h & 0 & 0 & -(1-\gamma)\mathbf{Q}_h^T & \mathbf{L}_h^T \\
0 & 0 & 0 & 0 & 0 & 0 \\
-(1-\gamma)v\mathbf{I} & 0 & 0 & (1-\gamma)v\mathbf{E} & 0 & 0 \\
0 & -(1-\gamma)\mathbf{Q}_h & 0 & 0 & (1-\gamma)\mathbf{K}_{qh} & 0 \\
\bar{\mathbf{L}} & \mathbf{L}_h & 0 & 0 & 0 & 0
\end{bmatrix}
\begin{Bmatrix}
\bar{\sigma} \\ \mathbf{a}_h \\ \mathbf{q}_r \\ \bar{\mathbf{e}}^u \\ \mathbf{q}_h \\ \mathbf{v}
\end{Bmatrix}
=
\begin{Bmatrix}
0 \\ 0 \\ \mathbf{f}_{qr} \\ \mathbf{f}_{qc} \\ \mathbf{f}_{qh} \\ \mathbf{f}_v
\end{Bmatrix}
\tag{63}
$$

Orthogonality Conditions. If the higher order stresses are divergence-free so that $\mathbf{P} \equiv \mathbf{Q}$, the relations (47) partition as

$$
\begin{bmatrix} 0 & v\mathbf{I} & 0 \\ 0 & 0 & \mathbf{Q}_h^T \end{bmatrix} = \begin{bmatrix} \bar{\mathbf{L}}^T \\ \mathbf{L}_h^T \end{bmatrix} [\mathbf{G}_r \quad \mathbf{G}_c \quad \mathbf{G}_h], \qquad \begin{bmatrix} 0 & v\mathbf{I} & 0 \\ 0 & 0 & \mathbf{Q}_h^T \end{bmatrix} \begin{bmatrix} \mathbf{H}_r \\ \mathbf{H}_c \\ \mathbf{H}_h \end{bmatrix} = \begin{bmatrix} \bar{\mathbf{L}}^T \\ \mathbf{L}_h^T \end{bmatrix},
\tag{64}
$$

whence the relations

$$
\begin{aligned}
\bar{\mathbf{L}}^T \mathbf{G}_r &= 0, & \bar{\mathbf{L}}^T \mathbf{G}_c &= v\mathbf{I}, & \bar{\mathbf{L}}^T \mathbf{G}_h &= 0, & \bar{\mathbf{L}}^T &= v\mathbf{H}_c, \\
\mathbf{L}_h^T \mathbf{G}_r &= 0, & \mathbf{L}_h^T \mathbf{G}_c &= 0, & \mathbf{L}_h^T \mathbf{G}_h &= \mathbf{Q}_h^T, & \mathbf{L}_h^T &= \mathbf{Q}_h^T \mathbf{H}_h.
\end{aligned}
\tag{65}
$$

The first four were obtained through other means by Bergan (1980) and Bergan and Nygård (1984), who called them the *force orthogonality* conditions on account of the physical interpretation of $\bar{\mathbf{L}}$ as a "boundary nodal force lumping" matrix in the free formulation studied below.

If the higher order stresses are not divergence free, the last four of (65) are replaced by

$$
\begin{aligned}
\mathbf{L}_h^T \mathbf{G}_r &= \mathbf{P}_{hr}^T, \qquad \mathbf{L}_h^T \mathbf{G}_c = \mathbf{P}_{hc}^T, \qquad \mathbf{L}_h^T \mathbf{G}_h = \mathbf{P}_{hh}^T, \\
\mathbf{L}_h^T &= \mathbf{P}_{hr}^T \mathbf{H}_r + \mathbf{P}_{hc}^T \mathbf{H}_c + \mathbf{P}_{hh}^T \mathbf{H}_h.
\end{aligned}
\tag{66}
$$

11 The Free Formulation

The free formulation of Bergan and Nygård (1984) was originally conceived as an incompatible finite-element displacement model that passes a cancelling-tractions version of the patch test which Bergan and Hanssen (1975) called the individual patch test. Here the formulation is re-interpreted in the context of the hybrid principle (19). The assumptions that lead to the FF are listed in the Introduction and studied in further detail below.

Constant Internal Stress. The internal stress field is *constant*. Consequently there are no a_h parameters, reducing (58) or (63) to

$$
\begin{bmatrix}
-\gamma \upsilon E^{-1} & 0 & -(1-\gamma)\upsilon I & 0 & \overline{L}^T \\
0 & 0 & 0 & 0 & 0 \\
-(1-\gamma)\upsilon I & 0 & (1-\gamma)\upsilon E & 0 & 0 \\
0 & 0 & 0 & (1-\gamma)K_{qh} & 0 \\
\overline{L} & 0 & 0 & 0 & 0
\end{bmatrix}
\begin{Bmatrix}
\bar{\sigma} \\ q_r \\ \bar{e}^u \\ q_h \\ v
\end{Bmatrix}
=
\begin{Bmatrix}
0 \\ f_{qr} \\ f_{qc} \\ f_{qh} \\ f_v
\end{Bmatrix}
\tag{67}
$$

Invertible G. Matrix G in (45) is constructed by *nodal collocation*, that is, by evaluating the expansion $\tilde{u} = Nq$ at the element boundary nodes. This establishes the transformation

$$
v = Gq = [\, G_r \quad G_c \quad G_h \,]
\begin{Bmatrix}
q_r \\ \bar{e}^u \\ q_h
\end{Bmatrix}.
\tag{68}
$$

According to the assumptions listed in the Introduction, matrix G is square and nonsingular so inverting (68) we get

$$
q = G^{-1} = Hv \qquad \text{or} \qquad
q =
\begin{Bmatrix}
q_r \\ \bar{e}^u \\ q_h
\end{Bmatrix}
=
\begin{bmatrix}
H_r \\ H_c \\ H_h
\end{bmatrix}
v =
\begin{bmatrix}
H_r \\ \upsilon^{-1}\overline{L}^T \\ H_h^T
\end{bmatrix}
v.
\tag{69}
$$

The FF Stiffness Equations. Eliminating $\bar{\sigma}$ and q from (67) yields the FF stiffness equations

$$
Kv = [K_b + (1-\gamma)K_h]\,v = f,
\tag{70}
$$

where

$$
K_b = \upsilon^{-1}\overline{L}E^{-1}\overline{L}^T, \quad K_h = H_h^T K_{qh} H_h, \quad f = f_v + H_r^T f_{qr} + \upsilon^{-1}\overline{L}f_{qc} + H_h f_{qh}.
\tag{71}
$$

In the free formulation, K_b and K_h receive the name *basic* and *higher order* stiffness matrices, respectively. A $\frac{1}{2}$ scaling of K_h derived from energy-balancing studies was recommended by Bergan and Felippa (1985) for a plane stress element. This corresponds to taking $\gamma = \frac{1}{2}$. But in general the value of γ can be expected to be dependent on the type and geometry of the element.

As K_b is rank-deficient (except for the simplex elements) choosing $\gamma = 1$, which corresponds to the d-generalized Hellinger-Reissner functional (17), is *not* admissible.

41

12 The Extended Free Formulation

In the extended free formulation (EFF) the number of internal displacement freedoms, $n_q = \dim(q)$, is allowed to exceed the number of nodal displacement connectors $n_v = \dim(v)$. We can establish the relation (68) as before, but matrix G will now be rectangular and cannot be directly inverted. One way of circumventing this difficulty is to retain $n_q - n_v = \dim(a_h)$ higher order stress modes; an alternative procedure is discussed in Section 13. The stress modes are assumed to be divergence free so (62) holds. The available relations are

$$v = Gq, \qquad C_h a_h = L_h^T v = Q_h^T q_h, \tag{72}$$

which can be combined to form the matrix system

$$\begin{Bmatrix} v \\ a_h \end{Bmatrix} = \begin{bmatrix} G_r & G_c & G_h \\ 0 & 0 & C_h^{-1}Q_h^T \end{bmatrix} \begin{Bmatrix} q_r \\ \bar{e}^u \\ q_h \end{Bmatrix}. \tag{73}$$

The matrix on the right side is square, and invertible if G, C_h and Q_h have full rank. Solving for q and eliminating a_h one obtains

$$q = \begin{Bmatrix} q_r \\ q_c \\ q_h \end{Bmatrix} = \begin{bmatrix} H_r & 0 \\ H_c & 0 \\ H_h' & J_h \end{bmatrix} \begin{Bmatrix} v \\ a_h \end{Bmatrix} = \begin{bmatrix} H_r \\ H_c \\ H_h' + J_h C_h^{-1}Q_h^T \end{bmatrix} v = \begin{bmatrix} H_r \\ H_c \\ H_h \end{bmatrix} v, \tag{74}$$

where H_h' and J_h result from the inversion process. Since $H_h'G_h + J_h C_h^{-1}Q_h^T = I$, we can express H_h as

$$H_h = H_h' + I - H_h'G_h. \tag{75}$$

Having H available, replacing into (48-50) we obtain the EFF stiffness equations

$$Kv = [K_b + K_{bh} + (1 - \gamma)K_h] v = f, \tag{76}$$

where K_b, K_h and f are the same as in (71), and

$$K_{bh} = L_h C_h^{-1}L_h. \tag{77}$$

Is $\gamma = 1$ now admissible? If $K_b + K_{bh}$ has correct rank, yes! Curiously enough, if the body force field b vanishes and $\gamma = 1$, (76) are precisely the stiffness equations for the original equilibrium-stress-assumed hybrid elements of Pian (1964), which can of course be constructed without any internal displacement assumptions.

42

13 Hierarchical Connector Augmentation

An alternative approach to building an invertible transformation such as (73) consists of augmenting $\mathbf{v}$ with $n_q - n_v$ connector degrees of freedom collected in subvector $\mathbf{v}_x$. These must be selected to give a square transformation of the form

$$\begin{Bmatrix} \mathbf{v} \\ \mathbf{v}_x \end{Bmatrix} = \begin{bmatrix} \mathbf{G}_r & \mathbf{G}_c & \mathbf{G}_h \\ 0 & 0 & \mathbf{G}_x \end{bmatrix} \begin{Bmatrix} \mathbf{q}_r \\ \bar{\mathbf{e}}^u \\ \mathbf{q}_h \end{Bmatrix} \tag{78}$$

If this approach is followed, it is important to choose $\mathbf{v}_x$ in *hierarchical* fashion so that the expanded G has the structure shown above. In other words, $\mathbf{v}_x$ *must not be "excited" by rigid body or constant strain motions*. Otherwise the interelement compatibility of boundary displacements is generally violated for such motions, and the patch test discussed in the Appendix fails.

Inversion of (78) provides the H matrix. The FF stiffness equations (70) can be constructed with the strain-energy contribution from $\mathbf{v}_x$ flowing to the higher order stiffness $\mathbf{K}_h$. Finally, the $\mathbf{v}_x$ freedoms can be statically condensed.

Which EFF approach is better? The decision seems to be element-dependent. The choice primarily hinges on whether it is easier to choose divergence-free stress modes than hierarchical connectors while preserving element invariance. If both approaches appear equally feasible, there is not presently enough experience to decide which one is preferable.

14 Concluding Remarks

The qualifier *free* in "free formulation" was meant to emphasize "freedom from conformity requirements" that are a pervasive part of the conventional displacement formulation, and the possibility of constructing the basic and higher order stiffness contributions through largely independent assumptions. But when the FF is studied from a variational standpoint, several constraints become immediately apparent. The extended FF releases the most troublesome one at the cost of buying more complicated stress assumptions, or additional hierarchical connectors. So it is fair to state that the admirable goal of absolute freedom has not yet been attained.

The development of the EFF as reported here was motivated by difficulties encountered in the construction of the following elements:

3-Node Plane Stress Triangle with Nodal Rotations. Similar to the element constructed by Bergan and Felippa (1985), but with a *fully quadratic* internal displacement field. Thus $n_v = 9$, $n_q = 12$ and three additional self-equilibrating stress fields are needed.

4-Node Tetrahedron with Nodal Rotations. The extension of the previous element to 3D has $n_v = 12$, $n_q = 18$ and six additional stress fields are needed.

Assuming fully quadratic internal displacement fields eliminates the higher-order mode selection difficulties discussed by Bergan and Felippa (1985). Progress in the derivation of these elements will be reported in subsequent papers.

Acknowledgements

References

Bergan, P. G. and Hanssen, L., 1976, "A new approach for deriving 'good' finite elements," MAFELAP II Conference, Brunel University, 1975, in *The Mathematics of Finite Elements and Applications – Volume II*, ed. by J. R. Whiteman, Academic Press, London

Bergan, P. G., 1980, "Finite Elements Based on Energy Orthogonal Functions," *Int. J. Num. Meth. Engrg.*, 15, pp. 1141–1555

Bergan, P. G. and Nygård, M. K., 1984, "Finite elements with increased freedom in choosing shape functions," *Int. J. Num. Meth. Engrg.*, 20, pp. 643–664

Bergan, P. G. and Wang X., 1984, "Quadrilateral plate bending elements with shear deformations," *Computer & Structures*, 19, pp. 25–34

Bergan, P. G. and Felippa, C. A., 1985, "A Triangular Membrane Element with Rotational Degrees of Freedom,' *Computer Methods in Applied Mechanics & Engineering*, 50, pp. 25–69

Bergan, P. G. and Nygård, M. K., 1985, "Nonlinear Shell Analysis Using Free Formulation Finite Elements," *Proc. Europe-US Symposium on Finite Element Methods for Nonlinear Problems*, held at Trondheim, Norway, August 1985, Springer-Verlag, Berlin

Chien, W. Z., 1983, "Method of High-Order Lagrange Multiplier and Generalized Variational Princiuples of Elasticity with More Forms of Functionals," *Applied Mathematics and Mechanics*, 4, pp. 143–159

Felippa, C. A. and Bergan, P. G., 1987, "A Triangular Plate Bending Element Based on an Energy-Orthogonal Free Formulation," *Computer Methods in Applied Mechanics & Engineering*, 61, pp. 129–160

Felippa, C. A., 1989a, "Parametrized Multifield Variational Principles in Elasticity: I. Mixed Functionals," to appear in *Communications in Applied Numerical Methods*

Felippa, C. A., 1989b, 'Parametrized Multifield Variational Principles in Elasticity: II. Hybrid Functionals and the Free Formulation,' to appear in *Communications in Applied Numerical Methods*

Fraeijs de Veubeke, B. M., 1974, "Variational Formulation and the Patch Test," *Int. J. Num. Meth. Engrg.*, 8, pp. 783–801

Gurtin, M., 1972, "The Linear Theory of Elasticity," in Volume VIa/2 of *Encyclopedia of Physics*, ed. by C. Truesdell, Springer-Verlag, Berlin

Hanssen, L., Syvertsen, T. G. and Bergan, P. G., 1979, "Stiffness Derivation Based on Element Convergence Requirements," MAFELAP III Conference, Brunel University, 1978, in *The Mathematics of Finite Elements and Applications – Vol III*, ed. by J. R. Whiteman, Academic Press, London

Nygård, M. K., 1986, *The Free Formulation for Nonlinear Finite Element Analysis with Applications to Shells*, Dr. Ing. Dissertation, isteport 86-1, Division of Structural Mechanics, The Norwegian Institute of Technology, Trondheim, Norway

44

Oden, J. T. and Reddy, J. N., 1983, *Variational Methods in Theoretical Mechanics*, 2nd ed., Springer-Verlag, Berlin

Pian, T. H. H., 1964, "Derivation of element stiffness matrices by assumed stress distributions," *AIAA Journal*, 2, pp. 1333–1336

Pian, T. H. H. and Tong, P., 1969, 'Basis of finite element methods for solid continua,' *Int. J. Numer. Meth. Engrg.*, 1, pp. 3–29

Pian, T. H. H., 1973, 'Finite element methods by variational principles with relaxed continuity requirements,' in *Variational Methods in Engineering*, Vol. 1, ed. by C. A. Brebbia and H. Tottenham, Southampton University Press, Southhampton, U.K.

Washizu, K., 1968, *Variational Methods in Elasticity and Plasticity*, Pergamon Press, Oxford

Appendix A. The Cancelling-Traction Patch Test

It is instructive to study whether this element class passes the patch test for an arbitrary γ. To investigate this question we use the sketch of Figure 1 and view the subvolumes V^+ and V^- as *two elements* connected along S_i with an external traction boundary S_t. Both elements are in a state of *constant stress* σ_0. The prescribed surface tractions are $[\hat{t} = \sigma_{0n}]_{S_t}$ and the body forces b vanish.

. First take (63) to be the governing discrete equations for the two-element assembly. The only nonzero forces are $f_v = [V^T \hat{t}]_{S_t}$. The key observation is that

$$\bar{L} = [V_n^T]_S = [V_n^T]_{S_t}, \tag{79}$$

because the integral over S_i vanishes as $(V_+ = V_-)_{S_i}$ on account of the interface compatibility conditions stated in Section 8, and $n^+ = -n^-$. Now for any γ it can be verified that the solution of (63) is that demanded by the patch test, namely

$$\bar{\sigma} = \sigma_0 = \bar{\sigma}^u, \quad a_h = 0, \quad q_r = arbitrary, \quad \bar{e}^u = E^{-1}\bar{\sigma}_0, \quad q_h = 0, \quad v = L^T\bar{\sigma}_0 + G_r q_r. \tag{80}$$

In checking this assertion one finds that the following relations, listed in (65), must be satisfied:

$$\bar{L}^T G_r = 0, \quad \bar{L}^T G_c = vI, \quad L_h^T G_c = 0, \quad L_h G_r = 0. \tag{81}$$

If instead we take the more general equations (59), verification of the solution (81) demands that

$$\bar{P}_r = 0, \quad \bar{P}_c = vI, \quad \bar{P}_h = 0, \quad P_{hr}^T = L_h^T G_r, \quad P_{hc}^T = L_h^T G_c, \quad P_{hh}^T = L_h^T G_h. \tag{82}$$

The first three follow from the divergence theorem as shown in (60). But the last three, listed in (66), are a consequence of the kinematic constraint (43), which is thus directly correlated to satisfaction of the patch test.

As noted by Fraeijs de Veubeke (1973), the physical meaning of this form of the patch test is that the *interface virtual work is zero* when the element patch is in a constant stress state.

DEVELOPMENTS IN VARIATIONAL METHODS FOR HIGH PERFORMANCE PLATE AND SHELL ELEMENTS

ABSTRACT

High performance elements are simple finite elements constructed to deliver engineering accuracy with coarse arbitrary grids. This paper is part of a series on the variational foundations of high-performance elements, with emphasis on plate and shell elements constructed with the free formulation (FF) and assumed natural strain (ANS) methods. In this paper, we study parametrized variational principles that provide a common foundation for the FF and ANS methods, as well as a combination of both. From this unified formulation a variant of the ANS formulation called the "assumed natural deviatoric strain" (ANDES) formulation, emerges as an important case. The first ANDES element, a high-performance 9-dof triangular Kirchhoff plate bending element, is briefly described to illustrate the use of the new formulation.

1. INTRODUCTION

For 25 years researchers have tried to construct "best" finite element models for problems in structural mechanics. The quest appeared to be nearly over in the late 1960s when high order displacement elements dominated the headlines. But these elements did not dominate the marketplace. The overwhelming preference of finite element code users has been for *simple elements that deliver engineering accuracy with coarse meshes*. These will be collectively called *high performance elements*, or HP elements.

1.1 Attributes of HP Elements

Approaching that general goal gives rise to a myriad of more concrete requirements which are supposed to be addressed in some degree during element development. Such requirements are listed in Table 1.

Some of these requirements are obvious. For example, *low distortion sensitivity* is a consequence of trying to achieve satisfactory accuracy with *arbitrary* meshes. But other items listed in Table 1 call for some explanation.

47

Table 1 -   Target Requirements for High-Performance Elements

- Simple: few freedoms, all physical, preferably at corners only

- Convergent

- Frame invariant

- No locking

- Rank sufficient: no spurious modes

- Balanced stiffness: not too rigid, not too flexible

- Stresses as accurate as displacements

- Low distortion sensitivity

- Mixable with other elements

- Economical to form

- Easily extendible to nonlinear and dynamic analyses

- Effective local error estimator for mesh adaptation

The first and foremost requirement is that the element be as *simple* as possible. This is in sharp contrast to the "baroque FE period" of 1965–1975 that lauded luxuriantly ornate elements and culminated with the development of very complex models, including elements with nonphysical degrees of freedom. One source of this retrenchment has been feedback from users of general purpose, finite element programs. As use of these programs expanded to more engineers without deep knowledge of "what's inside the black box" the trend in finite element model construction veered toward the "simplest elements that will do the job." Further impetus is provided by the gradual realization that high accuracy of complex elements in linear elastostatics does not necessarily carry over to dynamic and nonlinear analyses.

The *balanced stiffness* requirement also deserves comment. It follows from the goal of attaining reasonable accuracy with *coarse meshes*. This is illustrated in Fig. 1, which shows a convergence study of a classical model problem: the bending of a simply supported square plate under a concentrated central load. The mesh contains $2 \times N \times N$ triangles over a plate quadrant. A target "accuracy band" of $\pm 1\%$ is taken, somewhat arbitrarily, as representative of engineering accuracy for this rather simple problem. The convergence characteristics of several triangular elements are taken from the extensive study reported in Ref. 2. Although most elements converge, some are too stiff, while others are too flexible, and generally do not enter the accuracy band until
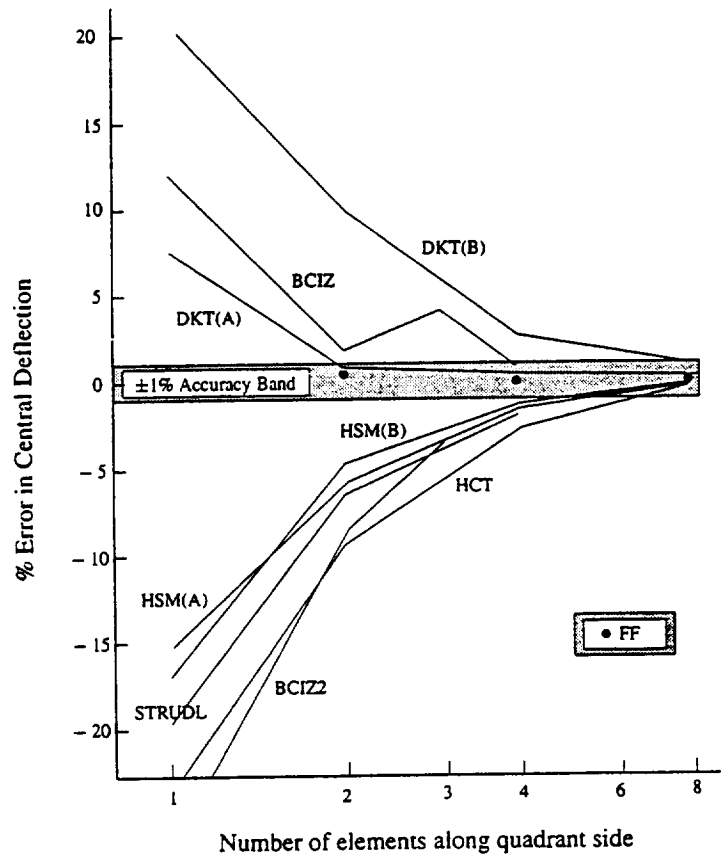
Fig. 1. Convergence study of several plate bending triangular elements as reported in Ref. 2. The FF results are from Ref. 8.

the mesh is fairly refined ($N \geq 8$). On the other hand, the results labeled 'FF', obtained with a plate element based on the free formulation (FF) discussed later, lie within the band for all meshes.

The balanced stiffness requirement should *not* be confused with fast asymptotic convergence for *fine* meshes. Simple elements cannot effectively compete with higher order elements in this regard, and are not effective in applications demanding very high accuracy. What is important is *how good are the results for coarse meshes*.

1.2 Constructing HP Elements

The search for HP elements began seriously in the mid-1970s and now represents an important area of finite element research in solid and structural mechanics. Many ingenious schemes have been tried: reduced and selective integration, incompatible modes, mixed and hybrid formulations, stress and strain projections, the (FF) formulation, and the (ANS) formulation. Many researchers are developing such elements. The common theme of the investigations is:

Abandon the conventional displacement formulation

Several techniques researchers use in their quest to build better elements are itemized in Table 2. Many of these were introduced over 20 years ago, but only recently a concerted effort has been made to *combine* several tools to produce HP elements. For example, the present work draws on items 1, 2, 3, 8, 10, 11, and 12 of Table 2.

Table 2 -   Tools of the Trade

	Technique	*Year Introduced*
1.	Incompatible shape functions	early 1960s
2.	Patch test	1965
3.	Mixed and hybrid variational principles	1965
4.	Projectors	1967
5.	Selective reduced integration	1969
6.	Uniform reduced integration	1970
7.	Assumed strains	1970
8.	Energy balancing	1974
9.	Directional integration	1978
10.	Limit differential equations	1982
11.	Free formulation	1984
12.	Assumed natural strains	1984

1.3   Objective of Present Work

This paper is part of a series (Refs. 9-12, 15-16) describing how several HP element construction methods can be embedded within an *extended* variational framework using parametrized hybrid functionals. Particular attention is focused on merging the last two items in Table 2.

The general plan of attack for this unification is flowcharted in Fig. 2. Box connections indicated with dashed lines are not dealt with in this paper. The variational extensions, shown on the left of Fig. 2, involve parametrization of the conventional elasticity functionals and treatment of element interfaces through generalizations of the hybrid approach of Refs. 20–23.
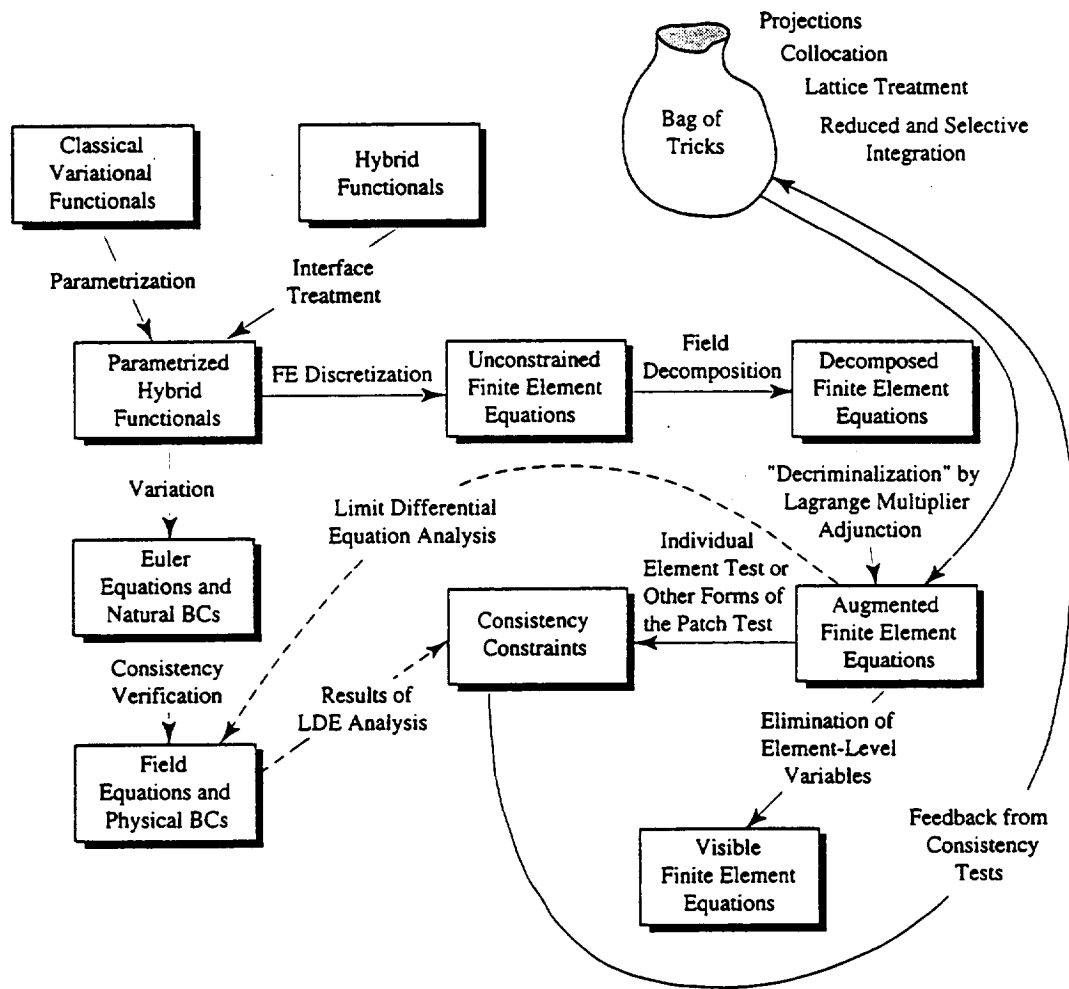
Fig. 2. Program of attack on the variational formulation of HP elements

The effective construction of HP elements relies on devices, sometimes derisively called "tricks" or "variational crimes," that do not fit *a priori* in the classical variational framework. The range of tricks spans innocuous collocation and finite difference constraints to more drastic remedies such as selective integration. Despite their unconventional nature, tricks are an essential part of the construction of high-performance elements. Collectively, they represent a fun-and-games ingredient that keeps the derivation of HP finite elements a surprisingly enjoyable task.

The present treatment "decriminalizes" kinematic constraint tricks by adjoining Lagrange multipliers, hence setting out the ensemble on proper variational foundations. Placing formulations within a variational framework has the great advantage of supplying the *general structure* of the stiffness matrices and forcing vectors of high performance elements, and providing theoretical coherence for the systematic derivation of element classes by a combination of techniques.

51

2. THE ELASTICITY PROBLEM

Consider a *linearly elastic body* under static loading that occupies the volume V. The body is bounded by the surface S, which is decomposed into $S : S_d \cup S_t$. Displacements are prescribed on S_d, whereas surface tractions are prescribed on S_t. The outward unit normal on S is denoted by $\mathbf{n} \equiv n_i$.

The three unknown volume fields are displacements $\mathbf{u} \equiv u_i$, infinitesimal strains $\mathbf{e} \equiv e_{ij}$, and stresses $\boldsymbol{\sigma} \equiv \sigma_{ij}$. The problem data include: the body force field $\mathbf{b} \equiv b_i$ in V, prescribed displacements $\hat{\mathbf{d}} \equiv \hat{d}_i$ on S_d, and prescribed surface tractions $\hat{\mathbf{t}} \equiv \hat{t}_i$ on S_t.

The relations between the volume fields are the strain-displacement equations:

$$\mathbf{e} = \tfrac{1}{2}(\nabla \mathbf{u} + \nabla^T \mathbf{u}) = \mathbf{Du} \qquad \text{or} \qquad e_{ij} = \tfrac{1}{2}(u_{i,j} + u_{j,i}) \quad \text{in } V, \tag{1}$$

the constitutive equations:

$$\boldsymbol{\sigma} = \mathbf{Ee} \qquad \text{or} \qquad \sigma_{ij} = E_{ijkl} e_{kl} \quad \text{in } V, \tag{2}$$

which will be assumed to be invertible, and the equilibrium (balance) equations:

$$-\mathbf{div}\,\boldsymbol{\sigma} = \mathbf{D}^* \boldsymbol{\sigma} = \mathbf{b} \qquad \text{or} \qquad \sigma_{ij,j} + b_i = 0 \quad \text{in } V, \tag{3}$$

in which $\mathbf{D}^* = -\mathbf{div}$ denotes the adjoint operator of $\mathbf{D} = \tfrac{1}{2}(\nabla + \nabla^T)$.

The stress vector with respect to a direction defined by the unit vector $\mathbf{v}$ is denoted as $\boldsymbol{\sigma}_v = \boldsymbol{\sigma} . \mathbf{v}$, or $\sigma_{vi} = \sigma_{ij} v_j$. On S the surface-traction stress vector is defined as

$$\boldsymbol{\sigma}_n = \boldsymbol{\sigma} . \mathbf{n}, \qquad \text{or} \qquad \sigma_{ni} = \sigma_{ij} n_j. \tag{4}$$

With this definition the traction boundary conditions may be stated as:

$$\boldsymbol{\sigma}_n = \hat{\mathbf{t}} \qquad \text{or} \qquad \sigma_{ij} n_j = \hat{t}_i \qquad \text{on } S_t, \tag{5}$$

and the displacement boundary conditions as

$$\mathbf{u} = \hat{\mathbf{d}} \qquad \text{or} \qquad u_i = \hat{d}_i \qquad \text{on } S_d. \tag{6}$$

3. NOTATION

3.1 Field Dependency

In variational methods of approximation we do not, of course, work with the exact fields that satisfy the governing Eqs. 1-3 and 5-6, but with *independent* (primary) fields, which are subject to variations, and *dependent* (secondary, associated, derived) fields, which are not. The approximation is determined by taking variations with respect to the independent fields.

Following the notation introduced in Refs. 9 and 10, an *independently varied* field will be identified by a superposed tilde, for example $\tilde{u}$. A dependent field is identified by writing the independent field symbol as superscript. For example, if the displacements are independently varied, the derived strain and stress fields are:

$$\mathbf{e}^u = \tfrac{1}{2}(\nabla + \nabla^T)\tilde{u} = \mathbf{D}\tilde{u}, \qquad \boldsymbol{\sigma}^u = \mathbf{Ee}^u = \mathbf{ED}\tilde{u}. \tag{7}$$

An advantage of this convention is that $\mathbf{u}$, $\mathbf{e}$ and $\boldsymbol{\sigma}$ may be reserved for the *exact* fields.
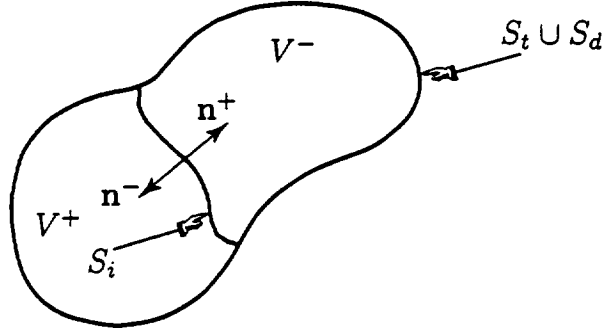
Fig. 3. Internal interface example.

3.2 Integral Abbreviations

Volume and surface integrals will be abbreviated by placing domain-subscripted parentheses and square brackets, respectively, around the integrand. For example:

$$(f)_V \overset{\text{def}}{=} \int_V f \, dV, \quad [f]_S \overset{\text{def}}{=} \int_S f \, dS, \quad [f]_{S_d} \overset{\text{def}}{=} \int_{S_d} f \, dS, \quad [f]_{S_t} \overset{\text{def}}{=} \int_{S_t} f \, dS. \tag{8}$$

If **f** and **g** are vector functions, and **p** and **q** are tensor functions, their inner product over V is denoted in the usual manner:

$$(\mathbf{f}, \mathbf{g})_V \overset{\text{def}}{=} \int_V \mathbf{f} \cdot \mathbf{g} \, dV = \int_V f_i g_i \, dV, \qquad (\mathbf{p}, \mathbf{q})_V \overset{\text{def}}{=} \int_V \mathbf{p} \cdot \mathbf{q} \, dV = \int_V p_{ij} q_{ij} \, dV, \tag{9}$$

and similarly for surface integrals, in which case square brackets are used.

3.3 Domain Assertions

The notation:

$$(a = b)_V, \qquad [a = b]_S, \qquad [a = b]_{S_d}, \qquad [a = b]_{S_t}, \tag{10}$$

is used to assert that the relation $a = b$ is valid at each point of V, S, S_d and S_t, respectively.

3.4 Internal Interfaces

In sections 4-5 we construct *hybrid variational principles* in which boundary displacements **d** can be varied independently from the internal displacements **u**. These displacements play the role of Lagrange multipliers that relax internal displacement continuity. Variational principles containing **d** will be called displacement-generalized, or "*d*-generalized" for short.

The choice of **d** as independent field is *not* variationally admissible on S_d or S_t. We must, therefore, extend the definition of boundary to include internal interfaces collectively designated as S_i. Thus:

$$S : S_d \cup S_t \cup S_i. \tag{11}$$

53

On S_i neither displacements nor tractions are prescribed. A simple case is illustrated in Fig. 3, in which the interface S_i divides V into two subvolumes: V^+ and V^-. An interface such as S_i on Fig. 3 has two "sides" called S_i^+ and S_i^-, which identify S_i viewed as boundary of V^+ and V^-, respectively. At smooth points of S_i the unit normals $\mathbf{n}^+$ and $\mathbf{n}^-$ point in opposite directions.

The integral abbreviations of Eqs. 8-9 generalize as follows, using Fig. 3 for definiteness. A volume integral is the sum of integrals over the subvolumes:

$$(f)_V \overset{\text{def}}{=} \int_{V^+} f\, dV + \int_{V^-} f\, dV. \tag{12}$$

An integral over S_i includes two contributions:

$$[g]_{S_i} \overset{\text{def}}{=} \int_{S_i^+} g^+\, dS + \int_{S_i^-} g^-\, dS, \tag{13}$$

where g^+ and g^- denote the value of the integrand g on S_i^+ and S_i^-, respectively. These two values may be different if g is discontinuous or involves a projection on the normals.

The appearance of S_i is a consequence of allowing elements with discontinuous displacements. Following a finite element discretization, the union of interelement boundaries becomes S_i. This boundary is generally nonphysical because it depends on the discretization.[1]

4. THE ELASTICITY FUNCTIONALS

The variational principles of linear elasticity are based on functionals of the form:

$$\Pi = U - P, \tag{14}$$

where U characterizes the internal energy stored in the body volume and P includes other contributions such as the work of applied loads and energy stored on internal interfaces. We shall call U the *generalized strain energy* and P the *forcing potential*.

The functionals in this section include *independently varied displacements*. The class of "equilibrium" functionals without independent displacements, such as the complementary energy, are briefly covered in section 5.5 for completeness, but are not required in the finite element developments of sections 6–11.

4.1 Generalized Strain Energy

The generalized strain energy has the following structure:

$$U = \tfrac{1}{2} j_{11}(\tilde{\sigma}, \mathbf{e}^\sigma)_V + j_{12}(\tilde{\sigma}, \tilde{\mathbf{e}})_V + j_{13}(\tilde{\sigma}, \mathbf{e}^u)_V + \tfrac{1}{2} j_{22}(\sigma^\epsilon, \tilde{\mathbf{e}})_V + j_{23}(\sigma^\epsilon, \mathbf{e}^u)_V + \tfrac{1}{2} j_{33}(\sigma^u, \mathbf{e}^u)_V \tag{15}$$

where j_{11} through j_{33} are numerical coefficients. For example, the Hu-Washizu principle is obtained by setting $j_{12} = -1$, $j_{13} = 1$, $j_{22} = 1$, all others being zero. The matrix representation of the general functional Eq. 15 and the relations that must exist between the coefficients are studied in section 5.1.

---

[1] If there are physical internal interfaces — for example, a sudden thickness or material change — it is common practice to select the mesh so that these natural interfaces are also interelement boundaries.

4.2 Hybrid Forcing Potentials

Variational principles of linear elasticity are constructed by combining the volume integral of Eq. 15 with the forcing potential P. Two forms of the forcing potential, called P^d and P^t in the sequel, are of interest in the hybrid treatment of interface discontinuities. The d-generalized forcing potential introduces, as described in section 3.4, an independent boundary displacement field $\bar{d}$ over S_i:

$$P^d(\bar{u}, \bar{\sigma}, \bar{d}) = (b, \bar{u})_V + [\bar{\sigma}_n, \bar{u} - \hat{d}]_{S_d} + [\hat{t}, \bar{u}]_{S_t} + [\bar{\sigma}_n, \bar{u} - \bar{d}]_{S_i}. \qquad (16)$$

The t-generalized (traction generalized) forcing potential introduces an independently varied traction displacement field $\bar{t}$ over S_i:

$$P^t(\bar{u}, \bar{\sigma}, \bar{t}) = (b, \bar{u})_V + [\bar{t}, \bar{u} - \hat{d}]_{S_d} + [\hat{t}, \bar{u}]_{S_t} + [\bar{t}, \bar{u}]_{S_i}. \qquad (17)$$

The conventional form P^c of the forcing potential is obtained if the interface integral vanishes and one sets $[t = \sigma_n]_S$. If so P^t and P^d coalesce into P^c, which retains only two independent fields:

$$P^c(\bar{u}, \bar{\sigma}) = (b, \bar{u})_V + [\bar{\sigma}_n, \bar{u} - \hat{d}]_{S_d} + [\hat{t}, \bar{u}]_{S_t}. \qquad (18)$$

4.3 Modified Forcing Potentials

Through various manipulations and assumptions detailed in Ref. 10 the forcing potential P^d may be transformed to

$$P^d(\bar{u}, \bar{\sigma}, \bar{d}) = (b, \bar{u})_V + [\hat{t}, \bar{d}]_{S_t} + [\bar{\sigma}_n, \bar{u} - \bar{d}]_S. \qquad (19)$$

where the all important surface dislocation integral is taken over S rather than S_i. One of the assumptions is that displacement boundary conditions, Eq. 6, are exactly satisfied on S_d. This expression of P^d is used in the sequel. A similar technique can be used to adjust P^t, but that modified formula will not be required in what follows.

4.4 Complete Functionals

Complete elasticity functionals are obtained by combining the generalized strain energy with one of the forcing potentials. For example, the d and t generalized versions of the Hu-Washizu functional are:

$$\Pi_W^d = U_W - P^d, \qquad \Pi_W^t = U_W - P^t. \qquad (20)$$

where U_W is obtained by setting $j_{22} = j_{13} = 1$, $j_{12} = -1$, others zero, in Eq. 15.

5. MATRIX REPRESENTATION OF ELASTICITY FUNCTIONALS

The generalized strain energy of Eq. 15 can be presented in the matrix form:

$$U = \tfrac{1}{2} \int_V \langle \bar{\sigma} \quad \sigma^\epsilon \quad \sigma^u \rangle \begin{bmatrix} j_{11} & j_{12} & j_{13} \\ & j_{22} & j_{23} \\ symm & & j_{33} \end{bmatrix} \begin{Bmatrix} e^\sigma \\ \tilde{e} \\ e^u \end{Bmatrix} \, dV. \tag{21}$$

The symmetric matrix[2]

$$\mathbf{J} = \begin{bmatrix} j_{11} & j_{12} & j_{13} \\ j_{12} & j_{22} & j_{23} \\ j_{13} & j_{23} & j_{33} \end{bmatrix} \tag{22}$$

characterizes the volume portion of the variational principle. Using the relations $\sigma^\epsilon = \mathbf{E}e$, $\sigma^u = \mathbf{E}\mathbf{D}\bar{u}$, $e^\sigma = \mathbf{E}^{-1}\sigma$, and $e^u = \mathbf{D}\bar{u}$, the above integral may be rewritten in terms of the independent fields as:

$$U = \tfrac{1}{2} \int_V \langle \bar{\sigma} \quad \tilde{e} \quad \bar{u} \rangle \begin{bmatrix} j_{11}\mathbf{E}^{-1} & j_{12}\mathbf{I} & j_{13}\mathbf{D} \\ j_{12}\mathbf{I} & j_{22}\mathbf{E} & j_{23}\mathbf{E}\mathbf{D} \\ j_{13}\mathbf{D}^T & j_{23}\mathbf{D}^T\mathbf{E} & j_{33}\mathbf{D}^T\mathbf{E}\mathbf{D} \end{bmatrix} \begin{Bmatrix} \bar{\sigma} \\ \tilde{e} \\ \bar{u} \end{Bmatrix} \, dV. \tag{23}$$

5.1 First Variation of Generalized Strain Energy

The first variation of Eq. 15 may be presented as:

$$\delta U = (\Delta e, \delta\bar{\sigma})_V + (\Delta\sigma, \delta\tilde{e})_V - (\mathbf{div}\,\sigma', \delta\bar{u})_V + [\sigma'_n, \delta\bar{u}]_S, \tag{24}$$

where

$$\begin{aligned} \Delta e &= j_{11}e^\sigma + j_{12}\tilde{e} + j_{13}e^u, \\ \Delta\sigma &= j_{12}\bar{\sigma} + j_{22}\sigma^\epsilon + j_{23}\sigma^u, \\ \sigma' &= j_{13}\bar{\sigma} + j_{23}\sigma^\epsilon + j_{33}\sigma^u. \end{aligned} \tag{25}$$

The last two terms combine with contributions from the forcing potential variation. For example, if $P \equiv P^c$, the complete variation of $\Pi^c = U - P^c$ is:

$$\delta\Pi^c = (\Delta e, \delta\bar{\sigma})_V + (\Delta\sigma, \delta\tilde{e})_V - (\mathbf{div}\,\sigma' + \mathbf{b}, \delta\bar{u})_V + [\sigma'_n - \hat{\mathbf{t}}, \delta\bar{u}]_{S_t} - [\bar{u} - \hat{\mathbf{d}}, \delta\bar{\sigma}_n]_{S_d}. \tag{26}$$

Using P^d or P^t does not change the volume terms. The first variations of Π^d and Π^t are studied in Refs. 9–11 for a more restrictive class of functionals, namely Π_γ. The Euler equations associated with the volume terms

$$\Delta e = 0, \qquad \Delta\sigma = 0, \qquad \mathbf{div}\,\sigma' + \mathbf{b} = 0, \tag{27}$$

are independent of the forcing potential. A "weighted residual" interpretation of Eqs. 27 in terms of the field equations is given in section 5.4. For consistency of the Euler equations with the field

---

[2] To justify the symmetry of $\mathbf{J}$ note, for example, that $j_{13}(\bar{\sigma}, e^u)_V = \tfrac{1}{2}j_{13}(\bar{\sigma}, e^u)_V + \tfrac{1}{2}j_{13}(e^\sigma, \sigma^u)_V$, and so on.

equations of section 2 we must have $\Delta e = 0$, $\Delta \sigma = 0$ and $\sigma' = \sigma$ if the assumed stress and strain fields reduce to the exact ones. Consequently,

$$j_{11} + j_{12} + j_{13} = 0,$$
$$j_{12} + j_{22} + j_{23} = 0, \qquad (28)$$
$$j_{13} + j_{23} + j_{33} = 1.$$

Because of these constraints, the maximum number of independent parameters defining the entries of $\mathbf{J}$ is three.

5.2 Specific Functionals

Expressions of $\mathbf{J}$ for some classical and parametrized variational principles of elasticity are tabulated below. The subscript of $\mathbf{J}$ is used to identify the functionals, which are listed roughly in order of ascending complexity. The fields in parentheses after the functional name are those subject to independent variations in V.

Potential energy $(\tilde{u})$:

$$\mathbf{J}_P = \begin{bmatrix} 0 & 0 & 0 \\ 0 & 0 & 0 \\ 0 & 0 & 1 \end{bmatrix}. \qquad (29)$$

Stress-displacement Reissner, also called Hellinger-Reissner, $(\tilde{\sigma}, \tilde{u})$:

$$\mathbf{J}_R = \begin{bmatrix} -1 & 0 & 1 \\ 0 & 0 & 0 \\ 1 & 0 & 0 \end{bmatrix}. \qquad (30)$$

Unnamed stress-displacement functional listed on p. 116 of Ref. 18 $(\tilde{\sigma}, \tilde{u})$:

$$\mathbf{J}_U = \begin{bmatrix} 1 & 0 & -1 \\ 0 & 0 & 0 \\ -1 & 0 & 2 \end{bmatrix}. \qquad (31)$$

Strain-displacement Reissner-type as listed on p. 116 of Ref. 18 $(\tilde{e}, \tilde{u})$:

$$\mathbf{J}_S = \begin{bmatrix} 0 & 0 & 0 \\ 0 & -1 & 1 \\ 0 & 1 & 0 \end{bmatrix}. \qquad (32)$$

Hu-Washizu[3] $(\tilde{\sigma}, \tilde{e}, \tilde{u})$:

$$\mathbf{J}_W = \begin{bmatrix} 0 & -1 & 1 \\ -1 & 1 & 0 \\ 1 & 0 & 0 \end{bmatrix}. \qquad (33)$$

---

[3] There are several functionals that carry this name, transformable from one to another through integration by parts. That corresponding to $\mathbf{J}_W$ is the third form listed in section 2.3 of Ref. 24.
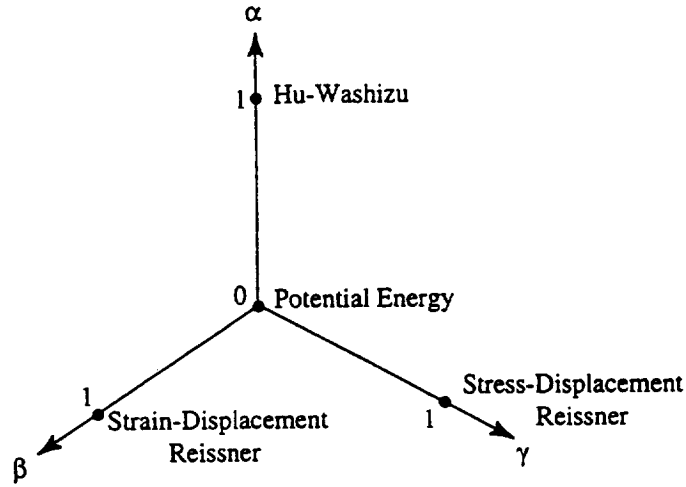
Fig. 4. Graphical representation of the $\mathbf{J}_{\alpha\beta\gamma}$ functionals

One-parameter stress-displacement family $(\bar{\sigma}, \bar{u})$ that includes U_P, U_R and U_U as special cases (Refs. 8–10)

$$\mathbf{J}_\gamma = \begin{bmatrix} -\gamma & 0 & \gamma \\ 0 & 0 & 0 \\ \gamma & 0 & 1-\gamma \end{bmatrix}. \tag{34}$$

One-parameter strain-displacement family $(\bar{e}, \bar{u})$ that includes U_P and U_S as special cases (Ref. 9):

$$\mathbf{J}_\beta = \begin{bmatrix} 0 & 0 & 0 \\ 0 & -\beta & \beta \\ 0 & \beta & 1-\beta \end{bmatrix}. \tag{35}$$

Two-parameter family $(\bar{\sigma}, \bar{e}, \bar{u})$ that includes U_β and U_γ as special cases (Ref. 9):

$$\mathbf{J}_{\beta\gamma} = (1-\beta)\mathbf{J}_\gamma + (1-\gamma)\mathbf{J}_\beta - (1-\beta-\gamma)\mathbf{J}_P$$
$$= \begin{bmatrix} -\gamma(1-\beta) & 0 & \gamma(1-\beta) \\ 0 & -\beta(1-\gamma) & \beta(1-\gamma) \\ \gamma(1-\beta) & \beta(1-\gamma) & 1-\beta-\gamma+2\beta\gamma \end{bmatrix}. \tag{36}$$

Three-parameter (α, β, γ) family $(\bar{\sigma}, \bar{e}, \bar{u})$ that includes U_W and $U_{\beta\gamma}$ as special cases (Ref. 9):

$$\mathbf{J}_{\alpha\beta\gamma} = \alpha\mathbf{J}_W + (1-\alpha)\mathbf{J}_{\beta\gamma}$$
$$= \begin{bmatrix} -\gamma(1-\beta)(1-\alpha) & -\alpha & \alpha+\gamma(1-\beta)(1-\alpha) \\ -\alpha & \alpha-\beta(1-\gamma)(1-\alpha) & \beta(1-\gamma)(1-\alpha) \\ \alpha+\gamma(1-\beta)(1-\alpha) & \beta(1-\gamma)(1-\alpha) & (1-\beta-\gamma+2\beta\gamma)(1-\alpha) \end{bmatrix}. \tag{37}$$

The last form, which contains three independent parameters, supplies all matrices $\mathbf{J}$ that satisfy the constraints of Eq. 28. It yields stress-displacement functionals for $\alpha = \beta = 0$, strain-displacement functionals for $\alpha = \gamma = 0$, and three-field (stress-strain-displacement) functionals otherwise. A graphic representation of this functional in (α, β, γ) space is given in Fig. 4.

The specialization $\gamma = 1$, $\beta = 0$ of $\mathbf{J}_{\alpha\beta\gamma}$ is of particular interest:

$$\mathbf{J}_\alpha = \begin{bmatrix} \alpha - 1 & -\alpha & 1 \\ -\alpha & \alpha & 0 \\ 1 & 0 & 0 \end{bmatrix}. \tag{38}$$

The associated functional Π_α might be called the generalized Hu-Washizu functional because it reduces to $\mathbf{J}_W$ for $\alpha = 1$. But because of its special relation with the ANDES formulation covered in section 8-11, Π_α will be herein referred to as the ANDES functional.

5.3 Energy Balancing

A prime motivation for introducing the j coefficients as free parameters is optimization of finite element performance in the balanced stiffness sense of Table 1. The determination of "best" parameters for specific elements relies on the concept of energy balance. Let $\mathcal{U}(\epsilon) = \frac{1}{2}(\mathbf{E}\epsilon, \epsilon)_V$ denote the strain energy associated with the strain field ϵ. If $\mathbf{E}$ is positive definite, $\mathcal{U}(\epsilon)$ is nonnegative. We may decompose the generalized strain energy into the following sum of strain energies:

$$U = \mathcal{U}(\mathbf{e}^u) + w_1 \mathcal{U}(\mathbf{e}^\sigma - \tilde{\mathbf{e}}) + w_2 \mathcal{U}(\tilde{\mathbf{e}} - \mathbf{e}^u) + w_3 \mathcal{U}(\mathbf{e}^u - \mathbf{e}^\sigma), \tag{39}$$

where $\mathcal{U}_P(\mathbf{e}^u) = U_P$ is the usual strain energy, and[4]

$$w_1 = \tfrac{1}{2}(j_{11} + j_{22} - j_{33} + 1), \quad w_2 = \tfrac{1}{2}(-j_{11} + j_{22} + j_{33} - 1), \quad w_3 = \tfrac{1}{2}(j_{11} - j_{22} + j_{33} - 1). \tag{40}$$

Eq. 39 is equivalent to decomposing $\mathbf{J}$ into the sum of four rank-one matrices:

$$\mathbf{J} = \begin{bmatrix} 0 & 0 & 0 \\ 0 & 0 & 0 \\ 0 & 0 & 1 \end{bmatrix} + w_1 \begin{bmatrix} 1 & -1 & 0 \\ -1 & 1 & 0 \\ 0 & 0 & 0 \end{bmatrix} + w_2 \begin{bmatrix} 0 & 0 & 0 \\ 0 & 1 & -1 \\ 0 & -1 & 1 \end{bmatrix} + w_3 \begin{bmatrix} 1 & 0 & -1 \\ 0 & 0 & 0 \\ -1 & 0 & 1 \end{bmatrix}. \tag{41}$$

Decompositions of this nature can be used to derive energy-balanced finite elements by considering element "patches" under simple load systems. This technique is discussed for the one-parameter functionals generated by $\mathbf{J}_\gamma$ in Refs. 6 and 8–11. It is important to note that the j coefficients *may vary from element to element*.

5.4 Interpretation of Euler Equations

Eqs. 27 gain physical meaning if they are rewritten as

$$\Delta \mathbf{e} = w_1(\mathbf{e}^\sigma - \tilde{\mathbf{e}}) + w_3(\mathbf{e}^u - \mathbf{e}^\sigma) = \mathbf{0},$$

$$\Delta \sigma = w_1(\tilde{\sigma} - \sigma^\epsilon) + w_2(\sigma^\epsilon - \sigma^u) = \mathbf{0}, \tag{42}$$

$$\mathbf{div}\,\sigma' = \mathbf{div}\left[\sigma^u + w_2(\sigma^\epsilon - \sigma^u) + w_3(\sigma^u - \tilde{\sigma})\right] = -\mathbf{b},$$

---

[4] As shown in section 5.4, these coefficients may be interpreted as field equation residual weights, hence the notation. It is conjectured that for stability the j coefficients should be confined so that $w_i \geq 0$, but this remains to be proven.

where the w_i are given by Eqs. 40. But $\mathbf{e}^\sigma - \bar{\mathbf{e}} = \mathbf{E}^{-1}\bar{\sigma} - \bar{\mathbf{e}} = 0$ as well as $\bar{\sigma} - \sigma^\epsilon = \bar{\sigma} - \mathbf{E}\bar{\mathbf{e}} = 0$ are representations of the constitutive equations, Eqs. 2. Likewise, $\sigma^\epsilon - \sigma^u = \mathbf{E}(\bar{\mathbf{e}} - \mathbf{D}\bar{\mathbf{u}}) = 0$ is a representation of the strain-displacement equations, Eqs. 1. Finally, $\mathbf{e}^u - \mathbf{e}^\sigma = \mathbf{D}\bar{\mathbf{u}} - \mathbf{E}^{-1}\bar{\sigma} = 0$, as well as $\sigma^u - \bar{\sigma} = 0$, are combinations of Eqs. 1-2. Thus, we conclude that the Euler equations $\Delta \mathbf{e} = 0$ and $\Delta \sigma = 0$ are weighted forms of the kinematic and constitutive field equations. On the other hand, $\mathbf{div}\,\sigma' + \mathbf{b} = 0$ is a weighted combination of the equilibrium equations, Eqs. 3, and the other two.

If the j coefficients are such that a weight vanishes (see also Footnote 4), that particular field equation drops out from the Euler equations and must be viewed as being satisfied *a priori*. For example, in the potential energy functional, $w_1 = w_2 = w_3 = 0$, and only the equilibrium condition in terms of σ^u remains in the Euler equations. This interpretation points the way for constructing U of Eq. 15 by the method of weighted residuals.

5.5 Functionals without Independent Displacements

The foregoing theory applies to functionals where the displacements $\mathbf{u}$ are independently varied. Although this case includes the more practically important functionals for our purposes, for completeness we present the general parametrization of stress-strain functionals. Decompose U of Eq. 15 as $U_c + U_u$, where U_u contains the strain energy due to displacement-derived strains:

$$U_u = (j_{13}\bar{\sigma} + j_{23}\sigma^\epsilon + \tfrac{1}{2}j_{33}\sigma^u, \mathbf{e}^u)_V = (\mathbf{div}\,\sigma', \mathbf{u})_V - [\sigma'_n, \mathbf{u}]_S. \tag{43}$$

If we now assume that the equilibrium equations $\mathbf{div}\,\sigma + \mathbf{b} = 0$ and traction boundary conditions $\sigma_n = \hat{\mathbf{t}}$ hold *a priori*, U_u may be dropped and we are left with the *generalized complementary energy* functional

$$U \rightarrow U_c = \tfrac{1}{2}j_{11}(\bar{\sigma}, \mathbf{e}^\sigma)_V + j_{12}(\bar{\sigma}, \bar{\mathbf{e}})_V + \tfrac{1}{2}j_{22}(\sigma^\epsilon, \bar{\mathbf{e}})_V. \tag{44}$$

Taking account of the *a priori* conditions, the first variation becomes:

$$\delta U_c = (j_{11}\mathbf{e}^\sigma + j_{12}\bar{\mathbf{e}} + \mathbf{e}^u, \delta\bar{\sigma})_V + (j_{12}\sigma + j_{22}\sigma^\epsilon, \delta\bar{\mathbf{e}})_V, \tag{45}$$

and for consistency we must have $j_{11} + j_{12} = -1$, $j_{12} + j_{22} = 0$. It follows that U_c may be represented as in the matrix form of Eq. 21 with a $\mathbf{J}$ that depends on a single parameter:

$$\mathbf{J}_\rho = \begin{bmatrix} \rho - 1 & -\rho & 0 \\ -\rho & \rho & 0 \\ 0 & 0 & 0 \end{bmatrix}. \tag{46}$$

Here $\rho = 0$ gives the classical principle of total complementary energy whereas $\rho = 1$ gives the functional $N(\bar{\sigma}, \bar{\mathbf{e}})$ listed on p. 117 of Ref. 18.

6. FINITE ELEMENT DISCRETIZATION

In this section assumptions invoked in the finite element discretization of the functional Π^d for arbitrary $\mathbf{J}$ are stated. Following usual practice in finite element work, the components of stresses and strains are arranged as one-dimensional arrays while the elastic moduli in $\mathbf{E}$ are arranged as a square symmetric matrix. In the sequel, and unless otherwise noted, we consider an *individual element* of volume V and surface $S : S_t \cup S_d \cup S_i$, where S_i is the portion of the boundary in common with other elements.

6.1 Boundary Displacement Assumption

The boundary displacement assumption is:

$$[\bar{\mathbf{d}} = \mathbf{N}_d \, \mathbf{v}]_S. \tag{47}$$

Here matrix $\mathbf{N}_d$ collects boundary shape functions for the boundary displacements $\mathbf{d}$ while vector $\mathbf{v}$ collects the "visible" degrees of freedom of the element, also called the *connectors*. These displacements must be unique on common element boundaries. This continuity condition is met if the displacement of a common boundary portion is uniquely specified by degrees of freedom located on that boundary. There are no derived fields associated with $\bar{\mathbf{d}}$.

6.2 Internal Displacement Assumption

The displacement assumption in the interior of the element is

$$(\bar{\mathbf{u}} = \mathbf{N}_u \mathbf{q})_V, \tag{48}$$

where matrix $\mathbf{N}_u$ collects the internal displacement shape functions and vector $\mathbf{q}$ collects generalized coordinates for the internal displacements. The assumed $\bar{\mathbf{u}}$ need not be continuous across interelement boundaries. The displacement derived fields are

$$(\mathbf{e}^u = \mathbf{D}\mathbf{N}\mathbf{q} = \mathbf{B}\mathbf{q})_V, \quad (\sigma^u = \mathbf{E}\mathbf{B}\mathbf{q})_V. \tag{49}$$

To link up with the FF and ANS formulations, we break up the internal displacement field as follows. The assumed $\bar{\mathbf{u}}$ is decomposed into rigid body, constant strain, and higher order displacements:

$$\bar{\mathbf{u}} = \mathbf{N}_r \mathbf{q}_r + \mathbf{N}_c \mathbf{q}_c + \mathbf{N}_h \mathbf{q}_h. \tag{50}$$

Applying the strain operator $\mathbf{D} = \frac{1}{2}(\nabla + \nabla^T)$ to $\bar{\mathbf{u}}$ we get the associated strain field:

$$\mathbf{e}^u = \mathbf{D}\mathbf{N}_r \mathbf{q}_r + \mathbf{D}\mathbf{N}_c \mathbf{q}_c + \mathbf{D}\mathbf{N}_h \mathbf{q}_h = \mathbf{B}_r \mathbf{q}_r + \mathbf{B}_c \mathbf{q}_c + \mathbf{B}_h \mathbf{q}_h. \tag{51}$$

But $\mathbf{B}_r = \mathbf{D}\mathbf{N}_r$ vanishes because $\mathbf{N}_r$ contains only rigid body modes. We are also free to select $\mathbf{B}_c = \mathbf{D}\mathbf{N}_c$ to be the identity matrix $\mathbf{I}$ if the generalized coordinates $\mathbf{q}_c$ are identified with the mean (volume-averaged) strain values $\bar{\mathbf{e}}^u$. Consequently Eq. 51 simplifies to

$$\mathbf{e}^u = \bar{\mathbf{e}}^u + \mathbf{e}_h^u = \bar{\mathbf{e}}^u + \mathbf{B}_h \mathbf{q}_h, \tag{52}$$

in which

$$\mathbf{q}_c \equiv \bar{\mathbf{e}}^u = (\mathbf{e}^u)_V / \upsilon, \quad (\mathbf{B}_h)_V = \mathbf{0}, \tag{53}$$

where $\upsilon = (1)_V$ is the element volume measure. The second relation is obtained by integrating both sides of Eq. 52 over V and noting that $\mathbf{q}_h$ is arbitrary. It says that the mean value of the higher order displacement-derived strains (also called the *deviatoric* displacement-derived strains) is zero over the element.

6.3 Stress Assumption

The stress field will be assumed to be *constant* over the element:

$$(\tilde{\sigma} = \overline{\sigma})_V. \tag{54}$$

This assumption is sufficient to construct high performance elements based on the free formulation developed in Refs. 4–8. As discussed in Ref. 11, the inclusion of higher order stress modes (deviatoric stresses) in Eq. 56 is computationally effective if these modes are divergence free, but such a requirement makes extension to geometrically nonlinear problems difficult. The only derived field is

$$(e^{\sigma} = \overline{e}^{\sigma} = E^{-1}\overline{\sigma})_V. \tag{55}$$

6.4 Strain Assumptions

The assumed strain field $\tilde{e}$ is split into a mean constant strain $\overline{e}$ and a higher order variation (the *deviatoric* strains):

$$(\tilde{e} = \overline{e} + e_d = \overline{e} + A_d a)_V, \tag{56}$$

where $\overline{e} = (\tilde{e})_V/v$, matrix A_d collects deviatoric strain modes with mean zero value over the element:

$$(A_d)_V = 0, \tag{57}$$

and a collects the corresponding strain mode amplitudes. The only derived field is:

$$(\sigma^{\epsilon} = E\tilde{e} = E\overline{e} + EA_d a)_V. \tag{58}$$

7. UNCONSTRAINED FINITE ELEMENT EQUATIONS

We shall assume that all elastic moduli in E are *constant* over the element. Inserting the above assumptions into Π^d with the modified forcing potential of Eq. 19, we obtain a quadratic algebraic form which is block-sparse because of the conditions stated in Eqs. 53 and 57. Rendering this form stationary yields the finite element equations.

$$
\begin{bmatrix}
j_{11}vE^{-1} & j_{12}vI & 0 & -P_r^T & j_{13}vI - P_u^T & -P_h^T & L^T \\
j_{12}vI & j_{22}vE & 0 & 0 & j_{23}vI & 0 & 0 \\
0 & 0 & j_{22}K_{ad} & 0 & 0 & j_{23}R^T & 0 \\
-P_r & 0 & 0 & 0 & 0 & 0 & 0 \\
j_{13}vI - P_u & j_{23}vI & 0 & 0 & j_{33}vE & 0 & 0 \\
-P_h & 0 & j_{13}R & 0 & 0 & j_{33}K_{qh} & 0 \\
L & 0 & 0 & 0 & 0 & 0 & 0
\end{bmatrix}
\begin{Bmatrix}
\overline{\sigma} \\ \overline{e} \\ a \\ q_r \\ \overline{e}^u \\ q_h \\ v
\end{Bmatrix}
=
\begin{Bmatrix}
0 \\ 0 \\ 0 \\ f_{qr} \\ f_{qu} \\ f_{qh} \\ f_v
\end{Bmatrix}, \tag{59}
$$

where:

$$K_{qh} = (B_h^T E B_h)_V = K_{qh}^T, \quad K_{ad} = (A_d^T E A_d)_V = K_{ad}^T, \quad R = (B_h^T E A_d)_V,$$

$$L = [N_{dn}^T]_S, \quad P_r = [N_{rn}^T]_S, \quad P_c = [N_{cn}^T]_S, \quad P_h = [N_{hn}^T]_S, \tag{60}$$

$$f_r = (N_r^T b)_V, \quad f_q = (N_q^T b)_V, \quad f_h = (N_h^T b)_V, \quad f_v = [N_d^T \hat{t}]_{S_t},$$

62

in which N_{dn} denotes the projection of shape functions N_d on the exterior normal $\mathbf{n}$, and similarly for N_r, N_c and N_h. Those coefficient matrix entries that do not depend on the j coefficients come from the last boundary term in Eq. 19.

7.1 The P Matrices

Application of the divergence theorem to the work of the mean stress on $\mathbf{e}^u$ yields:

$$(\bar{\sigma}, \mathbf{e}^u)_V = (\bar{\sigma}, \bar{\mathbf{e}}^u + \mathbf{B}_h \mathbf{q}_h)_V = v\bar{\sigma}^T \bar{\mathbf{e}}^u + \bar{\sigma}^T (\mathbf{B}_h)_V \mathbf{q}_h = v\bar{\sigma}^T \bar{\mathbf{e}}^u$$
$$= [\bar{\sigma}_n, \bar{\mathbf{u}}]_S = [\bar{\sigma}_n, N_r \mathbf{q}_r + N_c \bar{\mathbf{e}}^u + N_h \mathbf{q}_h]_S = \bar{\sigma}^T (\mathbf{P}_r \mathbf{q}_r + \mathbf{P}_c \bar{\mathbf{e}}^u + \mathbf{P}_h \mathbf{q}_h). \tag{61}$$

Hence $\mathbf{P}_r = 0$, $\mathbf{P}_c = v\mathbf{I}$, $\mathbf{P}_h = 0$, and the element equations simplify to:

$$\begin{bmatrix} j_{11}v\mathbf{E}^{-1} & j_{12}v\mathbf{I} & 0 & 0 & (j_{13}-1)v\mathbf{I} & 0 & \mathbf{L}^T \\ j_{12}v\mathbf{I} & j_{22}v\mathbf{E} & 0 & 0 & j_{23}v\mathbf{I} & 0 & 0 \\ 0 & 0 & j_{22}\mathbf{K}_{ad} & 0 & 0 & j_{23}\mathbf{R}^T & 0 \\ 0 & 0 & 0 & 0 & 0 & 0 & 0 \\ (j_{13}-1)v\mathbf{I} & j_{23}v\mathbf{I} & 0 & 0 & j_{33}v\mathbf{E} & 0 & 0 \\ 0 & 0 & j_{23}\mathbf{R} & 0 & 0 & j_{33}\mathbf{K}_{qh} & 0 \\ \mathbf{L} & 0 & 0 & 0 & 0 & 0 & 0 \end{bmatrix} \begin{Bmatrix} \bar{\sigma} \\ \bar{\mathbf{e}} \\ \mathbf{a} \\ \mathbf{q}_r \\ \bar{\mathbf{e}}^u \\ \mathbf{q}_h \\ \mathbf{v} \end{Bmatrix} = \begin{Bmatrix} 0 \\ 0 \\ 0 \\ \mathbf{f}_{qr} \\ \mathbf{f}_{qu} \\ \mathbf{f}_{qh} \\ \mathbf{f}_v \end{Bmatrix}. \tag{62}$$

The simplicity of the $\mathbf{P}$ matrices is essentially due to the mean-plus-deviator splitting of Eq. 52 for $\mathbf{e}^u$. If this decomposition is not enforced, $\mathbf{P}_r = 0$ but $\mathbf{P}_c = (\mathbf{B}_c)_V = v\mathbf{B}_c$ and $\mathbf{P}_h = (\mathbf{B}_h)_V$.

8. KINEMATIC CONSTRAINTS

The "tricks" we shall consider here are *kinematic constraints* that play a key role in the development of high-performance FF and ANS elements. These are matrix relations between kinematic quantities that are established *independently* of the variational equations. Two types of relations will be considered.

8.1 Constraints Between Internal and Boundary Displacements

Relations linking the generalized coordinates $\mathbf{q}$ of Eq. 48 and the connectors $\mathbf{v}$ were introduced by Bergan and coworkers in conjunction with the free formulation (FF) of finite elements (Ref. 5). For simplicity, we shall assume that the number of freedoms in $\mathbf{v}$ and $\mathbf{q}$ is the same; removal of this restriction is studied in Ref. 11. By collocation of $\mathbf{u}$ at the element node points one easily establishes the relation:

$$\mathbf{v} = \mathbf{G}_r \mathbf{q}_r + \mathbf{G}_c \mathbf{q}_c + \mathbf{G}_h \mathbf{q}_h = \mathbf{Gq}, \tag{63}$$

where $\mathbf{G}$ is a square transformation matrix that will be assumed to be nonsingular. On inverting this relation we obtain

$$\mathbf{q} = \mathbf{G}^{-1} = \mathbf{Hv}, \qquad \text{or} \qquad \mathbf{q} = \begin{Bmatrix} \mathbf{q}_r \\ \bar{\mathbf{e}}^u \\ \mathbf{q}_h \end{Bmatrix} = \begin{bmatrix} \mathbf{H}_r \\ \mathbf{H}_c \\ \mathbf{H}_h \end{bmatrix} \mathbf{v}. \tag{64}$$

The following relations between $\mathbf{L}$ (defined in Eq. 60) and the above submatrices hold as a consequence of the individual element test described in section 9.3:

$$\mathbf{L}^T \mathbf{G}_r = 0, \qquad \mathbf{L}^T \mathbf{G}_c = \upsilon \mathbf{I}, \qquad \upsilon \mathbf{H}_c = \mathbf{L}^T. \tag{65}$$

If the splitting of Eq. 52 is not enforced, however, the last two become:

$$\mathbf{L}^T \mathbf{G}_c = \upsilon \mathbf{B}_c, \qquad \mathbf{P}_c \mathbf{H}_c + \mathbf{P}_h \mathbf{H}_h = \mathbf{L}^T \quad \text{or} \quad \mathbf{P}_c = \mathbf{L}^T \mathbf{G}_c. \tag{66}$$

Since $\mathbf{P}_c = \upsilon \mathbf{B}_c$, these relations coalesce (see Ref. 5).

8.2 Constraints Between Assumed Deviatoric Strains and Boundary Displacements

Constraints linking $\tilde{\mathbf{e}}$ to $\mathbf{v}$ are fundamentally important in the ANS formulation. The effect of these constraints in a variational framework is analyzed in Refs. 15 and 16. In the present study we depart from previous work in that *only the deviatoric strains*, $\mathbf{e}_d$, *are assumed linked to* $\mathbf{v}$, *whereas the mean strains* $\bar{\mathbf{e}}$ *are obtained variationally*. Consequently, we shall postulate the following relation between assumed deviatoric strain amplitudes and nodal displacement connectors:

$$\mathbf{a} = \mathbf{Q}\mathbf{v}, \tag{67}$$

where $\mathbf{Q}$ is generally a rectangular matrix determined by collocation, least squares or other fitting methods. An example of the construction of $\mathbf{Q}$ is given in section 11.4. The individual element test described in section 9.3 requires that $\mathbf{Q}$ be orthogonal to $\mathbf{G}_r$ and $\mathbf{G}_c$:

$$\mathbf{Q}\mathbf{G}_r = 0, \qquad \mathbf{Q}\mathbf{G}_c = 0. \tag{68}$$

8.3 Limitation Principles

Strain assumptions made concurrently with displacement assumptions are confined by *limitation principles* similar to those stated by Fraeijs de Veubeke for stress-displacement mixed elements (Ref. 13). This issue was discussed in Ref. 15 for a more restricted strain displacement hybrid formulation. Limitation principles for the general formulation presented here remain to be studied.

9. VISIBLE STIFFNESS EQUATIONS

On enforcing the constraints $\mathbf{a} = \mathbf{Q}\mathbf{v}$, $\mathbf{q}_r = \mathbf{H}_r\mathbf{v}$, $\mathbf{q}_c = \mathbf{H}_c\mathbf{v} = \upsilon^{-1}\mathbf{L}^T\mathbf{v}$, and $\mathbf{q}_h = \mathbf{H}_h\mathbf{v}$, through Lagrange multiplier vectors λ_a, λ_r, λ_c, and λ_h, respectively, we get the augmented finite element equations

$$
\begin{bmatrix}
j_{11}\upsilon\mathbf{E}^{-1} & j_{12}\upsilon\mathbf{I} & 0 & 0 & (j_{13}-1)\upsilon\mathbf{I} & 0 & 0 & 0 & 0 & 0 & \mathbf{L}^T \\
j_{12}\upsilon\mathbf{I} & j_{22}\upsilon\mathbf{E} & 0 & 0 & j_{23}\upsilon\mathbf{I} & 0 & 0 & 0 & 0 & 0 & 0 \\
0 & 0 & j_{22}\mathbf{K}_{ad} & 0 & 0 & j_{23}\mathbf{R}^T & -\mathbf{I} & 0 & 0 & 0 & 0 \\
0 & 0 & 0 & 0 & 0 & 0 & 0 & -\mathbf{I} & 0 & 0 & 0 \\
(j_{13}-1)\upsilon\mathbf{I} & j_{23}\upsilon\mathbf{I} & 0 & 0 & j_{33}\upsilon\mathbf{E} & 0 & 0 & 0 & -\mathbf{I} & 0 & 0 \\
0 & 0 & j_{23}\mathbf{R} & 0 & 0 & j_{33}\mathbf{K}_{qh} & 0 & 0 & 0 & -\mathbf{I} & 0 \\
0 & 0 & -\mathbf{I} & 0 & 0 & 0 & 0 & 0 & 0 & 0 & \mathbf{Q} \\
0 & 0 & 0 & -\mathbf{I} & 0 & 0 & 0 & 0 & 0 & 0 & \mathbf{H}_r \\
0 & 0 & 0 & 0 & -\mathbf{I} & 0 & 0 & 0 & 0 & 0 & \upsilon^{-1}\mathbf{L}^T \\
0 & 0 & 0 & 0 & 0 & -\mathbf{I} & 0 & 0 & 0 & 0 & \mathbf{H}_h \\
\mathbf{L} & 0 & 0 & 0 & 0 & 0 & \mathbf{Q}^T & \mathbf{H}_r^T & \upsilon^{-1}\mathbf{L} & \mathbf{H}_h^T & 0
\end{bmatrix}
\begin{Bmatrix}
\bar{\sigma} \\ \bar{\mathbf{e}} \\ \mathbf{a} \\ \mathbf{q}_r \\ \bar{\mathbf{e}}^u \\ \mathbf{q}_h \\ \lambda_a \\ \lambda_r \\ \lambda_c \\ \lambda_h \\ \mathbf{v}
\end{Bmatrix}
=
\begin{Bmatrix}
0 \\ 0 \\ 0 \\ \mathbf{f}_{qr} \\ \mathbf{f}_{qu} \\ \mathbf{f}_{qh} \\ 0 \\ 0 \\ 0 \\ 0 \\ \mathbf{f}_v
\end{Bmatrix}
. \tag{69}
$$

Condensation of all degrees of freedom except v yields the visible[5] element stiffness equations:

$$\mathbf{K}\mathbf{v} = (\mathbf{K}_b + \mathbf{K}_h)\mathbf{v} = \mathbf{f}, \tag{70}$$

where

$$\mathbf{K}_b = v^{-1}\mathbf{L}\mathbf{E}\mathbf{L}^T, \tag{71}$$

$$\mathbf{K}_h = j_{33}\mathbf{H}_h^T\mathbf{K}_{qh}\mathbf{H}_h + j_{23}(\mathbf{H}_h^T\mathbf{R}\mathbf{Q} + \mathbf{Q}^T\mathbf{R}^T\mathbf{H}_h) + j_{22}\mathbf{Q}^T\mathbf{K}_{ad}\mathbf{Q}, \tag{72}$$

$$\mathbf{f} = \mathbf{f}_v + \mathbf{H}_r^T\mathbf{f}_{qr} + v^{-1}\mathbf{L}^T\mathbf{f}_{qc} + \mathbf{H}_h^T\mathbf{f}_{qh}. \tag{73}$$

Following the nomenclature of the free formulation, we shall call $\mathbf{K}_b$ the *basic stiffness matrix* and $\mathbf{K}_h$ the *higher order stiffness matrix*.

9.1 Relation to Previous HP Element Formulations

If $\mathbf{J} = \mathbf{J}_\gamma$ of Eq. 33, $j_{33} = 1 - \gamma$, $j_{22} = j_{23} = 0$, and we recover the *scaled free formulation* stiffness equations considered in Refs. 6, 8 and 10:

$$\mathbf{K}_h = (1 - \gamma)\,\mathbf{H}_h^T\mathbf{K}_{qh}\mathbf{H}_h, \qquad 1 - \gamma > 0. \tag{74}$$

On the other hand, if we take $\mathbf{J} = \mathbf{J}_\alpha$ as given in Eq. 38, $j_{22} = \alpha$, $j_{33} = j_{23} = 0$ and we obtain:

$$\mathbf{K}_h = \alpha\mathbf{Q}^T\mathbf{K}_{ad}\mathbf{Q}, \qquad \alpha > 0, \tag{75}$$

which is similar to the stiffness produced by the ANS hybrid variational formulation studied in Refs. 15–16, in which the forcing potential P^t was used instead of P^d. The variant of ANS considered herein will be called the *assumed natural deviatoric strain* (ANDES) formulation in the sequel. The name is apt in the sense that what is being assumed are deviatoric rather than total strains, and that this assumption only affects the higher order stiffness.

But the term with coefficient j_{23} in Eq. 72 is new. It may be viewed as coupling the FF and ANDES formulations. It is not known whether Eqs. 70–73 represent the most general structure of the visible stiffness equations of HP elements.

9.2 Recovery of Element Fields

For simplicity suppose that the *body forces vanish* and so do $\mathbf{f}_{qr}$, $\mathbf{f}_{qc}$ and $\mathbf{f}_{qh}$ because of Eqs. 60. If v is known following a finite element solution of the assembled system, solving Eqs. 69 for the internal degrees of freedom yields:

$$\bar{\mathbf{e}} = v^{-1}\mathbf{L}^T\mathbf{v}, \quad \bar{\sigma} = \mathbf{E}\bar{\mathbf{e}}, \quad \mathbf{a} = \mathbf{Q}\mathbf{v}, \quad \mathbf{q}_r = \mathbf{H}_r\mathbf{v}, \quad \bar{\mathbf{e}}^u = \bar{\mathbf{e}}, \quad \mathbf{q}_h = \mathbf{H}_h\mathbf{v},$$
$$\lambda_a = (j_{22}\mathbf{K}_{ad}\mathbf{Q} + j_{33}\mathbf{R}^T\mathbf{H}_h)\mathbf{v}, \quad \lambda_r = 0, \quad \lambda_c = 0, \quad \lambda_h = (j_{23}\mathbf{R}\mathbf{Q} + j_{33}\mathbf{K}_{qh}\mathbf{H}_h)\mathbf{v}. \tag{76}$$

---

[5] The qualifier "visible" emphasizes that these are the stiffness equations other elements "see", and, consequently, are the only ones that matter insofar as computer implementation on a displacement-based finite element program.

Eq. 76 show that the *mean* strains $\bar{\mathbf{e}}$, $\bar{\mathbf{e}}^u$ and $\bar{\mathbf{e}}^\sigma = \mathbf{E}^{-1}\bar{\sigma}$ coincide, and, of course, so do the mean stresses. But if the body forces do not vanish, the mean stresses and mean strains recovered from different fields will not generally agree.

We also note that a nonzero Lagrange multiplier vector flags a deviation of the associated fields from the *variationally consistent* fields that would result when using the unconstrained Eqs. 62 without "tricks".

9.3   The Individual Element Test

To conclude the general formulation, we investigate the conditions under which HP elements based on the foregoing setting pass the individual element test of Bergan and Hanssen described in Refs. 3–6. To carry out the test, assume that the "free floating" element[6] under zero body forces is in a *constant stress state* σ_0, which, of course, is also the mean stress. Insert the following data in the left-hand side vector of Eq. 69:

$$\bar{\sigma} = \sigma_0 = \bar{\sigma}^u, \quad \bar{\mathbf{e}} = \mathbf{E}^{-1}\sigma_0, \quad \mathbf{a}_h = \mathbf{0}, \quad \mathbf{q}_r = arbitrary, \quad \mathbf{e}^u = \bar{\mathbf{e}}^u = \mathbf{E}^{-1}\bar{\sigma}_0, \quad \mathbf{q}_h = \mathbf{0},$$

$$\lambda_a = \mathbf{0}, \quad \lambda_r = \mathbf{0}, \quad \lambda_c = \mathbf{0}, \quad \lambda_h = \mathbf{0}, \quad \mathbf{v} = \mathbf{G}_r\mathbf{q}_r + \mathbf{G}_c\bar{\mathbf{e}}^u = \mathbf{G}_r\mathbf{q}_r + \mathbf{G}_c\mathbf{E}^{-1}\sigma_0.$$

$$(77)$$

Premultiply by the coefficient matrix and demand that all terms on the right-hand side vanish except for $\mathbf{f}_v = \mathbf{L}\sigma_0$. Then the orthogonality conditions in Eqs. 65 and 68 emerge. This form of the patch test is very strong, and it may well be that relaxing circumstances can be found for specific problems such as shells.

10.   DISCUSSION

At this point it is useful to recapitulate key points and connect this material with some of the techniques of Table 2. The chief property of HP elements constructed with present methods is the decomposition of the element stiffness equations displayed in Eq. 70; a property that of course subsists at the assembly level.

The basic stiffness matrix has a *universal* character: as no j coefficients appear in Eq. 71, clearly $\mathbf{K}_b$ is independent of specific variational principles. Given the constant stress state introduced in Eq. 54, $\mathbf{K}_b$ depends only on the assumed boundary motions. It can be constructed (and programmed) once and for all for each element type. As emphasized in Ref. 5, the main function of $\mathbf{K}_b$ is to provide *convergence*.

The higher order stiffness in Eq. 72 serves two other functions: *stability* and *accuracy*. The basic stiffness is generally rank-deficient[7] because its rank cannot exceed that of $\mathbf{E}$; thus a key function of $\mathbf{K}_h$ is to stabilize $\mathbf{K}$ by raising its rank to the correct one. The second function, which has gained importance in recent work, is to increase solution accuracy for coarse grids. Here is where the j coefficients play the important role noted in section 5.3. *These coefficients may vary from element to element*, despite the fact that this variation implies that the variational principle changes from one element to another. Thus, the "element mixability" requirement of Table 1 is fulfilled without tears.

---

[6] Mathematically, the entire element boundary is traction-specified, *i.e.*, $S \equiv S_t$.

[7] Except in simplex elements, for which $\mathbf{K} \equiv \mathbf{K}_b$.

10.1 The Free Formulation

The present methodology was initially pursued to justify variationally the original FF ($\gamma = 0$) of Ref. 5, as well as the scaled FF ($\gamma \neq 0$) of Refs. 6–8. Thus, it is not surprising that those element construction techniques fit naturally in the present variational framework by simply taking $J = J_\gamma$. The extended FF described in Ref. 11 aims to remove the restriction that the dimension of vectors q and v be the same. One of the techniques advocated to allow $\dim(q) > \dim(v)$ involves extending Eq. 54 with deviatoric stress assumptions, and thus requires a generalization of Eqs. 59 and 62. Whether such a generalization is practically worthwhile is unclear.

10.2 The ANS Formulation

The conventional ANS formulation as presented in Refs. 1 and 19 constructs *total* strain fields $\bar{e}$ (not necessarily integrable into displacements u^e) gaged through generalized strain coordinates a as $e = Aa$. These coordinates are eventually linked to the connectors v via matrix expressions of the form $a = Qv$, leading to an element stiffness of the form $K = Q^T K_a Q$, where K_a is the generalized stiffness in terms of a. The restriction to deviatoric strains in section 6.4 is motivated by two interrelated factors: (a) the strain assumed stiffness "flows" to the higher order stiffness, where it can be naturally scaled by using $J = J_\alpha$, and even intermixed with FF contributions as Eq. 72 shows; and (b) the basic stiffness of the element, derived separately, can be used to insure convergence.

10.3 Projectors and S/R Integration

The so-called "B-bar" approach is based on expressing the element strains as[8]

$$e = \bar{\bar{B}}v \tag{78}$$

where $\bar{\bar{B}}$, which cuts off the "harmful" portion of B^u, is constructed by various ad-hoc devices such as strain projection, selective, and/or uniform reduced integration. These time-honored schemes are well covered in Ref. 14. They are easily included in the present setting if $\bar{\bar{B}}$ admits the decomposition

$$\bar{\bar{B}} = \bar{B} + A_d Q, \tag{79}$$

where Q is not position dependent and $\bar{e} = \bar{B}v$ provides the mean strains, which are discarded in favor of Eq. 76. This decomposition can be usually carried out in several ways.

11. EXAMPLE: A 9-DOF ANDES PLATE BENDING TRIANGLE

The first element constructed with the ANDES formulation is a three-node Kirchhoff plate-bending flat triangle with the usual nine degrees of freedom. The derivation is briefly covered to illustrate the essential steps in forming the higher order stiffness of such elements. These steps are outlined in "recipe" form in Table 3, which restates the arguments of section 6.4 in a more physically oriented sense closely aligned with the terminology of Ref. 19.

---

[8] This is a slight variation from the usual notation, necessitated by the use of the single overbar to denote average or mean values.

Table 3 - Construction of K_h by the ANDES Formulation

Step 1. Select *reference lines* (in 2D elements) or *reference planes* (in 3D elements) where "natural straingage" locations are to be chosen. By appropriate interpolation express the element natural strains $\widetilde{\epsilon}$ in terms of the "straingage readings" g at those locations:

$$\widetilde{\epsilon} = A_\epsilon \, g, \tag{80}$$

where $\widetilde{\epsilon}$ is a strain field in natural coordinates that must include all constant strain states. (For bending elements the term "strains" is to be interpreted in a generalized sense, *viz.* curvatures.)

Step 2. Relate the Cartesian strains $\bar{e}$ to the natural strains:

$$\bar{e} = T\widetilde{\epsilon} = TA_\epsilon g = Ag \tag{81}$$

at each point in the element. (If $e \equiv \epsilon$, or if it is possible to work throughout in natural coordinates, this step is skipped.)

Step 3. Split the Cartesian strain field into mean (volume-averaged) and deviatoric strains:

$$\bar{e} = \bar{\bar{e}} + e_d = (\bar{A} + A_d)g, \tag{82}$$

where $\bar{A} = (TA_\epsilon)_V/v$, and $e_d = A_d g$ has mean zero value over V. (This step may also be carried out on the natural strains if T is constant, as is the case for the element derived here.)

Step 4. Relate the natural straingage readings g to the visible degrees of freedom

$$g = Qv \tag{83}$$

where Q is a straingage-to-node displacement transformation matrix. Techniques by which this is accomplished vary from element to element and it is difficult to state rules that apply to every situation. In the element derived here Q is constructed by direct interpolation over the reference lines. (In general there is no internal displacement field u^e such that $\bar{e} = Du^e$, so this step cannot be done by simply integrating the field of Eq. 81 over the element and collocating u^e at the nodes.)

Step 5. The higher-order stiffness matrix is given by

$$K_h = \alpha Q^T K_{ad} Q, \quad \text{where} \quad K_{ad} = \int_V A_d^T E A_d \, dV, \tag{84}$$

where $\alpha > 0$ is the scaling coefficient supplied by the functional of Eq. 38.

68

11.1 Geometric Relations

The triangle has *straight sides*. Its geometry is completely defined by the location of its three corners, which are labeled 1,2,3, moving counterclockwise. The triangle is referred to a local Cartesian system (x, y) which is taken with origin at the centroid 0, whence the corner coordinates x_i, y_i satisfy the relations $x_1 + x_2 + x_3 = 0$ and $y_1 + y_2 + y_3 = 0$. Coordinate differences are abbreviated by writing $x_{ij} = x_i - x_j$, etc. The signed triangle area A is given by the formulas:

$$2A = x_{21}y_{31} - x_{31}y_{21} = x_{32}y_{12} - x_{12}y_{32} = x_{13}y_{23} - x_{23}y_{13}, \tag{85}$$

and we require that $A > 0$. We shall also make use of dimensionless triangular coordinates ζ_1, ζ_2, ζ_3 linked by the constraint $\zeta_1 + \zeta_2 + \zeta_3 = 1$. The following well known relation between the area and centroid-originated Cartesian coordinates of a straight-sided triangle is noted:

$$\zeta_i = \frac{1}{2A}(x_i y_k - x_k y_j + xy_{jk} + yx_{kj}), \tag{86}$$

where i, j and k denote positive cyclic permutations of 1, 2 and 3; for example, $i = 2$, $j = 3$, $k = 1$. Therefore $\partial\zeta_i/\partial x = y_{jk}/2A$ and $\partial\zeta_i/\partial y = x_{kj}/2A$. Other intrinsic dimensions and ratios used below are

$$\ell_{ij} = \sqrt{x_{ij}^2 + y_{ij}^2}, \quad a_{ij} = 2A/\ell_{ij}, \quad b_{ij} = (x_{ij}x_{ik} + y_{ij}y_{ik})/\ell_{ij}, \quad b_{ji} = \ell_{ij} - b_{ij},$$
$$\lambda_{ij} = b_{ij}/\ell_{ij} = (x_{ij}x_{ik} + y_{ji}y_{ki})/(x_{ij}^2 + y_{ij}^2), \quad \lambda_{ji} = b_{ji}/\ell_{ij} = 1 - \lambda_{ij}, \tag{87}$$

where ℓ_{ij} denote the triangle side lengths, a_{ij} are triangle heights, b_{ij} and b_{ji} are projections of sides ik and jk onto side ij, respectively, and the λs are ratios of these projections to the side lengths.

11.2 Displacements, Rotations, Side Coordinates

Because we are dealing with a Kirchhoff element, its displacement field is completely defined by the transverse displacement $w(x, y) \equiv w(\zeta_1, \zeta_2, \zeta_3)$, positive upwards. The midplane rotations about x and y are $\theta_x = \partial w/\partial y$ and $\theta_y = -\partial w/\partial x$. The visible degrees of freedom of the element collected in v are:

$$\mathbf{v}^T = [\, w_1 \quad \theta_{x1} \quad \theta_{y1} \quad w_2 \quad \theta_{x2} \quad \theta_{y2} \quad w_3 \quad \theta_{x3} \quad \theta_{y3} \,]. \tag{88}$$

Over the three sides 1-2, 2-3 and 3-1, traversed counterclockwise, we define the dimensionless side coordinates μ_{12}, μ_{23} and μ_{31} as follows: over side 1-2, μ_{12} varies from $\mu_{12} = 0$ at corner 1 to $\mu_{12} = 1$ at corner 2. Thus, $\mu_{12} \equiv \zeta_2$ when $\zeta_3 = 0$. Relations for the other sides follow from cyclic permutation of subscripts. Then:

$$\frac{\partial x}{\partial \mu_{12}} = x_{21}, \quad \frac{\partial x}{\partial \mu_{23}} = x_{32}, \quad \frac{\partial x}{\partial \mu_{31}} = x_{13},$$
$$\frac{\partial y}{\partial \mu_{12}} = y_{21}, \quad \frac{\partial y}{\partial \mu_{23}} = y_{32}, \quad \frac{\partial y}{\partial \mu_{31}} = y_{13}. \tag{89}$$

11.3 Natural Curvatures

The second derivatives of w with respect to the dimensionless side directions will be called the *natural curvatures* and denoted by $\chi_{ij} = \partial^2 w / \partial \mu_{ij}^2$. Note that they have dimensions of displacement. The natural curvatures can be related to the Cartesian plate curvatures $\kappa_{xx} = \partial^2 w / \partial x^2$, $\kappa_{yy} = \partial^2 w / \partial y^2$ and $\kappa_{xy} = 2\partial^2 w / \partial x \partial y$, by chain-rule application of Eqs. 89:

$$
\chi = \left\{ \begin{array}{c} \chi_{12} \\ \chi_{23} \\ \chi_{31} \end{array} \right\} = \left\{ \begin{array}{c} \dfrac{\partial^2 w}{\partial \mu_{12}^2} \\[2mm] \dfrac{\partial^2 w}{\partial \mu_{23}^2} \\[2mm] \dfrac{\partial^2 w}{\partial \mu_{31}^2} \end{array} \right\} = \begin{bmatrix} x_{21}^2 & y_{21}^2 & x_{21}y_{21} \\ x_{32}^2 & y_{32}^2 & x_{32}y_{32} \\ x_{13}^2 & y_{13}^2 & x_{13}y_{13} \end{bmatrix} \left\{ \begin{array}{c} \dfrac{\partial^2 w}{\partial x^2} \\[2mm] \dfrac{\partial^2 w}{\partial y^2} \\[2mm] 2\dfrac{\partial^2 w}{\partial x \partial y} \end{array} \right\} = \mathbf{T}^{-1} \kappa. \tag{90}
$$

The inverse of this relation is:

$$
\left\{ \begin{array}{c} \dfrac{\partial^2 w}{\partial x^2} \\[2mm] \dfrac{\partial^2 w}{\partial y^2} \\[2mm] 2\dfrac{\partial^2 w}{\partial x \partial y} \end{array} \right\} = \frac{1}{4A^2} \begin{bmatrix} y_{23}y_{13} & y_{31}y_{21} & y_{12}y_{32} \\ x_{23}x_{13} & x_{31}x_{21} & x_{12}x_{32} \\ y_{23}x_{31}+x_{32}y_{13} & y_{31}x_{12}+x_{13}y_{21} & y_{12}x_{23}+x_{21}y_{32} \end{bmatrix} \left\{ \begin{array}{c} \dfrac{\partial^2 w}{\partial \mu_{12}^2} \\[2mm] \dfrac{\partial^2 w}{\partial \mu_{23}^2} \\[2mm] \dfrac{\partial^2 w}{\partial \mu_{31}^2} \end{array} \right\}, \tag{91}
$$

or, in matrix form

$$
\kappa = \mathbf{T}\chi. \tag{92}
$$

11.4 Curvature Sampling

The *reference lines* referred to in Table 3 are the three triangle sides. The natural curvatures are assumed to vary linearly over each reference line, an assumption which is obviously consistent with cubic beam-like variations of w over the sides. A linear variation on each side is determined by two straingage sample points, which we chose to be at the corners.

On each triangle side chose the isoparametric coordinates ξ_{ij} that vary from -1 at corner i to $+1$ at corner j. These are related to the μ_{ij} coordinates as $\xi_{ij} = 2\mu_{ij} - 1$. Then the natural curvature over side ij is given by the beam formula

$$
\chi_{ij} = \frac{\partial^2 w}{\partial \mu_{ij}^2} = \ell_{ij} \left[\frac{6\xi_{ij}}{\ell_{ij}} \quad 3\xi_{ij} - 1 \quad \frac{-6\xi_{ij}}{\ell_{ij}} \quad 3\xi_{ij} + 1 \right] \left\{ \begin{array}{c} w_i \\ \theta_{ni} \\ w_j \\ \theta_{nj} \end{array} \right\}, \tag{93}
$$

where θ_n denotes the rotation about the external normal direction n on side ij. Evaluating these relations at the nodes by setting $\xi_{ij} = \pm 1$ and converting normal rotations to x-y rotations, we

build the transformation

$$
\begin{Bmatrix} \chi_{12}|_1 \\ \chi_{12}|_2 \\ \chi_{23}|_2 \\ \chi_{23}|_3 \\ \chi_{31}|_3 \\ \chi_{31}|_1 \end{Bmatrix} = \begin{bmatrix} -6 & -4y_{21} & 4x_{21} & 6 & -2y_{21} & 2x_{21} & 0 & 0 & 0 \\ 6 & 2y_{21} & -2x_{21} & -6 & 4y_{21} & -4x_{21} & 0 & 0 & 0 \\ 0 & 0 & 0 & -6 & -4y_{32} & 4x_{32} & 6 & -2y_{32} & 2x_{32} \\ 0 & 0 & 0 & 6 & 2y_{32} & -2x_{32} & -6 & 4y_{32} & -4x_{32} \\ 6 & -2y_{13} & 2x_{13} & 0 & 0 & 0 & -6 & -4y_{13} & 4x_{13} \\ -6 & 4y_{13} & -4x_{13} & 0 & 0 & 0 & 6 & 2y_{13} & -2x_{13} \end{bmatrix} \begin{Bmatrix} w_1 \\ \theta_{x1} \\ \theta_{y1} \\ w_2 \\ \theta_{x2} \\ \theta_{y2} \\ w_3 \\ \theta_{x3} \\ \theta_{y3} \end{Bmatrix}
$$

(94)

The left hand side is the natural strain-gage reading vector called **g** in Table 3 and so we can express this as the matrix relation

$$ \mathbf{g} = \mathbf{Q}\mathbf{v}. \tag{95} $$

11.5 Curvature Interpolation

The six gage readings collected in **g** provide curvatures along the three triangle side directions at two corners. But nine values are needed to recover the complete curvature field over the element. The three additional values are the natural curvatures at the missing corner. We obtain these values by adopting the following rule: *Cylindrical bending with linearly varying curvature along a side direction is to be exactly represented.* Another way of stating this is: the side curvature χ_{ij} is to be constant along lines normal to side ij. This makes the element insensitive to bad aspect ratios on "strip bending" if each element has a side oriented in the direction of the strip.

To apply this rule consider side 1-2. The natural curvature $\chi_{12} = \partial^2 w / \partial \mu_{12}^2$ along this side is defined at nodes 1 and 2 by the first two rows of Eq. 94. For node 3 take

$$ \chi_{12}|_3 = \left.\frac{\partial^2 w}{\partial \mu_{12}^2}\right|_3 = \lambda_{21}\, \chi_{12}|_1 + \lambda_{12}\, \chi_{12}|_2 , \tag{96} $$

where λ_{12} and λ_{21} are defined in Eq. 87. As we now know the values of $\chi_{12} = \partial^2 w / \partial \mu_{12}^2$ at the three corners, we can use the standard linear interpolation over the entire triangle:

$$ \chi_{12} = \chi_{12}|_1\, \zeta_1 + \chi_{12}|_2\, \zeta_2 + \chi_{12}|_3\, \zeta_3 = \chi_{12}|_1\, (\zeta_1 + \lambda_{21}\zeta_3) + \chi_{12}|_2\, (\zeta_2 + \lambda_{12}\zeta_3). \tag{97} $$

Proceeding analogously for the other two sides, we construct the matrix relation:

$$
\begin{Bmatrix} \chi_{12} \\ \chi_{23} \\ \chi_{31} \end{Bmatrix} = \begin{bmatrix} \zeta_1 + \lambda_{21}\zeta_3 & \zeta_2 + \lambda_{12}\zeta_3 & 0 & 0 & 0 & 0 \\ 0 & 0 & \zeta_2 + \lambda_{32}\zeta_1 & \zeta_3 + \lambda_{23}\zeta_1 & 0 & 0 \\ 0 & 0 & 0 & 0 & \zeta_3 + \lambda_{13}\zeta_2 & \zeta_1 + \lambda_{31}\zeta_2 \end{bmatrix} \mathbf{g},
$$

(98)

or

$$ \chi = \mathbf{A}_\chi \mathbf{g}, \qquad \kappa = \mathbf{T}\mathbf{A}_\chi \mathbf{g}. \tag{99} $$

71

Because T is constant we can do Step 3 of Table 3 directly on the natural curvatures. Now $A_\chi(\zeta_1, \zeta_2, \zeta_3)$ is a *linear* function of the triangular coordinates. Consequently, the mean natural curvatures can be simply obtained by evaluating A_χ at the centroid $\zeta_1 = \zeta_2 = \zeta_3 = 1/3$. Let the corresponding matrix be $\overline{A}_\chi$. Then $\overline{\chi} = \overline{A}_\chi g$, and the natural deviatoric curvatures are given by:

$$\chi_d = (A_\chi - \overline{A}_\chi)\, g, \qquad\qquad (100)$$

which transformed to deviatoric Cartesian curvatures $\kappa_d = \kappa - \overline{\kappa}$ gives finally:

$$\kappa_d = T(A_\chi - \overline{A}_\chi)g = A_d\, g. \qquad\qquad (101)$$

11.6 The Element Stiffness Matrix

The basic stiffness matrix K_b is the same derived in Ref. 8 using the conventional FF and need not be rederived here. The higher order stiffness matrix is given by Eqs. 84, which for a plate bending element specializes to

$$K_h = \alpha Q^T K_{ad} Q = \alpha Q^T \left[\int_A A_d^T DA_d\, dA \right] Q, \qquad\qquad (102)$$

where D is the Cartesian moment-curvature constitutive matrix resulting from the integration of E through the plate thickness:

$$m = \begin{Bmatrix} m_{xx} \\ m_{yy} \\ m_{xy} \end{Bmatrix} = \begin{bmatrix} D_{11} & D_{12} & D_{13} \\ D_{12} & D_{22} & D_{23} \\ D_{13} & D_{23} & D_{33} \end{bmatrix} \begin{Bmatrix} \kappa_{xx} \\ \kappa_{yy} \\ \kappa_{xy} \end{Bmatrix} = D\kappa. \qquad (103)$$

Because A_d varies linearly, if D is constant we could numerically integrate K_{ad} in Eq. 102 exactly with a three point Gauss rule, for example the three midpoint formula. The formation of the element stiffness is dominated by these calculations and it is of interest to derive K_{ad} in closed form. Such a derivation is found in Ref. 17.

11.7 Preliminary Evaluation

As of this writing, only a sketchy evaluation of the first ANDES element is available. We have found that for triangles with good aspect ratio their behavior is similar to that of the scaled FF element of Ref. 8, which is known to be an excellent performer. But the ANDES element shows less distortion sensitivity for high aspect ratio elements, as can be expected from its construction. Additional evaluation details will be reported in Ref. 17.

These preliminary results are encouraging in that we now have two good stand-alone components (FF and ANDES) of K_h. Thus, it is plausible that a weighted mix of these formulations as per Eq. 72 can be used to squeeze the ultimate in performance for this very simple element.

12. CONCLUSIONS

The results presented in this paper may be summarized as follows:

1. The classical variational principles of linear elasticity may be embedded in a parametrized matrix form.

2. The elasticity principles with independently varied displacements are members of a three-parameter family. Those principles without independent displacements are members of a one-parameter family.

3. Finite element assumptions for constructing high performance elements may be conveniently investigated in this family using hybrid forcing potentials.

4. Kinematic constraints established outside the realm of the variational principle may be incorporated through Lagrange multiplier adjunction.

5. The FF and ANS methods for constructing HP finite elements may be presented within this augmented variational setting. A variant of ANS, called ANDES, fits naturally in the decomposition of the stiffness equations into basic and higher order parts. In addition, combined FF/ANDES forms emerge from the general parametrized principle.

6. The satisfaction of the individual element test yields various orthogonality conditions that the kinematic constraints should satisfy *a priori*.

7. The first ANDES element based on this formulation displays an encouraging stand-alone performance regarding distortion sensitivity. The weighted combination of this element with its FF counterpart remains a topic for further investigation.

REFERENCES

1. Bathe, K. J. and Dvorkin, E. N., "A Four-Node Plate Bending Element Based on Mindlin/Reissner Plate Theory and a Mixed Interpolation," International Journal for Numerical Methods in Engineering, Vol. 21, 1985, pp. 367–383.

2. Batoz, J. L., Bathe, K. J. and Ho, L. W., "A Study of Three-Node Triangular Plate Bending Elements." International Journal for Numerical Methods in Engineering, Vol. 15, 1980, pp. 1771–1812.

3. Bergan, P. G. and Hanssen, L., "A New Approach for Deriving 'Good' Finite Elements," in MAFELAP 75 - The Mathematics of Finite Elements and Applications – Volume II, ed. by J. R. Whiteman, Academic Press, London, 1976, pp. 483–497.

4. Bergan, P. G., "Finite Elements Based on Energy Orthogonal Functions", International Journal for Numerical Methods in Engineering, Vol. 15, 1980, pp. 1141–1555.

5. Bergan, P. G. and Nygård, M. K., "Finite Elements with Increased Freedom in Choosing Shape Functions," International Journal for Numerical Methods in Engineering, Vol. 20, 1984, pp. 643–664.

6. Bergan, P. G. and Felippa, C. A., "A Triangular Membrane Element with Rotational Degrees of Freedom," Computer Methods in Applied Mechanics and Engineering, Vol. 50, 1985, pp. 25–69.

7. Bergan, P. G. and Nygård, M. K., "Nonlinear Shell Analysis Using Free Formulation Finite Elements," Proc. Europe-US Symposium on Finite Element Methods for Nonlinear Problems, ed. by P. G. Bergan et al., Springer-Verlag, Berlin, 1985, pp. 317–338.

8. Felippa, C. A. and Bergan, P. G., "A Triangular Plate Bending Element Based on an Energy-Orthogonal Free Formulation," Computer Methods in Applied Mechanics and Engineering, Vol. 61, 1987, pp. 129–160.

9. Felippa, C. A., "Parametrized Multifield Variational Principles in Elasticity: I. Mixed Functionals," Communications in Applied Numerical Methods, Vol. 5, 1989, pp. 79–88.

10. Felippa, C. A., "Parametrized Multifield Variational Principles in Elasticity: II. Hybrid Functionals and the Free Formulation," Communications in Applied Numerical Methods, Vol. 5, 1989, pp. 89–98.

11. Felippa, C. A., "The Extended Free Formulation of Finite Elements in Linear Elasticity," Journal of Applied Mechanics, in press.

12. Felippa, C. A. and Militello, C., "Variational Formulation of High Performance Finite Elements: Parametrized Variational Principles," Computers and Structures (to appear).

13. Fraeijs de Veubeke, B. M., "Displacement and Equilibrium Models in the Finite Element Method," Ch. 9 in Stress Analysis, ed. by O. C. Zienkiewicz and G. Hollister, Wiley, London, 1965, pp. 145–197.

14. Hughes, T. J. R., The Finite Element Method: Linear Static and Dynamic Finite Element Analysis, Prentice-Hall, Englewood Cliffs, N. J., 1987.

15. Militello, C. and Felippa, C. A., "A Variational Justification of the Assumed Natural Strain Formulation of Finite Elements: I. Variational Principles," Computers and Structures (to appear).

16. Militello, C. and Felippa, C. A., "A Variational Justification of the Assumed Natural Strain Formulation of Finite Elements: II. The Four-Node C^0 Plate Element," Computers and Structures (to appear).

17. Militello, C. and Felippa, C. A., "The First ANDES Element: A 9-Dof Plate Bending Triangle," Report CU-CSSC-89-15, Center for Space Structures and Controls, University of Colorado, Boulder, Co., 1989.

18. Oden, J. T. and Reddy, J. N., Variational Methods in Theoretical Mechanics, 2nd ed., Springer-Verlag, Berlin, 1983.

19. Park, K. C. and Stanley, G. M., "A Curved C^0 Shell Element Based on Assumed Natural-Coordinate Strains," Journal of Applied Mechanics, Vol. 53, 1986, pp. 278–290.

20. Pian, T. H. H., "Derivation of Element Stiffness Matrices by Assumed Stress Distributions," AIAA Journal, Vol. 2, 1964, pp. 1333–1336.

21. Pian, T. H. H. and Tong, P., "Basis of Finite Element Methods for Solid Continua," International Journal for Numerical Methods in Engineering, Vol. 1, 1969, pp. 3–29.

22. Pian, T. H. H., "Finite Element Methods by Variational Principles with Relaxed Continuity Requirements," in Variational Methods in Engineering — Volume I, ed. by C. A. Brebbia et al., Southampton University Press, Southampton, U.K., 1973, pp. 653–662.

23. Pian, T. H. H. and Chen, D. P., "Alternative Ways for Formulation of Hybrid Stress Elements," International Journal for Numerical Methods in Engineering, Vol. 18, 1982, pp. 1679–1684.

24. Washizu, K., Variational Methods in Elasticity and Plasticity, 3rd ed., Pergamon Press, Oxford, 1982.

A VARIATIONAL JUSTIFICATION OF THE ASSUMED NATURAL STRAIN FORMULATION OF FINITE ELEMENTS.
I. VARIATIONAL PRINCIPLES

SUMMARY

The *assumed natural strain* (ANS) formulation of finite elements has undergone rapid development over the past five years. The key formulation step is the replacement, in the potential energy principle, of selected displacement-related strains by independently assumed strain fields in *element natural coordinates*. These strains are not generally derivable from displacements. This procedure was conceived as one of several competing methods to solve the *element locking* problem. Its most noteworthy feature is that, unlike many forms of reduced integration, it produces no *rank deficiency*; furthermore, it is easily extendible to geometrically nonlinear problems. Many original formulations were not based on a variational principle. The objective of Part I is to study the ANS formulation from a variational standpoint. This study is based on two hybrid extensions of the Reissner-type functional that uses strains and displacements as independent fields. One of the forms is a genuine variational principle that contains an independent boundary traction field, whereas the other one represents a restricted variational principle. Two procedures for element-level elimination of the strain field are discussed, and one of them shown to be equivalent to the inclusion of incompatible displacement modes. In Part II, the 4-node C^0 plate bending quadrilateral element is used to illustrate applications of this theory.

1. INTRODUCTION

The assumed natural strain (ANS) formulation of finite elements is a relatively new development. A restricted form of the method was introduced in 1969 by Willam [1], who constructed a 4-node plane-stress element by assuming a constant shear strain independently of the direct strains and using a strain-displacement mixed variational principle. A different approach advocated by Ashwell [2] and coworkers regarded "strain elements" as a way to obtain appropriate displacement fields by integration of assumed compatible strain fields. These and other forms of assumed-strain techniques were overshadowed in the 1970s by developments in reduced and selective integration methods, but have recently begun to attract attention [3–7]. The primary motivation behind recent work has been the construction of simple and efficient finite elements for plates and shells that are locking-free, rank sufficient and distortion insensitive, yield accurate answers for coarse meshes, fit naturally into displacement-based programs, and can be easily extended to nonlinear and dynamic problems. Elements that attain these attributes are collectively known as *high performance* elements.

Over the past 20 years investigators have resorted to many ingenious devices to construct high-performance elements. Among the most successful ones we can mention patch-test-verified incompatible displacement models, reduced and selective integration, mixed and hybrid formulations, stress projectors, the free formulation, and assumed natural strains. The underlying theme is that although the final product may look like a standard displacement model so as to fit naturally into existing finite element programs, *the conventional displacement formulation is abandoned.* (By "conventional" we mean the use of conforming displacement assumptions into the total potential energy principle.)

Another common historic trend is that certain deviations from the conventional formulation were initially made without variational justification and in fact labelled as "variational crimes" by applied mathematicians. In some cases such as reduced numerical integration, reconciliation was achieved later after surprisingly good results prompted explanation. In other cases, notably non-conforming elements and the patch test, a comprehensive mathematical theory is still in the making.

The present paper seeks to interpret the assumed natural strain (ANS) formulation from a variational standpoint. The justification is based on hybrid extensions of the Reissner-type functional that uses the strains and displacements as independent fields. We restrict our considerations to linear elasticity although the straightforward extension to geometric nonlinearities is one of the strengths of the ANS formulation. In Part II, the 4-node C^0 plate-bending quadrilateral is used as a specific example to illustrate the application of the present variational interpretation.

2. PROBLEM DESCRIPTION

2.1 Governing Equations

Consider a *linearly elastic body* under *static* loading that occupies the volume V. The body is bounded by the surface S, which is decomposed into $S : S_u \cup S_t$. Displacements are prescribed on S_u whereas surface tractions are prescribed on S_t. The outward unit normal on S is denoted by $\mathbf{n} \equiv n_i$.

The three unknown volume fields are displacements $\mathbf{u} \equiv u_i$, infinitesimal strains $\epsilon \equiv \epsilon_{ij}$, and stresses $\sigma \equiv \sigma_{ij}$. The problem data include: the body force field $\mathbf{f} \equiv f_i$ in V, prescribed displacements $\hat{\mathbf{u}} = \hat{u}_i$ on S_u, and prescribed surface tractions $\hat{\mathbf{t}} \equiv \hat{t}_i$ on S_t.

The relations between the volume fields are the strain-displacement equations

$$\epsilon = \tfrac{1}{2}(\nabla \mathbf{u} + \nabla^T \mathbf{u}) = \mathbf{D}\mathbf{u} \qquad \text{or} \qquad \epsilon_{ij} = \tfrac{1}{2}(u_{i,j} + u_{j,i}) \quad \text{in } V, \tag{1}$$

(where superscript T denotes transposition), the constitutive equations

$$\sigma = \mathbf{E}\,\epsilon \qquad \text{or} \qquad \sigma_{ij} = E_{ijkl}\epsilon_{kl} \quad \text{in } V, \tag{2}$$

and the equilibrium (balance) equations

$$-\operatorname{div}\sigma = \mathbf{D}^*\sigma = \mathbf{f} \qquad \text{or} \qquad \sigma_{ij,j} + f_i = 0 \quad \text{in } V, \tag{3}$$

in which $\mathbf{D}^* = -\operatorname{div}$ (divergence) denotes the adjoint operator of the symmetric gradient $\mathbf{D} = \tfrac{1}{2}(\nabla + \nabla^T)$.

On S the surface stress vector is defined as

$$\sigma_n = \sigma.\mathbf{n}, \qquad \text{or} \quad \sigma_{ni} = \sigma_{ij}n_j. \tag{4}$$

With this definition the traction boundary conditions may be stated as

$$\sigma_n = \hat{\mathbf{t}} \qquad \text{or} \qquad \sigma_{ij}n_j = \hat{t}_i \qquad \text{on } S_t, \tag{5}$$

and the displacement boundary conditions as

$$\mathbf{u} = \hat{\mathbf{u}} \qquad \text{or} \qquad u_i = \hat{u}_i \qquad \text{on } S_u. \tag{6}$$

2.2 Notational Conventions

An *independently varied* field will be identified by a letter without superscript, for example $\mathbf{u}, \epsilon, \sigma$. A *dependent field* is identified by writing the independent field symbol as superscript. For example, if the displacements are independently varied, the derived strain and stress fields are denoted by

$$\epsilon^u = \tfrac{1}{2}(\nabla + \nabla^T)\mathbf{u} = \mathbf{D}\mathbf{u}, \qquad \sigma^u = \mathbf{E}\epsilon^u = \mathbf{E}\mathbf{D}\mathbf{u}. \tag{7}$$

Given a finite element subdivision of V, quantities pertaining to the eth element will be identified by superscript (e), for example $\mathbf{u}^{(e)}$, wherever appropriate. At an interface between two elements e and f, superscripts (ef) and (fe) will identify interface quantities considered as part of e and f, respectively.

77

3. THE HU-WASHIZU AND REISSNER FUNCTIONALS

In the conventional Hu-Washizu functional the displacements $\mathbf{u}$, stresses σ and strains ϵ are independently varied. Arranging the strain and stress components as vectors, and the elastic moduli in $\mathbf{E}$ as a matrix, the functional may be expressed as†

$$L(\mathbf{u}, \epsilon, \sigma) = \int_V \left[\tfrac{1}{2} \epsilon^T \mathbf{E}\, \epsilon + \sigma^T (\epsilon^u - \epsilon) - \mathbf{f}^T \mathbf{u} \right] dV - \int_{S_u} (\sigma_n)^T (\mathbf{u} - \hat{\mathbf{u}})\, dS - \int_{S_t} \hat{\mathbf{t}}^T \mathbf{u}\, dS. \quad (8)$$

From L one obtains the conventional stress-displacement Hellinger-Reissner functional by eliminating ϵ through the inverse of (2), namely $\epsilon = \epsilon^\sigma = \mathbf{E}^{-1}\sigma$. Another Reissner-type, strain-displacement functional is obtained by eliminating σ through the constitutive relation (2), namely $\sigma = \sigma^\epsilon = \mathbf{E}\epsilon$, which yields

$$R(\mathbf{u}, \epsilon) = \int_V \left[-\tfrac{1}{2} \epsilon^T \mathbf{E}\epsilon + \epsilon^T \mathbf{E}\epsilon^u - \mathbf{f}^T \mathbf{u} \right] dV - \int_{S_u} \left(\sigma_n^\epsilon \right)^T (\mathbf{u} - \hat{\mathbf{u}})\, dS - \int_{S_t} \hat{\mathbf{t}}^T \mathbf{u}\, dS. \quad (9)$$

Setting $\epsilon \equiv \epsilon^u$ reduces R to the potential energy functional

$$P(\mathbf{u}) = \int_V \left[\tfrac{1}{2} (\epsilon^u)^T \mathbf{E}\epsilon^u - \mathbf{f}^T \mathbf{u} \right] dV - \int_{S_u} \left(\sigma_n^u \right)^T (\mathbf{u} - \hat{\mathbf{u}})\, dS - \int_{S_t} \hat{\mathbf{t}}^T \mathbf{u}\, dS, \quad (10)$$

generalized with a S_u term over its usual expression.

4. HYBRID FUNCTIONALS

4.1 Independent Boundary Tractions

If the functional (9) is used to construct finite elements, the displacement field $\mathbf{u}$ should be *continuous* in V because of the presence of ϵ^u, whereas the assumed strain field may be discontinuous. To account rigorously for displacement discontinuities it is necessary to add the interelement surface tractions $\mathbf{t}$ as new independent field which plays the role of Lagrange multiplier. Let S_i denote the union of interelement boundaries traversed twice (one for each adjacent element); on S_i neither displacements nor tractions are prescribed. Then R expands to the *hybrid* functional

$$H(\mathbf{u}, \epsilon, \mathbf{t}) = R(\mathbf{u}, \epsilon) - \int_{S_i} \mathbf{t}^T \mathbf{u}\, dS. \quad (11)$$

For later reference we note the specialization $\epsilon \equiv \epsilon^u$ of (11) to the generalized potential energy functional of Jones [9]

$$P(\mathbf{u}, \mathbf{t}) = P(\mathbf{u}) - \int_{S_i} \mathbf{t}^T \tilde{\mathbf{u}}\, dS, \quad (12)$$

---

† There are several equivalent statements of this functional, differing from one another in transformations based on the divergence theorem. For example in Gurtin [8, p. 122] the stress divergence appears. Some authors attribute this specific functional to B. Fraeijs de Veubeke, who indeed published a version of it in 1951, four years before Hu and Washizu.
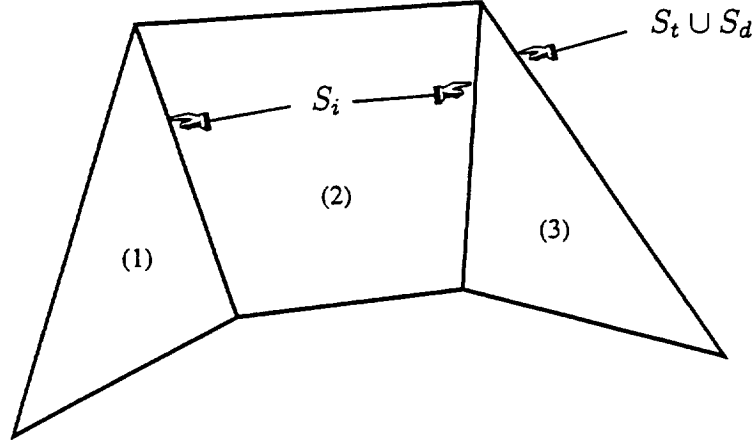
Figure 1. Sample finite element mesh to illustrate
computation of integrals in H

where $P(\mathbf{u})$ is given by (10).

The meaning of the integrals in H may be illustrated on the two-dimensional mesh of Figure 1:

$$\int_V \equiv \sum_e \int_{V^{(e)}} = \int_{V^{(1)}} + \int_{V^{(2)}} + \int_{V^{(3)}}$$

$$\int_{S_u} \equiv \sum_e \int_{S_u^{(e)}} = \int_{S_u^{(1)}} + \int_{S_u^{(1)}} + \int_{S_u^{(3)}}$$

$$\int_{S_t} \equiv \sum_e \int_{S_t^{(e)}} = \int_{S_t^{(1)}} + \int_{S_t^{(2)}} + \int_{S_t^{(3)}}$$

$$\int_{S_i} \equiv \sum_{e,f} \int_{S_i^{(ef)}} = \int_{S^{(1,2)}} + \int_{S^{(2,1)}} + \int_{S^{(2,3)}} + \int_{S^{(3,2)}}$$

(13)

where element identification conventions stated in Section 2.2 have been followed. It is seen that in the integrals over V, S_u and S_t each element appears once, whereas in S_i adjacent elements appear twice.

4.2 First Variation

The first variation of H:

$$\delta H = \delta_u H + \delta_\epsilon H + \delta_t H,$$

(14)

yields the Euler equations and interelement linking conditions, which are underlined in the expressions below. The three components of δH are

$$\delta_u H = \int_V \underline{(\nabla \sigma^\epsilon - \mathbf{f})^T} \, \delta \mathbf{u} \, dV + \int_{S_t} \underline{(\sigma_n^\epsilon - \hat{\mathbf{t}})^T} \, \delta \mathbf{u} \, dS + \int_{S_i} \underline{(\sigma_n^\epsilon - \mathbf{t})^T} \, \delta \mathbf{u} \, dS,$$

(15)

$$\delta_\epsilon H = \int_V \mathbf{E} \underline{(\epsilon^u - \epsilon)^T} \, \delta \epsilon^\epsilon \, dV - \int_{S_u} \underline{(\mathbf{u} - \hat{\mathbf{u}})^T} \delta(\mathbf{E}\epsilon)_n \, dS,$$

(16)

79

$$\delta_t H = \int_{S_i} \underline{\mathbf{u}^T} \delta \mathbf{t} \, dS. \tag{17}$$

Note that there are two contributions to the element interface integrals, one from $\delta_u H$ and another from $\delta_t H$. Putting the parts together and decomposing into element-pair contributions we get

$$\int_{S_i} \left[(\sigma_n^\epsilon - \mathbf{t})^T \delta \mathbf{u} + \mathbf{u}^T \, \delta \mathbf{t} \right] dS = \sum_{e,f} \int_{S^{(ef)}} \left[\sigma_n^{\epsilon\,(e)^T} \delta \mathbf{u}^{(e)} - \sigma_n^{\epsilon\,(f)^T} \delta \mathbf{u}^{(f)} \right.$$
$$\left. - \mathbf{t}^{(ef)^T} \delta \mathbf{u}^{(e)} - \mathbf{t}^{(fe)^T} \delta \mathbf{u}^{(f)} + \mathbf{u}^{(e)^T} \delta \mathbf{t}^{(ef)} + \mathbf{u}^{(f)^T} \delta \mathbf{t}^{(fe)} \right] dS. \tag{18}$$

In the absence of applied internal tractions, interelement equilibrium requires $\mathbf{t}^{(ef)} = -\mathbf{t}^{(fe)}$, which substituted into (16) reduces the right-hand side to

$$\sum_{e,f} \int_{S^{(e,f)}} \left[\sigma_n^{\epsilon\,(e)^T} \delta \mathbf{u}^{(e)} - \sigma_n^{\epsilon\,(f)^T} \delta \mathbf{u}^{(f)} - \mathbf{t}^{(ef)^T} \delta (\mathbf{u}^{(e)} - \mathbf{u}^{(f)}) + (\mathbf{u}^{(e)} - \mathbf{u}^{(f)})^T \delta \mathbf{t}^{(ef)} \right] dS. \tag{19}$$

If we assume a *compatible* displacement field, $\mathbf{u}^{(e)} = \mathbf{u}^{(f)}$, the above equation reduces to

$$\sum_{e,f} \int_{S^{(e,f)}} (\sigma_n^{\epsilon\,(e)} - \sigma_n^{\epsilon\,(f)})^T \delta \mathbf{u}^{(e)} \, dS, \tag{20}$$

which means that the interelement equilibrium condition appears as the Euler equation corresponding to the variation of the interface displacements.

4.3 A Restricted Variational Principle

If the displacement field is incompatible we should in principle retain $\mathbf{t}$ as an independent boundary-traction field satisfying $\mathbf{t}^{(ef)} = -\mathbf{t}^{(fe)}$ over interelement boundaries. One way to achieve this is to assume a continuous stress field σ^* over element boundaries, so that

$$\mathbf{t}^{(ef)} = \sigma^*.\mathbf{n}^{(e)} = \sigma_n^{*(e)}, \qquad \mathbf{t}^{(fe)} = \sigma^*.\mathbf{n}^{(f)} = \sigma^*.(-\mathbf{n}^{(e)}) = -\sigma_n^{*(e)}. \tag{21}$$

The presence of an independent boundary traction field is computationally disadvantageous because additional degrees of freedom must be retained on elements sides. This contradicts one of the tenets of high-performance element construction noted in the Introduction. It would be more convenient if σ^* could be identified with the *strain-derived stress field*, that is, $\sigma^* = \sigma^\epsilon = \mathbf{E}\epsilon$ on S_i, because we would have only two independent fields, $\mathbf{u}$ and ϵ, as in (9). The strain freedoms can be eliminated at the element level as explained in Section 6, and we are left with standard displacement connectors. The corresponding functional is

$$\widetilde{H}(\mathbf{u}, \epsilon) = R - \int_{S_i} (\sigma_n^\epsilon)^T \mathbf{u} \, dS. \tag{22}$$

But in general σ_n^ϵ is not continuous between elements. One can argue, however, that continuity is achieved in the limit of a converged solution. A variational statement such as $\delta \widetilde{H} = 0$ is

called a *restricted variational principle* [10, Ch. 11] because the governing field equations of §2.1 are satisfied only at the exact solution. Away from it, $\delta \tilde{H} = 0$ generally violates interelement-equilibrium field equations although it may provide satisfactory numerical approximations.

Stress-displacement (rather than strain-displacement) functionals of this form have been used by Pian and Chen [11,12], who transform the interface integral into an element volume integral and in doing so introduce a stress divergence term.

4.4 Finite Element Classification

Finite element models derivable from R, $\tilde{H}$ and H may be classified into several types according to the number of independent fields and the continuity conditions on those fields. Following are some general comments on the most interesting combinations, which are summarized in Table 1.

1. *Continuous displacements.* The independent boundary field t is not needed, and we can work with the mixed functional R. If the strain field is discontinuous, strain freedoms may be eliminated at the element level as explained in Section 6. Continuous strains are in principle possible but impractical in general structural applications where material interfaces, plasticity, and sudden thickness or area changes may occur.

2. *Discontinuous displacements.* The displacement field contains conforming and non-conforming portions. Assumed strains are discontinuous and may be eliminated at the element level. Displacement degrees of freedom associated with non-conforming modes may be also eliminated if separable. The governing functionals are $\tilde{H}$ or H. With the latter an independent traction field t is required; degrees of freedom associated with t must be retained at the assembly level.

In practice elements are often constructed as a combination of these types with conventional displacement models. Thus part of the strain field may be considered as completely derivable from displacements and part as independently assumed, as discussed in Section 8. This was in fact the scheme originally used by Willam [1]. The C^0 plate bending quadrilaterals studied in Part II provide another important example.

Table 1. Assumed-Strain Finite Element Models Derivable From R, H and $\widetilde{H}$

Element Type	Governing functional	Independent fields	Interelement continuity on*			Element connected fields	Element condensable fields
			u	ϵ	**t**		
(I)	R	$\mathbf{u}, \epsilon$	c	d		**u**	ϵ
(II)	R	$\mathbf{u}, \epsilon$	c	c		$\mathbf{u}, \epsilon$	
(III)	$\widetilde{H}$	$\mathbf{u}, \epsilon$	·	d	d	$\mathbf{u}^\dagger$	ϵ
(IV)	H	$\mathbf{u}, \epsilon, \mathbf{t}$	d	d	c	$\mathbf{u}^\dagger, \mathbf{t}$	ϵ

* c=continuous, d=discontinuous.   † conforming part only if separable as per (33)

5. DISCRETIZATION

5.1 Assumptions

In this section the finite element discretization of the hybrid functionals H and $\widetilde{H}$ is studied. That is, we focus attention on element types labelled (III) and (IV) in Table 1. In the sequel it will be assumed that the *displacement boundary conditions are identically satisfied* by **u**, whence the strain-displacement hybrid functionals reduce to

$$H(\mathbf{u}, \epsilon, \mathbf{t}) = \int_V \left[\epsilon^T \mathbf{E}(\epsilon^u - \tfrac{1}{2}\epsilon) - \mathbf{f}^T \mathbf{u} \right] dV - \int_{S_t} \hat{\mathbf{t}}^T \mathbf{u}\, dS - \int_{S_i} \mathbf{t}^T \mathbf{u}\, dS. \tag{23}$$

$$\widetilde{H}(\mathbf{u}, \epsilon) = \int_V \left[\epsilon^T \mathbf{E}(\epsilon^u - \tfrac{1}{2}\epsilon) - \mathbf{f}^T \mathbf{u} \right] dV - \int_{S_t} \hat{\mathbf{t}}^T \mathbf{u}\, dS - \int_{S_i} (\sigma_n^\epsilon)^T \mathbf{u}\, dS. \tag{24}$$

The framework used here accomodates both continuous and discontinuous displacements. The FE assumption may be written

$$\mathbf{u} = \mathbf{N}\mathbf{v} \quad \text{in } V, \qquad \epsilon = \mathbf{A}\mathbf{a} \quad \text{in } V, \qquad \mathbf{t} = \mathbf{T}\mathbf{s} \quad \text{on } S_i. \tag{25}$$

Here matrices **N**, **A** and **T** collect displacement shape functions, assumed natural strain functions and interface traction functions, respectively, whereas column vectors **v**, **a** and **s** collect nodal displacements, strain amplitudes, and interface tractions amplitudes, respectively. The derived fields in V are

$$\epsilon^u = \mathbf{D}\mathbf{N}\mathbf{v} = \mathbf{B}\mathbf{v}, \qquad \sigma^u = \mathbf{E}\mathbf{B}\mathbf{v}, \qquad \sigma^\epsilon = \mathbf{E}\epsilon = \mathbf{E}\mathbf{A}\mathbf{a}. \tag{26}$$

5.2 Discrete Equations

On inserting the assumptions (23-24) into (21-22) we obtain the bilinear algebraic forms

$$H(\mathbf{v}, \mathbf{a}, \mathbf{s}) = -\tfrac{1}{2}\mathbf{a}^T\mathbf{C}\mathbf{a} + \mathbf{a}^T\mathbf{P}\mathbf{v} - \mathbf{v}^T\mathbf{L}\mathbf{s} - \mathbf{v}^T\mathbf{p}, \tag{27}$$

$$\tilde{H}(\mathbf{v}, \mathbf{a}) = -\tfrac{1}{2}\mathbf{a}^T\mathbf{C}\mathbf{a} + \mathbf{a}^T(\mathbf{P} - \mathbf{R})\mathbf{v} - \mathbf{v}^T\mathbf{p} = -\tfrac{1}{2}\mathbf{a}^T\mathbf{C}\mathbf{a} + \mathbf{a}^T\tilde{\mathbf{P}}\mathbf{v} - \mathbf{v}^T\mathbf{p}. \tag{28}$$

where

$$\mathbf{C} = \int_V \mathbf{A}^T\mathbf{E}\mathbf{A}\,dV = \mathbf{C}^T, \quad \mathbf{P} = \int_V \mathbf{A}^T\mathbf{E}\mathbf{B}\,dV, \quad \mathbf{L} = \int_{S_i} \mathbf{N}^T\mathbf{T}\,dS,$$

$$\mathbf{R} = \int_{S_i} (\mathbf{E}\mathbf{A})_n^T\mathbf{N}\,dS, \quad \tilde{\mathbf{P}} = \mathbf{P} - \mathbf{R}, \quad \mathbf{p} = \int_V \mathbf{N}^T\mathbf{f}\,dV + \int_{S_t} \mathbf{N}^T\hat{\mathbf{t}}\,dS. \tag{29}$$

Observe that (28) results on substituting $\mathbf{L}\mathbf{s}$ by $\mathbf{R}^T\mathbf{a}$ in (27). Making these forms stationary yields the linear systems

$$\begin{bmatrix} -\mathbf{C} & \mathbf{P} & \mathbf{0} \\ \mathbf{P}^T & \mathbf{0} & -\mathbf{L} \\ \mathbf{0} & -\mathbf{L}^T & \mathbf{0} \end{bmatrix} \begin{Bmatrix} \mathbf{a} \\ \mathbf{v} \\ \mathbf{s} \end{Bmatrix} = \begin{Bmatrix} \mathbf{0} \\ \mathbf{p} \\ \mathbf{0} \end{Bmatrix}, \tag{30}$$

$$\begin{bmatrix} -\mathbf{C} & \tilde{\mathbf{P}} \\ \tilde{\mathbf{P}}^T & \mathbf{0} \end{bmatrix} \begin{Bmatrix} \mathbf{a} \\ \mathbf{v} \end{Bmatrix} = \begin{Bmatrix} \mathbf{0} \\ \mathbf{p} \end{Bmatrix}. \tag{31}$$

for (27) and (28), respectively. In both cases the first matrix equation is the discrete analog of (16), and expresses internal compatibility. The second matrix equation is the analog of (15) and expresses internal and boundary equilibrium, and, in the case of (31), approximate boundary compatibility. The third matrix equation in (30) is the analog of (17) and expresses boundary compatibility.

5.3 Displacement Field Decomposition

With view to further developments the assumed displacement field is decomposed as

$$\mathbf{u} = \mathbf{u}_c + \mathbf{u}_d. \tag{32}$$

where $\mathbf{u}_c$ is continuous (compatible, conforming) in V and $\mathbf{u}_d$ discontinuous (incompatible, non-conforming) on S_i. It will be further assumed that this decomposition can be effected in terms of the shape functions, i.e.,

$$\mathbf{u} = \mathbf{N}_c\mathbf{v}_c + \mathbf{N}_d\mathbf{v}_d, \tag{33}$$

where the $\mathbf{v}_d$ freedoms are defined element-by-element and may in principle be condensed out. This assumption holds for elements in which non-conforming shape functions are "injected" over a compatible set. For the H functional, as shown in Section 4.2 the S_i integral exactly vanishes for the conforming displacements:

$$\int_{S_i} \mathbf{t}^T\mathbf{u}_c = 0. \tag{34}$$

83

On the other hand, for $\tilde{H}$ the corresponding S_i integral also vanishes at the converged solution. Taking this into account, equations (30-31) expand to

$$
\begin{bmatrix}
-\mathbf{C} & \mathbf{P}_c & \mathbf{P}_d & \mathbf{0} \\
\mathbf{P}_c^T & \mathbf{0} & \mathbf{0} & \mathbf{0} \\
\mathbf{P}_d^T & \mathbf{0} & \mathbf{0} & -\mathbf{L}_d \\
\mathbf{0} & \mathbf{0} & -\mathbf{L}_d^T & \mathbf{0}
\end{bmatrix}
\begin{Bmatrix}
\mathbf{a} \\
\mathbf{v}_c \\
\mathbf{v}_d \\
\mathbf{s}
\end{Bmatrix}
=
\begin{Bmatrix}
\mathbf{0} \\
\mathbf{p}_c \\
\mathbf{p}_d \\
\mathbf{0}
\end{Bmatrix},
\tag{35}
$$

$$
\begin{bmatrix}
-\mathbf{C} & \mathbf{P}_c & \tilde{\mathbf{P}}_d \\
\mathbf{P}_c^T & \mathbf{0} & \mathbf{0} \\
\tilde{\mathbf{P}}_d^T & \mathbf{0} & \mathbf{0}
\end{bmatrix}
\begin{Bmatrix}
\mathbf{a} \\
\mathbf{v}_c \\
\mathbf{v}_d
\end{Bmatrix}
=
\begin{Bmatrix}
\mathbf{0} \\
\mathbf{p}_c \\
\mathbf{p}_d
\end{Bmatrix}.
\tag{36}
$$

in which $\tilde{\mathbf{P}}_d = \mathbf{P}_d - \mathbf{R}_d$, and where c- and d-subscripted matrices and vectors are given by integrals similar to (29) in which $\mathbf{N}$ is replaced by $\mathbf{N}_c$ and $\mathbf{N}_d$, respectively.

6. STRAIN ELIMINATION

The strain degrees of freedom may be eliminated *at the element level* by static condensation or by enforcing kinematic constraints. These two techniques are studied below.

6.1 Static Condensation

This is a well known *variationally consistent* procedure which will be illustrated for the system (30). From the first matrix equation get $\mathbf{a}$ at the element level:

$$
\mathbf{a} = \mathbf{C}^{-1}\mathbf{P}\mathbf{v} = \mathbf{Q}_s\mathbf{v}.
\tag{37}
$$

Substitution into the second equation gives

$$
\begin{bmatrix}
\mathbf{K} & -\mathbf{L} \\
-\mathbf{L}^T & \mathbf{0}
\end{bmatrix}
\begin{Bmatrix}
\mathbf{v} \\
\mathbf{t}
\end{Bmatrix}
=
\begin{Bmatrix}
\mathbf{p} \\
\mathbf{0}
\end{Bmatrix},
\tag{38}
$$

where $\mathbf{K} = \mathbf{P}^T\mathbf{C}^{-1}\mathbf{P} = \mathbf{P}^T\mathbf{Q}_s = \mathbf{Q}_s^T\mathbf{C}\mathbf{Q}_s$ is a stiffness matrix. Similarly, (31) condenses to

$$
\tilde{\mathbf{K}}\mathbf{v} = \mathbf{p},
\tag{39}
$$

where $\tilde{\mathbf{K}} = \tilde{\mathbf{P}}^T\mathbf{C}^{-1}\tilde{\mathbf{P}} = \tilde{\mathbf{Q}}_s^T\mathbf{C}\tilde{\mathbf{Q}}_s$ and $\tilde{\mathbf{Q}}_s = \mathbf{C}^{-1}\tilde{\mathbf{P}}$. The separable non-conforming degrees of freedom $\mathbf{v}_d$, if present, may be condensed out following a similar procedure.

6.2 Kinematic Constraints

A second elimination procedure has been used recently in the construction of ANS C^0 plate and shell elements. It will be described by considering the system (35) that displays separable conforming

and non-conforming displacement shape functions. A kinematic constraint that links strain to displacement degrees of freedom is established:

$$\mathbf{a} = \mathbf{Q}_c \mathbf{v}_c + \mathbf{Q}_d \mathbf{v}_d. \tag{40}$$

This relation may be constructed by collocation, least-square fitting or some other means. Often $\mathbf{Q}_d = 0$. For example, in the Bathe-Dvorkin element [2] studied in Part II collocation of natural shear strains is done at the quadrilateral midpoints.

If the following conditions hold:

(a) the dimension of $\mathbf{v}_d$ and $\mathbf{a}$ are the same so that $\mathbf{P}_d$ is square;

(b) matrix $\mathbf{P}_d - \mathbf{CQ}_d$ is nonsingular;

then the relation (40) may be interpreted *as a variationally-consistent constraint on non-conforming displacements*. In effect, the first equation of (35) becomes

$$(\mathbf{P}_c - \mathbf{CQ}_c)\,\mathbf{v}_c + (\mathbf{P}_d - \mathbf{CQ}_d)\mathbf{v}_d = 0, \tag{41}$$

whence

$$\begin{aligned}
\mathbf{v}_d &= -(\mathbf{P}_d - \mathbf{CQ}_d)^{-1}(\mathbf{P}_c - \mathbf{CQ}_c)\mathbf{v}_c = \mathbf{Wv}_c, \\
\mathbf{a} &= (\mathbf{Q}_c + \mathbf{Q}_d\mathbf{W})\mathbf{v}_c = \mathbf{Qv}_c.
\end{aligned} \tag{42}$$

If (as often happens) $\mathbf{Q}_d = 0$, $\mathbf{Q} \equiv \mathbf{Q}_c$. Replacing the constraints (42) into the discrete form $H(\mathbf{a}, \mathbf{v}_c, \mathbf{v}_d, \mathbf{t})$ and setting its first variation to zero yields†

$$\begin{bmatrix} \mathbf{K}^* & \mathbf{L}^* \\ (\mathbf{L}^*)^T & 0 \end{bmatrix} \begin{Bmatrix} \mathbf{v}_c \\ \mathbf{s} \end{Bmatrix} = \begin{Bmatrix} \mathbf{p}^* \\ 0 \end{Bmatrix}, \tag{43}$$

where

$$\mathbf{K}^* = \mathbf{Q}^T \mathbf{CQ}, \qquad \mathbf{L}^* = \mathbf{W}^T \mathbf{L}_d, \qquad \mathbf{p}^* = \mathbf{p}_c + \mathbf{W}^T \mathbf{p}_d. \tag{44}$$

Similarly, for (34) we get the stiffness equations

$$\widetilde{\mathbf{K}}^* \mathbf{v}_c = \widetilde{\mathbf{p}}^*, \tag{45}$$

where $\widetilde{\mathbf{K}}^* = \widetilde{\mathbf{Q}}^T \mathbf{C}\widetilde{\mathbf{Q}}$, in which $\widetilde{\mathbf{Q}}_d$ results on replacing $\mathbf{P}_d$ by $\widetilde{\mathbf{P}}_d$ in (41-42).

Note that condition (a) above may be relaxed if the dimension of $\mathbf{v}_d$ exceeds that of $\mathbf{a}$ by selecting a subset of $\mathbf{v}_d$ that satisfies (b), and statically condensing out the remainder.

---

† One obtains $\mathbf{K}^* = \mathbf{Q}^T(2\mathbf{P}_c + 2\mathbf{P}_d\mathbf{W} - \mathbf{CQ})$ which simplifies to (44) because $\mathbf{P}_d\mathbf{W} = \mathbf{CQ} - \mathbf{P}_c$.

6.3 Relation to the Strain Projection Approach

If the dimension of a exceeds that of v_d (in particular, if the assumed displacement field is conforming) the constraint (40) is in general inconsistent with a strain-displacement variational principle. In such a case a connection with other techniques for improving element performance can sometimes be established. For example, suppose that the assumed strains ϵ are *constant* and equal to $\bar{\epsilon}$ over each element, and that the displacements are continuous. We can choose $\mathbf{a} \equiv \bar{\epsilon}$, and $\mathbf{A} \equiv \mathbf{I}$ so that (40) may be written

$$\bar{\epsilon} = \overline{\mathbf{B}}\mathbf{v}. \tag{46}$$

This is the strain-projection approach, also called averaged-B or the $\overline{\mathbf{B}}$ approach. If $\overline{\mathbf{B}}$ is determined by collocation at the element center, (46) is equivalent to one-point reduced/selective integration on the potential energy functional, see *e.g.* Hughes's textbook [13, Ch. 4].

7. LIMITATION PRINCIPLE

The famous limitation principle of Fraeijs de Veubeke [14] was originally stated for stress-displacement mixed finite elements, but holds for many strain-displacement elements as well. The principle is applicable when the displacement-derived strain field ϵ^u is contained in the assumed strain field ϵ:

$$\epsilon \ni \epsilon^u = \mathbf{D}\mathbf{u} = \mathbf{B}\mathbf{v}. \tag{47}$$

This inclusion can be expressed in matrix form as

$$\epsilon = \mathbf{A}\mathbf{a} = \mathbf{B}\mathbf{a}_v + \mathbf{A}_x\mathbf{a}_x = [\, \mathbf{B} \quad \mathbf{A}_x \,] \begin{Bmatrix} \mathbf{a}_v \\ \mathbf{a}_x \end{Bmatrix}. \tag{48}$$

Here $\mathbf{a}_v$ contains the same number of entries as $\mathbf{v}$ whereas $\mathbf{A}_x$, which may be empty, contains "excess" strain modes. Consider elements of type (III) based on the functional H. Inserting (48) into (30) we get

$$\begin{bmatrix} -\mathbf{C}_{vv} & -\mathbf{C}_{vx} & \mathbf{C}_{vv} & 0 \\ -\mathbf{C}_{vx}^T & -\mathbf{C}_{xx} & \mathbf{C}_{vx}^T & 0 \\ \mathbf{C}_{vv} & \mathbf{C}_{xv} & 0 & -\mathbf{L} \\ 0 & 0 & -\mathbf{L}^T & 0 \end{bmatrix} \begin{Bmatrix} \mathbf{a}_v \\ \mathbf{a}_x \\ \mathbf{v} \\ \mathbf{s} \end{Bmatrix} = \begin{Bmatrix} 0 \\ 0 \\ \mathbf{p} \\ 0 \end{Bmatrix}, \tag{49}$$

where

$$\mathbf{C}_{vv} = \int_V \mathbf{B}^T \mathbf{E}\mathbf{B}\, dV, \qquad \mathbf{C}_{vx} = \int_V \mathbf{B}^T \mathbf{E}\mathbf{A}_x\, dV, \qquad \mathbf{C}_{xx} = \int_V \mathbf{A}_x^T \mathbf{E}\mathbf{A}\, dV. \tag{50}$$

The first two matrix equations give $\mathbf{a}_v = \mathbf{v}$ and $\mathbf{a}_x = 0$. Hence the system is equivalent to (38) in which $\mathbf{K} = \mathbf{C}_{vv}$ is simply the potential energy stiffness matrix. Consequently the stiffness equations may be directly constructed from the generalized potential energy functional (12) and the *independent strain assumption has no effect*. Of course the conclusion only applies if the strain degrees of freedom are solved for in a manner *consistent* with the variational equations (49); for example by static condensation. If the derived field ϵ^u varies over V, assuming a constant strain field $\bar{\epsilon}$ for ϵ is a safe way to guard against the limitation principle.

A similar analysis of type (IV) elements on the $\tilde{H}$-derived system (31) shows that the limitation principle does not generally hold unless $\mathbf{Rv} = 0$. For arbitrary $\mathbf{v}$ this implies that the interface integral vanishes, in which case $\tilde{H}$ reduces to the mixed functional R.

8. PARTIAL STRAIN ASSUMPTIONS

It is common practice to assume only part of the strains as independent fields. For example, in the C^0 plate bending element studied in Part II independent assumptions are only made for the transverse shear strains whereas the bending strains are entirely derived from displacements. The partial strain assumption may be expressed as

$$\epsilon = \left\{ \begin{array}{c} \epsilon_a \\ \epsilon_b \end{array} \right\}, \tag{51}$$

where independent strain assumptions are made only for $\epsilon_a = \mathbf{Aa}$. For ϵ_b one has $\epsilon_b = \epsilon_b^u$. The R and H functionals require obvious modification in the volume term; for example,

$$R(\mathbf{u}, \epsilon_a) = \int_V \left[\langle \, \epsilon_a^T \quad \epsilon_b^T \, \rangle \begin{bmatrix} \mathbf{E}_{aa} & \mathbf{E}_{ab} \\ \mathbf{E}_{ba} & \mathbf{E}_{bb} \end{bmatrix} \left\{ \begin{array}{c} \epsilon_a^u - \frac{1}{2}\epsilon_a \\ \frac{1}{2}\epsilon_b \end{array} \right\} - \mathbf{f}^T \mathbf{u} \right] dV + \text{surface terms} \tag{52}$$

while for $\tilde{H}$ an additional adjustment in the S_i integral is required. The resulting principles take a particularly simple form if the constitutive coupling term $\mathbf{E}_{ab}$ and $\mathbf{E}_{ba}$ vanish, in which case

$$R = R_a(\mathbf{u}, \epsilon_a) + P_b(\mathbf{u}) \tag{53}$$

where R_a is a mixed strain-displacement principle involving ϵ_a, and P_b is a potential-energy principle involving the ϵ_b^u strain energy.

9. CONCLUSIONS

The key results of the present study may be summarized as follows.

1. The mixed strain-displacement functional of Reissner type, R, can be expanded to two hybrid functionals, H and $\tilde{H}$, to account for incompatible displacements. Whereas $\delta R = 0$ and $\delta H = 0$ are genuine variational principles, $\delta \tilde{H} = 0$ represents a restricted variational principle.

2. Several types of assumed-strain finite elements may be constructed using R, H or $\tilde{H}$. The most practical elements for inclusion into existing displacement codes are those in which (1) strain and non-conforming-displacement degrees of freedom can be eliminated at the element level and (2) avoid surface traction connectors.

3. Strain degrees of freedom may be eliminated by static condensation or through kinematic constraints. The latter technique can be presented in a variationally consistent form if the conditions stated in Section 6.2 hold, in which case it can be interpreted as a constraint on non-conforming displacements. Special versions of this technique are closely related to the strain-projection approach.

4. DeVeubeke's limitation principle applies to finite element models derivable from functionals R and H if the strain elimination procedure is variationally consistent.

5. The present variational formulations may be readily modified to account for partial assumptions on the strain field.

ACKNOWLEDGEMENTS

REFERENCES

1. K. J. Willam, Finite element analysis of cellular structures, Ph. D. Dissertation, Dept. of Civil Engineering, University of California, Berkeley CA, 1969

2. D. G. Ashwell, Strain elements, with applications to arches, rings and cylindrical shells, in *Finite Elements for Thin Shells and Curved Members*, ed. by D. G. Ashwell and R. H. Gallagher, Wiley-Interscience, London, 1976

3. K. J. Bathe and E. N. Dvorkin, A four-node plate bending element based on Mindlin/Reissner plate theory and a mixed interpolation, *Int. J. Numer. Meth. Engrg.*, 21, 1985

4. T. J. R. Hughes and T.E. Tezduyar, Finite elements based upon Mindlin plate theory with particular reference to the four-node bilinear isoparametric element, *Journal of Applied Mechanics*, 1981, pp. 587–596

5. H. C. Huang and E. Hinton, A new nine node degenerated shell element with enhanced membrane and shear interpolation, *Int. J. Numer. Meth. Engrg.*, 22, 1986, pp. 73–92

6. K. C. Park and G. M. Stanley, A curved C^0 shell element based on assumed natural-coordinate strains, *Journal of Applied Mechanics*, 108, 1986, pp. 278–290

7. J. C. Simo and T.J.R. Hughes, On the variational foundations of assumed strain methods, *Journal of Applied Mechanics*, 53, 1986, pp. 51–54

8. M. Gurtin, The linear theory of elasticity, in Volume VIa/2 of *Encyclopedia of Physics*, ed. by C. Truesdell, Springer-Verlag, Berlin, 1972

9. R. E. Jones, A generalization of the direct stiffness method of structural analysis, *AIAA J.*, 2, 1964, pp. 821–826

10. B. A. Finlayson, *The Method of Weighted Residuals and Variational Principles*, Academic Press, New York, 1972

11. T. H. H. Pian and D. P. Chen, Alternative ways for formulation of hybrid stress elements, *Int. J. Numer. Meth. Engrg.*, 18, 1982, pp. 1679–1684

12. T. H. H. Pian and D. P. Chen, On the suppression of zero energy deformation modes, *Int. J. Numer. Meth. Engrg.*, 19, 1983, pp. 1741–1752

13. T. J. R. Hughes, *The Finite Element Method: Linear Static and Dynamic Finite Element Analysis*, Prentice-Hall, Englewood Cliffs, N. J., 1987

14. B. M. Fraeijs de Veubeke, Displacement and equilibrium models in the finite element method, Ch. 9 in *Stress Analysis*, ed. by O. C. Zienkiewicz and G. Hollister, Wiley, London, 1965

Appendix A. THE PATCH TEST

In this Section the conditions for this element to pass the *constant-traction patch test* are investigated. As discussed by Taylor *et al.* this is the most stringent form. The test is applied analytically to a single element in the form of the *individual element test* of Bergan and Hanssen closely following the procedures used in the standard and extended free formulation. No numerical studies are required.

Before undertaking the actual test some mathematical preliminaries are worked out below. Throughout the following derivations we work with an individual element; consequently V denotes the element volume, S its boundary, and so on.

A.1 Strain Decomposition

The assumed element strain field, ϵ, is decomposed into a constant value, $\bar{\epsilon}$, and a deviator:

$$\epsilon = \bar{\epsilon} + \epsilon_h = \bar{\epsilon} + A_h a_h, \tag{54}$$

in which

$$\bar{\epsilon} = \frac{1}{\upsilon} \int_V \epsilon \, dV, \qquad \int_V A_h \, dV = 0, \tag{55}$$

where $\upsilon = \int_V dV$ measures the element volume. The second relation in (55) is obtained by integrating (54) over V and noting that a_h is arbitrary.

A.2 Internal Displacement Decomposition

Borrowing from the standard techniques of the free formulation the element displacement field decomposition (33) is continued as follows

$$u = u_c + u_d = u_r + u_u + u_h + u_d = N_{qr}q_r + N_{qu}q_u + N_{qh}q_h + N_{qd}q_d, \tag{56}$$

where u_r, u_u and u_h denote the decomposition of u_c into rigid-body, uniform-strain and higher-order-compatible displacements, respectively. Corresponding displacement modes are collected in arrays N_{qr}, N_{qu}, and N_{qh}, and their amplitudes (generalized coordinates) are q_r, q_u and q_h. (Implicit in this decomposition is the assumption that the rigid-body and uniform state states are part of the *compatible* field.) As for u_d, N_{qh} collects nonconforming modes and q_d the corresponding generalized coordinates. If the separation (31) holds, we may obviously select $N_d \equiv N_{qd}$ and $v_d \equiv q_d$.

To illustrate the structure of (56), consider a 4-node plane stress rectangular element with 2 incompatible pure-bending modes, referred to a cartesian system x, y with origin at the rectangle center and parallel to the sides. Let the x, y displacement components be u_x and u_y. Then an admissible expansion is

$$\begin{Bmatrix} u_x \\ u_y \end{Bmatrix} = \begin{bmatrix} 1 & 0 & -y \\ 0 & 1 & x \end{bmatrix} \begin{Bmatrix} q_1 \\ q_2 \\ q_3 \end{Bmatrix} + \begin{bmatrix} x & 0 & y \\ 0 & y & x \end{bmatrix} \begin{Bmatrix} q_4 \\ q_5 \\ q_6 \end{Bmatrix} + \begin{bmatrix} xy & 0 \\ 0 & xy \end{bmatrix} \begin{Bmatrix} q_7 \\ q_8 \end{Bmatrix} + \begin{bmatrix} -xy & \frac{1}{2}y^2 \\ \frac{1}{2}x^2 & -xy \end{bmatrix} \begin{Bmatrix} q_9 \\ q_{10} \end{Bmatrix}$$

$$\underbrace{\qquad\qquad}_{\text{rigid-body}} \quad \underbrace{\qquad\qquad}_{\text{uniform strain}} \quad \underbrace{\qquad\qquad}_{\text{higher order}} \quad \underbrace{\qquad\qquad}_{\text{nonconforming}} \tag{57}$$

89

Applying the strain operator $\mathbf{D} = \frac{1}{2}(\nabla + \nabla^T)$ to $\mathbf{u}$ and noting that $\mathbf{B}_r = \mathbf{DN}_r$ vanishes because $\mathbf{N}_r$ contains only rigid-body modes we express the displacement derived strains as

$$\boldsymbol{\epsilon}^u = \mathbf{DN}_{qr}\mathbf{q}_r + \mathbf{DN}_{qu}\mathbf{q}_u + \mathbf{DN}_{qh}\mathbf{q}_h + \mathbf{DN}_{qd}\mathbf{q}_d = \mathbf{B}_u\mathbf{q}_u + \mathbf{B}_h\mathbf{q}_h + \mathbf{B}_d\mathbf{q}_d, \tag{58}$$

where matrix $\mathbf{B}_u$ is *constant* over the element.

The generalized coordinates $\mathbf{q}$ and displacement degrees of freedom $\mathbf{v}$ are linked by collocation of (56):

$$\mathbf{v} = \mathbf{G}_r\mathbf{q}_r + \mathbf{G}_u\mathbf{q}_u + \mathbf{G}_h\mathbf{q}_h + \mathbf{G}_d\mathbf{q}_d = \mathbf{Gq} \tag{59}$$

where matrix $\mathbf{G}$ is square and assumed nonsingular. The construction of $\mathbf{G}$ is illustrated for the sample expansion (57):

$$\mathbf{v} = \begin{Bmatrix} u_{x1} \\ u_{y1} \\ u_{x2} \\ u_{y2} \\ u_{x3} \\ u_{y3} \\ u_{x4} \\ u_{y4} \\ v_{d1} \\ v_{d2} \end{Bmatrix} = \begin{bmatrix} 1 & 0 & -y_1 & x_1 & 0 & y_1 & x_1y_1 & 0 & -x_1y_1 & \frac{1}{2}y_1^2 \\ 0 & 1 & x_1 & 0 & y_1 & x_1 & 0 & x_1y_1 & \frac{1}{2}x_1^2 & -x_1y_1 \\ 1 & 0 & -y_2 & x_2 & 0 & y_2 & x_2y_2 & 0 & -x_1y_1 & \frac{1}{2}y_1^2 \\ 0 & 1 & x_2 & 0 & y_2 & x_2 & 0 & x_2y_2 & \frac{1}{2}x_2^2 & -x_2y_2 \\ 1 & 0 & -y_3 & x_3 & 0 & y_3 & x_3y_3 & 0 & -x_1y_1 & \frac{1}{2}y_1^2 \\ 0 & 1 & x_3 & 0 & y_3 & x_3 & 0 & x_3y_3 & \frac{1}{2}x_3^2 & -x_3y_3 \\ 1 & 0 & -y_4 & x_4 & 0 & y_4 & x_4y_4 & 0 & -x_1y_1 & \frac{1}{2}y_1^2 \\ 0 & 1 & x_4 & 0 & y_4 & x_4 & 0 & x_4y_4 & \frac{1}{2}x_4^2 & -x_4y_4 \\ 0 & 0 & 0 & 0 & 0 & 0 & 0 & 0 & 1 & 0 \\ 0 & 0 & 0 & 0 & 0 & 0 & 0 & 0 & 0 & 1 \end{bmatrix} \begin{Bmatrix} q_1 \\ q_2 \\ \vdots \\ q_{10} \end{Bmatrix}, \tag{60}$$

in which we have chosen $v_{d1} = q_9$ and $v_{d2} = q_{10}$, as are are nodeless variables.

Inversion of (59) gives

$$\mathbf{q} = \begin{Bmatrix} \mathbf{q}_r \\ \mathbf{q}_u \\ \mathbf{q}_h \\ \mathbf{q}_d \end{Bmatrix} = \mathbf{G}^{-1}\mathbf{v} = \mathbf{Hv} = \begin{bmatrix} \mathbf{H}_r \\ \mathbf{H}_u \\ \mathbf{H}_h \\ \mathbf{H}_d \end{bmatrix} \mathbf{v}. \tag{61}$$

A.3 Equation Partitioning

Consider an element of type (III) with variational equations (30). For simplicity we assume that the elastic moduli in $\mathbf{E}$ are *constant* over the element and that there are no body forces. The element boundary is

$$S : S_t \cup \S_i$$

where S_i is the interface with other elements, and on S_t the traction $\hat{\mathbf{t}}$ is prescribed. The degree of freedom partition

$$\mathbf{a} = \begin{Bmatrix} \bar{\boldsymbol{\epsilon}} \\ \mathbf{a}_h \end{Bmatrix}, \qquad \mathbf{q} = \begin{Bmatrix} \mathbf{q}_r \\ \mathbf{q}_u \\ \mathbf{q}_h \\ \mathbf{q}_d \end{Bmatrix}, \tag{62}$$

in conjunction with (61) induces the following partition of the element equations

$$
\begin{bmatrix}
-\upsilon E & 0 & 0 & \bar{P}_u & \bar{P}_h & \bar{P}_d & 0 & 0 & 0 & 0 & 0 & 0 \\
0 & -C_{hh} & 0 & P_{hu} & P_{hh} & P_{hd} & 0 & 0 & 0 & 0 & 0 & 0 \\
0 & 0 & 0 & 0 & 0 & 0 & I & 0 & 0 & 0 & 0 & -L_r \\
\bar{P}_u^T & P_{hu}^T & 0 & 0 & 0 & 0 & 0 & I & 0 & 0 & 0 & -L_u \\
\bar{P}_h^T & P_{hh}^T & 0 & 0 & 0 & 0 & 0 & 0 & I & 0 & 0 & -L_h \\
\bar{P}_d^T & P_{hd}^T & 0 & 0 & 0 & 0 & 0 & 0 & 0 & I & 0 & -L_d \\
0 & 0 & I & 0 & 0 & 0 & 0 & 0 & 0 & 0 & -H_r & 0 \\
0 & 0 & 0 & I & 0 & 0 & 0 & 0 & 0 & 0 & -H_u & 0 \\
0 & 0 & 0 & 0 & I & 0 & 0 & 0 & 0 & 0 & -H_h & 0 \\
0 & 0 & 0 & 0 & 0 & I & 0 & 0 & 0 & 0 & -H_d & 0 \\
0 & 0 & 0 & 0 & 0 & 0 & -H_r^T & -H_u^T & -H_h^T & -H_d^T & 0 & 0 \\
0 & 0 & -L_r^T & -L_u^T & -L_h^T & -L_d^T & 0 & 0 & 0 & 0 & 0 & 0
\end{bmatrix}
\begin{Bmatrix}
\bar{\epsilon} \\ a_h \\ q_r \\ q_u \\ q_h \\ q_d \\ \lambda_r \\ \lambda_u \\ \lambda_h \\ \lambda_d \\ v \\ s
\end{Bmatrix}
=
\begin{Bmatrix}
0 \\ 0 \\ p_{qr} \\ p_{qu} \\ p_{qh} \\ p_{qd} \\ 0 \\ 0 \\ 0 \\ 0 \\ 0 \\ 0
\end{Bmatrix}
\tag{63}
$$

where $\lambda_r, \ldots \lambda_d$ are Lagrange multipliers that enforce the constraints (61), and

$$
C_{hh} = \int_V A_h^T E A_h \, dV, \qquad \bar{P}_u = \upsilon E B_u, \qquad \bar{P}_h = \int_V E B_h \, dV \qquad \bar{P}_d = \int_V E B_b \, dV
$$

$$
P_{hu} = \int_V A_h^T E B_h \, dV, \quad P_{hh} = \int_V A_h^T E B_h \, dV, \quad P_{hd} = \int_V A_h^T E B_d \, dV,
$$

$$
L_r = \int_{S_i} N_r^T T \, dS, \qquad L_u = \int_{S_i} N_u^T T \, dS, \qquad L_h = \int_{S_i} N_h^T T \, dS, \qquad L_d = \int_{S_i} N_d^T T \, dS,
\tag{64}
$$

$$
p_r = \int_{S_t} N_r^T \hat{t} \, dS \qquad p_u = \int_{S_t} N_u^T \hat{t} \, dS, \qquad p_h = \int_{S_t} N_h^T \hat{t} \, dS, \qquad p_d = \int_{S_t} N_d^T \hat{t} \, dS,
$$

Note that

$$
P_{hu} = \int_V A_h E B_u \, dV = \left(\int_V A_h \, dV \right) E B_u = 0,
\tag{65}
$$

on account of the second of (55), and

$$
p_r + L_r v = \int_{S_t} N_r^T \hat{t} \, dS = 0
\tag{66}
$$

on account of the theorem of work expended on rigid motions.

A.4 Integral Transformations

Suppose that the element is in a state of *constant* stress $\bar{\sigma} = E\bar{\epsilon}$. Application of the divergence theorem to the work of $\bar{\sigma}$ on the displacement-derived strains ϵ_x^u, where $x = r, u, h, d$, yields

$$
\int_V \bar{\sigma}^T \epsilon_x^u \, dV + \int_V (\text{div} \, \bar{\sigma})^T u_x \, dV = \int_V (\epsilon_x^u)^T \bar{\sigma} \, dV = \int_S u_x^T \bar{\sigma}_n \, dS.
\tag{67}
$$

Using (56) and (58):

$$
q_x^T \int_V B_x^T E \, dV \, \bar{\epsilon} = q_x^T \int_S N_x^T \bar{\sigma}_n \, dS, \quad \text{or} \quad \int_V B_x^T E \, dV \, \bar{\epsilon} = \int_S N_x^T \bar{\sigma}_n \, dV.
\tag{68}
$$

91

Comparing with (64) and noting that $\bar{\sigma}_n = \hat{t}$ on S_t and $\bar{\sigma} = t = Ts$ on S_i:

$$\bar{P}_x^T \bar{\epsilon} + \int_{S_i} N_x^T \bar{\sigma}_n \, dS = \bar{P}_x \bar{\epsilon} - L_x s = p_x \tag{69}$$

A.5 The Rigid Body Motions Test

The first part of the individual element test requires that no forces be produced in a rigid body motion. On the left-hand side vector of (63) prescribe $q_r = any$, $v_r = G_r q_r$, others zero. The only nonzero force on the right is

$$p_{qr} = \int_S N_{qr}^T \hat{t} \, dS = 0 \tag{70}$$

because of (66).

A.6 The Uniform Stress Test

The second part of the test requires that node forces among adjacent element pairs vanish when both elements are in a state of constant stress $\bar{\sigma}$. On the left-hand side vector of (63) prescribe the solution $q_u = \bar{\epsilon}$, $v = G_u \bar{\epsilon}$, $s = \sigma_n$, others zero. By virtue of (69) all forces on the right vanishes except for the S_i terms. These cancel identically with the forces of neighboring element. Hence the individual patch test is passed.

Elements of type (IV) also pass the constant stress patch test, as the interface integrals become identical to those for type (III). The patch test is trivial for types (I) and (II).

A.7 Effect of Strain Elimination

If the strain freedoms are not eliminated in a variational consistent manner the patch test is not generally passed. This happens if the constraint (40) is not verified by the constant stress state condition.

A VARIATIONAL JUSTIFICATION OF THE ASSUMED NATURAL STRAIN FORMULATION OF FINITE ELEMENTS. II. THE C^0 FOUR NODE PLATE ELEMENT

SUMMARY

In Part II we use the four-node C^0 plate bending element to explore some of the possibilities opened by the theory presented in Part I. This element is chosen because the version presented by Bathe and Dvorkin [1], *MITC4*, can be considered the simplest *assumed natural strain* element that allows several possibilities to be studied in a straightforward manner. We focus our attention on the governing functionals R and H presented in Part I, assuming independent strain fields only for the transverse shear strains. Besides *MITC4* we consider three formulations (two mixed and one hybrid) that collectively represent a variational justification for the assumed strain technique. In addition, we examine reduced and selective-integration elements to compare their behavior with that of the present strain-assumed elements.

1. INTRODUCTION

1.1 4-Node C^0 Bending Plate Element Formulation

We start with the formulation of the four-node Reissner-Mindlin plate element whose degrees of freedom (d.o.f) are the transverse displacement w and the two rotations θ_x and θ_y about the x and y axes, respectively, as shown in Figure 1. We expand the displacement field in the usual way:

$$
\begin{aligned}
w &= N_i(r, s)\, w_i \\
\theta_x &= N_i(r, s)\, \theta_{xi} \\
\theta_y &= N_i(r, s)\, \theta_{yi}
\end{aligned}
\qquad (1)
$$

where

$$
N_i(r, s) = \tfrac{1}{4}(1 + r_i r)(1 + s_i s), \qquad i = 1, 2, 3, 4
\qquad (2)
$$

are bilinear shape functions. The strain field derived from the displacement field is

$$
\begin{aligned}
\varepsilon^u_{xx} &= z\, \theta_{y,x} \\
\varepsilon^u_{yy} &= -z\, \theta_{x,y} \\
\varepsilon^u_{xy} &= \tfrac{1}{2}z\, (\theta_{y,y} - \theta_{x,x}) \\
\gamma^u_{yz} &= w_{,y} - \theta_x \\
\gamma^u_{xz} &= w_{,x} + \theta_y
\end{aligned}
\qquad (3)
$$

We take advantage of the decoupling between bending and shear energies by using different assumptions for each one. We assume that the bending strains coincide with the bending strains computed from the displacement field:

$$
\begin{aligned}
\varepsilon_{xx} &= \varepsilon^u_{xx} \\
\varepsilon_{yy} &= \varepsilon^u_{yy} \\
\varepsilon_{xy} &= \varepsilon^u_{xy}
\end{aligned}
\qquad (4)
$$

The shear strains components in the Cartesian basis x, y, z derived from the displacement field are

$$
\begin{aligned}
\gamma^u_{xz} &= w_{,x} + \theta_y \\
\gamma^u_{yz} &= w_{,y} - \theta_x
\end{aligned}
\qquad (5)
$$

After some manipulations we can obtain the covariant components of the shear strains in terms of the natural coordinates r and s as

$$
\gamma^u_{rz} = w_{,r} + \beta_r
\qquad (6)
$$

$$
\gamma^u_{sz} = w_{,s} + \beta_s
\qquad (7)
$$
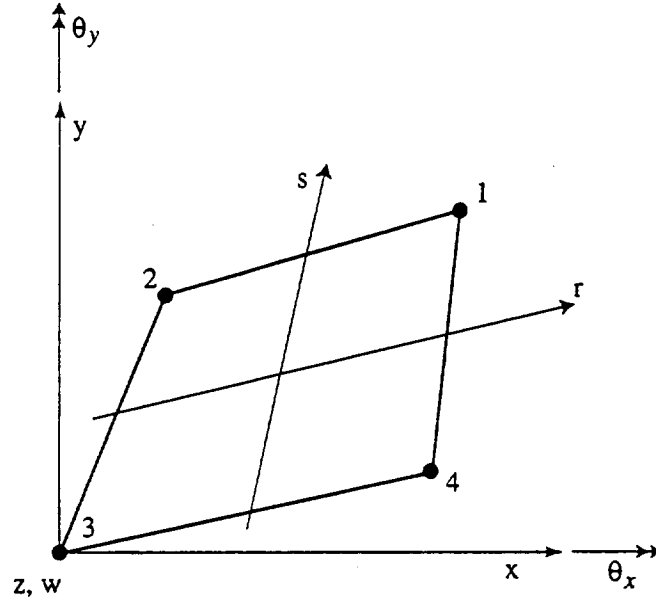
Figure 1. Element coordinate system and notational conventions

where

$$\beta_r = -\theta_x \, y_{,r} + \theta_y \, x_{,r} \qquad (8)$$

$$\beta_s = -\theta_x \, y_{,s} + \theta_y \, x_{,s} \qquad (9)$$

1.2 The Assumed Covariant Shear Strain

We consider two different assumptions for the covariant shear strains,

$$\gamma_{rz} = a_1 \frac{(1-s)}{2} + a_2 \frac{(1+s)}{2} \qquad (10)$$

$$\gamma_{sz} = a_3 \frac{(1-r)}{2} + a_4 \frac{(1+r)}{2} \qquad (11)$$

and

$$\gamma_{rz} = a_1 \qquad (12)$$

$$\gamma_{sz} = a_2 \qquad (13)$$

The bilinear assumption (10)–(11) is of the same form as that proposed in [1]. The constant strain assumption (12)–(13) is studied to see whether there are connections to the selective reduced integration (*SRI*) technique discussed by Hughes [2].

95

2. MIXED ELEMENT BASED ON THE FUNCTIONAL $R(u, \epsilon)$

Up to now we are working with a compatible displacement field and a discontinuous strain field. Hence we use the functional $R(u, \epsilon)$ presented in §3 of Part I. No boundary field is necessary and the constants a_i can be obtained at the element level.

The element displacement field is

$$\mathbf{u} = \left\{ \begin{array}{c} w \\ \theta_x \\ \theta_y \end{array} \right\} , \tag{14}$$

which can be expressed as

$$\mathbf{u} = \mathbf{N}_c \mathbf{v}_c \tag{15}$$

where

$$\mathbf{N}_c = \begin{bmatrix} N_1 & 0 & 0 & \dots & N_4 & 0 & 0 \\ 0 & N_1 & 0 & \dots & 0 & N_4 & 0 \\ 0 & 0 & N_1 & \dots & 0 & 0 & N_4 \end{bmatrix} \tag{16}$$

$$\mathbf{v}_c^T = (w_1 \quad \theta_{x1} \quad \theta_{y1} \quad \dots \quad w_4 \quad \theta_{x4} \quad \theta_{y4}) . \tag{17}$$

The strain fields derived from the displacements are

a) bending strains:

$$\boldsymbol{\epsilon}_b^u = \left\{ \begin{array}{c} \varepsilon_{xx}^u \\ \varepsilon_{yy}^u \\ 2\varepsilon_{xy}^u \end{array} \right\} = \mathbf{B}_b^c \mathbf{v}_c , \tag{18}$$

b) shear strains:

$$\boldsymbol{\gamma}^u = \left\{ \begin{array}{c} \gamma_{rz}^u \\ \gamma_{sz}^u \end{array} \right\} = \mathbf{B}_s^c \mathbf{v}_c . \tag{19}$$

The independently varied strains are:

a) bending strains: the same as obtained from the displacement field, i.e., (18).

b) shear strains:

$$\boldsymbol{\gamma} = \left\{ \begin{array}{c} \gamma_{rz} \\ \gamma_{sz} \end{array} \right\} = \mathbf{B}_s^a \mathbf{a} . \tag{20}$$

Replacing (18), (19) and (20) into the functional R and carrying out the integrations at the element level we obtain

$$R(\mathbf{v}_c, \mathbf{a}) = \tfrac{1}{2}\mathbf{v}_c^T \mathbf{K}_b^{cc} \mathbf{v}_c - \tfrac{1}{2}\mathbf{a}^T \mathbf{C}^{aa} \mathbf{a} + \mathbf{v}_c^T \mathbf{L}^{ca} \mathbf{a} - \mathbf{v}_c^T \mathbf{p}^c , \tag{21}$$

where

$$\mathbf{K}_b^{cc} = \int_{V^e} (\mathbf{B}_b^c)^T \mathbf{E}_b \mathbf{B}_b^c \, dV , \tag{22}$$

$$\mathbf{C}^{aa} = \int_{V^e} (\mathbf{B}_s^a)^T \mathbf{E}_s \mathbf{B}_s^a \, dV , \tag{23}$$
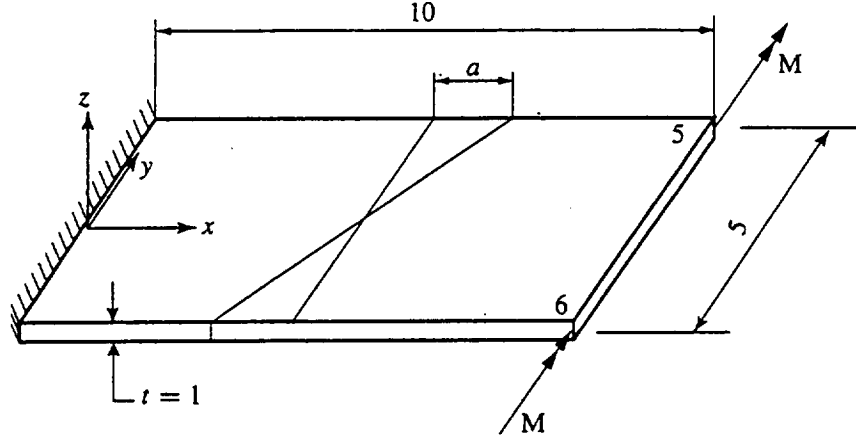
Figure 2. Bending test

$$L^{ca} = \int_{V^e} (B_s^c)^T E_s B_s^a \, dV, \tag{24}$$

$$p^c = \int_{V^e} N_c^T f \, dV + \int_{S_t^e} N_c^T \hat{t} \, dS \tag{25}$$

Here vector f collects applied distributed forces conjugate to w, θ_x and θ_y. On performing the variations we obtain the matrix equation

$$\begin{bmatrix} K_b^{cc} & L^{ca} \\ (L^{ca})^T & -C^{aa} \end{bmatrix} \begin{Bmatrix} v_c \\ a \end{Bmatrix} = \begin{Bmatrix} p^c \\ 0 \end{Bmatrix} \tag{26}$$

From the second equation we obtain the shear strain coefficients

$$a = (C^{aa})^{-1}(L^{ca})^T v_c = Q_c v_c \tag{27}$$

which replaced into (26) gives the statically condensed system

$$(K_b^{cc} + Q_c^T C^{aa} Q_c) v_c = p^c \tag{28}$$

Here K_b^{cc} is the bending stiffness matrix, which is also obtainable from the potential energy principle, and $Q_c^T C^{aa} Q_c$ stands for the new shear stiffness matrix; cf. §8 of Part I.

Equation (27) can also be obtained by minimizing the following shear energy error norm:

$$\Pi_s = \tfrac{1}{2} \int_{V^e} (\gamma - \gamma^\mu)^T E_s (\gamma - \gamma^\mu) \, dV$$

where vector γ collects the independent shear strains (10)-(11) or (12)-(13), and γ^μ collects the shear strains evaluated from the displacement field, equation (19). The minimization of this norm using an independent stress field instead of a strain field was proposed by Barlow [4] as a way of deriving stress-assumed hybrid elements.

97
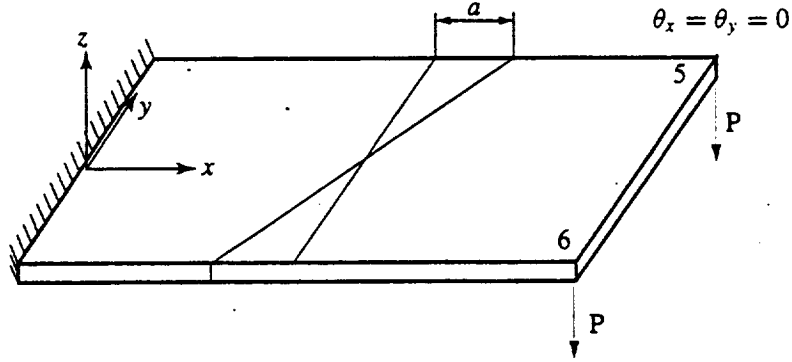
Figure 3. Shear test

We have implemented two elements based in the form (21) and the assumptions (10)–(11) and (12)–(13), which will be identified as *P4* and *P1*, respectively, in the sequel. The results obtained for the simple shear and bending tests illustrated in Figures 2 and 3 are summarized in Tables 1 and 2. We have compared these results to those obtained using *SRI* and *MITC4* elements. The results indicate that *P1* and *P4* behave poorly when elements are distorted and that *P1* is not equivalent to *SRI*.

An interesting result is that if we use one point reduced integration to compute $\mathbf{L}^{ca}$, both elements *P1* and *P4* yield the same results obtained using *SRI*.

We can obtain another expression for $\mathbf{Q}_c$, called $\mathbf{Q}_c^*$ in the sequel, from the field proposed by Bathe and Dvorkin [1] for the covariant shear strains. This expression relates four strain coefficients **a** to the nodal degrees of freedom $\mathbf{v}_c$. The elements of $\mathbf{Q}_c^*$ are given in Appendix A. It is important to realize that $\mathbf{Q}_c$ obtained for element *P4* matches the matrix $\mathbf{Q}_c^*$ only for rectangular shapes. Consequently, the variational principle based on the functional R justifies the assumed natural strain technique for rectangular shapes. However, what can we say about distorted shapes? We need $\mathbf{Q}_c = \mathbf{Q}_c^*$ for all possible configurations to generalize that justification.

3. INCOMPATIBLE DISPLACEMENTS. THE FUNCTIONAL $H(\mathbf{u}, \epsilon, t)$

Following the general procedure outlined in §6.2 of Part I, we add to the transverse displacement w the four midside *incompatible* shape functions of an eight node element. In this way the bending behavior is unchanged. We denote by $\mathbf{v}_d$ the nodal values associated with these "injected" incompatible shape functions. The new displacement field can be written as

$$\mathbf{u} = [\, \mathbf{N}_c \quad \mathbf{N}_d \,] \begin{Bmatrix} \mathbf{v}_c \\ \mathbf{v}_d \end{Bmatrix} \tag{29}$$

98

Table 1. Bending Test (FEM/Theory-Figure 2)

a	Node	MITC4		SRI		P1		P4	
		w	θ_y	w	θ_y	w	θ_y	w	θ_y
0.	5	1.00	1.00	1.00	1.00	1.00	1.00	1.00	1.00
	6	1.00	1.00	1.00	1.00	1.00	1.00	1.00	1.00
1.	5	1.00	1.00	0.90	1.00	0.88	1.00	0.44	0.44
	6	1.00	1.00	1.10	1.00	1.07	1.00	0.47	0.47
2.	5	1.00	1.00	0.80	1.00	0.74	1.00	0.23	0.23
	6	1.00	1.00	1.20	1.00	1.06	1.00	0.28	0.29

Table 2. Shear Test (FEM/Theory-Figure 3)

a	Node	MITC4	SRI	P1	P4
		w	w	w	w
0.	5	1.00	1.00	1.00	1.00
	6	1.00	1.00	1.00	1.00
1.	5	1.00	1.00	1.40	1.00
	6	1.00	1.00	0.85	1.00
2.	5	1.00	1.00	3.06	1.00
	6	1.00	1.00	0.99	1.00

where

$$\mathbf{N}_d = \begin{bmatrix} \frac{1}{2}(1+r)(1-s^2) & \frac{1}{2}(1-r)(1-s^2) & \frac{1}{2}(1+s)(1-r^2) & \frac{1}{2}(1-s)(1-r^2) \\ 0 & 0 & 0 & 0 \\ 0 & 0 & 0 & 0 \end{bmatrix}. \quad (30)$$

The bending strains do not change, and for the displacement derived shear strains we have

$$\gamma^\mu = \left\{ \begin{array}{c} \gamma^u_{rz} \\ \gamma^u_{sz} \end{array} \right\} = \mathbf{B}^c_s \mathbf{v}_c + \mathbf{B}^d_s \mathbf{v}_d. \quad (31)$$

If we introduce the new strains into the variational principle, we must use the functional $H(\mathbf{u}, \epsilon, \mathbf{t})$ because the displacement field will be discontinuous. Then, we have to introduce a traction field $\mathbf{t}$ over the boundary . This traction field is a (line) shear resultant, and for simplicity we shall assume that it is constant on each element side. On performing the variations, the following expression at

99

the element level is obtained:

$$
\begin{bmatrix}
\mathbf{K}_b^{cc} & 0 & \mathbf{P}^{ca} & \mathbf{L}^{ct} \\
0 & 0 & \mathbf{P}^{ca} & \mathbf{L}^{dt} \\
(\mathbf{P}^{ca})^T & (\mathbf{P}^{da})^T & -\mathbf{C}^{aa} & 0 \\
(\mathbf{L}^{ct})^T & (\mathbf{L}^{dt})^T & 0 & 0
\end{bmatrix}
\begin{Bmatrix}
\mathbf{v}_c \\
\mathbf{v}_d \\
\mathbf{a} \\
\mathbf{t}
\end{Bmatrix}
=
\begin{Bmatrix}
\mathbf{p}^c \\
\mathbf{p}^d \\
0 \\
0
\end{Bmatrix}
\tag{32}
$$

where

$$
\mathbf{P}^{ca} = \int_{V^e} (\mathbf{B}_s^c)^T \mathbf{E}_s \mathbf{B}_s^a \, dV
\tag{33}
$$

$$
\mathbf{P}^{da} = \int_{V^e} (\mathbf{B}_s^d)^T \mathbf{E}_s \mathbf{B}_s^a \, dV
\tag{34}
$$

$$
\mathbf{L}^{ct} = \int_{S^{ef}} \mathbf{N}_c^T \, dS
\tag{35}
$$

$$
\mathbf{L}^{dt} = \int_{S^{ef}} \mathbf{N}_d^T \, dS
\tag{36}
$$

$$
\mathbf{p}^d = \int_{S_t^e} \mathbf{N}_d^T \hat{\mathbf{t}} \, dS + \int_{V^e} \mathbf{N}_d^T \mathbf{f} \, dS
\tag{37}
$$

Now imposing the relation

$$
\mathbf{a} = \mathbf{Q}_c^* \mathbf{v}_c
\tag{38}
$$

we obtain

$$
\mathbf{v}_d = (\mathbf{P}^{da})^{-T} \left(\mathbf{C}^{aa} \mathbf{Q}_c^* - (\mathbf{P}^{ca})^T \right) \mathbf{v}_c = \mathbf{W}_c \mathbf{v}_c.
\tag{39}
$$

Replacing both relations in the variational principle and taking variations with respect to $\mathbf{v}_c$ and $\mathbf{t}$, the following expression at the element level is obtained:

$$
\begin{bmatrix}
\mathbf{K}_b^{cc} + \mathbf{Q}_c^{*T} \mathbf{C}^{aa} \mathbf{Q}_c^* & \mathbf{L}^{ct} + \mathbf{W}_c \mathbf{L}^{dt} \\
(\mathbf{L}^{ct} + \mathbf{W}_c \mathbf{L}^{dt})^T & 0
\end{bmatrix}
\begin{Bmatrix}
\mathbf{v}_c \\
\mathbf{t}
\end{Bmatrix}
=
\begin{Bmatrix}
\mathbf{p}^c + \mathbf{W}_c^T \mathbf{p}^d \\
0
\end{Bmatrix}
\tag{40}
$$

The stiffness matrix proposed in [1] for the plate element, namely, $\mathbf{K}_b^{cc} + \mathbf{Q}_c^{*T} \mathbf{C}^{aa} \mathbf{Q}_c^*$, can be clearly identified in the preceding expression. It is not necessary to compute the contribution $\mathbf{L}^{ct}$ because it comes from the compatible displacement and will cancel with the contribution of the neighboring element. On the other hand, the contribution $\mathbf{L}^{dt}$ from the incompatible mode does not vanish. If $\mathbf{t}$ vanishes the stiffness matrix reduces to that of [2] but the nodal force vector will generally be different. Thus it is worth emphasizing that the variational principle gives a *consistent treatment* for the distributed loads.

The matrix $\mathbf{P}^{da}$ is singular for rectangular elements, but we know that in this case $\mathbf{Q}_c$ is equal to $\mathbf{Q}_c^*$ and there is no need to introduce the incompatible displacement field.
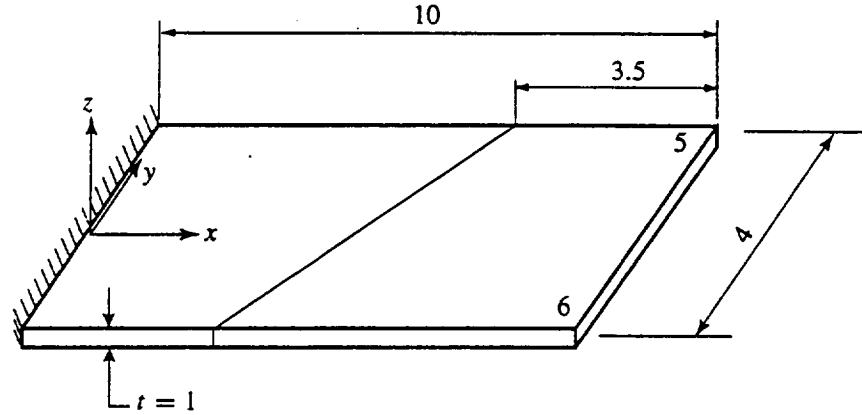
Figure 4. Cantilever beam discretization

Table 3. Normalized displacements (FEM/Theory) for bending, $t = 1.E - 12$

Node	MITC4		ANSH	
	w	θ_y	w	θ_y
5	1.000	1.000	1.000	1.000
6	1.000	1.000	1.000	1.000

Table 4. Normalized displacements (FEM/Theory) for shear, $t = -2.227$

Node	MITC4		ANSH	
	w	θ_y	w	θ_y
5	0.930	1.077	0.892	1.003
6	0.912	0.920	0.891	1.002

4. NUMERICAL EXAMPLE

To check the behavior of the functional $H(\mathbf{u}, \epsilon, \mathbf{t})$ we analyze a cantilever beam with two distorted elements, as depicted in Figure 4. The assumed independent shear strain corresponds to equations (10) and (11). We are interested in two load cases: a uniform bending moment at the tip (Figure 2); and a uniform transverse load at the tip (Figure 3). In both cases Poisson's ratio is set to zero to compare the results to those obtained through the Euler-Bernoulli beam theory.

Uniform Bending Moment. The theoretical solution for this problem requires a linear variation for

101

θ_y and a quadratic variation for the transverse displacement w. The results obtained with *MITC4* coincide with the theoretical results. So do those obtained with the present formulation labeled *ANSH* (for Assumed Natural Shear Hybrid).

The value obtained for t is of roundoff error order (1.10^{-12}). Then, in this case, both formulations are equivalent and the work of the incompatibility can be disregarded.

The external load vector is the same for both formulations because the external bending moment does not interact with the transverse displacement.

Uniform Transverse Load. The theoretical solution requires a quadratic variation in θ_y and a cubic one in w. In this case we must expect the computed solution to be approximate. The results obtained are shown in Table 4. Clearly the *ANSH* formulation is less sensitive to element distortion. The lack of symmetry can be observed at the third decimal position. The convergence and symmetry for the rotation is excellent. The value obtained for t is not negligible. Note that in this case the external load vector is not the same for the *MITC4* and *ANSH* formulations.

5. CONCLUSIONS

We have illustrated the theory presented in Part I [3] through the study of several 4-node C^0 plate elements with independently assumed shear strains. The following conclusions emerge from this study.

1. Elements *P1* and *P4* based on the mixed functional $R(u, \epsilon)$ are variationally impeccable. *P1* behaves well in the bending test and *P4* passes the shear patch test. Their performance deteriorates markedly, however, if the element geometry departs from the rectangular one.

2. The *MITC4* element imposes a shear strain- displacement relation (38) obtained by midpoint strain collocation. This kinematic relation is not *a priori* derivable from a mixed variational principle such as $\delta R = 0$.

3. A variationally consistent modification of *MITC4*, named *ANSH*, is obtained by introducing incompatible displacement modes and an independent surface traction t (in this case a shear line force), and using the hybrid functional $H(u, \epsilon, t)$ for the shear energy portion. The results are similar to those of *MITC4*. Although this element is more expensive to form, it does provide a consistent treatment of applied distributed loads.

4. The *MITC4* element stiffness matrix is recovered by setting the boundary traction field t of *ANSH* to zero. However, the nodal load vector for distributed applied forces will generally be different.

The techniques illustrated here are obviously applicable to the construction of other types of strain-assumed elements based on the various functionals presented in Part I [3]. In particular, the use of the restricted hybrid principle $\tilde{H}$, in which the boundary tractions are not retained as independent degrees of freedom, remain unexplored.

A key result of this investigation is that any change in the strain-displacement interpolation from the variationally consistent interpolation must be associated in some way to the addition of incompatible

displacement modes. This property is closely linked to the limitation principle stated in §7 of Part I.

ACKNOWLEDGEMENTS

REFERENCES

1.   K.J. Bathe and E.N. Dvorkin, A four-node plate bending element based on Mindlin-Reissner plate theory and a mixed interpolation, *Int. J. Numer. Meth. Engrg.*, **21**, pp. 367–383, 1985

2.   T. J. R. Hughes, *The Finite Element Method: Linear Static and Dynamic Finite Element Analysis*, Prentice-Hall, Englewood Cliffs, N. J., 1987

3.   C. Militello and C.A. Felippa, A variational justification of the assumed natural strain formulation of finite elements: I. Variational principles, Submitted to *Computers and Structures*, 1989

4.   J. Barlow, A different view of the assumed stress hybrid method, *Int. J. Numer. Meth. Engrg.*,**22**, pp. 11–16, 1986

Appendix A

Bathe and Dvorkin [1] proposed the same kind of shear strain interpolation we have used in equations (10)–(11). To determine the coefficients a_i they imposed the following midpoint-collocation relations:

$$a_1 = \frac{\gamma_{rz}^{u4} + \gamma_{rz}^{u3}}{2}, \qquad a_2 = \frac{\gamma_{rz}^{u1} + \gamma_{rz}^{u2}}{2},$$

$$a_3 = \frac{\gamma_{sz}^{u2} + \gamma_{sz}^{u3}}{2}, \qquad a_4 = \frac{\gamma_{sz}^{u1} + \gamma_{sz}^{u4}}{2},$$

where superscripts 1, 2, 3, 4 indicate the node where expressions (6) and (7) must be evaluated; see Figure 1. Through the application of the relations of Section 1 and after some algebra we obtain

$$\mathbf{a} = \mathbf{Q}_c^* \, \mathbf{v}_c$$

where

$$\mathbf{a}^T = (\, a_1 \quad a_2 \quad a_3 \quad a_4 \,)$$

$$\mathbf{v}_c^T = (\, w \quad \theta_{x1} \quad \theta_{y1} \quad \ldots \quad \theta_{y4} \,)$$

$$\mathbf{Q}_c^* = \begin{bmatrix} 0.5 & \frac{y_2 - y_1}{4} & \frac{x_1 - x_2}{4} & -0.5 & \frac{y_2 - y_1}{4} & \frac{x_1 - x_2}{4} & 0 & 0 & 0 & 0 & 0 & 0 \\ 0 & 0 & 0 & 0 & 0 & 0 & -0.5 & \frac{y_3 - y_4}{4} & \frac{x_4 - x_3}{4} & 0.5 & \frac{y_3 - y_4}{4} & \frac{x_4 - x_3}{4} \\ 0.5 & \frac{y_4 - y_1}{4} & \frac{x_1 - x_4}{4} & 0 & 0 & 0 & 0 & 0 & 0 & -0.5 & \frac{y_4 - y_1}{4} & \frac{x_1 - x_4}{4} \\ 0 & 0 & 0 & 0.5 & \frac{y_3 - y_2}{4} & \frac{x_2 - x_3}{4} & -0.5 & \frac{y_3 - y_2}{4} & \frac{x_2 - x_3}{4} & 0 & 0 & 0 \end{bmatrix}$$

MIXED VARIATIONAL FORMULATION OF FINITE ELEMENT ANALYSIS OF ACOUSTOELASTIC/SLOSH FLUID-STRUCTURE INTERACTION

ABSTRACT

A general three-field variational principle is obtained for the motion of an acoustic fluid enclosed in a rigid or flexible container by the method of canonical decomposition applied to a modified form of the wave equation in the displacement potential. The general principle is specialized to a mixed two-field principle that contains the fluid displacement potential and pressure as independent fields. This principle contains a free parameter α. Semidiscrete finite-element equations of motion based on this principle are displayed and applied to the transient response and free-vibrations of the coupled fluid-structure problem. It is shown that a particular setting of α yields a rich set of formulations that can be customized to fit physical and computational requirements. The variational principle is then extended to handle slosh motions in a uniform gravity field, and used to derived semidiscrete equations of motion that account for such effects.

105

1. INTRODUCTION

An elastic container (the *structure*) is totally or partly filled with a compressible liquid or gas (the *fluid*). The fluid structure system is initially in static equilibrium in a steady body force field such as gravity or centrifugal forces. We consider *small departures from equilibrium* that result in forced or free vibratory motions. To analyze these motions the fluid is treated as a linear acoustic fluid, *i.e.*, compressible but irrotational and inviscid. The purpose of the present work is

1. To derive variational equations of motion based on a mixed variational principle for the fluid subsystem.

2. To obtain semidiscrete equations of motion following spatial discretization of the coupled problem by the finite element method.

The derivation of the mixed variational principle for the fluid is based on the method of *canonical equations* advocated by Oden and Reddy [13] for mechanical applications. The most general dynamical principle derived in this paper contains three primary variables: pressure-momentum vector, dilatation-velocity vector, and displacement potential.

The general principle is specialized to a two-field functional of Reissner type that has pressure and displacement potential as primary variables, as well as a free coefficient α that parametrizes the application of the divergence theorem. The coupled variational equations are then discretized by the finite element method, and semidiscrete equations for a rigid container established. Linkage with the structure is then made to establish coupled semidiscrete equations of motion for a flexible container. By appropriate selection of the coefficient α a continuum of finite element formulations results. One particular setting yields a rich set of symmetric and unsymmetric formulations for the transient and free-vibrations elastoacoustic problems. From this set selections can be made to satisfy various physical and computational criteria. The implications of these selections as regards efficiency and numerical stability are discussed.

The variational formulation is then extented to cover slosh motions in a uniform gravity field. It is shown that the surface slosh equations may be incorporated as Galerkin terms in several forms, and that one of these forms merges naturally with the mixed variational principle to form an augmented functional. Semidiscretization of this functional produces finite element equations of motions that may be used for a rigid or flexible container.

2. GOVERNING EQUATIONS

The three-dimensional volume domain occupied by the fluid is denoted by V. This volume is assumed to be simply connected. The fluid boundary S consists generally of two portions

$$S : S_d \cup S_p. \tag{1}$$

S_d is the interface with the container at which the normal displacement d_n is prescribed (or found as part of the coupled fluid-structure problem) whereas S_p is the "free surface" at which the pressure

Table 1 Notation for Fluid States

Quantities	Domain	Original	Reference	Current	Transient
Displacements	V	0	$\mathbf{d}^0$	$\mathbf{d}'$	$\mathbf{d} = \mathbf{d}' - \mathbf{d}^0$
Velocities	V	0	$\dot{\mathbf{d}}^0$	$\dot{\mathbf{d}}'$	$\dot{\mathbf{d}} = \dot{\mathbf{d}}' - \dot{\mathbf{d}}^0$
Boundary displacements*	S	0	d_n^0	d_n^t	$d_n = d_n^t - d_n^0$
Displacement potential	V	0	ψ^0	ψ^t	$\psi = \psi^t - \psi^0$
Pressures (+ if compressive)	V	0	p^0	p'	$p = p' - p^0$
Body forces	V	0	$\mathbf{b} = \nabla\beta$	$\mathbf{b} = \nabla\beta$	
Density	V	ρ	ρ	ρ	

* Positive along outward normal

p is prescribed (or found as part of the "fluid slosh" problem). If the fluid is fully enclosed by the container, as is necessarily the case for a gas, then S_p is missing and $S \equiv S_d$. The domain is referred to a Cartesian coordinate system (x_1, x_2, x_3) grouped in vector $\mathbf{x}$.

The fluid is under a body force field $\mathbf{b}$ which is assumed to be the gradient of a *time independent* potential $\beta(\mathbf{x})$, *i.e.* $\mathbf{b} = \nabla\beta$. All displacements are taken to be infinitesimal and thus the fluid density ρ may be taken as invariant.

We consider three states or configurations: *original*, from which displacements, pressures and forces are measured, *current*, where the fluid is in dynamic equilibrium at time t, and *reference*, which is obtained in the static equilibrium limit of slow motions. *Transient* motions are the difference between current and reference states. It should be noted that in many situations the original configuration is not physically attainable. Table 1 summarizes the notation used in relation to these states.

2.1 FIELD EQUATIONS

The governing equations of the acoustic fluid are the momentum, state and continuity equations. They are stated below for the current configuration, and specialized to the reference configuration later. The momentum (balance) equation expresses Newton's second law for a fluid particle:

$$\rho\ddot{\mathbf{d}}' = -\nabla p' + \mathbf{b} = -\nabla p' + \nabla\beta. \tag{2}$$

The continuity equation may be combined with the linearized equation of state to produce the *constitutive equation* that expresses the small compressibility of a liquid:

$$p' = -K\nabla\mathbf{d}' = -\rho c^2 \nabla\mathbf{d}', \tag{3}$$

where K is the bulk modulus and $c = \sqrt{K/\rho}$ the fluid sound speed. If the fluid is incompressible, $K, c \to \infty$. This relation is also applicable to nonlinear elastic fluids such as gases undergoing

small excursions from the reference state, if the constitutive equation is linearized there so that $K = \rho_0 (dp/d\rho)_0$.

The boundary conditions are

$$d_n^t = \bar{d}_n^t \quad \text{on} \quad S_d, \qquad p^t = \bar{p}^t \quad \text{on} \quad S_p, \tag{4}$$

where $\bar{d}_n^t$ is either prescribed or comes from the solution of an auxiliary problem as in fluid-structure interaction, and $\bar{p}$ may be either prescribed or a function of d_n and $\mathbf{b}$, as in the surface-wave ("slosh") problem.

2.2 INTEGRAL ABBREVIATIONS

In the sequel the following abbreviations for the volume and surface integrals are used:

$$(f)_V \stackrel{\text{def}}{=} \int_V f \, dV, \qquad [g]_S \stackrel{\text{def}}{=} \int_S g \, dS, \qquad [g]_{S_d} \stackrel{\text{def}}{=} \int_{S_d} g \, dS, \quad \text{etc.} \tag{5}$$

That is, domain-subscripted parentheses (square brackets) are used to abbreviate volume (surface) integrals. Abbreviations for function innerproducts are illustrated by

$$(f, g)_V \stackrel{\text{def}}{=} \int_V fg \, dV, \qquad (f, g)_{V \times t} \stackrel{\text{def}}{=} \int_{t_0}^{t_1} \int_V fg \, dV \, dt, \qquad [f, g]_{S_d \times t} \stackrel{\text{def}}{=} \int_{t_0}^{t_1} \int_{S_d} fg \, dS \, dt, \quad \text{etc.} \tag{6}$$

3. THE DISPLACEMENT POTENTIAL

3.1 THE REFERENCE STATE

Taking the curl of both sides of (2) yields

$$\mathbf{curl}\, \ddot{\mathbf{d}}^t = 0. \tag{7}$$

The general integral of this equation for a simply connected domain is

$$\mathbf{d}^t = \nabla \psi^t + \mathbf{a} + \mathbf{b}t, \tag{8}$$

where $\psi^t = \psi^t(\mathbf{x}, t)$ is the displacement potential, $\mathbf{a} = \mathbf{a}(\mathbf{x})$ and $\mathbf{b} = \mathbf{b}(\mathbf{x})$ are time-independent vector functions, and t denotes the time. If accelerationless motions (for example, rigid body motions) are precluded by the boundary conditions, $\mathbf{a}$ and $\mathbf{b}$ vanish. Replacing $\ddot{\mathbf{d}}^t = \nabla \ddot{\psi}^t$ into the momentum equation (2) we get

$$\nabla p^t = -\rho \nabla \ddot{\psi}^t + \nabla \beta, \tag{9}$$

which spatially integrated gives

$$p^t = -\rho \ddot{\psi}^t + \beta + C(t), \tag{10}$$

where the scalar $C(t)$ is not spatially dependent. Next integrate the constitutive equation (3) over V and apply the divergence theorem to $\nabla \mathbf{d}$:

$$(p')_V + (\rho c^2 \nabla \mathbf{d}')_V = (p')_V + [\rho c^2 d_n']_S = 0. \tag{11}$$

Inserting p' from (10) into the above equation furnishes a condition on $C(t)$, which gives

$$C(t) = -\frac{\rho c^2}{\upsilon}[d_n']_S + \frac{\rho}{\upsilon}(\ddot{\psi}')_V - \frac{1}{\upsilon}(\beta)_V = -\frac{\rho c^2}{\upsilon}[d_n']_S + \rho\overline{\ddot{\psi}'} - \overline{\beta}, \tag{12}$$

where $\upsilon = (1)_V$ is the fluid volume and $\overline{f} = (f)_V/\upsilon$ denotes the volume average of a function f defined over V. Substituting $C(t)$ into (10) we get

$$p' = -\rho(\ddot{\psi}' - \overline{\ddot{\psi}'}) + (\beta - \overline{\beta}) - \frac{\rho c^2}{\upsilon}[d_n']_S. \tag{13}$$

In the static limit of very slow motions, the inertia terms may be neglected and we recover the reference solution

$$p^0 = (\beta - \overline{\beta}) - \frac{\rho c^2}{\upsilon}[d_n^0]_S. \tag{14}$$

For an incompressible fluid $[d_n]_S = 0$ but $c \to \infty$; thus it would be incorrect to conclude that $p^0 = \beta - \overline{\beta}$. A counterexample to this effect is provided in [14].

3.2 TRANSIENT MOTIONS

Subtracting the constitutive relations at the current and reference states we get

$$p = -\rho c^2 \nabla^2 \psi = \rho c^2 s, \tag{15}$$

where $s = -\nabla^2 \psi$ is called, following Lamb [10], the condensation. Subtracting (14) from (13) yields

$$p = -\rho(\ddot{\psi} - \overline{\ddot{\psi}}) - \frac{\rho c^2}{\upsilon}[d_n]_S. \tag{16}$$

On equating (15) and (16) we get modified forms of the wave equation that account for mean boundary surface motions:

$$s = \nabla^2 \psi = \frac{\ddot{\psi} - \overline{\ddot{\psi}}}{c^2} + \frac{1}{\upsilon}[d_n]_S, \quad \text{or} \quad c^2(\nabla^2 \psi - \overline{\nabla^2 \psi}) = \ddot{\psi} - \overline{\ddot{\psi}}. \tag{17}$$

The second form follows from $-\upsilon\overline{s} = [d_n]_S$, which is a consequence of the divergence theorem. For an incompressible fluid, $c \to \infty$ and $[d_n]_S = 0$, and from the first of (17) we recover the Laplace equation $\nabla^2 \psi = 0$.

3.3 ADJUSTING THE DISPLACEMENT POTENTIAL

If the transient displacement potential is modified by a function of time:

$$\psi = \hat{\psi} + P(t), \tag{18}$$

where $\hat{\psi}$ is the potential of (8)-(17), we may chose $P(t)$ so that $c^2\overline{\overline{\psi}} = \overline{\nabla^2\psi} = -\overline{s}$ for any t. Then we obtain the classical wave equation

$$c^2\nabla^2\psi = \ddot{\psi}, \qquad \text{or} \qquad \left(\frac{\partial^2}{\partial t^2} - c^2\nabla^2\right)\psi = 0. \tag{19}$$

In the sequel it is assumed that this adjustment has been made. If so, $C(t)$ vanishes and (16) reduces to

$$p = -\rho\ddot{\psi}. \tag{20}$$

4. MIXED VARIATIONAL PRINCIPLES

4.1 CANONICAL DECOMPOSITION

In this section we derive multifield variational principles for the fluid domain following the canonical decomposition method advocated by Oden and Reddy [13]. This method is applicable to self-adjoint boundary value problems (BVP) of the form

$$Au = f \qquad \text{in } D \tag{21}$$

where u is the unknown function, f the data, A a symmetric linear operator, and D the domain of existence of the solution. For time-dependent problems D is the tensor product of the time domain (typically 0 to t) and the volume V. To apply this method, the operator A is factored as

$$Au = W^*EWu = f, \tag{22}$$

where W and E are linear operators in V and W^* is the adjoint of W. This is called a *canonical decomposition*. This decomposition may be represented as the operator composition sequence

$$Wu = e, \qquad Ee = \sigma, \qquad W^*\sigma = f, \tag{23}$$

where e and σ denote intermediate field variables in D. The three equations (23) are called the kinematic, constitutive and balance equations, respectively, in mechanical applications. The canonical representation of boundary conditions on the surface $S = S_u \cup S_\sigma$ is

$$B_S u_S = g \quad \text{on} \quad S_u, \qquad B_S^* \sigma_S = h \quad \text{on} \quad S_\sigma. \tag{24}$$

where B_S and B_S^* are surface operators, g and h denote boundary data, and $u_S = \gamma_S u$ and $\sigma_S = \Gamma_S \sigma$ are extensions of u and σ to the boundary S. The extension operators γ_S and δ_S often involve normal derivatives.

4.2 THE WAVE EQUATION

The classical wave equation (19) is *not* a good basis for the canonical decomposition (22). Its principal drawback is that the pressure field does not appear naturally as an intermediate variable in (23). A better form for our purposes is obtained by taking the Laplacian of both sides of (19), and multiplying through by the density ρ:

$$\rho \nabla^2 (\ddot{\psi} - c^2 \nabla^2 \psi) = 0, \qquad \text{whence} \quad A = \rho \nabla^2 \left(\frac{\partial^2}{\partial t^2} - c^2 \nabla^2 \right), \quad f = 0. \tag{25}$$

A suitable canonical decomposition is $A = \mathbf{W}^* \mathbf{E} \mathbf{W}$, where

$$\mathbf{W} = \begin{bmatrix} i \nabla \frac{\partial}{\partial t} \\ -\nabla^2 \end{bmatrix}, \qquad \mathbf{E} = \rho \begin{bmatrix} \mathbf{I} & 0 \\ 0 & c^2 \end{bmatrix}, \qquad \mathbf{W}^* = [\, -i \nabla \frac{\partial}{\partial t} \quad \nabla^2 \,] = -\mathbf{W}^T, \tag{26}$$

in which $i = \sqrt{-1}$. Boldface symbols are used for $\mathbf{W}$ and $\mathbf{E}$ because these are 4×1 and 4×4 matrices, respectively. The operator product sequence (23) becomes

$$\mathbf{e} = \mathbf{W}\psi = \begin{bmatrix} i\nabla\dot{\psi} \\ -\nabla^2\psi \end{bmatrix} = \begin{bmatrix} i\mathbf{v} \\ s \end{bmatrix}, \quad \sigma = \mathbf{E}\mathbf{e} = \begin{bmatrix} i\rho\nabla\dot{\psi} \\ -\rho c^2\nabla^2\psi \end{bmatrix} = \begin{bmatrix} i\mathbf{m} \\ p \end{bmatrix}, \quad \mathbf{W}^*\sigma = \rho\nabla^2\ddot{\psi} - \rho c^2\nabla^4\psi = 0. \tag{27}$$

The intermediate fields $\mathbf{e}$ and σ are 4×1 column vectors. These vectors are partitioned into their temporal and spatial derivative subvectors for convenience in subsequent manipulations. Note that the transient pressure p appears naturally as the spatial component of σ. The temporal components of $\mathbf{e}$ and σ are the complex velocity $i\mathbf{v}$ and complex specific momentum $i\mathbf{m}$, respectively.

The boundary portions S_u and S_σ of (24) are relabeled S_d and S_p, respectively, to match the notation (1). Boundary and initial conditions may be stated as

$$\mathbf{B}\psi(\mathbf{x}, t) = \mathbf{g}(\mathbf{x}, t) \text{ on } S_d, \qquad \mathbf{B}^*\sigma(\mathbf{x}, t) = h(\mathbf{x}, t) \text{ on } S_p,$$
$$\mathbf{d}(\mathbf{x}, t_0) = \mathbf{d}_0(\mathbf{x}) \quad \text{or} \quad \mathbf{m}(\mathbf{x}, t_0) = \mathbf{m}_0(\mathbf{x}), \qquad \mathbf{d}(\mathbf{x}, t_1) = \mathbf{d}_1(\mathbf{x}) \quad \text{or} \quad \mathbf{m}(\mathbf{x}, t_1) = \mathbf{m}_1(\mathbf{x}). \tag{28}$$

Here $\mathbf{B}$ and $\mathbf{B}^*$ are time-independent 4×1 and 1×4 vectors, respectively, related to the canonical $\mathbf{B}_S$ and $\mathbf{B}_S^*$ operators of (24) by $\mathbf{B} = \mathbf{B}_S \gamma_S$ and $\mathbf{B}^* = \mathbf{B}_S^* \Gamma_S$, where γ_S (a scalar) and Γ_S (a 4×4 matrix) are boundary extension operators for ψ and σ, respectively. Comparison with (4) and the use of Green's function reveals that

$$\mathbf{B}_S^T = -\mathbf{B}_S^* = [\,0 \quad 0 \quad 0 \quad 1\,], \quad \mathbf{g}^T = [\,0 \quad 0 \quad 0 \quad \tilde{d}_n\,], \quad \gamma_S = \frac{\partial}{\partial n}, \quad \Gamma_S = \mathbf{I}, \quad h = -\tilde{p}. \tag{29}$$

4.3 THREE FIELD PRINCIPLE

The most general variational principle for the canonical decomposition (26) allows the three fields: ψ, $\mathbf{e}$, and σ, to be varied independently. The principle may be stated as $\delta L(\psi, \mathbf{e}, \sigma) = 0$, where the functional L is [13]

$$L(u, \mathbf{e}, \sigma) = L_V + L_S = \tfrac{1}{2}(\mathbf{Ee}, \mathbf{e})_{V \times t} + (\sigma, \mathbf{W}\psi - \mathbf{v})_{V \times t} - (f, \psi)_{V \times t} + (\sigma_S, \mathbf{B}\psi - \mathbf{g})_{S_d \times t} - (h, \psi_S)_{S_p \times t},$$
(30)

where L_V and L_S collect volume and surface terms, respectively. On inserting (27-29) into (30) we get

$$L_V = \tfrac{1}{2}(\mathbf{Ee}, \mathbf{e})_{V \times t} + (\sigma, \mathbf{W}\psi - \mathbf{e})_{V \times t} = \int_{t_0}^{t_1} \int_V \left[\tfrac{1}{2}\rho(-\mathbf{v}^T\mathbf{v} + c^2 s^2) - \mathbf{m}^T(\nabla\dot\psi - \mathbf{v}) - p(\nabla^2\psi + s) \right] dV\,dt,$$

$$L_S = (\sigma_S, \mathbf{B}\psi - \mathbf{g})_{S_d \times t} - (h, \psi_S)_{S_p \times t} = \int_{t_0}^{t_1} \left[\int_{S_d} p\left(\frac{\partial\psi}{\partial n} - \tilde d_n\right) dS + \int_{S_p} \bar p \frac{\partial\psi}{\partial n} dS \right] dt.$$
(31)

The term $(f, \psi)_{V \times t}$ vanishes and does not contribute to L_V.

4.4 TWO FIELD PRINCIPLES

A two field principle of Reissner type can be derived from the functional L by enforcing the inverse constitutive equations $\mathbf{e} = \mathbf{E}^{-1}\sigma$ *a priori*. The resulting principle, which allows ψ and σ to be varied simultaneously, is $\delta R(\psi, \sigma) = 0$, where

$$R(\psi, \sigma) = R_V + R_S = -\tfrac{1}{2}(\mathbf{E}^{-1}\sigma, \sigma)_{V \times t} + (\sigma, \mathbf{W}\psi)_{V \times t} - (f, \psi)_{V \times t} + (\sigma_S, \mathbf{B}\psi - \mathbf{g})_{S_d \times t} - (h, \psi_S)_{S_p \times t}.$$
(32)

where $R_S = L_S$ and

$$R_V(\psi, \sigma) = -\tfrac{1}{2}(\mathbf{E}^{-1}\sigma, \sigma)_{V \times t} + (\sigma, \mathbf{W}\psi)_{V \times t} = \int_{t_0}^{t_1} \int_V \left(\frac{1}{2\rho}\mathbf{m}^T\mathbf{m} - \frac{p^2}{2\rho c^2} - \mathbf{m}^T\nabla\dot\psi - p\nabla^2\psi\right) dV\,dt.$$
(33)

The specific momentum disappears as an independent field if we enforce $\mathbf{m} = \rho\nabla\dot\psi$ *a priori*, whereupon the functional R becomes a function of ψ and p only and the volume term contracts to

$$R_V(\psi, p) = \int_{t_0}^{t_1} \int_V \left(-\tfrac{1}{2}\rho(\nabla\dot\psi)^T\nabla\dot\psi - \tfrac{1}{2}\frac{p^2}{\rho c^2} - p\nabla^2\psi\right) dV\,dt.$$
(34)

To check $R = R_V(\psi, p) + R_S$ we form its first variation*

$$\delta R = -\left(\rho\nabla^2\ddot{\psi} + \nabla^2 p, \delta\psi\right)_{V\times t} - \left(\frac{1}{\rho c^2}p + \nabla^2\psi, \delta p\right)_{V\times t} + \left[\rho\frac{\partial\ddot{\psi}}{\partial n} + \frac{\partial p}{\partial n}, \delta\psi\right]_{S\times t}$$
$$- \left[p - \bar{p}, \delta\frac{\partial\psi}{\partial n}\right]_{S_p\times t} + \left[\frac{\partial\psi}{\partial n} - \bar{d}_n, \delta p\right]_{S_d\times t} - \left(\rho\nabla\dot{\psi}, \delta\nabla\psi\right)_V\Big|_{t_0}^{t_1}. \tag{35}$$

Setting $\delta R = 0$ provides the field equations, boundary and initial conditions.

4.5 PARAMETRIZATION

A one parameter family of variational principles can be obtained by transforming all or part of the last term in (34), viz. $p\nabla^2\psi$, by the divergence theorem (Green's first formula for the Laplace operator)

$$\int_V p\nabla^2\psi\, dV + \int_V (\nabla\psi)^T\nabla p\, dV = \int_S p\frac{\partial\psi}{\partial n}\, dS = \int_{S_d} p\frac{\partial\psi}{\partial n}\, dS + \int_{S_p} p\frac{\partial\psi}{\partial n}\, dS. \tag{36}$$

Let $0 \le \alpha \le 1$ be the portion of that term to be transformed. Insert $p\nabla^2\psi = \alpha p\nabla^2\psi + (1-\alpha)p\nabla^2\psi$ in (35) and apply (36) to $\alpha p\nabla^2\psi$ to get

$$R_{\alpha V} = \int_{t_0}^{t_1}\left[\int_V \left(\tfrac{1}{2}\rho(\nabla\dot{\psi})^T\nabla\dot{\psi} - \tfrac{1}{2}\frac{p^2}{\rho c^2} + \alpha(\nabla\psi)^T\nabla p - (1-\alpha)p\nabla^2\psi\right)dV - \alpha\int_{S_d} p\frac{\partial\psi}{\partial n}\, dS - \alpha\int_{S_p} p\frac{\partial\psi}{\partial n}\, dS\right]dt. \tag{37}$$

Finally, replace the Laplacian $\nabla^2\psi$ left over in (37) by $c^{-2}\ddot{\psi}$ to arrive at the parametrized two-field functional†

$$R_\alpha(\psi, p) = R_{\alpha V} + R_S = \int_{t_0}^{t_1}\left[\int_V\left(-\tfrac{1}{2}\rho(\nabla\dot{\psi})^T\nabla\dot{\psi} - \tfrac{1}{2}\frac{p^2}{\rho c^2} + \alpha(\nabla\psi)^T\nabla p - (1-\alpha)\frac{p\ddot{\psi}}{c^2}\right)dV\right.$$
$$\left. + \int_{S_d} p\left[(1-\alpha)\frac{\partial\psi}{\partial n} - \bar{d}_n\right]dS + \int_{S_p}(\bar{p} - \alpha p)\frac{\partial\psi}{\partial n}\, dS\right]dt. \tag{38}$$

---

* The variation of the kinetic energy integral term may be expressed in two different ways,

$$\delta\left(\rho\nabla\dot{\psi}^T, \nabla\dot{\psi}\right)_{V\times t} = \left(\rho\nabla^2\ddot{\psi}, \delta\psi\right)_{V\times t} - \left[\rho\frac{\partial\ddot{\psi}}{\partial n}, \delta\psi\right]_{S\times t} + \left(\rho\nabla\dot{\psi}, \delta\nabla\psi\right)_V\Big|_{t_0}^{t_1},$$

$$\delta\left(\rho\nabla\dot{\psi}^T, \nabla\dot{\psi}\right)_{V\times t} = \left(\rho\nabla^2\ddot{\psi}, \delta\dot{\psi}\right)_{V\times t} + \left[\rho\frac{\partial\dot{\psi}}{\partial n}, \delta\dot{\psi}\right]_{S\times t} - \left(\rho\nabla^2\dot{\psi}, \delta\psi\right)_V\Big|_{t_0}^{t_1}.$$

depending on whether integration by parts is performed first in time or space, respectively. The first form, which provides physically significant initial conditions, is used in constructing (35).

† If $\alpha \ne 1$, $\delta R_\alpha = 0$ is a *restricted* variational principle because the substitution $\nabla^2\psi = c^{-2}\ddot{\psi}$ holds only at the exact solution.

The highest spatial derivative index for both primary variables ψ and p is 1, except if $\alpha = 0$, in which case it is only 0 for p. The two interesting limit cases are of course $\alpha = 0$ and $\alpha = 1$, for which

$$R_0(\psi, p) = \int_{t_0}^{t_1} \left[\int_V \left(-\tfrac{1}{2}\rho(\nabla\dot{\psi})^T\nabla\dot{\psi} - \tfrac{1}{2}\frac{p^2}{\rho c^2} - \frac{p\ddot{\psi}}{c^2} \right) dV + \int_{S_d} p\left(\frac{\partial\psi}{\partial n} - \bar{d}_n \right) dS + \int_{S_p} \bar{p}\frac{\partial\psi}{\partial n} dS \right] dt, \tag{39}$$

$$R_1(\psi, p) = \int_{t_0}^{t_1} \left[\int_V \left(-\tfrac{1}{2}\rho(\nabla\dot{\psi})^T\nabla\dot{\psi} - \tfrac{1}{2}\frac{p^2}{\rho c^2} + (\nabla\psi)^T\nabla p \right) dV - \int_{S_d} p\bar{d}_n\, dS - \int_{S_p} (p-\bar{p})\frac{\partial\psi}{\partial n} dS \right] dt. \tag{40}$$

5. FINITE ELEMENT DISCRETIZATION

5.1 DISCRETIZATION OF R_α

In the following we derive semidiscrete finite-element equations of motion based on the R_α functional (38). The volume V is subdivided into fluid finite elements. Over each fluid element the state is represented by the primary variables ψ and p, which are defined as functions of position in the usual shape-function interpolation procedure. The finite element interpolation in V may be expressed as

$$\psi(\mathbf{x}, t) = N_\psi(\mathbf{x})\, \boldsymbol{\Psi}(t), \qquad p(\mathbf{x}, t) = N_p(\mathbf{x})\, \mathbf{p}(t), \tag{41}$$

where $\boldsymbol{\Psi}$ and $\mathbf{p}$ are computational column vectors that contain $n_p si$ and n_p nodal values of ψ and p, respectively, and N_ψ and N_p are corresponding row-vector arrays of dimensionless shape functions. The specified displacement over S_d is interpolated by

$$\bar{d}_n(\mathbf{x}, t) = \mathbf{n}^T d(\mathbf{x}, t) = \mathbf{n}^T N_d(\mathbf{x})\bar{\mathbf{d}}, = N_{dn}^T(\mathbf{x})\bar{\mathbf{d}}, \tag{42}$$

where $\mathbf{n}$ is the external-normal unit vector on S_d, N_d contains the displacement shape functions of the enclosing container, N_{dn} are these shape functions projected on the outward normal $\mathbf{n}$ on S_d, and $\bar{\mathbf{d}}$ contains nodal displacement values. For now the container displacements will be assumed to be prescribed, hence the superposed tilde.

In the following three Sections (5-8) we shall assume that *the prescribed-pressure boundary conditions are exactly satisfied* by the finite element interpolation, *i.e.* $p \equiv \bar{p}$ on S_p. If so the S_p integral of R_α simplifies to

$$\int_{S_p} (1 - \alpha)\bar{p}\frac{\partial\psi}{\partial n}\, dS, \tag{43}$$

which vanishes for $\alpha = 1$. Inserting (41)-(42) into the functional (38) with the simplified S_p integral (43) yields the semidiscrete quadratic form

$$R_\alpha(\boldsymbol{\Psi}, \mathbf{p}) = -\tfrac{1}{2}\rho\dot{\boldsymbol{\Psi}}^T H\dot{\boldsymbol{\Psi}} - \frac{1}{2\rho}\mathbf{p}^T G\mathbf{p} + \alpha\boldsymbol{\Psi}^T F\mathbf{p} + (1-\alpha)\left[\boldsymbol{\Psi}^T V\mathbf{p} - \ddot{\boldsymbol{\Psi}}^T D\mathbf{p} + \boldsymbol{\Psi}^T \mathbf{f}_\psi \right] - \mathbf{p}^T \widetilde{T}^T \bar{\mathbf{d}}, \tag{44}$$

114

where

$$H = \int_V \nabla N_\psi^T \nabla N_\psi \, dV = H^T, \qquad F = \int_V \nabla N_p^T \nabla N_\psi \, dV, \qquad G = \int_V c^{-2} N_p^T N_p \, dV = G^T,$$

$$D = \int_V c^{-2} N_\psi^T N_p \, dV, \quad V = \int_{S_d} (\nabla_n N_\psi)^T N_p \, dS, \quad \widetilde{T}^T = \int_{S_d} N_p^T N_{dn} \, dS, \quad f_\psi = \int_{S_p} \bar{p} \, \nabla_n N_\psi \, dS.$$

$$(45)$$

The integration with respect to time is dropped as it has no effect on the variation process described below.

5.2 CONTINUITY REQUIREMENTS

The interelement continuity requirements of the shape functions of ψ and p depend on the index of the highest spatial derivatives that appears in R_α. If $\alpha \neq 0$, this index is 1 for both ψ and p and consequently C^0 continuity is required. It is then natural to take the *same* shape functions for both variables:

$$N_\psi \equiv N_p \tag{46}$$

with both vectors Ψ and p of equal dimension and evaluated at the same nodes. Then some of the matrices in (45) coalesce as

$$H = F, \qquad G = D = D^T. \tag{47}$$

The case $\alpha = 0$ is exceptional in that no spatial derivatives of p appear. One can then chose C^{-1} (discontinuous) pressure shape functions; for example, constant over each fluid element. If this is done, obviously

$$N_\psi \neq N_p \tag{48}$$

because ψ must be C^0 continuous. Furthermore the dimensions of p and Ψ will not be generally the same.

5.3 SINGULARITY OF H

For later use, we note that matrix H (as well as F if different from H) before the application of any essential boundary conditions at fluid nodes, is singular because

$$He = 0 \tag{49}$$

where e denotes the vector of all ones. This follows from (45) and expresses the fact that a constant potential generates no pressures or displacements.

6. TRANSIENT RESPONSE EQUATIONS

6.1 THE RIGID-CONTAINER EQUATIONS OF MOTION

Since R_α contains time derivatives of of order up to 2 in Ψ, the appropriate Euler-Lagrange variational equation is

$$\delta R_\alpha = \left(\frac{\partial R_\alpha}{\partial \Psi} - \frac{\partial}{\partial t}\frac{\partial R_\alpha}{\partial \dot{\Psi}} + \frac{\partial^2}{\partial t^2}\frac{\partial R_\alpha}{\partial \ddot{\Psi}}\right)\delta\Psi + \frac{\partial R_\alpha}{\partial \mathbf{p}}\delta\mathbf{p} = 0, \tag{50}$$

which applied to (44) yields

$$\left[\rho\mathbf{H}\ddot{\Psi} + \alpha\mathbf{F}\mathbf{p} - (1-\alpha)\mathbf{D}\ddot{\mathbf{p}} + (1-\alpha)\mathbf{V}\mathbf{p} + (1-\alpha)\mathbf{f}_\psi\right]\delta\Psi = 0,$$

$$\left[-\rho^{-1}\mathbf{G}\mathbf{p} + \alpha\mathbf{F}^T\Psi - (1-\alpha)\mathbf{D}^T\ddot{\Psi} + (1-\alpha)\mathbf{V}^T\Psi - \tilde{\mathbf{T}}^T\tilde{\mathbf{d}}\right]\delta\mathbf{p} = 0. \tag{51}$$

These equations can be presented in partitioned matrix form as

$$\begin{bmatrix} \rho\mathbf{H} & -(1-\alpha)\mathbf{D} \\ -(1-\alpha)\mathbf{D}^T & 0 \end{bmatrix}\begin{Bmatrix} \ddot{\Psi} \\ \ddot{\mathbf{p}} \end{Bmatrix} + \begin{bmatrix} 0 & \mathbf{J} \\ \mathbf{J}^T & -\rho^{-1}\mathbf{G} \end{bmatrix}\begin{Bmatrix} \Psi \\ \mathbf{p} \end{Bmatrix} = \begin{Bmatrix} -(1-\alpha)\mathbf{f}_\psi \\ \tilde{\mathbf{T}}^T\tilde{\mathbf{d}} \end{Bmatrix}, \tag{52}$$

where $\mathbf{J} = (1-\alpha)\mathbf{V} + \alpha\mathbf{F}$.

6.2 THE FLEXIBLE-CONTAINER EQUATIONS OF MOTION

If the fluid is enclosed in a flexible container, the boundary displacements $\bar{\mathbf{d}}$ are no longer prescribed on S_d but must be incorporated in the problem by including them on the left hand side of the equations of motion. In the sequel, vector $\mathbf{d}$ collects *all structural node displacements*, of which $\bar{\mathbf{d}}$ is a subset on S_d. Matrix $\tilde{\mathbf{T}}$, suitably expanded with zeros to make it conform to $\mathbf{d}$, becomes $\mathbf{T}$. We shall only consider here the case in which the container is modelled as a *linear undamped* structure for which the standard mass/stiffness semidiscrete equation of motion is

$$\mathbf{M}\ddot{\mathbf{d}} + \mathbf{K}\mathbf{d} = \mathbf{f}_d + \mathbf{T}\mathbf{p}, \tag{53}$$

where $\mathbf{M}$ is the mass matrix, $\mathbf{K}$ the tangent stiffness matrix at the reference state, $\mathbf{T}\mathbf{p}$ is the pressure force on the structure, and $\mathbf{f}_d$ is the externally applied force on the structure. Note that $\mathbf{K}$ *in general must account for container prestress effects through the geometric stiffness*. Combining (52) and (53) we get the coupled system

$$\begin{bmatrix} \mathbf{M} & 0 & 0 \\ 0 & \rho\mathbf{H} & -(1-\alpha)\mathbf{D} \\ 0 & -(1-\alpha)\mathbf{D}^T & 0 \end{bmatrix}\begin{Bmatrix} \ddot{\mathbf{d}} \\ \ddot{\Psi} \\ \ddot{\mathbf{p}} \end{Bmatrix} + \begin{bmatrix} \mathbf{K} & 0 & -\mathbf{T} \\ 0 & 0 & \mathbf{J} \\ -\mathbf{T}^T & \mathbf{J}^T & -\rho^{-1}\mathbf{G} \end{bmatrix}\begin{Bmatrix} \mathbf{d} \\ \Psi \\ \mathbf{p} \end{Bmatrix} = \begin{Bmatrix} \mathbf{f}_d \\ -(1-\alpha)\mathbf{f}_\psi \\ 0 \end{Bmatrix}. \tag{54}$$

If $\alpha = 0$,

$$\begin{bmatrix} \mathbf{M} & 0 & 0 \\ 0 & \rho\mathbf{H} & \mathbf{D} \\ 0 & \mathbf{D}^T & 0 \end{bmatrix}\begin{Bmatrix} \ddot{\mathbf{d}} \\ \ddot{\Psi} \\ \ddot{\mathbf{p}} \end{Bmatrix} + \begin{bmatrix} \mathbf{K} & 0 & -\mathbf{T} \\ 0 & 0 & \mathbf{V} \\ -\mathbf{T}^T & \mathbf{V}^T & -\rho^{-1}\mathbf{G} \end{bmatrix}\begin{Bmatrix} \mathbf{d} \\ \Psi \\ \mathbf{p} \end{Bmatrix} = \begin{Bmatrix} \mathbf{f}_d \\ -\mathbf{f}_\psi \\ 0 \end{Bmatrix}. \tag{55}$$

There is little than can be done beyond this point, as the shape functions for p and ψ will be generally different. Although the pressure may be constant over each element, no condensation of $\mathbf{p}$ is possible in the dynamic case.

If $\alpha = 1$,

$$\begin{bmatrix} \mathbf{M} & 0 & 0 \\ 0 & \rho\mathbf{H} & 0 \\ 0 & 0 & 0 \end{bmatrix} \begin{Bmatrix} \ddot{\mathbf{d}} \\ \ddot{\Psi} \\ \ddot{\mathbf{p}} \end{Bmatrix} + \begin{bmatrix} \mathbf{K} & 0 & -\mathbf{T} \\ 0 & 0 & \mathbf{F} \\ -\mathbf{T}^T & \mathbf{F}^T & -\rho^{-1}\mathbf{G} \end{bmatrix} \begin{Bmatrix} \mathbf{d} \\ \Psi \\ \mathbf{p} \end{Bmatrix} = \begin{Bmatrix} \mathbf{f}_d \\ 0 \\ 0 \end{Bmatrix}. \tag{56}$$

Note that all these systems, (54) through (56), are *symmetric*.

6.3 IDENTICAL SHAPE FUNCTIONS

Further progress in the case $\alpha = 1$ can be made if we assume, as discussed in §5.2, that the shape functions for p and ψ coincide. Taking then (47) into account, (54) simplifies to

$$\begin{bmatrix} \mathbf{M} & 0 & 0 \\ 0 & \rho\mathbf{H} & 0 \\ 0 & 0 & 0 \end{bmatrix} \begin{Bmatrix} \ddot{\mathbf{d}} \\ \ddot{\Psi} \\ \ddot{\mathbf{p}} \end{Bmatrix} + \begin{bmatrix} \mathbf{K} & 0 & -\mathbf{T} \\ 0 & 0 & \mathbf{H} \\ -\mathbf{T}^T & \mathbf{H} & -\rho^{-1}\mathbf{G} \end{bmatrix} \begin{Bmatrix} \mathbf{d} \\ \Psi \\ \mathbf{p} \end{Bmatrix} = \begin{Bmatrix} \mathbf{f}_d \\ 0 \\ 0 \end{Bmatrix}. \tag{57}$$

The second matrix equation gives $\rho\mathbf{H}\ddot{\Psi} + \mathbf{Hp} = 0$. Since $\mathbf{H}$ is nonnegative definite we must have

$$\mathbf{p} = -\rho\ddot{\Psi}. \tag{58}$$

This is the discrete analog of the continuous relation (20) for the dynamic overpressure. For future use let us note that if the container is rigid, (57) reduces to

$$-\rho^{-1}\mathbf{Gp} + \mathbf{H}\Psi = \mathbf{G}\ddot{\Psi} + \mathbf{H}\Psi = \mathbf{T}^T\tilde{\mathbf{d}}. \tag{59}$$

6.4 UNSYMMETRIC ELIMINATION

If (58) is used to eliminate the pressure vector from (57) we obtain

$$\begin{bmatrix} \mathbf{M} & \rho\mathbf{T} \\ 0 & \mathbf{G} \end{bmatrix} \begin{Bmatrix} \ddot{\mathbf{d}} \\ \ddot{\Psi} \end{Bmatrix} + \begin{bmatrix} \mathbf{K} & 0 \\ -\mathbf{T}^T & \mathbf{H} \end{bmatrix} \begin{Bmatrix} \mathbf{d} \\ \Psi \end{Bmatrix} = \begin{Bmatrix} \mathbf{f}_d \\ 0 \end{Bmatrix}. \tag{60}$$

Conversely, eliminating the displacement potential vector gives

$$\begin{bmatrix} \mathbf{M} & 0 \\ \rho\mathbf{T}^T & \mathbf{G} \end{bmatrix} \begin{Bmatrix} \ddot{\mathbf{d}} \\ \ddot{\mathbf{p}} \end{Bmatrix} + \begin{bmatrix} \mathbf{K} & -\mathbf{T} \\ 0 & \mathbf{H} \end{bmatrix} \begin{Bmatrix} \mathbf{d} \\ \mathbf{p} \end{Bmatrix} = \begin{Bmatrix} \mathbf{f}_d \\ 0 \end{Bmatrix}. \tag{61}$$

Unlike previous systems, both (60) and (61) are *unsymmetric*. Thus the straightforward elimination of a field variable, be it p or ψ, causes symmetry to be lost. These forms will be called unsymmetric two-field forms, or U2 for short. System (60) reduces to (59) if the container is rigid.

7. REFORMULATIONS OF THE TRANSIENT RESPONSE EQUATIONS

7.1 S3 FORMS

Starting from (57) and (58) it is possible to derive three more symmetric forms that are formally equivalent. One is obtained by differentiating the last matrix equation twice in time, transforming the first equation via (57), and finally including (57) premultiplied by $\rho^{-1}G$ as third matrix equation:

$$\begin{bmatrix} M & \rho T & 0 \\ \rho T^T & -\rho H & G \\ 0 & G & 0 \end{bmatrix} \begin{Bmatrix} \ddot{d} \\ \ddot{\Psi} \\ \ddot{p} \end{Bmatrix} + \begin{bmatrix} K & 0 & 0 \\ 0 & 0 & 0 \\ 0 & 0 & \rho^{-1}G \end{bmatrix} \begin{Bmatrix} d \\ \Psi \\ p \end{Bmatrix} = \begin{Bmatrix} f_d \\ 0 \\ 0 \end{Bmatrix} \tag{62}$$

Another one is obtained by integrating the first matrix equation of (57) twice in time, using (58) to eliminate the pressure, and including $Kd - Kd = 0$ as trivial equation:

$$\begin{bmatrix} 0 & 0 & 0 \\ 0 & G & 0 \\ 0 & 0 & K \end{bmatrix} \begin{Bmatrix} \ddot{d} \\ \ddot{\Psi} \\ d \end{Bmatrix} + \begin{bmatrix} -M & -\rho T & -K \\ -\rho T^T & \rho H & 0 \\ -K & 0 & 0 \end{bmatrix} \begin{Bmatrix} d \\ \Psi \\ \overset{**}{d} \end{Bmatrix} = \begin{Bmatrix} -\overset{**}{f_d} \\ 0 \\ 0 \end{Bmatrix} \tag{63}$$

where superposed stars denote integration with respect to t. Finally, differentiating the first matrix equation of (63) twice in time, moving $\rho T^T d$ to the left, and including $Md - Md = 0$ as trivial equation, we get

$$\begin{bmatrix} 0 & 0 & -M \\ 0 & \rho G & -\rho T^T \\ -M & -\rho T & -K \end{bmatrix} \begin{Bmatrix} \ddot{d} \\ \ddot{\Psi} \\ d \end{Bmatrix} + \begin{bmatrix} M & 0 & 0 \\ 0 & \rho H & 0 \\ 0 & 0 & 0 \end{bmatrix} \begin{Bmatrix} d \\ \Psi \\ \overset{**}{d} \end{Bmatrix} = \begin{Bmatrix} 0 \\ 0 \\ -f_d \end{Bmatrix} \tag{64}$$

The four symmetric forms, (57), (62), (63) and (64), will be called *symmetric three field* forms, or S3 forms for short. It should be noted that there is no symmetric S3 form with a state vector consisting of d, p and $\overset{**}{d}$.

7.2 S2 FORMS

Each of the S3 forms has a statically condensable matrix equation that allows one field to be eliminated. For example, the last matrix equation of (57) is $-T^T d + H\Psi - \rho^{-1}Gp = 0$ which can be solved for the pressure vector p if G is nonsingular. Assuming that all matrix inverses indicated below exist (more will be said about this later), the condensation process yields four two-field symmetric forms:

$$\begin{bmatrix} M & 0 \\ 0 & \rho H \end{bmatrix} \begin{Bmatrix} \ddot{d} \\ \ddot{\Psi} \end{Bmatrix} + \begin{bmatrix} K + \rho TG^{-1}T^T & \rho TG^{-1}H \\ \rho HG^{-1}T^T & \rho HG^{-1}H \end{bmatrix} \begin{Bmatrix} d \\ \Psi \end{Bmatrix} = \begin{Bmatrix} f_d \\ 0 \end{Bmatrix}, \tag{65}$$

$$\begin{bmatrix} M + \rho TH^{-1}T^T & TH^{-1}G \\ GH^{-1}T^T & \rho^{-1}GH^{-1}G \end{bmatrix} \begin{Bmatrix} \ddot{d} \\ \ddot{p} \end{Bmatrix} + \begin{bmatrix} K & 0 \\ 0 & \rho^{-1}G \end{bmatrix} \begin{Bmatrix} d \\ p \end{Bmatrix} = \begin{Bmatrix} f_d \\ 0 \end{Bmatrix}, \tag{66}$$

$$\begin{bmatrix} \rho G & 0 \\ 0 & K \end{bmatrix} \begin{Bmatrix} \ddot{\Psi} \\ d \end{Bmatrix} + \begin{bmatrix} \rho H + \rho^2 T^T M^{-1}T & \rho T^T M^{-1}K \\ \rho KM^{-1}T & KM^{-1}K \end{bmatrix} \begin{Bmatrix} \Psi \\ \overset{**}{d} \end{Bmatrix} = -\begin{bmatrix} \rho T^T \\ K \end{bmatrix} M^{-1} \overset{**}{f_d}, \tag{67}$$

Table 2 Limit Conditions

Limit condition	Matrix expression	Recommended form(s)
Incompressible fluid ($c \to \infty$)	$\mathbf{G} \to \mathbf{0}$	(60), (61), (62), (66)
Cavitating fluid ($c \to 0$)	$\mathbf{G} \to \infty$	(57), (65)
Stiff container	$\mathbf{K} \to \infty$	(64), (68)
Hyperlight container	$\mathbf{M} \to \mathbf{0}$	(64), (68)

$$\begin{bmatrix} \mathbf{MK}^{-1}\mathbf{M} & \rho \mathbf{MK}^{-1}\mathbf{T} \\ \rho \mathbf{T}^T \mathbf{K}^{-1}\mathbf{M} & \rho \mathbf{G} + \rho^2 \mathbf{T}^T \mathbf{K}^{-1}\mathbf{T} \end{bmatrix} \begin{Bmatrix} \ddot{\mathbf{d}} \\ \ddot{\Psi} \end{Bmatrix} + \begin{bmatrix} \mathbf{M} & \mathbf{0} \\ \mathbf{0} & \rho \mathbf{H} \end{bmatrix} \begin{Bmatrix} \mathbf{d} \\ \Psi \end{Bmatrix} = - \begin{bmatrix} \mathbf{M} \\ \rho \mathbf{T}^T \end{bmatrix} \mathbf{K}^{-1} \mathbf{f}_d. \tag{68}$$

These will be called *symmetric two-field forms*, or S2 forms for brevity. The condensation process reduces the number of degrees of freedom but is detrimental to matrix sparsity. The last property may be recovered to some extent by taking advantage of *factored* forms of the matrices affected by the inverses; for example

$$\begin{bmatrix} \mathbf{K} + \rho \mathbf{TG}^{-1}\mathbf{T}^T & \rho \mathbf{TG}^{-1}\mathbf{H} \\ \rho \mathbf{HG}^{-1}\mathbf{T}^T & \rho \mathbf{HG}^{-1}\mathbf{H} \end{bmatrix} = \begin{bmatrix} \mathbf{I} & \mathbf{T} \\ \mathbf{0} & \mathbf{H} \end{bmatrix} \begin{bmatrix} \mathbf{K} & \mathbf{0} \\ \mathbf{0} & \rho \mathbf{G}^{-1} \end{bmatrix} \begin{bmatrix} \mathbf{I} & \mathbf{0} \\ \mathbf{T}^T & \mathbf{H} \end{bmatrix}. \tag{69}$$

Expressions for the matrices in (66)-(68) are given in [3].

7.3 ADVANTAGES AND RESTRICTIONS

The eight symmetric forms (S3 and S2), plus the two unsymmetric forms (U2), represent ten formulations of the R_1-based fluid-structure interaction problem for the identical-shape-function case. Although formally equivalent, they may have different behavior in terms of numerical stability and computational efficiency. The following items may affect the choice among the various forms.

Matrix sparseness retention. Matrices $\mathbf{G}$ and $\mathbf{M}$ are often diagonal. The S2 forms that involve $\mathbf{G}^{-1}$ and $\mathbf{K}^{-1}$, whether in direct or factored form, are (other things being equal) preferable to the others.

Existence of inverses. If the fluid does not have a free surface, $\mathbf{H}$ is singular on account of (49), and consequently (65) does not exist. If the container has some unsuppressed rigid body modes, $\mathbf{K}$ is singular and consequently (68) does not exist.

Applied force processing. Forms (63) and (67) require that the applied structural forces, $\mathbf{f}_d$, be integrated twice in time before being used. Both S2 forms (67) and (68) require additional matrix-vector operations on the force vectors. These disadvantages, however, disappear in the free-vibrations case discussed in §8.

Explicit versus implicit time integration. If $\mathbf{M}$ and $\mathbf{G}$ are diagonal, both unsymmetric forms (60) and (61) are attractive for explicit time integration because the leftmost coefficient matrices are upper and lower triangular, respectively. Therefore equations may be solved directly in a forward or backward direction without prior factorization. No symmetric form exhibits a similar property.

Physical limit conditions. Those collected in Table 2 are of interest in the applications. Recommended forms, if applicable (restrictions are analyzed in §7.3), are preferable because of numerical stability or suitability for perturbation analysis. Of all conditions listed in Table 2 the incompressible fluid case is of central importance. There must be a free surface S_p else the contained fluid would behave as a rigid body. Consequently $\mathbf{H}$ is nonsingular. Setting $\mathbf{G} = 0$ in (66) we obtain the so-called added mass equations

$$\mathbf{M}_a \ddot{\mathbf{d}} + \mathbf{K} \mathbf{d} = \mathbf{f}_d, \tag{70}$$

where $\mathbf{M}_a$ is the *added mass* of the coupled system:

$$\mathbf{M}_a = \mathbf{M} + \rho \mathbf{T} \mathbf{H}^{-1} \mathbf{T}^T. \tag{71}$$

Preservation of structural rigid body motions. This is discussed in more detail in §8.5 in conjunction with the free-vibration eigenproblem. Suffices to say that forms (63)-(64) and (67)-(68) do not generally preserve such motions and are inappropiate for treating unsupported structures (for example, liquid tanks in orbit).

Presence of constant potential mode (CPM). This is covered in detail in §8.6. If the fluid is totally enclosed by the container so that there is no free surface, forms (57) and (65) should not be used.

8. FREE VIBRATIONS

To obtain the elastoacoustic free-vibrations problem, we make the standard substitutions

$$\mathbf{d} = \mathbf{u} e^{j\omega t}, \quad \Psi = \mathbf{q} e^{j\omega t}, \quad \mathbf{p} = \mathbf{r} e^{j\omega t}, \quad \mathbf{f}_d = 0, \tag{72}$$

where $j = \sqrt{-1}$ and ω is the circular frequency, into the transient response equations. Thus we obtain ten algebraic eigenproblems, eight symmetric and two unsymmetric, which are displayed below. General properties of these eigensystems are summarized in the Appendix. In the following eigenproblem statements, subscript m is a mode index. The following eigenvector relations should be noted:

$$\mathbf{r}_m = -\rho \omega_m^2 \mathbf{q}_m, \quad \ddot{\mathbf{u}}_m = \omega_m^{-2} \mathbf{u}_m \quad (\omega_m \neq 0). \tag{73}$$

For the unsymmetric forms given in §8.3 one must distinguish between left and right eigenvectors. Supercript L is applied to left eigenvectors wherever necessary; otherwise right eigenvectors are assumed.

8.1 S3 FORMS

$$\omega_m^2 \begin{bmatrix} \mathbf{M} & 0 & 0 \\ 0 & \rho\mathbf{H} & 0 \\ 0 & 0 & 0 \end{bmatrix} \begin{Bmatrix} \mathbf{u}_m \\ \mathbf{q}_m \\ \mathbf{r}_m \end{Bmatrix} = \begin{bmatrix} \mathbf{K} & 0 & -\mathbf{T} \\ 0 & 0 & \mathbf{H} \\ -\mathbf{T}^T & \mathbf{H} & -\rho^{-1}\mathbf{G} \end{bmatrix} \begin{Bmatrix} \mathbf{u}_m \\ \mathbf{q}_m \\ \mathbf{r}_m \end{Bmatrix}, \tag{74}$$

$$\omega_m^2 \begin{bmatrix} \mathbf{M} & \rho\mathbf{T} & 0 \\ \rho\mathbf{T}^T & -\rho\mathbf{H} & \mathbf{G} \\ 0 & \mathbf{G} & 0 \end{bmatrix} \begin{Bmatrix} \mathbf{u}_m \\ \mathbf{q}_m \\ \mathbf{r}_m \end{Bmatrix} = \begin{bmatrix} \mathbf{K} & 0 & 0 \\ 0 & 0 & 0 \\ 0 & 0 & \rho^{-1}\mathbf{G} \end{bmatrix} \begin{Bmatrix} \mathbf{u}_m \\ \mathbf{q}_m \\ \mathbf{r}_m \end{Bmatrix}, \tag{75}$$

$$\omega_m^2 \begin{bmatrix} 0 & 0 & 0 \\ 0 & G & 0 \\ 0 & 0 & K \end{bmatrix} \begin{Bmatrix} \mathbf{u}_m \\ \mathbf{q}_m \\ \overset{**}{\mathbf{u}}_m \end{Bmatrix} = \begin{bmatrix} -M & -\rho T & -K \\ -\rho T^T & \rho H & 0 \\ -K & 0 & 0 \end{bmatrix} \begin{Bmatrix} \mathbf{u}_m \\ \mathbf{q}_m \\ \overset{**}{\mathbf{u}}_m \end{Bmatrix}, \tag{76}$$

$$\omega_m^2 \begin{bmatrix} 0 & 0 & -M \\ 0 & \rho G & -\rho T^T \\ -M & -\rho T & -K \end{bmatrix} \begin{Bmatrix} \mathbf{u}_m \\ \mathbf{q}_m \\ \overset{**}{\mathbf{u}}_m \end{Bmatrix} = \begin{bmatrix} M & 0 & 0 \\ 0 & \rho H & 0 \\ 0 & 0 & 0 \end{bmatrix} \begin{Bmatrix} \mathbf{u}_m \\ \mathbf{q}_m \\ \overset{**}{\mathbf{u}}_m \end{Bmatrix}. \tag{77}$$

8.2 S2 FORMS

$$\omega_m^2 \begin{bmatrix} M & 0 \\ 0 & \rho H \end{bmatrix} \begin{Bmatrix} \mathbf{u}_m \\ \mathbf{q}_m \end{Bmatrix} = \begin{bmatrix} K + \rho TG^{-1}T^T & \rho TG^{-1}H \\ \rho HG^{-1}T^T & \rho HG^{-1}H \end{bmatrix} \begin{Bmatrix} \mathbf{u}_m \\ \mathbf{q}_m \end{Bmatrix}, \tag{78}$$

$$\omega_m^2 \begin{bmatrix} M + \rho TH^{-1}T^T & TH^{-1}G \\ GH^{-1}T^T & \rho^{-1}GH^{-1}G \end{bmatrix} \begin{Bmatrix} \mathbf{u}_m \\ \mathbf{r}_m \end{Bmatrix} = \begin{bmatrix} K & 0 \\ 0 & \rho^{-1}G \end{bmatrix} \begin{Bmatrix} \mathbf{u}_m \\ \mathbf{r}_m \end{Bmatrix}, \tag{79}$$

$$\omega_m^2 \begin{bmatrix} \rho G & 0 \\ 0 & K \end{bmatrix} \begin{Bmatrix} \mathbf{q}_m \\ \overset{**}{\mathbf{u}}_m \end{Bmatrix} = \begin{bmatrix} \rho H + \rho^2 T^T M^{-1} T & \rho T^T M^{-1} K \\ \rho K M^{-1} T & K M^{-1} K \end{bmatrix} \begin{Bmatrix} \mathbf{q}_m \\ \overset{**}{\mathbf{u}}_m \end{Bmatrix}, \tag{80}$$

$$\omega_m^2 \begin{bmatrix} M K^{-1} M & \rho M K^{-1} T \\ \rho T^T K^{-1} M & \rho G + \rho^2 T^T K^{-1} T \end{bmatrix} \begin{Bmatrix} \mathbf{u}_m \\ \mathbf{q}_m \end{Bmatrix} = \begin{bmatrix} M & 0 \\ 0 & \rho H \end{bmatrix} \begin{Bmatrix} \mathbf{u}_m \\ \mathbf{q}_m \end{Bmatrix}. \tag{81}$$

8.3 U2 FORMS

$$\omega_m^2 \begin{bmatrix} M & \rho T \\ 0 & G \end{bmatrix} \begin{Bmatrix} \mathbf{u}_m \\ \mathbf{q}_m \end{Bmatrix} = \begin{bmatrix} K & 0 \\ -T^T & H \end{bmatrix} \begin{Bmatrix} \mathbf{u}_m \\ \mathbf{q}_m \end{Bmatrix}, \tag{82}$$

$$\omega_m^2 \begin{bmatrix} M & 0 \\ \rho T^T & G \end{bmatrix} \begin{Bmatrix} \mathbf{u}_m \\ \mathbf{r}_m \end{Bmatrix} = \begin{bmatrix} K & -T \\ 0 & H \end{bmatrix} \begin{Bmatrix} \mathbf{u}_m \\ \mathbf{r}_m \end{Bmatrix}. \tag{83}$$

8.4 COMPUTATIONAL CONSIDERATIONS

The considerations of §7.3 apply for the most part to these ten eigensystems. However, matrix symmetry is more important in free vibrations than in the transient response problem. This is because eigensolution extraction methods that take advantage of sparsity are more highly developed for the symmetric eigenproblem than for its unsymmetric counterpart. For an up-to-date exposition of those methods see Parlett [17].

The presence of zero eigenfrequencies ($\omega_m = 0$ roots) may cause serious numerical difficulties in some eigensystem formulations. Two sources of such roots may be distinguished: rigid body structural modes, and the constant-potential mode.

121

8.5 RIGID-BODY STRUCTURAL MODES

If the container is not fully supported, $\mathbf{Ku}_r = 0$ for structural rigid body eigenmodes $\mathbf{u}_r$. If $\mathbf{H}$ is nonsingular eigensystems (74)-(75), their condensed versions (78)-(79), as well as the two U2 eigensystems, preserve such modes. To verify this assertion, substitute

$$\mathbf{u}_m = \mathbf{u}_r, \quad \mathbf{q}_m = -\mathbf{H}^{-1}\mathbf{T}^T\mathbf{u}_r, \quad \mathbf{r}_m = 0, \tag{84}$$

into the Rayleigh quotients (A.12) or (A.15) of the eigensystems. If $\mathbf{H}$ is singular, form (79), which contains $\mathbf{H}^{-1}$, does not exist, whereas (74) preserves the modes if there exist $\mathbf{q}_r$ modes such that $\mathbf{Hq}_r + \mathbf{Tu}_r = 0$. Eigensystems (76)-(77) and (80) do not generally preserve rigid-body modes, whereas (81), which contains $\mathbf{K}^{-1}$, does not exist.

8.6 CONSTANT POTENTIAL MODE AND SPECTRUM CONTAMINATION

Suppose the container is supported so $\mathbf{K}$ is nonsingular but the enclosed fluid has no pressure-specified surface S_p. If so $\mathbf{H}$ is singular because of (49). Both U2 eigensystems then possess an $\omega = 0$ root which conventionally will be assigned modal index 0. This root is associated with the following left/right eigenvectors

$$\text{Eigensystem (82):} \quad \mathbf{u}_0 = 0, \quad \mathbf{q}_0 = \mathbf{e}, \quad \mathbf{u}_0^L = \mathbf{K}^{-1}\mathbf{Te}, \quad \mathbf{q}_0^L = \mathbf{e}, \tag{85}$$

$$\text{Eigensystem (83):} \quad \mathbf{u}_0 = \mathbf{K}^{-1}\mathbf{Te}, \quad \mathbf{r}_0 = \mathbf{e}, \quad \mathbf{u}_0^L = 0, \quad \mathbf{r}_0^L = \mathbf{e}, \tag{86}$$

This statement is readily verified by taking the Rayleigh quotients (A.12). The eigenpairs (85-86) are collectively called *constant potential mode* or CPM. The existence and computational implications of this mode have been discussed by Geradin *et. al.* [7]. The mathematical interpretation of (85) is "dual" to that of a structural rigid-body mode. Under a rigid-body motion the displacements are nonzero but the strains vanish. Under the CPM the potential is nonzero but all fluid displacements and dynamic pressures vanish. But unlike rigid-body modes, the CPM *has no physical significance*: it is spurious.

According to the eigenfunction theory summarized in the Appendix, all non-CPM modes $(\mathbf{u}_m, \mathbf{q}_m, \mathbf{r}_m)$ of (82) and (83) for $m \neq 0$, $\omega_m \neq 0$ satisfy the bi-orthogonality conditions

$$\langle 0 \quad \mathbf{e}^T \rangle \begin{bmatrix} \mathbf{M} & 0 \\ \rho\mathbf{T}^T & \mathbf{G} \end{bmatrix} \begin{Bmatrix} \mathbf{u}_m \\ \mathbf{r}_m \end{Bmatrix} = \mathbf{e}^T(\rho\mathbf{T}^T\mathbf{u}_m + \mathbf{Gr}_m) = 0, \tag{87}$$

$$\langle \mathbf{e}^T\mathbf{T}^T\mathbf{K}^{-1} \quad \mathbf{e}^T \rangle \begin{bmatrix} \mathbf{M} & \rho\mathbf{T}^T \\ 0 & \mathbf{G} \end{bmatrix} \begin{Bmatrix} \mathbf{u}_m \\ \mathbf{q}_m \end{Bmatrix} = \mathbf{e}^T(\mathbf{T}^T\mathbf{K}^{-1}\mathbf{Mu}_m + \rho\mathbf{T}^T\mathbf{K}^{-1}\mathbf{Tq}_m + \mathbf{Gq}_m) = 0. \tag{88}$$

As regards the symmetric forms, eigensystems (74) and (78) are adversely affected by the singularity of $\mathbf{H}$ and should not be used. This is because substituting the CPM left eigenvector (85) into either one, with $\mathbf{r}_m = 0$ for (74), produces a Rayleigh quotient for ω of the form 0/0. This means that both coefficient matrices have a common null space (the CPM) and every ω is an eigenvalue. Such an eigenproblem is called *defective* (see Appendix). If one attempts to numerically solve "untreated" defective eigenproblems, nonsensical results can be expected because the whole spectrum is likely to be contaminated.

9. SLOSH MOTIONS IN A GRAVITY FIELD

A liquid with a free surface in equilibrium in a time-independent acceleration field may exhibit *surface waves*, informally called "slosh" motions. From an applications standpoint the most important acceleration fields are gravity and rotational motion, the latter being of interest in rotating tanks. In this section we shall be content with formulating slosh effects in a uniform gravity field. More general fields, including time-dependent body forces, may be variationally treated by the method of canonical decomposition of the non-homogeneous wave equation, but that general method will not be followed here as it is not necessary for the gravity case.

The fluid volume V is in equilibrium in the reference state discussed in §3.1 under the time-invariant body force *per unit of volume* $\mathbf{b} = \nabla\beta$, where β is a potential field. As noted above we restrict developments here to a gravity field of strength g uniform in space and time. The boundary S_p is then the *equilibrium free surface* normal to the gravity field. The axes (x_1, x_2, x_3) are selected so that g acts along the $-x_3 \equiv -z$ axis. Hence $\beta = -\rho g z + B$, where B is an arbitrary constant. If we chose B so that β vanishes at the free surface $z = z_0$, then

$$\beta = -\rho g(z - z_0). \tag{89}$$

In the so-called *hydrostatic approximation* for small-amplitude gravity waves [9] sloshing is considered equivalent to a free surface pressure

$$p = \bar{p} + \rho g d_n = \bar{p} + \rho g \eta, \qquad \text{where} \qquad \eta = d_n = \frac{\partial \psi}{\partial n} \quad \text{on} \quad S_p. \tag{90}$$

Here $\bar{p}$ as before denotes the prescribed part of the pressure (for example, atmospheric pressure) and η is called the *elevation* of the liquid with respect to the equilibrium free surface. This approximation assumes that the displacements are infinitesimal and that the z-acceleration of the slosh motion is negligible.

9.1 VARIATIONAL PRINCIPLE

For the variational derivation of "slosh equations" it is advantageous to chose the elevation η as an independently varied field. This choice simplifies the reduction to surface unknowns as well as the treatment of more complex interface conditions such as capillary effects.

To incorporate slosh effects into the mixed variational principles based on the functionals studied in §4, it is convenient to follow a Galerkin technique by adding weighted forms of (88) to their first variation. The following combinations may be considered:

$$
\begin{aligned}
&\pm\left(p - \bar{p} - \rho g \eta, \delta\frac{\partial\psi}{\partial n}\right)_{S_p} \pm \left(\frac{\partial\psi}{\partial n} - \eta, \delta\eta\right)_{S_p}, && \pm\left(p - \bar{p} - \rho g \eta, \delta\frac{\partial\psi}{\partial n}\right)_{S_p} \pm \left(\frac{\partial\psi}{\partial n} - \eta, \delta p\right)_{S_p}, \\[2mm]
&\pm\left(p - \bar{p} - \rho g \eta, \delta p\right)_{S_p} \pm \left(\frac{\partial\psi}{\partial n} - \eta, \delta\frac{\partial\psi}{\partial n}\right)_{S_p}, && \pm\left(p - \bar{p} - \rho g \eta, \delta p\right)_{S_p} \pm \left(\frac{\partial\psi}{\partial n} - \eta, \delta\eta\right)_{S_p}, \qquad (91) \\[2mm]
&\pm\left(p - \bar{p} - \rho g \eta, \delta\eta\right)_{S_p} \pm \left(\frac{\partial\psi}{\partial n} - \eta, \delta p\right)_{S_p}, && \pm\left(p - \bar{p} - \rho g \eta, \delta\eta\right)_{S_p} \pm \left(\frac{\partial\psi}{\partial n} - \eta, \delta\frac{\partial\psi}{\partial n}\right)_{S_p}.
\end{aligned}
$$

Of these the first expression, with signs $-$ and $+$, offers two advantages: (1) it is derivable from a functional, and (2) it combines naturally with the S_p integral in the first variation (35). Of the "base" parametrized functional R_α the most computationally advantageous choice is again $\alpha = 1$. The expanded functional (40), denoted as $R_{1\eta}$ in the sequel, is

$$R_{1\eta}(p, \psi, \eta) = R_{1V} - \int_{t_0}^{t_1} \left[\int_{S_d} p \tilde{d}_n \, dS + \int_{S_p} (p - \bar{p} - \rho g \eta) \frac{\partial \psi}{\partial n} + \tfrac{1}{2} \rho g \eta^2 \, dS \right] dt. \qquad (92)$$

where R_{1V} is the volume integral of (40). Note that setting $\eta = 0$ restores R_1.

9.2 FINITE ELEMENT DISCRETIZATION

In addition to the assumptions (41), (42) and (46) we interpolate η as

$$\eta = N_\eta \eta \qquad \text{on} \quad S_p, \qquad (93)$$

where column vector η contains n_η fluid elevations at nodes on S_p, and row vector N_η contains the corresponding elevation shape functions. The semidiscrete quadratic form for (92), again excluding the time integral, is

$$R_{1\eta}(\Psi, p, \eta) = -\tfrac{1}{2} \rho \dot{\Psi}^T H \dot{\Psi} - \frac{1}{2\rho} p^T G p + p^T (H - Q_{p+}) \Psi - p^T \tilde{T}^T \tilde{d} + \rho g \eta^T (Q_{\eta+} \Psi - \tfrac{1}{2} S \eta) - \Psi^T f_\psi, \qquad (94)$$

where

$$Q_{\eta+} = \int_{S_p} N_\eta^T \nabla N_\psi \, dS, \quad Q_{p+} = \int_{S_p} N_p^T \nabla N_\psi \, dS, \quad S = \int_{S_p} N_\eta^T N_\eta \, dS = S^T, \quad f_\psi = \int_{S_p} \nabla N_\psi^T \bar{p}. \qquad (95)$$

The $+$ subscripts in $Q_{\eta+}$ and Q_{p+} convey that the nonzero, "surface" portion of these matrices is augmented with zeros to conform to vectors Ψ and p. To display this structure, Ψ, p and related matrices are partitioned as

$$\Psi = \left\{ \begin{array}{c} \Psi_s \\ \Psi_v \end{array} \right\}, \quad p = \left\{ \begin{array}{c} p_s \\ p_v \end{array} \right\}, \quad Q_{\eta+} = [Q_\eta \quad 0], \quad Q_{p+} = \begin{bmatrix} Q_p & 0 \\ 0 & 0 \end{bmatrix}, \quad H = \begin{bmatrix} H_{ss} & H_{sv} \\ H_{ss} & H_{vv} \end{bmatrix}, \qquad (96)$$

where Ψ_s contains potentials at $n_{\eta\psi}$ nodes of *elements* connected to S_p and p_s contains n_η pressures on S_p. The dimensions of Q_η and Q_p are $n_\eta \times n_{\eta\psi}$. In general $n_\eta < n_{\eta\psi}$ (in fact, about one half). Also typically $n_\eta \ll n_\psi = n_p$ as the latter pertain to a volume mesh. If η is interpolated by the same surface functions as p, i.e. $N_\eta \equiv N_p$ on S_p, then

$$Q_\eta = Q_p = Q, \qquad Q_{\eta+} = [Q \quad 0], \qquad Q_{p+} = \begin{bmatrix} Q & 0 \\ 0 & 0 \end{bmatrix}. \qquad (97)$$

9.3 THE RIGID CONTAINER

The following equations of motion for the rigid but mobile container are obtained on rendering (94) stationary:

$$
\begin{bmatrix} \rho H & 0 & 0 \\ 0 & 0 & 0 \\ 0 & 0 & 0 \end{bmatrix} \begin{Bmatrix} \ddot{\Psi} \\ \ddot{p} \\ \rho g \ddot{\eta} \end{Bmatrix} + \begin{bmatrix} 0 & H - Q_{p+}^T & Q_{\eta+}^T \\ H - Q_{p+} & -\rho^{-1}G & 0 \\ Q_{\eta+} & 0 & -S \end{bmatrix} \begin{Bmatrix} \Psi \\ p \\ \rho g \eta \end{Bmatrix} = \begin{Bmatrix} f_\psi \\ \widetilde{T}^T \tilde{d} \\ 0 \end{Bmatrix}.
\tag{98}
$$

Assuming G and S to be nonsingular and identical p and η shape functions so that (97) hols, the nodal pressures and elevations may be statically condensed from (98) thus producing the single matrix equation

$$
\rho H \ddot{\Psi} + (P + R_+)\Psi = f_\psi + \rho (H - Q_{p+})G^{-1}\widetilde{T}^T \tilde{d},
\tag{99}
$$

where

$$
R_+ = Q_{\eta+}^T S^{-1} Q_{\eta+} = \begin{bmatrix} Q^T S^{-1} Q & 0 \\ 0 & 0 \end{bmatrix} = \begin{bmatrix} R & 0 \\ 0 & 0 \end{bmatrix} = R_+^T, \quad P = \rho(H - Q_{p+}^T)G^{-1}(H - Q_{p+}) = P^T.
\tag{100}
$$

The rank of R_+ and R is the same as that of S, that is, n_η. For most real liquids, acoustic and slosh motions take place in very different time scales. This is the basis for the common assumption in slosh analysis that the fluid is *incompressible*, i.e. $c \to \infty$, $G \to 0$ and $R \to \infty$. If $G \to 0$ the response of the above system tends is forced to occur in the displacement-potential subspace defined by the second matrix equation of (98):

$$
(H - Q_{p+})\Psi = \widetilde{T}\tilde{d}.
\tag{101}
$$

For simplicity let us assume that the container is not only rigid but *motionless*, that is, $\tilde{d} = 0$. The incompressible-fluid equations become

$$
\rho \begin{bmatrix} H_{ss} & H_{sv} \\ H_{sv}^T & H_{vv} \end{bmatrix} \begin{Bmatrix} \ddot{\Psi}_s \\ \ddot{\Psi}_v \end{Bmatrix} + \begin{bmatrix} R & 0 \\ 0 & 0 \end{bmatrix} \begin{Bmatrix} \Psi_s \\ \Psi_v \end{Bmatrix} = \begin{Bmatrix} f_\psi \\ 0 \end{Bmatrix},
\tag{102}
$$

subject to the constraint $(H - Q_{p+})\Psi = 0$. Subvector Ψ_v may be statically condensed from these two relations, which may be combined as the system

$$
\begin{bmatrix} \rho H_s & 0 \\ 0 & 0 \end{bmatrix} \begin{Bmatrix} \ddot{\Psi}_s \\ \ddot{\lambda}_\psi \end{Bmatrix} + \begin{bmatrix} R & H_s - Q_s^T \\ H_s - Q_s & 0 \end{bmatrix} \begin{Bmatrix} \Psi_s \\ \lambda_\psi \end{Bmatrix} = \begin{Bmatrix} f_\psi \\ 0 \end{Bmatrix}.
\tag{103}
$$

where λ_ψ are Lagrangian multipliers (in fact, the pressures at nodes of Ψ_s), and

$$
H_s = H_{ss} - H_{sv}H_{vv}^{-1}H_{vs}, \qquad Q_s = \begin{bmatrix} Q \\ 0 \end{bmatrix}.
\tag{104}
$$

If $\tilde{d} \neq 0$ the force term in (103) must be appropriately modified.

9.4 THE FLEXIBLE CONTAINER

For a flexible container the equations of motion accounting for fluid compressibility are

$$
\begin{bmatrix} M & 0 & 0 & 0 \\ 0 & \rho H & 0 & 0 \\ 0 & 0 & 0 & 0 \\ 0 & 0 & 0 & 0 \end{bmatrix} \begin{Bmatrix} \ddot{d} \\ \ddot{\Psi} \\ \ddot{p} \\ \rho g \ddot{\eta} \end{Bmatrix} + \begin{bmatrix} K & 0 & -T & 0 \\ 0 & 0 & H - Q_{p+}^T & Q_{\eta+}^T \\ -T^T & H - Q_{p+} & -\rho^{-1}G & 0 \\ 0 & Q_{\eta+} & 0 & -S \end{bmatrix} \begin{Bmatrix} d \\ \Psi \\ p \\ \rho g \eta \end{Bmatrix} = \begin{Bmatrix} f_d \\ f_\psi \\ 0 \\ 0 \end{Bmatrix} .
$$

$$(105)$$

Eliminating η and p by static condensation yields

$$
\begin{bmatrix} M & 0 \\ 0 & \rho H \end{bmatrix} \begin{Bmatrix} \ddot{d} \\ \ddot{\Psi} \end{Bmatrix} = \begin{bmatrix} K_a & -Y \\ -Y^T & P+R \end{bmatrix} \begin{Bmatrix} d \\ \Psi \end{Bmatrix} = \begin{Bmatrix} f_d \\ f_\psi \end{Bmatrix} ,
$$

$$(106)$$

where

$$
K_a = K + \rho TG^{-1}T^T , \qquad Y = \rho TG^{-1}(H - Q_{p+}) .
$$

$$(107)$$

System (106) is the counterpart of (65). If the fluid is treated as incompressible, a subspace reduction procedure similar to that used in §9.3 can be invoked.

9.5 SLOSH VIBRATIONS

Algebraic eigenproblems to investigate slosh vibrations may be constructed following essentially the same techniques as in §8, and reduced to S_p node elevations and pressures. We illustrate the reduction technique for the incompressible fluid held in a motionless rigid container. The eigenproblem associated with (103), suppressing the modal index m for simplicity, may be written as

$$
\omega^2 \begin{bmatrix} \rho H_s & 0 \\ 0 & 0 \end{bmatrix} \begin{Bmatrix} q_s \\ r_\psi \end{Bmatrix} = \begin{bmatrix} R & H_s - Q^T \\ H - Q & 0 \end{bmatrix} \begin{Bmatrix} q_s \\ r_\psi \end{Bmatrix}
$$

$$(108)$$

where q_s and r_ψ are the modal amplitudes of Ψ_s and λ_ψ, respectively. The last matrix equation in (98) provides $Q\Psi_s = S\eta$, or $Qq_s = Sz$, where z is the vector of modal amplitudes of η, *i.e.* $\eta = ze^{j\omega t}$. Using these relations we can transform the eigenproblem (108) to

$$
\omega^2 \begin{bmatrix} \rho gS & 0 \\ 0 & 0 \end{bmatrix} \begin{Bmatrix} z \\ r_s \end{Bmatrix} = \begin{bmatrix} C & Q^T - C \\ Q - C & 0 \end{bmatrix} \begin{Bmatrix} z \\ r_s \end{Bmatrix}
$$

$$(109)$$

in which

$$
C = QH_s^{-1}Q^T
$$

$$(110)$$

and r_s are Lagrange-multiplier modal amplitudes at nodes of η. This generalized symmetric eigensystem of order $2n_\eta$ provides n_η solutions to the slosh eigenproblem. A similar technique may be followed for the flexible container case. This finite element reduction-to-surface technique provides an alternative to boundary integral methods [1,8].

10. CONCLUDING REMARKS

Displacement-potential formulations are of practical interest in fluid-structure transient-response and vibration analysis as they provide the basis for effective numerical computations. For some recent applications see [2,6,7,9,12,14] and references therein. The preceding treatment unifies a number of previous continuum-based and algebraic statements [3,4,5,9,11,12,14-16] of the coupled problem. It may be further extended in the following directions:

(1) The inhomogeneous wave equation $c^2 \nabla^2 \psi - \ddot{\psi} = f$, $f \neq 0$, when the body force field $b(x, t)$ is time-dependent and $\nabla 2b \neq 0$. Additional forcing terms appear in the equations of motion. These are of interest for slosh of fluids in rotating containers.

(2) Retaining the specific momentum m as independent field in functional (33).

(3) Inclusion of additional physical effects: capillarity, cavitation and viscosity.

Acknowledgements

REFERENCES

DeRuntz, J. A. and Geers, T. L., Added mass computation by the boundary integral method, *Int. J. Num. Meth. Engrg.*, 12, 1978, pp. 531–550

Felippa, C. A. and DeRuntz, J. A., Finite element analysis of shock-induced hull cavitation, *Computer Methods in Applied Mechanics & Engineering*, 44, 1984, pp. 297–337

Felippa, C. A., Symmetrization of the contained compressible fluid vibration eigenproblem, *Comm. Appl. Numer. Meth.*, 1, 1985, pp. 241–247

Felippa, C. A., Some aspects of the symmetrization of the contained compressible fluid eigenproblem, in *Proceedings Fourth International Symposium on Numerical Methods in Engineering*, Atlanta, Georgia, ed. by R.P. Shaw *et al.*, Computational Mechanics Pubs., Southampton, UK, 1986, pp. 249–255

Felippa, C. A., Symmetrization of coupled eigenproblems by eigenvector augmentation, *Comm. Appl. Numer. Meth.*, 4, 1988, pp. 561–563

Geers, T. L. and Ruzicka, G. C., Finite-element/boundary-element analysis of multiple structures excited by transient acoustic waves, in *Numerical Methods for Transient and Coupled Problems*, ed. by R. W. Lewis *et al.*, Pineridge Press, Swansea, U. K., 1984, pp. 150–162

Geradin, M., Roberts, G. and Huck, A., Eigenvalue analysis and transient response of fluid structure interaction problems, *Eng. Comp.*, 1, 1984, pp. 151–160

Khabbaz, G. R., Dynamic behavior of liquid in elastic tanks, *AIAA Journal*, 9, 1970, pp. 1985–1990

Kinsman, B., *Water Waves*, Dover, New York, 1965

Lamb, H., *Hydrodynamics*, Dover, New York, 6th ed. 1945

Morand, H. and Ohayon, R., Substructure variational analysis for the vibrations of coupled fluid-structure systems: finite element results, *Int. J. Num. Meth. Engrg.*, 14, 1979, pp. 741–755

Nicolas-Vullierme, B. and Ohayon, R., Fluid-structure interaction for bounded and unbounded medium vibration problems: Some recent advances at ONERA, in *Advances in Fluid-Structure Interaction*, ASME/AMD Volume 64, 1984

Oden, J. T. and Reddy, J. N., *Variational Methods in Theoretical Mechanics*, 2nd ed., Springer-Verlag, Berlin, 1983

Ohayon, R. and Valid, R., True symmetric variational formulations for fluid-structure interaction in bounded domains. Finite element results, Chap. 10 in *Numerical Methods in Coupled Systems*, ed. by R. W. Lewis, P. Bettess and E. Hinton, Wiley, 1984

Ohayon, R., Fluid-structure modal analysis. New symmetric continuum-based formulations. Finite element applications, Contribution T46 in *Proceedings International Conference on Numerical Methods in Engineering: Theory and Applications*, NUMETA 87, M. Nijhoff Pubs., Dordrecht, 1987

Ohayon, R., and Felippa, C. A., The effect of wall motion on the governing equations of contained fluids, submitted to *J. Applied Mechanics*

Parlett, B., *The Symmetric Eigenvalue Problem*, Prentice-Hall, Englewood Cliffs, N. J., 1980

Appendix A: THE GENERALIZED ALGEBRAIC EIGENPROBLEM

Some facts about the algebraic eigenproblem are collected here for convenient reference. These facts are relevant to the study of the free vibrations of the coupled fluid-structure system.

A.1 THE STANDARD UNSYMMETRIC EIGENPROBLEM

The standard eigenproblem for a *real unsymmetric* square matrix A may be stated as

$$Ax_i = \lambda_i x_i, \tag{A.1}$$

where λ_i the eigenvalues (which may be complex), and x_i the corresponding *right* eigenvectors *normalized to unit length*. The eigenproblem for the transposed matrix is

$$A^T y_i = \lambda_i y_i. \tag{A.2}$$

This problem has the same eigenvalues but in general the eigenvectors y_i will be different. The y_i are called *left* eigenvectors of A because they satisfy the problem $y_i^T A = \lambda_i y_i$; this in turn explains the qualifier 'right' applied to x_i. The system of left and right eigenvectors of A satisfies *bi-orthogonality* relations:

$$y_i^T x_j = \begin{cases} 0 & \text{if } i \neq j, \\ \mu_i & \text{if } i = j. \end{cases} \tag{A.3}$$

This μ_i is called the condition number of λ_i with respect to the eigenproblem (A.1); it is always less or equal than 1 in absolute value, and may be zero in pathological cases. (The closer to 1, the better conditioned λ_i is.)

Premultiplying (A.1) by y_i and assuming that $\mu_i \neq 0$ yields

$$\lambda_i = y_i^T A x_i / \mu_i = x_i^T A^T y_i / \mu_i, \tag{A.4}$$

which is the Rayleigh quotient for unsymmetric matrices. If $\mu_i = 0$ and $y_i^T A x_i = 0$, (A.5) takes the undetermined form 0/0 so every λ_i is an eigenvalue. In such a case the eigenproblem (A.1) is said to be *defective*.

A.2 THE STANDARD SYMMETRIC PROBLEM

If A is symmetric then $x_i = y_i$, $\mu_i = 1$ and (A.3) reduce to the usual orthogonality conditions

$$x_i^T x_j = \begin{cases} 0 & \text{if } i \neq j, \\ 1 & \text{if } i = j. \end{cases} \tag{A.5}$$

whereas (A.4) becomes the usual Rayleigh quotient for a unit length vector:

$$\lambda_i = x_i^T A x_i. \tag{A.6}$$

A.3 THE GENERALIZED UNSYMMETRIC EIGENPROBLEM

The generalized unsymmetric eigenproblem is

$$A x_i = \lambda_i B x_i, \tag{A.7}$$

where A and B are unsymmetric real matrices. Assuming that B^{-1} exists, this problem can be reduced to the standard problem

$$C x_i = \lambda_i x_i, \tag{A.8}$$

in which $C = B^{-1} A$. The transposed problem is

$$C^T z_i = A^T B^{-T} z_i = \lambda_i z_i. \tag{A.9}$$

Defining $B^T y_i = z_i$, (A.9) can be transformed to

$$A^T y_i = \lambda_i B^T y_i. \tag{A.10}$$

The bi-orthogonality conditions (A.3) become

$$z_i^T x_j = y_i^T B x_j = x_i^T B^T y_j = \begin{cases} 0 & \text{if } i \neq j, \\ \mu_i & \text{if } i = j. \end{cases} \tag{A.11}$$

The Rayleigh quotient (A.4) generalizes to

$$\lambda_i = \frac{y_i^T A x_i}{y_i^T B x_i} = \frac{y_i^T A x_i}{\mu_i}. \tag{A.12}$$

As in §A.1, if (A.12) takes on the form 0/0 for some i, every λ_i is an eigenvalue and the eigenproblem (A.7) is said to be *defective*; mathematically, A and B share a common null space. A defective eigenproblem cannot be solved numerically by conventional root-extraction methods because the 0/0 roots contaminate the entire spectrum.

A.4 THE GENERALIZED SYMMETRIC EIGENPROBLEM

If both A and B are symmetric,

$$x_i = y_i, \qquad z_i = B^{-1} y_i. \tag{A.13}$$

and we recover the usual orthonormality conditions

$$x_i^T B x_j = \begin{cases} 0 & \text{if } i \neq j, \\ \mu_i & \text{if } i = j. \end{cases} \tag{A.14}$$

In mechanical vibration problems for which B is the mass matrix, μ_i is called the *generalized mass*. Finally, (A.12) reduces to the usual Rayleigh quotient

$$\lambda_i = \frac{x_i^T A x_i}{x_i^T B x_i}. \tag{A.15}$$

129

VARIATIONAL FORMULATION OF HIGH PERFORMANCE FINITE ELEMENTS: PARAMETRIZED VARIATIONAL PRINCIPLES

SUMMARY

High performance elements are simple finite elements constructed to deliver engineering accuracy with coarse arbitrary grids. This paper is part of a series on the variational basis of high-performance elements, with emphasis on those constructed with the free formulation (FF) and assumed natural strain (ANS) methods. The present paper studies parametrized variational principles that provide a foundation for the FF and ANS methods, as well as for a combination of both,

1. INTRODUCTION

For 25 years researchers have tried to construct "best" finite element models for problems in structural mechanics. The quest appeared to be nearly over in the late 1960s when higher order displacement elements dominated the headlines. But these elements did not dominate the marketplace. The overwhelming preference of finite element code users has been for simple elements that deliver engineering accuracy with coarse meshes. The search for these "high-performance" (HP) elements began in the early 1970s and by now it represents an important area of finite element research in solid and structural mechanics. Many ingenious schemes have been tried: reduced and selective integration, incompatible modes, mixed and hybrid formulations, stress and strain projections, the free formulation (FF), and the assumed natural strain (ANS) method.

The present paper is part of a series [8-12] that studies how several high performance element construction methods can be embedded within an *extended* variational framework that uses parametrized hybrid functionals. The general plan of attack is sketched in Figure 1. Heavy

line boxes are those emphasized in the present paper. The extensions, shown on the left, involve parametrization of the conventional elasticity functionals and treatment of element interfaces through generalizations of the hybrid approach of Pian [14-16].

The effective construction of HP elements relies on devices, sometimes derisively called "tricks" or "variational crimes," that do not fit *a priori* in the classical variational framework. The range of tricks range from innocuous collocation and finite difference constraints to more drastic remedies such as selective integration. Despite their unconventional nature, tricks are an essential part of the construction of high-performance elements. They collectively represent a fun-and-games ingredient that keeps the derivation of HP finite elements as a surprisingly enjoyable task.

The present treatment "decriminalizes" kinematic constraint tricks by adjoining Lagrange multipliers, hence placing the ensemble in a proper variational setting. Placing formulations within a variational framework has the great advantage of supplying the *general structure* of the matrices and forcing vectors of high performance elements, and of allowing a systematic derivation of classes of elements by an array of powerful techniques.

Note the reliance of the program of Figure 1 on hybrid functionals. The original 1964 vision of Pian [14] is thus seen to acquire a momentous significance. It is perhaps appropriate to quote here the prediction of another great contributor to finite elements:

> *T. H. H. Pian responded to the problem of plate bending by inventing the "hybrid formulation", which avoids the problem of slope continuity. He assumed that the element responds not according to shape functions but according to element stress fields. These communicate with the outside world via the boundaries .... Hybrid elements can be the most competitive and we believe that the future lie in that direction. However, the formulation is more complicated. Therefore we advocate that researchers should try to cajole their formulation into shape function form, so that users do not have to struggle. In the form, hybrid elements are no more difficult to use than the iso-P elements ... Unfortunately at the time of writing we have no uniform technique to achieve this.*
>
> *B. Irons and S. Ahmad, Techniques of Finite Elements (1980), p. 159*

Fulfillment of the prophecy appears to be near.

2. THE ELASTICITY PROBLEM

Consider a *linearly elastic body* under static loading that occupies the volume V. The body is bounded by the surface S, which is decomposed into $S : S_d \cup S_t$. Displacements are prescribed on S_d whereas surface tractions are prescribed on S_t. The outward unit normal on S is denoted by $\mathbf{n} \equiv n_i$.

The three unknown volume fields are displacements $\mathbf{u} \equiv u_i$, infinitesimal strains $\mathbf{e} \equiv e_{ij}$,

131
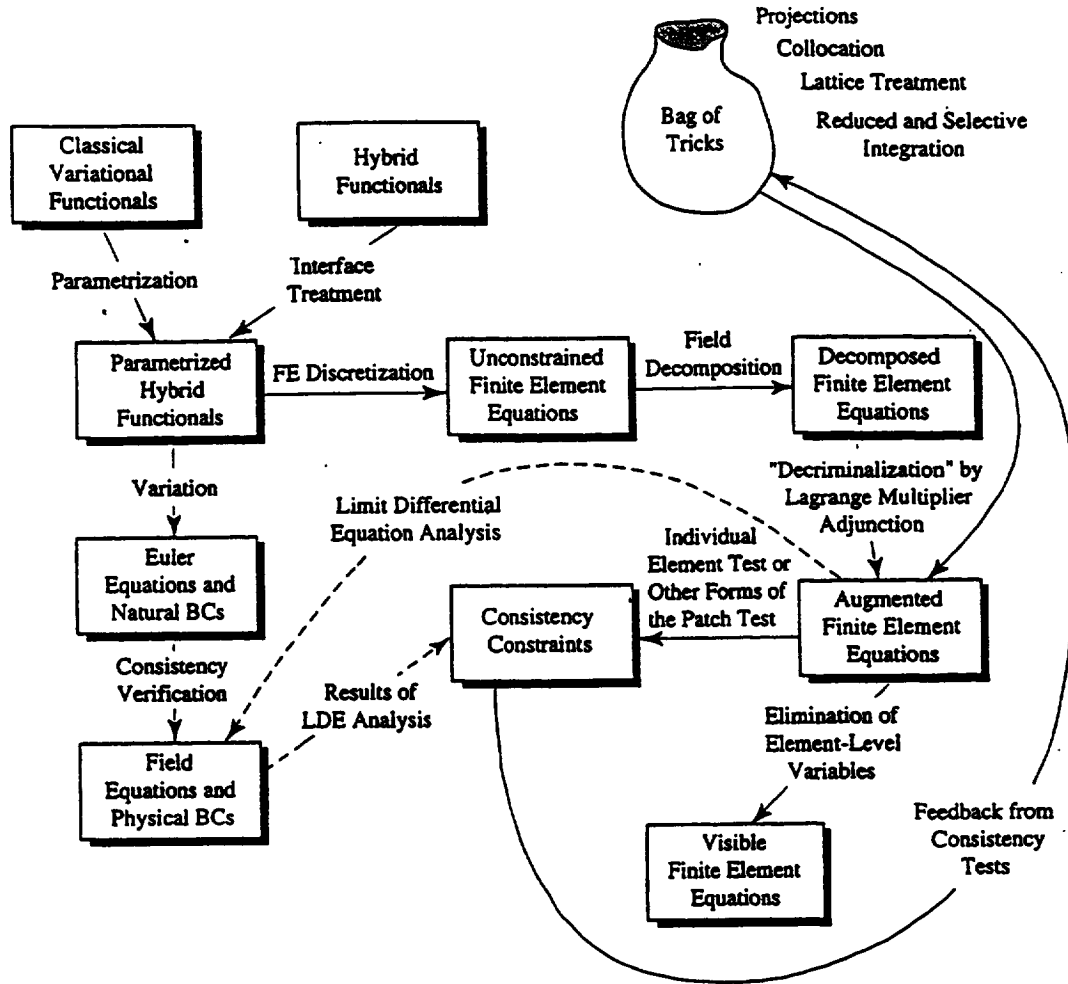
Figure 1. Program of attack on the variational formulation of HP elements

and stresses $\sigma \equiv \sigma_{ij}$. The problem data include: the body force field $\mathbf{b} \equiv b_i$ in V, prescribed displacements $\hat{\mathbf{d}}$ on S_d, and prescribed surface tractions $\hat{\mathbf{t}} \equiv \hat{t}_i$ on S_t.

The relations between the volume fields are the strain-displacement equations

$$\mathbf{e} = \tfrac{1}{2}(\nabla \mathbf{u} + \nabla^T \mathbf{u}) = \mathbf{D}\mathbf{u} \qquad \text{or} \qquad e_{ij} = \tfrac{1}{2}(u_{i,j} + u_{j,i}) \quad \text{in } V, \tag{1}$$

the constitutive equations

$$\sigma = \mathbf{E}\,\mathbf{e} \qquad \text{or} \qquad \sigma_{ij} = E_{ijkl}e_{kl} \quad \text{in } V, \tag{2}$$

and the equilibrium (balance) equations

$$-\mathbf{div}\,\sigma = \mathbf{D}^*\sigma = \mathbf{b} \qquad \text{or} \qquad \sigma_{ij,j} + b_i = 0 \quad \text{in } V, \tag{3}$$

in which $\mathbf{D}^* = -\mathbf{div}$ denotes the adjoint operator of $\mathbf{D} = \tfrac{1}{2}(\nabla + \nabla^T)$.

The stress vector with respect to a direction defined by the unit vector $\mathbf{v}$ is denoted as $\sigma_v = \sigma.\mathbf{v}$, or $\sigma_{vi} = \sigma_{ij}v_j$. On S the surface-traction stress vector is defined as

$$\sigma_n = \sigma.\mathbf{n}, \qquad \text{or} \quad \sigma_{ni} = \sigma_{ij}n_j. \tag{4}$$

With this definition the traction boundary conditions may be stated as

$$\sigma_n = \hat{\mathbf{t}} \qquad \text{or} \qquad \sigma_{ij}n_j = \hat{t}_i \qquad \text{on } S_t, \tag{5}$$

and the displacement boundary conditions as

$$\mathbf{u} = \hat{\mathbf{d}} \qquad \text{or} \qquad u_i = \hat{d}_i \qquad \text{on } S_d. \tag{6}$$

3. NOTATION

3.1 Field Dependency

In variational methods of approximation we do not work of course with the exact fields that satisfy the governing equations (1-3,5-6), but with *independent* (primary) fields, which are subject to variations, and *dependent* (secondary, associated, derived) fields, which are not. The approximation is determined by taking variations with respect to the independent fields.

An *independently varied* field will be identified by a superposed tilde, for example $\tilde{\mathbf{u}}$. A dependent field is identified by writing the independent field symbol as superscript. For example, if the displacements are independently varied, the derived strain and stress fields are

$$\mathbf{e}^u = \tfrac{1}{2}(\nabla + \nabla^T)\tilde{\mathbf{u}} = \mathbf{D}\tilde{\mathbf{u}}, \qquad \sigma^u = \mathbf{E}\mathbf{e}^u = \mathbf{ED}\tilde{\mathbf{u}}. \tag{7}$$

An advantage of this convention is that $\mathbf{u}$, $\mathbf{e}$ and σ may be reserved for the *exact* fields.

3.2 Integral Abbreviations

Volume and surface integrals will be abbreviated by placing domain-subscripted parentheses and square brackets, respectively, around the integrand. For example:

$$(f)_V \stackrel{\text{def}}{=} \int_V f\,dV, \quad [f]_S \stackrel{\text{def}}{=} \int_S f\,dS, \quad [f]_{S_d} \stackrel{\text{def}}{=} \int_{S_d} f\,dS, \quad [f]_{S_t} \stackrel{\text{def}}{=} \int_{S_t} f\,dS. \tag{8}$$

If $\mathbf{f}$ and $\mathbf{g}$ are vector functions, and $\mathbf{p}$ and $\mathbf{q}$ tensor functions, their inner product over V is denoted in the usual manner

$$(\mathbf{f}, \mathbf{g})_V \stackrel{\text{def}}{=} \int_V \mathbf{f}.\mathbf{g}\,dV = \int_V f_i g_i\,dV, \qquad (\mathbf{p}, \mathbf{q})_V \stackrel{\text{def}}{=} \int_V \mathbf{p}.\mathbf{q}\,dV = \int_V p_{ij}q_{ij}\,dV, \tag{9}$$

and similarly for surface integrals, in which case square brackets are used.

133

Figure 2. Internal interface example.

3.3 Domain Assertions

The notation

$$(a = b)_V, \qquad [a = b]_S, \qquad [a = b]_{S_d}, \qquad [a = b]_{S_t}, \tag{10}$$

is used to assert that the relation $a = b$ is valid at each point of V, S, S_d and S_t, respectively.

3.4 Internal Interfaces

In the following subsections we construct *hybrid variational principles* in which boundary displacements $\mathbf{d}$ can be varied independently from the internal displacements $\mathbf{u}$. These displacements play the role of Lagrange multipliers that relax internal displacement continuity. Variational principles containing P^d will be called *displacement-generalized*, or d-generalized for short.

The choice of $\mathbf{d}$ as independent field is *not* variationally admissible on S_d or S_t. We must therefore extend the definition of boundary to include *internal interfaces* collectively designated as S_i. Thus

$$S : S_d \cup S_t \cup S_i. \tag{11}$$

On S_i neither displacements nor tractions are prescribed. A simple case is illustrated in Figure 2, in which the interface S_i divides V into two subvolumes: V^+ and V^-. An interface such as S_i on Figure 2 has two "sides" called S_i^+ and S_i^-, which identify S_i viewed as boundary of V^+ and V^-, respectively. At smooth points of S_i the unit normals $\mathbf{n}^+$ and $\mathbf{n}^-$ point in opposite directions.

The integral abbreviations (8)-(9) generalize as follows, using Figure 2 for definiteness. A volume integral is the sum of integrals over the subvolumes:

$$(f)_V \overset{\text{def}}{=} \int_{V^+} f \, dV + \int_{V^-} f \, dV. \tag{12}$$

An integral over S_i includes two contributions:

$$[g]_{S_i} \overset{\text{def}}{=} \int_{S_i^+} g^+ \, dS + \int_{S_i^-} g^- \, dS, \tag{13}$$

134

where g^+ and g^- denotes the value of the integrand g on S_i^+ and S_i^-, respectively. These two values may be different if g is discontinuous or involves a projection on the normals.

Following a finite element discretization, the union of interelement boundaries becomes S_i.

4. THE ELASTICITY FUNCTIONALS

The variational principles of linear elasticity are based on functionals of the form

$$\Pi = U - P, \tag{14}$$

where U characterizes the internal energy stored in the body volume and P includes other contributions such as work of applied loads and energy stored on internal interfaces. We shall call U the *generalized strain energy* and P the *forcing potential*.

It must be pointed out that all functionals considered here include *independently varied displacements*. Thus, the class of dual functionals such as the complementary energy are *not* included in the following study.

4.1 Volume Integrals

The generalized strain energy has the following structure:

$$U = \tfrac{1}{2}j_{11}(\bar{\sigma}, e^\sigma)_V + j_{12}(\bar{\sigma}, \bar{e})_V + j_{13}(\bar{\sigma}, e^u)_V + \tfrac{1}{2}j_{22}(\sigma^e, \bar{e})_V + j_{23}(\sigma^e, e^u)_V + \tfrac{1}{2}j_{33}(\sigma^u, e^u)_V \tag{15}$$

where j_{11} through j_{33} are numerical coefficients. For example, the Hu-Washizu principle is obtained by setting $j_{12} = -1$, $j_{13} = 1$, $j_{22} = 1$, all others being zero. The matrix representation of the general functional (15) and the relations that must exist between the coefficients are studied in §5.1.

4.2 Hybrid Forcing Potentials

Variational principles of linear elasticity are constructed by combining the volume integral (15) with the forcing potential P. Two forms of the forcing potential, called P^d and P^t in the sequel, are of interest in the hybrid treatment of interface discontinuities. The d-generalized (displacement-generalized) forcing potential introduces an independent boundary displacement field $\bar{d}$ over S_i:

$$P^d(\bar{u}, \bar{\sigma}, \bar{d}) = (b, \bar{u})_V + [\bar{\sigma}_n, \bar{u} - \hat{d}]_{S_d} + [\hat{t}, \bar{u}]_{S_t} + [\bar{\sigma}_n, \bar{u} - \bar{d}]_{S_i}. \tag{16}$$

The t-generalized (traction generalized) forcing potential introduces an independently varied traction displacement field $\bar{t}$ over S_i:

$$P^t(\bar{u}, \bar{\sigma}, \bar{t}) = (b, \bar{u})_V + [\bar{t}, \bar{u} - \hat{d}]_{S_d} + [\hat{t}, \bar{u}]_{S_t} + [\bar{t}, \bar{u}]_{S_i}. \tag{17}$$

The "conventional" form P^c of the forcing potential is obtained if the interface integral vanishes and one sets $[t = \sigma_n]_S$. If so P^t and P^d coalesce into P^c, which retains only two independent fields:

$$P^c(\bar{u}, \bar{\sigma}) = (b, \bar{u})_V + [\bar{\sigma}_n, \bar{u} - \hat{d}]_{S_d} + [\hat{t}, \bar{u}]_{S_t}. \tag{18}$$

135

4.3 Modified Forcing Potentials

Through various manipulations and assumptions detailed in [10] the forcing potential P^d may be transformed to

$$P^d(\bar{u}, \bar{\sigma}, \bar{d}) = (b, \bar{u})_V + [\hat{t}, \bar{d}]_{S_t} + [\bar{\sigma}_n, \bar{u} - \bar{d}]_S. \tag{19}$$

where the all-important surface dislocation integral is taken over S rather than S_i. One of the assumptions is that displacement boundary conditions (6) are exactly satisfied. This expression of P^d is used in the sequel. A similar technique can be used to modify P^t, but that expression will not be required in what follows.

4.4 Complete Functionals

Complete elasticity functionals are obtained by combining the generalized strain energy with one of the forcing potentials. For example, the d and t generalized versions of the Hu-Washizu functional are

$$\Pi_W^d = U_W - P^d, \qquad \Pi_W^t = U_W - P^t. \tag{20}$$

where U_W is obtained by setting $j_{22} = j_{13} = 1$, $j_{12} = -1$, others zero, in (15).

5. MATRIX REPRESENTATION OF ELASTICITY FUNCTIONALS

The generalized strain energy (15) can be presented in matrix form as*

$$U = \frac{1}{2} \int_V \langle \bar{\sigma} \quad \sigma^\epsilon \quad \sigma^u \rangle \begin{bmatrix} j_{11} & j_{12} & j_{13} \\ & j_{22} & j_{23} \\ symm & & j_{33} \end{bmatrix} \left\{ \begin{array}{c} e^\sigma \\ \tilde{e} \\ e^u \end{array} \right\} dV. \tag{21}$$

The symmetric matrix

$$\mathbf{J} = \begin{bmatrix} j_{11} & j_{12} & j_{13} \\ & j_{22} & j_{23} \\ symm & & j_{33} \end{bmatrix} \tag{22}$$

characterizes the volume portion of the variational principle. Using the relations $\sigma^\epsilon = \mathbf{E}e$, $\sigma^u = \mathbf{E}\mathbf{D}\bar{u}$, $e^\epsilon = \mathbf{E}^{-1}e$, and $e^u = \mathbf{D}\bar{u}$, the above integral may be rewritten in terms of the independent fields as

$$U = \frac{1}{2} \int_V \langle \bar{\sigma} \quad \tilde{e} \quad \bar{u} \rangle \begin{bmatrix} j_{11}\mathbf{E}^{-1} & j_{12}\mathbf{I} & j_{13}\mathbf{D} \\ j_{12}\mathbf{I} & j_{22}\mathbf{E} & j_{23}\mathbf{E}\mathbf{D} \\ j_{13}\mathbf{D}^T & j_{23}\mathbf{D}^T\mathbf{E} & j_{33}\mathbf{D}^T\mathbf{E}\mathbf{D} \end{bmatrix} \left\{ \begin{array}{c} \bar{\sigma} \\ \tilde{e} \\ \bar{u} \end{array} \right\} dV. \tag{23}$$

---

* To justify the symmetry of $\mathbf{J}$ note, for example, that $j_{13}(\bar{\sigma}, e^u)_V = \frac{1}{2}j_{13}(\bar{\sigma}, e^u)_V + \frac{1}{2}j_{13}(e^\sigma, \sigma^u)_V$, and so on.

5.1 First Variation of Generalized Strain Energy

The first variation of the volume term (15) may be presented as

$$\delta U = (\Delta e, \delta \tilde{\sigma})_V + (\Delta \sigma, \delta \tilde{e})_V - (\text{div } \sigma', \delta \tilde{u})_V + [\sigma'_n, \delta \tilde{u}]_S. \tag{24}$$

where

$$\Delta e = j_{11} e^\sigma + j_{12} \tilde{e} + j_{13} e^u,$$
$$\Delta \sigma = j_{12} \tilde{\sigma} + j_{22} \sigma^e + j_{23} \sigma^u, \tag{25}$$
$$\sigma' = j_{13} \tilde{\sigma} + j_{23} \sigma^e + j_{33} \sigma^u.$$

The last two terms combine with contributions from the variation of P. For example, if $P = P^c$ the complete variation of $\Pi^c = U - P^c$ is

$$\delta \Pi^c = (\Delta e, \delta \tilde{\sigma})_V + (\Delta \sigma, \delta \tilde{e})_V - (\text{div } \sigma' + b, \delta \tilde{u})_V + [\sigma'_n - \hat{t}, \delta \tilde{u}]_{S_t} + -[\tilde{u} - \hat{d}, \delta \tilde{\sigma}_n]_{S_d}. \tag{26}$$

Using P^d or P^t does not change the volume terms. The Euler equations corresponding to P^d and P^t are studied in [10,11] for a more restrictive form of functionals U.

Since the Euler equations associated with the first two terms are $\Delta \sigma = 0$ and $\Delta e = 0$, these quantities may be regarded as deviations from stress-balance and strain-compatibility, respectively. For consistency of the Euler equations with the field equations of §2 we must have $\Delta e = 0$, $\Delta \sigma = 0$ and $\sigma' = \sigma$ if the assumed stress and strain fields reduce to the exact ones. Consequently

$$j_{11} + j_{12} + j_{13} = 0,$$
$$j_{12} + j_{22} + j_{23} = 0, \tag{27}$$
$$j_{13} + j_{23} + j_{33} = 1.$$

Because of these constraints, the maximum number of independent parameters that define the entries of J is three.

5.2 Specific Functionals

Expressions of J for some classical and parametrized variational principles of elasticity are tabulated below. The subscript of J is used the identify the functionals, which are listed roughly in order of ascending complexity. The fields included in parentheses after the functional name are those subject to independent variations.

Potential energy $(\tilde{u})$:

$$J_P = \begin{bmatrix} 0 & 0 & 0 \\ 0 & 0 & 0 \\ 0 & 0 & 1 \end{bmatrix}. \tag{28}$$

Stress-displacement Reissner, also called Hellinger-Reissner, $(\tilde{\sigma}, \tilde{u})$:

$$J_R = \begin{bmatrix} -1 & 0 & 1 \\ 0 & 0 & 0 \\ 1 & 0 & 0 \end{bmatrix}. \tag{29}$$

Unnamed stress-displacement functional listed in Oden and Reddy [13] $(\bar{\sigma}, \bar{u})$:

$$\mathbf{J}_U = \begin{bmatrix} 1 & 0 & -1 \\ 0 & 0 & 0 \\ -1 & 0 & 2 \end{bmatrix}. \tag{30}$$

Strain-displacement Reissner-type [13] $(\bar{e}, \bar{u})$:

$$\mathbf{J}_S = \begin{bmatrix} 0 & 0 & 0 \\ 0 & -1 & 1 \\ 0 & 1 & 0 \end{bmatrix}. \tag{31}$$

Hu-Washizu $(\bar{\sigma}, \bar{e}, \bar{u})$:

$$\mathbf{J}_W = \begin{bmatrix} 0 & -1 & 1 \\ -1 & 1 & 0 \\ 1 & 0 & 0 \end{bmatrix}. \tag{32}$$

One-parameter stress-displacement family $(\bar{\sigma}, \bar{u})$ that includes U_P, U_R and U_U as special cases [9,10,11]:

$$\mathbf{J}_\gamma = \begin{bmatrix} -\gamma & 0 & \gamma \\ 0 & 0 & 0 \\ \gamma & 0 & 1-\gamma \end{bmatrix}. \tag{33}$$

One-parameter strain-displacement family $(\bar{e}, \bar{u})$ that includes U_P and U_S as special cases [9]:

$$\mathbf{J}_\beta = \begin{bmatrix} 0 & 0 & 0 \\ 0 & -\beta & \beta \\ 0 & \beta & 1-\beta \end{bmatrix}. \tag{34}$$

Two-parameter strain-displacement family $(\bar{\sigma}, \bar{e}, \bar{u})$ that includes U_β and U_γ as special cases [9]:

$$\begin{aligned} \mathbf{J}_{\beta\gamma} &= (1-\beta)\mathbf{J}_\gamma + (1-\gamma)\mathbf{J}_\beta - (1-\beta-\gamma)\mathbf{J}_P \\ &= \begin{bmatrix} -\gamma(1-\beta) & 0 & \gamma(1-\beta) \\ 0 & -\beta(1-\gamma) & \beta(1-\gamma) \\ \gamma(1-\beta) & \beta(1-\gamma) & 1-\beta-\gamma+2\beta\gamma \end{bmatrix}. \end{aligned} \tag{35}$$

Three-parameter (α, β, γ) family $(\bar{\sigma}, \bar{e}, \bar{u})$ that includes U_W and $U_{\beta\gamma}$ as special cases [9]:

$$\begin{aligned} \mathbf{J}_{\alpha\beta\gamma} &= \alpha\mathbf{J}_W + (1-\alpha)\mathbf{J}_{\beta\sigma} \\ &= \begin{bmatrix} -\gamma(1-\beta)(1-\alpha) & -\alpha & \alpha+\gamma(1-\beta)(1-\alpha) \\ -\alpha & \alpha-\beta(1-\gamma)(1-\alpha) & \beta(1-\gamma)(1-\alpha) \\ \alpha+\gamma(1-\beta)(1-\alpha) & \beta(1-\gamma)(1-\alpha) & (1-\beta-\gamma+2\beta\gamma)(1-\alpha) \end{bmatrix}. \end{aligned} \tag{36}$$

The last form, which contains three independent parameters, supplies all matrices $\mathbf{J}$ that satisfy the constraints (21). It yields stress-displacement functionals for $\alpha = \beta = 0$, strain displacement functionals for $\alpha = \gamma = 0$, and 3-field functionals otherwise. A graphic representation of $\mathbf{J}_{\alpha\beta\gamma}$ in (α, β, γ) space is given in Figure 3.
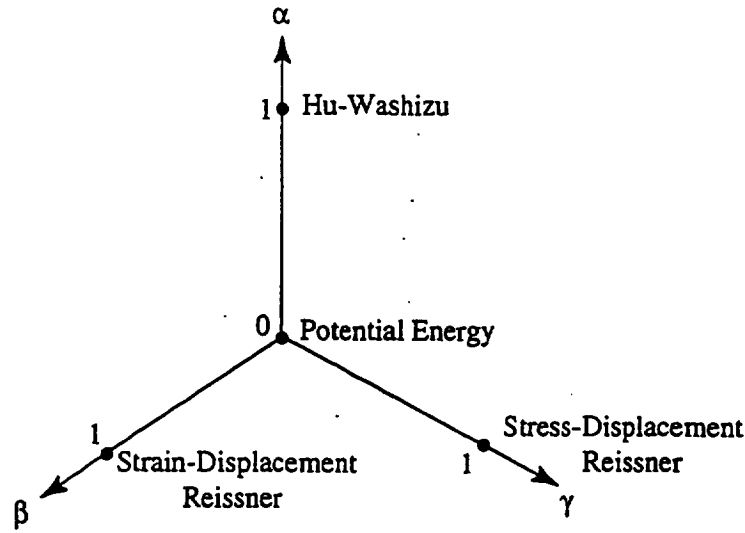
Figure 3.   Graphical representation of the $J_{\alpha\beta\gamma}$ functionals

5.3 Energy Balancing

A prime motivation for introducing the j coefficients as free parameters is optimization of finite element performance. The determination of "best" parameters for specific elements relies on the concept of energy balance. Let $\mathcal{U}(\epsilon) = \frac{1}{2}(E\epsilon, \epsilon)_V$ denote the strain energy associated with the strain field ϵ. If E is positive definite, $\mathcal{U}(\epsilon)$ is nonnegative. We may decompose the generalized strain energy into the following sum of strain energies:

$$U = j_{33}\mathcal{U}(e^u) + c_1\mathcal{U}(e^\sigma - \bar{e}) + c_2\mathcal{U}(\bar{e} - e^u) + c_3\mathcal{U}(e^u - e^\sigma), \qquad (37)$$

where $\mathcal{U}_P(e^u) = U_P$ is the usual strain energy, $c_1 = \frac{1}{2}(j_{11} + j_{22} - j_{33} + 1)$, $c_2 = \frac{1}{2}(-j_{11} + j_{22} + j_{33} - 1)$, and $c_3 = \frac{1}{2}(j_{11} - j_{22} + j_{33} - 1)$. Equation (37) is equivalent to decomposing J into the sum of four rank-one matrices:

$$J = j_{33}\begin{bmatrix} 0 & 0 & 0 \\ 0 & 0 & 0 \\ 0 & 0 & 1 \end{bmatrix} + c_1\begin{bmatrix} 1 & -1 & 0 \\ -1 & 1 & 0 \\ 0 & 0 & 0 \end{bmatrix} + c_2\begin{bmatrix} 0 & 0 & 0 \\ 0 & 1 & -1 \\ 0 & -1 & 1 \end{bmatrix} + c_3\begin{bmatrix} 1 & 0 & -1 \\ 0 & 0 & 0 \\ -1 & 0 & 1 \end{bmatrix}. \qquad (38)$$

Decompositions of this nature can be used to derive energy balanced finite elements by considering element "patches" under simple load systems. This technique is discussed for the one-parameter functionals generated by (34) in [5,7,8].

6. FINITE ELEMENT DISCRETIZATION

In this section assumptions invoked in the finite element discretization of the functional Π^d for arbitrary J are stated. Following usual practice in finite element work, the components of stresses and strains are arranged as one-dimensional arrays whereas the elastic moduli in E are arranged as a square symmetric matrix. In the sequel we shall consider an *individual element* of volume V and surface $S : S_t \cup S_d \cup S_i$, where S_i is the portion of the boundary in common with other elements.

6.1 Boundary Displacement Assumption

The boundary displacement assumption is

$$[\tilde{\mathbf{d}} = \mathbf{N}_d\,\mathbf{v}]_S. \tag{39}$$

Here matrix $\mathbf{N}_d$ collects the boundary shape functions for the boundary displacement $\mathbf{d}$ whereas vector $\mathbf{v}$ collects the degrees of freedom of the element, also called the *connectors*. These boundary displacements must be unique on common element boundaries. This condition is verified if the displacement of the common boundary portion is uniquely specified by degrees of freedom located on that boundary. There are no derived fields associated with $\tilde{\mathbf{d}}$.

6.2 Internal Displacement Assumption

The displacement assumption in the interior of the element is

$$(\tilde{\mathbf{u}} = \mathbf{N}_u\mathbf{q})_V, \tag{40}$$

where matrix $\mathbf{N}_u$ collects the internal displacement shape functions and vector $\mathbf{q}$ collects generalized coordinates for the internal displacements. The assumed $\tilde{\mathbf{u}}$ need not be continuous across interelement boundaries.

The displacement derived fields are

$$(\mathbf{e}^u = \mathbf{D}\mathbf{N}\mathbf{q} = \mathbf{B}\mathbf{q})_V, \quad (\sigma^u = \mathbf{E}\mathbf{B}\mathbf{q})_V. \tag{41}$$

To link up with the FF and ANS formulations, we proceed to break up the internal displacement field as follows. The assumed $\tilde{\mathbf{u}}$ is decomposed into rigid body, constant strain, and higher order displacements:

$$\tilde{\mathbf{u}} = \mathbf{N}_r\mathbf{q}_r + \mathbf{N}_c\mathbf{q}_c + \mathbf{N}_h\mathbf{q}_h. \tag{42}$$

Applying the strain operator $\mathbf{D} = \frac{1}{2}(\nabla + \nabla^T)$ to $\tilde{\mathbf{u}}$ we get the associated strain field:

$$\mathbf{e}^u = \mathbf{D}\mathbf{N}_r\mathbf{q}_r + \mathbf{D}\mathbf{N}_c\mathbf{q}_c + \mathbf{D}\mathbf{N}_h\mathbf{q}_h = \mathbf{B}_r\mathbf{q}_r + \mathbf{B}_c\mathbf{q}_c + \mathbf{B}_h\mathbf{q}_h. \tag{43}$$

But $\mathbf{B}_r = \mathbf{D}\mathbf{N}_r$ vanishes because $\mathbf{N}_r$ contains only rigid-body modes. We are also free to select $\mathbf{B}_c = \mathbf{D}\mathbf{N}_c$ to be the identity matrix $\mathbf{I}$ if the generalized coordinates $\mathbf{q}_c$ are identified with the mean (volume-averaged) strain values $\bar{\mathbf{e}}^u$. Consequently (44) simplifies to

$$\mathbf{e}^u = \bar{\mathbf{e}}^u + \mathbf{e}^u_h = \bar{\mathbf{e}}^u + \mathbf{B}_h\mathbf{q}_h, \tag{44}$$

in which

$$\mathbf{q}_c \equiv \bar{\mathbf{e}}^u = (\mathbf{e}^u)_V/\upsilon, \qquad (\mathbf{B}_h)_V = 0. \tag{45}$$

where $\upsilon = (1)_V$ is the element volume measure. The second relation is obtained by integrating (44) over V and noting that $\mathbf{q}_h$ is arbitrary. It says that the mean value of the higher-order displacement-derived strains is zero over the element.

6.3 Stress Assumption

The stress field will be assumed to be *constant* over the element:

$$(\tilde{\sigma} = \bar{\sigma})_V. \tag{46}$$

This assumption is sufficient to construct high-performance elements based on the free formulation [1-10]. Higher order stress variations are computationally effective if they are divergence free [10] but such a requirement makes extension to geometrically nonlinear problems difficult. The only derived field is

$$(\tilde{e}^{\sigma} = E^{-1}\bar{\sigma})_V \tag{47}$$

6.4 Strain Assumptions

The assumed strain field $\tilde{e}$ is decomposed into a mean constant strain $\bar{e}$ and a higher order variation:

$$(\tilde{e} = \bar{e} + Aa)_V. \tag{48}$$

where $\bar{e} = (\tilde{e})_V/v$, A collects higher order strain modes with mean zero value over the element:

$$(A)_V = 0, \tag{49}$$

and a collects the corresponding strain parameters. The only derived field is

$$(\sigma^{\epsilon} = E\tilde{e} = E\bar{e} + EAa)_V. \tag{50}$$

7. UNCONSTRAINED FINITE ELEMENT EQUATIONS

For simplicity we shall assume that all elastic moduli in **E** are *constant* over the element. Inserting the above assumptions into Π^d with the forcing potential (19), we obtain a quadratic algebraic form, which is fairly sparse on account of the conditions (45) and (49). Making this form stationary yields the finite element equations

$$
\begin{bmatrix}
j_{11}vE^{-1} & j_{12}vI & 0 & -P_r^T & j_{13}vI - P_u^T & -P_h^T & L^T \\
j_{12}vI & j_{22}vE & 0 & 0 & j_{23}vI & 0 & 0 \\
0 & 0 & j_{22}C_h & 0 & 0 & j_{23}R^T & 0 \\
-P_r & 0 & 0 & 0 & 0 & 0 & 0 \\
j_{13}vI - P_u & 0 & 0 & 0 & j_{33}vE & 0 & 0 \\
-P_h & 0 & j_{13}R & 0 & 0 & j_{33}K_{qh} & 0 \\
L & 0 & 0 & 0 & 0 & 0 & 0
\end{bmatrix}
\begin{Bmatrix} \bar{\sigma} \\ \bar{e} \\ a \\ q_r \\ \bar{e}^u \\ q_h \\ v \end{Bmatrix}
=
\begin{Bmatrix} 0 \\ 0 \\ 0 \\ f_{qr} \\ f_{qu} \\ f_{qh} \\ f_v \end{Bmatrix}. \tag{51}
$$

where

$$K_{qh} = (B_h^T E B_h)_V = K_{qh}^T, \quad C_h = (A^T E A)_V = C^T, \quad R = (B_h^T E A)_V,$$

$$L = [N_{dn}^T]_S, \quad P_r = [N_{rn}^T]_S, \quad P_c = [N_{cn}^T]_S, \quad P_h = [N_{hn}^T]_S, \tag{52}$$

$$f_r = (N_r^T b)_V, \quad f_q = (N_q^T b)_V, \quad f_h = (N_h^T b)_V, \quad f_v = [N_d^T \hat{t}]_{S_t}.$$

in which N_{dn} denotes the projection of shape functions N_d on the exterior normal **n**, and similarly for N_r, N_c and N_h. Coefficient matrix entries that do not depend on the j's come from the last boundary term in (19).

7.1 The P matrices

Application of the divergence theorem to the work of the mean stress on e^u yields

$$(\bar{\sigma}, e^u)_V = (\bar{\sigma}, \bar{e}^u + B_h q_h)_V = v\bar{\sigma}^T \bar{e}^u + \bar{\sigma}^T (B_h)_V q_h = v\bar{\sigma}^T \bar{e}^u \qquad (53)$$
$$= [\bar{\sigma}_n, \bar{u}]_S = [\bar{\sigma}_n, N_r q_r + N_c \bar{e}^u + N_h q_h]_S = \bar{\sigma}^T (P_r q_r + P_c \bar{e}^u + P_h q_h).$$

Hence $P_r = 0$, $P_c = vI$, $P_h = 0$, and the element equations simplify to

$$
\begin{bmatrix}
j_{11}vE^{-1} & j_{12}vI & 0 & 0 & (j_{13}-1)vI & 0 & L^T \\
j_{12}vI & j_{22}vE & 0 & 0 & j_{23}vI & 0 & 0 \\
0 & 0 & j_{22}C_h & 0 & 0 & j_{23}R^T & 0 \\
0 & 0 & 0 & 0 & 0 & 0 & 0 \\
(j_{13}-1)vI & j_{23}vI & 0 & 0 & j_{33}vE & 0 & 0 \\
0 & 0 & j_{23}R & 0 & 0 & j_{33}K_{qh} & 0 \\
L & 0 & 0 & 0 & 0 & 0 & 0
\end{bmatrix}
\begin{Bmatrix}
\bar{\sigma} \\ \bar{e} \\ a \\ q_r \\ \bar{e}^u \\ q_h \\ v
\end{Bmatrix}
=
\begin{Bmatrix}
0 \\ 0 \\ 0 \\ f_{qr} \\ f_{qu} \\ f_{qh} \\ f_v
\end{Bmatrix}. \qquad (54)
$$

The simplicity of the P matrices comes from the mean-plus-deviator expression (44) for e^u. If this decomposition is not enforced, $P_r = 0$ but $P_c = (B_c)_V$ and $P_h = (B_h)_V$.

8. KINEMATIC CONSTRAINTS

The "tricks" we shall consider here are *kinematic constraints* that play a key role in the development of high-performance FF and ANS elements. These are matrix relations between kinematic quantities that are established *independently* of the variational equations. Two types of relations will be studied.

8.1 Constraints Between Internal and Boundary Displacements

Relations linking the generalized coordinates q and the nodal connectors v were introduced by Bergan and coworkers in conjunction with the free formulation (FF) of finite elements [2-3]. For simplicity we shall assume that the number of freedoms in v and q is the same; removal of this restriction is discussed in [10]. By collocation of u at the element node points one easily establishes the relation

$$v = G_r q_r + G_c q_c + G_h q_h = Gq, \qquad (55)$$

where G is a square transformation matrix that will be assumed to be nonsingular. On inverting this relation we obtain

$$q = G^{-1} = Hv, \qquad \text{or} \qquad q = \begin{Bmatrix} q_r \\ \bar{e}^u \\ q_h \end{Bmatrix} = \begin{bmatrix} H_r \\ H_c \\ H_h \end{bmatrix} v. \qquad (56)$$

The following relations between L and the above submatrices hold as a consequence of the individual element test performed in §9.3:

$$L^T G_r = 0, \qquad L^T G_c = vI, \qquad vH_c = L^T. \qquad (57)$$

If the decomposition (44) is not enforced, the last two should read $L^T G_c = vB_c$, a relation first stated in [3], and $P_c H_c + P_h H_h = L^T$.

8.2 Constraints Between Assumed Higher Order Strains and Boundary Displacements

Constraints linking $\tilde{\mathbf{e}}_h$ to $\mathbf{v}$ are of fundamental importance in the assumed natural strain (ANS) formulation. The effect of these constraints in a variational framework is analyzed in some detail in [11-12]. Here we shall simply postulate the following relation between higher order strains and nodal displacements:

$$\mathbf{a} = \mathbf{Q}\mathbf{v}. \tag{58}$$

where $\mathbf{Q}$ is generally a rectangular matrix determined by collocation and/or interpolation. The individual element test in §9.3 requires that $\mathbf{Q}$ be orthogonal to $\mathbf{G}_r$ and $\mathbf{G}_c$:

$$\mathbf{Q}\mathbf{G}_r = \mathbf{0}, \qquad \mathbf{Q}\mathbf{G}_c = \mathbf{0}. \tag{59}$$

The constraint (58) still leaves the independently varied mean strain $\bar{\mathbf{e}}$ to be determined variationally.

9. VISIBLE STIFFNESS EQUATIONS

Enforcing the constraints $\mathbf{a} = \mathbf{Q}\mathbf{v}$, $\mathbf{q}_r = \mathbf{H}_r\mathbf{v}$, $\mathbf{q}_c = \mathbf{H}_c\mathbf{v} = \upsilon^{-1}\mathbf{L}^T\mathbf{v}$, $\mathbf{q}_h = \mathbf{H}_h\mathbf{v}$, through Lagrange multiplier vectors λ_a, λ_r, λ_c, and λ_h, respectively, we get the augmented finite element equations

$$
\begin{bmatrix}
j_{11}\upsilon\mathbf{E}^{-1} & j_{12}\upsilon\mathbf{I} & 0 & 0 & (j_{13}-1)\upsilon\mathbf{I} & 0 & 0 & 0 & 0 & 0 & \mathbf{L}^T \\
j_{12}\upsilon\mathbf{I} & j_{22}\upsilon\mathbf{E} & 0 & 0 & j_{23}\upsilon\mathbf{I} & 0 & 0 & 0 & 0 & 0 & 0 \\
0 & 0 & j_{22}\mathbf{C}_h & 0 & 0 & j_{23}\mathbf{R}^T & -\mathbf{I} & 0 & 0 & 0 & 0 \\
0 & 0 & 0 & 0 & 0 & 0 & 0 & -\mathbf{I} & 0 & 0 & 0 \\
(j_{13}-1)\upsilon\mathbf{I} & j_{23}\upsilon\mathbf{I} & 0 & 0 & j_{33}\upsilon\mathbf{E} & 0 & 0 & 0 & -\mathbf{I} & 0 & 0 \\
0 & 0 & j_{23}\mathbf{R} & 0 & 0 & j_{33}\mathbf{K}_{qh} & 0 & 0 & 0 & -\mathbf{I} & 0 \\
0 & 0 & -\mathbf{I} & 0 & 0 & 0 & 0 & 0 & 0 & 0 & \mathbf{Q} \\
0 & 0 & 0 & -\mathbf{I} & 0 & 0 & 0 & 0 & 0 & 0 & \mathbf{H}_r \\
0 & 0 & 0 & 0 & -\mathbf{I} & 0 & 0 & 0 & 0 & 0 & \upsilon^{-1}\mathbf{L}^T \\
0 & 0 & 0 & 0 & 0 & -\mathbf{I} & 0 & 0 & 0 & 0 & \mathbf{H}_h \\
\mathbf{L} & 0 & 0 & 0 & 0 & 0 & \mathbf{Q}^T & \mathbf{H}_r^T & \upsilon^{-1}\mathbf{L} & \mathbf{H}_h^T & 0
\end{bmatrix}
\begin{Bmatrix}
\bar{\sigma} \\
\bar{\mathbf{e}} \\
\mathbf{a} \\
\mathbf{q}_r \\
\bar{\mathbf{e}}^u \\
\mathbf{q}_h \\
\lambda_a \\
\lambda_r \\
\lambda_c \\
\lambda_h \\
\mathbf{v}
\end{Bmatrix}
=
\begin{Bmatrix}
0 \\
0 \\
0 \\
\mathbf{f}_{qr} \\
\mathbf{f}_{qu} \\
\mathbf{f}_{qh} \\
0 \\
0 \\
0 \\
0 \\
\mathbf{f}_v
\end{Bmatrix}. \tag{60}
$$

Condensation of all degrees of freedom except $\mathbf{v}$ yields the visible * element stiffness equations

$$\mathbf{K}\mathbf{v} = (\mathbf{K}_b + \mathbf{K}_h)\mathbf{v} = \mathbf{f} \tag{61}$$

where

$$\mathbf{K}_b = \upsilon^{-1}\mathbf{L}\mathbf{E}\mathbf{L}^T, \tag{62}$$

$$\mathbf{K}_h = j_{33}\mathbf{H}_h^T\mathbf{K}_{qh}\mathbf{H}_h + j_{23}(\mathbf{H}_h^T\mathbf{R}\mathbf{Q} + \mathbf{Q}^T\mathbf{R}^T\mathbf{H}_h) + j_{22}\mathbf{Q}^T\mathbf{C}_h\mathbf{Q}, \tag{63}$$

$$\mathbf{f} = \mathbf{f}_v + \mathbf{H}_r^T\mathbf{f}_{qr} + \upsilon^{-1}\mathbf{L}^T\mathbf{f}_{qc} + \mathbf{H}_h^T\mathbf{f}_{qh}. \tag{64}$$

Adopting the nomenclature of the free formulation [3], we shall call $\mathbf{K}_b$ the *basic stiffness matrix* and $\mathbf{K}_h$ the *higher order stiffness matrix*.

---

* The qualifier *visible* emphasizes that these are the stiffness equations other elements "see", and consequently are the only ones that matter insofar as computer implementation on a displacement-based finite element program.

9.1 Relation to Previous HP Element Formulations

If $\mathbf{J} = \mathbf{J}_\gamma$ of (33), $j_{33} = 1 - \gamma$, $j_{22} = j_{23} = 0$, and we recover the scaled *free formulation* stiffness equations studied in [5,7,9,10]:

$$\mathbf{K}_h = (1 - \gamma) \mathbf{H}_h^T \mathbf{K}_{qh} \mathbf{H}_h. \tag{65}$$

If we take $\mathbf{J} = \mathbf{J}_W$ of (32), $j_{22} = 1$, $j_{33} = j_{23} = 0$ and we obtain

$$\mathbf{K}_h = \mathbf{Q}^T \mathbf{C}_h \mathbf{Q}. \tag{66}$$

This is similar to the stiffness produced by the ANS hybrid variational formulation studied in [11-12], in which the potential P^t was used instead of P^d.

But the term with coefficient j_{23} in (63) is new. It may be viewed as coupling the FF and ANS formulations. It is not known at this time whether (61-64) represents the most general structure of the visible stiffness equations of HP elements.

9.2 Recovery of Element Fields

For simplicity suppose that the *body forces vanish* and so do $\mathbf{f}_{qr}$, $\mathbf{f}_{qc}$ and $\mathbf{f}_{qh}$. If $\mathbf{v}$ is known following a finite element solution of the assembled system, solving the equations (60) for the internal degrees of freedom yields

$$\bar{\mathbf{e}} = \upsilon^{-1} \mathbf{L}^T \mathbf{v}, \quad \bar{\sigma} = \mathbf{E}\bar{\mathbf{e}}, \quad \mathbf{a} = \mathbf{Q}\mathbf{v}, \quad \mathbf{q}_r = \mathbf{H}_r \mathbf{v}, \quad \bar{\mathbf{e}}^u = \bar{\mathbf{e}}, \quad \mathbf{q}_h = \mathbf{H}_h \mathbf{v},$$
$$\lambda_a = (j_{22}\mathbf{C}_h\mathbf{Q} + j_{33}\mathbf{R}^T\mathbf{H}_h)\mathbf{v}, \quad \lambda_r = 0, \quad \lambda_c = 0, \quad \lambda_h = (j_{23}\mathbf{R}\mathbf{Q} + j_{33}\mathbf{K}_{qh}\mathbf{H}_h)\mathbf{v}. \tag{67}$$

It is seen that the *mean* strains $\bar{\mathbf{e}}$, $\bar{\mathbf{e}}^u$ and $\bar{\mathbf{e}}^\sigma = \mathbf{E}^{-1}\bar{\sigma}$ agree, and so would the mean stresses. This is not the case, however, if the body forces are not zero. It is also worthwhile to mention that a nonzero Lagrange multiplier vector flags a deviation of the associated fields from the *variationally consistent* fields that would result on using the unconstrained FE equations (54) without "tricks".

9.3 The Individual Element Test

To conclude the paper, we investigate the conditions under which HP elements based on the foregoing general formulation pass the individual element test of Bergan and Hanssen [1-3]. To carry out the test, assume that the "free floating" element* under zero body forces is in a *constant stress state* σ_0, which of course is also the mean stress. Insert the following data in the left-hand side vector of (60):

$$\bar{\sigma} = \sigma_0 = \bar{\sigma}^u, \quad \bar{\mathbf{e}} = \mathbf{E}^{-1}\sigma_0, \quad \mathbf{a}_h = 0, \quad \mathbf{q}_r = arbitrary, \quad \mathbf{e}^u = \bar{\mathbf{e}}^u = \mathbf{E}^{-1}\bar{\sigma}_0, \quad \mathbf{q}_h = 0,$$
$$\lambda_a = 0, \quad \lambda_r = 0, \quad \lambda_c = 0, \quad \lambda_h = 0, \quad \mathbf{v} = \mathbf{G}_r\mathbf{q}_r + \mathbf{G}_c\bar{\mathbf{e}}^u = \mathbf{G}_r\mathbf{q}_r + \mathbf{G}_c\mathbf{E}^{-1}\sigma_0. \tag{68}$$

Premultiply by the coefficient matrix, and demand that all terms on the right-hand side vanish but for $\mathbf{f}_v = \mathbf{L}\sigma_0$. Then the orthogonality conditions in (57) and (59) emerge. This form of the patch test is very strong, and it may well be that relaxing circumstances can be found for specific problems such as shells.

---

* Mathematically, the entire element boundary is traction-specified, *i.e.*, $S \equiv S_t$.

10. CONCLUSIONS

The results of the present paper may be summarized as follows.

1. The classical variational principles of linear elasticity may be embedded in a parametrized matrix form.

2. The elasticity principles with assumed displacements are members of a three-parameter family.

3. Finite element assumptions for constructing high-performance elements may be conveniently investigated on this family.

4. Kinematic constraints established outside the realm of the variational principle may be incorporated through Lagrange multiplier adjunction.

5. The FF and ANS methods for constructing HP finite elements may be presented within this variational setting. In addition, combined forms emerge naturally from the general parametrized principle.

6. The satisfaction of the individual element test yields various orthogonality conditions that the kinematic constraints should satisfy *a priori*.

The construction of high performance elements based on a weighted mix of FF and ANS "ingredients" will be examined in sequel papers, and specific examples given to convey the power and flexibility of the present methods. .

Acknowledgements

References

1. P. G. Bergan and L. Hanssen, A new approach for deriving 'good' finite elements, MAFELAP II Conference, Brunel University, 1975, in *The Mathematics of Finite Elements and Applications – Volume II*, ed. by J. R. Whiteman, Academic Press, London, 1976

2. P. G. Bergan, Finite elements based on energy orthogonal functions, *Int. J. Num. Meth. Engrg.*, 15, 1980, pp. 1141–1555

3. P. G. Bergan and M. K. Nygård, Finite elements with increased freedom in choosing shape functions, *Int. J. Num. Meth. Engrg.*, 20, 1984, pp. 643–664

4. P. G. Bergan and X. Wang, Quadrilateral plate bending elements with shear deformations, *Computer & Structures*, 19, 1984, pp. 25–34

5. P. G. Bergan and C. A. Felippa, A triangular membrane element with rotational degrees of freedom, *Computer Methods in Applied Mechanics & Engineering*, 50, 1985, pp. 25–69

6. P. G. Bergan and M. K. Nygård, Nonlinear shell analysis using free formulation finite elements, *Proc. Europe-US Symposium on Finite Element Methods for Nonlinear Problems*, held at Trondheim, Norway, August 1985, Springer-Verlag, Berlin, 1985

7. C. A. Felippa and P. G. Bergan, A triangular plate bending element based on an energy-orthogonal free formulation, *Computer Methods in Applied Mechanics & Engineering*, 61, 1987, pp. 129–160

8. C. A. Felippa, Parametrized multifield variational principles in elasticity: I. Mixed functionals, *Communications in Applied Numerical Methods*, in press

9. C. A. Felippa, Parametrized multifield variational principles in elasticity: II. Hybrid functionals and the free formulation, *Communications in Applied Numerical Methods*, in press

10. C. A. Felippa, The extended free formulation of finite elements in linear elasticity, *Journal of Applied Mechanics*, in press

11. C. Militello and C. A. Felippa, A variational justification of the assumed natural strain formulation of finite elements: I. Variational principles, submitted to *Computers and Structures*

12. C. Militello and C. A. Felippa, A variational justification of the assumed natural strain formulation of finite elements: I. The four node C^0 plate element, submitted to *Computers and Structures*

13. J. T. Oden and J. N. Reddy, *Variational Methods in Theoretical Mechanics*, 2nd ed., Springer-Verlag, Berlin, 1983

14. T. H. H. Pian, Derivation of element stiffness matrices by assumed stress distributions, *AIAA Journal*, 2, 1964, pp. 1333–1336

15. T. H. H. Pian and P. Tong, Basis of finite element methods for solid continua, *Int. J. Numer. Meth. Engrg.*, 1, 1969, pp. 3–29

16. T. H. H. Pian, Finite element methods by variational principles with relaxed continuity requirements, in *Variational Methods in Engineering*, Vol. 1, ed. by C. A. Brebbia and H. Tottenham, Southampton University Press, Southhampton, U.K., 1973

THE ANDES FORMULATION OF FINITE ELEMENTS

SUMMARY. – ANDES is an acronym for *Assumed Natural DEviatoric Strains*. This is a brand new variant of the *Assumed Natural Strain* (ANS) formulation of finite elements, which has recently attracted attention as an effective method for constructing high-performance plate and shell elements for linear and nonlinear analysis. The ANDES formulation is based on an extended parametrized variational principle developed in recent publications. The key concept is that only the deviatoric part of the strains is assumed over the element whereas the mean strain part is discarded in favor of a constant stress assumption. Unlike conventional ANS elements, ANDES elements satisfy the individual element test (a stringent form of the patch test) *a priori* while retaining the favorable distortion-insensitivity properties of ANS elements. The first application of this new formulation has been the development of several Kirchhoff plate bending triangular elements with the standard nine degrees of freedom. Numerical experiments indicate that one of the ANDES element is relatively insensitive to distortion compared to previously derived high-performance plate-bending elements, while retaining accuracy for nondistorted elements..

INTRODUCTION

Despite almost three decades of work, plates and shells remain a important area of research in finite element methods. Challenging topics include:

1. The construction of high performance elements.

2. The modeling of composite and stiffened wall constructions.

3. The treatment of prestress, imperfections, nonlinear, dissipative and dynamic effects.

4. The development of practical error estimators and adaptive discretization methods.

5. The interaction with nonstructural components, for example external and internal fluids.

This paper reports progress in the first challenge, although it must be recognized that advances in this direction are shaped to a large extent by thinking of the others.

The main motivation behind our recent finite element work has been the construction of simple and efficient finite elements for plates and shells that are lock-free, rank sufficient and distortion insensitive, yield accurate answers for coarse meshes, fit naturally into displacement-based programs, and can be easily extended to nonlinear and dynamic problems. Elements that possess these attributes to some noticeable degree are collectively known as *high performance* or HP elements.

Over the past three decades investigators have resorted to many ingenious devices to construct HP elements. The most important ones are listed in Table 1. The underlying theme is that although the final product may look like a standard displacement model so as to fit naturally into existing finite element programs, *the conventional displacement formulation is aban-*

doned. (By "conventional" we mean the use of conforming displacement assumptions into the total potential energy principle.)

Table 1. Tools for Constructing HP Elements

Technique		Year introduced
1.	Incompatible shape functions	1961
2.	Patch test	1965
3.	Mixed and hybrid principles	1965
4.	Projectors	1967
5.	Selective reduced integration	1969
6.	Uniform reduced integration	1970
7.	Partial strain assumptions	1970
8.	Energy balancing	1974
9.	Directional integration	1978
10.	Limit differential equations	1982
11.	Free formulation	1984
12.	Assumed natural strains	1984

Box 1 Decomposition of the Element Stiffness Equations

Let K be the element stiffness matrix, v the visible element degrees of freedom (those degrees of freedom in common with other elements, also called the *connectors*) and f the corresponding element node forces. Then the element stiffness equations decompose as

$$K v = (K_b + K_h) v = f. \tag{1}$$

K_b and K_h are called the *basic* and *higher order* stiffness matrices, respectively. The basic stiffness matrix, which is usually rank deficient, is constructed for *convergence*. The higher order stiffness matrix is constructed for *stability* and (in more recent work) *accuracy*. A decomposition of this nature, which also holds at the assembly level, was first obtained by Bergan and Nygård (1984) in the derivation of the free formulation.

In the unified formulation presented by Felippa and Militello (1989, 1990a, 1990b) the following key properties of the decomposition (1) are derived.

1. K_b is *formulation independent* and is defined entirely by an assumed constant stress state working on element boundary displacements. No knowledge of the interior displacements is necessary (Box 2). The extension of this statement to C^0 plate and shell elements is not straightforward, however, and special considerations are necessary in order to obtain K_b for those elements.

2. K_h has the general form

$$K_h = j_{33} K_{h33} + j_{22} K_{h22} + j_{23} K_{h23}. \tag{2}$$

The three parameters j_{22}, j_{23} and j_{33} characterize the source variational principle in the following sense:

   (a) The FF is recovered if $j_{22} = j_{23} = 0$ and $j_{33} = 1 - \gamma$, where γ is a K_h scaling coefficient studied in Bergan and Felippa (1985) and Felippa and Bergan (1987). The original FF of Bergan and Nygård (1984) is obtained if $\gamma = 0$. The source variational principle is a one-parameter form that includes the potential energy and stress-displacement Reissner functionals as special cases; see Felippa (1989a, 1989b, 1989c).

   (b) The ANDES variant of ANS is recovered if $j_{22} = j_{23} = 0$ whereas $j_{22} = \alpha$ is a scaling parameter. The source variational principle is a one-parameter form that includes Reissner's stress-displacement and Hu-Washizu's functionals as special cases; see Felippa and Militello (1989, 1990a, 1990b).

   (c) If j_{23} is nonzero, the last term in (2) may be viewed as being produced by a FF/ANDES combination. Such a combination remains unexplored.

A Unified Variational Framework

Table 1 conveys the feeling of a bewildering array of tools. The question arises as to whether some of them are just facets of the same thing. Limited progress has been made in this regard. One notable advance in the 1970s has been the equivalence of reduced/selective integration and mixed methods achieved by Malkus and Hughes (1978).

The present work has benefited from the unplanned confluence of two unification efforts. An initial attempt to place the free formulation developed in Bergan and Hanssen (1976), Bergan (1980), Bergan and Nygård (1984), within the framework of parametrized hybrid variational principles was successful, as reported in Felippa (1989a, 1989b, 1989c). The free formulation in turn "dragged" incompatible shape functions, the patch test, and energy balancing into the scene. Concurrently a separate effort was carried out to set out the assumed natural strain (ANS) (as well as related techniques such as projection methods) in a mixed/hybrid variational framework as described in Militello and Felippa (1990a, 1990b). Comparison of the results led to the rather unexpected conclusion that

a parametrized variational framework was able to encompass ANS *and* the free formulation as well as some hitherto untried methods; see Felippa and Militello (1989, 1990a, 1990b).

The common theme emerging from this unification is that a wide class of HP elements can be constructed using two ingredients:

(1) A parametrized functional that contains all variational principles of elasticity as special cases.

(2) Additional assumptions (which are sometimes called "variational crimes" or "tricks") that can be placed on a variational setting through Lagrange multipliers.

As of this writing it is not known whether the "wide class" referred to above encompasses all HP elements or at least the most interesting ones. Some surprising coalescences, such as DKT and ANS bending elements, however, have emerged from this study.

Box 2 Construction of the Basic Stiffness Matrix K_b

Step B.1.   Assume a *constant* stress field, $\bar{\sigma}$, inside the element. (This should be the element stress field that holds in the convergence limit; for structural elements the assumption would be on *independent* stress resultants.) The associated boundary tractions are $\bar{\sigma}_n = \bar{\sigma}.n$, where n denotes the unit external normal on the element boundary S.

Step B.2.   Assume boundary displacements, d, over S. This field is described in terms of the *visible* element node displacements v (also called the *connectors*) as

$$d = N_d\, v, \tag{3}$$

where N_d is an array of boundary shape functions. The boundary motions (3) must satisfy interelement continuity (or at least, zero mean discontinuity so that no energy is lost at interfaces) and contain rigid-body and constant-strain motions exactly.

Step B.3.   Construct the "lumping matrix" L that consistently "lumps" the boundary tractions $\bar{\sigma}_n$ into element node forces, $\bar{f}$, conjugate to v in the virtual work sense. That is,

$$\bar{f} = \int_S N_{dn}\bar{\sigma}_n\, dS = L\bar{\sigma}. \tag{4}$$

In the above, N_{dn} are boundary-system projections of N_d conjugate to the surface tractions $\bar{\sigma}_n$.

Step B.4.   The basic stiffness matrix for a 3D element is

$$K_b = v^{-1}\, LEL^T, \tag{5}$$

where E is the stress-strain constitutive matrix of elastic moduli, which are assumed to be constant over the element, and $v = \int_V dV$ is the element volume measure.

For a Kirchhoff plate bending element, stresses, strains and stress-strain moduli become bending moments, curvatures and moment-curvature moduli, respectively, and the integration is performed over the element area A:

$$K_b = A^{-1}\, LDL^T, \tag{6}$$

where D is the matrix of moment-curvature moduli. Specific examples for L are provided in the 'Stiffness Matrix Computation' section.

The Assumed Natural Strain Formulation

The assumed natural strain (ANS) formulation of finite elements is a relatively new development. A restricted form of the assumed strain method (not involving natural strains) of the assumed strain method (not involving natural strains) was introduced by Willam (1969), who constructed a 4-node plane-stress element by assuming a constant shear strain independently of the direct strains and using a strain-displacement mixed variational principle. (The resulting element is identical to that derivable by selective one-point integration.) A different approach advocated by Ashwell (1974) and coworkers viewed "strain elements" as a convenient way to generate 'good' displacement fields by integration of appropriately assumed compatible strain fields. [In fact, this was the technique originally used by Turner *et al.* (1956) for deriving the constant-strain membrane triangle in their celebrated paper.]

These and other forms of assumed-strain techniques were overshadowed in the 1970s by developments in reduced and selective integration methods. The assumed strain approach in natural coordinates, however, has recently attracted substantial attention; particularly in view of its effectiveness in geometrically nonlinear analysis. Important contributions have been made by Bathe and Dvorkin (1985), Huang and Hinton (1986), Jang and Pinsky (1986), MacNeal (1978), Park (1986), Park and Stanley (1986), and Simo and Hughes (1986).

As noted above, the unification achieved by Felippa and Militello (1989, 1990a, 1990b) merges two HP element construction schemes: the free formulation (FF) of Bergan and Nygård (1984), and a variant of ANS called ANDES (acronym for Assumed Natural Deviatoric Strains) described in further detail below. The stiffness equations produced by the unified formulation enjoy the fundamental decomposition property summarized in Box 1.

In the ANDES variant of ANS, assumptions are made only on the *deviatoric* portion of the element strains, namely that portion that integrates to zero over each element. This assumption produces the higher order stiffness labeled K_{h22} in Box 1. The mean strains are left to be determined variationally and have no effect on the stiffness equations.

149

Box 3   Construction of K_h by the ANDES Formulation

Step H.1.   Select *reference lines* (in 2D elements) or *reference planes* (in 3D elements) where "natural straingage" locations are to be chosen. By appropriate interpolation express the element natural strains ϵ in terms of the "straingage readings" g at those locations:

$$\epsilon = A_\epsilon \, g, \tag{7}$$

where ϵ is a strain field in natural coordinates that must include all constant strain states. (For structural elements the term "strain" is to be interpreted in a generalized sense.)

Step H.2.   Relate the Cartesian strains e to the natural strains:

$$e = T\epsilon = TA_\epsilon g = Ag \tag{8}$$

at each point in the element. (If $e \equiv \epsilon$, or if it is possible to work throughout in natural coordinates, this step is skipped.)

Step H.3.   Relate the natural straingage readings g to the visible degrees of freedom

$$g = Qv, \tag{9}$$

where Q is a straingage-to-node displacement transformation matrix. Techniques for doing this vary from element to element and it is difficult to state rules that apply to every situation. In the elements derived here Q is constructed by direct interpolation over the reference lines. (In general there is no unique internal displacement field u whose symmetric gradient is e or ϵ, so this step cannot be done by simply integrating the strain field over the element and collocating u at the nodes.)

Step H.4.   Split the Cartesian strain field into mean (volume-averaged) and deviatoric strains:

$$e = \bar{e} + e_d = (\overline{A} + A_d)\, g, \tag{10}$$

where $\overline{A} = \int_V TA_\epsilon \, dV / v$, and $e_d = A_d\, g$ has mean zero value over V. This step may also be carried out on the natural strains if T is constant, as is the case for the elements here.

Step H.5.   The higher-order stiffness matrix is given by

$$K_h = \alpha Q^T K_d Q, \qquad \text{with} \qquad K_d = \int_V A_d^T EA_d \, dV, \tag{11}$$

where $\alpha = j_{22} > 0$ is a scaling coefficient (see Box 1).

It is often convenient to combine the product of A and Q into a single strain-displacement matrix called (as usual) B, which splits into $\overline{B}$ and B_d:

$$e = AQv = (\overline{A} + A_d)Qv = (\overline{B} + B_d)v = B\,v, \tag{12}$$

in which case

$$K_h = \int_V B_d^T EB_d \, dV. \tag{13}$$

The notation $B_\epsilon = A_\epsilon Q$ is also used in the sequel.

150

Box 4   Construction of K by the Conventional ANS Formulation

Steps S.1 to S.3.   Identical to the first three steps *H.1* through *H.3*, in Box 3. The fourth step: strain splitting, is omitted.

Step S.4.   The element stiffness matrix is given by

$$K = Q^T K_a Q, \qquad \text{with} \qquad K_a = \int_V A^T EA \, dV. \tag{14}$$

or, if $B = AQ$ is readily available

$$K = \int_V B^T EB \, dV. \tag{15}$$

In general this stiffness matrix does not pass the *individual element test* of Bergan and Hanssen (1976), which is a strong form of the patch test that demands pairwise cancellation of node forces between adjacent elements subjected to constant stress states. For this to happen, K must admit the decomposition

$$K = K_b + K_h = v^{-1} LEL^T + K_h, \tag{16}$$

where L is a force-lumping matrix derivable as per Box 2 and K_h is orthogonal to the rigid body and constant strain test motions. In other words, the ANS element must coalesce with the ANDES formulation with $\alpha = 1$. The equivalence may be checked by requiring that

$$\overline{B} = \overline{A}Q = v^{-1} L^T, \tag{17}$$

where $\overline{A}$ is the mean part of A (see Box 3). At the present there are no known general techniques for explicitly constructing strain fields that satisfy these conditions *a priori*.

If the patch test is not satisfied, one should switch to the ANDES formulation by replacing the basic stiffness constructed from constant strain, namely $v\overline{B}^T E\overline{B}$, with one constructed from constant stress as in Box 2.

The basic steps in the construction of K_b and K_h for a general three-dimensional element are summarized in Boxes 2 and 3, respectively. For justification of these "recipes" the reader is referred to Felippa and Militello (1989, 1990a, 1990b).

The derivation of the element stiffness matrix for *conventional* ANS elements is summarized in Box 4. In this case there is no splitting into basic and higher order parts.

This paper reports briefly (because of space constraints) on the construction and testing of the first ANDES elements. These are Kirchhoff plate-bending triangular elements with the standard 9 degrees of freedom (one displacement and two rotations at each corner). This choice is made because of the following reasons:

1. High-performance three-node triangular plate bending elements, whether based on Kirchhoff or Reissner-Mindlin mathematical models, have not been previously obtained through the ANS formulation. [Although the DKT element presented by Batoz, Bathe and Ho (1980) and Batoz (1982) qualifies as high-performance and is in fact an ANS element as shown later, it has not been derived as such.] The situation is in sharp contrast to four-node quadrilateral bending elements, for which HP elements have been constructed through a greater variety of tools;

see *e.g.* Bathe and Dvorkin (1985), Crisfield (1983), Hughes and Tezduyar (1981), Kang (1986), MacNeal (1978) and Park and Stanley (1986).

2. High performance elements of this type have been obtained through the FF and ancestors of the FF as described in Bergan and Hanssen (1976), Bergan (1980), Bergan and Nygård (1984) and Felippa and Bergan (1987). These elements are considered among the best performers available. It is therefore intriguing whether elements based on the ANDES variant can match or exceed this performance.

THE TRIANGULAR PLATE ELEMENT

Geometric Relations

We consider here an individual triangle with *straight sides*. Its geometry is completely defined by the location of its three corners, which are labeled 1,2,3, traversed counterclockwise. The element is referred to a local Cartesian system (x, y) which is usually taken with origin at the centroid 0, whence the corner coordinates x_i, y_i satisfy the relations

$$x_1 + x_2 + x_3 = 0, \qquad y_1 + y_2 + y_3 = 0. \tag{18}$$

Coordinate differences are abbreviated by writing $x_{ij} = x_i - x_j$, and $y_{ij} = y_i - y_j$. The signed triangle area A is given by

$$2A = \begin{vmatrix} 1 & 1 & 1 \\ x_1 & x_2 & x_3 \\ y_1 & y_2 & y_3 \end{vmatrix} = x_{21}y_{31} - x_{31}y_{21} \qquad (19)$$

$$= x_{32}y_{12} - x_{12}y_{32} = x_{13}y_{23} - x_{23}y_{13},$$

and we require that $A > 0$. We shall make use of dimensionless triangular coordinates ζ_1, ζ_2 and ζ_3, linked by $\zeta_1 + \zeta_2 + \zeta_3 = 1$. The following well known relations between the triangular and Cartesian coordinates of a straight-sided triangle are noted for further use:

$$x = x_1\zeta_1 + x_2\zeta_2 + x_3\zeta_3, \quad y = y_1\zeta_1 + y_2\zeta_2 + y_3\zeta_3, \quad (20)$$

$$\zeta_i = \frac{1}{2A}\left[x_iy_k - x_ky_j + (x - x_0)y_{jk} + (y - y_0)x_{kj}\right], \quad (21)$$

in which i, j and k denote positive cyclic permutations of $1, 2$ and 3; for example, $i = 2, j = 3, k = 1$. (If the origin is taken at the centroid, $x_0 = y_0 = 0$.) It follows that

$$2A\frac{\partial\zeta_1}{\partial x} = y_{23}, \quad 2A\frac{\partial\zeta_2}{\partial x} = y_{31}, \quad 2A\frac{\partial\zeta_3}{\partial x} = y_{12},$$

$$2A\frac{\partial\zeta_1}{\partial y} = x_{32}, \quad 2A\frac{\partial\zeta_2}{\partial y} = x_{13}, \quad 2A\frac{\partial\zeta_3}{\partial y} = x_{21}. \quad (22)$$

Other intrinsic dimensions and ratios of use in future derivations are

$$\ell_{ij} = \ell_{ji} = \sqrt{x_{ij}^2 + y_{ij}^2}, \quad c_{ij} = x_{ji}/\ell_{ij}, \quad s_{ij} = y_{ji}/\ell_{ij},$$

$$a_k = 2A/\ell_{ij}, \quad b_{ij} = (x_{ij}x_{ik} + y_{ji}y_{ki})/\ell_{ij} = \ell_{ij} - b_{ji},$$

$$\lambda_{ij} = b_{ij}/\ell_{ij} = (x_{ij}x_{ik} + y_{ji}y_{ki})/(x_{ij}^2 + y_{ij}^2),$$

$$\lambda_{ji} = 1 - \lambda_{ij} = b_{ji}/\ell_{ij}. \quad (23)$$

Here $\ell_{ij} = \ell_{ji}$ is the length of side $i-j$ and c_{ij} and s_{ij} the cosine and sine, respectively, of angle $(i \rightarrow j, x)$. Furthermore b_{ij} and b_{ji} are the projections of sides $i-k$ and $k-j$, respectively, onto $i-j$; λ_{ij} and λ_{ji} being the corresponding projection ratios. On each side $i-j$, define the dimensionless natural coordinates μ_{ij} as varying from 0 at i to 1 at j. The coordinate μ_{ij} of a point not on the side is that of its projection on $i-j$. Obviously

$$\frac{\partial x}{\partial\mu_{ij}} = x_{ji}, \quad \frac{\partial y}{\partial\mu_{ij}} = y_{ji}. \quad (24)$$

Displacements, Rotations, Curvatures

As we are dealing with a Kirchhoff element, its displacement field is completely defined by the transverse displacement $w(x, y) \equiv w(\zeta_1, \zeta_2, \zeta_3)$, positive upwards. In the present section we assume that w is unique and known inside the element; this assumption is relaxed later. The midplane (covariant) rotations about x and y are $\theta_x = \partial w/\partial y$ and $\theta_y = -\partial w/\partial x$, respectively. Along side $i-j$ with tangential direction t and

external-normal n the tangential and normal rotations are defined as

$$\theta_n = \frac{\partial w}{\partial t} = \theta_x s_{ij} - \theta_y c_{ij},$$

$$\theta_t = -\frac{\partial w}{\partial n} = \theta_x c_{ij} + \theta_y s_{ij}. \quad (25)$$

The visible degrees of freedom of the element collected in $\mathbf{v}$ (see Boxes 2–3) are

$$\mathbf{v}^T = [\, w_1 \; \theta_{x1} \; \theta_{y1} \; w_2 \; \theta_{x2} \; \theta_{y2} \; w_3 \; \theta_{x3} \; \theta_{y3} \,]. \quad (26)$$

The Cartesian second derivatives are given by

$$\frac{\partial^2 w}{\partial x^2} = \frac{\partial^2 w}{\partial\zeta_i\partial\zeta_j}\frac{\partial\zeta_i}{\partial x}\frac{\partial\zeta_j}{\partial x} + \frac{\partial w}{\partial\zeta_i}\frac{\partial^2\zeta_i}{\partial x^2} = \frac{1}{4A^2}\frac{\partial^2 w}{\partial\zeta_i\partial\zeta_j}y_{jk}y_{ki},$$

$$\frac{\partial^2 w}{\partial x\partial y} = \frac{\partial^2 w}{\partial\zeta_i\partial\zeta_j}\frac{\partial\zeta_i}{\partial x}\frac{\partial\zeta_j}{\partial y} + \frac{\partial w}{\partial\zeta_i}\frac{\partial^2\zeta_i}{\partial x\partial y} = \frac{1}{4A^2}\frac{\partial^2 w}{\partial\zeta_i\partial\zeta_j}y_{jk}x_{ik},$$

$$\frac{\partial^2 w}{\partial y^2} = \frac{\partial^2 w}{\partial\zeta_i\partial\zeta_j}\frac{\partial\zeta_i}{\partial y}\frac{\partial\zeta_j}{\partial y} + \frac{\partial w}{\partial\zeta_i}\frac{\partial^2\zeta_i}{\partial y^2} = \frac{1}{4A^2}\frac{\partial^2 w}{\partial\zeta_i\partial\zeta_j}x_{kj}x_{ik}, \quad (27)$$

since $\partial^2\zeta_i^2/\partial x^2$, $\partial^2\zeta_i^2/\partial x\partial y$ and $\partial^2\zeta_i^2/\partial y^2$ vanish on a straight-sided triangle, cf. Eq. (21).

Natural Curvatures

The second derivatives of w with respect to the dimensionless side directions defined above will be called the *natural curvatures* and denoted by $\chi_{ij} = \partial^2 w/\partial\mu_{ij}^2$. Note that these curvatures have dimensions of displacement. The natural curvatures can be related to the Cartesian plate curvatures $\kappa_{xx} = \partial^2 w/\partial x^2$, $\kappa_{yy} = \partial^2 w/\partial y^2$ and $\kappa_{xy} = 2\partial^2 w/\partial x\partial y$, by chain-rule application of Eqs. (24):

$$\begin{Bmatrix} \chi_{12} \\ \chi_{23} \\ \chi_{31} \end{Bmatrix} = \begin{Bmatrix} \dfrac{\partial^2 w}{\partial\mu_{12}^2} \\[6pt] \dfrac{\partial^2 w}{\partial\mu_{23}^2} \\[6pt] \dfrac{\partial^2 w}{\partial\mu_{31}^2} \end{Bmatrix} = \begin{bmatrix} x_{21}^2 & y_{21}^2 & x_{21}y_{21} \\ x_{32}^2 & y_{32}^2 & x_{32}y_{32} \\ x_{13}^2 & y_{13}^2 & x_{13}y_{13} \end{bmatrix} \begin{Bmatrix} \dfrac{\partial^2 w}{\partial x^2} \\[6pt] \dfrac{\partial^2 w}{\partial y^2} \\[6pt] 2\dfrac{\partial^2 w}{\partial x\partial y} \end{Bmatrix}. \quad (28)$$

or $\chi = \mathbf{T}^{-1}\kappa$. The inverse of this relation is

$$\begin{Bmatrix} \dfrac{\partial^2 w}{\partial x^2} \\[6pt] \dfrac{\partial^2 w}{\partial y^2} \\[6pt] 2\dfrac{\partial^2 w}{\partial x\partial y} \end{Bmatrix} = \frac{1}{4A^2} \begin{bmatrix} y_{23}y_{13} & y_{31}y_{21} & y_{12}y_{32} \\ x_{23}x_{13} & x_{31}x_{21} & x_{12}x_{32} \\ y_{23}x_{31} + x_{32}y_{13} & y_{31}x_{12} + x_{13}y_{21} & y_{12}x_{23} + x_{21}y_{32} \end{bmatrix} \begin{Bmatrix} \dfrac{\partial^2 w}{\partial\mu_{12}^2} \\[6pt] \dfrac{\partial^2 w}{\partial\mu_{23}^2} \\[6pt] \dfrac{\partial^2 w}{\partial\mu_{31}^2} \end{Bmatrix}. \quad (29)$$

or, in compact matrix notation

$$\kappa = T\chi. \tag{30}$$

At this point we relax the requirement that the curvatures be derivable from a displacement field w; consequently the partial derivative notation will be discontinued. However, the foregoing transformations will be assumed to hold even if the curvature fields κ and χ are not derivable from w.

DIRECT CURVATURE INTERPOLATION

The Straingage Readings

ANS and ANDES plate bending elements are based on direct interpolation of natural curvatures. All elements discussed here adopt the three triangle sides as the *reference lines* defined in Box 3. The natural curvatures are assumed to vary linearly over each reference line, an assumption which is obviously consistent with cubic beam-like variations of w over the sides. A linear variation on each side is determined by two straingage sample points, which we chose to be at the corners.

Over each triangle side chose the isoparametric coordinates ξ_{ij} that vary from -1 at corner i to $+1$ at corner j. These are related to the natural μ_{ij} coordinates by $\xi_{ij} = 2\mu_{ij} - 1$. The Hermite interpolation of w over $i-j$ is

$$w = \tfrac{1}{4}[(1-\xi_{ij})^2(2+\xi_{ij}) \quad \tfrac{1}{2}\ell_{ij}(1-\xi_{ij})^2(1+\xi_{ij})$$
$$(1+\xi_{ij})^2(2-\xi_{ij}) \quad -\tfrac{1}{2}\ell_{ij}(1+\xi_{ij})^2(1-\xi_{ij})]\, v_{ij} \tag{31}$$

where $v_{ij} = \{\, w_i \quad \theta_{ni} \quad w_j \quad \theta_{nj}\,\}^T$ and θ_n denotes the rotation about the external normal n on side ij. The natural curvature over side ij is given by

$$\chi_{ij} = \frac{\partial^2 w}{\partial \mu_{ij}^2} = [\,6\xi_{ij}\ \ 3\ell_{ij}(\xi_{ij}-1)\ \ -6\xi_{ij}\ \ 3\ell_{ij}(\xi_{ij}+1)\,]\, v_{ij}, \tag{32}$$

Evaluating these relations at the nodes by setting $\xi_{ij} = \pm 1$ and converting normal rotations to x-y rotations through (25), we build the transformation

$$
\begin{Bmatrix} \chi_{12}|_1 \\ \chi_{12}|_2 \\ \chi_{23}|_2 \\ \chi_{23}|_3 \\ \chi_{31}|_3 \\ \chi_{31}|_1 \end{Bmatrix} =
\begin{bmatrix}
-6 & -4y_{21} & 4x_{21} & 6 & -2y_{21} \\
6 & 2y_{21} & -2x_{21} & -6 & 4y_{21} \\
0 & 0 & 0 & -6 & -4y_{32} \\
0 & 0 & 0 & 6 & 2y_{32} \\
6 & -2y_{13} & 2x_{13} & 0 & 0 \\
-6 & 4y_{13} & -4x_{13} & 0 & 0
\end{bmatrix}
$$

$$
\begin{bmatrix}
2x_{21} & 0 & 0 & 0 \\
-4x_{21} & 0 & 0 & 0 \\
4x_{32} & 6 & -2y_{32} & 2x_{32} \\
-2x_{32} & -6 & 4y_{32} & -4x_{32} \\
0 & -6 & -4y_{13} & 4x_{13} \\
0 & 6 & 2y_{13} & -2x_{13}
\end{bmatrix}
\begin{Bmatrix} w_1 \\ \theta_{x1} \\ \theta_{y1} \\ w_2 \\ \theta_{x2} \\ \theta_{y2} \\ w_3 \\ \theta_{x3} \\ \theta_{y3} \end{Bmatrix}. \tag{33}
$$

The left hand side is the natural straingage reading vector called g in Box 3 and thus we can express (33) as

$$g = Qv. \tag{34}$$

This relation holds for all elements discussed here.

The six gage readings collected in g provide curvatures along the three triangle side directions at two corners. But *nine* values are needed to recover the complete curvature field over the element. The three additional values are the natural curvatures χ_{23}, χ_{31} and χ_{12} at corners 1, 2 and 3, respectively. Three possibilities for the missing values are discussed below.

The Average-Curvature Rule

To each corner k assign the average natural curvature χ_{ij} of the opposite side. This average is given by (34) evaluated at $\xi_{ij} = 0$. For example

$$\chi_{12}|_3 = \tfrac{1}{2}(\chi_{12}|_1 + \chi_{12}|_2) = y_{21}(\theta_{x2} - \theta_{x1}) + x_{12}(\theta_{y2} - \theta_{y1}). \tag{35}$$

The natural curvature now can be interpolated linearly over the triangle:

$$
\begin{aligned}
\chi_{12} &= \chi_{12}|_1\, \zeta_1 + \chi_{12}|_2\, \zeta_2 + \chi_{12}|_3\, \zeta_3 \\
&= \chi_{12}|_1\, (\zeta_1 + \tfrac{1}{2}\zeta_3) + \chi_{12}|_2\, (\zeta_2 + \tfrac{1}{2}\zeta_3).
\end{aligned} \tag{36}
$$

It is readily verified that under this rule the natural curvature χ_{12} is constant over lines parallel to the triangle *median* that passes through node 3. Formulas for the other curvatures follow by cyclic permutation, from which we construct the matrix relation

$$
\begin{Bmatrix} \chi_{12} \\ \chi_{23} \\ \chi_{31} \end{Bmatrix} =
\begin{bmatrix}
\zeta_1 + \tfrac{1}{2}\zeta_3 & \zeta_2 + \tfrac{1}{2}\zeta_3 & 0 \\
0 & 0 & \zeta_2 + \tfrac{1}{2}\zeta_1 \\
0 & 0 & 0
\end{bmatrix}
$$

$$
\begin{bmatrix}
0 & 0 & 0 \\
\zeta_3 + \tfrac{1}{2}\zeta_1 & 0 & 0 \\
0 & \zeta_3 + \tfrac{1}{2}\zeta_2 & \zeta_1 + \tfrac{1}{2}\zeta_2
\end{bmatrix} g
$$

$$
=
\begin{bmatrix}
6\zeta_{21} & (3\zeta_{21}-1)y_{21} & (3\zeta_{12}+1)x_{21} \\
0 & 0 & 0 \\
6\zeta_{31} & (3\zeta_{13}+1)y_{13} & (3\zeta_{31}-1)y_{13}
\end{bmatrix}
$$

$$
\begin{bmatrix}
6\zeta_{12} & (3\zeta_{21}+1)y_{21} & (3\zeta_{12}-1)y_{21} \\
6\zeta_{32} & (3\zeta_{32}-1)y_{32} & (3\zeta_{23}+1)x_{32} \\
0 & 0 & 0 \\
0 & 0 & 0 \\
6\zeta_{23} & (3\zeta_{32}+1)y_{32} & (3\zeta_{23}-1)y_{32} \\
6\zeta_{13} & (3\zeta_{13}-1)y_{13} & (3\zeta_{31}+1)x_{13}
\end{bmatrix} v, \tag{37}
$$

in which $\zeta_{12} = \zeta_1 - \zeta_2$, etc.

In the notation of Box 3,

$$\chi = \mathbf{A}_{\chi a}\mathbf{g} = \mathbf{A}_{\chi a}\mathbf{Q}\mathbf{v} = \mathbf{B}_{\chi a}\mathbf{v}. \qquad (38)$$

where subscript a identifies the "averaging" rule (35). Since the natural curvatures vary linearly over the triangle, their mean values are obtained by evaluating (37) at the centroid $\zeta_1 = \zeta_2 = \zeta_3 = 1/3$:

$$\overline{\chi} = \begin{Bmatrix} \overline{\chi}_{12} \\ \overline{\chi}_{23} \\ \overline{\chi}_{31} \end{Bmatrix} = \begin{bmatrix} 0 & -y_{21} & x_{21} & 0 & y_{21} & -x_{21} \\ 0 & 0 & 0 & 0 & -y_{32} & x_{32} \\ 0 & y_{13} & -x_{13} & 0 & 0 & 0 \end{bmatrix}$$

$$\begin{bmatrix} 0 & 0 & 0 \\ 0 & y_{32} & -x_{32} \\ 0 & -y_{13} & x_{13} \end{bmatrix}\mathbf{v} = \overline{\mathbf{B}}_{\chi a}\mathbf{v}. \qquad (39)$$

Finally, the Cartesian curvatures are given by

$$\kappa = \mathbf{T}\mathbf{B}_{\chi a}\mathbf{v} = \mathbf{B}_a\mathbf{v}, \qquad (40)$$

An explicit expression of these relations is easily obtained, but not required in what follows; however, that of the mean Cartesian curvatures $\overline{\kappa} = \mathbf{T}\overline{\mathbf{B}}_{\chi a}\mathbf{v} = \overline{\mathbf{B}}_a\mathbf{v}$ (a relation valid because $\mathbf{T}$ is constant over the triangle) is enlightening:

$$\overline{\kappa} = \begin{Bmatrix} \overline{\kappa}_{xx} \\ \overline{\kappa}_{yy} \\ 2\overline{\kappa}_{xy} \end{Bmatrix} = \frac{1}{2A}\begin{bmatrix} 0 & 0 & y_{32} & 0 & 0 & y_{13} \\ 0 & x_{32} & 0 & 0 & x_{13} & 0 \\ 0 & y_{23} & x_{23} & 0 & y_{31} & x_{31} \end{bmatrix}$$

$$\begin{bmatrix} 0 & 0 & y_{21} \\ 0 & x_{21} & 0 \\ 0 & y_{12} & x_{12} \end{bmatrix}\mathbf{v} = \overline{\mathbf{B}}_a\mathbf{v}. \qquad (41)$$

The Projection Rule

To each corner k assign the natural curvature χ_{ij} of its projection onto the opposite side. This results in χ_{ij} being constant along lines *normal* to side ij. For equilateral triangles this agrees with the averaging rule, but not otherwise. The underlying motivation is to make the element insensitive to bad aspect ratios in cylindrical bending along side directions.

To illustrate the application of this rule consider side 1–2. For node 3 take

$$\chi_{12}|_3 = \left.\frac{\partial^2 w}{\partial\mu_{12}^2}\right|_3 = \lambda_{12}\,\chi_{12}|_1 + \lambda_{21}\,\chi_{12}|_2, \qquad (42)$$

where λ_{12} and λ_{21} are defined in Eqs. (23). Proceeding in the same manner along the other sides we construct the matrix relation

$$\begin{Bmatrix} \chi_{12} \\ \chi_{23} \\ \chi_{31} \end{Bmatrix} = \begin{bmatrix} \zeta_1 + \lambda_{12}\zeta_3 & \zeta_2 + \lambda_{21}\zeta_3 & 0 \\ 0 & 0 & \zeta_2 + \lambda_{23}\zeta_1 \\ 0 & 0 & 0 \end{bmatrix}$$

$$\begin{bmatrix} 0 & 0 & 0 \\ \zeta_3 + \lambda_{32}\zeta_1 & 0 & 0 \\ 0 & \zeta_3 + \lambda_{31}\zeta_2 & \zeta_1 + \lambda_{13}\zeta_2 \end{bmatrix}\mathbf{g}, \qquad (43)$$

or

$$\chi = \mathbf{A}_{\chi p}\,\mathbf{g}, \qquad \kappa = \mathbf{T}\mathbf{A}_{\chi p}\,\mathbf{g}, \qquad (44)$$

where subscript p identifies the "projection" rule. As in the preceding rule, since $\mathbf{T}$ is constant we can do the strain-splitting step of Box 3 directly on the natural curvatures by evaluating at the centroid:

$$\mathbf{A}_{\chi p} = (\overline{\mathbf{A}}_{\chi p} + \mathbf{A}_{\chi dp}) = \begin{bmatrix} \frac{1}{3}(1 + \lambda_{12}) & \frac{1}{3}(1 + \lambda_{21}) \\ 0 & 0 \\ 0 & 0 \end{bmatrix}$$

$$\begin{bmatrix} 0 & 0 & 0 & 0 \\ \frac{1}{3}(1 + \lambda_{23}) & \frac{1}{3}(1 + \lambda_{32}) & 0 & 0 \\ 0 & 0 & \frac{1}{3}(1 + \lambda_{31}) & \frac{1}{3}(1 + \lambda_{13}) \end{bmatrix}$$

$$= \begin{bmatrix} \zeta_{10} + \lambda_{12}\zeta_{30} & \zeta_{20} + \lambda_{21}\zeta_{30} & 0 \\ 0 & 0 & \zeta_{20} + \lambda_{23}\zeta_{10} \\ 0 & 0 & 0 \end{bmatrix}$$

$$\begin{bmatrix} 0 & 0 & 0 \\ \zeta_{30} + \lambda_{32}\zeta_{10} & 0 & 0 \\ 0 & \zeta_{30} + \lambda_{31}\zeta_{20} & \zeta_{10} + \lambda_{13}\zeta_{20} \end{bmatrix}. \qquad (45)$$

in which $\zeta_{i0} = \zeta_i - \frac{1}{3}$. Then

$$\mathbf{B}_p = \mathbf{T}\mathbf{A}_{\chi p}\mathbf{Q} = \mathbf{T}(\overline{\mathbf{A}}_{\chi p} + \mathbf{A}_{dp})\mathbf{Q} = \overline{\mathbf{B}}_p + \mathbf{B}_{dp}. \qquad (46)$$

The explicit expression of these matrices is not revealing. For the construction of the stiffness matrix it is better to leave (46) in product form and to carry out the operations with a symbolic algebra package such as MACSYMA. The explicit expression of $\mathbf{K}_{hp}$ obtained in this manner is presented in Appendix B of Militello and Felippa (1989). Observe that if all λ coefficients are $\frac{1}{2}$, which happens for the equilateral triangle, the expressions reduce to those of the averaging rule.

The 'Sliding Beam' Rule

This is a refinement of the average-curvature rule. Consider a fictitious beam parallel to side $i - j$ sliding towards corner k. The end displacements and rotation of this beam are obtained by interpolating w cubically, θ_n quadratically, and θ_t linearly, along sides i–k and j–k. Compute the mean natural curvature of this beam and assign to node k the limit as the beam reaches that corner.

The calculations can be simplified if we observe that the mean curvature of the sliding beam varies linearly as it moves from i–j, where it coincides with (35), to corner k. At $1/3$ of the way this mean is the natural centroidal curvature, which can then be readily extrapolated to k. These centroidal curvatures are given by $\overline{\chi} = \overline{\mathbf{B}}_{\chi s}\mathbf{v}$, where subscript s identifies the 'sliding' rule. A symbolic calculation yields the explicit form

$$\overline{\mathbf{B}}_{\chi s}^T = \begin{bmatrix} 2\lambda_{13} & -2(\lambda_{21} + \lambda_{31}) & 2\lambda_{12} \\ a_2 c_{13} & a_3 c_{21} + a_2 c_{13} & a_3 c_{21} \\ a_2 s_{13} & a_3 s_{21} + a_2 s_{13} & a_3 s_{21} \\ 2\lambda_{23} & 2\lambda_{21} & -2(\lambda_{12} + \lambda_{32}) \\ a_1 c_{32} & a_3 c_{21} & a_1 c_{32} + a_3 c_{21} \\ a_1 s_{32} & a_3 s_{21} & a_1 s_{32} + a_3 s_{21} \\ -2(\lambda_{13} + \lambda_{23}) & 2\lambda_{31} & 2\lambda_{32} \\ a_2 c_{13} + a_1 c_{32} & a_2 c_{13} & a_1 c_{32} \\ a_2 s_{13} + a_1 s_{32} & a_2 s_{13} & a_1 s_{32} \end{bmatrix}. \qquad (47)$$

154

where a_i, c_{ij} and s_{ij} are defined in Eqs. (23). Extrapolating this equation to the opposite corners and linearly

interpolating over the triangle we construct the relation $\chi = B_{\chi s} v$, with

$$B_{\chi s}^T = \begin{bmatrix} 6(-\zeta_1 + \zeta_2 + \lambda_{13}\zeta_3) & -6(\lambda_{21} + \lambda_{31})\zeta_1 & 6(\zeta_3 - \zeta_1 + \lambda_{12}\zeta_2) \\ 2y_{21}(1 - 3\zeta_1) + 3a_2 c_{13}\zeta_3 & (3a_3 c_{21} + 3a_2 c_{13})\zeta_1 & 2y_{13}(3\zeta_1 - 1) + 3a_3 c_{21}\zeta_2 \\ 2x_{21}(3\zeta_1 - 1) + 3a_2 s_{13}\zeta_3 & (3a_3 s_{21} + 3a_2 s_{13})\zeta_1 & 2x_{13}(1 - 3\zeta_1) + 3a_3 s_{21}\zeta_2 \\ 6(\zeta_1 - \zeta_2 + \lambda_{23}\zeta_3) & 6(-\zeta_2 + \zeta_3 + \lambda_{21}\zeta_1) & -6(\lambda_{12} + \lambda_{32})\zeta_2 \\ 2y_{21}(3\zeta_2 - 1) + 3a_1 c_{32}\zeta_3 & 2y_{32}(1 - 3\zeta_2) + 3a_3 c_{21}\zeta_1 & (3a_1 c_{32} + 3a_3 c_{21})\zeta_2 \\ 2x_{21}(1 - 3\zeta_2) + 3a_1 s_{32}\zeta_3 & 2x_{32}(3\zeta_2 - 1) + 3a_3 s_{21}\zeta_1 & (3a_1 s_{32} + 3a_3 s_{21})\zeta_2 \\ -6(\lambda_{23} + \lambda_{13})\zeta_3 & 6(\zeta_2 - \zeta_3 + \lambda_{31}\zeta_1) & 6(-\zeta_3 + \zeta_1 + \lambda_{32}\zeta_2) \\ (3a_2 c_{13} + 3a_1 c_{32})\zeta_3 & 2y_{32}(3\zeta_3 - 1) + 3a_2 c_{13}\zeta_1 & 2y_{13}(1 - 3\zeta_3) + 3a_1 c_{32}\zeta_2 \\ (3a_2 s_{13} + 3a_1 s_{32})\zeta_3 & 2x_{32}(1 - 3\zeta_3) + 3a_2 s_{13}\zeta_1 & 2x_{13}(3\zeta_3 - 1) + 3a_1 s_{32}\zeta_2 \end{bmatrix}. \tag{48}$$

It should be noted that $A\chi$ and Q are inextricably enmeshed in the above formula and cannot be easily separated. Premultiplication by T yields $\kappa = B_s v$. Evaluation of B_s at the centroid yields $\overline{B}_s = L_q^T/A$, where $L_q^T = A T \overline{B}_{\chi s}$ is the force lumping matrix given in Eq. (54).

A variation on the sliding-beam theme would consist of interpolating the normal rotation θ_n along i–k and j–k linearly rather than quadratically. This scheme turns out to be identical, however, to the average curvature rule and thus it provides nothing new.

The ANS Elements

Three ANS elements based on the preceding interpolation rules may be constructed by following the prescription of Box 4. Their stiffnesses are identified as K_a, K_p, and K_s, for averaging, projection, and sliding-beam, respectively. The following properties hold for these elements.

Patch Test. Assuming that the element has constant thickness and material properties, K_a and K_s pass the individual element test, but K_p does not. This claim can be analytically confirmed by applying the criterion of Eqs. (16)-(17), and noting that $\overline{B}_a = L_\ell^T/A$ and $\overline{B}_s = L_q^T/A$, where L_ℓ and L_q are the force lumping matrices (51) and (54).

Equivalence with DKT. K_s turns out to be identical to the stiffness matrix of the Discrete Kirchhoff Triangle (DKT) element, which was originally constructed in a completely different way that involves assumed rotation fields; see Batoz, Bathe and Ho (1980). *Thus DKT is an ANS element, and also (because of the equivalence noted below) an ANDES element.* This equivalence provides the first variational justification of DKT, as well as the proof that DKT passes the patch test without any numerical verification.

ANS/ANDES Equivalence. If the basic stiffness matrices $K_{b\ell}$ and K_{bq} derived in the next section are used in conjunction with the averaging and sliding-beam rules, and $\alpha = 1$, the ANDES formulation yields the same results as ANS if the element has constant thickness and material properties. (If the element has variable thickness, or the material properties vary, the equivalence does not hold.) The ANDES formulation used with the projection rule yields two elements, called ALR and AQR in the sequel, which differ in their basic stiffnesses. Both of these elements pass the patch test and are not equivalent to

the ANS formulation.

STIFFNESS MATRIX COMPUTATION

The Basic Stiffness

As explained on Box 2, the basic stiffness is obtained by constructing the lumping matrix L. In our case this is a 9×3 matrix that "lumps" an internal constant bending-moment field ($\overline{m}_{xx}$, $\overline{m}_{yy}$, $\overline{m}_{xy}$) to node forces $\overline{f}$ conjugate to v.

On each element side, the constant moment field produces boundary moments $\overline{m}_{nn}$ and $\overline{m}_{nt}$ referred to a local edge coordinate system n, t are

$$\left\{ \begin{array}{c} \overline{m}_{nn} \\ \overline{m}_{nt} \end{array} \right\}_{ij} = \begin{bmatrix} s_{ij}^2 & c_{ij}^2 & -2s_{ij}c_{ij} \\ s_{ij}c_{ij} & -s_{ij}c_{ij} & s_{ij}^2 - c_{ij}^2 \end{bmatrix} \left\{ \begin{array}{c} \overline{m}_{xx} \\ \overline{m}_{yy} \\ \overline{m}_{xy} \end{array} \right\} \tag{49}$$

The boundary motions d conjugate to m_{nn} and m_{nt} are $\partial w/\partial n = -\theta_t$ and $\partial w/\partial t = \theta_n$. Given the degree of freedom configuration (26), the normal slope $\partial w/\partial n = -\theta_t$ along side i–j can at most vary linearly (it could be also taken as constant and equal to $\frac{1}{2}(\theta_{ti} + \theta_{tj})$ but the results are the same as for a linear variation).

For the tangential slope (the rotation about the normal) $\partial w/\partial t = \theta_n$ there are three options: constant, linear and quadratic variation. But a constant $\theta_n = (w_j - w_i)/\ell_{ij}$ turns out to be equivalent to the quadratic variation and a constant $\theta_n = \frac{1}{2}(\theta_{ni} + \theta_{nj})$ equivalent to the linear variation. Consequently only the linear and quadratic cases need to be examined.

Linear Normal Rotation. The variation of θ_t and θ_n along each side is linear:

$$\left\{ \begin{array}{c} \theta_t \\ \theta_n \end{array} \right\}_{ij} = \frac{1}{2} \begin{bmatrix} 0 & 1-\xi & 0 & 0 & 1+\xi & 0 \\ 0 & 0 & 1-\xi & 0 & 0 & 1+\xi \end{bmatrix} \left\{ \begin{array}{c} w_i \\ \theta_{ti} \\ \theta_{ni} \\ w_j \\ \theta_{tj} \\ \theta_{nj} \end{array} \right\}, \tag{50}$$

where $\xi \equiv \xi_{ij}$.

Under this assumption Felippa and Bergan (1987) obtained the lumping matrix

$$\mathbf{L}_\ell^T = \tfrac{1}{2} \begin{bmatrix} 0 & 0 & y_{32} & 0 & 0 & y_{13} & 0 & 0 & y_{21} \\ 0 & x_{32} & 0 & 0 & x_{13} & 0 & 0 & x_{21} & 0 \\ 0 & y_{23} & x_{23} & 0 & y_{31} & x_{31} & 0 & y_{12} & x_{12} \end{bmatrix},$$

(51)

where superscript ℓ stands for 'linear θ_n.' The corresponding basic stiffness is

$$\mathbf{K}_{b\ell} = A^{-1}\mathbf{L}_\ell \mathbf{D} \mathbf{L}_\ell^T,$$

(52)

where $\mathbf{D}$ is the Cartesian moment-curvature constitutive matrix resulting from the integration of $\mathbf{E}$ through the plate thickness. This matrix been used as component of the free formulation (FF) element presented in that reference.

$$\mathbf{L}_q = \begin{bmatrix} -c_{12}s_{12} + c_{31}s_{31} & -c_{31}s_{31} + c_{12}s_{12} & (s_{31}^2 - c_{31}^2) - (s_{12}^2 - c_{12}^2) \\ \tfrac{1}{2}(s_{12}^2 x_{12} + s_{31}^2 x_{31}) & \tfrac{1}{2}(c_{12}^2 x_{12} + c_{31}^2 x_{31}) & c_{12}^2 y_{21} + c_{31}^2 y_{13} \\ -\tfrac{1}{2}(s_{12}^2 y_{21} + s_{31}^2 y_{13}) & -\tfrac{1}{2}(c_{12}^2 y_{21} + c_{31}^2 y_{13}) & -s_{12}^2 x_{12} - s_{31}^2 x_{31} \\ -c_{23}s_{23} + c_{12}s_{12} & -c_{12}s_{12} + c_{23}s_{23} & (s_{12}^2 - c_{12}^2) - (s_{23}^2 - c_{23}^2) \\ \tfrac{1}{2}(s_{12}^2 x_{12} + s_{23}^2 x_{23}) & \tfrac{1}{2}(c_{12}^2 x_{12} + c_{23}^2 x_{23}) & c_{12}^2 y_{21} + c_{23}^2 y_{32} \\ -\tfrac{1}{2}(s_{12}^2 y_{21} + s_{23}^2 y_{32}) & -\tfrac{1}{2}(c_{12}^2 y_{21} + c_{23}^2 y_{23}) & -s_{12}^2 x_{12} - s_{23}^2 x_{23} \\ -c_{31}s_{31} + c_{23}s_{23} & -c_{23}s_{23} + c_{31}s_{31} & (s_{23}^2 - c_{23}^2) - (s_{31}^2 - c_{31}^2) \\ \tfrac{1}{2}(s_{23}^2 x_{23} + s_{31}^2 x_{31}) & \tfrac{1}{2}(c_{23}^2 x_{23} + c_{31}^2 x_{31}) & c_{23}^2 y_{32} + c_{31}^2 y_{13} \\ -\tfrac{1}{2}(s_{23}^2 y_{32} + s_{31}^2 y_{13}) & -\tfrac{1}{2}(c_{23}^2 y_{32} + c_{31}^2 y_{13}) & -s_{23}^2 x_{23} - s_{31}^2 x_{31} \end{bmatrix}.$$

(54)

The corresponding basic stiffness matrix is denoted by

$$\mathbf{K}_{bq} = A^{-1}\mathbf{L}_q \mathbf{D}\mathbf{L}_q^T.$$

(55)

The Higher Order Stiffness

The higher order stiffness for the ANDES elements described previously is

$$\mathbf{K}_{hx} = \alpha \mathbf{Q}^T \mathbf{K}_{dx} \mathbf{Q}$$
$$= \alpha \mathbf{Q}^T \left[\int_A \mathbf{A}_{dx}^T \mathbf{D}\mathbf{A}_{dx} \, dA \right] \mathbf{Q} = \alpha \int_A \mathbf{B}_{dx}^T \mathbf{D}\mathbf{B}_{dx} \, dA,$$

(56)

where $x = a, p, s$ for the average, projection and sliding-beam rules, respectively. (The last expression is appropriate when $\mathbf{B}_{dx}$ is not easily factored into $\mathbf{A}_{dx}\mathbf{Q}$, as in the sliding-beam rule.) Since $\mathbf{A}_{dx}$ varies linearly, if $\mathbf{D}$ is constant we could numerically integrate $\mathbf{K}_{dx}$ in (56) exactly with a three point Gauss rule; for example the three-midpoint formula. But as the element stiffness formation time is dominated by these calculations it is of interest to derive $\mathbf{K}_h$ in closed form. This is done in Appendix B of Militello and Felippa (1989) for $\mathbf{K}_{hp}$, which from the numerical experiments discussed below appears to be the best performer.

NUMERICAL EXPERIMENTS

An extensive set of numerical experiments has been run to assess the performance of the new ANDES elements based on

Quadratic Normal Rotation. A quadratic variation of θ_n can be accommodated in conjunction with the cubic variation of w along the side:

$$\begin{Bmatrix} \theta_t \\ \theta_n \end{Bmatrix}_{ij} = \tfrac{1}{2} \begin{bmatrix} 0 & 1-\xi & 0 \\ 3(\xi^2-1)/\ell & 0 & \tfrac{1}{2}(3\xi+1)(\xi-1) \end{bmatrix}$$

$$\begin{bmatrix} 0 & 1+\xi & 0 \\ 3(\xi^2-1)/\ell & 0 & \tfrac{1}{2}(3\xi-1)(\xi+1) \end{bmatrix} \begin{Bmatrix} w_i \\ \theta_{ti} \\ \theta_{ni} \\ w_j \\ \theta_{tj} \\ \theta_{nj} \end{Bmatrix},$$

(53)

where $\xi \equiv \xi_{ij}$ and $\ell \equiv \ell_{ij}$. Then the resulting lumping matrix can be presented as

the projection rule (ALR and AQR) and to compare them with other existing high-performance elements. These experiments are reported in Militello and Felippa (1989). Four elements were considered in this study:

ALR   Stiffness defined as $\mathbf{K} = \mathbf{K}_{b\ell} + 1.5\mathbf{K}_{hp}$. This combines the linear-rotation basic stiffness (52) with the higher order stiffness given by the projection rule. The value $\alpha = 1.5$ was established through simple energy balance techniques similar to those discussed in Felippa and Bergan (1987) for the free formulation elements.

AQR   Stiffness defined as $\mathbf{K} = \mathbf{K}_{bq} + \mathbf{K}_{hp}$. This combines the quadratic-rotation basic stiffness (55) with the higher order stiffness given by the projection rule. The coefficient α is unity.

DKT   Stiffness defined as $\mathbf{K} = \mathbf{K}_{bq} + \mathbf{K}_{hs}$. As previously noted, this combination is identical to the well known Discrete Kirchhoff Triangle (DKT) element.

FF   The free formulation triangle described in Felippa and Bergan (1987), with multiparameter scaling of the higher order stiffness matrix. The basic stiffness matrix is $\mathbf{K}_{b\ell}$.

All of them qualify as high performance elements in the standard plate bending "obstacle" problems.

Traditionally tests for new finite elements are reported in the following sequence:

(I)   Patch tests, usually carried out numerically on arbitrarily chosen mesh configurations.

(II) Regular-mesh tests such as circular, square, skew and cantilever plates under concentrated and distributed loads.

(III) High-aspect ratio and geometric distortion tests.

For the present investigation (I) was unnecessary because all elements pass the patch test (in fact, a strong form of it) *a priori* by construction.

As for (II)-(III), the traditional order was reversed. First all four elements were subject to highly demanding distortion tests. This decision was taken to "weed" consistently weak performers and thus reduce the number of test runs on batch (II). The approach paid off in that AQR and DKT (the two elements that use the quadratic-rotation basic stiffness) consistently outperformed ALR and FF on distorted meshes, with AQR exhibiting an edge in extreme distortion cases.

Then a "run off" contest between AQR and DKT was carried out on the regular-mesh tests (II). On these the performance was similar with an advantage to AQR in problems involving concentrated loads. These results are reported in detail in Militello and Felippa (1989).

CONCLUSIONS

The main conclusions of the present study can be summarized as follows.

1. The ANDES formulation represents a variant of the ANS formulation that merits serious study. The key advantages of ANDES over ANS are:

    (a) *a priori* satisfaction of the patch test. Although this advantage is less clear for elements where ANS and ANDES coalesce for constant thickness and material properties, it reappears for more general cases.

    (b) The separation of the higher order stiffness allows the application of a scaling parameter. Furthermore it opens the possibility for the energy-balanced combination with other formulations as per Eq. (2), although this possibility presently remains unexplored.

2. The study of plate bending elements shows that the widely used DKT element is both an ANS and ANDES element. This discovery provides a variational foundation hereto lacking and analytically proves (because of the ANDES connection) that DKT passes the patch test.

3. The numerical results clearly demonstrate that the choice of basic stiffness is of paramount importance in the behavior of elements based on the ANDES formulation. Of the two elements sharing the quadratic-rotation basic stiffness, namely AQR and DKT, the former has excelled in

geometric distortion tests and in convergence studies that involve concentrated forces. For other cases the performance of AQR and DKT is similar, and superior to those elements that use the linear-rotation basic stiffness.

The numerical experiments have not addressed questions of *material sensitivity* such as element performance for highly anisotropic and composite plates. This behavior, as well as the possibility of applying this technology to C^0 bending elements, is currently under investigation.

REFERENCES

Ashwell, D. G. (1976). Strain elements, with applications to arches, rings and cylindrical shells, in *Finite Elements for Thin Shells and Curved Members*, ed. by D. G. Ashwell and R. H. Gallagher, Wiley-Interscience, London, pp. 91–112

Bathe, K.-J., and E. N. Dvorkin (1985). A four-node plate bending element based on Mindlin/Reissner plate theory and a mixed interpolation, *International Journal of Numerical Methods in Engineering*, 21, pp. 367–383

Batoz, J. L., Bathe, K.-J., and L. W. Ho (1980). A study of three-node triangular plate bending elements, *International Journal of Numerical Methods in Engineering*, 15, pp. 1771–1812

Batoz, J. L. (1982). An explicit formulation for an efficient triangular plate-bending element, *International Journal of Numerical Methods in Engineering*, 18, pp. 1077–1089

Bergan, P. G. and L. Hanssen (1976). A new approach for deriving 'good' finite elements, MAFELAP II Conference, Brunel University, 1975, in *The Mathematics of Finite Elements and Applications – Volume II*, ed. by J. R. Whiteman, Academic Press, London

Bergan, P. G. (1980). Finite elements based on energy orthogonal functions, *International Journal of Numerical Methods in Engineering*, 15, pp. 1141–1555

Bergan, P. G., and M. K. Nygård (1984). Finite elements with increased freedom in choosing shape functions, *International Journal of Numerical Methods in Engineering*, 20, pp. 643–664

Bergan, P. G., and Felippa, C. A. (1985). A triangular membrane element with rotational degrees of freedom, *Computer Methods in Applied Mechanics & Engineering*, 50, pp. 25–69

1. Crisfield, M. A. (1983). A four-noded thin plate element using shear constraints — a modified version of Lyons' element, *Computer Methods in Applied Mechanics & Engineering*, **38**, pp. 93–120

2. Felippa, C. A., and Bergan, P. G. (1987). A triangular plate bending element based on an energy-orthogonal free formulation, *Computer Methods in Applied Mechanics & Engineering*, **61**, pp. 129–160

3. Felippa, C. A. (1989a). Parametrized multifield variational principles in elasticity: I. Mixed functionals, *Communications in Applied Numerical Methods*, **5**, pp. 69–78

4. Felippa, C. A. (1989b). Parametrized multifield variational principles in elasticity: II. Hybrid functionals and the free formulation, *Communications in Applied Numerical Methods*, **5**, pp. 79–88

5. Felippa, C. A. (1989c). The extended free formulation of finite elements in linear elasticity, *Journal of Applied Mechanics*, **56**, pp. 609–616

6. Felippa, C. A., and C. Militello (1989). Developments in variational methods for high performance plate and shell elements, in *Analytical and Computational Models for Shells*, CED Vol. 3, ed. by A. K. Noor, T. Belytschko and J. C. Simo, American Society of Mechanical Engineers, ASME, New York, pp. 191–216

7. Felippa, C. A., and C. Militello (1990a). Principios variacionales parametrizados en elasticidad linear, *Revista Internacional de Métodos Numéricos para Cálculo y Diseño en Ingeniería*, **6**, pp. 333–342 (1990)

8. Felippa, C. A., and C. Militello (1990b). Variational formulation of high performance finite elements: parametrized variational principles, *Computers & Structures*, **36**, pp. 1–11 (1990)

9. Huang, H. C., and E. Hinton (1986). A new nine node degenerated shell element with enhanced membrane and shear interpolation, *International Journal of Numerical Methods in Engineering*, **22**, pp. 73–92

10. Hughes, T. J. R., and T. E. Tezduyar, (1981). Finite elements based upon Mindlin plate theory with particular reference to the four-node bilinear isoparametric element, *J. Applied Mechanics*, **48**, pp. 587–596

11. Hughes, T. J. R. (1987). *The Finite Element Method: Linear Static and Dynamic Finite Element Analysis*, Prentice-Hall, Englewood Cliffs, New Jersey

12. Jang, J., and P. M. Pinsky (1987). An assumed covariant strain based 9-node shell element, *International Journal of Numerical Methods in Engineering*, **24**, pp. 2389–2411

13. Kang, D. S. S. (1986). Hybrid stress finite element method, Ph. D. Dissertation, Dept. of Aeronautics and Astronautics, Massachusetts Institute of Technology

14. MacNeal, R. H. (1978). Derivation of element stiffness matrices by assumed strain distribution, *Nuclear Engineering & Design*, **70**, pp. 3-12

15. Malkus, D. S., and T. J. R. Hughes (1978). Mixed finite element methods — reduced and selective integration techniques: a unification of concepts, *Computer Methods in Applied Mechanics & Engineering*, **15**, pp. 68–81

16. Militello, C. and C. A. Felippa (1989). The first ANDES elements: 9-DOF plate bending triangles, Center for Space Structures and Controls Report CU-CSSC-89-22, University of Colorado, Boulder, Colorado; submitted to *Computer Methods in Applied Mechanics & Engineering*

17. Militello, C., and C. A. Felippa (1990a). A variational justification of the assumed natural strain formulation of finite elements: I. Variational principles, *Computers & Structures*, **34**, pp. 431–438

18. Militello, C., and C. A. Felippa (1990b). A variational justification of the assumed natural strain formulation of finite elements: II. The four node C^0 plate element, *Computers & Structures*, **34**, pp. 439–444

19. Park, K. C., and G. M. Stanley (1986). A curved C^0 shell element based on assumed natural-coordinate strains, *Journal of Applied Mechanics*, **53**, pp. 278–290

20. Park, K. C. (1986). An improved strain interpolation for curved C^0 elements, *International Journal of Numerical Methods in Engineering*, **22**, pp. 281–288

21. Simo, J. C., and T. J. R. Hughes (1986). On the variational foundations of assumed strain methods, *Journal of Applied Mechanics*, **53**, pp. 51–54

22. Turner, M. J., Clough, R. W., Martin, H. C., and L. J. Topp (1956). Stiffness and deflection analysis of complex structures, *Journal of Aeronautical Sciences*, **23**, pp. 805–824

23. Willam, K. J. (1969). Finite element analysis of cellular structures, Ph. D. Dissertation, Dept. of Civil Engineering, University of California, Berkeley, CA

ELECTROMAGNETIC FINITE ELEMENTS BASED ON A FOUR-POTENTIAL VARIATIONAL PRINCIPLE

SUMMARY

We derive electromagnetic finite elements based on a variational principle that uses the electromagnetic four-potential as primary variable. This choice is used to construct elements suitable for downstream coupling with mechanical and thermal finite elements for the analysis of electromagnetic/mechanical systems that involve superconductors. The key advantages of the four-potential are: the number of degrees of freedom per node remain modest as the problem dimensionality increases, jump discontinuities on interfaces are naturally accomodated, and static as well as dynamics are included without any *a priori* approximations. The new elements are tested on an axisymmetric problem under steady-state forcing conditions. The results are in excellent agreement with analytical solutions.

1. INTRODUCTION

The present work is part of a research program for the numerical simulation of electromagnetic/mechanical systems that involve superconductors. The simulation involves the interaction of the following four components:

(1) *Mechanical Fields*: displacements, stresses, strains and mechanical forces.

(2) *Thermal Fields*: temperature and heat fluxes.

(3) *Electromagnetic (EM) Fields*: electric and magnetic field strengths and fluxes, currents and charges.

(4) *Coupling Fields*: the foundamental coupling effect is the constitutive behavior of the materials involved. Particularly important are the metallurgical phase change phenomena triggered by thermal, mechanical and EM fields.

1.1 Finite Element Treatment

The first three fields (mechanical, thermal and electromagnetic) are treated by the finite element method. This treatment produces the spatial discretization of the continuum into mechanical, thermal and electromagnetic meshes of finite number of degrees of freedom. The finite element discretization may be developed in two ways:

(1) *Simultaneous Treatment*. The whole problem is treated as an indivisible whole. The three meshes noted above become tightly coupled, with common nodes and elements.

(2) *Staged Treatment*. The mechanical, thermal and electromagnetic components of the problem are treated separately. Finite element meshes for these components may be developed separately. Coupling effects are viewed as information that has to be transferred between these three meshes.

The present research follows the staged treatment. More specifically, *we develop finite element models for the fields in isolation, and then treat coupling effects as interaction forces between these models*. This "divide and conquer" strategy is ingrained in the partitioned treatment of coupled problems [4,16], which offers significant advantages in terms of computational efficiency and software modularity. Another advantage relates to the way research into complex problems can be made more productive. It centers on the observation that some aspects of the problem are either better understood or less physically relevant than others. These aspects may be then temporarily left alone while efforts are concentrated on the less developed and/or more physically important aspects. The staged treatment is better suited to this approach.

1.2 Mechanical Elements

Mechanical elements for this research have been derived using general variational principles that decouple the element boundary from the interior thus providing efficient ways to work out coupling

with non-mechanical fields. The point of departure was previous research into the free-formulation variational principles reported in Ref. [5]. A more general formulation for the mechanical elements, which includes the assumed natural strain formulation, was established and reported in Refs. [5,6,14,15]. New representations of thermal fields have not been addressed as standard formulations are considered adequate for the coupled-field phases of this research.

2. ELECTROMAGNETIC ELEMENTS

The development of electromagnetic (EM) finite elements has not received to date the same degree of attention given to mechanical and thermal elements. Part of the reason is the widespread use of analytical and semianalytical methods in electrical engineering. These methods have been highly refined for specialized but important problems such as circuits and waveguides. Thus the advantages of finite elements in terms of generality have not been enough to counterweight established techniques. Much of the EM finite element work to date has been done in England and is well described in the surveys by Davies [1] and Trowbridge [21]. The general impression conveyed by these surveys is one of an unsettled subject, reminiscent of the early period (1960-1970) of finite elements in structural mechanics. A great number of formulations that combine flux, intensity, and scalar potentials are described with the recommended choice varying according to the application, medium involved (polarizable, dielectric, semiconductors, etc.) number of space dimensions, time-dependent characteristics (static, quasi-static, harmonic or transient) as well as other factors of lesser importance. The possibility of a general variational formulation has not apparently been recognized.

In the present work, the derivation of electromagnetic (EM) elements is based on a variational formulation that uses the four-potential as primary variable. The electric field is represented by a scalar potential and the magnetic field by a vector potential. The formulation of these variational principle proceeds along lines previously developed for the acoustic fluid problem [7,8].

The main advantages of using potentials as primary variables as opposed to the more conventional EM finite elements based on intensity and/or flux fields are, in order or importance:

1. Interface discontinuities are automatically taken care of without any special intervention.

2. No approximations are invoked *a priori* since the general Maxwell equations are used.

3. The number of degrees of freedom per finite element node is kept modest as the problem dimensionality increases.

4. Coupling with the mechanical and thermal fields, which involves derived fields, can be naturally evaluated at the Gauss points at which derivatives of the potentials are evaluated.

Following a recapitulation of the basic field equations, the variational principle is stated. The discretization of these principle into finite element equations produces semidiscrete dynamical equations, which are specialized to the axisymmetric case. These equations are validated in a simulation of a cylindrical conductor wire.

161

Table 1 Electric and Magnetic Quantities

Quantities	Symbol	MKS-Weber Units
Electric charge density	ρ	coulomb/m^2
Electric field intensity	E	newton/coulomb
Electric flux density	D	coulomb/m^2
Electric resistance	R	ohm
Electric conductivity	g	mho
Displacement current density	$\dot{D}$	coulomb/(sec.m^2)
Susceptibility*	ϵ	coulomb/(joule.m)
Current	j	coulomb/sec
Magnetic field intensity	H	newton/weber or amperes/m
Magnetic flux density	B	weber/m^2
Magnetic permeability†	μ	weber/(joule.m) or henry/m

* Also called capacitivity and permittivity
† Also called inductivity

3. ELECTROMAGNETIC FIELD EQUATIONS

3.1 The Maxwell Equations

The original Maxwell equations (1873) involve four spatial fields: **B, D, E** and **H**. Vectors **E** and **H** represents the electric and magnetic field strengths (also called intensities), respectively, whereas **D** and **B** represent the electric and magnetic flux densities, respectively. All of these are three-vector quantities, that is, vector fields in three-dimensional space ($x_1 \equiv x$, $x_2 \equiv y$, $x_3 \equiv z$):

$$\mathbf{E} = \begin{Bmatrix} E_1 \\ E_2 \\ E_3 \end{Bmatrix}, \quad \mathbf{D} = \begin{Bmatrix} D_1 \\ D_2 \\ D_3 \end{Bmatrix}, \quad \mathbf{E} = \begin{Bmatrix} E_1 \\ E_2 \\ E_3 \end{Bmatrix}, \quad \mathbf{H} = \begin{Bmatrix} H_1 \\ H_2 \\ H_3 \end{Bmatrix}. \tag{1}$$

Other quantities are the electric current 3-vector **j** and the electric charge density ρ (a scalar). Units for these and other quantities of interest in this work are summarized in Tables 1-2.

With this notation, and using superposed dots to denote differentiation with respect to time t, we can state Maxwell equations as*

$$\begin{aligned} \dot{\mathbf{B}} + \nabla \times \mathbf{E} = 0, \quad & \nabla \times \mathbf{H} - \dot{\mathbf{D}} = \mathbf{j}, \\ \nabla \cdot \mathbf{D} = \rho, \quad & \nabla \cdot \mathbf{B} = 0. \end{aligned} \tag{2}$$

The first and second equation are also known as Faraday's and Ampère-Maxwell laws, respectively.

The system (2) supplies a total of eight partial differential equations, which as stated are independent of the properties of the underlying medium.

---

* Some authors, for example Eyges [2], include 4π factors and the speed of light c in the Maxwell equation. Other textbooks [19,20], follow Heaviside's advice in using technical units that eliminate such confusing factors.

Table 2   Equivalences Between Various MKS-Giorgi Units

$$1 \text{ newton} \equiv 1 \text{ kg.m/sec}^2$$
$$1 \text{ joule} \equiv 1 \text{ newton.m}$$
$$1 \text{ watt} \equiv 1 \text{ joule/sec}$$
$$1 \text{ coulomb} \equiv 1 \text{ ampere.sec}$$
$$1 \text{ ohm} \equiv 1 \text{ volt/ampere}$$
$$1 \text{ farad} \equiv 1 \text{ coulomb/volt}$$
$$1 \text{ henry} \equiv 1 \text{ (volt.sec)/ampere}$$
$$1 \text{ weber} \equiv 1 \text{ volt.sec}$$
$$1 \text{ mho} \equiv 1 \text{ ohm}^{-1}$$

3.2 Constitutive Equations

The field intensities E and H and the corresponding flux densities D and B are not independent but are connected by the EM constitutive equations. For an electromagnetically isotropic, non-polarized material the equations are

$$\boxed{B = \mu H, \qquad D = \epsilon E,}$$

(3)

where μ and ϵ are the permeability and susceptibility, respectively, of the material†. These coefficients are functions of position but (for static or harmonic fields) do not depend on time. In the general case of a non-isotropic material both μ and ϵ become tensors. Even in isotropic media μ in general is a complicated function of H; in ferromagnetic materials it depends on the previous history (hysteresis effect).

In free space $\mu = \mu_0$ and $\epsilon = \epsilon_0$, which are connected by

$$c_0^2 = \frac{1}{\mu_0 \epsilon_0}$$

(4)

where c_0 is the speed of light in a free vacuum. In MKS-A units, $c_0 = 3.10^9$ m/sec and

$$\mu_0 = 4\pi \times 10^{-7} \text{ henry/m}, \quad \epsilon_0 = \mu_0^{-1} c_0^{-2} = (36\pi)^{-1} \times 10^{-11} \text{ sec}^2/\text{(henry.m)}$$

(5)

The condition $\mu \approx \mu_0$ holds well for most practical purposes in such media as air and copper; in fact $\mu_{air} = 1.0000004\mu_0$ and $\mu_{copper} = .99999\mu_0$.

The electrical field strength E is further related to the current density j by Ohm's law:

$$j = gE$$

(6)

where g is the conductivity of the material. Again for an non-isotropic material g is generally a tensor which may also contain real and imaginary components; in which case the above relation becomes the generalized Ohm's law. For good conductors $g >> \epsilon$; for bad conductors $g << \epsilon$. In free space, $g = 0$.

---

† Other names are often used, see Table 1.

3.3 Maxwell Equations in Terms of E and B

To pass to the four-potential considered in Section 4 it is convenient to express Maxwell's equations in terms of the electrical field strength **E** and the magnetic flux **B**. In fact this is the pair most frequently used in electromagnetic work that involve arbitrary media. On eliminating **D** and **H** through the constitutive equations (3) we obtain

$$\boxed{\begin{aligned} \dot{\mathbf{B}} + \nabla \times \mathbf{E} = 0, \qquad & \nabla \times \mathbf{B} - \mu\epsilon\dot{\mathbf{E}} = \mu\mathbf{j}, \\ \nabla \cdot \mathbf{E} = \rho/\epsilon, \qquad & \nabla \cdot \mathbf{B} = 0. \end{aligned}} \tag{7}$$

The second equation assumes that ϵ is independent of time; otherwise $\epsilon\dot{\mathbf{E}} = \epsilon\, d\mathbf{E}/dt$ should be replaced by $d(\epsilon\mathbf{E})/dt$. In charge-free vacuum the equations reduce to

$$\dot{\mathbf{B}} + \nabla \times \mathbf{E} = 0, \qquad \nabla \times \mathbf{B} - \frac{1}{c_0^2}\dot{\mathbf{E}} = 0,$$

$$\nabla \cdot \mathbf{E} = 0, \qquad \nabla \cdot \mathbf{B} = 0. \tag{8}$$

3.4 The Electromagnetic Potentials

The electric scalar potential Φ and the magnetic vector potential **A** are introduced by the definitions

$$\boxed{\mathbf{E} = -\nabla\Phi - \dot{\mathbf{A}}, \qquad \mathbf{B} = \nabla \times \mathbf{A}.} \tag{9}$$

This definition satisfies the two homogeneous Maxwell equations in (7). The definition of **A** leaves its divergence $\nabla \cdot \mathbf{A}$ arbitrary. We shall use the Lorentz gauge

$$\nabla \cdot \mathbf{A} + \mu\epsilon\dot{\Phi} = 0. \tag{10}$$

With this choice the two non-homogeneous Maxwell equations in terms of Φ and **A** separate into the wave equations

$$\nabla^2\Phi - \mu\epsilon\ddot{\Phi} = -\rho/\epsilon, \qquad \nabla^2\mathbf{A} - \mu\epsilon\ddot{\mathbf{A}} = -\mu\mathbf{j}. \tag{11}$$

4. THE ELECTROMAGNETIC FOUR-POTENTIAL

Maxwell's equations can be presented in a compact manner* in the four-dimensional spacetime defined by the coordinates

$$x_1 \equiv x, \quad x_2 \equiv y, \quad x_3 \equiv z, \quad x_4 = ict \tag{12}$$

where x_1, x_2, x_3 are spatial Cartesian coordinates, $i^2 = -1$ is the imaginary unit, and $c = 1/\sqrt{\mu\epsilon}$ is the speed of EM waves in the medium under consideration. In the sequel Roman subscripts will consistently go from 1 to 4 and the summation convention over repeated indices will be used unless otherwise stated.

---

* A form compatible with special relativity.

164

4.1 The Field Strength Tensor

The unification can be expressed most conveniently in terms of the *field-strength tensor* F, which is a four-dimensional *antisymmetric* tensor constructed from the components of E and B as follows:

$$
\mathbf{F} = \begin{pmatrix} 0 & F_{12} & F_{13} & F_{14} \\ -F_{12} & 0 & F_{23} & F_{24} \\ -F_{13} & -F_{23} & 0 & F_{34} \\ -F_{14} & -F_{23} & -F_{34} & 0 \end{pmatrix} \overset{\text{def}}{=} \beta \begin{pmatrix} 0 & cB_3 & -cB_2 & -iE_1 \\ -cB_3 & 0 & cB_1 & -iE_2 \\ cB_2 & -cB_1 & 0 & -iE_3 \\ iE_1 & iE_2 & iE_3 & 0 \end{pmatrix}.
\tag{13}
$$

Here β is an adjustment factor to be determined later. Similarly, introduce the *four-current* vector J as

$$
\mathbf{J} = \begin{Bmatrix} J_1 \\ J_2 \\ J_3 \\ J_4 \end{Bmatrix} \overset{\text{def}}{=} \beta \begin{Bmatrix} c\mu j_1 \\ c\mu j_2 \\ c\mu j_3 \\ i\rho/\epsilon \end{Bmatrix} = \beta c \begin{Bmatrix} \mu j_1 \\ \mu j_2 \\ \mu j_3 \\ i\sqrt{\mu/\epsilon}\,\rho \end{Bmatrix}.
\tag{14}
$$

Then, for arbitrary β, the non-homogeneous Maxwell equations, namely $\nabla \times \mathbf{B} - \mu\epsilon\dot{\mathbf{E}} = \mu\mathbf{j}$ and $\nabla \cdot \mathbf{E} = \rho/\epsilon$, may be presented in the compact "continuity" form†

$$
\frac{\partial F_{ik}}{\partial x_k} = J_i.
\tag{15}
$$

The other two Maxwell equations, $\nabla \cdot \mathbf{B} = 0$ and $\nabla \times \mathbf{E} + \dot{\mathbf{B}} = 0$, can be presented as

$$
\frac{\partial F_{ik}}{\partial x_m} + \frac{\partial F_{mi}}{\partial x_k} + \frac{\partial F_{km}}{\partial x_i} = 0,
\tag{16}
$$

where the index triplet (i, j, k) takes on the values (1,2,3), (4,2,3), (4,3,1) and (4,1,2).

4.2 The Four-Potential

The EM "four-potential" ϕ is a four-vector whose components are constructed with the electric and magnetic potential components of A and Φ:

$$
\phi = \beta \begin{Bmatrix} \phi_1 \\ \phi_2 \\ \phi_3 \\ \phi_4 \end{Bmatrix} \overset{\text{def}}{=} \begin{Bmatrix} cA_1 \\ cA_2 \\ cA_3 \\ i\Phi \end{Bmatrix}.
\tag{17}
$$

It may then be verified that F can be expressed as the four-curl of ϕ, that is

$$
F_{ik} = \frac{\partial \phi_k}{\partial x_i} - \frac{\partial \phi_i}{\partial x_k},
\tag{18}
$$

or in more detail and using commas to abbreviate partial derivatives:

$$
\mathbf{F} = \begin{pmatrix} 0 & \phi_{2,1} - \phi_{1,2} & \phi_{3,1} - \phi_{1,3} & \phi_{4,1} - \phi_{1,4} \\ \phi_{1,2} - \phi_{2,1} & 0 & \phi_{3,2} - \phi_{2,3} & \phi_{4,2} - \phi_{2,4} \\ \phi_{1,3} - \phi_{3,1} & \phi_{2,3} - \phi_{3,2} & 0 & \phi_{4,3} - \phi_{3,4} \\ \phi_{1,4} - \phi_{4,1} & \phi_{2,4} - \phi_{4,2} & \phi_{3,4} - \phi_{4,3} & 0 \end{pmatrix}.
\tag{19}
$$

---

† The covariant form of these two equations.

4.3 The Lagrangian

With these definitions, the basic Lagrangian of electromagnetism can be stated as[‡]

$$L = \tfrac{1}{4} F_{ik} F_{ik} - J_i \phi_i = \tfrac{1}{4}\beta^2 \left(\frac{\partial \phi_k}{\partial x_i} - \frac{\partial \phi_i}{x_k} \right)^2 - J_i \phi_i$$

$$= \tfrac{1}{2}\beta^2 \left(c^2 B^2 - E^2 \right) - \frac{\beta^2}{\epsilon}(j_1 A_1 + j_2 A_2 + j_3 A_3 - \rho\Phi), \tag{20}$$

in which

$$B^2 = \mathbf{B}^T \mathbf{B} = B_1^2 + B_2^2 + B_3^2, \quad E^2 = \mathbf{E}^T \mathbf{E} = E_1^2 + E_2^2 + E_3^2. \tag{21}$$

Comparing the first term with the magnetic and electric energy densities [2,19,20]

$$u_m = \tfrac{1}{2}\mathbf{B}^T \mathbf{H} = \frac{1}{2\mu}B^2, \quad u_e = \tfrac{1}{2}\mathbf{D}^T \mathbf{E} = \tfrac{1}{2}\epsilon E^2, \tag{22}$$

we must have $\beta^2 c^2 = \beta^2/(\mu\epsilon) = 1/\mu$, from which

$$\beta = \sqrt{\epsilon}. \tag{23}$$

Consequently the required Lagrangian is

$$\boxed{L = \frac{1}{2\mu}B^2 - \tfrac{1}{2}\epsilon E^2 - (j_1 A_1 + j_2 A_2 + j_3 A_3 - \rho\Phi).} \tag{24}$$

The associated variational form is

$$R = \int_{t_0}^{t_1} \int_V L\, dV dt \tag{25}$$

where V is the integration volume considered in the analysis. In theory V extends over the whole space, but in the numerical simulation the integration is truncated at a distant boundary or special devices are used to treat the decay behavior at infinity.

4.4 The Four-Field Equations

On setting the variation of the functional (24) to zero we recover the field equations (15–16). Taking the divergence of both sides of (15) and observing that $\mathbf{F}$ is an antisymmetric tensor so that its divergence vanishes we get

$$\frac{\partial J_i}{\partial x_i} = c\mu(\nabla \cdot \mathbf{j} + \dot{\rho}) = 0, \tag{26}$$

[‡] Lanczos [12] presents this Lagrangian for free space, but the expression (24) for an arbitrary material was found in none of the textbooks on electromagnetism listed in the References.

The vanishing term in parenthesis is the equation of continuity, which expresses the law of conservation of charge. The Lorentz gauge condition (10) may be stated as $\nabla \cdot \phi = 0$. Finally, the potential wave equations (11) may be expressed in compact form as

$$\Box \phi_i = -J_i \tag{27}$$

where $\Box$ denotes the "four-wave-operator", also called the D'Alembertian:

$$\Box \stackrel{\text{def}}{=} \frac{\partial^2}{\partial x_k \partial x_k} = \frac{\partial^2}{\partial x_1^2} + \frac{\partial^2}{\partial x_2^2} + \frac{\partial^2}{\partial x_3^2} - \frac{\partial^2}{c^2 \partial t^2}. \tag{28}$$

Hence each component of the four-potential ϕ satisfies an inhomogeneous wave equation. In free space, $J_i = 0$ and each component satisfies the homogeneous wave equation.

5. THE AXISYMMETRIC TEST EXAMPLE

The simplest example for testing the finite element formulation based on the four-potential variational principle is provided by the axisymmetric magnetic field generated by a uniform, steady current flowing through a straight, infinitely long conducting wire of circular cross section. In the present Section we derive expressions for the magnetostatic fields outside and within the conductor. These analytical solutions will be later compared with the finite element numerical solutions.

5.1 The Free-Space Magnetic Field

To take advantage of the axisymmetric geometry we choose a cylindrical coordinate system with the wire centerline as the longitudinal z-axis. The vector components in the cylindrical coordinate directions r, θ and z are denoted by

$$A_1, \; B_1, \; E_1 \quad \text{in the } r \text{ direction}$$
$$A_2, \; B_2, \; E_2 \quad \text{in the } \theta \text{ direction}$$
$$A_3, \; B_3, \; E_3 \quad \text{in the } z \text{ direction}$$

The electromagnetic fields will then vary in the radial direction (r) but not in the angular (θ) and axial (z) directions. Similarly, the current density that flows in the wire has only one nonzero component acting in the positive or negative z direction; conventionally we select the positive direction.

In Cartesian coordinates the radial component of the electrostatic potential in free space can be calculated from the expression (see, e.g., [2,10,18,19,20])

$$A_z = A_3 = \frac{\mu_0}{4\pi} \int_V \frac{j_3}{|\mathbf{r}|} \, dV, \tag{29}$$

where $|\mathbf{r}|$ is the distance between the elemental charge $j_3 \, dV$ and the point in space at which we wish to find the field potential. The integral extends over the volume containing charges. This expression serves equally well in cylindrical coordinates. In fact, the transformation of z components will be one to one if the center of the systems coincide.

As noted above the only non-vanishing component of the current vector is $j_3\,dS$ where dS is the elemental cross sectional area of the conductor and j_3 is the current density in the z direction. If $d\ell$ represents the differential length of the wire, then $\int_S j_3\,dV = \int_S j_3\,dS\,d\ell = I\,d\ell = I\,dz$ and $|\mathbf{r}| = \sqrt{r^2 + z^2}$. Substitution into Eq. (29) yields

$$A_3(r) = \frac{\mu_0 I}{4\pi} \int_{-\infty}^{\infty} \frac{dz}{\sqrt{r^2 + z^2}}. \tag{30}$$

This integral diverges, but this difficulty can be overcome by taking the wire to have a finite length $2L$ symmetric with respect to the field point, that is large with respect to its diameter. Integrating between $-L$ and $+L$ we get

$$A_3(r) = \frac{\mu_0 I}{4\pi} \int_{-L}^{L} \frac{dz}{\sqrt{r^2 + z^2}} = \frac{\mu_0 I}{4\pi} \ln\left(z + \sqrt{r^2 + z^2}\right)\Big|_{-L}^{+L}. \tag{31}$$

Expanding this equation in powers of r/L and retaining only first-order terms gives

$$A_3 = -\left(\frac{\mu_0 I}{2\pi}\right) \ln r + C. \tag{32}$$

where C is an arbitrary constant. For subsequent developments it is convenient to select $C = (\mu_0 I/2\pi)\ln R_T$, where R_T is the "truncation radius" of the finite element mesh in the radial direction. Then

$$A_3 = -\left(\frac{\mu_0 I}{2\pi}\right) \ln\left(\frac{r}{R_T}\right). \tag{33}$$

With this normalization $A_3 = 0$ at $r = R_T$. Taking the curl of $\mathbf{A}$ gives the $\mathbf{B}$ field in cylindrical coordinates:

$$\mathbf{B} = \nabla \times \mathbf{A} = \left\{ \begin{array}{c} B_1 \\ B_2 \\ B_3 \end{array} \right\} = \left\{ \begin{array}{c} B_r \\ B_\theta \\ B_z \end{array} \right\} = \left\{ \begin{array}{c} \frac{1}{r}\frac{\partial A_3}{\partial\theta} - \frac{\partial A_2}{\partial z} \\ \frac{\partial A_1}{\partial z} - \frac{\partial A_3}{\partial r} \\ \frac{1}{r}\frac{\partial(r A_2)}{\partial r} - \frac{1}{r}\frac{\partial A_1}{\partial\theta} \end{array} \right\} = \left\{ \begin{array}{c} 0 \\ -\frac{\partial A_3}{\partial r} \\ 0 \end{array} \right\}. \tag{34}$$

It is seen that the only non-vanishing component of the magnetic flux density is

$$B_\theta \equiv B_2 = \mu_0 H_2 = -\frac{\partial A_3}{\partial r} = \frac{\mu_0 I}{2\pi r}. \tag{35}$$

This expression is called the law of Biot-Savart in the EM literature.

5.2 Magnetic Field Within the Conductor

Again restricting our consideration to the static case, we have from Maxwell's equations in their integral flux form

$$\oint_C \mathbf{H} \cdot ds = \oint_C \mu^{-1}\mathbf{B} \cdot ds = \int_S \mathbf{j} \cdot d\mathbf{S}, \tag{36}$$

THIS PAGE INTENTIONALLY LEFT BLANK

where C is a contour around the field point traversed counterclockwise with an oriented differential arclength ds and dS is the oriented surface element inside the contour. The term for the electric field disappears in this analysis because $\dot{E} = 0$. From before we know that the right hand side of Eq. (35) is equal to the normal component of the current that flows through the cross sectional area evaluated by the integral. In the free space case, this is the total current that flows through the conductor. But in the conductor the amount of current is a function of the distance r from the center. Again using I to represent the total current carried by the conductor, and R the radius of the conductor, and assuming an *uniform* current density $j_3 = I/(\pi R^2)$, the right hand side of (35) become A

$$\int_S \mathbf{j} \cdot d\mathbf{S} = \int_S j_3 \, dS = \frac{I}{\pi R^2} \int_S dS = I \frac{r}{R^2}. \tag{37}$$

Evaluating the left hand side of the integral and solving for B_2 gives:

$$2\pi r \mu^{-1} B_2 = I \frac{r^2}{R^2}, \qquad B_2 = \frac{\mu I r}{2\pi R^2}. \tag{38}$$

Comparing with (34) we see that if $\mu = \mu_0$ then B_2 is continuous at the wire surface $r = R$ and has the value $\mu_0 I/(2\pi R)$. But if $\mu \neq \mu_0$ there is a jump $(\mu - \mu_0)I/(2\pi R)$ in B_2.

The magnetic potential A_3 within the conductor is easily computed by integrating $-B_2$ with respect to r:

$$A_3 = -\frac{\mu I r^2}{4\pi R^2} + C. \tag{39}$$

The value of C is determined by matching (33) at $r = R$, since the potential must be continuous. The result can be written

$$A_3 = \frac{I}{2\pi} \left[\tfrac{1}{2}\mu \left(1 - \frac{r^2}{R^2} \right) - \mu_0 \ln \left(\frac{R}{R_T} \right) \right]. \tag{40}$$

The preceding expressions (33)-(40) for A_3 could also be derived in a somewhat more direct fashion by integrating the ordinary differential equation $\nabla^2 A_3 = r^{-1}(\partial(r\partial A_3/\partial r)\partial r) = \mu j_3$ to which the second of (11) reduces.

6. FINITE ELEMENT DISCRETIZATION

6.1 The Lagrangian in Cylindrical Coordinates

To construct finite element approximations we need to express the Lagrangian (24)

$$L = \frac{1}{2\mu} B^2 - \tfrac{1}{2}\epsilon E^2 - (\mathbf{j}^T \mathbf{A} - \rho\Phi), \tag{41}$$

in terms of the potentials written in cylindrical coordinates. For B^2 we can use the expression of the curl (33)

$$B^2 = \left(\frac{1}{r}\frac{\partial A_3}{\partial\theta} - \frac{\partial A_2}{\partial z} \right)^2 + \left(\frac{\partial A_1}{\partial z} - \frac{\partial A_3}{\partial r} \right)^2 + \left(\frac{1}{r}\frac{\partial(rA_2)}{\partial r} - \frac{1}{r}\frac{\partial A_1}{\partial\theta} \right)^2, \tag{42}$$

For E^2 we need the cylindrical-coordinate gradient formulas

$$\mathbf{E} = \begin{Bmatrix} E_1 \\ E_2 \\ E_3 \end{Bmatrix} = \begin{Bmatrix} E_r \\ E_\theta \\ E_z \end{Bmatrix} = - \begin{Bmatrix} \frac{\partial \Phi}{\partial r} + \dot{A}_1 \\ \frac{1}{r} \frac{\partial \Phi}{\partial \theta} + \dot{A}_2 \\ \frac{\partial \Phi}{\partial z} + \dot{A}_3 \end{Bmatrix} \qquad (43)$$

so that

$$E^2 = \left(\frac{\partial \Phi}{\partial r} + \frac{\partial A_1}{\partial t} \right)^2 + \left(\frac{1}{r} \frac{\partial \Phi}{\partial \theta} + \frac{\partial A_2}{\partial t} \right)^2 + \left(\frac{\partial \Phi}{\partial z} + \frac{\partial A_3}{\partial t} \right)^2 . \qquad (44)$$

In the axisymmetric case, $A_1 = A_2 = 0$; furthermore $A_z = A_3$ is only a function of the radial distance from the wire. Therefore $\partial A_3 / \partial \theta = \partial A_3 / \partial z = 0$. From symmetry considerations we also know that the electric field cannot vary in the θ and z directions, which gives $\partial \Phi / \partial z = \partial \Phi / \partial \theta = 0$. Finally, the only nonvanishing current density component is j_3. Consequently the Lagrangian (41) simplifies to

$$L = \frac{1}{2\mu} \left(\frac{\partial A_3}{\partial r} \right)^2 - \frac{1}{2}\epsilon \left[\left(\frac{\partial \Phi}{\partial r} \right)^2 + \left(\frac{\partial A_3}{\partial t} \right)^2 \right] - (j_3 A_3 - \rho \Phi) . \qquad (45)$$

6.2 Constructing EM Finite Elements

To deal with this particular axisymmetric problem a two-node "line" finite element extending in the radial r direction is sufficient. In the following we deal with an individual element identified by superscript e. The two element end nodes are denoted by i and j. The electric potential Φ and the magnetic potential $A_3 \equiv A_z$ are interpolated over each element as

$$\Phi^e = \mathbf{N}_\Phi^e \Phi^e, \qquad A_3^e = \mathbf{N}_A^e \mathbf{A}_3^e, \qquad (46)$$

Here row vectors $\mathbf{N}_\Phi^e$ and $\mathbf{N}_A^e$ contain the finite element shape functions for Φ^e and A_3^e, respectively, which are only functions of the radial coordinate r:

$$\mathbf{N}_\Phi^e = \langle N_{\Phi i}^e(r) \quad N_{\Phi j}^e(r) \rangle, \qquad \mathbf{N}_A^e = \langle N_{Ai}^e(r) \quad N_{Aj}^e(r) \rangle, \qquad (47)$$

and column vectors Φ^e and $\mathbf{A}_3^e$ contain the nodal values of Φ and A_3, respectively, which are only functions of time t:

$$\Phi^e = \begin{Bmatrix} \Phi_i(t) \\ \Phi_j(t) \end{Bmatrix}, \qquad \mathbf{A}_3^e = \begin{Bmatrix} A_{3i}(t) \\ A_{3j}(t) \end{Bmatrix} . \qquad (48)$$

Substitution of these finite element assumptions into the Lagrangian (45) and then into Eq. (25) yields the variational integral as sum of element contributions $R = \sum_e R^e$, where

$$R^e = \int_{t_0}^{t_1} \int_{V^e} \frac{1}{2\mu} \left(\frac{\partial \mathbf{N}_A^e}{\partial r} \mathbf{A}_3^e \right)^2 - \frac{1}{2}\epsilon \left[\left(\frac{\partial \mathbf{N}_\Phi^e}{\partial r} \Phi^e \right)^2 + \left(\frac{\partial \mathbf{N}_A^e}{\partial t} \dot{\mathbf{A}}_3^e \right)^2 \right]$$
$$- \left(j_3 \mathbf{N}_A^e \mathbf{A}_3^e - \rho \mathbf{N}_\Phi^e \Phi^e \right) dV^e \, dt. \qquad (49)$$

169

where V^e denotes the volume of the element. Taking the variation with respect to the element node values gives

$$
\delta R^e = \int_{t_0}^{t_1} \int_{V^e} \left(\delta A_3^e\right)^T \left[\frac{1}{\mu} \left(\frac{\partial N_A^e}{\partial r}\right)^T \frac{\partial N_A^e}{\partial r} A_3^e + \epsilon \left(N_A^e\right)^T N_A^e \ddot{A}_3^e - j_3 \left(N_A^e\right)^T \right]
$$
$$
+ \int_{t_0}^{t_1} \int_{V^e} \left(\delta \Phi^e\right)^T \left[-\epsilon \left(\frac{\partial N_\Phi^e}{\partial r}\right)^T \frac{\partial N_\Phi^e}{\partial r} \Phi^e + \rho \left(N_\Phi^e\right)^T \right] dV^e\, dt.
$$
(50)

On applying fixed-end initial conditions at $t = t_0$ and $t = t_1$ and the lemma of the calculus of variations, we proceed to equate each of the expressions in brackets to zero. From the first bracket we obtain for each element the following second-order dynamic equations for the magnetic potential at the nodes, which are purposedly written in a notation resembling the mass-stiffness-force equations of mechanics:

$$
M_A^e \ddot{A}_3^e + K_A^e A_3^e = f_A^e,
$$
(51)

where

$$
M_A^e = \int_{V^e} \epsilon \left(N_A^e\right)^T N_A^e\, dV^e, \qquad K_A^e = \int_{V^e} \frac{1}{\mu} \left(\frac{\partial N_A^e}{\partial r}\right)^T \frac{\partial N_A^e}{\partial r}\, dV^e,
$$
(52)

$$
f_A^e = \int_{V^e} j_3 N_A^{e\,T}\, dV^e.
$$
(53)

From the second bracket we obtain for the electric potential a simpler relation which does not involve time derivatives, i.e, is static in nature:

$$
K_\Phi^e \Phi^e = f_\Phi^e,
$$
(54)

where

$$
K_\Phi^e = \int_{V^e} \epsilon \left(\frac{\partial N_\Phi^e}{\partial r}\right)^T \frac{\partial N_\Phi^e}{\partial r}\, dV^e, \qquad f_\Phi^e = \int_{V^e} \rho \left(N_\Phi^e\right)^T\, dV^e.
$$
(55)

Assembling these equations in the usual way we obtain the semidiscrete *master finite element equations*:

$$
M_A \ddot{A}_3 + K_A A_3 = f_A,
$$
$$
K_\Phi \Phi = f_\Phi.
$$
(56)

6.3 The Static Case

In time-independent (static, steady state) problems, the term $\ddot{A}_3$ disappears and the master finite element equations of electromagnetostatics become

$$
K_A A_3 = f_A, \qquad K_\Phi \Phi = f_\Phi.
$$
(57)

If the current density and charge distributions are known *a priori* then these two equations may be solved separately. If only the charge distribution is known then the second equation should be solved first to obtain the electric field $\mathbf{E}$ as gradient of the computed electric potential; then

170

the current density j obtained from Ohm's law (6) and used to computed the force vector of the first equation. Conversely if only the current density distribution is known *a priori* the process is reversed.

In the present study the current distribution is assumed to be known and we will be content with solving the first equation for the magnetic flux.

6.4 An Alternative Semidiscretization

If upon setting the brackets of the variation (50) to zero we multiply them through by μ and $1/\epsilon$, respectively, the expressions for the mass, stiffness and force matrices become

$$\mathbf{M}_A^e = \int_{V^e} \frac{1}{c^2} (\mathbf{N}_A^e)^T \mathbf{N}_A^e \, dV^e, \quad \mathbf{K}_A^e = \int_{V^e} \left(\frac{\partial \mathbf{N}_A^e}{\partial r}\right)^T \frac{\partial \mathbf{N}_A^e}{\partial r} dV^e, \quad \mathbf{f}_A^e = \int_{V^e} \mu \, j_3 \mathbf{N}_A^{e\,T} \, dV^e,$$

$$\mathbf{K}_\Phi^e = \int_{V^e} \left(\frac{\partial \mathbf{N}_\Phi^e}{\partial r}\right)^T \frac{\partial \mathbf{N}_\Phi^e}{\partial r} dV, \qquad \mathbf{f}_\Phi^e = \int_{V^e} \frac{1}{\epsilon} \rho \, (\mathbf{N}_\Phi^e)^T \, dV. \tag{58}$$

The matrices M and K above are quite similar to the capacitance and reactance matrices, respectively, obtained in the potential analysis of acoustic fluids [7,8]. Another attractive feature of (58) is that $\mathbf{K}_A = \mathbf{K}_\Phi$ if the shape functions of both potentials coalesce, as is natural to assume. These advantages are, however, more than counterbalanced by the fact that "jump forces" contributions to $\mathbf{f}_A$ and $\mathbf{f}_\Phi$ arise on material interfaces where μ and ϵ change abruptly, and the proper handling of such forces substantially complicates the programming logic. Note that this issue does not arise in the treatment of homogeneous acoustic fluids.

6.5 Applying Boundary Conditions

The finite element mesh is necessarily terminated at a finite size, which for the test problem is defined as the truncation radius R_T alluded to in Section 5.1. In static calculations the material outside the FE mesh may be viewed as having zero permeability μ, or, equivalently, infinite stiffness or zero potential. It follows that the potential value at the node located on the truncation radius may be prescribed to be zero. This is the only essential boundary condition necessary for this particular problem.

7. NUMERICAL VALIDATION

7.1 Finite Element Model

The test problem consists of a wire conductor of radius R transporting a unit current density. For this problem the finite element mesh is completely defined if we specify the radial node coordinates $r_i^e = r_n^e$ and $r_j^e = r_{n+1}^e$ for each element e. If the mesh contains N_{ec} elements inside the conductor, those elements are numbered $e = 1, 2, \ldots N_{ec}$ and nodes $n = 1, 2, \ldots N_{ec} + 1$ starting from the conductor center outwards. The first node ($n = 1$) is at the conductor center $r = 0$ and node $n = N_{ec} + 1$ is placed at the conductor boundary $r = R$. The mesh is then continued with N_{ef}

171
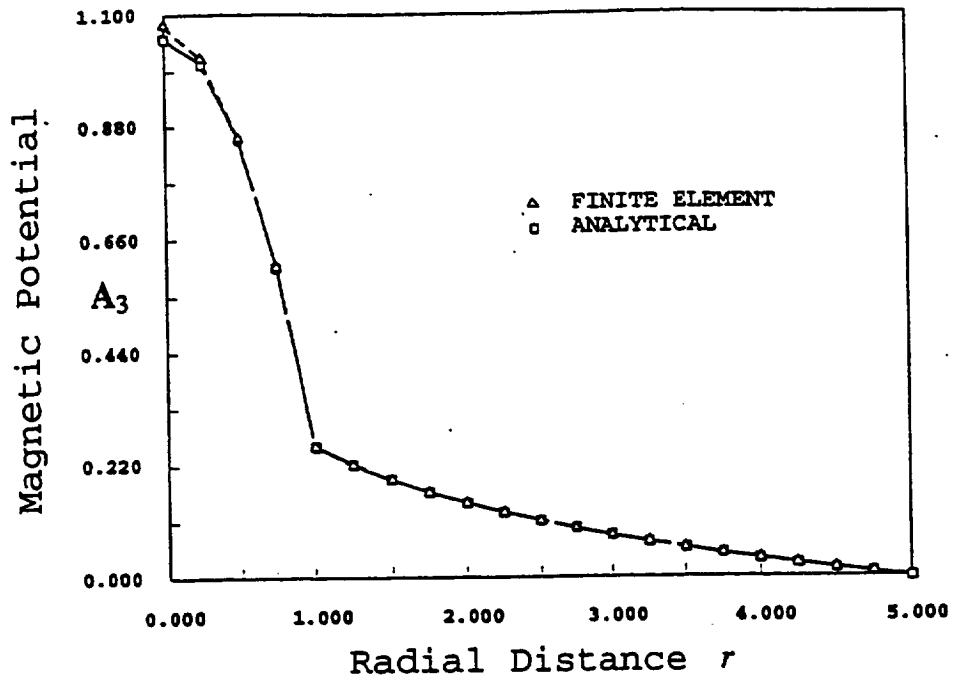
Figure 1. Magnetic potential A_3 vs. distance from center r, $\mu_{wire} = 10.0$: finite element values (triangles) and analytical values (squares).
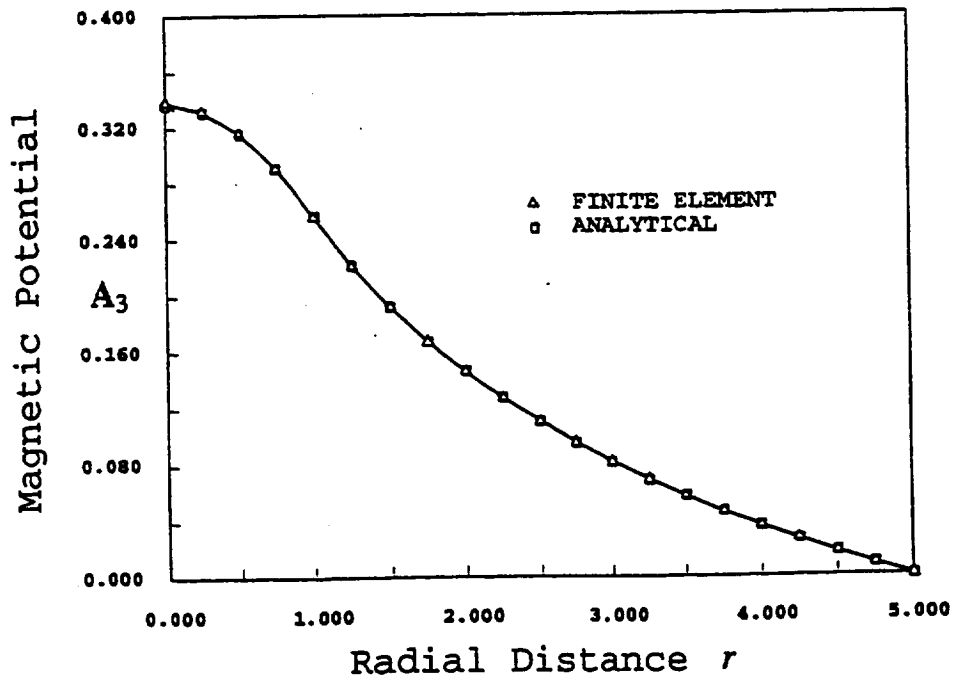
Figure 2. Magnetic potential A_3 vs. distance from center r, $\mu_{wire} = 1.0$: finite element values (triangles) and analytical values (squares).
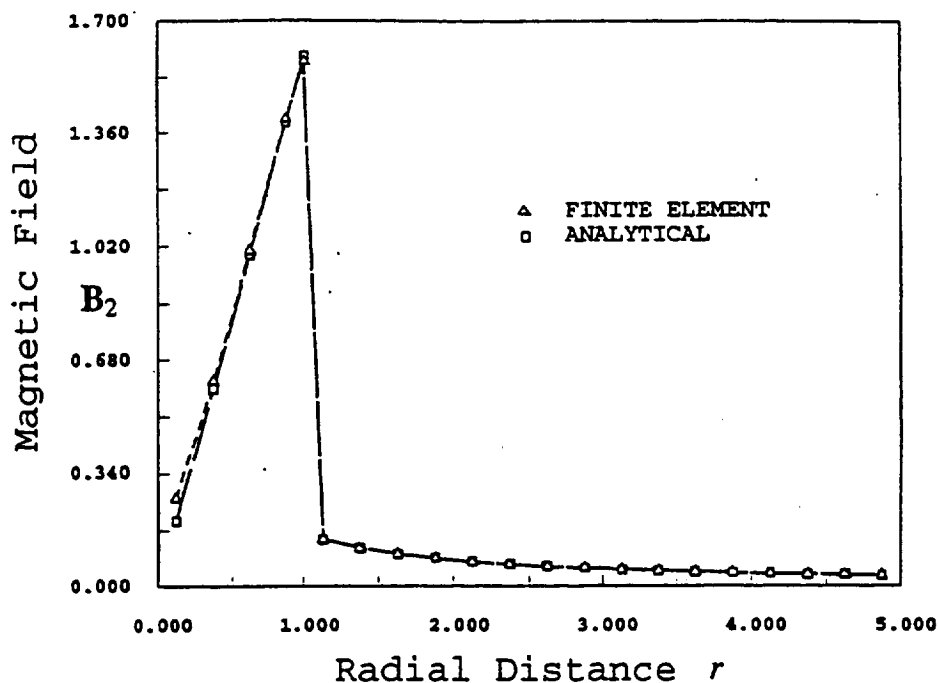
Figure 3. Magnetic flux density B_2 vs. distance from center r, $\mu_{wire} = 10.0$: finite element values (triangles) and analytical values (squares). Values shown on the interface $r = 1$ with dark symbols have been extrapolated from element center values to display the jump more accurately; this extrapolation scheme has not been used elsewhere.
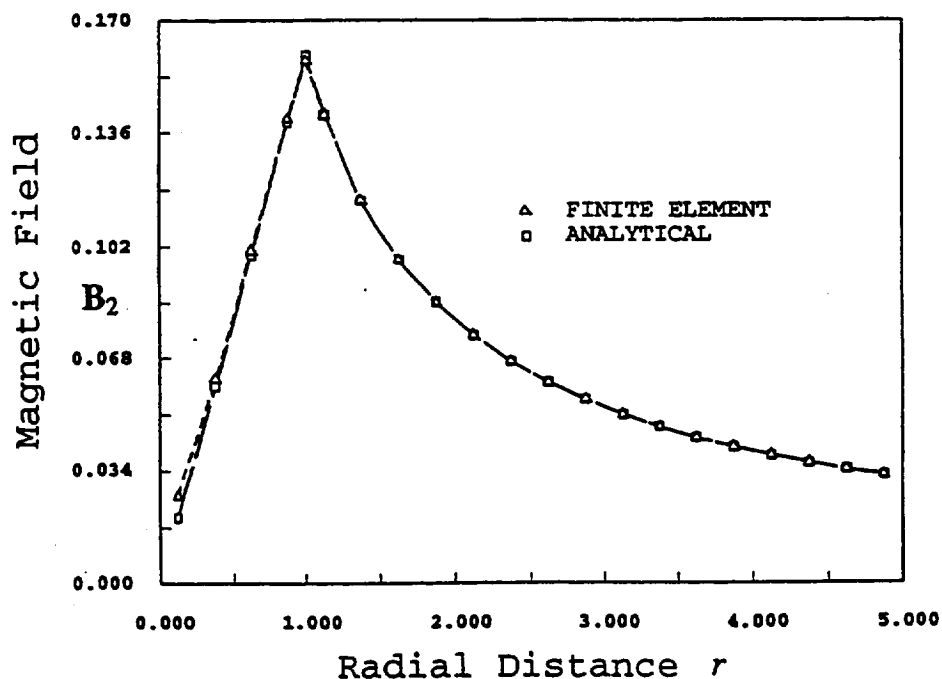
Figure 4. Magnetic flux density B_2 vs. distance from center r, $\mu_{wire} = 1.0$: finite element values (triangles) and analytical values (squares).
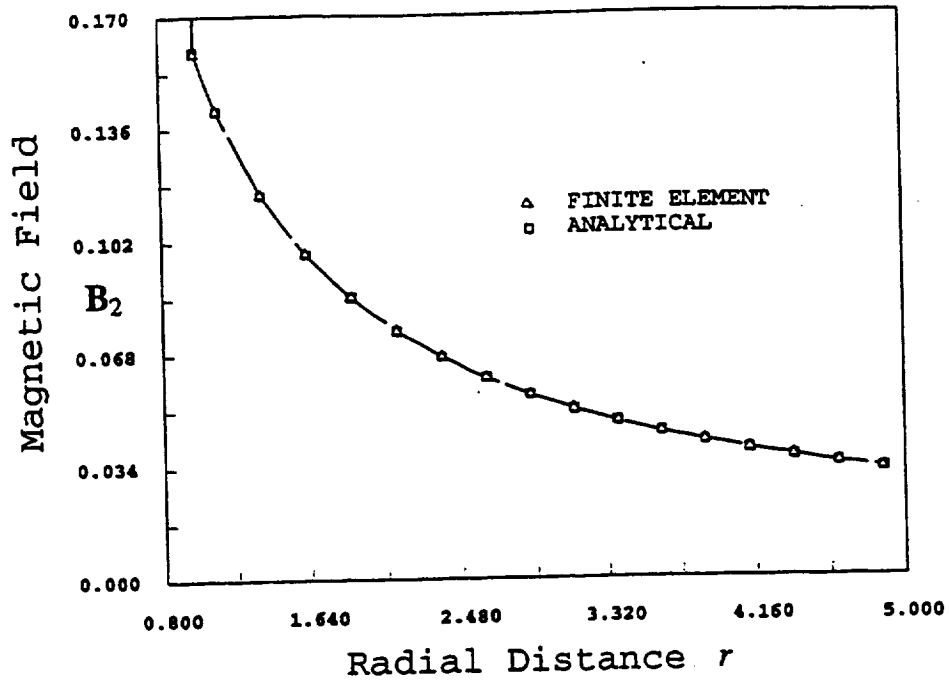
Figure 5. Restriction of Figure 3 to $r > R = 1$, $\mu_{wire} = 10.0$, showing free space magnetic flux density in more detail.
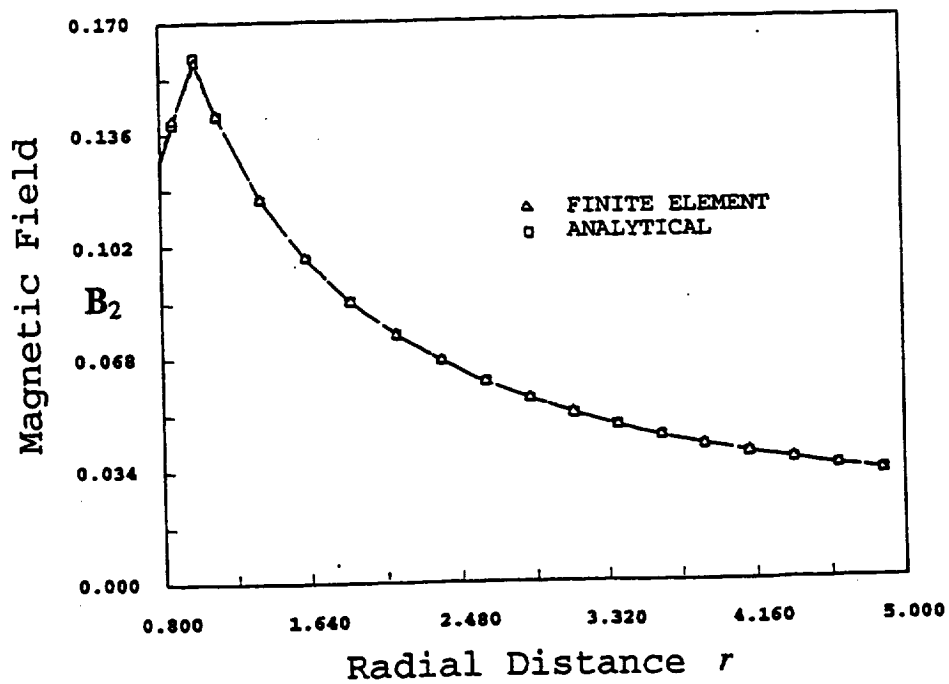

Figure 6. Restriction of Figure 4 to $r > R = 1$, $\mu_{wire} = 1.0$, showing free space magnetic flux density in more detail.

174

elements into free space, with a double node at the counductor boundary. The last node is placed at $r = R_T$ at which point the free space mesh is truncated; usually $R_T = 4R$ to $5R$. Although the mesh appears to be one-dimensional, a typical element actually forms a "tube" of longitudinal axis z, internal radius r_i^e and external radius r_j^e, extending a unit distance along z.

For the present study the magnetic potential was linearly interpolated in r, using the linear shape functions

$$\mathbf{N}_A^e = \langle \tfrac{1}{2}(1-\xi) \quad \tfrac{1}{2}(1+\xi) \rangle,\tag{59}$$

where ξ is the dimensionless isoparametric coordinate that varies from -1 at node i to $+1$ at node j. This interpolation provides for C^0 continuity of the potential inside the conductor and in free space.

For the calculation of the element stiffnesses and force vectors, it was assumed that the permeability μ and the current density j_3 were uniform over the element. Then analytical integration over the element geometry gives

$$\mathbf{K}_A^e = \frac{\mu\, r_m}{\ell} \begin{bmatrix} 1 & -1 \\ -1 & 1 \end{bmatrix}, \qquad \mathbf{f}_A^e = j_3 \ell \left\{ \begin{array}{l} \tfrac{1}{6}(2r_i^e + r_j^e) \\ \tfrac{1}{6}(r_i^e + 2r_j^e) \end{array} \right\},\tag{60}$$

where $r_m = \tfrac{1}{2}(r_i^e + r_j^e)$ is the mean radius and $\ell = r_j^e - r_i^e$ the radial length. For the test problem, μ is constant inside the conductor whereas outside it $\mu = \mu_0$ was assumed to be unity. The longitudinal current density is $j_3 = I/(\pi R^2)$ inside the conductor whereas outside it j_3 vanishes.

The master stiffness matrix and force vector were assembled following standard finite element techniques. The only essential boundary condition was the setting of the nodal potential on the truncation boundary to zero, as explained in Section 6.5. The modified master equations were processed by a conventional symmetric skyline solver, which provided the value of the magnetic potential at the mesh nodes. The magnetic flux density B_2, which is constant over each element, was recovered in element by element fashion through the simple finite difference scheme

$$B_2^e = -\frac{\partial A_3}{\partial r} \approx \frac{A_{3i}^e - A_{3j}^e}{\ell}.\tag{61}$$

This value is assigned to the center of element e.

7.2 Numerical Results

The numerical results shown in Figures 1 through 6 pertain to a unit radius conductor ($R = 1$), with the external (free space) mesh truncated at $R_T = 5$. The element radial lengths $r_j^e - r_i^e$ were kept constant and equal to 0.25, which corresponds to 4 internal and 16 external elements.

The computed values of the potential A_3 are compared with the analytical solution given by Eqs. (33) and (40). As can be seen the agreement is excellent. The comparison between computed and analytical values of the magnetic flux density B_2 shows excellent agreement except for the last element near the wire center, at which point the difference scheme (61) loses accuracy. The permeability of free space is conventionally selected to be unity. Figures 1, 3, and 5 illustrate the case where the wire permeability μ_{wire} is set to 10.0, whereas Figures 2, 4, and 6 are for the

case in which μ_{wire} is 1.0, that is, same as in free space. (The value of the susceptibility ϵ does not appear in these magnetostatic computations.) Figures 1 and 2 show computed and analytical magnetic potentials. The slope discontinuity at $r = 1$ in Figure 1 is a consequence of the change in permeability μ from the wire material to free space. Figures 3 and 4 show the computed and analytical magnetic flux densities. As discussed in Section 5.2, the jump at $r = 1$ in Figure 3 is due to the change in permeability μ from the material to free space. Figures 5 and 6 show the computed and analytical magnetic flux densities in free space with more detail. Note that Figures 5 and 6 for $r > 1$ are identical; this is the expected result because, as shown in Section 5.1, the free-space magnetic flux field depends only upon the current enclosed by a surface integral around the wire and not on the details of the interior field distribution.

In summary, the finite element model performed very accurately in the test problem and converged, as expected, to the analytical solution as the size of the elements decreased.

8. CONCLUSIONS

The results obtained in the one-dimensional steady-state case are encouraging, and appear to be extensible to two- and three-dimensional problems without major difficulties. The electric field remains effectively decoupled from the magnetic field except through Ohm's law. Care must be taken, however, in modeling the forcing function terms so as to avoid the appearance of discontinuity-induced forces at physical interfaces.

The next step in achieving the goal of a finite element model for a superconductor field is to study the time-dependent case, starting with harmonic currents and proceeding eventually to general transients. The code for this is currently written, but a suitable analytical solution for comparison with computed responses is still being developed.

If encouraging results are obtained in the dynamic case, thermocoupling effects will be added to the code. References [3,17,22] discuss several different approaches applicable to various contexts (e.g. eddy currents) and these will have to be investigated for suitability for capturing the couplings effects that are relevant to the superconducting problem.

After modeling the coupling effects, the next step will be to model the superconducting fields. The feasibility of using the current model for superconductor applications is great, as the current density of a superconductor can be approximated by the standard current density multiplied by a constant squared. This constant is called the *London penetration depth*. Other analytical models that possess similar characteristics have been developed and are presented in Ref. [11].

REFERENCES

1. Davies, J. B., The Finite Element Method, Chapter 2 in *Numerical Techniques for Microwave and Millimeter-Wave Passive Structures*, T. Itoh (ed.), Wiley, New York, 1989

2. Eyges, L. *The Classical Electromagnetic Field*, Dover, New York, 1980

3. Fano, R.M., Chu, L.J., and Adler, R.B., *Electromagnetic Fields, Energy, and Forces*, John Wiley and Sons, Inc., New York, 1960

4. Felippa, C. A. and Geers, T. L., Partitioned Analysis of Coupled Mechanical Systems, *Engineering Computations*, 5, 1988, pp. 123–133

5. Felippa, C. A., The Extended Free Formulation of Finite Elements in Linear Elasticity, *Journal of Applied Mechanics*, 56, 3, 1989, pp. 609–616

6. Felippa, C. A. and Militello, C., The Variational Formulation of High-Performance Finite Elements: Parametrized Variational Principles, (with C. Militello), submitted to *Computers & Structures*, 1989

7. Felippa, C. A. and Militello, C., Developments in Variational Methods for High-Performance Plate and Shell Elements, to be presented at the ASME Winter Annual Meeting, San Francisco, December 1989

8. Felippa, C. A. and Ohayon, R. Treatment of Coupled Fluid-Structure Interaction Problems by a Mixed Variational Principle, *Proceedings 7th International Conference on Finite Element Methods in Fluids*, ed. by T.J. Chung *et.al.*, University of Alabama Press, Huntsville, Alabama, April 1989, pp. 555-563

9. Felippa, C. A. and Ohayon, R. Mixed Variational Formulation of Finite Element Analysis of Acousto-elastic Fluid-Structure Interaction, submitted to *Journal of Fluids & Structures*, 1989

10. Grant, I.S., and Phillips, W.R., *Electromagnetism*, John Wiley and Sons, Inc., New York, 1975

11. Kittel, C., *Introduction to Solid State Physics*, 6th. ed, John Wiley and Sons, Inc., New York, 1986

12. Lanczos, C. *The Variational Principles of Mechanics*, Univ. of Toronto Press, Toronto, 1949

13. Lorentz, H. A., *Theory of Electrons*, 2nd. ed, Dover, New York, 1952

14. Militello, C. and Felippa, C. A., A Variational Justification of the Assumed Natural Strain Formulation of Finite Elements: I. Variational Principles, (with C. Militello), submitted to *Computers & Structures*, 1988

15. Militello, C. and Felippa, C. A., A Variational Justification of the Assumed Natural Strain Formulation of Finite Elements: II. The C^0 4-Node Plate Element, submitted to *Computers & Structures*, 1988

16. Park, K. C. and Felippa, C. A., Partitioned Analysis of Coupled Systems, Chapter 3 in *Computational Methods for Transient Analysis*, T. Belytschko and T. J. R. Hughes, eds., North-Holland, Amsterdam-New York, 1983

17. Parkus, H., ed., *Electromagnetic Interactions in Elastic Solids*, Springer-Verlag, Berlin, 1979

18. Purcell, E.M., *Electricity and Magnetism*, Vol. 2, McGraw-Hill, New York, 1985

19. Rojanski, V., *The Electromagnetic Field*, Dover, New York, 1979

20. Shadowitz, A. *The Electromagnetic Field*, Dover, New York, 1975

21. Trowbridge, C. W., Numerical Solution of Electromagnetic Field Problems in Two and Three Dimensions, Chapter 18 in *Numerical Methods in Coupled Problems*, ed. by R. Lewis *et.al.*, Wiley, London, 1984

22. Yuan, K.-Y., Moon, F. C. and Abel, J. F., Elastic Conducting Structures in Pulsed magnetic Fields, Chapter 19 in *Numerical Methods in Coupled Problems*, ed. by R. Lewis *et.al.*, Wiley, London, 1984

AN UNCONDITIONALLY STABLE STAGGERED ALGORITHM
FOR TRANSIENT FINITE ELEMENT ANALYSIS
OF COUPLED THERMOELASTIC PROBLEMS

Abstract — An unconditionally stable second order accurate implicit-implicit staggered procedure for the finite element solution of fully coupled thermoelasticity transient problems is proposed. The procedure is stabilized with a semi-algebraic augmentation technique. A comparative cost analysis reveals the superiority of the proposed computational strategy to other conventional staggered procedures. Numerical examples of one and two-dimensional thermomechanical coupled problems demonstrate the accuracy of the proposed numerical solution algorithm.

I. INTRODUCTION

Transient response prediction of thermally loaded structures is of considerable importance in many aerospace engineering problems, and it has been the subject of intense research. Finite element formulations of the classical heat conduction problem without mechanical coupling have been presented by Wilson and Nickell [1]. Ritz type methods for the solution of linear dynamic problems in coupled thermoelasticity were given by Nickell and Sackman [2]. Oden [3] has formulated finite element models for the analysis of a class of nonlinear problems in dynamic coupled thermoelasticity, and Oden and Armstrong [4] have developed explicit quadratic numerical schemes for the integration of nonlinear unpartitioned systems of difference equations arising from the analysis of dynamic coupled thermoviscoelastic problems. Recently, Ting and Chen [5] have introduced a unified numerical approach for the analysis of thermal stress waves. They have derived their algorithm from the concept of heat displacement and a variational formulation in Lagrangian form. They have proposed to integrate the resulting semi-discrete equations with conditionally stable

explicit schemes. Liu and Zhang [6] have described an implicit-explicit procedure for the prediction of thermal stress waves in coupled thermoelasticity problems. They have adopted the explicit rational Runge-Kutta method [7, 8] for approximately solving the heat conduction equation and have claimed that their solution procedure is unconditionally stable. However, their computational strategy requires the manipulation of a full matrix. In a sequel note, Liu and Chang [9] have slightly modified the original procedure of Liu and Zhang to involve a banded rather than full matrix, and have numerically verified the unconditional stability on one dimensional problems.

However, several practical issues must be resolved before unconditionally stable explicit rational Runge-Kutta schemes can become suitable for the analysis of real thermomechanical coupled problems. First, when unconditional stability is achieved for explicit time integration algorithms, typically consistency becomes conditional (see for example Hughes and Belytschko [10]). Second, most rational Runge-Kutta algorithms involve some divide operations by the difference between intermediate solution quantities, which can significantly damage accuracy. Finally, these algorithms do not appear to accomodate staggered solution procedures for thermal/structure interaction problems, as they are not implemented in many existing production-level thermal computer programs.

The semi-discrete equations governing soil-pore fluid interaction dynamic problems and those resulting from a mixed pressure-velocity formulation for fluid/structure problems are similar to those governing thermoelastic coupled transient problems. In this sense, the work of Liu and Chang [11] and the very recent work of Zienkiewicz, Paul and Chan [12] could be extended to the response analysis of thermally loaded structures.

In the present work, we present an unconditionally stable and robust implicit-implicit partitioned procedure for the solution of transient thermoelastic coupled problems. In Section II, we briefly review the basic equations for the linearized coupled thermoelasticity theory. A conventional implicit-implicit staggered solution procedure is summarized in Section III. The thermal coupling term in the structural dynamics equation is treated as an applied force. However, while being very simple to implement, the resulting time integration algorithm suffers from conditional stability. In Section IV, we introduce an augmented implicit-implicit staggered solution procedure for the partitioned problem. We establish the unconditional stability and second order accuracy of the resulting numerical algorithm in Section V. In Section VI, we discuss the computer implementation aspects of the proposed computational strategy; we conduct a comparative cost analysis which demonstrates the superiority of the proposed solution procedure to other conventional staggered schemes. Finally in Section VII, we apply our partitioned algorithm to the solution of the one-dimensional Second Danilovskaya [13] and two-dimensional Youngdahl-Sternberg [14] problems. For both problems, the results generated by the proposed stabilized procedure are shown to be in excellent agreement with the analytical "exact" solutions.

II. FINITE ELEMENT FORMULATION

Let B denote the body of the structure to be analyzed, and $\partial B = \partial B_u \cup \partial B_s \cup \partial B_\theta \cup \partial B_q$ the surface enclosing it. The basic equations for the linearized isotropic coupled thermoelasticity theory are:

$$
\begin{aligned}
\rho\ddot{\mathbf{u}} &= div\,\sigma + \mathbf{b} \quad \text{in } B \\
c\dot{\theta} &= -div(-k\nabla\theta) - \alpha(3\lambda + 2\mu)\theta_0 tr(\dot{\epsilon}) + r \quad \text{in } B \\
\sigma &= 2\mu\epsilon + \lambda(tr\epsilon)\mathbf{I} - \alpha(3\lambda + 2\mu)(\theta - \theta_0)\mathbf{I} \\
\epsilon &= \frac{1}{2}(\nabla\mathbf{u} + \nabla\mathbf{u}^T)
\end{aligned}
$$

and

$$
\begin{aligned}
\mathbf{u} &= \hat{\mathbf{u}} \quad \text{on } \partial B_u \\
\sigma\mathbf{n} &= \hat{\mathbf{s}} \quad \text{on } \partial B_s \\
\theta &= \hat{\theta} \quad \text{on } \partial B_\theta \\
-k\nabla\theta &= \hat{q} \quad \text{on } \partial B_q
\end{aligned}
$$

(1)

where $\mathbf{u}, \epsilon, \sigma, \theta, \theta_0, \mathbf{b}$, and r are the displacement, strain, stress, temperature, reference temperature chosen such that $(\theta - \theta_0)/\theta_0 << 1$, body force, and heat supply fields, respectively, while $\mu, \lambda, c, \alpha, \rho, k$ and $\mathbf{n}$ are the Lame' moduli, the shear modulus, the specific heat, the coefficient of thermal expansion, the mass per unit volume, the thermal diffusivity, and the normal to the surface at a given point, respectively. $\mathbf{I}$ is the identity tensor. The dot and T superscripts denote a time derivative and a transpose operation, and tr denotes the trace of a given tensor.

If now we express the dependent variables $\mathbf{u}$ and θ by suitable shape functions as:

$$
\mathbf{u} = \mathbf{N}\bar{\mathbf{u}} \quad \text{and} \quad \theta = \hat{\mathbf{N}}\bar{\theta}
$$

then a standard Galerkin procedure transforms (1) in the following algebraic coupled system of differential equations:

$$
\begin{aligned}
\mathbf{M}\ddot{\mathbf{u}} + \mathbf{D}\dot{\mathbf{u}} + \mathbf{K}\mathbf{u} - \mathbf{C}\theta &= \mathbf{f} \\
\mathbf{Q}\dot{\theta} + \mathbf{H}\theta + \theta_0\mathbf{C}^T\dot{\mathbf{u}} &= \mathbf{r}
\end{aligned}
$$

(2)

where $\mathbf{M}, \mathbf{D}$ and $\mathbf{K}$ are the usual mass, damping and stiffness matrices, $\mathbf{f}$ is the prescribed structural loading vector, and $\mathbf{Q}, \mathbf{H}$, and $\mathbf{r}$ are respectively the capacity and conductivity matrices and the nodal source vector. If $\mathbf{L}$ denotes the differential operator corresponding to strain, the coupling matrix is expressed as $\mathbf{C} = \int_B (\mathbf{L}\mathbf{N})^T[1, 1, 1, 0, 0, 0]\hat{\mathbf{N}}dB$.

III. CONVENTIONAL IMPLICIT-IMPLICIT PROCEDURE

In many applications, the coupling term $C^T\dot{u}$ that appears in the heat equation and which is induced by the effect of the strain rate is negligible. Therefore, one expects the second of equations (2) to remain parabolic and the temperature response to remain close to the uncoupled solution. Consequently, the dependent variable θ is easier to predict than the displacement u, so that the most natural way of solving (2) would be:

$$M\ddot{u}^{n+1} + D\dot{u}^{n+1} + Ku^{n+1} = f^{n+1} + C\theta^{n+1^P}$$
$$Q\dot{\theta}^{n+1} + H\theta^{n+1} = r^{n+1} - \theta_0 C^T\dot{u}^{n+1}$$

(3)

where θ^{n+1^P} is the predicted temperature. Unfortunately, the above numerical procedure is only conditionally stable, even when each field is integrated with an unconditionally stable algorithm. Proofs of this result are given by Dubois-Pelerin [15] for various consistent predictors. Next, we introduce an augmentation technique that stabilizes the staggered solution of (2).

IV. AN AUGMENTED IMPLICIT-IMPLICIT PARTITIONED PROCEDURE

Park, Felippa and DeRuntz [16] have introduced a differential augmentation concept that was successfully used in the stabilization of staggered solution procedures for fluid-structure interaction problems. Basically, one of the coupled equations is injected into the other in order to "soften" the system, either by reducing the large eigenvalues of the uncoupled stiff equation, or by introducing some damping into it. Here, we adopt a different strategy. We perform a semi-algebraic augmentation — that is, we augment one of the two coupled equations while integrating both fields.

First, the structural equation is integrated with the trapezoidal rule:

$$\dot{u}^{n+1} = \dot{u}^n + \frac{\Delta t}{2}(\ddot{u}^{n+1} + \ddot{u}^n)$$
$$= \dot{u}^n + \frac{\Delta t}{2}[\ddot{u}^n + M^{-1}(f^{n+1} - D\dot{u}^{n+1} - Ku^{n+1} + C\theta^{n+1})]$$
$$u^{n+1} = u^n + \frac{\Delta t}{2}(\dot{u}^{n+1} + \dot{u}^n)$$
$$= u^n + \Delta t\dot{u}^n + \frac{\Delta t^2}{4}[\ddot{u}^n + M^{-1}(f^{n+1} - D\dot{u}^{n+1} - Ku^{n+1} + C\theta^{n+1})]$$

(4)

and the velocity vector is extracted as:

$$(I + \frac{\Delta t}{2}M^{-1}D)\dot{u}^{n+1} = \dot{u}^n + \frac{\Delta t}{2}[\ddot{u}^n + M^{-1}(f^{n+1} - Ku^{n+1} + C\theta^{n+1})]$$

(5)

Next, the heat equation is also integrated with the trapezoidal rule:

$$\theta^{n+1} = \theta^n + \frac{\Delta t}{2}(\dot{\theta}^{n+1} + \dot{\theta}^n)$$

$$= \theta^n + \frac{\Delta t}{2}[\dot{\theta}^n + Q^{-1}(r^{n+1} - H\theta^{n+1} - \theta_0 C^T \dot{u}^{n+1})]$$

(6)

Finally, the system is augmented by recasting (5) in (6) to obtain:

$$\theta^{n+1} = \theta^n + \frac{\Delta t}{2}\{\dot{\theta}^n + Q^{-1}[r^{n+1} - H\theta^{n+1} - \theta_0 C^T(I + \frac{\Delta t}{2}M^{-1}D)^{-1}$$

$$(\dot{u}^n + \frac{\Delta t}{2}(\ddot{u}^n + M^{-1}(f^{n+1} - Ku^{n+1} + C\theta^{n+1})))]\}$$

(7)

Substituting (5) into the second of equations (4) and re-arranging (7) leads to:

$$(I + \frac{\Delta t^2}{4}B(\Delta t)M^{-1}K)\,u^{n+1} - \frac{\Delta t^2}{4}B(\Delta t)M^{-1}C\,\theta^{n+1} = F^{n+1}$$

$$(-\frac{\Delta t^2}{4}\theta_0 AK)\,u^{n+1} + (I + \frac{\Delta t}{2}Q^{-1}H + \frac{\Delta t^2}{4}\theta_0 AC)\,\theta^{n+1} = R^{n+1}$$

(8)

where

$$A = Q^{-1}C^T M^{-1}$$

$$B(\Delta t) = (I + \frac{\Delta t}{2}M^{-1}D)^{-1}$$

$$F^{n+1} = u^n + \frac{\Delta t}{2}(I + B(\Delta t))\dot{u}^n + \frac{\Delta t^2}{4}(B(\Delta t)\ddot{u}^n + M^{-1}B(\Delta t)f^{n+1})$$

$$R^{n+1} = \theta^n + \frac{\Delta t}{2}[\dot{\theta}^n + Q^{-1}(r^{n+1} - \theta_0 C^T B(\Delta t)\dot{u}^n)]$$

$$- \frac{\Delta t^2}{4}[\theta_0 Q^{-1}C^T(B(\Delta t)\ddot{u}^n + B(\Delta t)M^{-1}f^{n+1})]$$

(9)

Now, a displacement predicted staggered procedure for the solution of (8) is:

1. Predict the displacement field:

$$u^{n+1^P} = u^n$$

(10)

2. Solve for the temperature field:

$$(I + \frac{\Delta t}{2}Q^{-1}H + \frac{\Delta t^2}{4}\theta_0 AC)\,\theta^{n+1} = R^{n+1} + \frac{\Delta t^2}{4}\theta_0 AK\,u^{n+1^P}$$

(11)

3. Correct the displacement field:

$$(I + \frac{\Delta t^2}{4} B(\Delta t) M^{-1} K)\, u^{n+1} = F^{n+1} + \frac{\Delta t^2}{4} B(\Delta t) M^{-1} C\, \theta^{n+1} \tag{12}$$

4. Compute velocity, acceleration and flux fields:

$$\dot{u}^{n+1} = B(\Delta t)\{\dot{u}^n + \frac{\Delta t}{2}[\ddot{u}^n + M^{-1}(f^{n+1} - Ku^{n+1} + C\theta^{n+1})]\}$$

$$\ddot{u}^{n+1} = M^{-1}(f^{n+1} + C\theta^{n+1} - D\dot{u}^{n+1} - Ku^{n+1}) \tag{13}$$

$$\dot{\theta}^{n+1} = Q^{-1}(r^{n+1} - \theta_0 C^T \dot{u}^{n+1} - H\theta^{n+1})$$

Remarks:

1. The predictor $u^{n+1\,P}$ is simply the previous step solution. It has been found (see, for example, [17]) that this is the most stable predictor when used in conjunction with the trapezoidal rule, while still maintaining a second-order accuracy.

2. The injection of (5) into (6) is not arbitrary. It will be shown in Section VI that this is more economical than injecting (6) into (5).

3. Equations (13) define the computational path of the staggered procedure.

V. STABILITY AND ACCURACY ANALYSES

In this section, we establish that equations (10)-(13) result in a unconditionally stable second order accurate transient algorithm for the time integration of the coupled system (2). To avoid lengthy expressions, we consider the undamped ($D = 0$) and unforced ($f = r = 0$) case. Note however that even when $D = 0$, the quantity $C\theta$ still transmits a rate dependent damping effect to the structural equation.

Stability. The stability of the proposed staggered procedure can be examined by seeking a nontrivial solution in the form:

$$\begin{bmatrix} u^{n+1} \\ \dot{u}^{n+1} \\ \ddot{u}^{n+1} \\ \theta^{n+1} \\ \dot{\theta}^{n+1} \end{bmatrix} = \frac{1+z}{1-z} \begin{bmatrix} u^n \\ \dot{u}^n \\ \ddot{u}^n \\ \theta^n \\ \dot{\theta}^n \end{bmatrix} \tag{14}$$

and determining under what condition the real part of z is positive. Substitution of (10) into (11) and (14) into (11)-(13) yields, after some algebraic manipulations:

$$\begin{bmatrix} z^2 I + \frac{\Delta t^2}{4} M^{-1} K & -\frac{\Delta t^2}{4} M^{-1} C \\ -(1 - z^2)\frac{\Delta t^2}{4}\theta_0 AK & z^2 I + z\frac{\Delta t}{2}Q^{-1}H + \frac{\Delta t^2}{4}\theta_0 AC \end{bmatrix} \begin{bmatrix} u^n \\ \theta^n \end{bmatrix} = \begin{bmatrix} 0 \\ 0 \end{bmatrix} \tag{15}$$

184

Therefore, the characteristic equation associated with (15) is:

$$| \, \mathbf{M}z^3 + \mathbf{VM}\frac{\Delta t}{2}z^2 + (\mathbf{K} + \theta_0 \mathbf{CQ}^{-1}\mathbf{C}^T + \frac{\Delta t^2}{4}\theta_0 \mathbf{CQ}^{-1}\mathbf{C}^T\mathbf{M}^{-1}\mathbf{K})\frac{\Delta t^2}{4}z + \mathbf{VK}\frac{\Delta t^3}{8} \, | \; = \; 0 \quad (16)$$

where

$$\mathbf{V} \, = \, \mathbf{CUC}^T, \qquad \mathbf{U} \, = \, \mathbf{Q}^{-1}\mathbf{H}(\mathbf{C}^T\mathbf{C})^{-1}$$

and $|\,\,|$ denotes the matrix determinant. If the matrices $\mathbf{M}$, $\mathbf{K}$, $\mathbf{Q}$ and $\mathbf{H}$ are positive definite, and the coupling matrix $\mathbf{C}$ has full column rank, then $\mathbf{U}$, $\mathbf{V}$ and each matrix coefficient of the determinant expression (16) is positive definite. If $\mathbf{C}$ is column rank deficient, $\mathbf{U}$ and $\mathbf{V}$ are positive semi-definite. In any case, all coefficients of the stability polynomial are non-negative. Consequently, the first part of the Routh-Hurwitz criterion [18] for unconditional stability is satisfied. In order to check the second component of this criterion, we consider a 2-d.o.f. model problem for (2). The corresponding scalar form of (16) is:

$$a_3 z^3 + a_2 z^2 + a_1 z + a_0 \; = \; 0 \tag{17}$$

where

$$a_3 = 1, \quad a_2 = \frac{\Delta t h}{2q}, \quad a_1 = \frac{\Delta t^2}{4}[\omega^2 + \frac{\theta_0 c^2}{qm}(1 + \frac{\Delta t^2}{4}\omega^2)], \quad a_0 = \frac{\Delta t^3 h}{8q}\omega^2$$

Since $\Delta t, h, q, w^2, \theta_0, c^2$, and $m \, > \, 0$, then all the coefficients of the polynomial (17) in z are positive. Morevoer, the quantity

$$a_1 a_2 - a_0 a_3 \; = \; \frac{\theta_0 h c^2 \Delta t^3}{8mq^2}(1 + \frac{\Delta t^2}{4}w^2)$$

is also positive, which demonstrates that the staggered solution procedure is unconditionally stable for the 2-d.o.f. model problem.

For the general multi-dimensional case, it turns out that the limiting case $\mathbf{K} = 0$ which states that the structural system will grow quadratically in time, provides a sufficient test. For this case, (16) reduces to:

$$| \, \mathbf{M}z^2 + \frac{\Delta t}{2}\mathbf{VM}z + \frac{\Delta t^2}{4}\theta_0 \mathbf{CQ}^{-1}\mathbf{C}^T \, | \; = \; 0$$

Since $\mathbf{M}$ is positive definite and $\mathbf{VM}$ and $\mathbf{CQ}^{-1}\mathbf{C}^T$ are at least positive semi-definite, the procedure is unconditionally stable for the limiting case $\mathbf{K} = 0$, as discussed in Bellman [19]. This argument has been extensively utilized in [17] during the analysis of several partitioned procedures. Therefore, we conclude that the procedure given by (10)-(13) is unconditionally stable.

185

Remarks:

1. The characteristic equation (16) reveals that the proposed procedure (10)-(13) is algorithmically identical to the one obtained by first differentiating the second of equations (2):

$$Q\ddot{\theta} + H\dot{\theta} + \theta_0 C^T \ddot{u} = \dot{r}$$

then substituting $\ddot{u}$ from the first of equations (2) into the above equation:

$$Q\ddot{\theta} + H\dot{\theta} + \theta_0 C^T M^{-1} C\theta = = \dot{r} - \theta_0 C^T M^{-1}(f - Ku)$$

However, differentiating the nodal source vector may be not practical, for example, if r is a discontinuous function of time. In our present derivation (11)-(13) we avoid this problem.

2. The first-order thermal equation is algorithmically modified to behave as a damped second-order system. It should be emphasized that the described stabilization technique has *not* introduced any artificial damping. The only augmentation that is used is part of the governing equation of motion itself.

Accuracy. After differentiation, the third of equations (13) in the unforced case reads:

$$\ddot{\theta}^{n+1} = -\theta_0 Q^{-1} C^T \ddot{u}^{n+1} - Q^{-1} H \dot{\theta}^{n+1} \tag{18}$$

Expanding the various terms in (8) around the time $n\Delta t$ and injecting (13) and (18) when needed leads to:

$$M\ddot{u}^n + Ku^n = C\theta^n + O(\Delta t^2)$$
$$Q\dot{\theta}^n + H\theta^n = -\theta_0 C^T \dot{u}^n + O(\Delta t^2) \tag{19}$$

Comparing (2) and (19) demonstrates that the staggered procedure is second order accurate. The same result can be proved for the damped ($D \neq 0$) and forced ($f \neq 0$, $r \neq 0$) case.

VI. COMPUTATIONAL ASPECTS

In the remainder of this paper, we consider the case where the structure is undamped ($D = 0$) and the mass and capacity matrices are lumped (M, Q are diagonal). The unconditionally stable staggered procedure (10)-(13) can be implemented as:

1. Form:

$$R^{n+1*} = \frac{\Delta t}{2} r^{n+1} + Q[\theta^n + \frac{\Delta t}{2}(\dot{\theta}^n - \theta_0 C^T \dot{u}^n)] - \frac{\Delta t^2}{4}\theta_0 C^T [\ddot{u}^n + M^{-1}(f^{n+1} - Ku^{n+1^P})] \tag{20}$$

186

2. Solve:

$$(Q + \frac{\Delta t}{2} H + \frac{\Delta t^2}{4} \theta_0 C^T M^{-1} C) \theta^{n+1} = R^{n+1*} \tag{21}$$

3. Form:

$$F^{n+1*} = M[u^n + \Delta t (\dot{u}^n + \frac{\Delta t}{4} \ddot{u}^n)] + \frac{\Delta t^2}{4} (f^{n+1} + C\theta^{n+1}) \tag{22}$$

4. Solve:

$$(M + \frac{\Delta t^2}{4} K) u^{n+1} = F^{n+1*} \tag{23}$$

5. Update:

$$\ddot{u}^{n+1} = M^{-1} (f^{n+1} + C\theta^{n+1} - Ku^{n+1})$$

$$\dot{u}^{n+1} = \dot{u}^n + \frac{\Delta t}{2} (\ddot{u}^n + \ddot{u}^{n+1}) \tag{24}$$

$$\dot{\theta}^{n+1} = Q^{-1} (r^{n+1} - \theta_0 C^T \dot{u}^{n+1} - H\theta^{n+1})$$

Equations (20) to (24) involve algebraic computations that are common to most implicit algorithms, when applied to the uncoupled problem. Only the quantity $C^T M^{-1} C$ deserves special attention. In particular, it is important to note that:

- $C^T M^{-1} C$ is not a full matrix. It is a symmetric banded operator. Let n_s, n_h, b_s and b_h denote the sizes and the semi-bandwidths of the structural and heat matrices, respectively. Typically, n_s and b_s are two to six times larger than n_h and b_h. The matrix product $C^T M^{-1} C$ is n_h by n_h and has a semi-bandwidth close to $2b_h$. Therefore, equation (21) entails the solution of an n_h by n_h symmetric banded system. On the other hand, if equation (6) had been injected into equation (5) — that is, if the temperature field had been eliminated from the structural equation — the resulting augmentation term would have been $CQ^{-1}C^T$ which is n_s by n_s and has a semi-bandwidth close to $2bs$. The latter would have entailed the solution of a symmetric system that is several times larger and denser than (21). For a rectilinear mesh composed of two-dimensional truss elements, the patterns of matrices C, C^T, $C^T M^{-1} C$ and $CQ^{-1}C^T$ are depicted in Figure 1.

- the additional cost incurred by the augmentation term is restricted to the factorization and subsequent solutions of equation (21). The precise value of this additional cost (with respect to the conventional procedure (3)) depends on the cleverness of the implementation.

At this point we also note that the quantity $C^T M^{-1} C$ is common to several coupled field problems. Its pattern, storage and computational properties have also been recognized and analyzed by previous investigators in different areas (see for example Liu and Chang [12]).
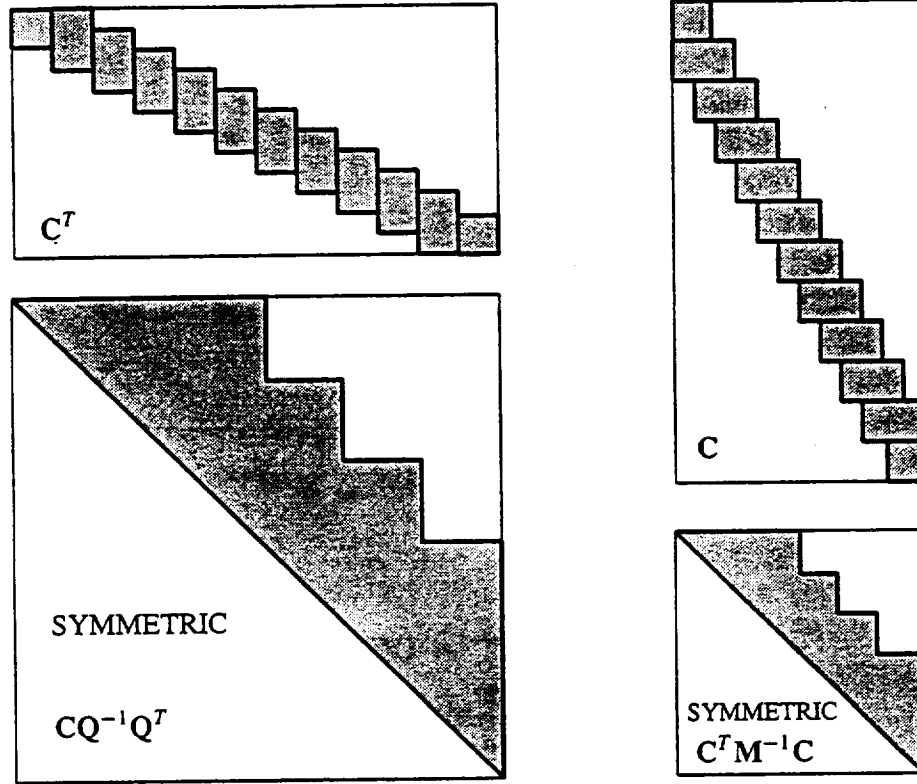
Figure 1. Patterns of the coupling matrices for a
rectilinear mesh with 2D truss elements

In order to illustrate the computational costs of the proposed numerical procedure, we consider the problem of a clamped square plate where the edges are exposed to a sudden heating. The finite element mesh is composed of N by N 4-node regular elements. The stiffness and conductivity matrices $\mathbf{K}$ and $\mathbf{Q}$ are assumed to be stored in banded form so that operation counting is facilitated. In practice, these matrices are compacted in skyline data structures. We denote by d and p, respectively the number of structural degrees of freedom per node ($d \leq 6$) and the number of integration steps.

The assumption of an N by N regular mesh with a number of fixed degrees of freedom at each node is unlikely in practice. However, it is the worst case as far as the computational effort required for the evaluation of the product $\mathbf{C}^T \mathbf{M}^{-1} \mathbf{C}$.

For the above problem, the formation and factorization of equations (21) and (23) require respectively $(2+d)N^4$ and $d^3 N^4 / 2$ multiplications. The resolution of equations (20)-(24) requires $(7d^2 + 6d + 3)N^3$ multiplications for each time step. Therefore, the total computational effort needed for the transient coupled solution using the proposed stabilized procedure is:

$$E^s \sim (\frac{d^3}{2} + d + 2)N^4 + p^s(7d^2 + 6d + 3)N^3 \qquad (25)$$

For the same problem, the computational cost associated with a conventional second-order accurate conditionally stable procedure (3) is:

$$E^c \sim (\frac{d^3+1}{2})N^4 + p^c(7d^2 + 6d + 3)N^3 \qquad (26)$$

Clearly, unconditional stability is obtained at the cost of $(d+3/2)N^4$ additional floating point operations. For linear problems, this computational effort is needed once. In the following, we show that this overhead is compensated by a much larger time step.

The natural frequencies of the clamped square plate are given by:

$$\omega_{mn} = \pi^2 \sqrt{\frac{El^3}{12(1-\nu^2)\rho}}(\frac{m^2+n^2}{a^2}) \qquad (27)$$

where E, ν, l, and a are respectively Young modulus, Poisson's coefficient, the plate thickness and its edge size [20]. Therefore, the lowest frequency is:

$$\omega_{min} = \frac{2\pi^2}{a^2} \sqrt{\frac{El^3}{12(1-\nu^2)\rho}} \qquad (28)$$

and a good approximation of the highest element frequency is:

$$\omega_{max}^{(e)} = \frac{2\pi^2}{a^2}N^2 \sqrt{\frac{El^3}{12(1-\nu^2)\rho}} \qquad (29)$$

An adequate time step for the stabilized procedure is given by $\omega_{min}\Delta t^s = \pi/10$. For the conventional conditionally stable staggered procedure where both u and θ are integrated with the trapezoidal rule, the stable time step is expressed as a multiple of the time step based on the Courant condition associated with the hyperbolic structural equation. Hence, $\Delta t^c = m \times 2/\omega_{max}^{(e)}$, where $m \geq 1$. Using (28) and (29) we have:

$$\Delta t^s = \frac{a^2}{20\pi} \sqrt{\frac{12(1-\nu^2)\rho}{El^3}}, \qquad \Delta t^c = \frac{ma^2}{\pi^2 N^2} \sqrt{\frac{12(1-\nu^2)\rho}{El^3}} \qquad (30)$$

so that

$$p^s = 40, \qquad p^c = \frac{2\pi N^2}{m} \qquad (31)$$

are the number of steps which would cover twice the largest period of the problem. The computational costs for both procedures become:

$$E^s \sim (\frac{d^3}{2} + d + 2)N^4, \qquad E^c \sim \frac{2\pi}{m}(7d^2 + 6d + 3)N^5 \qquad (32)$$

which demonstrates the superiority of the proposed stabilized staggered procedure for N sufficiently large ($N > m/14$).

VII. NUMERICAL EXAMPLES

First, we consider the Second Danilovskaya problem [13]. An elastic half-space ($x > 0$) with the surface plane $x = 0$ assumed free of tractions for all time is exposed to a sudden high ambient temperature θ_∞. The continuum is assumed to be mechanically constrained and thermally insulated so that the displacement and temperature fields are given by:

$$u_x = u_x(x, t), \qquad u_y = 0, \qquad u_z = 0, \qquad \theta = \theta(x, t) \tag{33}$$

The boundary and initial conditions for this problem are:

$$\sigma_{xx}(0, t) = 0, \qquad k\frac{\partial\theta}{\partial x}(0, t) = h(\theta(0, t) - \theta_\infty)$$

and

$$\tag{34}$$

$$u_x(x, 0) = 0, \qquad \dot{u}_x(x, 0) = 0, \qquad \theta(x, 0) = \theta_0$$

where h is the boundary-layer conductance. The following dimensionless variables are introduced:

$$\bar{x} = \frac{ax}{\kappa}, \qquad \bar{t} = \frac{a^2 t}{\kappa}, \qquad \bar{\sigma} = \frac{\sigma_{xx}}{\beta\theta_0}, \qquad \bar{\theta} = \frac{\theta - \theta_0}{\theta_0}, \qquad \bar{u} = \frac{a(\lambda + 2\mu)u_x}{\kappa\beta\theta_0} \tag{35}$$

where

$$\kappa = \frac{k}{\rho c}, \qquad a^2 = \frac{\lambda + 2\mu}{\rho}, \qquad \beta = \frac{\alpha}{3\lambda + 2\mu} \tag{36}$$

The thermomechanical coupling parameter is defined by:

$$\delta = \frac{\beta^2\theta_0}{\rho c(\lambda + 2\mu)} = \frac{\beta^2\theta_0}{\rho^2 a^2 c} \tag{37}$$

The exact solution for this problem can be obtained using the Laplace transform (see Nickell and Sackman [21]). The finite element solution is carried out using 2-node linear elements. The ratio $\kappa h/ak$ is fixed to 0.5 and the thermomechanical coupling parameter δ is set to 1. We report on the generated results for two time integration steps, $\Delta t^{(1)} = \pi/5\omega_{min}$ and $\Delta t^{(2)} = \Delta t^{(1)}/2 = \pi/10\omega_{min}$. These correspond to sampling the largest period of the mechanical problem into 10 and 20 steps, respectively. Figure 2 depicts the dimensionless temperature $\bar{\theta}$ at $\bar{x} = 1.0$ as a function of

SECOND DANILOVSKAYA PROBLEM
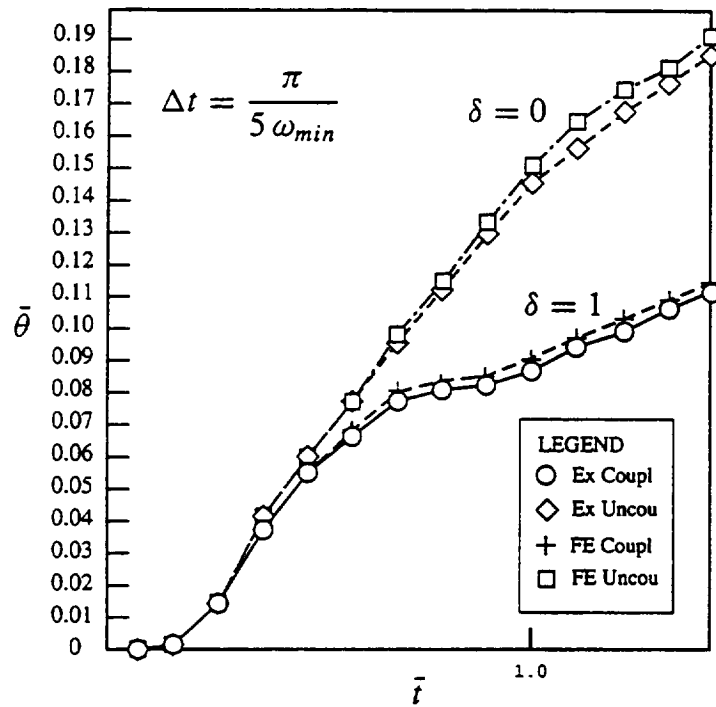
Figure 2. Dimensionless temperature at $\bar{x} = 1.0$

SECOND DANILOVSKAYA PROBLEM
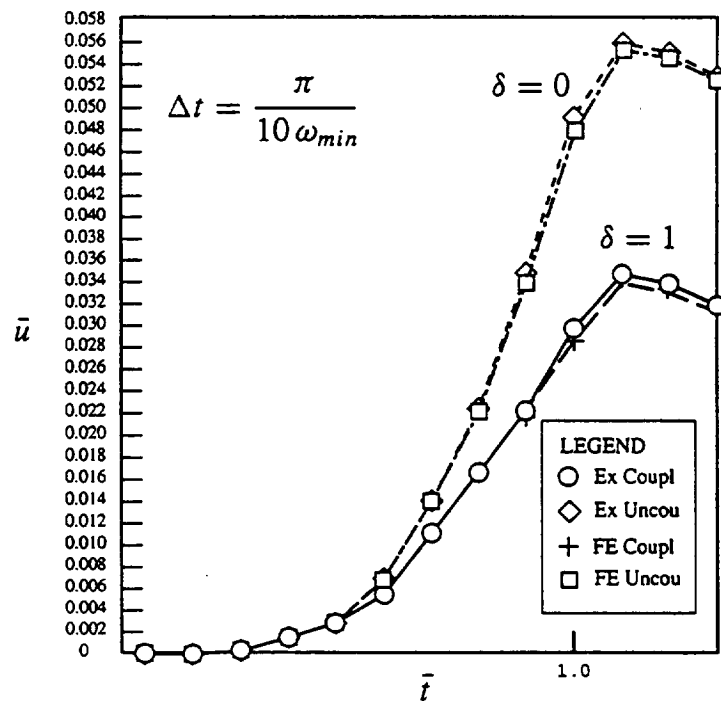
Figure 3. Dimensionless displacement at $\bar{x} = 1.0$

191

the dimensionless time $\bar{t}$, for $\Delta t = \Delta t^{(1)}$. Figure 3 reports the dimensionless displacement $\bar{u}(\bar{t})$ at $\bar{x} = 1.0$, for $\Delta t = \Delta t^{(2)}$. As expected, the results for $\Delta t = \Delta t^{(2)}$ are more accurate than those for $\Delta t = \Delta t^{(1)}$. However in both cases, the generated solutions are in good agreement with the exact ones.
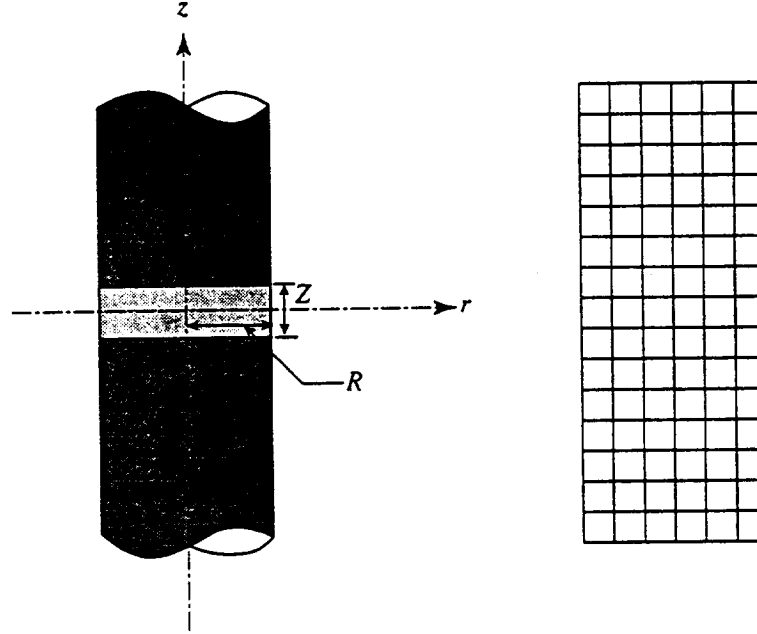
Figure 4. Problem geometry and finite element discretization

Next, we consider the case of an infinitely long elastic circular shaft of radius R, where the surface temperature undergoes a sudden uniform change over a finite band of length Z, and is steadily maintained thereafter (Fig. 4). Youngdahl and Sternberg have presented in [14] an exact solution for the transient temperature and thermal stresses distributions in the shaft, when thermomechanical coupling is neglected, in the form of definite integrals and infinite series. In cylindrical co-ordinates (r, ϕ, z), the axisymmetric torsionless displacement and temperature fields are given as:

$$u_r = u_r(r, z, t), \qquad u_\phi = 0, \qquad u_z = u_z(r, z, t), \qquad \theta = \theta(r, z, t) \qquad (38)$$

The boundary and initial conditions for this problem are:

$$\sigma_{rr}(R, z, t) = 0, \qquad \sigma_{rz}(R, z, t) = 0,$$

$$\sigma_{rr} \to 0 \text{ as } |z| \to \infty, \qquad \sigma_{\phi\phi} \to 0 \text{ as } |z| \to \infty, \qquad \sigma_{zz} \to 0 \text{ as } |z| \to \infty, \qquad \sigma_{rz} \to 0 \text{ as } |z| \to \infty,$$

$$\theta(R, z, t) = \theta_\infty \quad |z| < \frac{Z}{2}, \qquad \theta(R, z, t) = 0 \quad |z| > \frac{Z}{2}$$

and

$$u_r(r, z, 0) = 0, \qquad u_z(r, z, 0) = 0, \qquad \dot{u}_r(r, z, 0) = 0, \qquad \dot{u}_z(r, z, 0) = 0, \qquad \theta(r, z, 0) = 0$$

$$(39)$$

192

YOUNGDAHL-STERNBERG PROBLEM
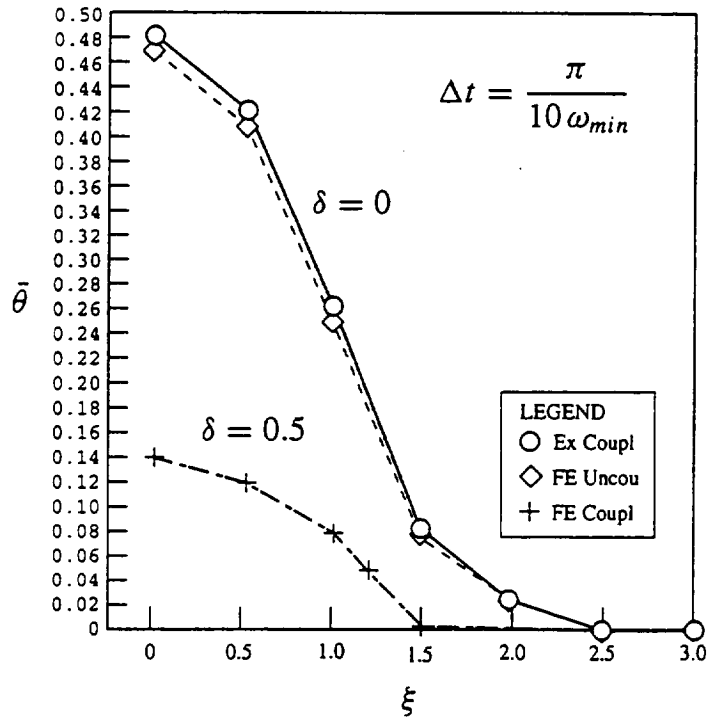
Figure 5. Dimensionless temperature at $\rho = 0$ for $\bar{t} = 0.2$

YOUNGDAHL-STERNBERG PROBLEM
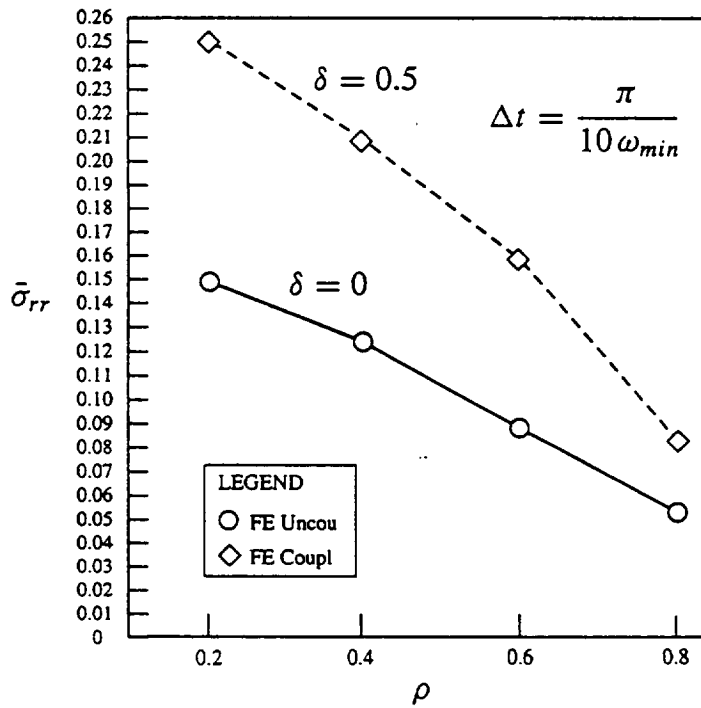
Figure 6. Dimensionless radial stress at $\xi = 0.1$ for $\bar{t} = 0.2$

The following new dimensionless variables (there should be no confusion over the present definition of these variables and their earlier use) are introduced:

$$\rho = \frac{r}{R}, \qquad \xi = \frac{2z}{L}, \qquad \bar{\theta} = \frac{\theta}{\theta_\infty}, \qquad \bar{t} = \frac{kt}{R^2} \qquad (40)$$

For all computations, we set $L = 2R$ and $\nu = 1/4$. The finite element solution is carried out using 4-node axisymmetric linear elements, and a time step $\Delta t = \pi/10 w_{min}$. Figure 5 compares the predicted temperatures at the center of the shaft ($\rho = 0$) with the exact ones for $\delta = 0$, and reports on the effect of thermocoupling ($\delta = 0.5$) on temperature distribution. Clearly, the stabilized procedure provides accurate solutions. The variations of the radial stress at $\xi = 0.1$ for $\delta = 0$ and $\delta = 0.5$ are depicted in Figure 6. All numerical results are reported at $\bar{t} = 0.2$. It is interesting to note that when the thermocoupling effect is neglected the temperature field is overestimated, but the radial stress distribution is underestimated.

VIII. CONCLUSION

An implicit-implicit staggered procedure for the solution of thermoelastic problems is presented. It is stabilized with a cost-effective semi-algebraic augmentation scheme. The resulting transient algorithm is unconditionally stable and second-order accurate.

ACKNOWLEDGMENTS

REFERENCES

[1] E. L. Wilson and R. E. Nickell, "Application of the Finite Element Method to Heat Conduction Analysis", *Nucl. Eng. Des.*, Vol. 4, pp. 276-286 (1966)

[2] R. E. Nickell and J. L. Sackman, "Approximate Solutions in Linear Coupled Thermoelasticity", *J. Appl. Mech.*, Vol. 35, pp. 255-266 (1968)

[3] J. T. Oden, "Finite Element Analysis of Nonlinear Problems in the Dynamical Theory of Coupled Thermoelasticity", *Nucl. Eng. Des.*, Vol. 10, pp. 465-475 (1969)

[4] J. T. Oden and W. H. Armstrong, "Analysis of Nonlinear Dynamic Coupled Thermoviscoelasticity Problems by the Finite Element Method", *Computers & Structures*, Vol. 1, pp. 603-621 (1971)

[5] E. C. Ting and H. C. Chen, "A Unified Numerical Approach for Thermal Stress Waves", *Computers & Structures*, Vol. 15, No. 2, pp. 165-175 (1982)

[6] W. K. Liu and Y. F. Zhang, "Unconditionally Stable Implicit-Explicit Algorithms for Coupled Thermal Stress Waves", *Computers & Structures*, Vol. 17, No. 3, pp. 371-374 (1983)

[7] A. Wamberg, "Rational Runge Kutta Methods for Solving Systems of O. D. E.", *Computing*, Vol. 20, pp. 333-342 (1978)

[8] E. Hairen, "Unconditionally Stable Explicit Methods for Parabolic Equation", Numerical Math., Vol. 35, pp. 57-68 (1980)

[9] W. K. Liu and H. G. Chang, "A Note on Numerical Analysis of Dynamic Coupled Thermoelasticity", *J. Appl. Mech.*, Vol. 52, pp. 483-485 (1985)

[10] T. J. R. Hughes and T. Belytschko, "A Precis of Developments in Computational Methods for Transient Analysis", *J. Appl. Mech.*, Vol. 50, pp. 1033-1041 (1983)

[11] O. C. Zienkiewicz, D. K. Paul and A. H. C. Chan, "Unconditionally Stable Staggered Solution Procedure for Soil-Pore Fluid Interaction Problems", *Int. J. Num. Meth. Eng.*, Vol. 26, pp. 1039-1055 (1988)

[12] W. K. Liu and H. Chang, "On a Numerical Method for Liquid Filled Systems", *Computers & Structures*, Vol. 23, No. 5, pp. 671-677 (1986)

[13] V. I. Danilovskaya, "On a Dynamical Problem of Thermoelasticity", *Prikladnaya Matematika i Mechanika*, Vol. 14, No. 3, pp. 341-344 (1952)

[14] C. K. Youngdahl and E. Sternberg, "Transient Thermal Stresses in a Circular Cylinder", *J. Appl. Mech.*, Vol. 28, pp. 25-34 (1961)

[15] Y. Dubois-Pelerin, "Linear Thermomechanical Coupling by the Staggered Method", *IREM Internal Report*, Ecole Polytechnique Federale de Lausanne (1989)

[16] K. C. Park, C. A. Felippa and J. A. DeRuntz, "Stabilization of Staggered Solution Procedures for Fluid-Structure Interaction Analysis", *Computational Methods for Fluid-Structure Interaction Problems*, ed. by Belytshcko and Geers, ASME Applied Mechanics Symposia Series, AMD, Vol. 26, pp. 94-124 (1977)

[17] K. C. Park, "Partitioned Transient Analysis Procedures for Coupled-Field Problems: Stability Analysis", *J. Appl. Mech.*, Vol. 47, No. 2, pp. 370-376 (1980)

[18] F. R. Gantmacher, "The Theory of Matrices", 2, Chelsea Publication Co., New York, pp. 190-196 (1959)

[19] R. Bellman, "Introduction to Matrix Analysis", 2nd ed., McGraw-Hill, New York, pp. 249-262 (1970)

[20] L. Meirovitch, "Analytical Methods in Vibrations", The Macmillan Company, New York, p. 185 (1967)

[21] R. E. Nickell and J. L. Sackman, "The Extended Ritz Method Applied to Transient Coupled Thermoelastic Boundary-Value Problems", *Rep. No. 67-3, Structures and Materials Research*, University of California at Berkeley (1967) Linear Coupled Thermoelasticity", *J. Appl. Mech.*, Vol. 35, pp. 255-266 (1968)

ELECTROMAGNETIC AXISYMMETRIC FINITE ELEMENTS BASED ON A GAUGED FOUR-POTENTIAL VARIATIONAL PRINCIPLE

ABSTRACT

We derive electromagnetic finite elements based on a variational principle that uses the electro-magnetic four-potential as primary variable. The Lorentz gauge normalization is incorporated as a constraint condition through a Lagrange multiplier field λ. This "gauged principle" is used to construct elements suitable for downstream coupling with mechanical and thermal finite elements for the analysis of high-temperature superconductor devices of potential use in aerospace applications. The main advantages of the four-potential formulation are: jump discontinuities on interfaces are naturally handled, no *a priori* approximations are invoked, and the number of degrees of freedom per node remain modest as the problem dimensionality increases. The new elements are tested on two magnetostatic axisymmetric problems. The results are in excellent agreement with analytical solutions and previous "ungauged" finite element solutions for the one-dimensional problem of a conducting infinite wire, in which case the multiplier field has no effect. For the two-dimensional problem of a hollow cylinder connected to an infinite cylindrical feed wire, the results make physical sense although there is no known analytical solution. In this case, the multiplier field λ couples the potentials in the radial and axial directions. The effect of full and selective integration on λ, as well as that of leaving λ out of the problem, are assessed. For materials of widely different permeability, jump conditions are found to be naturally accommodated by the present formulation.

NOMENCLATURE

Symbol	Meaning
A	Magnetic potential vector; also computational vector of finite element node values of magnetic potentials
B	Magnetic flux density vector
C	Damping matrix of finite element discretization
c	Speed of light in arbitrary material
c_0	Speed of light in vacuum
D	Electric flux density vector
$\dot{B}$ $\mathcal{D}$ $\partial D/\partial t$	Displacement current density vector
E	Electric field intensity vector
e	Element identifier (as superscript)
F	Field strength tensor
f	Force vector of finite element discretization
G_A, G_8, G_λ	Matrices relating element magnetic, electric and multiplier fields, respectively, to node values
g	Electric conductivity
H	Magnetic field intensity
I	Total current intensity carried by a conductor
i	When not used as suscript, imaginary unit
J	Four-current vector
j	Current density vector
K	Stiffness matrix of finite element discretization
L	Lagrangian
L_g	Gauged Lagrangian
M	Mass matrix of finite element discretization
N	Finite element shape function vector
R	Governing functional
r	Radial coordinate in cylindrical coordinate system
u	Finite element node value computational vector containing magnetic potentials, electric potential and λ
t	Time
x_1, x_2, x_3, x_4	Four-space coordinates
z	Longitudinal coordinate in cylindrical coordinate system
$\mathcal{U}_M, \mathcal{U}_E$	Magnetic and electric energy density, respectively
β	Normalization factor in Lagrangian
δ	Variation symbol

NOMENCLATURE (Cont'd)

Symbol	Meaning
ϵ	Susceptibility (also called capacitivity and permittivity)
ϵ_0	Susceptibility of vacuum
θ	Circumferential (longitude) coordinate in cylindrical coordinate system
λ	Lagrangian multiplier field for Lorentz gauge constraint
λ	Finite element vector of Lagrange multipliers
μ	Magnetic permeability (also called inductivity)
μ_0	Magnetic permeability of vacuum
ρ	Electric charge density
8	Electric potential
Φ	Finite element node value vector of electric potentials
ϕ	Four-potential vector
∇	Gradient operator
$\nabla \cdot$	Divergence operator
$\nabla \times$	Curl operator
$\square$	D'Alambertian (four-wave) operator
$\Re$	Abbreviation for temporal derivative
$\bowtie^T$	Matrix transposition

1. MOTIVATION AND APPROACH

The present work is part of a research program for the numerical simulation of electromagnetic/mechanical systems that involve high-temperature superconductors (HTS). These are composite materials whose structural and environmental properties are presently the subject of intensive experimental research. Devices fabricated with these materials are expected to have major impact in space propulsion, power, digital computing and communication systems in the next century. Some potential applications[1] of this rapidly evolving technology to aerospace systems are listed in Table 1.

The computer simulation of HTS devices involves the interaction of the following four components:

(1) *Mechanical Fields*: displacements, stresses, strains and mechanical forces.

(2) *Thermal Fields*: temperature and heat fluxes.

198

Table 1   Potential Aerospace Applications of HTS Devices[1]

```
Magnetic Thrusters
Microwave Power Transmission
Superconducting Magnetic Energy Storage
Electromagnetic Launch and Braking
Aircraft Power Systems
```

(3) *Electromagnetic (EM) Fields*: electric and magnetic field strengths and fluxes, currents and charges.

(4) *Coupling Fields*: the fundamental coupling effect is the constitutive behavior of the materials involved. Particularly important are the metallurgical and superconducting phase change phenomena triggered by thermal, mechanical and EM fields.

1.1   Finite Element Treatment

The first three fields (mechanical, thermal and electromagnetic) are treated by the finite element method. This treatment produces the spatial discretization of the continuum into mechanical, thermal and electromagnetic meshes of a finite number of degrees of freedom. The finite element discretization may be developed in two ways:

(1) *Simultaneous Treatment*. The whole problem is treated as an indivisible whole. The three meshes noted above become tightly coupled, with common nodes and elements.

(2) *Staged Treatment*. The mechanical, thermal and electromagnetic components of the problem are treated separately. Finite element meshes for these components may be developed separately. Coupling effects are viewed as information that has to be transferred between these three meshes.

The present research follows the staged treatment. More specifically, *we develop finite element models for the fields in isolation, and then treat coupling effects as interaction forces between these models*. This "divide and conquer" strategy is ingrained in the partitioned treatment of coupled problems[2,3], which offers significant advantages in terms of computational efficiency and software modularity. Another advantage relates to the way research into complex problems can be made more productive. It centers on the observation that some aspects of the problem are either better understood or less physically relevant than others. These aspects may be then temporarily left alone while efforts are concentrated on the less developed and/or more physically important aspects. The staged treatment is better suited to this approach.

1.2 Mechanical Elements

Mechanical elements for this research have been derived using general variational principles that decouple the element boundary from the interior thus providing efficient ways to work out coupling with non-mechanical fields. The point of departure was previous research into the free-formulation variational principles presented in Felippa[4]. A more general formulation for the mechanical elements, which includes the assumed natural strain formulation, was established and presented by Felippa and Militello[5-8]. New representations of thermal fields have not been addressed as standard formulations are considered adequate for the coupled-field phases of this research. However, research in thermomechanical interaction supported by this program has resulted in the construction of robust and efficient staggered solution procedures[9].

1.3 Electromagnetic Elements

The development of electromagnetic (EM) finite elements has not received to date the same degree of attention given to mechanical and thermal elements. Part of the reason is the widespread use of analytical and semianalytical methods in electrical engineering. These methods have been highly refined for specialized but important problems such as circuits and waveguides. Thus the advantages of finite elements in terms of generality have not been enough to counterweight established techniques. Much of the EM finite element work to date has been done in England and is well described in the surveys by Davies[10] and Trowbridge[11]. The general impression conveyed by these surveys is one of an unsettled subject, reminiscent of the early period (1960-1970) of finite elements in structural mechanics. A great number of formulations that combine flux, intensity, and scalar potentials are described with the recommended choice varying according to the application, medium involved (polarizable, dielectric, semiconductors, etc.) number of space dimensions, time-dependent characteristics (static, quasi-static, harmonic or transient) as well as other factors of lesser importance. The possibility of a general variational formulation has not apparently been recognized.

In the present work, the derivation of electromagnetic (EM) elements is based on a variational formulation that uses the four-potential as primary variable. The electric field is represented by a scalar potential and the magnetic field by a vector potential. The formulation of this variational principle proceeds along lines previously developed for the acoustic fluid problem[12,13]. The Lorentz gauge normalization is incorporated in the variational (weak) form through the adjunction of a Lagrange multiplier field.

The main advantages of using potentials as primary variables in contrast to existing EM finite elements based on intensity and/or flux fields are, in order of importance:

1. Interface discontinuities are automatically taken care of without any special intervention.

2. No approximations are invoked *a priori* since the general Maxwell equations are used.

3. The number of degrees of freedom per finite element node is kept modest as the problem dimensionality increases.

4. Coupling with the mechanical and thermal fields, which involves derived fields, can be naturally evaluated at the Gauss points where derivatives of the potentials are evaluated.

Following a recapitulation of the basic field equations, the variational principle is stated and specialized to an axisymmetric geometry. The discretization of this principle into finite element equations produces semidiscrete dynamical equations, which reduce to the electromagnetostatic equations in the time-independent case. These equations are tested in the simulation of a cylindrical conductor wire and of a hollow conducting "can" connected to an infinite feed wire.

2. ELECTROMAGNETIC FIELD EQUATIONS

2.1 The Maxwell Equations

The original Maxwell equations (1873) involve four spatial fields: **B**, **D**, **E** and **H**. Vectors **E** and **H** represents the electric and magnetic field strengths (also called intensities), respectively, whereas **D** and **B** represent the electric and magnetic flux densities, respectively. All of these are three-vector quantities, that is, vector fields in three-dimensional space ($x_1 \equiv x$, $x_2 \equiv y$, $x_3 \equiv z$):

$$\mathbf{B} \equiv \begin{Bmatrix} B_1 \\ B_2 \\ B_3 \end{Bmatrix}, \quad \mathbf{D} \equiv \begin{Bmatrix} D_1 \\ D_2 \\ D_3 \end{Bmatrix}, \quad \mathbf{E} \equiv \begin{Bmatrix} E_1 \\ E_2 \\ E_3 \end{Bmatrix}, \quad \mathbf{H} \equiv \begin{Bmatrix} H_1 \\ H_2 \\ H_3 \end{Bmatrix}. \qquad \rhd 1 \lhd$$

Other quantities are the electric current three-vector **j** and the electric charge density ρ (a scalar).

Using superposed dots to denote differentiation with respect to time t, we can state Maxwell equations as†

$$\boxed{\begin{array}{ll} \dot{\mathbf{B}} C \, \nabla \times \mathbf{E} \equiv 0, & \nabla \times \mathbf{H} - \dot{\mathbf{B}} \equiv \mathbf{j}, \\ \nabla \cdot \mathbf{D} \equiv \rho, & \nabla \cdot \mathbf{B} \equiv 0. \end{array}} \qquad \rhd 2 \lhd$$

The first and second equation are also known as Faraday's and Ampère-Maxwell laws, respectively.

The system (2) supplies a total of eight partial differential equations, which as stated are independent of the properties of the underlying medium.

2.2 Constitutive Equations

The field intensities **E** and **H** and the corresponding flux densities **D** and **B** are not independent but are connected by the electromagnetic constitutive equations. For an electromagnetically isotropic, non-polarized material the equations are

$$\boxed{\mathbf{B} \equiv \mu\mathbf{H}, \qquad \mathbf{D} \equiv \epsilon\mathbf{E}} \qquad \rhd 3 \lhd$$

---

† Some authors, for example Eyges[14], include 4π factors and the speed of light c in the Maxwell equations. Other textbooks, e.g. Rojanski[15] and Shadowitz[16], follow Heaviside's advice in using technical units that eliminate such confusing factors.

where μ and ϵ are the permeability and susceptibility, respectively, of the material (other names are often used, cf. Nomenclature Section). These coefficients are functions of position but (for static or harmonic fields) do not depend on time. In the general case of a non-isotropic material both μ and ϵ become tensors. Even in isotropic media μ may be a complicated function of H; in ferromagnetic materials exhibiting hysteretic effects μ depends on the previous history.

In free space $\mu \, \mathcal{D} \, \mu_0$ and $\epsilon \, \mathcal{D} \, \epsilon_0$, which are connected by

$$c_0^2 \, \mathcal{D} \, \frac{1}{\mu_0 \epsilon_0},$$

$\triangleright 4 \triangleleft$

where c_0 is the speed of light in free-space vacuum.

The electrical field strength E is further related to the current density j by Ohm's law:

$$j \, \mathcal{D} \, gE,$$

$\triangleright 5 \triangleleft$

where g is the conductivity of the material. Again for a non-isotropic material g is generally a tensor which may also contain real and imaginary components; in which case the above relation becomes the generalized Ohm's law. For good conductors $g \gg \epsilon$; for bad conductors $g \ll \epsilon$. In free space, $g \, \mathcal{D} \, 0$.

2.3 Maxwell Equations in Terms of E and B

To pass to the four-potential formulation it is convenient to express Maxwell's equations in terms of the electrical field strength E and the magnetic flux B. In fact this is the pair most frequently used in electromagnetic work that involve arbitrary media. On eliminating D and H through the constitutive equations (3) we obtain

$$\dot{B} C \, \nabla \times E \, \mathcal{D} \, 0, \qquad \nabla \times B - \mu \epsilon \dot{E} \, \mathcal{D} \, \mu j,$$
$$\nabla \cdot E \, \mathcal{D} \, \rho/\epsilon, \qquad \nabla \cdot B \, \mathcal{D} \, 0.$$

$\triangleright 6 \triangleleft$

The second equation assumes that ϵ is independent of time; otherwise $\epsilon \dot{E} \, \mathcal{D} \, \epsilon \, dE/dt$ should be replaced by $d\triangleright \epsilon E \triangleleft/dt$. In charge-free vacuum the equations (6) reduce to

$$\dot{B} C \, \nabla \times E \, \mathcal{D} \, 0, \qquad \nabla \times B - \frac{1}{c_0^2}\dot{E} \, \mathcal{D} \, 0,$$
$$\nabla \cdot E \, \mathcal{D} \, 0, \qquad \nabla \cdot B \, \mathcal{D} \, 0.$$

$\triangleright 7 \triangleleft$

2.4 The Electromagnetic Potentials

The electric scalar potential 8 and the magnetic vector potential A are introduced by the definitions

$$E \, \mathcal{D} \, -\nabla 8 - \dot{A}, \qquad B \, \mathcal{D} \, \nabla \times A.$$

$\triangleright 8 \triangleleft$

This definition satisfies the two homogeneous Maxwell equations in (7). The definition of A leaves its divergence $\nabla \cdot A$ arbitrary. We shall use the Lorentz gauge[17]

$$\boxed{\nabla \cdot A\, C\, \mu\epsilon\dot{\mathcal{B}}\, \mathcal{D}\, 0.}$$

▷9◁

With this choice the two non-homogeneous Maxwell equations written in terms of 8 and A separate into the wave equations

$$\nabla^2 8 - \mu\epsilon\ddot{\mathcal{B}}\mathcal{D} -\rho/\epsilon, \qquad \nabla^2 A - \mu\epsilon\ddot{A}\,\mathcal{D} -\mu j,$$

▷10◁

which are only coupled on the right-hand side through Ohm's law (5).

3. THE ELECTROMAGNETIC FOUR-POTENTIAL

Maxwell's equations can be presented in a compact manner (a form compatible with special relativity) in the four-dimensional spacetime defined by the coordinates

$$x_1 \equiv x, \quad x_2 \equiv y, \quad x_3 \equiv z, \quad x_4\, \mathcal{D}\, ict$$

▷11◁

where x_1, x_2, x_3 are spatial Cartesian coordinates, $i^2\, \mathcal{D}\, -1$ is the imaginary unit, and $c\, \mathcal{D}\, 1/\sqrt{\mu\epsilon}$ is the speed of EM waves in the medium under consideration. In the sequel Roman subscripts will consistently go from 1 to 4 and the summation convention over repeated indices will be used unless otherwise stated.

3.1 The Field Strength Tensor

The unification can be expressed most conveniently in terms of the *field-strength tensor* F, which is a four-dimensional *antisymmetric* tensor constructed from the components of E and B as follows[14,16]

$$\mathbf{F}\, \mathcal{D}\, \begin{pmatrix} 0 & F_{12} & F_{13} & F_{14} \\ -F_{12} & 0 & F_{23} & F_{24} \\ -F_{13} & -F_{23} & 0 & F_{34} \\ -F_{14} & -F_{23} & -F_{34} & 0 \end{pmatrix} \overset{\text{def}}{\mathcal{D}} \beta \begin{pmatrix} 0 & cB_3 & -cB_2 & -iE_1 \\ -cB_3 & 0 & cB_1 & -iE_2 \\ cB_2 & -cB_1 & 0 & -iE_3 \\ iE_1 & iE_2 & iE_3 & 0 \end{pmatrix}.$$

▷12◁

Here β is an adjustment factor to be determined later. Similarly, introduce the *four-current* vector J as

$$\mathbf{J}\, \mathcal{D}\, \begin{Bmatrix} J_1 \\ J_2 \\ J_3 \\ J_4 \end{Bmatrix} \overset{\text{def}}{\mathcal{D}} \beta \begin{Bmatrix} c\mu j_1 \\ c\mu j_2 \\ c\mu j_3 \\ i\rho/\epsilon \end{Bmatrix} \mathcal{D}\, \beta c \begin{Bmatrix} \mu j_1 \\ \mu j_2 \\ \mu j_3 \\ i\sqrt{\mu/\epsilon}\,\rho \end{Bmatrix}.$$

▷13◁

Then, for arbitrary β, the non-homogeneous Maxwell equations, namely $\nabla \times B - \mu\epsilon\dot{E}\, \mathcal{D}\, \mu j$ and $\nabla \cdot E\, \mathcal{D}\, \rho/\epsilon$, may be presented in the compact "continuity" form (the covariant form of these two equations):

$$\frac{\partial F_{ik}}{\partial x_k}\, \mathcal{D}\, J_i.$$

▷14◁

The other two Maxwell equations, $\nabla \cdot \mathbf{B} \, \mathcal{D} \, 0$ and $\nabla \times \mathbf{E} \, C \, \dot{\mathbf{B}} \, \mathcal{D} \, 0$, can be presented as

$$\frac{\partial F_{ik}}{\partial x_m} \, C \, \frac{\partial F_{mi}}{\partial x_k} \, C \, \frac{\partial F_{km}}{\partial x_i} \, \mathcal{D} \, 0, \qquad \triangleright 15 \triangleleft$$

where the index triplet (i, k, m) takes on the values (1,2,3), (4,2,3), (4,3,1) and (4,1,2).

3.2 The Four-Potential

The *electromagnetic four-potential* ϕ is a four-vector whose components are constructed with the electric and magnetic potential components of $\mathbf{A}$ and Φ:

$$\phi \, \mathcal{D} \, \beta \left\{ \begin{array}{c} \phi_1 \\ \phi_2 \\ \phi_3 \\ \phi_4 \end{array} \right\} \overset{\text{def}}{\mathcal{D}} \left\{ \begin{array}{c} cA_1 \\ cA_2 \\ cA_3 \\ i8 \end{array} \right\}. \qquad \triangleright 16 \triangleleft$$

It may then be verified that $\mathbf{F}$ can be expressed as the four-curl of ϕ, that is

$$F_{ik} \, \mathcal{D} \, \frac{\partial \phi_k}{\partial x_i} - \frac{\partial \phi_i}{\partial x_k}, \qquad \triangleright 17 \triangleleft$$

or in more detail and using commas to abbreviate partial derivatives:

$$\mathbf{F} \, \mathcal{D} \begin{pmatrix} 0 & \phi_{2,1} - \phi_{1,2} & \phi_{3,1} - \phi_{1,3} & \phi_{4,1} - \phi_{1,4} \\ \phi_{1,2} - \phi_{2,1} & 0 & \phi_{3,2} - \phi_{2,3} & \phi_{4,2} - \phi_{2,4} \\ \phi_{1,3} - \phi_{3,1} & \phi_{2,3} - \phi_{3,2} & 0 & \phi_{4,3} - \phi_{3,4} \\ \phi_{1,4} - \phi_{4,1} & \phi_{2,4} - \phi_{4,2} & \phi_{3,4} - \phi_{4,3} & 0 \end{pmatrix}. \qquad \triangleright 18 \triangleleft$$

3.3 The Ungauged Lagrangian

With these definitions, the basic Lagrangian of electromagnetism† can be stated as[19]

$$L \, \mathcal{D} \, \tfrac{1}{4} F_{ik} F_{ik} - J_i \phi_i \, \mathcal{D} \, \tfrac{1}{4} \beta^2 \left(\frac{\partial \phi_k}{\partial x_i} - \frac{\partial \phi_i}{\partial x_k} \right)^2 - J_i \phi_i \qquad \triangleright 19 \triangleleft$$

$$\mathcal{D} \, \tfrac{1}{2} \beta^2 \left(c^2 B^2 - E^2 \right) - \frac{\beta^2}{\epsilon} \triangleright j_1 A_1 \, C \, j_2 A_2 \, C \, j_3 A_3 - \rho 8 \triangleleft,$$

in which

$$B^2 \, \mathcal{D} \, \mathbf{B}^T \mathbf{B} \, \mathcal{D} \, B_1^2 \, C \, B_2^2 \, C \, B_3^2, \quad E^2 \, \mathcal{D} \, \mathbf{E}^T \mathbf{E} \, \mathcal{D} \, E_1^2 \, C \, E_2^2 \, C \, E_3^2. \qquad \triangleright 20 \triangleleft$$

Comparing the first term with the magnetic and electric energy densities[14,15,16]

$$U_M \, \mathcal{D} \, \tfrac{1}{2} \mathbf{B}^T \mathbf{H} \, \mathcal{D} \, \frac{1}{2\mu} B^2, \qquad U_E \, \mathcal{D} \, \tfrac{1}{2} \mathbf{D}^T \mathbf{E} \, \mathcal{D} \, \tfrac{1}{2} \epsilon E^2, \qquad \triangleright 21 \triangleleft$$

---

† L is an extension of the free-space Lagrangian given by Lanczos[18] to a material obeying the more general constitutive equations (3).

we must have $\beta^2 c^2 \; \mathcal{D} \; \beta^2/{\triangleright}\mu\epsilon{\triangleleft} \; \mathcal{D} \; 1/\mu$, from which

$$\beta \; \mathcal{D} \; \sqrt{\epsilon}. \qquad\qquad {\triangleright}22{\triangleleft}$$

Consequently the required Lagrangian is

$$\boxed{L \; \mathcal{D} \; \frac{1}{2\mu}B^2 - \tfrac{1}{2}\epsilon E^2 - {\triangleright}j_1 A_1 \; C \; j_2 A_2 \; C \; j_3 A_3 - \rho 8{\triangleleft}.} \qquad {\triangleright}23{\triangleleft}$$

The associated variational form is

$$R \; \mathcal{D} \int_{t_0}^{t_1} \int_V L \, dV \, dt \qquad\qquad {\triangleright}24{\triangleleft}$$

where V is the integration volume considered in the analysis. In theory V extends over the whole space, but in the numerical simulation the integration is truncated at a distant boundary or special devices are used to treat the decay behavior at infinity.

3.4 The Gauged Lagrangian

If the fields A and 8 to be inserted into L do not satisfy the Lorentz gauge relation (9) *a priori*, this condition has to be imposed as a constraint using a Lagrange multiplier field $\lambda{\triangleright}x_i{\triangleleft}$, leading to the modified or "gauged" Lagrangian:

$$\boxed{L_g \; \mathcal{D} \; L \; C \; \lambda{\triangleright}\nabla \cdot \mathbf{A} \; C \; \mu\epsilon 8{\triangleleft}.} \qquad {\triangleright}25{\triangleleft}$$

3.5 The Four-Field Equations

On setting the variation of the functional (25) to zero we recover the field equations (14–15) as well as the gauge constraint (9) as Euler-Lagrange equations. Taking the divergence of both sides of (14) and observing that F is an antisymmetric tensor so that its divergence vanishes we get

$$\frac{\partial J_i}{\partial x_i} \; \mathcal{D} \; c\mu{\triangleright}\nabla \cdot \mathbf{j} \; C \; \dot{\rho}{\triangleleft} \; \mathcal{D} \; 0, \qquad\qquad {\triangleright}26{\triangleleft}$$

The vanishing term in parenthesis is the equation of continuity, which expresses the law of conservation of charge. The Lorentz gauge condition (9) may be stated as $\nabla \cdot \phi \; \mathcal{D} \; 0$. Finally, the potential wave equations (10) may be expressed in compact form as

$$\Box \phi_i \; \mathcal{D} \; -J_i \qquad\qquad {\triangleright}27{\triangleleft}$$

where $\Box$ denotes the "four-wave-operator", also called the D'Alembertian:

$$\Box \; \overset{\text{def}}{\mathcal{D}} \; \frac{\partial^2}{\partial x_k \partial x_k} \; \mathcal{D} \; \frac{\partial^2}{\partial x_1^2} \; C \; \frac{\partial^2}{\partial x_2^2} \; C \; \frac{\partial^2}{\partial x_3^2} - \frac{\partial^2}{c^2 \partial t^2}. \qquad {\triangleright}28{\triangleleft}$$

Hence each component of the four-potential ϕ satisfies an inhomogeneous wave equation. In free space, $\mathbf{J} \; \mathcal{D} \; 0$ and each component satisfies the homogeneous wave equation.

4. FINITE ELEMENT DISCRETIZATION

In a previous paper[19] the ungauged Lagrangian (23) was used to construct *one-dimensional* axisymmetric finite elements. These elements were successfully tested on a magnetostatic problem. In the present investigation we extend the technique to *two-dimensional* axisymmetric problems. In doing so we find that the finite element discretization does not necessarily satisfies the gauge condition (9) *a priori* and consequently the gauged Lagrangian (25) must be used.

4.1 The Lagrangian in Cylindrical Coordinates

To take advantage of the axisymmetric geometry we choose a cylindrical coordinate system with the rotational axis as z-axis. The vector components in the cylindrical coordinate directions r, θ and z are denoted by

$$A_1, \; B_1, \; E_1 \equiv A_r, \; B_r, \; E_r \quad \text{in the } r \text{ (radial) direction,}$$

$$A_2, \; B_2, \; E_2 \equiv A_\theta, \; B_\theta, \; E_\theta \quad \text{in the } \theta \text{ (circumferential) direction,}$$

$$A_3, \; B_3, \; E_3 \equiv A_z, \; B_z, \; E_z \quad \text{in the } z \text{ (longitudinal) direction.}$$

The electromagnetic fields will then vary in the radial (r) and axial (z) directions but not in the circumferential (θ) direction.

To construct finite element approximations we need to express the gauged Lagrangian

$$L_g = \frac{1}{2\mu}B^2 - \tfrac{1}{2}\epsilon E^2 - j^T A - \rho\phi + \lambda \nabla \cdot A + \mu\epsilon\dot\phi, \qquad (29)$$

in terms of the potentials written in cylindrical coordinates. For B^2 we use the expression of the curl (see *e.g.*, p. 54 of Shadowitz[16])

$$B^2 = \left(\frac{1}{r}\frac{\partial A_3}{\partial \theta} - \frac{\partial A_2}{\partial z}\right)^2 + \left(\frac{\partial A_1}{\partial z} - \frac{\partial A_3}{\partial r}\right)^2 + \left(\frac{1}{r}\frac{\partial r A_2}{\partial r} - \frac{1}{r}\frac{\partial A_1}{\partial \theta}\right)^2, \qquad (30)$$

For E^2 we use the cylindrical-coordinate gradient formulas

$$E = \begin{Bmatrix} E_1 \\ E_2 \\ E_3 \end{Bmatrix} = \begin{Bmatrix} E_r \\ E_\theta \\ E_z \end{Bmatrix} = - \begin{Bmatrix} \dfrac{\partial \phi}{\partial r} + \dot{A}_1 \\[4pt] \dfrac{1}{r}\dfrac{\partial \phi}{\partial \theta} + \dot{A}_2 \\[4pt] \dfrac{\partial \phi}{\partial z} + \dot{A}_3 \end{Bmatrix}, \qquad (31)$$

so that

$$E^2 = E^T E = \left(\frac{\partial \phi}{\partial r} + \frac{\partial A_1}{\partial t}\right)^2 + \left(\frac{1}{r}\frac{\partial \phi}{\partial \theta} + \frac{\partial A_2}{\partial t}\right)^2 + \left(\frac{\partial \phi}{\partial z} + \frac{\partial A_3}{\partial t}\right)^2. \qquad (32)$$

For the Lorentz gauge we use the gradient formula again to get

$$\nabla \cdot A + \mu\epsilon\dot\phi = \frac{1}{r}\frac{\partial r A_1}{\partial r} + \frac{\partial A_3}{\partial z} + \mu\epsilon\dot\phi. \qquad (33)$$

In the axisymmetric case the partials of any potential with respect to θ should vanish. Consequently the gauged Lagrangian (30) simplifies to

$$
\begin{aligned}
L_g \; = \; & \frac{1}{2\mu}\left[\left(\frac{\partial A_1}{\partial z} - \frac{\partial A_3}{\partial r}\right)^2 + \left(\frac{\partial A_2}{\partial z}\right)^2 + \left(\frac{1}{r}\frac{\partial \triangleright r A_2 \triangleleft}{\partial r}\right)^2\right] \\
& - \tfrac{1}{2}\epsilon\left[\left(\frac{\partial 8}{\partial r} + \frac{\partial A_1}{\partial t}\right)^2 + \left(\frac{\partial A_2}{\partial t}\right)^2 + \left(\frac{\partial 8}{\partial z} + \frac{\partial A_3}{\partial t}\right)^2\right] \\
& + \lambda\left(\frac{1}{r}\frac{\partial \triangleright r A_1 \triangleleft}{\partial r} + \frac{\partial A_3}{\partial z} + \mu\epsilon\dot{8}\right) - \left(j_1 A_1 + j_2 A_2 + j_3 A_3 - \rho 8\right).
\end{aligned}
\qquad \triangleright 34 \triangleleft
$$

Note that this Lagrangian involves *all* components of the four-potential although the independence from θ has introduced some simplifications with respect to the full three-dimensional case.

4.2 Constructing EM Finite Elements

For the finite element discretization of the two-dimensional case we have constructed quadrilateral and triangular axisymmetric elements defined by their geometry on the r-z plane. We have used isoparametric elements with corner node points only. Additional construction details are provided in Section 5.

In the following we consider an *individual element* identified by superscript e. The element nodes are locally numbered $i = 1, \ldots, n$, where n is the number of corner nodes ($n = 3$ for triangles and $n = 4$ for quadrilaterals). The electric potential 8 and the magnetic potential components, $A_1 \equiv A_r$, $A_2 \equiv A_\theta$, and $A_3 \equiv A_z$, are interpolated over each element as

$$
8^e = \mathbf{N}_8^e \Phi^e, \qquad A_i^e = \mathbf{N}_{A_i}^e \mathbf{A}_i^e,
\qquad \triangleright 35 \triangleleft
$$

Here row vectors $\mathbf{N}_8^e$ and $\mathbf{N}_{A_i}^e$ contain the (isoparametric) finite element shape functions for 8^e and A_i^e, respectively, which are only functions of the radial and longitudinal coordinates r and z:

$$
\mathbf{N}_8^e = [\, N_{8_1}^e \triangleright r, z \triangleleft \;\; \cdots \;\; N_{8_n}^e \triangleright r, z \triangleleft \,], \qquad
\mathbf{N}_{A_i}^e = [\, N_{A_{i1}}^e \triangleright r, z \triangleleft \;\; \cdots \;\; N_{A_{in}}^e \triangleright r, z \triangleleft \,],
\qquad \triangleright 36 \triangleleft
$$

and column vectors Φ^e and $\mathbf{A}^e$ contain the nodal values of 8 and A_i, respectively, which are only functions of time t:

$$
\Phi^e = \left(8_1 \triangleright t \triangleleft \;\; \cdots \;\; 8_n \triangleright t \triangleleft\right)^T,
$$
$$
\mathbf{A}^e = \left(A_{11} \triangleright t \triangleleft \;\; \cdots \;\; A_{1n} \triangleright t \triangleleft \;\; A_{21} \triangleright t \triangleleft \;\; \cdots \;\; A_{2n} \triangleright t \triangleleft \;\; A_{31} \triangleright t \triangleleft \;\; \cdots \;\; A_{3n} \triangleright t \triangleleft\right)^T.
$$
$$\triangleright 37 \triangleleft$$

The Lagrangian multiplier field $\lambda \triangleright r, z \triangleleft$ will be assumed to be constant over each element since the variational principle associated with (34) allows interelement discontinuities in this field. This value, denoted by λ^e, may therefore be associated with an internal node.

To facilitate a more compact formulation, we introduce the following matrix and vector notations:

$$G_A^e \; \mathcal{D} \; \frac{1}{\sqrt{\mu}} \begin{bmatrix} 0 & -\frac{\partial N_{A_2}^e}{\partial z} & 0 \\ \frac{\partial N_{A_1}^e}{\partial z} & 0 & -\frac{\partial N_{A_1}^e}{\partial r} \\ 0 & \left(\frac{\partial}{\partial r} C \frac{1}{r}\right) N_{A_2}^e & 0 \end{bmatrix}, \quad N_A^e \; \mathcal{D} \; \sqrt{\epsilon} \begin{bmatrix} N_{A_1}^e & 0 & 0 \\ 0 & N_{A_2}^e & 0 \\ 0 & 0 & N_{A_3}^e \end{bmatrix}, \quad \triangleright 38 \triangleleft$$

$$G_8^e \; \mathcal{D} \; \sqrt{\epsilon} \left\{ \begin{array}{c} \frac{\partial N_8^e}{\partial r} \\ 0 \\ \frac{\partial N_8^e}{\partial z} \end{array} \right\}, \quad G_\lambda^e \; \mathcal{D} \; \left\{ \begin{array}{c} \left(\frac{\partial}{\partial r} C \frac{1}{r}\right) N_{A_1}^e \\ 0 \\ \frac{\partial N_{A_1}^e}{\partial z} \end{array} \right\}, \quad j^e \; \mathcal{D} \; \left\{ \begin{array}{c} j_1^e \\ j_2^e \\ j_3^e \end{array} \right\}. \quad \triangleright 39 \triangleleft$$

Substitution of the finite element assumptions and our new notation into (35) and (25) yields the variational integral as a sum of element contributions $R \; \mathcal{D} \; \sum_e R^e$, where

$$R^e \; \mathcal{D} \; R_1^e - R_2^e - R_3^e \; C \; R_4^e, \qquad \triangleright 40 \triangleleft$$

in which

$$R_1^e \; \mathcal{D} \; \int_{t_0}^{t_1} \int_{V^e} \tfrac{1}{2} A^{eT} G_A^{eT} G_A^e A^e \, dV^e \, dt,$$

$$R_2^e \; \mathcal{D} \; \int_{t_0}^{t_1} \int_{V^e} \tfrac{1}{2} \left\{ \left(\Phi^{eT} G_8^{eT} C \, \mathcal{R}^{eT} N_A^{eT} \right) \left(G_8^e \Phi^e \, C \, N_A^e \mathcal{R}^e \right) \right\} dV^e \, dt,$$

$$R_3^e \; \mathcal{D} \; \int_{t_0}^{t_1} \int_{V^e} \left(A^{eT} N_A^{eT} j^e - \rho \Phi^{eT} N_8^{eT} \right) dV^e \, dt,$$

$$R_4^e \; \mathcal{D} \; \int_{t_0}^{t_1} \int_{V^e} \lambda^e \left(A^{eT} G_\lambda \, C \, \mu \epsilon \mathcal{P}^{eT} N_8^{eT} \right) dV^e \, dt, \qquad \triangleright 41 \triangleleft$$

where V^e denotes the volume of the element. On taking the variation with respect to the element node values we get $\delta R^e \; \mathcal{D} \; \delta R_1^e - \delta R_2^e - \delta R_3^e \; C \; \delta R_4^e \; \mathcal{D} \; 0$, with

$$\delta R_1^e \; \mathcal{D} \; \int_{t_0}^{t_1} \int_{V^e} \delta A^{eT} G_A^{eT} G_A^e A^e \, dV^e \, dt,$$

$$\delta R_2^e \; \mathcal{D} \; \int_{t_0}^{t_1} \int_{V^e} \left\{ \delta \Phi^{eT} G_8^{eT} \left(G_8^e \Phi^e \, C \, N_A^e \mathcal{R}^e \right) - \delta \mathcal{R}^{eT} N_A^{eT} \left(G_8^e \Phi^e \, C \, N_A^e \mathcal{R}^e \right) \right\} dV^e \, dt$$

$$C \int_{V^e} \delta A^{eT} N_A^{eT} \left(G_8^e \Phi^e \, C \, N_A^e \mathcal{R}^e \right) dV^e \Big|_{t_0}^{t_1},$$

$$\delta R_3^e \; \mathcal{D} \; \int_{t_0}^{t_1} \int_{V^e} \left(\delta A^{eT} N_A^{eT} j^e - \rho \, \delta \Phi^{eT} N_8^{eT} \right) dV^e \, dt, \qquad \triangleright 42 \triangleleft$$

$$\delta R_4^e \; \mathcal{D} \; \int_{t_0}^{t_1} \int_{V^e} \lambda^e \left(\delta A^{eT} G_\lambda \right) dV^e \, dt \; C \int_{t_0}^{t_1} \int_{V^e} \delta \lambda^e \left(G_\lambda A^e \, C \, \mu \epsilon N_8^e \mathcal{P}^e \right) dV^e \, dt$$

$$- \int_{t_0}^{t_1} \int_{V^e} \mathcal{R}^e \mu \epsilon N_8^{eT} \, \delta \Phi^e \, dV^e \, dt \; C \int_{V^e} \lambda^e \mu \epsilon N_8^{eT} \, \delta \Phi^e \, dV^e \Big|_{t_0}^{t_1}.$$

On applying fixed-end initial conditions at $t = t_0$ and $t = t_1$ and the lemma of the calculus of variations, we proceed to equate each of the volume integrals to zero. We thus obtain for each element the following second-order dynamic equations for the magnetic and electric potentials at the nodes, which are purposely written in a notation resembling the mass-damping-stiffness-force equations of mechanics:

$$\mathbf{M}^e \ddot{\mathbf{u}}^e + \mathbf{C}^e \dot{\mathbf{u}}^e + \mathbf{K}^e \mathbf{u}^e = \mathbf{f}^e; \tag{43}$$

where

$$\mathbf{M}^e = \int_{V^e} \begin{bmatrix} \mathbf{N}_A^{eT}\mathbf{N}_A^e & 0 & 0 \\ 0 & 0 & 0 \\ 0 & 0 & 0 \end{bmatrix} dV^e, \tag{44}$$

$$\mathbf{C}^e = \int_{V^e} \begin{bmatrix} 0 & \mathbf{N}_A^{eT}\mathbf{G}_8^e & 0 \\ \mathbf{G}_8^{eT}\mathbf{N}_A^e & 0 & \mu\epsilon\mathbf{N}_8^{eT} \\ 0 & \mu\epsilon\mathbf{N}_8^e & 0 \end{bmatrix} dV^e, \tag{45}$$

$$\mathbf{K}^e = \int_{V^e} \begin{bmatrix} \mathbf{G}_A^{eT}\mathbf{G}_A^e & 0 & \mathbf{G}_\lambda^e \\ 0 & \mathbf{G}_8^{eT}\mathbf{G}_8^e & 0 \\ \mathbf{G}_\lambda^{eT} & 0 & 0 \end{bmatrix} dV^e, \tag{46}$$

$$\mathbf{f}^e = \int_{V^e} \begin{Bmatrix} \mathbf{N}_A^{eT}\mathbf{j}^e \\ -\rho\mathbf{N}_8^{eT} \\ 0 \end{Bmatrix} dV^e, \qquad \mathbf{u}^e = \begin{Bmatrix} \mathbf{A}^e \\ \Phi^e \\ \lambda^e \end{Bmatrix}. \tag{47}$$

Considering (43) as a set of three matrix differential equations, we observe that the first two are the discrete analog of the wave equations (10). These equations are coupled, however, in the damping and stiffness terms as a consequence of the discretization of the gauge condition (9). We can find an expression for Φ in terms of $\mathbf{A}$, but the reverse is not generally possible.

4.3 The Static Case

For the numerical experiments reported here, we are primarily concerned with static solutions for the magnetic fields. If the time dependence disappears, the magnetic and electric fields uncouple and the element equations reduce to

$$\mathbf{K}_M^e \mathbf{u}^e = \mathbf{f}_M^e, \qquad \mathbf{K}_E^e \mathbf{u}_E^e = \mathbf{f}_E^e, \tag{48}$$

where

$$\mathbf{K}_M^e = \int_{V^e} \begin{bmatrix} \mathbf{G}_A^{eT}\mathbf{G}_A^e & \mathbf{G}_\lambda^e \\ \mathbf{G}_\lambda^{eT} & 0 \end{bmatrix} dV^e, \quad \mathbf{f}_M^e = \int_{V^e} \begin{Bmatrix} \mathbf{N}_A^{eT}\mathbf{j}^e \\ 0 \end{Bmatrix} dV^e, \quad \mathbf{u}_M^e = \begin{Bmatrix} \mathbf{A}^e \\ \lambda^e \end{Bmatrix}, \tag{49}$$

$$\mathbf{K}_E^e = \int_{V^e} [\mathbf{G}_8^{eT}\mathbf{G}_8^e] \, dV^e, \qquad \mathbf{f}_E^e = \int_{V^e} -\rho\mathbf{N}_8^{eT} \, dV^e, \qquad \mathbf{u}_E^e = \{ \Phi^e \}. \tag{50}$$

Assembling these element equations in the usual manner we obtain the discrete finite element equations of electromagnetostatics:

$$K_M u_M \; \mathcal{D} \; f_M , \qquad K_E u_E \; \mathcal{D} \; f_E . \qquad \qquad \triangleright 51 \triangleleft$$

If both the current density and charge distribution are known *a priori* then these two equations may be solved separately. If only the charge distribution ρ is known then the electrostatic equation should be solved first to obtain the electric field E as gradient of the computed electric potential 8; then the current density j can be obtained from Ohm's law (5) and used to computed the force vector f_M of the magnetic equation, which is then solved for the magnetic potential. Conversely, if only the current density distribution is known *a priori* the preceding steps are reversed.

For the two test problems presented here the current density distribution is assumed to be known, and we shall be content with solving the equations for the magnetic flux.

5. NUMERICAL EXPERIMENTS

5.1 The Finite Element Model

The finite element formulation described in the previous Section has been applied to the solution of two test problems described below. Both problems are treated with quadrilateral elements. Each quadrilateral element has four corner points and one interior node. These nodes are defined by their radial and axial positions r_j^e and z_j^e. At each corner j we have four degrees of freedom, namely A_{1j}, A_{2j}, A_{3j} and 8_j. From these values the potential components are interpolated with the standard bilinear shape functions, which provide the C^0 continuity required by the variational formulation. The centroidal node carries no physical significance and is solely used to provide the extra degree of freedom assigned to the Lagrangian multiplier λ^e. Thus each quadrilateral element has $4 \times 4 C \; 1 \; \mathcal{D} \; 17$ degrees of freedom.

For the calculation of the element stiffnesses and force vectors, it is assumed that the permeability μ and the current densities are uniform over the element. The desired stiffness matrix and force vector are calculated by numerical quadrature using Gauss formulas. The portion associated with potentials is always evaluated with 2×2 rule. Three different schemes, on the other hand, were tried on the entries associated with λ:

Full Integration. The same 2×2 rule as for the potentials is used.

Selective Integration. A one-point rule is used for G_λ^e.

Zero Integration. The effect of λ is ignored by omitting the integration of the associated terms and placing ones on the diagonal. This numerical device effectively forces $\lambda^e \; \mathcal{D} \; 0$, and thus "releases" the gauge constraint.

5.2 Applying Boundary Conditions

The finite element mesh is necessarily terminated at a finite size. For the two test problems, the outer radial end of the mesh is defined as the truncation radius $r \; \mathcal{D} \; R_T$. In static calculations the

material outside the FE mesh may be viewed as having zero permeability μ, or, equivalently, infinite stiffness or zero potential. It follows that the z component of the potential at the nodes located on the truncation radius may be prescribed to be zero. We do this because, no matter what the shape of an axisymmetric conductor, it will appear to be straight to the far field potential. Because of the coupling provided by the Lorentz gauge, the gradient of the r component of the potential must be a constant in the axial direction. For this reason, we constrain A_r at the top and the bottom of the mesh. A_r must also be constrained to zero on the axis if the field is to decay to zero since the gradient of A_z in the radial direction should also be zero.

5.3   Assembly, Solution and Field Recovery

The master stiffness matrix and force vector are assembled following standard finite element techniques. The boundary conditions are set as explained previously. The modified master equations modified for B.C. are processed by a standard symmetric skyline solver, which provides the value of the potentials at the mesh nodes.

The physical quantities of interest are not the potentials but the magnetic flux and electric strength densities B_i and E_i, and most especially the circumferential magnetic flux density $B_2 \equiv B_\theta$. This is calculated by discretizing the curl of A as follows. Since $\frac{\partial A_i}{\partial \theta} \mathcal{D} 0$, the magnetic fields become after discretization:

$$\left\{ \begin{array}{c} B_r \\ B_\theta \\ B_z \end{array} \right\} \mathcal{D} \left\{ \begin{array}{c} -\frac{\partial N_{A_2}^e}{\partial z} A_2^e \\ \frac{\partial N_{A_1}^e}{\partial z} A_1^e - \frac{\partial N_{A_1}^e}{\partial r} A_3^e \\ \frac{1}{r^e} \frac{\partial \triangleright r N_{A_2}^e \triangleleft}{\partial r} A_2^e \end{array} \right\} .$$ ▷52◁

The nodal values for **B** are obtained by evaluation at the Gauss point followed by extrapolation to node locations. The average of these quantities is also reported as the centroidal value. As discussed below this value was found to be more accurate than interelement-averaged node values. Consequently the centroidal value was used to report results.

For both test problems, the magnetic permeability $\mu \mathcal{D} \mu_{wire}$ is constant inside the conductor whereas outside it the free-space permeability $\mu_{free} \mathcal{D} \mu_0$ was assumed to be unity. The current densities are assumed to be uniformly distributed and consequently are calculated by dividing the assumed total current flowing through the conductor by the total cross-sectional areas of the conductors.

5.4   Problem 1: A Conducting Infinite Wire

The first test problem is identical to that reported in Schuler and Felippa[19] with a one-dimensional axisymmetric discretization. As shown in Figure 1, it consists of a wire conductor of radius a transporting a total current $I \mathcal{D} 1$ in the z direction. This current is assumed to be uniformly distributed over the wire cross section. For this problem one layer of quadrilateral elements in the z direction, extending from $z \mathcal{D} 0$ through $z \mathcal{D} d$, is sufficient; here the distance d is chosen arbitrarily. The radial direction is discretized with N_{wire} elements inside the wire and N_{free}
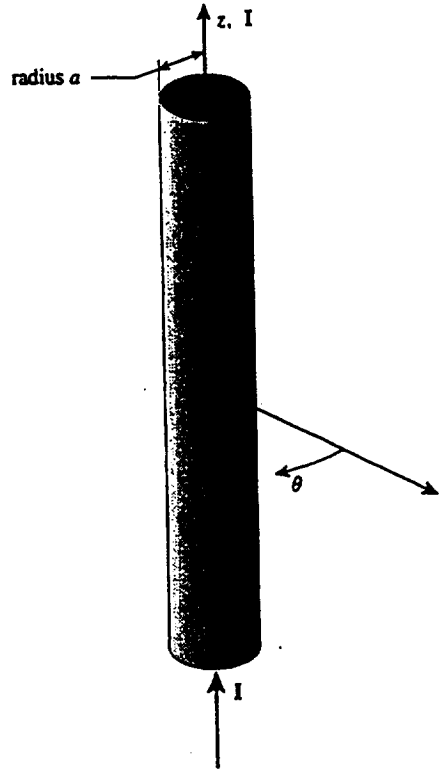
Fig. 1. Diagram of the first test problem: infinite cylindrical wire conducting total current I, assumed to be uniformly distributed over the cross section.

elements outside the wire in free space. The mesh is terminated at a "truncation radius" $r_T \gg a$ where the potential component $A_3 \equiv A_z$ is arbitrarily set to zero. Other boundary conditions are $A_2 \equiv A_r \, \mathcal{D} \, 0$ on the nodes at $z \, \mathcal{D} \, 0$ and $z \, \mathcal{D} \, d$.

The results obtained with $r_T \, \mathcal{D} \, 5a$, $N_{wire} \, \mathcal{D} \, 4$ and $N_{free} \, \mathcal{D} \, 10$ for the potentials were identical to those reported previously[19] thus providing a check on the element calculations. The same results were obtained with the three integration schemes noted above for the λ term, which verifies that the Lorentz gauge constraint (9) is automatically satisfied by the finite element shape function for one-dimensional magnetostatic fields.

The computed magnetic flux density B_2 at node points was not as accurate as it could be expected, especially at $r \, \mathcal{D} \, 0$. The centroidal values, on the other hand, were considerably more accurate as regards matching analytical results. Thus for the second problem we decided to report field values at the element centroids.

5.5 Problem 2: A Conducting Hollow Can

The second test problem, shown in Figure 2, brings two-dimensional features. It is a hollow conducting cylindrical "can" with infinite feed wires connected to the center of its top and bottom faces. These wires carry a total current $I \, \mathcal{D} \, 1$ going in the Cz direction; this current is assumed to be uniformly distributed over the varying cross sections it traverses. The wire radius a and the can
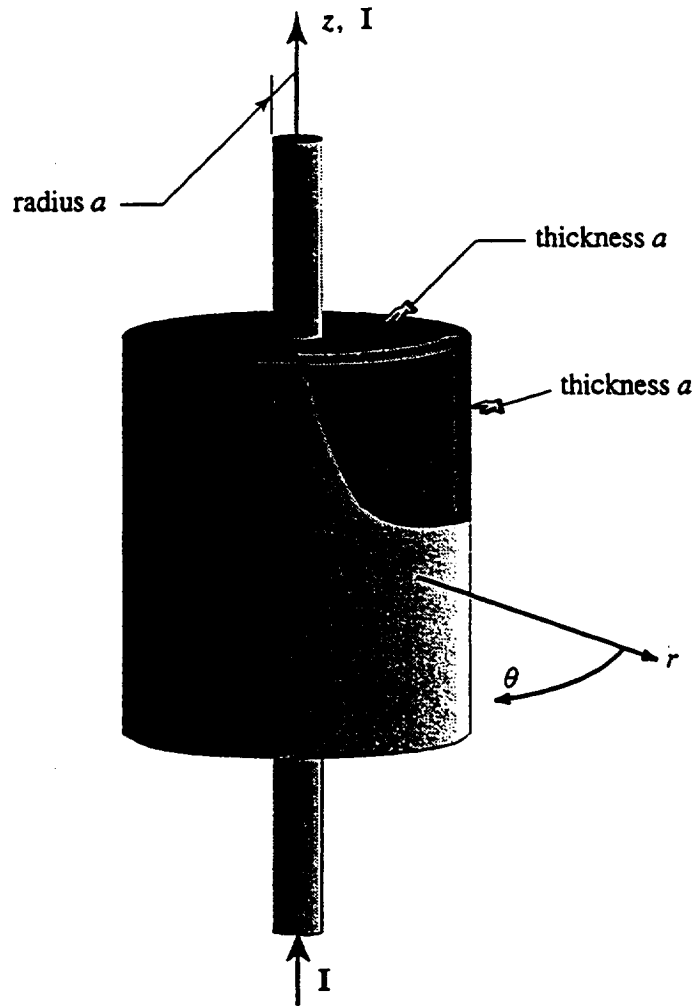
Fig. 2. Diagram of second test problem: a cylindrical "can" connected to an infinite feed wire conducting total current I, which is assumed to be uniformly distributed over the varying cross sections. The feed wire radius and can wall thicknesses are identical.

wall thicknesses are assumed to be identical.

Because of the symmetry of the problem it is sufficient to model only the upper half $z \geq 0$. The results presented here were obtained using a 25 × 25 element mesh of square elements. Within this mesh the wire as well as the can walls are modeled with only one element across the radius or thickness, respectively.

The uniform mesh indeed represents an "overkill" for the free space while it is insufficiently refined to capture field distribution details inside and near the conducting material. It was actually chosen to expedite the preparation of inputs to three-dimensional plotting software given the limited time available for obtaining displays.

The problem was run using full, selective and zero integration schemes for the λ freedoms. The magnetic permeability μ_{free} $\mathcal{D}$ μ_0 in the free space outside the conducting material is chosen as
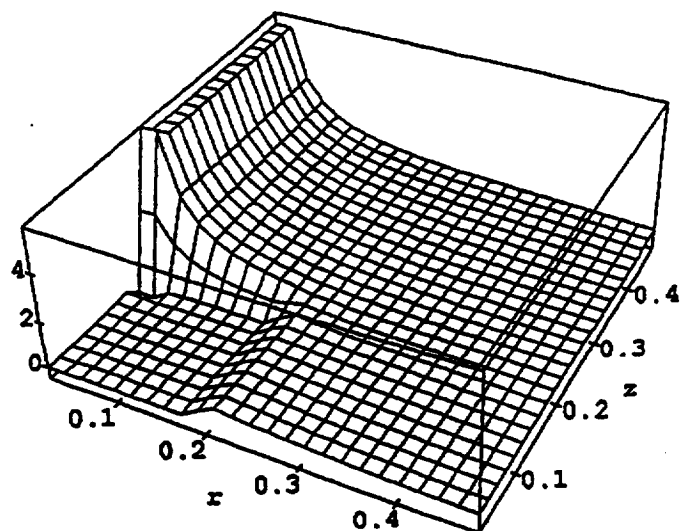
Fig. 3. Magnetic field $B_2 \equiv B_\theta$ vs. radial and axial coordinates r and z for $\mu_{wire} = 1$. Full integration scheme for λ. Intersections of mesh represent element centroids.
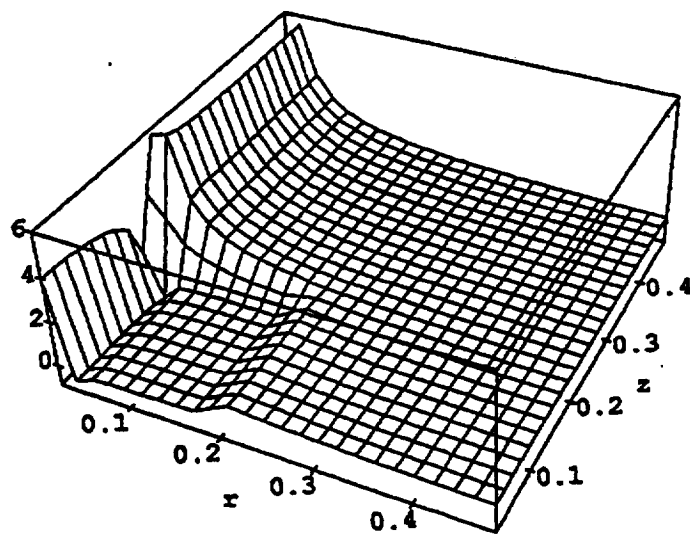
Fig. 4. Magnetic field $B_2 \equiv B_\theta$ vs. radial and axial coordinates r and z for $\mu_{wire} = 1$. Zero integration scheme for λ ($\equiv$ gauge constraint not enforced). Intersections of mesh represent element centroids.

214
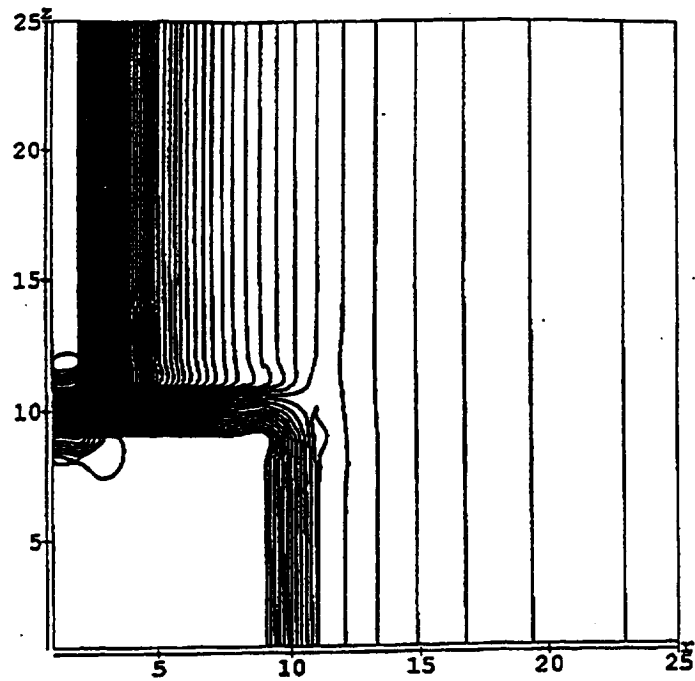
Fig. 5. Contour plot of magnetic field $B_2 \equiv B_\theta$, $\mu_{wire} = 1.0$. Full integration scheme for λ. Numbers on axes represent the number of element centroids traversed from the center of the "can". Each element is .02 x .02 square. All contours are equally spaced and range from minimum to maximum values of the field.
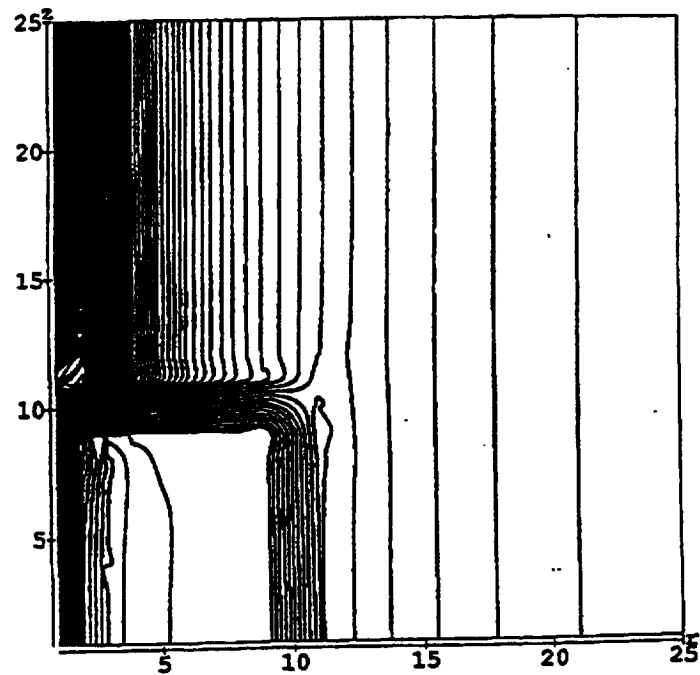
Fig. 6. Contour plot of magnetic field $B_2 \equiv B_\theta$, $\mu_{wire} = 1.0$. Zero integration scheme for λ ($\equiv$ gauge constraint not enforced). Numbers on axes represent the number of element centroids traversed from the center of the "can". Each element is .02 x .02 square. All contours are equally spaced and range from minimum to maximum values of the field.

215
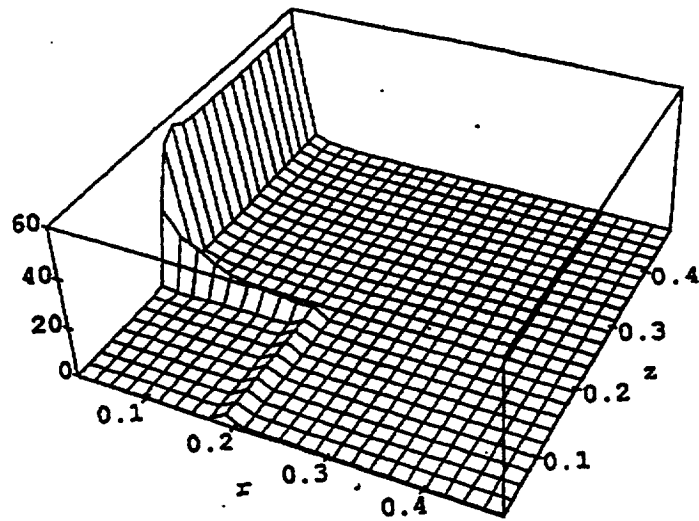
Fig. 7. Magnetic field $B_2 = B_\theta$ vs. radial and axial coordinates r and z for $\mu_{wire} = 10$. Full integration scheme for λ. Intersections of mesh represent element centroids. Note sharp field jump on conductor surfaces
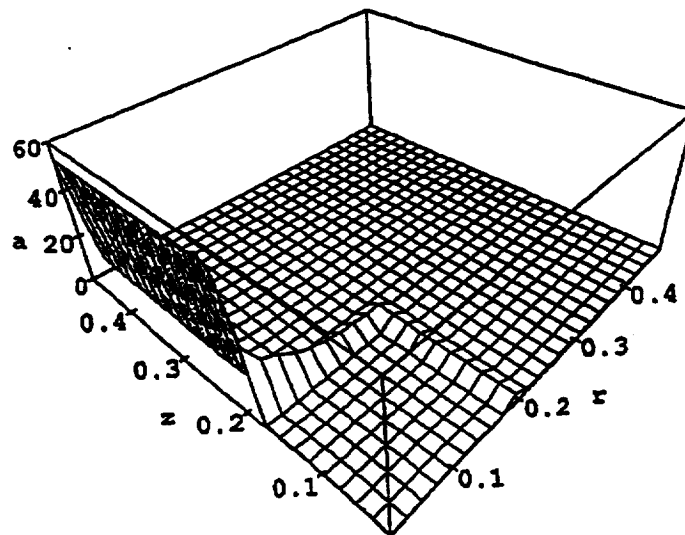
Fig. 8. The same case as Figure 7 shown from a different viewing point to emphasize how magnetic field in feed wire fails to go to zero as r approaches zero because of the coarse conductor discretization.

216

unity. For the conducting material two different values for the permeability $\mu = \mu_{wire}$ were tried: 1.0 and 10.0; the latter to check whether flux jump conditions are automatically accommodated by the potential formulation.

Selective results are reported graphically in Figures 3 through 8. Figures 3 and 4 show the magnitude of $B_2 \equiv B_\theta$ for $\mu_{wire} = \mu_{free} = \mu_0 = 1$ obtained for the full and zero order integration schemes, respectively. Figures 5 and 6 show these results in contour plot form. Figures 7 and 8 correspond to $\mu_{wire} = 10$ and show the magnitude of B_θ from different viewing points. A general discussion of the results follow.

The full integration scheme for λ performed well outside the conductor. Results were compared with those of the analytical solution for the infinite straight wire (the first test problem) to determine whether they were physically reasonable. As r becomes large compared to the can cross dimension (towards the outer radial edge of the mesh), the answers agreed. This is the expected behavior, because as $r \to \infty$ the general axisymmetric problem should appear as an infinite straight conductor. As one moves towards the top of the mesh, the solution again approaches that for an infinite wire as can be observed in Figures 3 through 8. This behavior was expected because as we move parallel to the wire in the z direction, the effects of the current in the can ends should tend to zero and the only far-field effects should be from the total current. The results for the magnetic field within the feed wire are not accurate as it did not vanish for $r = 0$; this behavior is due to the use of only one element across the radius and the fact that we report only centroidal values as noted above.

The selective integration scheme gave answers of the same general shape as the full integration scheme, but they only agreed to one or two significant digits; these results are not shown here as they are hard to distinguish in plots. The zero integration scheme (which in fact releases the Lorentz gauge coupling), gave solutions for the field that were larger than expected at the conductor boundary and a physically unrealizable field inside of the "can". This field grows sharply as the can axis is approached, as shown in Figures 4 and 6.

The finite element model also provided results for the electric potential 8 and associated electric field strength E, but such results have not been analyzed as of the time of this writing.

6. CONCLUSIONS AND FUTURE WORK

The results obtained from our two dimensional axisymmetric model for magnetostatic fields are particularly encouraging. They show that our variational approach can provide good models of electromagnetic fields outside of the conductor and appear to be extensible to three-dimensional static problems without major difficulties.

The results obtained for fields inside of the conductor in the second test problem can be improved by using a finer (graded) mesh, higher order finite elements, or elements based on a Hellinger-Reissner principle in which both potentials and fields are primary variables. In our experiments with one-dimensional elements, the finer mesh gave excellent results, and it is expected that the two-dimensional element being based upon the same variational principle will converge upon the exact solution in the same manner.

One unsettled aspect of our results is the damping type matrix C that appears in the dynamic equations (43) for the multidimensional case. It appears than in time-dependent problems we will either be forced to work with a set of equations that are coupled on the left-hand side or find a gauge transformation that will provide for the desired uncoupling. The treatment of time-dependent effects, however, represents an important step in the construction of a finite element model for superconductors. We plan to concentrate on harmonic currents rather than general transients as the former are more important in envisioned applications such as communication systems.

If encouraging results are obtained in the dynamic case, thermocoupling effects will be added to the code. Recent textbooks and surveys[20,21,22] discuss several different approaches applicable to various contexts (*e.g.* eddy currents) and these will have to be investigated for suitability for capturing the couplings effects that are relevant to the superconducting problem. Fano, Chu and Adler[20] present an interesting discussion on the coupling of electric and magnetic forces to mechanical effects through the Lorentz force and it is expected that this will be the next addition to our code.

After accounting for coupling effects, the following step will be to model the superconducting fields. The feasibility of using the current model for superconductor applications is high, as the current density of a superconductor can be approximated by the standard current density multiplied by a constant squared. This constant is called the *London penetration depth*. Other analytical models that possess similar characteristics have been developed and are described, for example, in the books of Kittel[23] and Tinkham[24].

ACKNOWLEDGEMENTS

REFERENCES

1. D. J. Connolly, "Aerospace applications of high-temperature superconductors," SSTAC/ARTS Briefing, Space Electronics Division, NASA Lewis Research Center, 1989

2. C. A. Felippa and T. L. Geers, "Partitioned analysis of coupled mechanical systems," *Engineering Computations*, 5, 1988, pp. 123–133

3. K. C. Park and C. A. Felippa, "Partitioned analysis of coupled systems," Chapter 3 in *Computational Methods for Transient Analysis*, ed. by T. Belytschko and T. J. R. Hughes, North-Holland, Amsterdam– New York, 1983

4. C. A. Felippa, "The extended free formulation of finite elements in linear elasticity," *Journal of Applied Mechanics*, 56, 3, 1989, pp. 609–616

5. C. A. Felippa and C. Militello, "Developments in variational methods for high-performance plate and shell elements," in *Analytical and Computational Models for Shells*, CED Vol. 3, ed. by A. K. Noor, T. Belytschko and J. C. Simo, The American Society of Mechanical Engineers, ASME, New York, 1989, pp. 191–216

6. C. A. Felippa and C. Militello, "The variational formulation of high-performance finite elements: parametrized variational principles," (with C. Militello), *Computers & Structures* 36, 1991, pp. 1–11

7. C. Militello and C. A. Felippa, "A variational justification of the assumed natural strain formulation of finite elements: I. Variational principles," (with C. Militello), *Computers & Structures* 34, 1990, pp. 439–444

8. C. Militello and C. A. Felippa, "A variational justification of the assumed natural strain formulation of finite elements: II. The C^0 4-node plate element," *Computers & Structures*, 34, 1990, pp. 445–453

9. C. Farhat and K. C. Park, "An Unconditionally Stable Staggered Algorithm for Transient Finite Element Analysis of Coupled Thermoelastic Problems," to appear in *Int. J. Numer. Meth. Engrg*, 1990

10. J. B. Davies, "The finite element method," Chapter 2 in *Numerical Techniques for Microwave and Millimeter-Wave Passive Structures*, ed. by T. Itoh, Wiley, New York, 1989

11. C. W. Trowbridge, "Numerical solution of electromagnetic field problems in two and three dimensions," Chapter 18 in *Numerical Methods in Coupled Problems*, ed. by R. Lewis *et.al.*, Wiley, London, 1984

12. C. A. Felippa and R. Ohayon, "Treatment of coupled fluid-structure interaction problems by a mixed variational principle," *Proceedings 7th International Conference on Finite Element Methods in Fluids*, ed. by T. J. Chung *et.al.*, University of Alabama Press, Huntsville, Alabama, April 1989, pp. 555–563

13. C. A. Felippa and R. Ohayon, "Mixed variational formulation of finite element analysis of acousto-elastic fluid-structure interaction," *Journal of Fluids & Structures*, 4, pp. 35-57, 1990

14. L. Eyges, *The Classical Electromagnetic Field*, Dover, New York, 1980

15. V. Rojanski, *The Electromagnetic Field*, Dover, New York, 1979

16. A. Shadowitz, *The Electromagnetic Field*, Dover, New York, 1975

17. H. A. Lorentz, *Theory of Electrons*, 2nd. ed, Dover, New York, 1952

18. C. Lanczos, *The Variational Principles of Mechanics*, Univ. of Toronto Press, Toronto, 1949

19. J. Schuler and C. A. Felippa, "Electromagnetic Finite Elements Based On A Four-Potential Variational Principle", *Finite Elements in Analysis and Design*, in press

20. R. M. Fano, L. J. Chu and R. B. Adler, *Electromagnetic Fields, Energy, and Forces*, Wiley, New York, 1960

21. H. Parkus (ed.), *Electromagnetic Interactions in Elastic Solids*, Springer-Verlag, Berlin, 1979

22. K.-Y. Yuan, F. C. Moon and J. F. Abel, "Elastic conducting structures in pulsed magnetic fields," Chapter 19 in *Numerical Methods in Coupled Problems*, ed. by R. Lewis *et.al.*, Wiley, London, 1984

23. C. Kittel, *Introduction to Solid State Physics*, 6th. ed, Wiley, New York, 1986

24. M. Tinkham, *Introduction to Superconductivity*, Krieger Pub. Co., Malabar, Florida, 1975

THE FIRST ANDES ELEMENTS:
9-DOF PLATE BENDING TRIANGLES

SUMMARY

New elements are derived to validate and assess the *assumed natural deviatoric strain* (ANDES) formulation. This is a brand new variant of the *assumed natural strain* (ANS) formulation of finite elements, which has recently attracted attention as an effective method for constructing high-performance elements for linear and nonlinear analysis. The ANDES formulation is based on an extended parametrized variational principle developed in recent publications. The key concept is that only the deviatoric part of the strains is assumed over the element whereas the mean strain part is discarded in favor of a constant stress assumption. Unlike conventional ANS elements, ANDES elements satisfy the individual element test (a stringent form of the patch test) *a priori* while retaining the favorable distortion-insensitivity properties of ANS elements. The first application of this new formulation is the development of several Kirchhoff plate bending triangular elements with the standard nine degrees of freedom. Linear curvature variations are sampled along the three sides with the corners as "gage reading" points. These sample values are interpolated over the triangle using three schemes. Two schemes merge back to conventional ANS elements, one being identical to the Discrete Kirchhoff Triangle (DKT), whereas the third one produces two new ANDES elements. Numerical experiments indicate that one of the ANDES element is relatively insensitive to distortion compared to previously derived high-performance plate-bending elements, while retaining accuracy for nondistorted elements.

1. INTRODUCTION

Despite almost three decades of work, plates and shells remain a important area of research in finite element methods. Challenging topics include:

1. The construction of high performance elements.

2. The modeling of composite and stiffened wall constructions.

3. The treatment of prestress, imperfections, nonlinear, dissipative and dynamic effects.

4. The development of practical error estimators and adaptive discretization methods.

5. The interaction with nonstructural components, for example external and internal fluids.

This paper addresses primarily the first challenge, although it must be recognized that progress in this direction is shaped to some extent by thinking of the others. The main motivation here is the construction of simple and efficient finite elements for plates and shells that are lock-free, rank sufficient and distortion insensitive, yield accurate answers for coarse meshes, fit into displacement-based programs, and can be easily extended to nonlinear and dynamic problems. Elements that possess these attributes to some noticeable degree are collectively known as *high performance* or HP elements.

Over the past three decades investigators have resorted to many ingenious devices to construct HP elements. The most important ones are listed in Table 1. The underlying theme is that although the final product may look like a standard displacement model so as to fit easily into existing finite element programs, *the conventional displacement formulation is abandoned*. (By "conventional" we mean the use of conforming displacement assumptions into the total potential energy principle.)

1.1 A Unified Variational Framework

Table 1 conveys the feeling of a bewildering array of tools. The question arises as to whether some of them are just facets of the same thing. Limited progress has been made in this regard. One notable advance in the 1970s has been the unification of reduced/selective integration and mixed methods achieved by Malkus and Hughes [1].

The present work has benefited from the unplanned confluence of two unification efforts. An initial attempt to place the free formulation [2–5] within the framework of parametrized hybrid variational principles was successful [6–8]. The free formulation in turn "dragged" incompatible shape functions, the patch test, and energy balancing into the scene. Concurrently a separate effort was carried out to set out the assumed natural strain (ANS) and projection methods in a mixed/hybrid variational framework [9,10]. Comparison of the results led to the rather unexpected conclusion that a parametrized variational framework was able to encompass ANS *and* the free formulation as well as some hitherto untried methods [11,12].

The common theme emerging from this unification is that a wide class of HP elements can be constructed using two ingredients:

(1) A parametrized functional that contains all variational principles of elasticity as special cases.

(2) Additional assumptions (sometimes called "variational crimes" or "tricks") that can be placed on a variational setting through Lagrange multipliers.

As of this writing it is not known whether the "wide class" referred to above encompasses all HP elements or at least the most interesting ones. Some surprising coalescences, such as DKT and ANS bending elements, however, have emerged from this study.

Table 1. Tools for Constructing HP Elements

	Technique	Year introduced
1.	Incompatible shape functions	early 1960s
2.	Patch test	1965
3.	Mixed and hybrid variational principles	1965
4.	Projectors	1967
5.	Selective reduced integration	1969
6.	Uniform reduced integration	1970
7.	Partial strain assumptions	1970
8.	Energy balancing	1974
9.	Directional integration	1978
10.	Limit differential equations	1982
11.	Free formulation	1984
12.	Assumed natural strains	1984

1.2 The Assumed Natural Strain Formulation

The assumed natural strain (ANS) formulation of finite elements is a relatively new development. A restricted form of the assumed strain method (not involving natural strains) was introduced in 1969 by Willam [13], who constructed a 4-node plane-stress element by assuming a constant shear strain independently of the direct strains and using a strain-displacement mixed variational principle. (The resulting element is identical to that derivable by selective one-point integration.) A different approach advocated by Ashwell [14] and coworkers viewed "strain elements" as a convenient way to generate appropriate displacement fields by integration of appropriately assumed compatible strain fields. (In fact, this was the technique originally used by Turner et al. [15] for deriving the constant-strain membrane triangle in their celebrated 1956 paper.)

These and other forms of assumed-strain techniques were overshadowed in the 1970s by developments in reduced and selective integration methods. The assumed strain approach in natural coordinates, however, has recently attracted substantial attention [16,17,18,19,20,21,22,23], particularly in view of its effectiveness in geometrically nonlinear analysis. One of the key ingredients in this approach is the concept of natural coordinates developed by Argyris and coworkers in the early 1960s [24–27]. Another important ingredient is the idea of reference lines introduced by Park and Stanley [21].

As noted above, the unification presented in [11,12] merges two HP element construction schemes: the free formulation (FF) of Bergan and Nygård [4] and a variant of ANS called ANDES (acronym for Assumed Natural Deviatoric Strains) described in further detail below. The stiffness equations produced by the unified formulation enjoy the fundamental decomposition property summarized in Box 1.

In the ANDES variant of ANS, assumptions are made only on the *deviatoric* portion of the element strains, namely that portion that integrates to zero over each element. This assumption produces the higher order stiffness labeled K_{h22} in Box 1. The mean portion of the strains is left to be determined variationally from assumptions on the limit stress field, and has no effect on the stiffness equations.

223

This paper describes the construction of the first ANDES elements. These are Kirchhoff plate-bending triangular elements with the standard 9 degrees of freedom (one displacement and two rotations at each corner). This choice is made because of the following reasons:

1. High-performance three-node triangular plate bending elements, whether based on Kirchhoff or Reissner-Mindlin mathematical models, have not been previously obtained through the ANS formulation. (Although the DKT element [28,29] qualifies as high-performance and is in fact an ANS element as shown later, it has not been derived as such.) The situation is in sharp contrast to four-node quadrilateral bending elements, for which HP elements have been constructed through a greater variety of tools; see *e.g.* [17,30,31,20,21].

2. High performance elements of this type have been obtained through the FF and ancestors of the FF [2,3,4,36], and they are considered among the best performers available. It is therefore intriguing whether elements based on the ANDES variant can match or exceed this performance.

The basic steps in the construction of K_b and K_h for a general three-dimensional element are summarized in Boxes 2 and 3, respectively. For justification of these "recipees" the reader is referred to [11,12]. The derivation of conventional ANS elements is summarized in Box 4.

Box 1   Decomposition of the Element Stiffness Equations

Let K be the element stiffness matrix, v the visible element degrees of freedom (those degrees of freedom in common with other elements, also called the *connectors*) and f the corresponding element node forces. Then the element stiffness equations decompose as

$$Kv = (K_b + K_h)\, v = f. \tag{1}$$

K_b and K_h are called the *basic* and *higher order* stiffness matrices, respectively. The basic stiffness matrix, which is usually rank deficient, is constructed for *convergence*. The higher order stiffness matrix is constructed for *stability* and (in more recent work) *accuracy*. A decomposition of this nature, which also holds at the assembly level, was first obtained by Bergan and Nygård in the derivation of the free formulation [4].

In the unified formulation presented in [11,12] the following key properties of the decomposition (1) are derived.

1. K_b is *formulation independent* and is defined entirely by an assumed constant stress state working on element boundary displacements. No knowledge of the interior displacements is necessary (Box 2). The extension of this statement to C^0 plate and shell elements is not straightforward, however, and special considerations are necessary in order to obtain K_b for those elements.

2. K_h has the general form
    $$K_h = j_{33}K_{h33} + j_{22}K_{h22} + j_{23}K_{h23}. \tag{2}$$

    The three parameters j_{22}, j_{23} and j_{33} characterize the source variational principle in the following sense:

    (a) The FF is recovered if $j_{22} = j_{23} = 0$ and $j_{33} = 1 - \gamma$, where γ is a K_h scaling coefficient studied in [5,32,33]. The original FF of [4] is obtained if $\gamma = 0$. The source variational principle is a one-parameter form that includes the potential energy and stress-displacement Reissner functionals as special cases [6–8].

    (b) The ANDES variant of ANS is recovered if $j_{22} = j_{23} = 0$ whereas $j_{22} = \alpha$ is a scaling parameter. The source variational principle is a one-parameter form that includes Reissner's stress-displacement and Hu-Washizu's functionals as special cases [12].

    (c) If j_{23} is nonzero, the last term in (2) may be viewed as being produced by a FF/ANDES combination. Such a combination remains unexplored.

Box 2 Construction of the Basic Stiffness Matrix K_b

Step B.1.   Assume a *constant* stress field, $\overline{\sigma}$, inside the element. (This should be the element stress field that holds in the convergence limit; for structural elements the assumption would be on *independent* stress resultants.) The associated boundary tractions are $\overline{\sigma}_n = \overline{\sigma}.n$, where n denotes the unit external normal on the element boundary S.

Step B.2.   Assume boundary displacements, d, over S. This field is described in terms of the *visible* element node displacements v (also called the *connectors*) as

$$d = N_d\, v, \tag{3}$$

where N_d is an array of boundary shape functions. The boundary motions (3) must satisfy interelement continuity (or at least, zero mean discontinuity so that no energy is lost at interfaces) and contain rigid-body and constant-strain motions exactly.

Step B.3.   Construct the "lumping matrix" L that consistently "lumps" the boundary tractions $\overline{\sigma}_n$ into element node forces, $\bar{f}$, conjugate to v in the virtual work sense. That is,

$$\bar{f} = \int_S N_{dn}\overline{\sigma}_n\, dS = L\overline{\sigma}. \tag{4}$$

In the above, N_{dn} are boundary-system projections of N_d conjugate to the surface tractions $\overline{\sigma}_n$.

Step B.4.   The basic stiffness matrix for a 3D element is

$$K_b = \upsilon^{-1}\, LEL^T, \tag{5}$$

where E is the stress-strain constitutive matrix of elastic moduli, which are assumed to be constant over the element, and $\upsilon = \int_V dV$ is the element volume measure.

For a Kirchhoff plate bending element, stresses, strains and stress-strain moduli become bending moments, curvatures and moment-curvature moduli, respectively, and the integration is performed over the element area A:

$$K_b = A^{-1}\, LDL^T, \tag{6}$$

where D is the matrix of moment-curvature moduli. Specific examples for L are provided in Section 4.

Box 3 Construction of K_h by the ANDES Formulation

Step H.1. Select *reference lines* (in 2D elements) or *reference planes* (in 3D elements) where "natural straingage" locations are to be chosen. By appropriate interpolation express the element natural strains ϵ in terms of the "straingage readings" g at those locations:

$$\epsilon = A_\epsilon g, \tag{7}$$

where ϵ is a strain field in natural coordinates that must include all constant strain states. (For structural elements the term "strain" is to be interpreted in a generalized sense.)

Step H.2. Relate the Cartesian strains e to the natural strains:

$$e = T\epsilon = TA_\epsilon g = Ag \tag{8}$$

at each point in the element. (If $e \equiv \epsilon$, or if it is possible to work throughout in natural coordinates, this step is skipped.)

Step H.3. Relate the natural straingage readings g to the visible degrees of freedom

$$g = Qv, \tag{9}$$

where Q is a straingage-to-node displacement transformation matrix. Techniques for doing this vary from element to element and it is difficult to state rules that apply to every situation. In the elements derived here Q is constructed by direct interpolation over the reference lines. (In general there is no unique internal displacement field u whose symmetric gradient is e or ϵ, so this step cannot be done by simply integrating the strain field over the element and collocating u at the nodes.)

Step H.4. Split the Cartesian strain field into mean (volume-averaged) and deviatoric strains:

$$e = \bar{e} + e_d = (\overline{A} + A_d) g, \tag{10}$$

where $\overline{A} = \int_V TA_\epsilon \, dV / v$, and $e_d = A_d g$ has mean zero value over V. This step may also be carried out on the natural strains if T is constant, as is the case for the elements here.

Step H.5. The higher-order stiffness matrix is given by

$$K_h = \alpha Q^T K_d Q, \qquad \text{with} \qquad K_d = \int_V A_d^T E A_d \, dV, \tag{11}$$

where $\alpha = j_{22} > 0$ is a scaling coefficient (see Box 1).

It is often convenient to combine the product of A and Q into a single strain-displacement matrix called (as usual) B, which splits into $\overline{B}$ and B_d:

$$e = AQv = (\overline{A} + A_d)Qv = (\overline{B} + B_d)v = Bv, \tag{12}$$

in which case

$$K_h = \int_V B_d^T E B_d \, dV. \tag{13}$$

The notation $B_\epsilon = A_\epsilon Q$ is also used in the sequel.

227

2. THE TRIANGULAR ELEMENT

2.1 Geometric Relations

The geometry of an individual triangle is illustrated in Figure 1. The triangle has *straight sides*. Its geometry is completely defined by the location of its three corners, which are labelled 1,2,3, traversed counterclockwise. The element is referred to a local Cartesian system (x, y) which is usually taken with origin at the centroid 0, whence the corner coordinates x_i, y_i satisfy the relations

$$x_1 + x_2 + x_3 = 0, \qquad y_1 + y_2 + y_3 = 0. \tag{18}$$

Coordinate differences are abbreviated by writing $x_{ij} = x_i - x_j$, and $y_{ij} = y_i - y_j$. The signed triangle area A is given by

$$2A = \begin{vmatrix} 1 & 1 & 1 \\ x_1 & x_2 & x_3 \\ y_1 & y_2 & y_3 \end{vmatrix} = x_{21}y_{31} - x_{31}y_{21} = x_{32}y_{12} - x_{12}y_{32} = x_{13}y_{23} - x_{23}y_{13}, \tag{19}$$
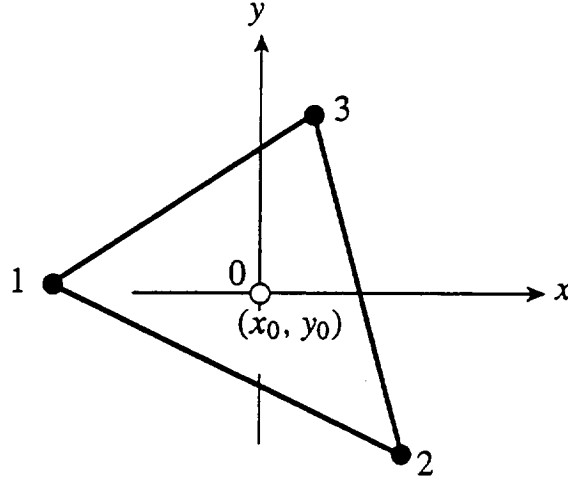
Figure 1. The triangular element.

and we require that $A > 0$.

We shall make use of dimensionless triangular coordinates ζ_1, ζ_2 and ζ_3, linked by $\zeta_1 + \zeta_2 + \zeta_3 = 1$. The following well known relations between the triangular and Cartesian coordinates of a straight-sided triangle are noted for further use:

$$x = x_1\zeta_1 + x_2\zeta_2 + x_3\zeta_3, \qquad y = y_1\zeta_1 + y_2\zeta_2 + y_3\zeta_3, \tag{20}$$

$$\zeta_i = \frac{1}{2A}\left[x_j y_k - x_k y_j + (x - x_0)y_{jk} + (y - y_0)x_{kj}\right], \tag{21}$$

in which i, j and k denote positive cyclic permutations of 1, 2 and 3; for example, $i = 2$, $j = 3$, $k = 1$. (If the origin is taken at the centroid as in Figure 1, $x_0 = y_0 = 0$.) It follows that

$$2A\frac{\partial\zeta_1}{\partial x} = y_{23}, \qquad 2A\frac{\partial\zeta_2}{\partial x} = y_{31}, \qquad 2A\frac{\partial\zeta_3}{\partial x} = y_{12},$$

$$2A\frac{\partial\zeta_1}{\partial y} = x_{32}, \qquad 2A\frac{\partial\zeta_2}{\partial y} = x_{13}, \qquad 2A\frac{\partial\zeta_3}{\partial y} = x_{21}. \tag{22}$$

Other intrinsic dimensions and ratios of use in future derivations are (see Figure 2)

$$\ell_{ij} = \ell_{ji} = \sqrt{x_{ij}^2 + y_{ij}^2}, \qquad c_{ij} = x_{ji}/\ell_{ij}, \qquad s_{ij} = y_{ji}/\ell_{ij},$$

$$a_k = 2A/\ell_{ij}, \qquad b_{ij} = (x_{ij}x_{ik} + y_{ji}y_{ki})/\ell_{ij} = \ell_{ij} - b_{ji},$$

$$\lambda_{ij} = b_{ij}/\ell_{ij} = (x_{ij}x_{ik} + y_{ji}y_{ki})/(x_{ij}^2 + y_{ij}^2), \qquad \lambda_{ji} = 1 - \lambda_{ij} = b_{ji}/\ell_{ij}. \tag{23}$$

Here $\ell_{ij} = \ell_{ji}$ is the length of side $i-j$ and c_{ij} and s_{ij} the cosine and sine, respectively, of angle $(i \rightarrow j, x)$. Furthermore b_{ij} and b_{ji} are the projections of sides $i-k$ and $k-j$, respectively, onto $i-j$; λ_{ij} and λ_{ji} being the corresponding projection ratios.

On each side $i-j$, define the dimensionless natural coordinates μ_{ij} as varying from 0 at i to 1 at j. The coordinate μ_{ij} of a point not on the side is that of its projection on $i-j$. Obviously

$$\frac{\partial x}{\partial \mu_{ij}} = x_{ji}, \qquad \frac{\partial y}{\partial \mu_{ij}} = y_{ji}. \tag{24}$$

Figure 2. Intrinsic dimensions of triangle.

2.2 Displacements, Rotations, Curvatures

As we are dealing with a Kirchhoff element, its displacement field is completely defined by the transverse displacement $w(x, y) \equiv w(\zeta_1, \zeta_2, \zeta_3)$, positive upwards. In the present section we assume that w is unique and known inside the element; this assumption is relaxed later. The midplane (covariant) rotations about x and y are $\theta_x = \partial w/\partial y$ and $\theta_y = -\partial w/\partial x$, respectively. Along side i–j with tangential direction t and external-normal n (see Figure 3) the tangential and normal rotations are defined as

$$\theta_n = \frac{\partial w}{\partial t} = \theta_x s_{ij} - \theta_y c_{ij},$$
$$\theta_t = -\frac{\partial w}{\partial n} = \theta_x c_{ij} + \theta_y s_{ij}.$$

(25)

The visible degrees of freedom of the element collected in v (see Boxes 2–3) are

$$\mathbf{v}^T = [\, w_1 \quad \theta_{x1} \quad \theta_{y1} \quad w_2 \quad \theta_{x2} \quad \theta_{y2} \quad w_3 \quad \theta_{x3} \quad \theta_{y3} \,].$$

(26)

The first and second derivatives of the displacement w with respect to the Cartesian and triangular coordinates are linked by the relations (summation convention used)

$$\frac{\partial w}{\partial x} = \frac{\partial w}{\partial \zeta_i}\frac{\partial \zeta_i}{\partial x} = \frac{1}{2A}\frac{\partial w}{\partial \zeta_i} y_{jk},$$
$$\frac{\partial w}{\partial y} = \frac{\partial w}{\partial \zeta_i}\frac{\partial \zeta_i}{\partial y} = \frac{1}{2A}\frac{\partial w}{\partial \zeta_i} x_{kj}.$$

(27)

$$\frac{\partial^2 w}{\partial x^2} = \frac{\partial^2 w}{\partial \zeta_i \partial \zeta_j}\frac{\partial \zeta_i}{\partial x}\frac{\partial \zeta_j}{\partial x} + \frac{\partial w}{\partial \zeta_i}\frac{\partial^2 \zeta_i}{\partial x^2} = \frac{1}{4A^2}\frac{\partial^2 w}{\partial \zeta_i \partial \zeta_j} y_{jk} y_{ki},$$
$$\frac{\partial^2 w}{\partial x \partial y} = \frac{\partial^2 w}{\partial \zeta_i \partial \zeta_j}\frac{\partial \zeta_i}{\partial x}\frac{\partial \zeta_j}{\partial y} + \frac{\partial w}{\partial \zeta_i}\frac{\partial^2 \zeta_i}{\partial x \partial y} = \frac{1}{4A^2}\frac{\partial^2 w}{\partial \zeta_i \partial \zeta_j} y_{jk} x_{ik}$$
$$\frac{\partial^2 w}{\partial y^2} = \frac{\partial^2 w}{\partial \zeta_i \partial \zeta_j}\frac{\partial \zeta_i}{\partial y}\frac{\partial \zeta_j}{\partial y} + \frac{\partial w}{\partial \zeta_i}\frac{\partial^2 \zeta_i}{\partial y^2} = \frac{1}{4A^2}\frac{\partial^2 w}{\partial \zeta_i \partial \zeta_j} x_{kj} x_{ik}$$

(28)

since $\partial^2 \zeta_i^2/\partial x^2$, $\partial^2 \zeta_i^2/\partial x \partial y$ and $\partial^2 \zeta_i^2/\partial y^2$ vanish on a straight-sided triangle, cf. Eq. (22). We can represent the second
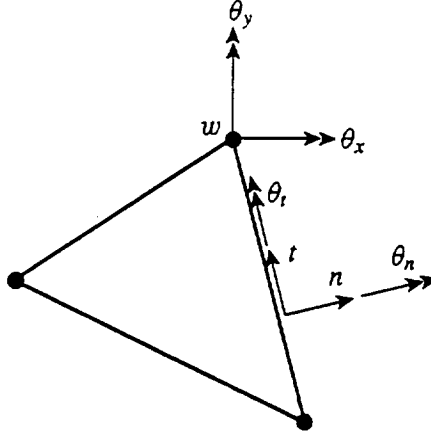
Figure 3. Local coordinate systems over a element side.

derivative relations in matrix form as

$$
\left\{ \begin{array}{c} \dfrac{\partial^2 w}{\partial x^2} \\[6pt] \dfrac{\partial^2 w}{\partial y^2} \\[6pt] 2\dfrac{\partial^2 w}{\partial x \partial y} \end{array} \right\} = \dfrac{1}{4A^2} \left[\begin{array}{ccc} y_{23}^2 & x_{32}^2 & 2x_{32}y_{23} \\ y_{31}^2 & x_{13}^2 & 2x_{13}y_{31} \\ y_{12}^2 & x_{21}^2 & 2x_{21}y_{12} \\ 2y_{23}y_{31} & 2x_{32}x_{13} & x_{32}y_{31}+x_{13}y_{23} \\ 2y_{31}y_{12} & 2x_{13}x_{21} & x_{13}y_{12}+x_{21}y_{31} \\ 2y_{12}y_{23} & 2x_{21}x_{32} & x_{21}y_{23}+x_{32}y_{12} \end{array} \right]^T \left\{ \begin{array}{c} \dfrac{\partial^2 w}{\partial \zeta_1^2} \\[6pt] \dfrac{\partial^2 w}{\partial \zeta_2^2} \\[6pt] \dfrac{\partial^2 w}{\partial \zeta_3^2} \\[6pt] \dfrac{\partial^2 w}{\partial \zeta_1 \partial \zeta_2} \\[6pt] \dfrac{\partial^2 w}{\partial \zeta_2 \partial \zeta_3} \\[6pt] \dfrac{\partial^2 w}{\partial \zeta_3 \partial \zeta_1} \end{array} \right\},
\tag{29}
$$

or

$$
\kappa = \mathbf{W} \mathbf{w}_{\zeta\zeta}.
\tag{30}
$$

The inverse relation does not exist.

2.3 Natural Curvatures

The second derivatives of w with respect to the dimensionless side directions defined in Section 2.1 will be called the *natural curvatures* and denoted by $\chi_{ij} = \partial^2 w/\partial \mu_{ij}^2$. Note that these curvatures have dimensions of displacement. The natural curvatures can be related to the Cartesian plate curvatures $\kappa_{xx} = \partial^2 w/\partial x^2$, $\kappa_{yy} = \partial^2 w/\partial y^2$ and $\kappa_{xy} = 2\partial^2 w/\partial x \partial y$, by chain-rule application of (22):

$$
\chi = \left\{ \begin{array}{c} \chi_{12} \\ \chi_{23} \\ \chi_{31} \end{array} \right\} = \left\{ \begin{array}{c} \dfrac{\partial^2 w}{\partial \mu_{12}^2} \\[6pt] \dfrac{\partial^2 w}{\partial \mu_{23}^2} \\[6pt] \dfrac{\partial^2 w}{\partial \mu_{31}^2} \end{array} \right\} = \left[\begin{array}{ccc} x_{21}^2 & y_{21}^2 & x_{21}y_{21} \\ x_{32}^2 & y_{32}^2 & x_{32}y_{32} \\ x_{13}^2 & y_{13}^2 & x_{13}y_{13} \end{array} \right] \left\{ \begin{array}{c} \dfrac{\partial^2 w}{\partial x^2} \\[6pt] \dfrac{\partial^2 w}{\partial y^2} \\[6pt] 2\dfrac{\partial^2 w}{\partial x \partial y} \end{array} \right\} = \mathbf{T}^{-1}\kappa.
\tag{31}
$$

231

The inverse of this relation is

$$
\left\{
\begin{array}{c}
\dfrac{\partial^2 w}{\partial x^2} \\[2ex]
\dfrac{\partial^2 w}{\partial y^2} \\[2ex]
2\dfrac{\partial^2 w}{\partial x \partial y}
\end{array}
\right\}
= \dfrac{1}{4A^2}
\left[
\begin{array}{ccc}
y_{23}y_{13} & y_{31}y_{21} & y_{12}y_{32} \\[1ex]
x_{23}x_{13} & x_{31}x_{21} & x_{12}x_{32} \\[1ex]
y_{23}x_{31}+x_{32}y_{13} & y_{31}x_{12}+x_{13}y_{21} & y_{12}x_{23}+x_{21}y_{32}
\end{array}
\right]
\left\{
\begin{array}{c}
\dfrac{\partial^2 w}{\partial \mu_{12}^2} \\[2ex]
\dfrac{\partial^2 w}{\partial \mu_{23}^2} \\[2ex]
\dfrac{\partial^2 w}{\partial \mu_{31}^2}
\end{array}
\right\},
\tag{32}
$$

or, in compact matrix notation

$$
\kappa = T\chi.
\tag{33}
$$

A comparison of (29) with (31)–(32) displays the advantages of natural curvatures over triangle-coordinate curvatures when the curvature field is to be constructed directly. On the other hand, (29) is useful when the transverse displacement w over the element is built as a function of the triangular coordinates.

At this point we relax the requirement that the curvatures be derivable from a displacement field w; consequently the partial derivative notation will be discontinued. However, the foregoing transformations will be assumed to hold even if the curvature fields κ and χ are not derivable from w.

3. DIRECT CURVATURE INTERPOLATION

3.1 The Straingage Readings

ANS and ANDES plate bending elements are based on direct interpolation of natural curvatures. All elements discussed here adopt the three triangle sides as the *reference lines* defined in Box 3. The natural curvatures are assumed to vary linearly over each reference line, an assumption which is obviously consistent with cubic beam-like variations of w over the sides. A linear variation on each side is determined by two straingage sample points, which we chose to be at the corners.

Over each triangle side chose the isoparametric coordinates ξ_{ij} that vary from -1 at corner i to $+1$ at corner j. These are related to the μ_{ij} coordinates introduced in Section 2.1 by $\xi_{ij} = 2\mu_{ij} - 1$. The Hermite interpolation of w over i–j is

$$
w = \tfrac{1}{4}[\,(1-\xi_{ij})^2(2+\xi_{ij}) \quad \tfrac{1}{2}\ell_{ij}(1-\xi_{ij})^2(1+\xi_{ij}) \quad (1+\xi_{ij})^2(2-\xi_{ij}) \quad -\tfrac{1}{2}\ell_{ij}(1+\xi_{ij})^2(1-\xi_{ij})\,]
\left\{
\begin{array}{c}
w_i \\ \theta_{ni} \\ w_j \\ \theta_{nj}
\end{array}
\right\}
$$

where θ_n denotes the rotation about the external normal n on side ij. The natural curvature over side ij is given by

$$
\chi_{ij} = \frac{\partial^2 w}{\partial \mu_{ij}^2} = [\,6\xi_{ij} \quad \ell_{ij}(3\xi_{ij}-1) \quad -6\xi_{ij} \quad \ell_{ij}(3\xi_{ij}+1)\,]
\left\{
\begin{array}{c}
w_i \\ \theta_{ni} \\ w_j \\ \theta_{nj}
\end{array}
\right\},
\tag{34}
$$

Evaluating these relations at the nodes by setting $\xi_{ij} = \pm 1$ and converting normal rotations to x-y rotations through (25), we build the transformation

$$
\left\{
\begin{array}{c}
\chi_{12}|_1 \\ \chi_{12}|_2 \\ \chi_{23}|_2 \\ \chi_{23}|_3 \\ \chi_{31}|_3 \\ \chi_{31}|_1
\end{array}
\right\}
=
\left[
\begin{array}{ccccccccc}
-6 & -4y_{21} & 4x_{21} & 6 & -2y_{21} & 2x_{21} & 0 & 0 & 0 \\
6 & 2y_{21} & -2x_{21} & -6 & 4y_{21} & -4x_{21} & 0 & 0 & 0 \\
0 & 0 & 0 & -6 & -4y_{32} & 4x_{32} & 6 & -2y_{32} & 2x_{32} \\
0 & 0 & 0 & 6 & 2y_{32} & -2x_{32} & -6 & 4y_{32} & -4x_{32} \\
6 & -2y_{13} & 2x_{13} & 0 & 0 & 0 & -6 & -4y_{13} & 4x_{13} \\
-6 & 4y_{13} & -4x_{13} & 0 & 0 & 0 & 6 & 2y_{13} & -2x_{13}
\end{array}
\right]
\left\{
\begin{array}{c}
w_1 \\ \theta_{x1} \\ \theta_{y1} \\ w_2 \\ \theta_{x2} \\ \theta_{y2} \\ w_3 \\ \theta_{x3} \\ \theta_{y3}
\end{array}
\right\}
\tag{35}
$$

The left hand side is the natural straingage reading vector called $\mathbf{g}$ in Box 3 and thus we can express (35) as

$$\mathbf{g} = \mathbf{Qv}. \tag{36}$$

This relation holds for all elements discussed here.

The six gage readings collected in $\mathbf{g}$ provide curvatures along the three triangle side directions at two corners. But nine values are needed to recover the complete curvature field over the element. The three additional values are the natural curvatures χ_{23}, χ_{31} and χ_{12} at corners 1, 2 and 3, respectively. Three possibilities for the missing values are discussed below.

3.2 The Average-Curvature Rule

To each corner k assign the average natural curvature χ_{ij} of the opposite side. This average is given by (34) evaluated at $\xi_{ij} = 0$. For example

$$\chi_{12}|_3 = \tfrac{1}{2}(\chi_{12}|_1 + \chi_{12}|_2) = y_{21}(\theta_{x2} - \theta_{x1}) + x_{12}(\theta_{y2} - \theta_{y1}). \tag{37}$$

The natural curvature now can be interpolated linearly over the triangle:

$$\chi_{12} = \chi_{12}|_1\,\zeta_1 + \chi_{12}|_2\,\zeta_2 + \chi_{12}|_3\,\zeta_3 = \chi_{12}|_1\,(\zeta_1 + \tfrac{1}{2}\zeta_3) + \chi_{12}|_2\,(\zeta_2 + \tfrac{1}{2}\zeta_3). \tag{38}$$

It is readily verified that under this rule the natural curvature χ_{12} is constant over lines parallel to the triangle *median* that passes through node 3. Formulas for the other curvatures follow by cyclic permutation, from which we construct the matrix relation

$$
\begin{Bmatrix} \chi_{12} \\ \chi_{23} \\ \chi_{31} \end{Bmatrix} =
\begin{bmatrix}
\zeta_1 + \tfrac{1}{2}\zeta_3 & \zeta_2 + \tfrac{1}{2}\zeta_3 & 0 & 0 & 0 & 0 \\
0 & 0 & \zeta_2 + \tfrac{1}{2}\zeta_1 & \zeta_3 + \tfrac{1}{2}\zeta_1 & 0 & 0 \\
0 & 0 & 0 & 0 & \zeta_3 + \tfrac{1}{2}\zeta_2 & \zeta_1 + \tfrac{1}{2}\zeta_2
\end{bmatrix} \mathbf{g}
$$

$$
=
\begin{bmatrix}
6\zeta_{21} & (3\zeta_{21}-1)y_{21} & (3\zeta_{12}+1)x_{21} & 6\zeta_{12} & (3\zeta_{21}+1)y_{21} & (3\zeta_{12}-1)y_{21} \\
0 & 0 & 0 & 6\zeta_{32} & (3\zeta_{32}-1)y_{32} & (3\zeta_{23}+1)x_{32} \\
6\zeta_{31} & (3\zeta_{13}+1)y_{13} & (3\zeta_{31}-1)y_{13} & 0 & 0 & 0
\end{bmatrix}
\tag{39}
$$

$$
\begin{bmatrix}
0 & 0 & 0 \\
6\zeta_{23} & (3\zeta_{32}+1)y_{32} & (3\zeta_{23}-1)y_{32} \\
6\zeta_{13} & (3\zeta_{13}-1)y_{13} & (3\zeta_{31}+1)x_{13}
\end{bmatrix} \mathbf{v},
$$

in which $\zeta_{12} = \zeta_1 - \zeta_2$, etc. In the notation of Box 3,

$$\chi = \mathbf{A}_{\chi a}\mathbf{g} = \mathbf{A}_{\chi a}\mathbf{Qv} = \mathbf{B}_{\chi a}\,\mathbf{v}. \tag{40}$$

where subscript a identifies the "averaging" rule (37). Since the natural curvatures vary linearly over the triangle, their mean values are obtained by evaluating (39) at the centroid $\zeta_1 = \zeta_2 = \zeta_3 = 1/3$:

$$
\overline{\chi} = \begin{Bmatrix} \overline{\chi}_{12} \\ \overline{\chi}_{23} \\ \overline{\chi}_{31} \end{Bmatrix} =
\begin{bmatrix}
0 & -y_{21} & x_{21} & 0 & y_{21} & -x_{21} & 0 & 0 & 0 \\
0 & 0 & 0 & 0 & -y_{32} & x_{32} & 0 & y_{32} & -x_{32} \\
0 & y_{13} & -x_{13} & 0 & 0 & 0 & 0 & -y_{13} & x_{13}
\end{bmatrix} \mathbf{v} = \overline{\mathbf{B}}_{\chi a}\mathbf{v}. \tag{41}
$$

Finally, the Cartesian curvatures are given by

$$\kappa = \mathbf{TB}_{\chi a}\mathbf{v} = \mathbf{B}_a\mathbf{v}, \tag{42}$$

An explicit expression of these relations is easily obtained, but not required in what follows; however, that of the mean Cartesian curvatures $\overline{\kappa} = \mathbf{T}\overline{\mathbf{B}}_{\chi a}\mathbf{v} = \overline{\mathbf{B}}_a\mathbf{v}$ (a relation valid because $\mathbf{T}$ is constant over the triangle) is enlightening:

$$
\overline{\kappa} = \begin{Bmatrix} \overline{\kappa}_{xx} \\ \overline{\kappa}_{yy} \\ 2\overline{\kappa}_{xy} \end{Bmatrix} = \frac{1}{2A}
\begin{bmatrix}
0 & 0 & y_{32} & 0 & 0 & y_{13} & 0 & 0 & y_{21} \\
0 & x_{32} & 0 & 0 & x_{13} & 0 & 0 & x_{21} & 0 \\
0 & y_{23} & x_{23} & 0 & y_{31} & x_{31} & 0 & y_{12} & x_{12}
\end{bmatrix} \mathbf{v} = \overline{\mathbf{B}}_a\mathbf{v}. \tag{43}
$$

233

3.3 The Projection Rule

To each corner k assign the natural curvature χ_{ij} of its projection onto the opposite side. This results in χ_{ij} being constant along lines *normal* to side ij. For equilateral triangles this agrees with the averaging rule, but not otherwise. The underlying motivation is to make the element insensitive to bad aspect ratios in cylindrical bending along side directions.

To illustrate the application of this rule consider side 1–2. For node 3 take

$$\chi_{12}|_3 = \left.\frac{\partial^2 w}{\partial \mu_{12}^2}\right|_3 = \lambda_{12}\,\chi_{12}|_1 + \lambda_{21}\,\chi_{12}|_2, \tag{44}$$

where λ_{12} and λ_{21} are defined in (23). Proceeding similarly along the other sides we construct the matrix relation

$$\begin{Bmatrix} \chi_{12} \\ \chi_{23} \\ \chi_{31} \end{Bmatrix} = \begin{bmatrix} \zeta_1 + \lambda_{12}\zeta_3 & \zeta_2 + \lambda_{21}\zeta_3 & 0 & 0 & 0 & 0 \\ 0 & 0 & \zeta_2 + \lambda_{23}\zeta_1 & \zeta_3 + \lambda_{32}\zeta_1 & 0 & 0 \\ 0 & 0 & 0 & 0 & \zeta_3 + \lambda_{31}\zeta_2 & \zeta_1 + \lambda_{13}\zeta_2 \end{bmatrix} \mathbf{g}, \tag{45}$$

or

$$\chi = \mathbf{A}_{\chi p}\,\mathbf{g}, \qquad \kappa = \mathbf{T}\mathbf{A}_{\chi p}\,\mathbf{g}. \tag{46}$$

where subscript p identifies the "projection" rule. As in the preceding rule, since $\mathbf{T}$ is constant we can do the strain-splitting step of Box 3 directly on the natural curvatures by evaluating at the centroid:

$$
\begin{aligned}
\mathbf{A}_{\chi p} &= (\overline{\mathbf{A}}_{\chi p} + \mathbf{A}_{\chi dp}) \\
&= \begin{bmatrix} \tfrac{1}{3}(1+\lambda_{12}) & \tfrac{1}{3}(1+\lambda_{21}) & 0 & 0 & 0 & 0 \\ 0 & 0 & \tfrac{1}{3}(1+\lambda_{23}) & \tfrac{1}{3}(1+\lambda_{32}) & 0 & 0 \\ 0 & 0 & 0 & 0 & \tfrac{1}{3}(1+\lambda_{31}) & \tfrac{1}{3}(1+\lambda_{13}) \end{bmatrix} \\
&\quad + \begin{bmatrix} \zeta_{10}+\lambda_{12}\zeta_{30} & \zeta_{20}+\lambda_{21}\zeta_{30} & 0 & 0 & 0 & 0 \\ 0 & 0 & \zeta_{20}+\lambda_{23}\zeta_{10} & \zeta_{30}+\lambda_{32}\zeta_{10} & 0 & 0 \\ 0 & 0 & 0 & 0 & \zeta_{30}+\lambda_{31}\zeta_{20} & \zeta_{10}+\lambda_{13}\zeta_{20} \end{bmatrix},
\end{aligned}
\tag{47}
$$

in which $\zeta_{i0} = \zeta_i - \tfrac{1}{3}$. Then

$$\mathbf{B}_p = \mathbf{T}\mathbf{A}_{\chi p}\mathbf{Q} = \mathbf{T}(\overline{\mathbf{A}}_{\chi p} + \mathbf{A}_{dp})\mathbf{Q} = \overline{\mathbf{B}}_p + \mathbf{B}_{dp}. \tag{48}$$

The explicit expression of these matrices is not revealing and for the construction of the stiffness matrix given in Appendix B it is better to leave (48) in product form. If all λ coefficients are $\tfrac{1}{2}$, which happens for the equilateral triangle, the expressions reduce to those of the averaging rule.

3.4 The 'Sliding Beam' Rule

This is a refinement of the average-curvature rule. Consider a fictitious beam parallel to side $i - j$ sliding towards corner k. The end displacements and rotation of this beam are obtained by interpolating w cubically, θ_n quadratically, and θ_t linearly, along sides i–k and j–k. Compute the mean natural curvature of this beam and assign to node k the limit as the beam reaches that corner.

The required calculations can be simplified if we observe that the mean curvature of the sliding beam varies linearly as it moves from i–j, where it coincides with (41), to corner k. At one third of the way this mean is the natural centroidal curvature, which can then be readily extrapolated to k. These centroidal curvatures are given by $\overline{\chi} = \overline{\mathbf{B}}_{\chi s}\mathbf{v}$, where subscript s identifies the 'sliding' rule. A symbolic calculation yields the explicit form

$$\overline{\mathbf{B}}_{\chi s}^T = \begin{bmatrix} 2\lambda_{13} & -2(\lambda_{21} + \lambda_{31}) & 2\lambda_{12} \\ a_2c_{13} & a_3c_{21} + a_2c_{13} & a_3c_{21} \\ a_2s_{13} & a_3s_{21} + a_2s_{13} & a_3s_{21} \\ 2\lambda_{23} & 2\lambda_{21} & -2(\lambda_{12} + \lambda_{32}) \\ a_1c_{32} & a_3c_{21} & a_1c_{32} + a_3c_{21} \\ a_1s_{32} & a_3s_{21} & a_1s_{32} + a_3s_{21} \\ -2(\lambda_{13} + \lambda_{23}) & 2\lambda_{31} & 2\lambda_{32} \\ a_2c_{13} + a_1c_{32} & a_2c_{13} & a_1c_{32} \\ a_2s_{13} + a_1s_{32} & a_2s_{13} & a_1s_{32} \end{bmatrix}, \tag{49}$$

where a_i, c_{ij} and s_{ij} are defined in Eqs. (23). Extrapolating to the opposite corners and interpolating over the triangle we get $\chi = \mathbf{B}_{\chi s} \mathbf{v}$, with

$$\mathbf{B}_{\chi s}^T = \begin{bmatrix} 6(-\zeta_1 + \zeta_2 + \lambda_{13}\zeta_3) & -6(\lambda_{21} + \lambda_{31})\zeta_1 & 6(\zeta_3 - \zeta_1 + \lambda_{12}\zeta_2) \\ 2y_{21}(1 - 3\zeta_1) + 3a_2c_{13}\zeta_3 & (3a_3c_{21} + 3a_2c_{13})\zeta_1 & 2y_{13}(3\zeta_1 - 1) + 3a_3c_{21}\zeta_2 \\ 2x_{21}(3\zeta_1 - 1) + 3a_2s_{13}\zeta_3 & (3a_3s_{21} + 3a_2s_{13})\zeta_1 & 2x_{13}(1 - 3\zeta_1) + 3a_3s_{21}\zeta_2 \\ 6(\zeta_1 - \zeta_2 + \lambda_{23}\zeta_3) & 6(-\zeta_2 + \zeta_3 + \lambda_{21}\zeta_1) & -6(\lambda_{12} + \lambda_{32})\zeta_2 \\ 2y_{21}(3\zeta_2 - 1) + 3a_1c_{32}\zeta_3 & 2y_{32}(1 - 3\zeta_2) + 3a_3c_{21}\zeta_1 & (3a_1c_{32} + 3a_3c_{21})\zeta_2 \\ 2x_{21}(1 - 3\zeta_2) + 3a_1s_{32}\zeta_3 & 2x_{32}(3\zeta_2 - 1) + 3a_3s_{21}\zeta_1 & (3a_1s_{32} + 3a_3s_{21})\zeta_2 \\ -6(\lambda_{23} + \lambda_{13})\zeta_3 & 6(\zeta_2 - \zeta_3 + \lambda_{31}\zeta_1) & 6(-\zeta_3 + \zeta_1 + \lambda_{32}\zeta_2) \\ (3a_2c_{13} + 3a_1c_{32})\zeta_3 & 2y_{32}(3\zeta_3 - 1) + 3a_2c_{13}\zeta_1 & 2y_{13}(1 - 3\zeta_3) + 3a_1c_{32}\zeta_2 \\ (3a_2s_{13} + 3a_1s_{32})\zeta_3 & 2x_{32}(1 - 3\zeta_3) + 3a_2s_{13}\zeta_1 & 2x_{13}(3\zeta_3 - 1) + 3a_1s_{32}\zeta_2 \end{bmatrix}. \tag{50}$$

It should be noted that $A\chi$ and $\mathbf{Q}$ are inextricably enmeshed in the above formula and cannot be easily separated. Premultiplication by T yields $\kappa = \mathbf{B}_s \mathbf{v}$. Evaluation of $\mathbf{B}_s$ at the centroid yields $\overline{\mathbf{B}}_s = \mathbf{L}_q^T/A$, where $\mathbf{L}_q^T = A T \overline{\mathbf{B}}_{\chi s}$ is the force lumping matrix given in Eq. (56).

A variation on the sliding-beam theme would consist of interpolating the normal rotation θ_n along $i-k$ and $j-k$ linearly rather than quadratically. This scheme turns out to be identical, however, to the average curvature rule and thus it provides nothing new.

3.5 The Six Beam Lattice Rule

In addition to the sides, consider three fictitious beams along the triangle medians. Determine the displacements and rotations at the triangle midpoints by the same interpolation procedure as in the sliding beam rule. The linear curvatures along the medians are thus readily computed. At each triangle corner we now know the curvatures in three directions: the two sides and the median. We can therefore transform to $x - y$ curvatures using Eq. (32), and interpolate these linearly over the element. This apparently new model gives, however, identical results to the projection rule, a result that can be *a posteriori* justified by geometric reasoning. Consequently this scheme will not be pursued further.

3.6 The ANS Elements

Three ANS elements based on the previous interpolation rules may be constructed by following the prescription of Box 4. Their stiffness matrices are identified as $\mathbf{K}_a$, $\mathbf{K}_p$, and $\mathbf{K}_s$, for averaging, projection, and sliding-beam, respectively. The following properties hold for these elements.

Patch Test. Assuming that the element has constant thickness and material properties, $\mathbf{K}_a$ and $\mathbf{K}_s$ pass the individual element test, but $\mathbf{K}_p$ does not. This claim can be analytically confirmed by applying the criterion of Eqs. (16)-(17), and noting that $\overline{\mathbf{B}}_a = \mathbf{L}_l^T/A$ and $\overline{\mathbf{B}}_s = \mathbf{L}_q^T/A$, where $\mathbf{L}_l$ and $\mathbf{L}_q$ are the force lumping matrices derived in Section 4.

Equivalence with DKT. $\mathbf{K}_s$ turns out to be identical to the stiffness matrix of the Discrete Kirchhoff Triangle (DKT) element, which was originally constructed in a completely different way [28,29] that involves assumed rotation fields. Thus *DKT is an ANS element, and also (because of the equivalence noted below) an ANDES element.* This equivalence provides the first variational justification of DKT, as well as the proof that DKT passes the patch test without any numerical verification.

235

ANS/ANDES Equivalence. If the basic stiffness matrices $\mathbf{K}_{bl}$ and $\mathbf{K}_{bq}$ derived in Section 4.1 are used in conjunction with the averaging and sliding-beam rules, and $\alpha = 1$, the ANDES formulation yields the same results as ANS if the element has constant thickness and material properties. (If the element has variable thickness, or the material properties vary, the equivalence does not hold.) The ANDES formulation used with the projection rule yields two elements, called ALR and AQR in the sequel, which differ in their basic stiffnesses. Both of these elements pass the patch test and are not equivalent to the ANS formulation.

4. STIFFNESS MATRIX COMPUTATION

4.1 The Basic Stiffness

As explained on Box 2, the basic stiffness is obtained by constructing the lumping matrix L. In our case this is a 9×3 matrix that "lumps" an internal constant bending-moment field $(\overline{m}_{xx}, \overline{m}_{yy}, \overline{m}_{xy})$ to node forces $\tilde{\mathbf{f}}$ conjugate to v.

On each element side, the constant moment field produces boundary moments $\overline{m}_{nn}$ and $\overline{m}_{nt}$ referred to a local edge coordinate system n, t (see Figure 3):

$$\left\{ \begin{matrix} \overline{m}_{nn} \\ \overline{m}_{nt} \end{matrix} \right\}_{ij} = \begin{bmatrix} s_{ij}^2 & c_{ij}^2 & -2s_{ij}c_{ij} \\ s_{ij}c_{ij} & -s_{ij}c_{ij} & s_{ij}^2 - c_{ij}^2 \end{bmatrix} \left\{ \begin{matrix} \overline{m}_{xx} \\ \overline{m}_{yy} \\ \overline{m}_{xy} \end{matrix} \right\} \tag{51}$$

The boundary motions d conjugate to m_{nn} and m_{nt} are $\partial w/\partial n = -\theta_t$ and $\partial w/\partial t = \theta_n$ (see Figure 3). Given the degree of freedom configuration (25), the normal slope $\partial w/\partial n = -\theta_t$ along side $i-j$ can at most vary linearly (it could be also taken as constant and equal to $\frac{1}{2}(\theta_{ti} + \theta_{tj})$ but the results are the same as for a linear variation).

For the tangential slope (the rotation about the normal) $\partial w/\partial t = \theta_n$ there are three options: constant, linear and quadratic variation. But a constant $\theta_n = (w_j - w_i)/\ell_{ij}$ turns out to be equivalent to the quadratic variation and a constant $\theta_n = \frac{1}{2}(\theta_{ni} + \theta_{nj})$ equivalent to the linear variation. Consequently only the linear and quadratic cases need to be examined.

Linear Normal Rotation. The variation of θ_t and θ_n along each side is linear:

$$\left\{ \begin{matrix} \theta_t \\ \theta_n \end{matrix} \right\}_{ij} = \frac{1}{2} \begin{bmatrix} 0 & 1-\xi & 0 & 0 & 1+\xi & 0 \\ 0 & 0 & 1-\xi & 0 & 0 & 1+\xi \end{bmatrix} \left\{ \begin{matrix} w_i \\ \theta_{ti} \\ \theta_{ni} \\ w_j \\ \theta_{tj} \\ \theta_{nj} \end{matrix} \right\}, \tag{52}$$

where $\xi \equiv \xi_{ij}$. Under this assumption one obtains [33]

$$\mathbf{L}_l^T = \frac{1}{2} \begin{bmatrix} 0 & 0 & y_{32} & 0 & 0 & y_{13} & 0 & 0 & y_{21} \\ 0 & x_{32} & 0 & 0 & x_{13} & 0 & 0 & x_{21} & 0 \\ 0 & y_{23} & x_{23} & 0 & y_{31} & x_{31} & 0 & y_{12} & x_{12} \end{bmatrix}, \tag{53}$$

where superscript l stands for "linear θ_n." The corresponding basic stiffness is

$$\mathbf{K}_{bl} = A^{-1}\mathbf{L}_l \mathbf{D} \mathbf{L}_l^T, \tag{54}$$

where D is the Cartesian moment-curvature constitutive matrix resulting from the integration of E through the plate thickness. This matrix been used as component of the free formulation (FF) element presented in Ref. [33].

Quadratic Normal Rotation. A quadratic variation of θ_n can be accomodated in conjunction with the cubic variation of w along the side:

$$\left\{\begin{array}{c} \theta_t \\ \theta_n \end{array}\right\}_{ij} = \frac{1}{2}\left[\begin{array}{cccccc} 0 & 1-\xi & 0 & 0 & 1+\xi & 0 \\ 3(\xi^2-1)/\ell & 0 & \frac{1}{2}(3\xi+1)(\xi-1) & 3(\xi^2-1)/\ell & 0 & \frac{1}{2}(3\xi-1)(\xi+1) \end{array}\right]\left\{\begin{array}{c} w_i \\ \theta_{ti} \\ \theta_{ni} \\ w_j \\ \theta_{tj} \\ \theta_{nj} \end{array}\right\} \tag{55}$$

where $\xi \equiv \xi_{ij}$ and $\ell \equiv \ell_{ij}$. Then the resulting lumping matrix can be presented as

$$\mathbf{L}_q = \left[\begin{array}{ccc} -c_{12}s_{12} + c_{31}s_{31} & -c_{31}s_{31} + c_{12}s_{12} & (s_{31}^2 - c_{31}^2) - (s_{12}^2 - c_{12}^2) \\ \frac{1}{2}(s_{12}^2 x_{12} + s_{31}^2 x_{31}) & \frac{1}{2}(c_{12}^2 x_{12} + c_{31}^2 x_{31}) & c_{12}^2 y_{21} + c_{31}^2 y_{13} \\ -\frac{1}{2}(s_{12}^2 y_{21} + s_{31}^2 y_{13}) & -\frac{1}{2}(c_{12}^2 y_{21} + c_{31}^2 y_{13}) & -s_{12}^2 x_{12} - s_{31}^2 x_{31} \\ -c_{23}s_{23} + c_{12}s_{12} & -c_{12}s_{12} + c_{23}s_{23} & (s_{12}^2 - c_{12}^2) - (s_{23}^2 - c_{23}^2) \\ \frac{1}{2}(s_{12}^2 x_{12} + s_{23}^2 x_{23}) & \frac{1}{2}(c_{12}^2 x_{12} + c_{23}^2 x_{23}) & c_{12}^2 y_{21} + c_{23}^2 y_{32} \\ -\frac{1}{2}(s_{12}^2 y_{21} + s_{23}^2 y_{32}) & -\frac{1}{2}(c_{12}^2 y_{21} + c_{23}^2 y_{23}) & -s_{12}^2 x_{12} - s_{23}^2 x_{23} \\ -c_{31}s_{31} + c_{23}s_{23} & -c_{23}s_{23} + c_{31}s_{31} & (s_{23}^2 - c_{23}^2) - (s_{31}^2 - c_{31}^2) \\ \frac{1}{2}(s_{23}^2 x_{23} + s_{31}^2 x_{31}) & \frac{1}{2}(c_{23}^2 x_{23} + c_{31}^2 x_{31}) & c_{23}^2 y_{32} + c_{31}^2 y_{13} \\ -\frac{1}{2}(s_{23}^2 y_{32} + s_{31}^2 y_{13}) & -\frac{1}{2}(c_{23}^2 y_{32} + c_{31}^2 y_{13}) & -s_{23}^2 x_{23} - s_{31}^2 x_{31} \end{array}\right]. \tag{56}$$

The corresponding basic stiffness matrix is denoted by

$$\mathbf{K}_{bq} = A^{-1}\mathbf{L}_q \mathbf{D} \mathbf{L}_q^T. \tag{57}$$

4.2 The Higher Order Stiffness

The higher order stiffness for the ANDES elements described in Section 3 is

$$\mathbf{K}_{hx} = \alpha \mathbf{Q}^T \mathbf{K}_{dx} \mathbf{Q} = \alpha \mathbf{Q}^T \left[\int_A \mathbf{A}_{dx}^T \mathbf{D} \mathbf{A}_{dx}\, dA\right]\mathbf{Q} = \alpha \int_A \mathbf{B}_{dx}^T \mathbf{D} \mathbf{B}_{dx}\, dA, \tag{58}$$

where $x = a, p, s$ for the average, projection and sliding-beam rules, respectively. (The last expression is appropriate when $\mathbf{B}_{dx}$ is not easily factored into $\mathbf{A}_{dx}\mathbf{Q}$, as in the sliding-beam rule.) Since $\mathbf{A}_{dx}$ varies linearly, if $\mathbf{D}$ is constant we could numerically integrate $\mathbf{K}_{dx}$ in (58) exactly with a three point Gauss rule; for example the three-midpoint formula. But as the element stiffness formation time is dominated by these calculations it is of interest to derive $\mathbf{K}_h$ in closed form. This is done in Appendix B for $\mathbf{K}_{hp}$, which from the numerical experiments appears to be the best performer.

5. NUMERICAL EXPERIMENTS: GENERAL DESCRIPTION

An extensive set of numerical experiments has been run to assess the performance of the new ANDES elements based on the projection rule (ALR and AQR) and to compare them with other existing high-performance elements. Table 2 lists the tests, material properties and some relevant geometrical properties, whereas Table 3 lists elements, loading and mesh identifiers.

An inspection of the element identifiers in Table 3 displays two important points: the difference in the results obtained with AQR and ALR can be attributed to their basic stiffness, whereas differences between AQR and DKT can be attributed to their higher order stiffness. With these facts in mind, we conducted first a set of distortion tests so that the less distortion sensitive combinations can be identified. Then, the best performers are submitted to a set of representative thin-plate bending problems in linear elasticity.

The scaling $\alpha = 1.5$ for ALR and $\alpha = 1.0$ for AQR have been chosen to obtain energy balance in some simple cylindrical bending tests. No further adjustment of these parameters was made. In the distortion tests we included the results obtained with the free formulation (FF) element presented in [33], since that reference did not report such tests.

Whenever the simply supported condition appears it implies that only the transverse displacement w is restrained. It is equivalent to the SS1 condition described in Hughes' textbook [34].

For tests involving an uniform distributed load q, two node-force computation schemes are usually reported:

1. Triangular lumping (TL), in which one third of the load qA is assigned to each triangle corners, and nodal moments are set to zero.

$$\mathbf{f}^T = \frac{qA}{3}[1 \quad 0 \quad 0 \quad 1 \quad 0 \quad 0 \quad 1 \quad 0 \quad 0].\qquad(59)$$

2. Consistent lumping (CL), in which the element node force vector is

$$\mathbf{f}^T = \frac{qA}{3}\left[1 \quad \frac{y_{31}+y_{21}}{8} \quad \frac{x_{13}+x_{12}}{8} \quad 1 \quad \frac{y_{23}+y_{32}}{8} \quad \ldots\right].\qquad(60)$$

This lumping was obtained using the transverse displacement w of the FF element in [33]. It is used for the ANS and ANDES elements as a matter of expediency, since for such elements a unique internal transverse displacement does not exist.

Inasmuch as the present elements pass the linear patch test by virtue of their construction, no validation experiments along these lines are necessary once the elements are correctly programmed.

6. DISTORTION TESTS

6.1 Simply Supported Square Plate under Central Load

This distortion test was proposed by Kang [31]. The use of a coarse mesh exacerbates the distortion effect when far from of the converged solution. (In a fine mesh the distortion effect would be diluted.) The mesh and distortion parameter are shown in Figure 4. When the distortion parameter a approaches 2.5 the mesh converges to a four element cross-diagonal mesh. Results are reported as a percentage of the deterioration with respect to the undistorted mesh.

The results given in Table 4 show that AQR is superior in this test. FF and ALR are the worst for $a > 2$. DKT and AQR display low deterioration rate from $a = 2$ up to $a = 2.49$, but DKT behaves poorly for $a < 2$.

6.2 Cantilever Beam

A cantilever beam with a transverse load at the tip was selected for this test. Two meshes shown in Figure 5, A and B, are used to observe the effect of the element orientation under a linear bending state. The results are reported in Table 5. Also shown in this table is the ratio of the computed tip deflection to the exact value w_{ex} for zero distortion.

For mesh A, AQR is the best performer closely followed by DKT. FF and ALR behave poorly.

For mesh B FF is the best performer in terms of deterioration, followed by AQR, DKT and ALR. However it must be noted that FF and ALR recover only 77% of the exact solution. This is a serious drawback in elements supposedly capable of providing an appropriate response for linear bending. This shortcoming can be attributed to the basic stiffness K_{bl} which is the same for both elements. AQR and DKT recover almost 99% of the response for both meshes.

6.3 Twisted Ribbon

This test has been selected to assess the distortion effect under a field which combines bending and twisting. The test uses mesh B of Figure 5. The results shown in Table 6 indicate that AQR and DKT are the least distortion sensitive elements for this problem.

Table 2. Key to Material and Geometrical Data

Test	Description
Square plate	Isotropic material $\nu = 0$, $E = 1$; thickness $t = 1$, plate span $a = 10$; load scaled so that center deflection $w_c = 100$
Cantilever beam	Isotropic material $\nu = 0$, $E = 1$; thickness $t = 1$; load scaled so that center deflection $w_c = 100$
Twisted ribbon	Isotropic material $\nu = 0.25$, $E = 10^7$; thickness $t = 0.05$; transverse load at tip so that $P_B = -P_A = 1$
Rhombic cantilever	Isotropic material $\nu = 0.3$, $E = 10.5\,10^6$; thickness $t = 0.125$; uniform transverse load $q = 0.26066$
Rhombic plate	Isotropic material $\nu = 0.3$, $E = 1$; thickness $t = 1$, plate side $a = 100$, uniform transverse load q scaled so that $w_c = 100$

Table 3. Key to Element, Loading and Mesh Identifiers

Key	Explanation
ALR	ANDES element $K_{bl} + 1.5K_{hp}$
AQR	ANDES element $K_{bq} + K_{hp}$
FF	FF element of [33] with 3-parameter scaling of K_h
DKT	ANS/ANDES element $K_{bq} + K_{hs}$: identical to DKT
CL	Consistent lumping (59) of uniform load q
TL	Triangular lumping (60) of uniform load q
SDC	In rhombic meshes, triangles obtained by splitting quadrilateral mesh units with short diagonal cuts
LDC	In rhombic meshes, triangles obtained by splitting quadrilateral mesh units with long diagonal cuts

239
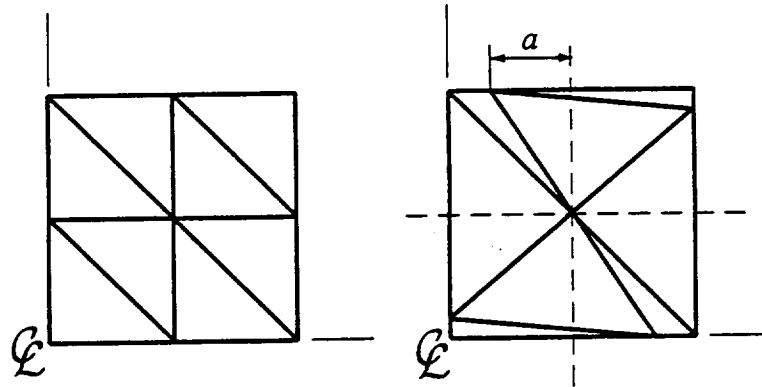
Figure 4. Square plate: mesh for distortion analysis.

Table 4. Distortion Analysis of Centrally Loaded SS Square Plate: Percent
Error of Center Deflection with Respect to Undistorted Mesh

Element	Distortion parameter				
type	0.50	1.00	1.50	2.00	2.49
ALR	0.83	2.65	5.05	7.88	10.38
AQR	0.17	−0.14	−1.59	−3.29	−4.40
DKT	−0.95	−3.46	−6.29	−8.06	−8.42
FF	0.81	2.27	3.69	4.85	−13.50

7. CONVERGENCE STUDIES

From the distortion test results, it can be concluded that elements whose basic stiffness is K_{bq} are less distortion sensitive. Consequently only results for the AQR and DKT elements are presented in the following studies.

7.1 Square Plate

In this analysis a square plate with either simply-supported or clamped edges is considered. Due to symmetry only one quarter of the plate is modeled. The two different mesh orientations, A and B, used in the analysis are illustrated in Figure 6. The number of elements used is $2N^2$, where N is the number of side subdivisions.

For the cases involving a concentrated load, Figures 7 and 8 show that for both meshes AQR converges faster and is less sensitive to mesh orientation than DKT.

In the case of uniform loading with triangular lumping, Figures 9 and 10, the convergence is uniform for all the meshes and elements. For the simply-supported condition all answers are within the 5% error limit for $N = 4$. Clearly DKT converges faster in this case. For the clamped condition and $N = 4$, DKT(A) is outside the 5% error limit.

For consistent force lumping, the results shown in Table 7 indicate a dramatic improvement of AQR. DKT also improves in the sense that becomes less mesh sensitive and that all the results are within 5% error for $N = 4$.

240
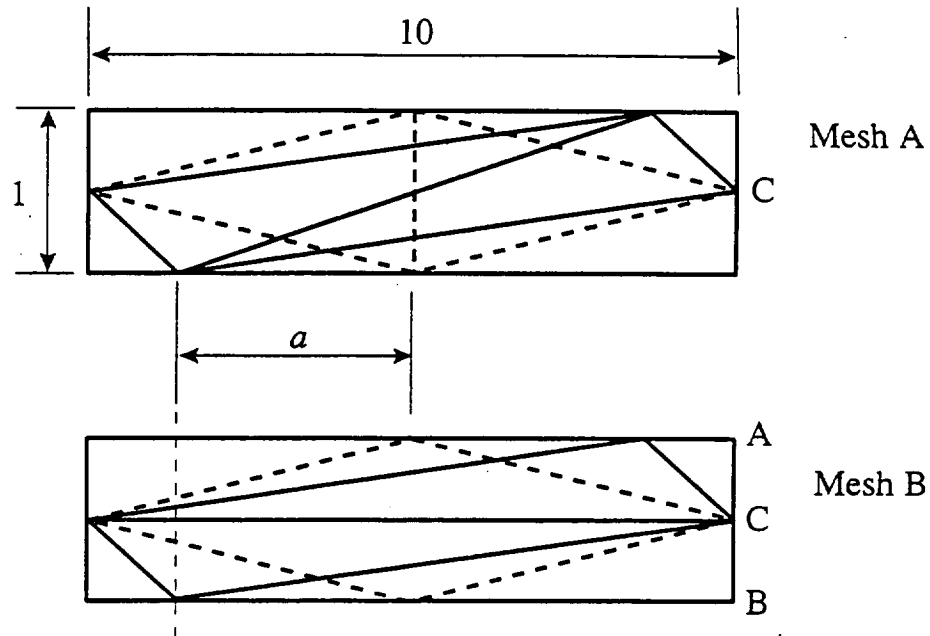
Figure 5. Distorted meshes for cantilever beam and twisted ribbon.

Table 5. Distortion Analysis of Cantilever Beam: Percent
Error at Node C with Respect to Undistorted Mesh

Mesh	Element type	Distortion parameter			w_C/w_{Cex} (no distortion)
		1.00	3.00	4.90	
A	ALR	−10.70	−19.80	8.40	1.031
A	AQR	0.15	0.10	−2.05	0.995
A	DKT	0.20	−0.59	3.41	0.982
A	FF	−7.75	−17.30	−18.35	0.974
B	ALR	0.20	3.00	45.90	0.764
B	AQR	−0.10	0.40	−2.85	0.995
B	DKT	−0.13	−1.09	−3.49	0.979
B	FF	−0.05	−0.15	2.20	0.769

241

Table 6. Distortion Analysis of Twisted Ribbon:
Loss of Symmetry under Distortion (Mesh B)

Element type	Node	Distortion parameter		
		1.00	3.00	4.90
ALR	A	1.016	1.122	1.363
	B	1.013	1.098	1.076
AQR	A	0.989	0.966	0.945
	B	1.010	1.029	0.995
DKT	A	0.993	0.978	0.940
	B	1.006	1.015	1.018
FF	A	0.983	0.933	0.789
	B	0.994	0.877	0.877

Mesh A   Mesh B
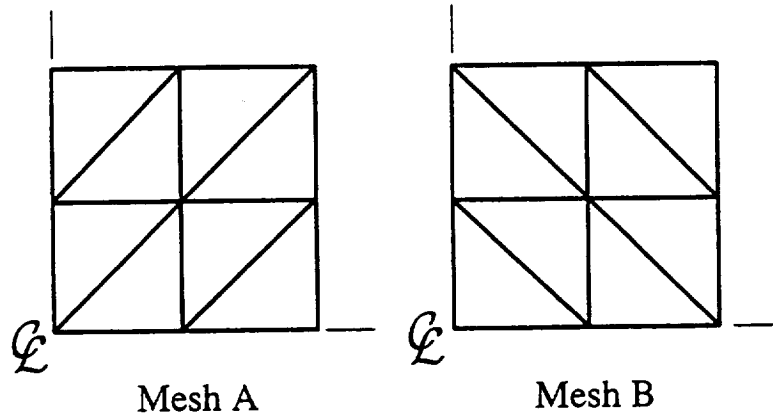
Figure 6.   Meshes for square plate convergence studies.
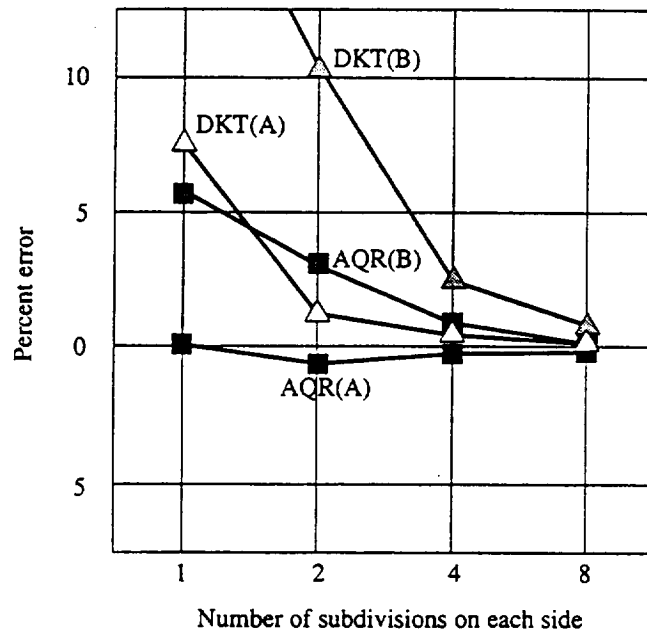
Figure 7. Central deflection of centrally loaded SS square plate.
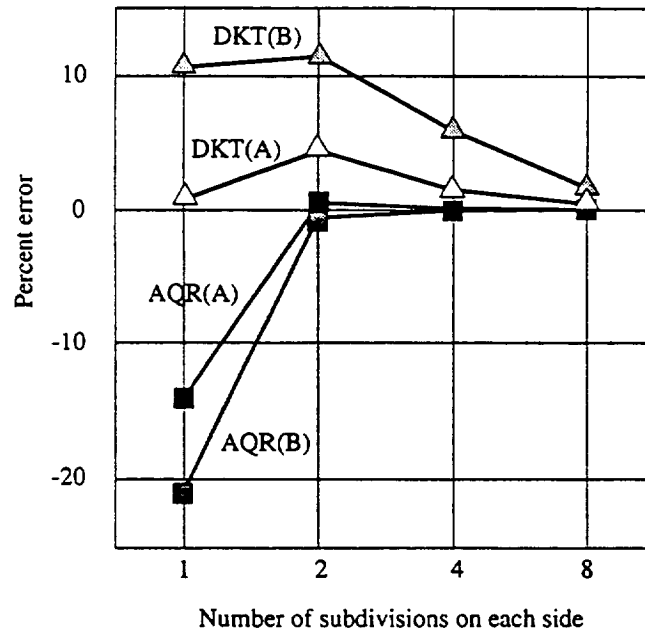
Figure 8. Central deflection of centrally loaded clamped square plate.
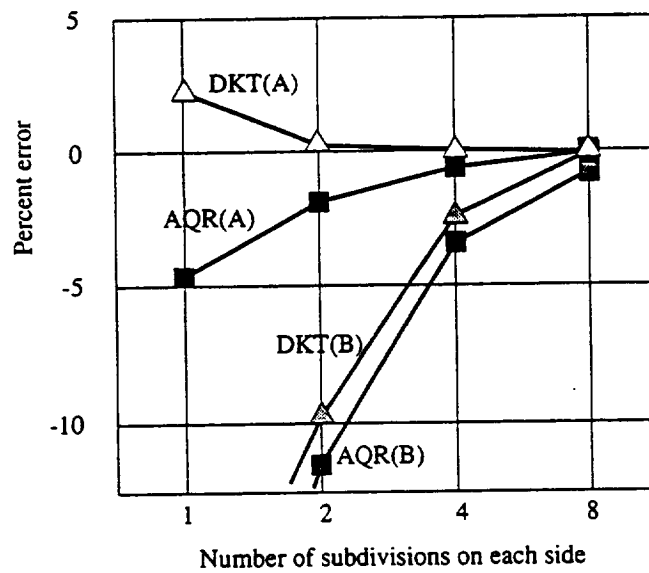
Figure 9. Central deflection of uniformly loaded SS square plate with TL force lumping.
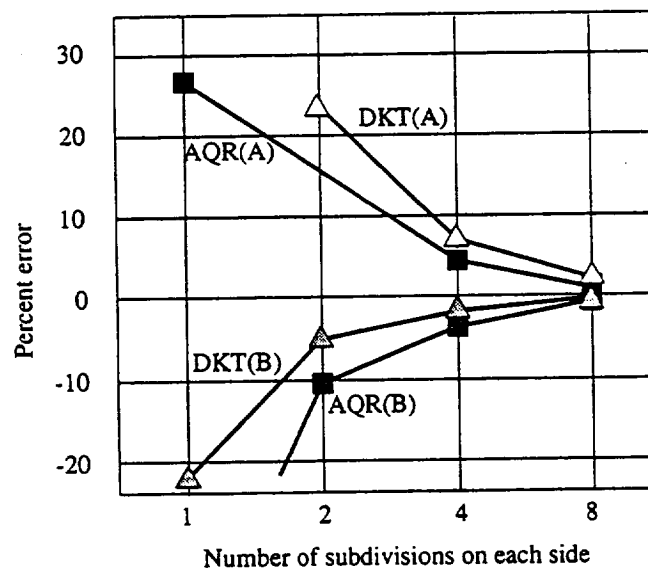
Figure 10. Central deflection of uniformly loaded clamped square plate with TL force lumping.

244

Table 7. Uniformly Loaded Square Plate with CL Force Lumping:
Percent Error of Central Deflection

Support	Element type	Mesh type	Mesh over quarter plate			
			1×1	2×2	4×4	8×8
SS	DKT	A	31.73	4.49	1.01	0.24
		B	4.55	5.37	1.56	0.41
	AQR	A	16.28	2.20	0.47	0.11
		B	−1.55	2.30	0.74	0.20
Clamped	DKT	A	46.35	14.90	4.10	1.03
		B	−21.60	2.08	1.30	0.36
	AQR	A	26.65	8.26	1.87	0.44
		B	−41.20	−3.22	−0.28	−0.05
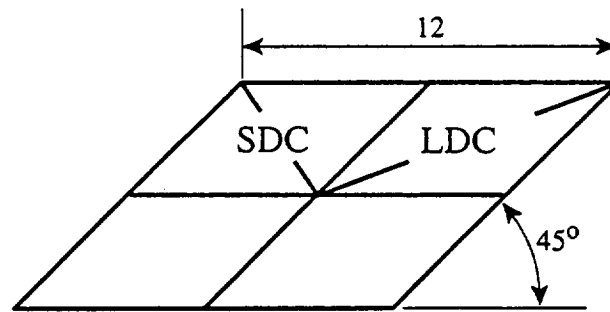
Figure 11. Rhombic cantilever: meshes for convergence studies

245

Table 8. Rhombic Cantilever: Percent Difference
of Tip-A Deflection with Respect to Experimental Value Reported in [28]

Mesh type	Element type	Subdivision of whole plate		
		4 × 4	8 × 8	16 × 16
LDC	DKT	2.3	−3.7	−4.0
	AQR	−17.8	−10.4	−6.0
SDC	DKT	−6.7	−5.0	−4.0
	AQR	−6.3	−5.0	−4.0

7.2 Rhombic Cantilever

The test involves a rhombic cantilevered plate subjected to uniform load. This problem was used in [28] to test the DKT element with reference given to an experimental deflection result; however, no convergence analysis was performed. This has been done here taking into account the two possible mesh subdivision patterns, SDC and LDC, depicted in Figure 11. Triangular force lumping has been used.

The results are shown in Table 8. For the LDC mesh DKT converges from above to an answer 4% below the experimental value quoted in [28]. On the other hand, AQR converges from below. For the SDC mesh both elements behave identically and converge to a value 4% under the experimental one.

It is clear from these results that the experimental tip deflection given in [28] is in error by about +4% with respect to the analytical value for the material properties quoted. The apparently small error for the 2 × 2 DKT/LDC mesh is thus fortuitous.

Table 9. Uniformly Loaded SS Rhombic Plate with TL Force
Lumping: Percent Error in Center Deflection

Mesh type	Element type	Subdivision of whole plate		
		4 × 4	8 × 8	16 × 16
SDC	DKT	11.05	4.07	2.86
	AQR	13.86	4.56	2.89
LDC	DKT	80.97	22.64	7.51
	AQR	6.85	−0.36	−2.91

7.3 Simply Supported Rhombic Plate

This problem poses severe difficulties for ordinary finite element methods because of the presence of a singularity in the bending moments at the obtuse corner. A detailed description of this problem may be seen for example in [33]. The acute angle $\alpha = 30°$ was selected for the test. Again both SDC and LDC meshes were tried.

The results are shown in Table 9. For the SDC meshes AQR and DKT show slight difference and almost the same rate of convergence. For the LDC meshes DKT is too flexible whereas AQR converges faster.

8. CONCLUSIONS

The main conclusions of the present study can be summarized as follows.

1. The ANDES formulation represents a variant of the ANS formulation that merits serious study. The key advantages of ANDES over ANS are:

    (a) *a priori* satisfaction of the patch test. Although this advantage is less clear for elements where ANS and ANDES coalesce for constant thickness and material properties, it reappears for more general cases.

    (b) The separation of the higher order stiffness allows the application of a scaling parameter. Furthermore it opens the possibility for an energy-balanced combination with other formulations as per Eq. (2), although this possibility presently remains unexplored.

2. The study of plate bending elements shows that the widely used DKT element is both an ANS and ANDES element. This discovery provides a variational foundation hereto lacking and analytically proves (because of the ANDES connection) that DKT passes the patch test.

3. The numerical results clearly demonstrate that the choice of basic stiffness is of paramount importance in the behavior of elements based on the ANDES formulation. Of the two elements sharing the quadratic-rotation basic stiffness, namely AQR and DKT, the former has excelled in geometric distortion tests and in convergence studies that involve concentrated forces. For other cases the performance of AQR and DKT is similar, and generally superior to those elements that use the linear-rotation basic stiffness.

The numerical experiments have not addressed questions of *material sensitivity* such as element performance for highly anisotropic and composite plates. This behavior, as well as the possibility of applying this technology to C^0 bending elements, is currently under investigation.

References

1. D. S. Malkus and T. J. R. Hughes, Mixed finite element methods — reduced and selective integration techniques: a unification of concepts, *Computer Methods in Applied Mechanics and Engineering*, 15, 1978, pp. 68–81

2. P. G. Bergan and L. Hanssen, A new approach for deriving 'good' finite elements, MAFELAP II Conference, Brunel University, 1975, in *The Mathematics of Finite Elements and Applications - Volume II*, ed. by J. R. Whiteman, Academic Press, London, 1976

3. P. G. Bergan, Finite elements based on energy orthogonal functions, *Int. J. Num. Meth. Engrg.*, 15, 1980, pp. 1141–1555

4. P. G. Bergan and M. K. Nygård, Finite elements with increased freedom in choosing shape functions, *Int. J. Num. Meth. Engrg.*, 20, 1984, pp. 643–664

5. P. G. Bergan and C. A. Felippa, A triangular membrane element with rotational degrees of freedom, *Computer Methods in Applied Mechanics & Engineering*, 50, 1985, pp. 25–69

6. C. A. Felippa, Parametrized multifield variational principles in elasticity: I. Mixed functionals, *Communications in Applied Numerical Methods*, 5, 1989, pp. 69–78

7. C. A. Felippa, Parametrized multifield variational principles in elasticity: II. Hybrid functionals and the free formulation, *Communications in Applied Numerical Methods*, 5, 1989, pp. 79–88

8. C. A. Felippa, The extended free formulation of finite elements in linear elasticity, *Journal of Applied Mechanics*, 56, 3, 1989, pp. 609–616

9. C. Militello and C. A. Felippa, A variational justification of the assumed natural strain formulation of finite elements: I. Variational principles, *Computers and Structures*, 34, 1990, pp. 431–438

10. C. Militello and C. A. Felippa, A variational justification of the assumed natural strain formulation of finite elements: II. The four node C^0 plate element, *Computers and Structures*, 34, 1990, pp. 439–444

11. C. A. Felippa and C. Militello, Variational formulation of high performance finite elements: parametrized variational principles, *Computers & Structures*, 36, 1990, pp. 1–11

12. C. A. Felippa and C. Militello, Developments in variational methods for high performance plate and shell elements, in *Analytical and Computational Models for Shells*, CED Vol. 3, Eds. A. K. Noor, T. Belytschko and J. C. Simo, The American Society of Mechanical Engineers, ASME, New York, 1989, pp. 191–216

13. K. J. Willam, Finite element analysis of cellular structures, Ph. D. Dissertation, Dept. of Civil Engineering, University of California, Berkeley CA, 1969

14. D. G. Ashwell, Strain elements, with applications to arches, rings and cylindrical shells, in *Finite Elements for Thin Shells and Curved Members*, ed. by D. G. Ashwell and R. H. Gallagher, Wiley-Interscience, London, 1976

15. M. J. Turner, R. W. Clough, H. C. Martin, and L. J. Topp, Stiffness and deflection analysis of complex structures, *Journal of Aeronautical Sciences*, 23, 1956, pp. 805–824

16. K. J. Bathe and E. N. Dvorkin, A four-node plate bending element based on Mindlin/Reissner plate theory and a mixed interpolation, *Int. J. Numer. Meth. Engrg.*, 21, 1985, pp. 367–383

17. M. A. Crisfield, A four-noded thin plate element using shear constraints — a modified version of Lyons' element, *Computer Methods in Applied Mechanics & Engineering*, 38, 1983, pp. 93–120

18. H. C. Huang and E. Hinton, A new nine node degenerated shell element with enhanced membrane and shear interpolation, *Int. J. Numer. Meth. Engrg.*, 22, 1986, pp. 73–92

19. J. Jang and P. M. Pinsky, An assumed covariant strain based 9-node shell element, *Int. J. Numer. Meth. Engrg.*, 24, 1987, pp. 2389–2411

20. R. H. MacNeal, Derivation of element stiffness matrices by assumed strain distribution, *Nuclear Engrgr. Design*, 70, 1978, pp. 3–12

21. K. C. Park and G. M. Stanley, A curved C^0 shell element based on assumed natural-coordinate strains, *Journal of Applied Mechanics*, 53, 1986, pp. 278–290

22. K. C. Park, An improved strain interpolation for curved C^0 elements, *Int. J. Numer. Meth. Engrg.*, 22, 1986, pp. 281–288

23. J. C. Simo and T. J. R. Hughes, On the variational foundations of assumed strain methods, *Journal of Applied Mechanics*, 53, 1986, pp. 51–54

24. J. H. Argyris, Recent advances in matrix methods of structural analysis, *Progress in Aeronautical Sciences*, 4, Pergamon Press, Oxford, 1964

25. J. H. Argyris, Three-dimensional anisotropic and inhomogeneous elastic media, Matrix analysis for small and large displacements, *Ingenieur Archiv*, 34, 1965, pp. 33–65

26. J. H. Argyris, Continua and discontinua, Opening Address, in *Proceedings 1st Conference on Matrix Methods in Structural Mechanics*, AFFDL-TR-66-80, Air Force Institute of Technology, Dayton, Ohio, 1966, pp. 11–189

27. J. H. Argyris, M. Haase, and G. A. Malejannis, Natural geometry of surfaces with specific references to the matrix displacement analysis of shells, *Proc. Kon. Neder. Akad. Wet. Ser. B*, 5, 76, 1973

28. J. L. Batoz, K. J. Bathe and L. W. Ho, A study of three-node triangular plate bending elements, *Int. J. Numer. Meth. Engng*, 15, 1980, pp. 1771–1812

29. J. L. Batoz, An explicit formulation for an efficient triangular plate-bending element, *Int. J. Numer. Meths. Engrg.*, 18, pp. 1077–1089, 1982

30. T. J. R. Hughes and T.E. Tezduyar, Finite elements based upon Mindlin plate theory with particular reference to the four-node bilinear isoparametric element, *Journal of Applied Mechanics*, 48, 1981, pp. 587–596

31. D. S. S. Kang, Hybrid stress finite element method, Ph. D. Dissertation, Dept. of Aeronautics and Astronautics, Massachusetts Institute of Technology, 1986

32. P. G. Bergan and C. A. Felippa, Efficient implementation of a triangular membrane element with drilling freedoms, Finite Element Handbook series, ed. by T. J. R. Hughes and E. Hinton, Pineridge Press, 1986, pp. 139–152

33. C. A. Felippa and P. G. Bergan, A triangular plate bending element based on an energy-orthogonal free formulation, *Computer Methods in Applied Mechanics & Engineering*, 61, 1987, pp. 129–160

34. T. J. R. Hughes, *The Finite Element Method: Linear Static and Dynamic Finite Element Analysis*, Prentice-Hall, Englewood Cliffs, N. J., 1987

35. G. P. Bazeley, Y. K. Cheung, B. M. Irons and O. C. Zienkiewicz, Triangular elements in plate bending: conforming and non-conforming solutions, in *Proceedings 1st Conference on Matrix Methods in Structural Mechanics*, AFFDL-TR-66-80, Air Force Institute of Technology, Dayton, Ohio, 1966, pp. 547–576

36. C. A. Felippa, Refined finite element analysis of linear and nonlinear two-dimensional structures, Ph. D. Dissertation, Department of Civil Engineering, University of California at Berkeley, Berkeley, CA, 1966

Appendix A. SANITIZING INCOMPATIBLE ELEMENTS

The stiffness-splitting technique summarized in Box 1 provides a systematic way for "sanitizing" existing nonconforming bending elements that do not pass the patch test. The technique amounts to the replacement of the basic stiffness. The main steps will be briefly outlined for the simplest such element: the BCIZ triangle proposed in 1965 by Bazeley et al [35]. The assumed transverse displacement is given explicitly in [36] as

$$
w = \left\{
\begin{array}{c}
\zeta_1^2(3 - 2\zeta_1) + 2\zeta_1\zeta_2\zeta_3 \\
\zeta_1^2(y_{12}\zeta_2 - y_{31}\zeta_3) + \tilde{y}_1\zeta_1\zeta_2\zeta_3 \\
\zeta_1^2(x_{21}\zeta_2 - x_{13}\zeta_3) + \tilde{x}_1\zeta_1\zeta_2\zeta_3 \\
\zeta_2^2(3 - 2\zeta_2) + 2\zeta_1\zeta_2\zeta_3 \\
\zeta_2^2(y_{23}\zeta_3 - y_{12}\zeta_1) + \tilde{y}_2\zeta_1\zeta_2\zeta_3 \\
\zeta_2^2(x_{32}\zeta_3 - x_{21}\zeta_1) + \tilde{x}_2\zeta_1\zeta_2\zeta_3 \\
\zeta_3^2(3 - 2\zeta_3) + 2\zeta_1\zeta_2\zeta_3 \\
\zeta_3^2(y_{31}\zeta_1 - y_{23}\zeta_2) + \tilde{y}_3\zeta_1\zeta_2\zeta_3 \\
\zeta_3^2(x_{13}\zeta_1 - x_{32}\zeta_2) + \tilde{x}_3\zeta_1\zeta_2\zeta_3
\end{array}
\right\}^T \mathbf{v}
\tag{61}
$$

where $\tilde{y}_1 = y_{12} - y_{31}$, $\tilde{y}_2 = y_{23} - y_{12}$, $\tilde{y}_3 = y_{31} - y_{23}$, $\tilde{x}_1 = x_{21} - x_{13}$, $\tilde{x}_2 = x_{32} - x_{21}$, $\tilde{x}_3 = x_{13} - x_{32}$. The strain-displacement matrix $\mathbf{B}$ is obtained by double differentiation with respect to the triangular coordinates and application of (30):

$$
\kappa = \left\{
\begin{array}{c}
\kappa_{xx} \\
\kappa_{yy} \\
2\kappa_{xy}
\end{array}
\right\} = \mathbf{WRv} = \mathbf{Bv} = (\mathbf{B}_0 + \mathbf{B}_1\zeta_1 + \mathbf{B}_2\zeta_2 + \mathbf{B}_3\zeta_3)\mathbf{v},
\tag{62}
$$

in which $\mathbf{W}$ is given by (29), and

$$
\mathbf{R}^T = 2
\begin{bmatrix}
3(1 - \zeta_1) & 0 & 0 & \zeta_3 & \zeta_1 & \zeta_2 \\
y_{12}\zeta_2 - y_{31}\zeta_3 & 0 & 0 & y_{12}\zeta_1 + \frac{1}{2}\tilde{y}_1\zeta_3 & \frac{1}{2}\tilde{y}_1\zeta_1 & -y_{31}\zeta_1 + \frac{1}{2}\tilde{y}_1\zeta_2 \\
x_{12}\zeta_2 - x_{31}\zeta_3 & 0 & 0 & x_{21}\zeta_1 + \frac{1}{2}\tilde{x}_1\zeta_3 & \frac{1}{2}\tilde{x}_1\zeta_1 & -x_{13}\zeta_1 + \frac{1}{2}\tilde{x}_1\zeta_2 \\
0 & 3(1 - \zeta_2) & 0 & \zeta_3 & \zeta_1 & \zeta_2 \\
0 & y_{23}\zeta_3 - y_{12}\zeta_1 & 0 & -y_{12}\zeta_2 + \frac{1}{2}\tilde{y}_2\zeta_3 & y_{23}\zeta_2 + \frac{1}{2}\tilde{y}_2\zeta_1 & \frac{1}{2}\tilde{y}_2\zeta_2 \\
0 & x_{32}\zeta_3 - x_{21}\zeta_1 & 0 & -x_{21}\zeta_2 + \frac{1}{2}\tilde{x}_2\zeta_3 & x_{32}\zeta_2 + \frac{1}{2}\tilde{x}_2\zeta_1 & \frac{1}{2}\tilde{x}_2\zeta_2 \\
0 & 0 & 3(1 - \zeta_3) & \zeta_3 & \zeta_1 & \zeta_2 \\
0 & 0 & y_{31}\zeta_1 - y_{23}\zeta_2 & \frac{1}{2}\tilde{y}_3\zeta_3 & -y_{23}\zeta_3 + \frac{1}{2}\tilde{y}_3\zeta_2 & y_{31}\zeta_3 + \frac{1}{2}\tilde{y}_3\zeta_1 \\
0 & 0 & x_{13}\zeta_1 - x_{32}\zeta_2 & \frac{1}{2}\tilde{x}_3\zeta_3 & -x_{32}\zeta_3 + \frac{1}{2}\tilde{x}_3\zeta_2 & x_{13}\zeta_3 + \frac{1}{2}\tilde{x}_3\zeta_1
\end{bmatrix}
\tag{63}
$$

Split the strain-displacement equations as

$$
\kappa = \bar{\kappa} + \kappa_d = (\bar{\mathbf{B}} + \mathbf{B}_d)\mathbf{v},
\tag{64}
$$

where $\bar{\mathbf{B}} = \mathbf{B}_0 + \frac{1}{3}(\mathbf{B}_1 + \mathbf{B}_2 + \mathbf{B}_3)$, $\mathbf{B}_d = \mathbf{B} - \bar{\mathbf{B}}$. Then the "sanitized" stiffness matrix is

$$
\mathbf{K} = \mathbf{K}_b + \alpha \int_A \mathbf{B}_d^T \mathbf{D}_b \mathbf{B}_d \, dA,
\tag{65}
$$

where $\mathbf{K}_b$ is one of the basic stiffness matrices derived in Section 4.1. The free formulation leads to the same result but in a less direct manner, because w would have to be decomposed into rigid body, constant curvature and higher order states. Although the corrected element passes the patch test it is unlikely to be competitive with ANDES elements in distortion insensitivity as this property appears to depend on relaxing curvature compatibility conditions.

Appendix B. EXPLICIT REPRESENTATION OF HIGHER ORDER STIFFNESS

To obtain an explicit representation of K_{hp}, begin by defining

$$C = T^T D T = \begin{bmatrix} C_{11} & C_{12} & C_{13} \\ & C_{22} & C_{23} \\ symm & & C_{23} \end{bmatrix}, \tag{66}$$

which can be interpreted as a constitutive matrix that relates the natural moments $T^T m$ to the natural curvatures χ. Then

$$K_{dp} = \int_A A_d^T C A_d \, dA = \frac{A}{36} \begin{bmatrix} r_{11} & -r_{11} & r_{12} & -r_{12} & r_{13} & -r_{13} \\ & r_{11} & -r_{12} & r_{12} & -r_{13} & r_{13} \\ & & r_{22} & -r_{22} & r_{23} & -r_{23} \\ & & & r_{22} & -r_{23} & r_{23} \\ & & & & r_{33} & -r_{33} \\ symm & & & & & r_{33} \end{bmatrix} \tag{67}$$

where $r_{ij} = \beta_{ij} C_{ij}$ for $i = 1, 2, 3$, $j = 1, 2, 3$, and

$$\beta_{11} = 2(\lambda_{12}^2 - \lambda_{12} + 1), \quad \beta_{22} = 2(\lambda_{23}^2 - \lambda_{23} + 1), \quad \beta_{33} = 2(\lambda_{31}^2 - \lambda_{31} + 1),$$

$$\beta_{12} = (2 - \lambda_{12})\lambda_{23} - \lambda_{12} - 1, \quad \beta_{23} = (2 - \lambda_{23})\lambda_{31} - \lambda_{23} - 1, \quad \beta_{13} = (2 - \lambda_{31})\lambda_{12} - \lambda_{31} - 1. \tag{68}$$

Carrying out the congruential transformation $K_{hp} = Q^T K_{dp} Q$ with MACSYMA yields

$K_{11} = 4(r_{33} - r_{13} - r_{13} + r_{11})$,

$K_{12} = 2((r_{11} - r_{13})y_{21} + (r_{13} - r_{33})y_{13})$

$K_{13} = 2((r_{13} - r_{11})x_{21} + (r_{33} - r_{13})x_{13})$,

$K_{14} = 4(-r_{23} + r_{13} + r_{12} - r_{11})$

$K_{15} = 2((r_{12} - r_{23})y_{32} + (r_{11} - r_{13})y_{21})$,

$K_{16} = 2((r_{23} - r_{12})x_{32} + (r_{13} - r_{11})x_{21})$

$K_{17} = 4(-r_{33} + r_{23} + r_{13} - r_{12})$,

$K_{18} = 2((r_{12} - r_{23})y_{32} + (r_{13} - r_{33})y_{13})$

$K_{19} = 2((r_{23} - r_{12})x_{32} + (r_{33} - r_{13})x_{13})$,

$K_{22} = r_{11}y_{21}^2 + 2r_{13}y_{13}y_{21} + r_{33}y_{13}^2$

$K_{23} = (-r_{11}x_{21} - r_{13}x_{13})y_{21} + (-r_{13}x_{21} - r_{33}x_{13})y_{13}$,

$K_{24} = 2((r_{12} - r_{11})y_{21} + (r_{23} - r_{13})y_{13})$

$K_{25} = (r_{12}y_{21} + r_{23}y_{13})y_{32} + r_{11}y_{21}^2 + r_{13}y_{13}y_{21}$,

$K_{26} = (-r_{12}x_{32} - r_{11}x_{21})y_{21} + (-r_{23}x_{32} - r_{13}x_{21})y_{13}$

$K_{27} = 2((r_{13} - r_{12})y_{21} + (r_{33} - r_{23})y_{13})$,

$K_{28} = (r_{12}y_{21} + r_{23}y_{13})y_{32} + r_{13}y_{13}y_{21} + r_{33}y_{13}^2$

$K_{29} = (-r_{12}x_{32} - r_{13}x_{13})y_{21} + (-r_{23}x_{32} - r_{33}x_{13})y_{13}$,

$K_{33} = r_{11}x_{21}^2 + 2r_{13}x_{13}x_{21} + r_{33}x_{13}^2$

$K_{34} = 2((r_{11} - r_{12})x_{21} + (r_{13} - r_{23})x_{13})$,

$K_{35} = (-r_{12}x_{21} - r_{23}x_{13})y_{32} + (-r_{11}x_{21} - r_{13}x_{13})y_{21}$

$K_{36} = (r_{12}x_{21} + r_{23}x_{13})x_{32} + r_{11}x_{21}^2 + r_{13}x_{13}x_{21}$,

$K_{37} = 2((r_{12} - r_{13})x_{21} + (r_{23} - r_{33})x_{13})$

$K_{38} = (-r_{12}x_{21} - r_{23}x_{13})y_{32} + (-r_{13}x_{21} - r_{33}x_{13})y_{13}$,

$K_{39} = (r_{12}x_{21} + r_{23}x_{13})x_{32} + r_{13}x_{13}x_{21} + r_{33}x_{13}^2$

$K_{44} = 4(r_{22} - r_{12} - r_{12} + r_{11})$,

$K_{45} = 2((r_{22} - r_{12})y_{32} + (r_{12} - r_{11})y_{21})$

$K_{46} = 2((r_{12} - r_{22})x_{32} + (r_{11} - r_{12})x_{21})$,

$K_{47} = 4(r_{23} - r_{22} - r_{13} + r_{12})$

$K_{48} = 2((r_{22} - r_{12})y_{32} + (r_{23} - r_{13})y_{13})$,

$K_{49} = 2((r_{12} - r_{22})x_{32} + (r_{13} - r_{23})x_{13})$

$K_{55} = r_{22}y_{32}^2 + 2r_{12}y_{21}y_{32} + r_{11}y_{21}^2$,

$K_{56} = (-r_{22}x_{32} - r_{12}x_{21})y_{32} + (-r_{12}x_{32} - r_{11}x_{21})y_{21}$

$K_{57} = 2((r_{23} - r_{22})y_{32} + (r_{13} - r_{12})y_{21})$,

$K_{58} = r_{22}y_{32}^2 + (r_{12}y_{21} + r_{23}y_{13})y_{32} + r_{13}y_{13}y_{21}$

$K_{59} = (-r_{22}x_{32} - r_{23}x_{13})y_{32} + (-r_{12}x_{32} - r_{13}x_{13})y_{21}$,

$K_{66} = r_{22}x_{32}^2 + 2r_{12}x_{21}x_{32} + r_{11}x_{21}^2$

$K_{67} = 2((r_{22} - r_{23})x_{32} + (r_{12} - r_{13})x_{21})$,

$K_{68} = (-r_{22}x_{32} - r_{12}x_{21})y_{32} + (-r_{23}x_{32} - r_{13}x_{21})y_{13}$

$K_{69} = r_{22}x_{32}^2 + (r_{12}x_{21} + r_{23}x_{13})x_{32} + r_{13}x_{13}x_{21}$,

$K_{77} = 4(r_{33} - r_{23} - r_{23} + r_{22})$

$K_{78} = 2((r_{23} - r_{22})y_{32} + (r_{33} - r_{23})y_{13})$,

$K_{79} = 2((r_{22} - r_{23})x_{32} + (r_{23} - r_{33})x_{13})$

$K_{88} = r_{22}y_{32}^2 + 2r_{23}y_{13}y_{32} + r_{33}y_{13}^2$,

$K_{89} = (-r_{22}x_{32} - r_{23}x_{13})y_{32} + (-r_{23}x_{32} - r_{33}x_{13})y_{13}$

$K_{99} = r_{22}x_{32}^2 + 2r_{23}x_{13}x_{32} + r_{33}x_{13}^2$.

The same stiffness expression applies for K_{ha}, if one sets $\lambda_{12} = \lambda_{23} = \lambda_{31} = \frac{1}{2}$.

251

PARAMETRIZED VARIATIONAL PRINCIPLES ENCOMPASSING COMPRESSIBLE AND INCOMPRESSIBLE ELASTICITY

SUMMARY

Abstract — A parametrized five-field variational principle that can accomodate both compressible and incompressible hyperelasticity is presented. The primary variables are mean and deviatoric stresses, mean and deviatoric strains, and displacements. Through appropriate selection of parameters the functional of this general principle specializes to those previously presented by Atluri-Reissner, Herrmann, and Franca.

1. GOVERNING EQUATIONS

Consider a *linearly hyperelastic body* under static loading that occupies the volume V. The body is bounded by the surface S, which is decomposed into $S : S_d \cup S_t$. Displacements are prescribed on S_d while surface tractions are prescribed on S_t. The outward unit normal on S is denoted by $\mathbf{n} \equiv n_i$.

The three unknown volume fields are displacements $\mathbf{u} \equiv u_i$, infinitesimal strains $\mathbf{e} \equiv e_{ij}$, and stresses $\sigma \equiv \sigma_{ij}$. The problem data include: the body force field $\mathbf{b} \equiv b_i$ in V, prescribed displacements $\hat{\mathbf{d}} \equiv \hat{d}_i$ on S_d, and prescribed surface tractions $\hat{\mathbf{t}} \equiv \hat{t}_i$ on S_t.

The relations between the volume fields are the strain-displacement equations

$$\mathbf{e} = \tfrac{1}{2}(\nabla \mathbf{u} + \nabla^T \mathbf{u}) = \mathbf{D}\mathbf{u} \qquad \text{or} \qquad e_{ij} = \tfrac{1}{2}(u_{i,j} + u_{j,i}) \quad \text{in } V, \tag{1}$$

the constitutive equations

$$\sigma = \mathbf{E}\mathbf{e} \qquad \text{or} \qquad \sigma_{ij} = E_{ijkl}e_{kl} \quad \text{in } V, \tag{2}$$

and the equilibrium (balance) equations

$$-\operatorname{div}\sigma = \mathbf{D}^*\sigma = \mathbf{b} \qquad \text{or} \qquad \sigma_{ij,j} + b_i = 0 \quad \text{in } V, \tag{3}$$

in which $\mathbf{D}^* = -\operatorname{div}$ denotes the adjoint operator of the symmetric gradient $\mathbf{D} = \tfrac{1}{2}(\nabla + \nabla^T)$.

The stress vector with respect to a direction defined by the unit vector $\mathbf{v}$ is denoted as $\sigma_v = \sigma.\mathbf{v}$, or $\sigma_{vi} = \sigma_{ij}v_j$. On S the surface-traction stress vector is defined as $\sigma_n = \sigma.\mathbf{n}$ or $\sigma_{ni} = \sigma_{ij}n_j$. With this notation the traction and displacement boundary conditions may be stated as

$$\sigma_n = \hat{\mathbf{t}} \quad \text{or} \quad \sigma_{ij}n_j = \hat{t}_i \quad \text{on } S_t, \qquad \text{and} \qquad \mathbf{u} = \hat{\mathbf{d}} \quad \text{or} \quad u_i = \hat{d}_i \quad \text{on } S_d. \tag{4}$$

252

2. NOTATION

Field Dependency

In the following investigation of variational methods, the notational conventions used in References [1–5] are followed. An *independently varied* field will be identified by a superposed tilde, for example $\tilde{u}$. A dependent field is identified by writing the independent field symbol as superscript. For example, if the displacements are independently varied, the derived strain and stress fields are

$$e^{\tilde{u}} = \tfrac{1}{2}(\nabla + \nabla^T)\tilde{u} = D\tilde{u}, \qquad \sigma^{\tilde{u}} = Ee^{\tilde{u}} = ED\tilde{u}. \tag{5}$$

Using this convention, tildeless symbols such as u, e and σ are reserved for the *exact* or for *generic* fields.

Integral Abbreviations

Volume and surface integrals may be abbreviated by placing domain-subscripted parentheses and square brackets, respectively, around the integrand. For example:

$$(f)_V \stackrel{\text{def}}{=} \int_V f\, dV, \qquad [f]_S \stackrel{\text{def}}{=} \int_S f\, dS, \qquad [f]_{S_d} \stackrel{\text{def}}{=} \int_{S_d} f\, dS, \qquad [f]_{S_t} \stackrel{\text{def}}{=} \int_{S_t} f\, dS. \tag{6}$$

If f and g are vector functions, and p and q tensor functions, their inner product over V is denoted in the usual manner

$$(f, g)_V \stackrel{\text{def}}{=} \int_V f_i g_i\, dV, \qquad (p, q)_V \stackrel{\text{def}}{=} \int_V p_{ij} q_{ij}\, dV, \tag{7}$$

and similarly for surface integrals, in which case square brackets are used.

Stress and Strain Vectors

To facilitate the construction of variational matrix expressions, stresses and strains will be arranged as 6-component column vectors constructed from the tensors σ_{ij} and e_{ij} following the usual conventions of structural mechanics:

$$\sigma = \begin{Bmatrix} \sigma_{11} \\ \sigma_{22} \\ \sigma_{33} \\ \sigma_{12} \\ \sigma_{23} \\ \sigma_{31} \end{Bmatrix}, \qquad e = \begin{Bmatrix} e_{11} \\ e_{22} \\ e_{33} \\ 2e_{12} \\ 2e_{23} \\ 2e_{31} \end{Bmatrix}. \tag{8}$$

Then $(\sigma, e)_V = (\sigma_{ij} e_{ij})_V = (\sigma^T e)_V$, and so on. Similarly, fourth order constitutive tensors such as $E_{ijk\ell}$ are arranged as symmetric 6×6 matrices (resulting from their restriction to the space of symmetric stress-strain tensors) in the usual manner.

3. STRESS-STRAIN SPLITTINGS

For incompressible materials, in which $\text{div}\, u = \text{tr}\, \nabla u = u_{i,i} = 0$, the stress-strain relation (2) only holds in the space of traceless strain tensors, and its inverse does not exist. With a view to including both compressible and incompressible elasticity in the variational principles, some general splittings of the strain and stress

fields are studied below. Define (actual) pressure p and total strain condensation (negative of the volumetric strain) θ as

$$p = -\tfrac{1}{3} \operatorname{tr} \sigma = -\tfrac{1}{3}(\sigma_{11} + \sigma_{22} + \sigma_{33})$$
$$\theta = -\operatorname{tr} e = -(e_{11} + e_{22} + e_{33}) = -\operatorname{div} u. \tag{9}$$

Throughout this paper it shall be assumed that the material is *volumetrically isotropic* in the sense

$$p = k\theta, \tag{10}$$

where $k > 0$ is the modulus of compression (one third of the bulk modulus K). In the incompressible limit, $k \to \infty$.

Parametrized Splitting

A family of stress-strain splittings considered here is

$$\sigma_{ij} = s(\xi)_{ij} - \xi p\, \delta_{ij}, \qquad e_{ij} = g(\eta)_{ij} - \tfrac{1}{3}\eta\theta\delta_{ij}, \tag{11}$$

where δ_{ij} is the Kronecker delta, and ξ and η are scalars in the range $[0, 1]$ that determine the splitting. If $\xi = 0$, $s(0)_{ij} \equiv \sigma_{ij}$, whereas if $\xi = 1$, $s(1)_{ij}$ reduce to the usual deviatoric stresses s_{ij} and the argument ξ will be omitted. If $\eta = 0$, $g(0)_{ij} \equiv e_{ij}$, whereas if $\eta = 1$, $g(1)_{ij}$ reduce to the usual deviatoric strains g_{ij} and the argument η will be omitted.

Using the matrix notation (8) for strains and stresses (11) is represented as

$$\sigma = s(\xi) - \xi p\mathbf{h}, \qquad e = g(\eta) - \eta\theta\mathbf{h}, \tag{12}$$

where $\mathbf{h}$ is the 6-component column vector

$$\mathbf{h} = \{1 \quad 1 \quad 1 \quad 0 \quad 0 \quad 0\}^T. \tag{13}$$

Note that $\mathbf{h}^T\mathbf{h} = 3$, $\mathbf{h}^T\sigma = \operatorname{tr}\sigma = -3p$, $\mathbf{h}^Te = \operatorname{tr}e = -\theta$, $\mathbf{h}^Ts(\xi) = \operatorname{tr}s(\xi) = -3(1 - \xi)p$, $\mathbf{h}^Tg(\eta) = \operatorname{tr}g(\eta) = -(1 - \eta)\theta$, and $\mathbf{h}^Ts = \mathbf{h}^Tg = 0$.

Constraints on ξ and η

Parameters ξ and η are not independent but chosen so that $s(\xi)$ and $g(\eta)$ are connected by an invertible "deviatoric" constitutive equation

$$s(\xi) = \mathbf{C}g(\eta), \qquad \text{or} \quad s(\xi)_{ij} = C_{ijk\ell}\, g(\eta)_{k\ell}, \tag{14}$$

where matrix $\mathbf{C}$ is finite and nonsingular. This condition is assumed to hold if $\xi = \eta = 1$ for any material. For other values of ξ and η the choice is possible if the material is fully isotropic because if so (2) may be written (see *e.g.* Section 22 of Gurtin [6])

$$\sigma_{ij} = 2\mu e_{ij} + \lambda e_{kk}, \qquad \text{or} \quad \sigma = 2\mu e - \lambda\,\theta\mathbf{h}, \tag{15}$$

where μ and λ are the Lamé coefficients (μ is the same as the shear modulus G), so that $\mathbf{C} = 2\mu\mathbf{I}$. Furthermore, μ, λ and k are related to the elastic modulus E and Poisson's ratio ν through

$$k = \frac{\lambda(1 + \nu)}{3\nu} = \frac{E}{3(1 - 2\nu)} = \tfrac{1}{3}(3\lambda + 2\mu), \qquad \mu = \frac{\lambda(1 - 2\nu)}{2\nu} = \tfrac{3}{2}(k - \lambda) = \frac{E}{2(1 + \nu)}. \tag{16}$$

254

Substituting these relations into (15) and (14) one obtains the condition

$$(1 + v)\xi - (1 - 2v)\eta = 3v. \tag{17}$$

The pair $\xi = \eta = 1$ satisfies this constraint for any v. If $v \neq 0.5$, specifying $0 \leq \xi < 1$ or η determines the other; for example if $\eta = 0, \xi = 3v/(1 + v)$. If the material is incompressible, *i.e.* $v = 0.5, \xi = 1$ regardless of the value of η.

Deviatoric Split

The usual deviatoric stress-strain splitting is obtained by taking $\xi = \eta = 1$:

$$\sigma = s - p\mathbf{h}, \qquad e = g - \tfrac{1}{3}\theta\mathbf{h}. \tag{18}$$

As noted above, this choice satisfies the condition (14) for isotropic or anisotropic materials.

Lamé Split

The Lamé splitting for isotropic materials — so called because of its intimate relationship with the constitutive form (15) that displays the two Lamé coefficients — is obtained if $\eta = 0$ so that $g = e$. Then ξ is chosen so that $\tau = s(\xi) = 2\mu e$:

$$\sigma = \mathbf{C}e - \xi p\mathbf{h} = 2\mu e - \frac{3v}{1 + v}p\mathbf{h} = \tau - q\mathbf{h}. \tag{19}$$

In the literature $q = \xi p$ is called the pseudo pressure whereas $\tau = s(\xi) = 2\mu e = \mathbf{C}e$ is called the extra stress, although a better name would be pseudo deviatoric stress. In the incompressible limit, pseudo pressure q and extra stress τ reduce to ordinary pressure p and deviatoric stress s, respectively.

Although the Lamé split may in principle be extended to anisotropic materials, parameter ξ then becomes a matrix: $\mathbf{I} - (3k)^{-1}\mathbf{C}$, which complicates derivations substantially. The same is true of (12) unless $\xi = \eta = 1$. It follows that splittings other than (18) are of limited value for non-isotropic behavior.

4. THE GENERALIZED STRAIN ENERGY

The variational principles of linear elasticity studied here have the general form

$$\Pi = U - P. \tag{20}$$

Here U is the generalized strain energy, which characterizes the stored energy of deformation, and P is the forcing potential, which characterizes all other contributions. The conventional form of P is

$$P^c = (\mathbf{b}, \mathbf{u})_V + [\mathbf{u} - \hat{\mathbf{d}}, \sigma_n]_{S_d} + [\hat{\mathbf{t}}, \mathbf{u}]_{S_t}. \tag{21}$$

Other two forms of P, which are of interest in hybrid finite element formulations, called P^d and P^t for displacement-generalized and traction-generalized, respectively, are studied in other papers [1–5]. As this term is not affected by material behavior attention will be focused on U.

For a *compressible* material, the generalized strain energy introduced in References [4,5] has the following parametrized structure:

$$U = \tfrac{1}{2}j_{11}(\bar{\sigma}, \mathbf{e}^\sigma)_V + j_{12}(\bar{\sigma}, \bar{\mathbf{e}})_V + j_{13}(\bar{\sigma}, \mathbf{e}^u)_V + \tfrac{1}{2}j_{22}(\sigma^\epsilon, \bar{\mathbf{e}})_V + j_{23}(\sigma^\epsilon, \mathbf{e}^u)_V + \tfrac{1}{2}j_{33}(\sigma^u, \mathbf{e}^u)_V, \tag{22}$$

255

where j_{11} through j_{33} are numerical coefficients. The three independent fields are stresses $\bar{\sigma}$, strains $\bar{e}$ and displacements $\bar{u}$. Following the notational conventions stated in Section 2, the derived fields that appear in (22) are

$$\sigma^e = E\bar{e}, \quad \sigma^u = ED\bar{u}, \quad e^\sigma = E^{-1}\bar{\sigma}, \quad e^u = D\bar{u}. \tag{23}$$

As an example, the U of Hu-Washizu's functional is obtained by setting $j_{12} = -1$, $j_{13} = 1$, $j_{22} = 1$, all others being zero:

$$U_H(\bar{\sigma}, \bar{e}, \bar{u}) = \tfrac{1}{2}(\sigma^e, \bar{e})_V + \tfrac{1}{2}(\bar{\sigma}, e^u - \bar{e})_V + \tfrac{1}{2}(\sigma^u - \sigma^e, e^\sigma)_V = \tfrac{1}{2}(\sigma^e, \bar{e})_V + (\bar{\sigma}, e^u - \bar{e})_V. \tag{24}$$

Equation (22) can be rewritten in matrix form as

$$U = \tfrac{1}{2}\int_V \begin{Bmatrix} \bar{\sigma} \\ \sigma^e \\ \sigma^u \end{Bmatrix}^T \begin{bmatrix} j_{11}I & j_{12}I & j_{13}I \\ & j_{22}I & j_{23}I \\ symm & & j_{33}I \end{bmatrix} \begin{Bmatrix} e^\sigma \\ \bar{e} \\ e^u \end{Bmatrix} dV. \tag{25}$$

where I denotes the 6×6 identity matrix. The functional-generating symmetric matrix (to justify the symmetry note, for example, that $j_{13}(\bar{\sigma}, e^u)_V = \tfrac{1}{2}j_{13}(\bar{\sigma}, e^u)_V + \tfrac{1}{2}j_{13}(e^\sigma, \sigma^u)_V$, and so on)

$$\mathbf{J}_3 = \begin{bmatrix} j_{11} & j_{12} & j_{13} \\ j_{12} & j_{22} & j_{23} \\ j_{13} & j_{23} & j_{33} \end{bmatrix} \tag{26}$$

is seen to fully characterize (22) hence, once the forcing potential P is selected, the functional (20). (The subscript of $\mathbf{J}$ identifies the number of independent parameters, as shown below.)

On replacing (23) into (22), U may be expressed in terms of the independent fields as

$$U = \tfrac{1}{2}\int_V \begin{Bmatrix} \bar{\sigma} \\ \bar{e} \\ \bar{u} \end{Bmatrix}^T \begin{bmatrix} j_{11}E^{-1} & j_{12}I & j_{13}D \\ j_{12}I & j_{22}E & j_{23}ED \\ j_{13}D^T & j_{23}D^TE & j_{33}D^TED \end{bmatrix} \begin{Bmatrix} \bar{\sigma} \\ \bar{e} \\ \bar{u} \end{Bmatrix} dV, \tag{27}$$

which verifies the symmetry of $\mathbf{J}_3$. Using (27) the first variation of U may be presented as

$$\delta U = (\Delta e, \delta\bar{\sigma})_V + (\Delta\sigma, \delta\bar{e})_V - (\operatorname{div}\sigma', \delta\bar{u})_V + [\sigma'_n, \delta\bar{u}]_S, \tag{28}$$

where

$$\Delta e = j_{11}e^\sigma + j_{12}\bar{e} + j_{13}e^u, \quad \Delta\sigma = j_{12}\bar{\sigma} + j_{22}\sigma^e + j_{23}\sigma^u, \quad \sigma' = j_{13}\bar{\sigma} + j_{23}\sigma^e + j_{33}\sigma^u. \tag{29}$$

The last two terms in (28) combine with contributions from the forcing potential variation. For example, if P is the conventional forcing potential (21), the complete variation of $\Pi^c = U - P^c$ is

$$\delta\Pi^c = (\Delta e, \delta\bar{\sigma})_V + (\Delta\sigma, \delta\bar{e})_V - (\operatorname{div}\sigma' + b, \delta\bar{u})_V + [\sigma'_n - \hat{t}, \delta\bar{u}]_{S_t} - [\bar{u} - \hat{d}, \delta\bar{\sigma}_n]_{S_d}. \tag{30}$$

Using P^d or P^t does not change the volume terms. Consequently the Euler equations associated with the volume terms of the first variation

$$\Delta e = 0, \quad \Delta\sigma = 0, \quad \operatorname{div}\sigma' + b = 0, \tag{31}$$

256

are independent of the forcing potential.

For consistency of the Euler equations with the field equations (1–3) one must have $\Delta e = 0$, $\Delta \sigma = 0$ and $\sigma' = \sigma$ if the assumed stress and strain fields reduce to the exact ones. Therefore

$$
\begin{aligned}
j_{11} + j_{12} + j_{13} &= 0, \\
j_{12} + j_{22} + j_{23} &= 0, \\
j_{13} + j_{23} + j_{33} &= 1.
\end{aligned}
\tag{32}
$$

Because of these constraints, the maximum number of independent parameters that define the entries of $\mathbf{J}_3$ is three as claimed. The specialization of these functionals to conventional and parametrized forms is discussed in References [4,5].

5. SPLIT FORM OF GENERALIZED STRAIN ENERGY

The expression (22) for U is not suitable for incompressible materials. To construct a parametrized form that encompasses incompressibility the generalized strain energy is augmented with additional independent fields, one of which must be the pressure. There are several ways of accomplishing this objective. In this Section the starting point is the conventional deviatoric splitting (18); the Lamé splitting (19) is considered in Section 7.

An augmented generalized strain energy U_{ds} (subscripts stand for "deviatoric split") is constructed in terms of the five independent fields $\bar{s}$, $\bar{g}$, $\bar{u}$, $\bar{p}$ and $\bar{\theta}$. Using (25) as a "template" the following quadratic form is postulated:

$$
U_{ds} = \tfrac{1}{2} \int_V
\left\{ \begin{array}{c} \bar{s} \\ s^g \\ s^u \\ \bar{p} \\ p^\theta \\ p^u \end{array} \right\}^T
\left[\begin{array}{cccccc}
j_{11}\mathbf{I} & j_{12}\mathbf{I} & j_{13}\mathbf{I} & j_{14}\mathbf{h} & j_{15}\mathbf{h} & j_{16}\mathbf{h} \\
j_{21}\mathbf{I} & j_{22}\mathbf{I} & j_{23}\mathbf{I} & j_{24}\mathbf{h} & j_{25}\mathbf{h} & j_{26}\mathbf{h} \\
j_{31}\mathbf{I} & j_{32}\mathbf{I} & j_{33}\mathbf{I} & j_{34}\mathbf{h} & j_{35}\mathbf{h} & j_{36}\mathbf{h} \\
j_{41}\mathbf{h}^T & j_{42}\mathbf{h}^T & j_{43}\mathbf{h}^T & j_{44} & j_{45} & j_{46} \\
j_{51}\mathbf{h}^T & j_{52}\mathbf{h}^T & j_{53}\mathbf{h}^T & j_{54} & j_{55} & j_{56} \\
j_{61}\mathbf{h}^T & j_{62}\mathbf{h}^T & j_{63}\mathbf{h}^T & j_{64} & j_{65} & j_{66}
\end{array} \right]
\left\{ \begin{array}{c} \mathbf{g}^s \\ \bar{\mathbf{g}} \\ \mathbf{g}^u \\ \theta^p \\ \bar{\theta} \\ \theta^u \end{array} \right\} dV,
\tag{33}
$$

in which the derived fields are

$$
\mathbf{g}^u = (\mathbf{D} - \tfrac{1}{3}\mathbf{h} \, \mathrm{div}\,)\bar{u} = \mathbf{D}_g \bar{u}, \quad \mathbf{g}^s = \mathbf{C}^{-1}\bar{s}, \quad \theta^p = k^{-1}\bar{p}, \quad \theta^u = -\,\mathrm{div}\,\bar{u},
$$

$$
s^g = \mathbf{C}\bar{g}, \quad s^u = \mathbf{C}\mathbf{g}^u = \mathbf{C}\mathbf{D}_g \bar{u}, \quad p^\theta = k\bar{\theta}, \quad p^u = k\theta^u = -k \, \mathrm{div}\,\bar{u}.
\tag{34}
$$

The kernel matrix of the quadratic form (33) is now 21×21 and is characterized by the thirty-six j coefficients. Unlike the treatment in Section 4, coefficient symmetry conditions are not set *ab initio*. Substituting (34)

into (33), U_{ds} may be expressed in terms of the five independent fields as the quadratic form

$$U_{ds} = \frac{1}{2} \int_V \begin{Bmatrix} \tilde{s} \\ \tilde{g} \\ \tilde{u} \\ \tilde{p} \\ \tilde{\theta} \end{Bmatrix}^T \begin{bmatrix} j_{11}\mathbf{C}^{-1} & j_{12}\mathbf{I} \\ j_{21}\mathbf{I} & j_{22}\mathbf{C} \\ j_{31}\mathbf{D}_g^T + j_{61}k\,\mathrm{grad}\,\mathbf{h}^T\mathbf{C}^{-1} & j_{32}\mathbf{D}_g^T\mathbf{C} + j_{62}k\,\mathrm{grad}\,\mathbf{h}^T \\ j_{41}\mathbf{h}^T\mathbf{C}^{-1} & j_{42}\mathbf{h}^T \\ j_{51}k\mathbf{h}^T\mathbf{C}^{-1} & j_{52}k\mathbf{h}^T \end{bmatrix}$$

$$\begin{bmatrix} j_{13}\mathbf{D}_g + j_{16}\mathbf{h}\,\mathrm{div} & j_{14}k^{-1}\mathbf{h} & j_{15}\mathbf{h} \\ j_{23}\mathbf{C}\mathbf{D}_g + j_{26}\mathbf{C}\mathbf{h}\,\mathrm{div} & j_{24}k^{-1}\mathbf{C}\mathbf{h} & j_{25}\mathbf{C}\mathbf{h} \\ \mathbf{D}_g^T\mathbf{C}(j_{33}\mathbf{D}_g + j_{36}\mathbf{h}\,\mathrm{div}) & j_{34}k^{-1}\mathbf{D}_g^T\mathbf{C}\mathbf{h} + j_{64}\,\mathrm{grad} & j_{35}\mathbf{D}_g^T\mathbf{C}\mathbf{h} + j_{65}k\,\mathrm{grad} \\ +k\,\mathrm{grad}\,(j_{63}\,\mathbf{h}^T\mathbf{D}_g + j_{66}\,\mathrm{div}) & & \\ j_{43}\,\mathbf{h}^T\mathbf{D}_g + j_{46}\,\mathrm{div} & j_{44}k^{-1} & j_{45} \\ j_{53}k\mathbf{h}^T\mathbf{D}_g + j_{56}k\,\mathrm{div} & j_{54} & j_{55}k \end{bmatrix} \begin{Bmatrix} \tilde{s} \\ \tilde{g} \\ \tilde{u} \\ \tilde{p} \\ \tilde{\theta} \end{Bmatrix} dV. \tag{35}$$

in which $\mathrm{grad} \equiv \mathrm{div}^T = \{\partial/\partial x_1 \quad \partial/\partial x_2 \quad \partial/\partial x_3\}^T$ when applied to a scalar function. The kernel matrix in (35) must be symmetric, a condition that provides the following symmetry relations:

$$j_{mn} = j_{nm}, \quad m = 1,2,3 \quad n = 1,2,3 \qquad j_{mn} = j_{nm}, \quad m = 4,5,6 \quad n = 4,5,6$$
$$j_{mn}\mathbf{I} = j_{nm}k^{-1}\mathbf{C}, \quad m = 4,5,6 \quad n = 1,2,3. \tag{36}$$

If these conditions are imposed on (33) that kernel matrix becomes

$$\begin{bmatrix} j_{11}\mathbf{I} & j_{12}\mathbf{I} & j_{13}\mathbf{I} & j_{14}\mathbf{h} & j_{15}\mathbf{h} & j_{16}\mathbf{h} \\ j_{12}\mathbf{I} & j_{22}\mathbf{I} & j_{23}\mathbf{I} & j_{24}\mathbf{h} & j_{25}\mathbf{h} & j_{26}\mathbf{h} \\ j_{13}\mathbf{I} & j_{32}\mathbf{I} & j_{33}\mathbf{I} & j_{34}\mathbf{h} & j_{35}\mathbf{h} & j_{36}\mathbf{h} \\ j_{14}k^{-1}\mathbf{C}\mathbf{h}^T & j_{24}k^{-1}\mathbf{C}\mathbf{h}^T & j_{34}k^{-1}\mathbf{C}\mathbf{h}^T & j_{44} & j_{45} & j_{46} \\ j_{15}k^{-1}\mathbf{C}\mathbf{h}^T & j_{25}k^{-1}\mathbf{C}\mathbf{h}^T & j_{35}k^{-1}\mathbf{C}\mathbf{h}^T & j_{45} & j_{55} & j_{56} \\ j_{16}k^{-1}\mathbf{C}\mathbf{h}^T & j_{26}k^{-1}\mathbf{C}\mathbf{h}^T & j_{36}k^{-1}\mathbf{C}\mathbf{h}^T & j_{46} & j_{56} & j_{66} \end{bmatrix}, \tag{37}$$

This is fully characterized by the 6×6 functional-generating symmetric matrix

$$\mathbf{J}_{12} = \begin{bmatrix} j_{11} & j_{12} & j_{13} & j_{14} & j_{15} & j_{16} \\ j_{12} & j_{22} & j_{23} & j_{24} & j_{25} & j_{26} \\ j_{13} & j_{23} & j_{33} & j_{34} & j_{35} & j_{36} \\ j_{14} & j_{24} & j_{34} & j_{44} & j_{45} & j_{46} \\ j_{15} & j_{25} & j_{35} & j_{45} & j_{55} & j_{56} \\ j_{16} & j_{26} & j_{36} & j_{46} & j_{56} & j_{66} \end{bmatrix}. \tag{38}$$

(the $\mathbf{J}$ subscript denotes the number of free parameters, as explained below). The kernel matrix of (35) becomes

$$\begin{bmatrix} j_{11}\mathbf{C}^{-1} & j_{12}\mathbf{I} & j_{13}\mathbf{D}_g - j_{16}\mathbf{h}\,\mathrm{div} & j_{14}k^{-1}\mathbf{h} & j_{15}\mathbf{h} \\ & j_{22}\mathbf{C} & j_{23}\mathbf{C}\mathbf{D}_g - j_{26}\mathbf{C}\mathbf{h}\,\mathrm{div} & j_{24}k^{-1}\mathbf{C}\mathbf{h} & j_{25}\mathbf{C}\mathbf{h} \\ & & j_{33}\mathbf{D}_g^T\mathbf{C}\mathbf{D}_g + j_{66}k\,\mathrm{grad}\,\mathrm{div}) & j_{34}k^{-1}\mathbf{D}_g^T\mathbf{C}\mathbf{h} & j_{35}\mathbf{D}_g^T\mathbf{C}\mathbf{h} \\ & & -j_{36}(\mathbf{D}_g^T\mathbf{C}\mathbf{h}\,\mathrm{div} + \mathrm{grad}\,\mathbf{h}^T\mathbf{C}\mathbf{D}_g) & -j_{46}\,\mathrm{grad} & -j_{56}k\,\mathrm{grad} \\ & & & j_{44}k^{-1} & j_{45} \\ symm & & & & j_{55}k \end{bmatrix} \tag{39}$$

The first variation of (35) is

$$\delta U_{ds} = (\Delta g, \delta \tilde{s})_V + (\Delta s, \delta \tilde{g})_V - (\operatorname{div} \sigma', \delta \bar{u})_V + (\Delta \theta, \delta \bar{p})_V + (\Delta p, \delta \bar{\theta})_V + [\sigma'_n, \delta \bar{u}]_S, \qquad (40)$$

where

$$\Delta g = j_{11} g^s + j_{12} \tilde{g} + j_{13} g^u + \mathbf{h}(j_{14} \theta^p + j_{15} \bar{\theta} + j_{16} \theta^u),$$

$$\Delta s = j_{12} \tilde{s} + j_{22} \tilde{s}^s + j_{23} s^u + \mathbf{Ch}(j_{24} \theta^p + j_{25} \bar{\theta} + j_{26} \theta^u),$$

$$\sigma' = j_{13} \tilde{s} + j_{23} s^s + j_{33} s^u + \mathbf{B}(j_{34} \theta^p + j_{35} \bar{\theta} + j_{36} \theta^u)$$
$$\qquad + \mathbf{h}\mathbf{h}^T (j_{16} \tilde{s} + j_{26} s^s + j_{36} s^u) - \mathbf{h}(j_{46} p + j_{56} p^\theta + j_{66} p^u) \qquad (41)$$
$$\qquad = j_{13} \tilde{s} + j_{23} s^s + j_{33} s^u + \mathbf{B}(j_{34} \theta^p + j_{35} \theta + j_{36} \theta^u) - \mathbf{h}(j_{46} p + j_{56} p^\theta + j_{66} p^u),$$

$$\Delta \theta = \mathbf{h}^T k^{-1}(j_{14} \tilde{s} + j_{24} s^s + j_{34} s^u) + j_{44} \theta^p + j_{45} \bar{\theta} + j_{46} \theta^u = j_{44} \theta^p + j_{45} \bar{\theta} + j_{46} \theta^u,$$

$$\Delta p = \mathbf{h}^T (j_{15} \tilde{s} + j_{25} s^s + j_{35} s^u) + j_{45} \bar{p} + j_{55} p^\theta + j_{56} p^u = j_{45} \bar{p} + j_{55} p^\theta + j_{56} p^u.$$

where $\mathbf{B} = (\mathbf{I} - \frac{1}{3}\mathbf{h}\mathbf{h}^T)\mathbf{Ch}$, and the simplifications in σ', $\Delta \theta$ and Δp result from $\mathbf{h}^T s = \mathbf{h}^T s^s = \mathbf{h}^T s^u = 0$ since the deviatoric stress tensor is traceless. Applying again the consistency argument and noting that mean and deviatoric parts may vary independently one obtains the constraint conditions

$$j_{11} + j_{12} + j_{13} = 0, \qquad j_{14} + j_{15} + j_{16} = 0, \qquad j_{12} + j_{22} + j_{23} = 0,$$

$$j_{24} + j_{25} + j_{26} = 0, \qquad j_{13} + j_{23} + j_{33} = 1, \qquad j_{34} + j_{35} + j_{36} = 0, \qquad (42)$$

$$j_{46} + j_{56} + j_{66} = 1, \qquad j_{44} + j_{45} + j_{46} = 0, \qquad j_{45} + j_{55} + j_{56} = 0.$$

Because of these nine constraints the maximum number of independent parameters that define the coefficients of matrix (38) is $21 - 9 = 12$ as claimed.

6. SIMPLIFICATIONS

Having a ∞^{12} family of functionals for constructing numerical approximation methods such as finite elements leaves the selection wide open. In the absence of other information it appears prudent to reduce the number of free parameters by setting to zero all coefficients that couple mean and deviatoric quantities:

$$\mathbf{J}_6 = \begin{bmatrix} j_{11} & j_{12} & j_{13} & 0 & 0 & 0 \\ j_{12} & j_{22} & j_{23} & 0 & 0 & 0 \\ j_{13} & j_{32} & j_{33} & 0 & 0 & 0 \\ 0 & 0 & 0 & j_{44} & j_{45} & j_{46} \\ 0 & 0 & 0 & j_{45} & j_{55} & j_{56} \\ 0 & 0 & 0 & j_{46} & j_{56} & j_{66} \end{bmatrix} \qquad (43)$$

subject to the constraints that the row (implying column) sums be 0, 0, 1, 0, 0 and 1, respectively. This simplified form exhibits six independent parameters.

The next question is how to include exact incompressibility, for which $k \to \infty$. A study of the matrix (39) reveals that the only coefficients affecting terms multiplied by k are j_{55} and j_{66}. One solution would be to take $j_{55} = j'_{55}/k$, and $j_{66} = j'_{66}/k$ with the primed coefficients as source data. A more expedient solution

is to set those coefficients to zero, which reduces (43) to

$$
\mathbf{J}_4 =
\begin{bmatrix}
j_{11} & j_{12} & j_{13} & 0 & 0 & 0 \\
j_{12} & j_{22} & j_{23} & 0 & 0 & 0 \\
j_{13} & j_{32} & j_{33} & 0 & 0 & 0 \\
0 & 0 & 0 & 2\omega - 1 & -\omega & 1 - \omega \\
0 & 0 & 0 & -\omega & 0 & \omega \\
0 & 0 & 0 & 1 - \omega & \omega & 0
\end{bmatrix}
\tag{44}
$$

where ω is a free parameter that determines the lower 3×3 principal minor. The total number of parameters is reduced to four, just one more than in compressible elasticity. Thus the following practical rule emerges: any compressible-elasticity principle characterized by the coefficients (26) can be extended to embody incompressibility by modifying U as follows:

(I) Replace σ and e by s and g, respectively. (In fact, only the first modification is actually needed, since $s^T g = s^T e$, etc.)

(II) Add the pressure and volumetric strain terms characterized by the lower 3×3 principal minor in (44). If ω is zero the volumetric strain drops out as independent field and the additional terms reduce to

$$
\tfrac{1}{2}(\bar{p}, \theta^u - \theta^p)_V + \tfrac{1}{2}(p^u, \theta^p)_V = -\int_V \left(\frac{\bar{p}^2}{2k} + \bar{p} \operatorname{div} \bar{u} \right) dV.
\tag{45}
$$

Furthermore, in exact incompressibility only the term $-\bar{p} \operatorname{div} u$ survives.

7. LAMÉ SPLIT

Consideration of the Lamé split (19) is of interest because of historical reasons, since the first mixed variational principle encompassing compressible and incompressible isotropic elasticity constructed by Herrmann [7] was based on it. Again one can start by postulating a quadratic form for the generalized strain energy U_{Ls} (where subscripts stand for "Lamé split"):

$$
U_{Ls} = \tfrac{1}{2} \int_V
\begin{Bmatrix} \bar{\tau} \\ \tau^e \\ \tau^u \\ \bar{q} \\ q^\theta \\ q^u \end{Bmatrix}^T
\begin{bmatrix}
\ell_{11}\mathbf{I} & \ell_{12}\mathbf{I} & \ell_{13}\mathbf{I} & \ell_{14}\mathbf{h} & \ell_{15}\mathbf{h} & \ell_{16}\mathbf{h} \\
\ell_{21}\mathbf{I} & \ell_{22}\mathbf{I} & \ell_{23}\mathbf{I} & \ell_{24}\mathbf{h} & \ell_{25}\mathbf{h} & \ell_{26}\mathbf{h} \\
\ell_{31}\mathbf{I} & \ell_{32}\mathbf{I} & \ell_{33}\mathbf{I} & \ell_{34}\mathbf{h} & \ell_{35}\mathbf{h} & \ell_{36}\mathbf{h} \\
\ell_{41}\mathbf{h}^T & \ell_{42}\mathbf{h}^T & \ell_{43}\mathbf{h}^T & \ell_{44} & \ell_{45} & \ell_{46} \\
\ell_{51}\mathbf{h}^T & \ell_{52}\mathbf{h}^T & \ell_{53}\mathbf{h}^T & \ell_{54} & \ell_{55} & \ell_{56} \\
\ell_{61}\mathbf{h}^T & \ell_{62}\mathbf{h}^T & \ell_{63}\mathbf{h}^T & \ell_{64} & \ell_{65} & \ell_{66}
\end{bmatrix}
\begin{Bmatrix} e^\tau \\ \bar{e} \\ e^u \\ \theta^q \\ \bar{\theta} \\ \theta^u \end{Bmatrix} dV,
\tag{46}
$$

in which the ℓ's coefficients take the place of the j's, and where the new terms are

$$
\bar{\tau} = \sigma - q\mathbf{h}, \qquad \tau^e = \mathbf{C}\bar{e}, \qquad \tau^u = \mathbf{C}\mathbf{D}u, \qquad e^\tau = \mathbf{C}^{-1}\bar{\tau},
$$
$$
\xi = 3v/(1 + v), \qquad \bar{q} = \xi \bar{p}, \qquad q^\theta = \xi \lambda \bar{\theta}, \qquad q^u = -\xi \lambda \operatorname{div} \bar{u}, \qquad \theta^q = q/\lambda.
\tag{47}
$$

Going through the same mechanics one obtains relations similar to (35) through (40) with s, g, p, k and $\mathbf{D}_g$ replaced by τ, e, q, λ and $\mathbf{D}$, respectively. But now $\mathbf{h}^T \tau$ is not necessarily zero and so the counterpart of (41)

260

retains more terms:

$$\Delta e = \ell_{11} e^\tau + \ell_{12} \tilde{e} + \ell_{13} e^u + \mathbf{h}(\ell_{14} \theta^q + \ell_{15} \bar{\theta} + \ell_{16} \theta^u),$$

$$\Delta \tau = \ell_{12} \bar{\tau} + \ell_{22} \bar{\tau}^\prime + \ell_{23} \tau^u + \mathbf{Ch}(\ell_{24} \theta^q + \ell_{25} \bar{\theta} + \ell_{26} \theta^u),$$

$$\sigma' = \ell_{13} \bar{\tau} + \ell_{23} \tau^\prime + \ell_{33} \tau^u + \mathbf{Ch}(\ell_{34} \theta^q + \ell_{35} \theta + \ell_{36} \theta^u)$$

$$\qquad + \mathbf{h}\mathbf{h}^T(\ell_{16} \bar{\tau} + \ell_{26} \tau^\prime + \ell_{36} \tau^u) - \mathbf{h}(\ell_{46} p + \ell_{56} p^\theta + \ell_{66} p^u), \tag{48}$$

$$\Delta \theta = \mathbf{h}^T \lambda^{-1}(\ell_{14} \bar{\tau} + \ell_{24} \tau^\prime + \ell_{34} \tau^u) + \ell_{44} \theta^q + \ell_{45} \bar{\theta} + \ell_{46} \theta^u,$$

$$\Delta q = \mathbf{h}^T(\ell_{15} \bar{\tau} + \ell_{25} \tau^\prime + \ell_{35} \tau^u) + \ell_{45} \bar{q} + \ell_{55} q^\theta + \ell_{56} q^u.$$

Consistency provides the twelve constraints

$$\ell_{11} + \ell_{12} + \ell_{13} = 0, \qquad \ell_{14} + \ell_{15} + \ell_{16} = 0, \qquad \ell_{12} + \ell_{22} + \ell_{23} = 0,$$

$$\ell_{24} + \ell_{25} + \ell_{26} = 0, \qquad \ell_{13} + \ell_{23} + \ell_{33} = 1, \qquad \ell_{34} + \ell_{35} + \ell_{36} = 0,$$

$$\ell_{16} + \ell_{26} + \ell_{36} = 0, \qquad \ell_{46} + \ell_{56} + \ell_{66} = 1, \qquad \ell_{14} + \ell_{24} + \ell_{34} = 0, \tag{49}$$

$$\ell_{44} + \ell_{45} + \ell_{46} = 0, \qquad \ell_{15} + \ell_{25} + \ell_{35} = 0, \qquad \ell_{45} + \ell_{55} + \ell_{56} = 0.$$

This leaves $21 - 12 = 9$ independent parameters in the functional-generating symmetric matrix

$$\mathbf{L_9} = \begin{bmatrix} \ell_{11} & \ell_{12} & \ell_{13} & \ell_{14} & \ell_{15} & \ell_{16} \\ \ell_{12} & \ell_{22} & \ell_{23} & \ell_{24} & \ell_{25} & \ell_{26} \\ \ell_{13} & \ell_{23} & \ell_{33} & \ell_{34} & \ell_{35} & \ell_{36} \\ \ell_{14} & \ell_{24} & \ell_{34} & \ell_{44} & \ell_{45} & \ell_{46} \\ \ell_{15} & \ell_{25} & \ell_{35} & \ell_{45} & \ell_{55} & \ell_{56} \\ \ell_{16} & \ell_{26} & \ell_{36} & \ell_{46} & \ell_{56} & \ell_{66} \end{bmatrix}. \tag{50}$$

If the off-diagonal blocks of this matrix are set to zero as in (43), $\mathbf{L_9}$ becomes $\mathbf{L_6}$ and the conditions on the remaining nonzero coefficients are identical to those of $\mathbf{J_6}$.

Treatment of the more general splitting (12) with $\eta \neq 0$ does not cause any particular difficulties. However, as splittings other than (18) do not accomodate anisotropic materials naturally, they will not be investigated further.

8. SPECIALIZATIONS

The simplest principle (in the sense of having the sparsest $\mathbf{J}$ matrix) that accomodates both compressible and incompressible elasticity is obtained by specializing (44) to

$$\mathbf{J}_P = \begin{bmatrix} 0 & 0 & 0 & 0 & 0 & 0 \\ 0 & 0 & 0 & 0 & 0 & 0 \\ 0 & 0 & 1 & 0 & 0 & 0 \\ 0 & 0 & 0 & -1 & 0 & 1 \\ 0 & 0 & 0 & 0 & 0 & 0 \\ 0 & 0 & 0 & 1 & 0 & 0 \end{bmatrix}. \tag{51}$$

This choice leaves only displacements and pressures as independent field variables and yields

$$U_P(\bar{\mathbf{u}}, \bar{p}) = \tfrac{1}{2}(\mathbf{s}^u, \mathbf{g}^u)_V - \left(\bar{p}, \frac{\bar{p}}{2k} + \operatorname{div} \bar{\mathbf{u}}\right)_V = \tfrac{1}{2}(\mathbf{s}^u, \mathbf{e}^u)_V - \left(\frac{\bar{p}^2}{2k} + \bar{p} \operatorname{div} \bar{\mathbf{u}}\right)_V, \tag{52}$$

which may be viewed as an modification of the minimum potential energy functional. For practical use it is important to note that $\mathbf{g}^u$ may be replaced by $\mathbf{e}^u$ in the first integral because tensor s^u_{ij} is traceless. In the incompressible limit U_P collapses to $\frac{1}{2}(\mathbf{s}^u, \mathbf{e}^u)_V - (\bar{p}, \operatorname{div}\bar{\mathbf{u}})_V$.

The specialization

$$\mathbf{J}_{AR} = \begin{bmatrix} 0 & -1 & 1 & 0 & 0 & 0 \\ -1 & 1 & 0 & 0 & 0 & 0 \\ 1 & 0 & 0 & 0 & 0 & 0 \\ 0 & 0 & 0 & 0 & -1 & 1 \\ 0 & 0 & 0 & -1 & 1 & 0 \\ 0 & 0 & 0 & 1 & 0 & 0 \end{bmatrix} \tag{53}$$

reduces $U_{ds} - P$ to the five-field functional presented by Atluri and Reissner [8] (in that paper p and θ are defined as the negatives of the quantities used here). Notice that since both 3×3 principal minors of $\mathbf{J}_{AR}$ display the numerical structure of the Hu-Washizu principle of compressible elasticity, use of (24) yields

$$U_{AR} = U_H(\bar{\mathbf{s}}, \bar{\mathbf{g}}, \bar{\mathbf{u}}) + U_H(\bar{p}\mathbf{h}, \bar{\theta}\mathbf{h}, \theta^u\mathbf{h}) = \frac{1}{2}(\mathbf{s}^s, \bar{\mathbf{g}})_V + (\bar{\mathbf{s}}, \mathbf{g}^u - \bar{\mathbf{g}})_V + \frac{1}{2}(p^\theta, \bar{\theta})_V + \bar{p}(\theta^u - \bar{\theta})_V, \tag{54}$$

in which again $\mathbf{g}^u$ and $\bar{\mathbf{g}}$ may be replaced by $\mathbf{e}^u$ and $\bar{\mathbf{e}}$, respectively. As $j_{ss} \neq 0$, this functional does not accomodate exact incompressibility. This drawback can be easily corrected, however, through the techniques discussed in Section 6.

Finally, specialization of (50) to

$$\mathbf{L}_H = \begin{bmatrix} 0 & 0 & 0 & 0 & 0 & 0 \\ 0 & 0 & 0 & 0 & 0 & 0 \\ 0 & 0 & 1 & 0 & 0 & 0 \\ 0 & 0 & 0 & -1 & 0 & 1 \\ 0 & 0 & 0 & 0 & 0 & 0 \\ 0 & 0 & 0 & 1 & 0 & 0 \end{bmatrix}, \quad \mathbf{L}_F = \begin{bmatrix} 0 & -1 & 1 & 0 & 0 & 0 \\ -1 & 1 & 0 & 0 & 0 & 0 \\ 1 & 0 & 0 & 0 & 0 & 0 \\ 0 & 0 & 0 & -1 & 0 & 1 \\ 0 & 0 & 0 & 0 & 0 & 0 \\ 0 & 0 & 0 & 1 & 0 & 0 \end{bmatrix}, \tag{55}$$

reduces the functional $U_{Ls} - P$ to those presented by Herrmann [7] and Franca [9], respectively; which are identified as $U_H - P$ and $U_F - P$ in the sequel.

Herrmann's functional, which as noted above has historical importance, contains two independent fields: displacements $\mathbf{u}$ and pseudo pressure q. Its U functional is

$$U_H(\bar{\mathbf{u}}, \bar{q}) = \frac{1}{2}(\tau^u, \mathbf{e}^u)_V - \left(\frac{\bar{q}^2}{2\lambda} + \bar{q}\operatorname{div}\bar{\mathbf{u}}\right)_V. \tag{56}$$

The upper and lower 3×3 principal minors of $\mathbf{L}_H$ display the numerical structure of the minimum potential energy and stress-displacement Reissner compressible-elasticity functionals, respectively.

Franca's functional contains four independent fields: extra stress τ, total strains $\mathbf{e}$, displacements $\mathbf{u}$ and pseudo pressure q. Its U functional is

$$U_F(\bar{\tau}, \bar{\mathbf{e}}, \bar{\mathbf{u}}, \bar{q}) = \frac{1}{2}(\tau^e, \bar{\mathbf{e}})_V + (\bar{\tau}, \mathbf{e}^u - \bar{\mathbf{e}})_V - \left(\frac{\bar{q}^2}{2\lambda} + \bar{q}\operatorname{div}\bar{\mathbf{u}}\right)_V. \tag{57}$$

The upper and lower 3×3 principal minors of $\mathbf{L}_F$ display the numerical structure of the Hu-Washizu and stress-displacement Reissner functionals of compressible elasticity, respectively.

9. CONCLUSIONS

The parametrized formulations presented here extend the parametrized functionals of References [4,5] to accommodate incompressibility. In doing so a wider and perhaps bewildering range of possibilities is encountered, which raises some questions as regards the usefulness of parametrization techniques.

The formulation of parametrized variational principles offers conceptual and practical advantages. From a conceptual standpoint the technique is intellectually satisfying in that all possible variational forms are obtained once and for all. This should be contrasted to the conventional case-by-case derivation, which can only take "potshots" at the infinite domain of possible functionals. The key practical advantage is that generating matrix coefficients may be left free in finite element applications down to the element level, and use to enhance the quality of the numerical approximations as discussed in References [1–5].

But coming face to face with twelve free parameters as in Section 5 may be confusing and negate the claimed benefits of generality. The simplifications of Section 6 appear reasonable from an applications standpoint because (1) they cut the number of independent parameters while retaining flexibility in the weighting of the participating fields, and (2) all important specific functionals proposed to date are still covered.

Finally, the simplicity and generality of the functionals based on the deviatoric splitting (18) should be kept in mind. It is difficult to understand why the finite element literature is still preoccupied with the Lamé split and associated functionals. Not only is this split unnatural for anisotropic materials but note that associated functionals such as (56) and (57) degenerate for $\lambda = 0$, which happens if $\nu = 0$. At this value, $\xi = 0$, q vanishes identically, and $0/0$ terms requiring special treatment appear in U. As a zero Poisson's ratio is physically realizable the claim to generality of application, even with restriction to isotropic behavior, is seriously weakened.

REFERENCES

1. C. A. Felippa, Parametrized multifield variational principles in elasticity: I. Mixed functionals, *Communications in Applied Numerical Methods*, 5, 79–88 (1989)

2. C. A. Felippa, Parametrized multifield variational principles in elasticity: II. Hybrid functionals and the free formulation, *Communications in Applied Numerical Methods*, 5, 89–98 (1989)

3. C. A. Felippa, The extended free formulation of finite elements in linear elasticity, *Journal of Applied Mechanics*, 56, 609–616 (1989)

4. C. A. Felippa and C. Militello, The variational formulation of high-performance finite elements: parametrized variational principles, *Computers & Structures*, in press

5. C. A. Felippa and C. Militello, Developments in variational methods for high-performance plate and shell elements, in *Analytical and Computational Methods for Shells*, CAD Vol. 3, ed. by A. K. Noor, T. Belytschko and J. C. Simo, American Society of Mechanical Engineers, ASME, New York, 191–216 (1989)

6. M. Gurtin, The linear theory of elasticity, in Volume VIa/2 of *Encyclopedia of Physics*, ed. by C. Truesdell, Springer-Verlag, Berlin (1972)

7. L. R. Herrmann, Elasticity equations for nearly incompressible materials by a variational theorem, *AIAA Journal*, 3, 1896–1900 (1965)

8. S. N. Atluri and E. Reissner, On the formulation of variational theorems involving volume constraints, *Computational Mechanics*, 5, 337–344 (1989)

9. L. P. Franca, Analysis and finite element approximation of compressible and incompressible linear isotropic elasticity based upon a variational principle, *Computer Methods in Applied Mechanics and Engineering*, 76, 259–273 (1989)

THE INDIVIDUAL ELEMENT TEST REVISITED

SUMMARY

The subject of the patch test for finite elements retains several unsettled aspects. In particular, the issue of one-element versus multielement tests needs clarification. Following a brief historical review, we present the individual element test (IET) of Bergan and Hanssen in an expanded context that encompasses several important classes of new elements. The relationship of the IET to the multielement forms A, B and C of the patch test and to the single element test are clarified.

1. BACKGROUND

The patch test for convergence is a fascinating area in the development of nonconforming finite element methods. It grew up of the brilliant intuition of Bruce Irons. Initially developed in the mid-1960s at Rolls Royce and then at the Swansea group headed by Olek Zienkiewicz, by the early 1970s the test had became a powerful and practical tool for evaluating and checking nonconforming elements. And yet today it remains a controversial issue: accepted by most finite element developers while ignored by others, welcomed by element programmers, distrusted by mathematicians. For tracing down the origins of the test there is no better source than a 1973 survey article by Irons and Razzaque [12]. Added remarks to the quoted material are inserted in footnotes, and reference numbers have been altered to match those of the present paper.

Origins of the Patch Test

In 1965 even engineering intuition dared not predict the behavior of certain finite elements. Experience force those engineers who doubted it to admit that interelement continuity was important: the senior author[1] believed that it was necessary for convergence. It is not known which ideas inspired a numerical experiment by Tocher and Kapur [25], which demonstrated convergence within 0.3% in a biharmonic problem of plate bending, using equal rectangular elements with 1, x, y, x^2, xy, y^2, y^2, x^3, x^2y, xy^2, y^3, and x^3y and xy^3, as functional basis. The nodal variable of this Ari Adini rectangle [1] are w, $\partial w/\partial x$ and $\partial w/\partial y$ at the four corners, and this element guarantees only C^0 conformity.

Some months later, research at Rolls-Royce on the Zienkiewicz nonconforming triangle [2], — a similar plate-bending element[2]— clarified the situation. Three elements with C^1 continuity were simultaneously available, and, because the shape function subroutine used for numerical integration had been exhaustively tested,

---

[1] Bruce Irons

[2] This element is that identified by 'BCIZ' in the present paper

the results were trustworthy. It was observed: (a) that every problem giving constant curvature over the whole domain was accurately solved by the conforming elements whatever the mesh pattern, as was expected, and (b) that the nonconforming element was also successful, but only for one particular mesh pattern.[3]

Thus the patch test was born. For if the external nodes of any sub-assembly of a successful assembly of elements are given prescribed values corresponding to an arbitrary state of constant curvature, then the internal nodes must obediently take their correct values. (An internal node is defined as one completely surrounded by elements.) Conversely, if two overlapping patches can reproduce any given state of constant curvature, they should combine into a larger successful patch, provided that every external node lost is internal to one of the original patches. For such nodes are in equilibrium at their correct values, and should behave correctly as internal nodes of the extended patch. In an unsuccessful patch test, the internal nodes take unsuitable values, which introduce interelement discontinuities. The errors in deflection may be slight, but the errors in curvature may be ±20%. We must recognize two distinct types of errors:

(i) The finite element equations would not be exactly satisfied by the correct values at the internal nodes — in structural terms, we have disequilibrium;

(ii) The answers are nonunique because the matrix of coefficients K is semidefinite.

Role of the Patch Test

Clearly the patch test provides a *necessary* condition for convergence with fine mesh. We are less confident that it provides a *sufficient* condition. The argument is that if the mesh is fine, the patches are also small. Over any patch the correct solution gives almost uniform conditions to which the patch is known to respond correctly — provided that the small perturbations from uniform conditions do not cause a disproportionate response in the patch: we hope to prevent this by insisting that K is positive definite.

The patch test is invaluable to the research worker. Already, it has made respectable

(i)   Elements that do not conform,

(ii)   Elements that contain singularities,

(iii)   Elements that are approximately integrated,

(iv)   Elements that have no clear physical basis.

In short, the patch test will help a research worker to exploit and justify his wildest ideas. It largely restores the freedom enjoyed by the early unsophisticated experimenters.

The late 1960s and early 1970s were a period of unquestionable success for the test. That optimism is evident in the article quoted above, and prompted Gilbert Strang to develop a mathematical version popularized in the Strang-Fix textbook [21].

Confidence was shaken in the late 1970s by several developments. Numerical experiments, for example, those of Sander and Beckers [20] suggested that the test is not necessary for convergence, thus disproving Irons' belief stated above. Then a counterexample by Stummel [22] purported to show that the test is not even sufficient.[4] This motivated defensive responses by Irons [13] shortly before his untimely death, and by Taylor, Simo, Zienkiewicz and Chan [24]. These papers tried to set out the engineering version of the test on a more precise basis.

Despite these ruminations many questions persist, as noted in the lucid review article by Griffiths and Mitchell [11]. Some of them are listed below.

---

[3] The bending element test referred to in this sentence appears in the Addendum to [2]. This Addendum was not part of the original paper presented at the First Wright-Patterson Conference held in September 1965; it was added to the Proceedings that appeared in 1966. The name "patch test" will not be found there; see the Appendix of [21] for further historical details.

[4] Stummel has constructed [23] a *generalized patch test* that is mathematically impeccable in that it provides necessary and sufficient conditions for convergence. Unfortunately such test lacks important side benefits of Irons' patch test, such as element checkout by computer, because it is administered as a mathematically limiting process in function spaces. Furthermore, it does not apply to a mixture of different element types, or to situations such as a side shared by more than two elements.

Q1. What is a patch? Is it the ensemble of all possible meshes? Are some meshes excluded? Can these meshes contain different types of elements?

Q2. The test was originally developed for harmonic and biharmonic compressible elasticity problems, for which the concept of "constant strains" or "constant curvatures" is unambiguous. But what is the equivalent concept for shells? Even Reissner-Mindlin plates (which lead to the so-called C^0 elements) pose difficulties.

Q3. What are the modifications required for incompressible media? Is the test applicable to dynamic or nonlinear problems?

Q4. Are single-element versions of the test equivalent to the conventional, multielement versions?

Q5. Is the test restricted to nonconforming assumed-displacement elements? Can it be extended to encompass assumed-stress or assumed-strain mixed and hybrid elements? (For initial attempts in this direction, see [10])

The following treatment is aimed primarily at answering the last two questions. No position as to the mathematical relevance of the test is taken.

2. THE INDIVIDUAL ELEMENT TEST

Because of practical difficulties incurred in testing all possible patches there have been efforts directed toward translating the original test into statements involving a single element. These will be collectively called *one-element tests*.

The first step along this path was taken by Strang [21], who using integration by parts recast the original test in terms of "jump" contour integrals over element interfaces. An updated account is given by Griffiths and Mitchell [11], who remark that Strang's test can be passed in three different ways:

JCS: Jump integrals cancel over common sides of adjacent elements (*e.g.* DeVeubeke's 3-midside-node triangle, Morley's plate elements).

JOS: Jump integrals cancel over opposite element sides (*e.g.* Wilson's incompatible plane rectangle [26]).

JEC: Jump integrals cancel over the element contour (see examples in [11]).

Another important development, not so well publicized as Strang's, was undertaken by Bergan and coworkers at Trondheim over the period 1975–1984. The so called *individual element test*, or IET, was proposed by Bergan and Hanssen [4] in 1975. The underlying goal was to establish a test that could be directly carried out on the stiffness equations of a *single* element — an obvious improvement over the multielement form. In addition the test was to be constructive, *i.e.*, used as an *a priori* guide during element formulation, rather than as a post-facto check.

The IET has a simple physical motivation: to demand pairwise cancellation of tractions among adjacent elements that are subjected to a common uniform stress state. This is precisely the 'JCS' case of the Strang test noted above. Because of this inclusion, the IET is said to be a *strong* version

267

of the patch test in the following sense: any element passing the IET also verifies the conventional multielement form of the patch test, but the converse is not necessarily true.

The IET has formed the basis of the free formulation (FF) later developed by Bergan and Nygård [6]. It has also played an important part in the development of high performance finite elements undertaken by the authors [7–9,15–18].

In an important paper written in response to Stummel's counterexample, Taylor, Simo, Zienkiewicz and Chan [24] defined multielement patch tests in more precise terms, introducing the so-called A, B and C versions. They also discussed a one-element test called the "single element test," herein abbreviated to SET. They used the BCIZ plate bending element [2] to show that an element may pass the SET but fail multielement versions, and consequently that tests involving single elements are to be viewed with caution. In what follow we try to clarify this apparent contradiction and to establish precisely what the individual element test entails. In particular *it is shown that the IET contains a crucial condition that the SET lacks*, and that the two tests are not therefore equivalent.

Furthermore, we extend the IET to conditions beyond those considered by Bergan and Nygård by including elements with unknown internal displacement fields. The most important sources of such elements are: stress-assumed hybrids, and elements constructed through the assumed natural strain (ANS) and assumed natural deviatoric strain (ANDES) formulations.

3. ASSUMPTIONS FOR ELEMENT CONSTRUCTION

Suppose that we want to test an individual element of volume V and boundary S with exterior normal $\mathbf{n}$. The element satisfies the following assumptions.

A1. The element shares displacement degrees of freedom collected in $\mathbf{v}$ (the so called *visible* degrees of freedom) with adjacent elements. The boundary displacement field $\mathbf{d}$ is uniquely determined by $\mathbf{v}$ as

$$\mathbf{d} = \mathbf{N}_d \mathbf{v}, \tag{1}$$

where $\mathbf{N}_d$ are boundary shape functions.

The term "boundary displacement field" is meant to include normal derivatives (side rotations or slopes) in bending problems. More generally, in a problem governed by a variational principle of index $m > 1$, $\mathbf{d}$ includes normal derivatives up to the $(m-1)^{th}$ order.

This assumption says nothing about the internal displacement field $\mathbf{u}$. In free-formulation elements $\mathbf{u}$ is known and agrees with $\mathbf{d}$ only at the nodes. In the ANS [3,14,19,] and ANDES [8,9,17,18] formulations, $\mathbf{u}$ is unknown because the deviatoric strain field ϵ_h introduced in A2 below is not generally integrable.

A2. The strain field ϵ within the element is expressible as

$$\epsilon = \mathbf{B}\mathbf{v}, \tag{2}$$

which admits the following decomposition into mean and deviatoric parts:

$$\epsilon = \bar{\epsilon} + \epsilon_h = \overline{\mathbf{B}}\,\mathbf{v} + \mathbf{B}_h\mathbf{v} = (\overline{\mathbf{B}} + \mathbf{B}_h)\mathbf{v}, \tag{3}$$

268

where

$$\bar{\epsilon} = \frac{1}{V} \int_V \epsilon \, dV, \qquad \epsilon_h = \epsilon - \bar{\epsilon}. \tag{4}$$

We note that

$$\int_V \mathbf{B}_h \, dV = 0, \qquad \int_V \mathbf{A}\mathbf{B}_h \, dV = 0. \tag{5}$$

in which $\mathbf{A}$ is an arbitrary matrix constant over the element.

Subscript h stands for "high order." The strain field ϵ_h is not generally integrable, that is, associable with an internal displacement field u such that $\epsilon_h = \mathbf{D}u$, where $\mathbf{D} = \frac{1}{2}(\nabla + \nabla^T)$ is the symmetric vector gradient operator. On the other hand, the mean strain field $\bar{\epsilon}$, being constant, is integrable, as discussed under assumption A4.

A3. Suppose the element is under a constant stress state σ_0. Then a nodal force system $\mathbf{p}_0$ conjugate to $\mathbf{v}$ in the sense of virtual work develops. These forces are connected to $\mathbf{v}$ through the relation

$$\mathbf{p}_0 = \mathbf{L}\sigma_0, \qquad \mathbf{L} = \int_S \mathbf{N}_{dn} \, dS, \tag{6}$$

where $\mathbf{L}$ is called the *force lumping matrix* and $\mathbf{N}_{dn}$ denotes the projection of the shape functions $\mathbf{N}_d$ over the normal to the element side.

Matrix $\mathbf{L}$ was introduced by Bergan and coworkers in their studies leading to the free formulation [5,6], and plays a crucial role in the individual element test.

A4. The constant stress field σ_0 is associated with a given displacement field called $\mathbf{u}_{rc}$, such that the associated strain and stress fields are

$$\bar{\epsilon}^u = \mathbf{D}(\mathbf{u}_{rc}), \qquad \sigma^0 = \mathbf{E}\bar{\epsilon}^u, \tag{7}$$

where $\mathbf{E}$ is the symmetric matrix of elastic moduli, assumed constant over the element. This constitutive assumption excludes incompressibility, which must receive special treatment.

Field $\mathbf{u}_{rc}$ cannot be immediately linked to $\mathbf{v}$ because it spans a subspace of the possible boundary motions. We must start by expressing $\mathbf{u}_{rc}$ in the modal or generalized-coordinate form

$$\mathbf{u}_{rc} = \mathbf{N}_{rc}^q \mathbf{q}_{rc}, \tag{8}$$

where $\mathbf{N}_{rc}^q$ are modal functions and $\mathbf{q}_{rc}$ their amplitudes. The projection $\mathbf{v}_{rc}$ of $\mathbf{u}_{rc}$ over the space of boundary motions spanned by $\mathbf{v}$ can be most easily obtained by collocation, that is, evaluating $\mathbf{u}_{rc}$ at the nodal points. This process yields

$$\mathbf{v}_{rc} = \mathbf{G}_{rc} \mathbf{q}_{rc}, \tag{9}$$

in which $\mathbf{G}_{rc}$ will generally be a rectangular matrix with more rows than columns.

Subscripts r and c mean that $\mathbf{u}_{rc}$ is supposed to include rigid-body and constant-strain modes. In mathematical terms, $\mathbf{u}_{rc}$ is a polynomial of degree $m - 1$ when the variational index is m.

269

4. THE STIFFNESS MATRIX

Under the previous assumptions, the stiffness matrix is given by

$$\mathbf{K} = \int_V \mathbf{B}^T \mathbf{E} \mathbf{B} \, dV. \tag{10}$$

Using the strain decomposition (3), $\mathbf{K}$ splits as follows:

$$\mathbf{K} = \mathbf{K}_b + \mathbf{K}_h = \int_V \overline{\mathbf{B}}^T \mathbf{E} \overline{\mathbf{B}} \, dV + \int_V \mathbf{B}_h^T \mathbf{E} \mathbf{B}_h \, dV = V \overline{\mathbf{B}}^T \mathbf{E} \overline{\mathbf{B}} + \int_V \mathbf{B}_h^T \mathbf{E} \mathbf{B}_h \, dV \tag{11}$$

because of the *energy orthogonality condition*

$$\int_V \overline{\mathbf{B}}^T \mathbf{E} \mathbf{B}_h \, dV = 0, \tag{12}$$

which results on taking $\mathbf{A} = \overline{\mathbf{B}}^T \mathbf{E}$ on the second of (5). Matrices $\mathbf{K}_b$ and $\mathbf{K}_h$ receive the name of *basic·stiffness* and *higher order stiffness*, respectively.

5. FIRST CONDITION: CONSTANT STRAIN STATES

Bergan and Nygård [6] state two constraints for FF elements, which taken together represent the satisfaction of the IET. The first one is

$$\mathbf{K} \mathbf{v}_{rc} = \mathbf{L} \sigma_0, \tag{13}$$

which is essentially an equilibrium statement at the element level. Premultiplying (13) by $\mathbf{v}_{rc}^T$ we get $\mathbf{v}_{rc}^T \mathbf{K} \mathbf{v}_{rc} = \mathbf{v}_{rc}^T \mathbf{L} \sigma_0$, which on introducing (9) and (11) becomes

$$\mathbf{q}_{rc}^T \mathbf{G}_{rc}^T \overline{\mathbf{B}}^T \mathbf{E} \overline{\mathbf{B}} \mathbf{G}_{rc} \mathbf{q}_{rc} V + \mathbf{q}_{rc}^T \mathbf{G}_{rc}^T \mathbf{K}_h \mathbf{G}_{rc} \mathbf{q}_{rc} = \mathbf{q}_{rc}^T \mathbf{G}_{rc}^T \mathbf{L} \sigma_0. \tag{14}$$

If we request that $\mathbf{K}_h$ cannot contribute to the internal energy under a constant strain state we must have $\mathbf{G}_{rc}^T \mathbf{K}_h \mathbf{G}_{rc} = 0$, or, since $\mathbf{K}_h = \int_V \mathbf{B}_h \mathbf{E} \mathbf{B}_h \, dV$,

$$\mathbf{B}_h \mathbf{G}_{rc} = 0, \tag{15}$$

This may be called the *higher order strain cancellation condition*. Taking into account that $\sigma_0 = \mathbf{E} \mathbf{B}_{rc}^q \mathbf{q}_{rc}$, where $\mathbf{B}_{rc}^q = \mathbf{D}(\mathbf{N}_{rc}^q)$, the above equation becomes $\overline{\mathbf{B}}^T \mathbf{E} \overline{\mathbf{B}} \mathbf{G}_{rc} = V^{-1} \mathbf{L} \mathbf{E} \mathbf{B}_{rc}^q$. This can be split into $\overline{\mathbf{B}}^T = V^{-1} \mathbf{L}$ and $\overline{\mathbf{B}} \mathbf{G}_{rc} = \mathbf{B}_{rc}^q$. Replacing the former in the latter we obtain

$$V^{-1} \mathbf{L}^T \mathbf{G}_{rc} = \mathbf{B}_{rc}^q. \tag{16}$$

These conditions were introduced by Bergan and Nygård [6] in the context of the free formulation. They state that equation (16) should be used to check that the matrix $\mathbf{L}$ is correct. Then (16) is the first consistency constraint on $\mathbf{L}$. Equations (15) and (16) are necessary *in order that a single*
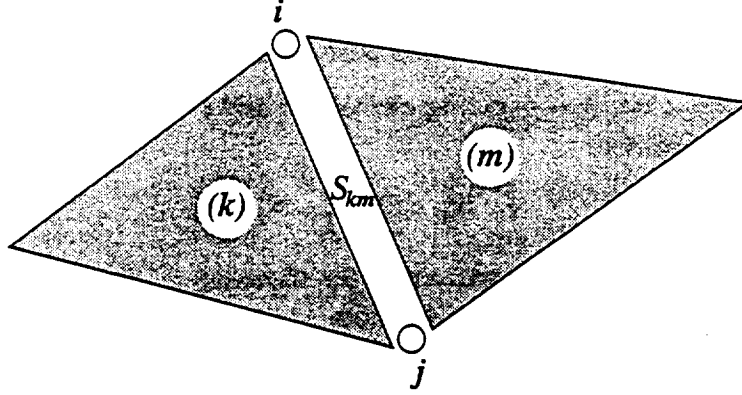
Figure 1. A common side $i - j$ shared by two elements.

element, which is in equilibrium, be capable of copying a constant strain state. To prove that they are also sufficient conditions is straightforward.

An important consequence of (16) can be investigated as follows. Rewrite it as $V^{-1} L^T G_{rc} q_{rc} = Du_{rc}$. Multiplying both sides by σ_0^T and integrating over the element volume we obtain

$$\sigma_0^T L^T G_{rc} q_{rc} = \int_V \sigma_0^T Du_{rc} \, dV. \tag{17}$$

Integration by parts of the right hand side yields

$$\sigma_0^T L^T G_{rc} q_{rc} = \sigma_0^T \int_S N_{un} \, dS \, q_{rc}, \tag{18}$$

where N_{un} are the the projections of the modal functions over the normal to the element side. From the definition of L in (6) we conclude that

$$\int_S N_{dn}^T \, dS \, G_{rc} q_{rc} = \int_S N_{un} \, dS \, q_{rc}. \tag{19}$$

This result may be stated as follows: the force lumping produced by the boundary displacement field should be energy consistent (in the sense of virtual work) with that produced by the displacement field u_{rc} over the element side. Although B_{rc}^q is unique for a given problem, since G_{rc} is generally a rectangular matrix, equation (16) clearly shows that L is not necessarily unique. Examples that illustrate this property may be found in [17]. L is unique for simplex elements where we have the same number of nodal connectors v and rc-modal amplitudes q_{rc}, because in this case G_{rc} is square and non-singular. For these elements the total and basic stiffness matrices coalesce. An obvious example is provided by the constant strain triangle (CST).

6. SECOND CONDITION: PAIRWISE FORCE CANCELLATION

Quoting from [4]: "The basis for the individual element test is that the element, when interacting with its neighbors, should be capable of identically reproducing an arbitrary rigid-body/constant

271

strain field ... The interelement forces transferred at nodes should cancel out in a pairwise manner for adjacent elements during such state." This establishes a second key constraint on **L**.

Suppose we have a side $i - j$ joining elements k and $k + 1$, as illustrated in Figure 1. The second condition requires that

$$\int_i^j \mathbf{N}_{dn}^k \, dS = \int_i^j \mathbf{N}_{dn}^{k+1} \, dS. \tag{20}$$

The easiest way of enforcing this condition is by choosing a boundary displacement **d** that is uniquely defined over $i - j$ by degrees of freedom on that interface.

This rule can be extended to cases in which more than two elements share a side, as is the case in many practical structures. Note that (20) does not involve the internal displacement field in any way. Consequently it establishes the *mixability* of elements of different types (for example, FF with ANDES elements). The SET discussed in [24] omits this important condition.

7. MULTIELEMENT PATCH TESTS AND THE IET

Bergan and coworkers called conditions (13) and (20) the IET. We now prove that if the element under consideration satisfies these conditions, it will also pass the so-called forms A and B of the multielement patch test [24]. Furthermore, if the element is rank sufficient it will also pass form C.
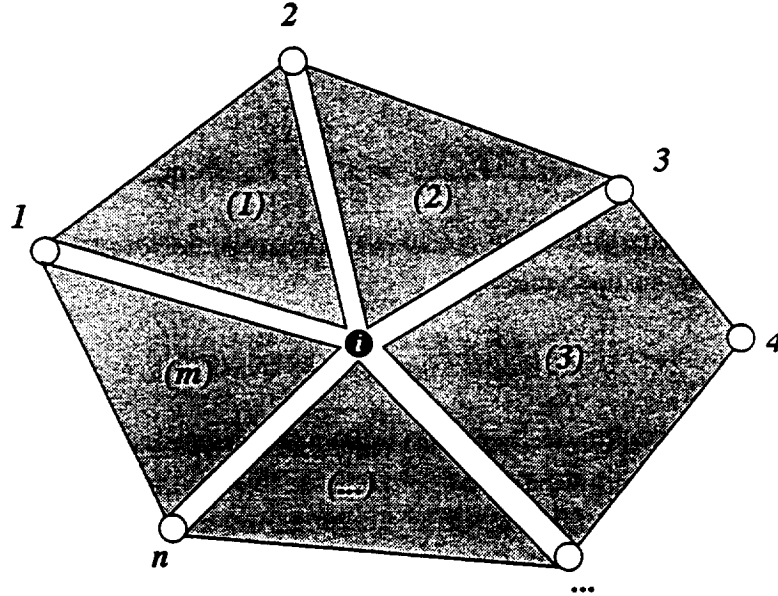
Figure 2. An assemblage of elements

Let us consider the assemblage of elements shown in Figure 2 as a patch. The global displacement field consistent with a constant strain field is $\mathbf{v}_{rc}^g = \mathbf{G}_{rc}^g \mathbf{q}_{rc}$ The stiffness matrix of the kth element satisfies equation (13), or its equivalent global form

$$(\mathbf{P}^k)^T \mathbf{K}^k \mathbf{P}^k \mathbf{v}_{rc}^g = (\mathbf{P}^k)^T \mathbf{L}^k \sigma_0, \tag{21}$$

272

REFERENCES

1. ADINI, A. – *Analysis of Shell Structures by the Finite Element Method*, Ph. D. Dissertation, Dept. of Civil Engineering, University of California, Berkeley, CA, 1961.

2. BAZELEY, G.P., CHEUNG, Y.K., IRONS, B.M. and ZIENKIEWICZ, O.C. – Triangular Elements in Plate Bending – Conforming and Nonconforming Solutions, *Proceedings 1st Conference on Matrix Methods in Structural Mechanics*, AFFDL-TR-66-80, Air Force Institute of Technology, Dayton, Ohio, 1966, p. 547.

3. BATHE, K.J. and DVORKIN, E.N. – A Four-node Plate Bending Element Based on Mindlin/Reissner Plate Theory and a Mixed Interpolation, Int. J. Numer. Meth. Engrg., $\underline{21}$, 367–383 (1985)

4. BERGAN, P.G. and HANSSEN, L. – A New Approach for Deriving 'Good' Finite Elements, MAFELAP II Conference, Brunel University, 1975, in *The Mathematics of Finite Elements and Applications – Volume II*, ed. by J. R. Whiteman, Academic Press, London, 1976.

5. BERGAN, P.G. – Finite Elements Based on Energy Orthogonal Functions, Int. J. Num. Meth. Engrg., $\underline{15}$, 1141–1555 (1980)

6. BERGAN, P.G. and NYGÅRD, M.K. – Finite Elements with Increased Freedom in Choosing Shape Functions, Int. J. Num. Meth. Engrg., $\underline{20}$, 643–664 (1984)

7. FELIPPA, C.A. – Parametrized Multifield Variational Principles in Elasticity: II. Hybrid Functionals and the Free Formulation, Communications in Applied Numerical Methods, $\underline{5}$, 79–88 (1989)

8. FELIPPA, C.A. and MILITELLO, C. – Variational Formulation of High Performance Finite Elements: Parametrized Variational Principles, Computers & Structures, $\underline{36}$, 1–11 (1990)

9. FELIPPA, C.A. and MILITELLO, C. – 'Developments in Variational Methods for High Performance Plate and Shell Elements', in *Analytical and Computational Models for Shells*, CED Vol. 3, Eds. A. K. Noor, T. Belytschko and J. C. Simo, The American Society of Mechanical Engineers, ASME, New York, 1989, p. 191.

10. FRAEIJS DE VEUBEKE, B.M. – Variational Principles and the Patch Test, Int. J. Numer. Meth. Engrg, $\underline{8}$, 783–801 (1974)

11. GRIFFITHS, D.F. and MITCHELL, A.R. – 'Nonconforming Elements', in *The Mathematical Basis of Finite Element Methods*, Ed. Griffiths, D. F., Clarendon Press, Oxford, 1984, p. 41.

12. IRONS, B.M. and RAZZAQUE, A. – 'Experiences with the Patch Test for Convergence of Finite Elements', in *The Mathematical Foundations of the Finite Element Method with Applications to Partial Differential Equations*, Ed. Aziz, A. K., Academic Press, New York, 1972, p. 557.

13. IRONS, B.M. and LOIKKANEN, M. – An Engineer's Defense of the Patch Test, Int. J. Numer. Meth. Engrg., $\underline{19}$, 1391–1401 (1983)

14. MacNEAL, R.H. – Derivation of Element Stiffness Matrices by Assumed Strain Distribution, Nuclear Engrg. Design, $\underline{70}$, 3–12 (1978)

where $\mathbf{P}^k$ are Boolean localization matrices. Upon assembly we obtain

$$\mathbf{K}^g \mathbf{v}_{rc}^g = \mathbf{L}^g \sigma_0 = \mathbf{p}, \tag{22}$$

but because of the satisfaction of equation (20) the force vector $\mathbf{p}$ has only components in nodes $j, \ldots j + n$. Then, for the ith internal degree of freedom we have

$$K_{ij}^g v_{rcj}^g = p_i = 0, \tag{23}$$

which is the statement of the form A of the patch test. If an element satisfies A, form B is also satisfied because from (22) we can obtain the displacement of the internal node i as:

$$v_{rc_i} = (K_{ii}^g)^{-1}(p_i - K_{ij}v_{rc_j}^g), \qquad j \neq i. \tag{24}$$

Because the element satisfies (13), $\mathbf{v}_{rc}$ can be obtained if upon removing the rigid body motions $\mathbf{K}^k$ is nonsingular and can be inverted. Consequently $\mathbf{K}^k$ should be rank sufficient in order to satisfy form C.

8. CONCLUSIONS

It has been shown that the IET constraints plus rank sufficiency provide sufficient conditions to pass any form of the multielement patch test. The main practical advantages of the IET are:

1. By applying rules (13) and (20) elements can be constructed that will pass any multielement patch test *a priori*, provided that they are rank sufficient, while being capable of copying constant strain states. No such possibility exists in the conventional patch test, which must be necessarily applied *a posteriori*.

2. Element mixability is immediately established.

3. A "surgical operation" can be established to "sanitize" elements that fail the IET, as discussed in the Appendix of [17]. The operation essentially amounts to the replacement of the basic stiffness.

The price paid for these advantages is that the test is occasionally stronger than strictly necessary. For example, the BCIZ nonconforming triangle [2] fails the IET but passes the multielement test for certain mesh configurations.

A potential difficulty in the application of the IET to *existing* elements is the need for extracting the force-lumping matrix $\mathbf{L}$. This matrix may not be readily available and, as mentioned in Section 5, is not necessarily unique.

Finally, as remarked in several places, the present statement of the IET is not restricted to the free formulation, and has actually been used in this expanded form for constructing high-performance elements based on the ANDES formulation [8, 9,17,18].

15. MILITELLO, C. and FELIPPA, C.A. – A Variational Justification of the Assumed Natural Strain Formulation of Finite Elements: I. Variational Principles, Computers & Structures, 34, 431–438 (1990)

16. MILITELLO, C. and FELIPPA, C.A. – A Variational Justification of the Assumed Natural Strain Formulation of Finite Elements: II. The Four Node C^0 Plate Element, Computers & Structures, 34, 439–444 (1990)

17. MILITELLO, C. and FELIPPA, C.A. – The First ANDES Elements: 9-DOF Plate Bending Triangles, to appear in Comp. Meth. Appl. Mech. Engrg. (1991)

18. MILITELLO, C. – *Application of Parametrized Variational Principles to the Finite Element Method*, Ph. D. Dissertation, Department of Aerospace Engineering Sciences, University of Colorado, Boulder, CO, 1991.

19. PARK, K.C. and STANLEY, G.M. – A Curved C^0 Shell Element Based on Assumed Natural-Coordinate Strains, Journal of Applied Mechanics, 53, 278–290 (1986)

20. SANDER, G. and BECKERS, P. – 'The Influence of the Choice of Connectors in the Finite Element Method', in *The Mathematical Aspects of the Finite Element Method*, Lecture Notes in Mathematics, Vol. 606, Springer-Verlag, Berlin, 1977, p. 316.

21. STRANG, G. and FIX, G. – *An Analysis of the Finite Element Method*, Prentice-Hall, Englewood Cliffs, N.J., 1973.

22. STUMMEL, F. – The Limitations of the Patch Test, Int. J. Numer. Meth. Engrg., 15, 177–188 (1980)

23. STUMMEL, F. – The Generalized Patch Test, SIAM J. Numer. Anal., 16, 449–471 (1979)

24. TAYLOR, R.L., SIMO, J.C., ZIENKIEWICZ, O.C. and CHAN, A.C. – The Patch Test: A Condition for Assessing FEM Convergence, Int. J. Numer. Meth. Engrg, 22, 39–62 (1986)

25. TOCHER, J.L. and KAPUR, K.K. – Discussion of 'Basis for derivation of matrices for the direct stiffness method' by R. J. Melosh, J. AIAA, 3, 1215–1216 (1965)

26. WILSON, E.L., TAYLOR, R.L., DOHERTY, W.P. and GHABOUSSI, J. – 'Incompatible Displacement Models', in *Numerical and Computer Models in Structural Mechanics*, Eds. S. J. Fenves *et.al.*, Academic Press, New York, 1973, p. 43.

MEMBRANE TRIANGLES WITH CORNER DRILLING FREEDOMS: I. THE EFF ELEMENT

SUMMARY

This paper is the first of a three-Part series that studies the formulation of 3-node, 9-dof membrane elements with normal-to-element-plane rotations (the so-called drilling freedoms) within the context of parametrized variational principles. These principles supply a unified basis for several advanced element-construction techniques; in particular: the free formulation (FF), the extended free formulation (EFF) and the assumed natural deviatoric strain (ANDES) formulation. In Part I we construct an element of this type using the EFF. This derivation illustrates the basic steps in the application of that formulation to the construction of high-performance, rank-sufficient, nonconforming elements with corner rotations. The element is initially given the 12 degrees of freedom of the linear strain triangle (LST), which allows the displacement expansion to be a complete quadratic in each component. The expansion basis contains the 6 linear basic functions and 6 energy-orthogonal quadratic higher order functions. Three degrees of freedom, defined as the midpoint deviations from linearity along the triangle-median directions, are eliminated by kinematic constraints. The remaining hierarchical midpoint freedoms are transformed to corner rotations. The performance of the resulting element is evaluated in Part III.

1. INTRODUCTION

The idea of including normal-rotation degrees of freedom at corner points of plane-stress finite elements — the so-called *drilling freedoms* — is an old one. The main motivations behind this idea are:

1. To improve the element performance while avoiding the use of midpoint degrees of freedom. Midpoint nodes have lower valency than corner nodes, demand extra effort in mesh definition and generation, and can cause modeling difficulties in nonlinear analysis and dynamics.

2. To solve the "normal rotation problem" of smooth shells analyzed with finite elements programs that carry six degrees of freedom per node.

3. To simplify the modeling of connections between plates, shells and beams, as well as the treatment of junctures between shells and/or plates.

Many efforts to develop membrane elements with drilling freedoms were made during the period 1964–1975 with inconclusive results. A summary of this early work is given in the Introduction of an article by Bergan and Felippa [1], where it is remarked that Irons and Ahmad in their 1980 book [2] had dismissed the task as hopeless. In fact, the subject laid largely dormant during the late 1970s, but it has been revived in recent publications [3,1,4–8] that present several solutions to this challenge. Especially noteworthy is the study by Hughes and Brezzi [9] of variational principles that include independent displacement and rotation fields. A membrane element with drilling freedoms based on these principles has recently been constructed by Ibrahimbegovic [10].

The first successful triangles with drilling freedoms were presented by Allman in 1984 [3] and Bergan and Felippa in 1985 [1]. Both elements are nonconforming and pass displacement-specified patch tests. In addition the Bergan-Felippa triangle, being rank sufficient, passes traction-specified patch tests. The original Allman element, based on the concept of *vertex* rotations, had remaining problems such as rank deficiency, which were corrected in an improved version published in 1988 [7]. The two approaches share procedural similarities, such as the use of incompatible displacement functions. But the element construction methods are entirely different: Allman used the conventional potential energy formulation whereas Bergan and Felippa used the free formulation (FF) of Bergan and Nygård [11]. Furthermore Bergan and Felippa, following mid-1960s work at Berkeley and Trondheim [12–15] exploited the concept of continuum-mechanics rotations, sometimes referred to as *true* rotations. A discussion of the relative performance of these elements is given in Part III of this series [16].

Both approaches can be extended to *quadrilateral* elements with drilling freedoms for plane stress and shell analysis. Extensive experience with Allman-type quadrilateral shell elements is reported by Frey and coworkers; see the excellent survey article [17] and references therein. A FF-based quadrilateral called FFQ was constructed by Nygård in his thesis [18] using quadratic and cubic higher order functions; this is presenly a workhorse shell element in the nonlinear program FENRIS [19].

277

At the time the Bergan-Felippa element was constructed (summer 1984) the free formulation lacked a variational basis. This deficiency was remedied five years later by the introduction of parametrized variational principles in a series of recent publications [20–23]. Therein it is shown that the energy-orthogonal FF with scaled higher order stiffness can be accommodated in the framework of a one-parameter d-generalized hybrid variational principle that reduces to hybrid versions of the potential energy and Hellinger-Reissner's principle as special cases. This rigorous justification of the FF opened the door to a variant called the extended free formulation or EFF [24], which circumvents a major kinematic restriction of the FF.

The present work may be viewed as a continuation of two mid-80 papers [1,6] but now on firmer theoretical grounds. Our main objective is to illustrate the application of the EFF to the construction of a triangular membrane element with drilling freedoms that initially has *complete* quadratic polynomial expansions in each displacement component. The use of complete quadratic expansions as departure point requires a total of 12 degrees of freedom. Nine freedoms are defined at the corner nodes in the usual fashion, *i.e.*, six translations and three drilling rotations. Three additional degrees of freedoms, to be subsequently eliminated, are needed. In the EFF such additional freedoms can be eliminated in three ways: duality pairing with divergence-free stresses, static condensation of augmenting degrees of freedom, or *a posteriori* application of kinematic constraints. The present derivation uses the last technique.

Four choices of "eliminable midpoint freedoms" intrinsically related to the triangle geometry were considered: side directions, normal-to-sides, median directions and normal-to-medians. It was found that only the third choice provides for stable elimination. Once this key discovery was made, the remaining element derivation steps, though laborious, could be followed in a systematic way.

2. THE STIFFNESS EQUATIONS

The stiffness equations derived from the parametrized variational principles referenced in the Introduction enjoy the fundamental decomposition property summarized in Box 1. The element stiffness matrix can be additively decomposed into $\mathbf{K} = \mathbf{K}_b + \mathbf{K}_h$ where $\mathbf{K}_b$ is the *basic* stiffness matrix, which is constructed for *convergence*, and $\mathbf{K}_h$ is the *higher order* stiffness matrix, which is constructed for *stability* and *accuracy*. As discussed in Box 1, for free-formulated elements $\mathbf{K}_h$ can be scaled by $(1 - \gamma)$, where γ is a scaling coefficient < 1 that may be used to increase the element performance for coarse meshes. This value may vary from element to element without affecting convergence. This scaling is justified variationally in [20,21]. Multiparameter scaling is discussed in [25] to improve the performance of a specific plate bending element.

The basic stiffness part of the present element (as well as that of the element derived in Part II [26]) is identical to that presented in Bergan and Felippa [1,6]. The higher order stiffness is initially based on a modification of the twelve shape functions of the linear strain triangle (LST). The modification makes the higher order (quadratic) shape functions energy orthogonal to the lower order (linear) ones. The coefficients of these quadratic shape functions are generalized coordinates in terms of which a generalized higher order stiffness matrix is readily constructed in closed form. A chain of transformations follows in which these generalized coordinates are first transformed to midpoint degrees of freedom of the hierarchical LST, and then to three drilling freedoms at corners and three median hierarchical displacements at the midpoints. Finally the latter are eliminated by invoking a parametrized boundary constraint.

The main advantages sought for this element over the FF element of [1,6] are:

1. The higher order stiffness matrix is obtained in explicit form without need of numerical inversion. Explicitness is expected to facilitate the direct derivation of energy-balancing formulas to attain high performance under in-plane bending. This is especially true for orthotropic or anisotropic material behavior.

2. Shorter formation time for $\mathbf{K}_h$, which dominates the computation of $\mathbf{K}$.

3. The coarse-mesh performance should be comparable to that of the linear strain triangle (LST) without the encumbrance of midpoint nodes.

Experience with the EFF element, as reported in Part III [16], indicates that the first two advantages were realized, but the last one was not. Its performance turned out to be similar to that of the original FF element, except for some regular-mesh problems where explicit energy balancing was able to make a difference. The performance is, however, substantially better than all other elements tested for large element aspect ratios.

Aside from its intrinsic value as illustration of a powerful new technique for constructing high-performance elements, the present derivation serves as prelude to a far more challenging task: the construction of a rank-sufficient element in three dimensions (a 24-dof, rank-18 tetrahedron with 12 corner rotations).

3. THE FREE FORMULATION

The original free formulation (FF) was developed by Bergan and Nygård [11] for the construction of displacement-based, incompatible finite elements. This work consolidated a decade of research of Bergan and coworkers at Trondheim, milestones of which may be found in [27,28,19]. The products of this research have been finite elements of high performance, especially for linear and nonlinear analysis of plate and shell structures. As noted in the Introduction, a theoretical justification based on parametrized hybrid variational principles is provided in references [20–23].

The original FF was based on nonconforming displacement assumptions, the principle of virtual work and a specialized form of Irons' patch test that Bergan and Hanssen [27] called the individual element test. The basic and higher order stiffness are constructed in largely independent fashion by following the procedures outlined in Boxes 2 to 4.

Box 2 lists the main steps for constructing the basic stiffness matrix; for justification the reader is referred to the previously cited references. The key steps in constructing the higher order stiffness matrix using the standard free formulation (FF) are listed in Box 3.

The extended free formulation (EFF) presented in [24] removes the restriction $n_v = n_q$ of Step H.1(b) in Box 3 by three methods: (1) injection of higher order divergence-free stress fields, (2) freedom augmentation with elimination by static condensation or (3) freedom augmentation with elimination by kinematic constraints. The last method, which is the one used for the present element, is outlined in Box 4.

Box 1 Decomposition of the Element Stiffness Equations

Let $\mathbf{K}$ be the element stiffness matrix, $\mathbf{v}$ the visible element degrees of freedom (those degrees of freedom in common with other elements, also called the *connectors*) and $\mathbf{p}$ the corresponding element node forces. Then the element stiffness equations decompose as

$$\mathbf{K}\mathbf{v} = (\mathbf{K}_b + \mathbf{K}_h)\,\mathbf{v} = \mathbf{p}. \tag{1}$$

$\mathbf{K}_b$ and $\mathbf{K}_h$ are called the *basic* and *higher order* stiffness matrices, respectively. The basic stiffness matrix, which is usually rank deficient, is constructed for *convergence*. The higher order stiffness matrix is constructed for *stability* and (in more recent work) *accuracy*. A decomposition of this nature, which also holds at the assembly level, was first obtained by Bergan and Nygård in the derivation of the free formulation [11].

In the unified formulation presented in [22, 23] the following key properties of the decomposition (1) are derived.

1. $\mathbf{K}_b$ is *formulation independent* and is defined entirely by an assumed constant stress state working on element boundary displacements. As detailed in Box 2, no knowledge of the interior displacements is necessary for this stiffness component. The extension of this statement to C^0 plate and shell elements is not straightforward, however, and special considerations are necessary in order to obtain $\mathbf{K}_b$ for those elements.

2. $\mathbf{K}_h$ has the general form

$$\mathbf{K}_h = j_{33}\mathbf{K}_{h33} + j_{22}\mathbf{K}_{h22} + j_{23}\mathbf{K}_{h23}. \tag{2}$$

The three parameters j_{22}, j_{23} and j_{33} characterize the source variational principle in the following sense:

   (a) The FF is recovered if $j_{22} = j_{23} = 0$ and $j_{33} = 1 - \gamma$, where γ is a $\mathbf{K}_h$ scaling coefficient studied in [1,6,25]. The original FF of [11] is obtained if $\gamma = 0$. The source variational principle is a one-parameter form that includes the potential energy and stress-displacement Reissner functionals as special cases.

   (b) The ANDES variant of ANS is recovered if $j_{23} = j_{33} = 0$ whereas j_{22} is a scaling parameter. The source variational principle is a one-parameter form that includes Reissner's stress-displacement and Hu-Washizu's functionals as special cases.

   (c) If j_{23} is nonzero, the last term in (2) may be viewed as being produced by a FF/ANDES combination. Such a combination remains unexplored.

Box 2   Construction of the Basic Stiffness K_b

Step B.1.   Assume a *constant* stress field, $\bar{\sigma}$, inside the element. The associated boundary tractions are $\bar{\sigma}_n = \bar{\sigma}.n$, where n denotes the unit external normal on the boundary S.

Step B.2.   Assume boundary displacements, d, over S. This field is described in terms of the *visible* element node displacements v (also called the *connectors*) as

$$d = N_d v, \tag{3}$$

where N_d is an array of boundary shape functions. The boundary motions (2) must satisfy interelement continuity and contain rigid-body and constant-strain motions exactly.

Step B.3.   Construct the "force lumping matrix"

$$L = \int_S N_{dn} \, dS, \tag{4}$$

that consistently maps the boundary tractions $\bar{\sigma}_n = \bar{\sigma}.n$ into element node forces, $\bar{p}$, conjugate to v in the virtual work sense. That is,

$$\bar{p} = \int_S N_n \sigma_n \, dS = L\bar{\sigma}. \tag{5}$$

In the above, $N_{dn} = N_d.n$ are boundary-system projections of N_d that work on the surface tractions $\bar{\sigma}_n$.

Step B.4.   The basic stiffness matrix for a three-dimensional element is

$$K_b = \frac{1}{v} LEL^T, \tag{6}$$

where E is the stress-strain constitutive matrix of elastic moduli, which are assumed to be constant over the element, and $v = \int_V dV$ is the element volume measure. For two-dimensional or one-dimensional elements, v is replaced by the element area A or length ℓ, respectively, if the remaining dimensions are incorporated in the constitutive matrix E.

Box 3   Construction of K_h by FF

Step H.1.   Assume an *internal displacement field* over the element volume V:

$$\mathbf{u} = \mathbf{N}_u\,\mathbf{q} = \underset{rigid\,body}{\mathbf{N}_r\mathbf{q}_r} + \underset{constant\text{-}strain}{\mathbf{N}_c\mathbf{q}_c} + \underset{higher\,order}{\mathbf{N}_h\mathbf{q}_h} \tag{7}$$

where array $\mathbf{N}_u$ collects shape functions and $\mathbf{q}$ collects generalized coordinates. This assumption must satisfy the following conditions:

(a) linear independence with respect to $\mathbf{v}$;

(b) the dimensions n_q and n_v of vectors $\mathbf{q}$ and $\mathbf{v}$, respectively, are the same;

(c) the rigid motions and constant-strain fields are complete;

(d) the higher order displacements are energy orthogonal with respect to the constant-strain displacements. (Although this requirement was not mandatory in the original FF, it is an essential part of the variationally formulated FF.)

Often (7) is written so that the rigid body and constant strain shape functions are combined:

$$\mathbf{u} = \mathbf{N}_{rc}\mathbf{q}_{rc} + \mathbf{N}_h\mathbf{q}_h. \tag{8}$$

Step H.2.   The internal strain field derived from $\mathbf{u}$ is $\mathbf{e}^u = \mathbf{D}\mathbf{u}$, where $\mathbf{D}$ is the strain-displacement operator. Decompose this field as

$$\mathbf{e}^u = \mathbf{D}\mathbf{N}_u\mathbf{q} = \mathbf{e}_c^u + \mathbf{e}_h^u = \mathbf{B}_c\mathbf{q}_c + \mathbf{B}_h\mathbf{q}_h, \tag{9}$$

since the strains associated with rigid body motions, $\mathbf{B}_r\mathbf{q}_r$, must vanish.

Step H.3.   By collocation at the node points assemble the square nonsingular transformation

$$\mathbf{v} = \mathbf{G}\mathbf{q} = \mathbf{G}_r\mathbf{q}_r + \mathbf{G}_c\mathbf{q}_c + \mathbf{G}_h\mathbf{q}_h, \tag{10}$$

which inverted gives

$$\mathbf{q} = \left\{ \begin{array}{c} \mathbf{q}_r \\ \mathbf{q}_c \\ \mathbf{q}_h \end{array} \right\} = \mathbf{H}\mathbf{v} = \left[\begin{array}{c} \mathbf{H}_r \\ \mathbf{H}_c \\ \mathbf{H}_h \end{array} \right] \mathbf{v}. \tag{11}$$

Step H.4.   The higher order stiffness matrix is given by

$$\mathbf{K}_h = (1 - \gamma)\mathbf{H}_h^T\mathbf{K}_{qh}\mathbf{H}_h, \qquad \text{where} \qquad \mathbf{K}_{qh} = \int_V \mathbf{B}_h^T\mathbf{E}\mathbf{B}_h\,dV. \tag{12}$$

$\mathbf{K}_{qh}$ is the generalized stiffness in terms of the $\mathbf{q}_h$ coordinates, and $(1 - \gamma)$ is a scaling parameter (see Box 1).

Box 4   Construction of K_h by EFF with Freedom Augmentation

Step E.1.   The internal displacement expansion is written as in (7) or (8) but now $n_q > n_v$ is allowed. The general prescription is to augment vector v with $n_q - n_v$ degrees of freedom collected in subvector v_x. These additional degrees of freedom must be chosen so as to produce an invertible square transformation matrix with the following hierarchical structure:

$$\left\{ \begin{array}{c} v \\ v_x \end{array} \right\} = \begin{bmatrix} G_r & G_c & G_h \\ 0 & 0 & G_x \end{bmatrix} \left\{ \begin{array}{c} q_r \\ q_c \\ q_h \end{array} \right\} = Gq. \tag{13}$$

Step E.2.   Solving (13) for q one obtains an inverse relation of the form

$$q = \left\{ \begin{array}{c} q_r \\ q_c \\ q_h \end{array} \right\} = \begin{bmatrix} H_r & 0 \\ H_c & 0 \\ H_h' & H_x \end{bmatrix} \left\{ \begin{array}{c} v \\ v_x \end{array} \right\}. \tag{14}$$

Step E.3.   Eliminate v_x through a kinematic constraint, say

$$v_x = Tv \tag{15}$$

Then

$$q = \begin{bmatrix} H_r \\ H_c \\ H_h' + H_x T \end{bmatrix} v = \begin{bmatrix} H_r \\ H_c \\ H_h \end{bmatrix} v. \tag{16}$$

Having H_h available, proceed as in step H.4 of Box 3.

Many variations and shortcuts are possible. For example, often H_h can be expressed as the product of k transformation matrices:

$$H_h = H_{h1} H_{h2} \dots H_{hk}. \tag{17}$$

some of which can be directly constructed whereas others result from solving simpler inverse problems. If all matrices in (17) can be determined in closed form the numerical inversion of G is avoided. This is the approach followed in the element constructed here.

4. ELEMENT GEOMETRY

The geometry of an individual triangle is illustrated in Figures 1 and 2. The triangle has *straight sides*. Its geometry is completely defined by the location of its three corners, which are labeled 1,2,3, traversed counterclockwise. The element is referred to a local Cartesian system (x, y). The Cartesian distances from the nodes to the triangle centroid $x_0 = (x_1 + x_2 + x_3)/3$, $y_0 = (y_1 + y_2 + y_3)/3$ are denoted by $x_{i0} = x_i - x_0$ and $y_{i0} = y_i - y_0$. It follows that

$$x_{10} + x_{20} + x_{30} = 0, \qquad y_{10} + y_{20} + y_{30} = 0. \tag{18}$$

Node coordinate differences are abbreviated by writing $x_{ij} = x_i - x_j$, etc. The signed triangle area A is given by the formulas

$$2A = x_{21}y_{31} - x_{31}y_{21} = x_{32}y_{12} - x_{12}y_{32} = x_{13}y_{23} - x_{23}y_{13}, \tag{19}$$

and we require that $A > 0$. We shall also make use of dimensionless triangular area coordinates ζ_1, ζ_2, ζ_3 linked by the constraint

$$\zeta_1 + \zeta_2 + \zeta_3 = 1. \tag{20}$$

The following well known relation between the area and Cartesian coordinates of a straight-sided triangle is noted for further use:

$$\zeta_i = \frac{1}{2A}\left[x_i y_k - x_k y_j + (x - x_0)y_{jk} + (y - y_0)x_{kj} \right], \tag{21}$$

where i, j and k denote positive cyclic permutations of 1, 2 and 3; for example, $i = 2$, $j = 3$, $k = 1$. (If the origin is taken at the centroid, $x_0 = y_0 = 0$.) It follows that

$$2A\frac{\partial \zeta_1}{\partial x} = y_{23}, \qquad 2A\frac{\partial \zeta_2}{\partial x} = y_{31}, \qquad 2A\frac{\partial \zeta_3}{\partial x} = y_{12},$$
$$2A\frac{\partial \zeta_1}{\partial y} = x_{32}, \qquad 2A\frac{\partial \zeta_2}{\partial y} = x_{13}, \qquad 2A\frac{\partial \zeta_3}{\partial y} = x_{21}. \tag{22}$$

Other intrinsic dimensions of use in subsequent derivations are

$$\ell_{ij} = \ell_{ji} = \sqrt{x_{ij}^2 + y_{ij}^2}, \qquad a_{ij} = a_{ji} = \tfrac{3}{2}\sqrt{x_{k0}^2 + y_{k0}^2}, \qquad b_{ij} = 2A/a_{ij},$$
$$S_1 = \tfrac{1}{4}(\ell_{12}^2 - \ell_{31}^2), \qquad S_2 = \tfrac{1}{4}(\ell_{23}^2 - \ell_{12}^2), \qquad S_3 = \tfrac{1}{4}(\ell_{13}^2 - \ell_{23}^2). \tag{23}$$

in which j and k denote the positive cyclic permutations of i; for example $i = 2$, $j = 3$, $k = 1$. The a_{ij} are the lengths of the triangle medians (see Figure 2).

In addition to the corner nodes 1, 2 and 3 we shall also use the element midpoints 4, 5 and 6 for intermediate derivations although these nodes will not appear in the final equations. These are located opposite corners 3, 1 and 2, respectively. As shown in Figures 1 and 2, two intrinsic coordinate systems are used on each side:

$$n_{21}, s_{21}, \qquad n_{32}, s_{32}, \qquad n_{13}, s_{13}, \tag{24}$$

285
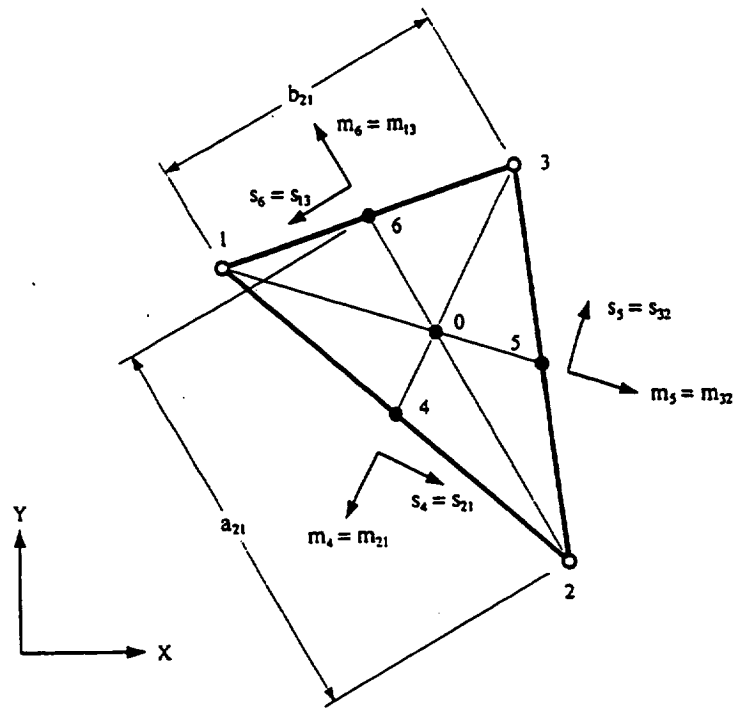
Figure 1. Triangle geometry, showing Cartesian and normal/tangential coordinate systems.
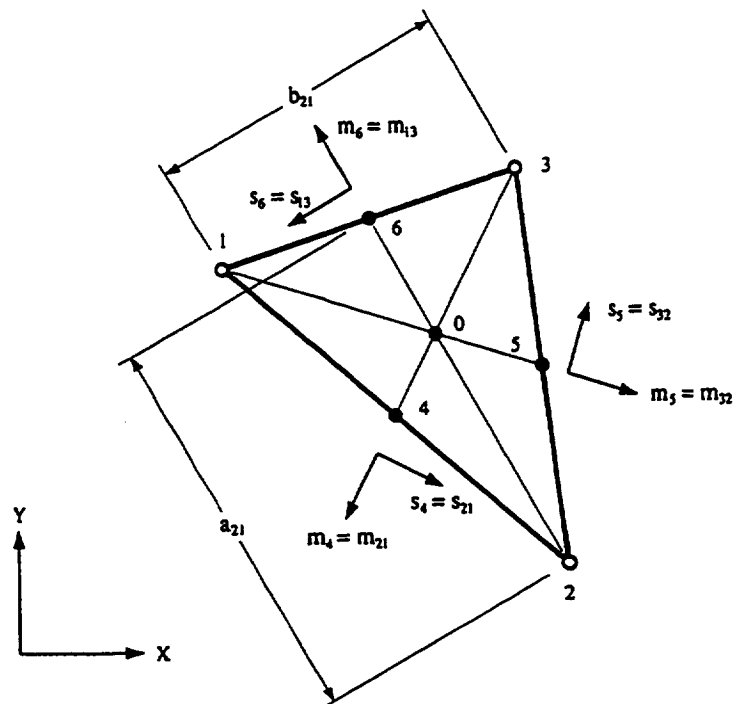

Figure 2. Intrinsic triangle dimensions and median/normal-to-median coordinate systems.

$$m_{21}, t_{21}, \quad m_{32}, t_{32}, \quad m_{13}, t_{13}. \tag{25}$$

Here n and s are oriented along the external normal-to-side and side directions, respectively, whereas m and t are oriented along the triangle median and normal-to-median directions, respectively. Note that the two coordinate sets (24)-(25) coincide only for equilateral triangles. The origin of these systems is left "floating" and may be adjusted as appropriate. If the origin is placed at the midpoints, subscripts 4, 5 and 6 may be used instead of 21, 32 and 13, respectively, as illustrated in Figure 2.

The visible degrees of freedom of the element collected in vector v are

$$\mathbf{v}^T = [\, v_{x1} \quad v_{y1} \quad \theta_1 \quad v_{x2} \quad v_{y2} \quad \theta_2 \quad v_{x3} \quad v_{y3} \quad \theta_3 \,]. \tag{26}$$

Here v_{xi} and v_{yi} denote the nodal values of the translational displacements u_x and u_y along x and y, respectively, and θ are the "drilling rotations" about z defined by

$$\theta = \theta_z = \tfrac{1}{2}\left(\frac{\partial u_y}{\partial x} - \frac{\partial u_x}{\partial y} \right). \tag{27}$$

5. THE BASIC STIFFNESS

The assumed constant stress field of Step B.1 of Box 2 is

$$\sigma_{xx} = \overline{\sigma}_{xx}, \qquad \sigma_{yy} = \overline{\sigma}_{yy}, \qquad \tau_{xy} = \overline{\tau}_{xy}. \tag{28}$$

For Step B.2, the boundary displacements (d_n, d_s) along side $j-k$ opposite corner i in the normal/tangential side coordinate system (n_{jk}, s_{jk}) may be expressed in terms of the visible node displacements as

$$\begin{Bmatrix} d_n \\ d_s \end{Bmatrix} = \begin{bmatrix} \psi_{nj} & 0 & \alpha_b \psi_{\theta j} & \psi_{nk} & 0 & \alpha_b \psi_{\theta k} \\ 0 & \psi_{sj} & 0 & 0 & \psi_{sk} & 0 \end{bmatrix} \begin{Bmatrix} v_{nj} \\ v_{sj} \\ \theta_j \\ v_{nk} \\ v_{sk} \\ \theta_k \end{Bmatrix} \tag{29}$$

with the shape functions

$$\begin{aligned}
\psi_{nj} &= \tfrac{1}{4}(1-\xi)^2(2+\xi), & \psi_{\theta j} &= \tfrac{1}{8}\ell(1-\xi)^2(1+\xi), \\
\psi_{nk} &= \tfrac{1}{4}(1+\xi)^2(2-\xi) & \psi_{\theta k} &= -\tfrac{1}{8}\ell(1+\xi)^2(1-\xi), \\
\psi_{sj} &= \tfrac{1}{2}(1-\xi), & \psi_{sk} &= \tfrac{1}{2}(1+\xi).
\end{aligned} \tag{30}$$

Here ξ is the isoparametric side coordinate $\xi = (2s/\ell) - 1$, which varies from -1 at node j $(s=0)$ to $+1$ at node k $(s=\ell)$; s being the side distance from node j and $\ell = \ell_{jk}$ the triangle side length. A scaling factor α_b has been introduced on the shape functions that relate boundary normal

displacements to the corner rotations. The significance of this factor is discussed by Bergan and Felippa [1]. (In that work this parameter is called α. The subscript b is used here to distinguish this parameter from a similar one that appears in the derivation of the higher order stiffness.)

The surface tractions along a side of the element are

$$\overline{\sigma}_n = \left\{ \begin{array}{c} \overline{\sigma}_{nn} \\ \overline{\sigma}_{ns} \end{array} \right\} = \left[\begin{array}{ccc} \cos^2 \omega & \sin^2 \omega & 2\sin\omega\cos\omega \\ -\sin\omega\cos\omega & \sin\omega\cos\omega & \cos^2\omega - \sin^2\omega \end{array} \right] \left\{ \begin{array}{c} \overline{\sigma}_{xx} \\ \overline{\sigma}_{yy} \\ \overline{\sigma}_{xy} \end{array} \right\}, \qquad (31)$$

in which $\omega = \omega_{jk}$ is the angle of the external normal with x. In [1] it is shown that on carrying out the boundary integrals of Eq. (4) one obtains the force lumping matrix

$$\mathbf{L} = \tfrac{1}{2} \left[\begin{array}{ccc} y_{23} & 0 & x_{32} \\ 0 & x_{32} & y_{23} \\ \tfrac{1}{6}\alpha_b y_{23}(y_{13} - y_{21}) & \tfrac{1}{6}\alpha_b x_{32}(x_{31} - x_{12}) & \tfrac{1}{3}\alpha_b(x_{31}y_{13} - x_{12}y_{21}) \\ y_{31} & 0 & x_{13} \\ 0 & x_{13} & y_{31} \\ \tfrac{1}{6}\alpha_b y_{31}(y_{21} - y_{32}) & \tfrac{1}{6}\alpha_b x_{13}(x_{12} - x_{23}) & \tfrac{1}{3}\alpha_b(x_{12}y_{21} - x_{23}y_{32}) \\ y_{12} & 0 & x_{21} \\ 0 & x_{21} & y_{12} \\ \tfrac{1}{6}\alpha_b y_{12}(y_{32} - y_{13}) & \tfrac{1}{6}\alpha_b x_{21}(x_{23} - x_{31}) & \tfrac{1}{3}\alpha_b(x_{23}y_{32} - x_{31}y_{13}) \end{array} \right] . \qquad (32)$$

If $\alpha_b = 0$ the force lumping matrix of the constant strain triangle (CST) results, in which case all nodal forces are associated with translations only. Once $\mathbf{L}$ is available, it is a simple matter to form the basic stiffness $\mathbf{K}_b$ according to the prescription (6), which for a two-dimensional element becomes

$$\mathbf{K}_b = \frac{1}{A} \mathbf{L}\,(h\mathbf{E})\,\mathbf{L}^T, \qquad (33)$$

where h is the mean thickness of the element and $\mathbf{E}$ the plane stress constitutive matrix arranged as a symmetric 3×3 matrix in the usual manner:

$$\mathbf{E} = \left[\begin{array}{ccc} E_{11} & E_{12} & E_{13} \\ E_{21} & E_{22} & E_{23} \\ E_{13} & E_{23} & E_{33} \end{array} \right] \qquad (34)$$

Often the *thickness-integrated constitutive matrix* $\mathbf{D}_m = h\mathbf{E}$ is specified instead of $\mathbf{E}$. This is particularly useful for nonhomogeneous plates where $\mathbf{E}$ varies through the thickness.

6. THE HIGHER ORDER STIFFNESS

6.1 The Internal Displacement Field

The construction of the EFF higher order stiffness requires a considerable amount of analytical derivations, the details of which are given in the Appendix. In the present Section only the key results are reported. One starts by expressing the internal displacement field u of Boxes 3–4 as

$$\begin{Bmatrix} u_x \\ u_y \end{Bmatrix} = \begin{bmatrix} q_{x1} & q_{x2} & q_{x3} & q_{x4} & q_{x5} & q_{x6} \\ q_{y1} & q_{y2} & q_{y3} & q_{y4} & q_{y5} & q_{y6} \end{bmatrix} \begin{Bmatrix} \phi_1 \\ \phi_2 \\ \phi_3 \\ \phi_4 \\ \phi_5 \\ \phi_6 \end{Bmatrix} \tag{35}$$

where the q's are generalized coordinates, and

$$\phi_1 = \zeta_1, \qquad \phi_2 = \zeta_2, \qquad \phi_3 = \zeta_3,$$

$$\phi_4 = (\zeta_1 - \zeta_2)^2 = \zeta_{12}^2, \quad \phi_5 = (\zeta_2 - \zeta_3)^2 = \zeta_{23}^2, \quad \phi_6 = (\zeta_3 - \zeta_1)^2 = \zeta_{31}^2. \tag{36}$$

This expansion befits the form (7), with

$$\mathbf{q}_{rc}^T = [\, q_{x1} \quad q_{x2} \quad q_{x3} \quad q_{y1} \quad q_{y2} \quad q_{y3} \,] \tag{37}$$

$$\mathbf{q}_h^T = [\, q_{x4} \quad q_{x5} \quad q_{x6} \quad q_{y4} \quad q_{y5} \quad q_{y6} \,] \tag{38}$$

Note that rigid body and constant strain terms coalesce into one set of linear shape functions. It is shown in Section A.2 of the Appendix that the six basis functions (36) enjoy the following properties:

1. They span a complete quadratic basis.

2. The higher order base functions ϕ_4, ϕ_5 and ϕ_6 are energy orthogonal to the basic functions ϕ_1, ϕ_2 and ϕ_3.

6.2 Gradients and Strains

The displacement gradients are obtained by differentiating (35) with respect to x and y:

$$\begin{Bmatrix} \dfrac{\partial u_x}{\partial x} \\[4pt] \dfrac{\partial u_x}{\partial y} \\[4pt] \dfrac{\partial u_y}{\partial x} \\[4pt] \dfrac{\partial u_y}{\partial y} \end{Bmatrix} = \frac{1}{2A} \begin{bmatrix} q_{x1} & q_{x2} & q_{x3} & 0 & 0 & 0 & q_{x4} & q_{x5} & q_{x6} & 0 & 0 & 0 \\ 0 & 0 & 0 & q_{x1} & q_{x2} & q_{x3} & 0 & 0 & 0 & q_{x4} & q_{x5} & q_{x6} \\ q_{y1} & q_{y2} & q_{y3} & 0 & 0 & 0 & q_{y4} & q_{y5} & q_{y6} & 0 & 0 & 0 \\ 0 & 0 & 0 & q_{y1} & q_{y2} & q_{y3} & 0 & 0 & 0 & q_{y4} & q_{y5} & q_{y6} \end{bmatrix} \begin{Bmatrix} y_{23} \\ y_{31} \\ y_{12} \\ x_{32} \\ x_{13} \\ x_{21} \\ 6\zeta_{21}y_{30} \\ 6\zeta_{32}y_{10} \\ 6\zeta_{13}y_{20} \\ 6\zeta_{21}x_{30} \\ 6\zeta_{32}x_{10} \\ 6\zeta_{13}x_{20} \end{Bmatrix} \tag{39}$$

where use of (18) has been made in the derivation of the last six entries in the rightmost vector. The displacement-derived element strains may be conveniently split as in (9):

$$\mathbf{e}^u = \begin{Bmatrix} \epsilon_{xx} \\ \epsilon_{yy} \\ \gamma_{xy} \end{Bmatrix} = \begin{Bmatrix} \partial u_x/\partial x \\ \partial u_y/\partial y \\ \partial u_x/\partial y + \partial u_y/\partial x \end{Bmatrix} = \mathbf{e}_c^u + \mathbf{e}_h^u = \mathbf{B}_{rc}\mathbf{q}_{rc} + \mathbf{B}_h\mathbf{q}_h \qquad (40)$$

where $\mathbf{e}_c^u$ and $\mathbf{e}_h^u$ are associated with constant strain and higher order terms, respectively, as discussed in Box 3. The strain-displacement matrices are

$$\mathbf{B}_{rc} = \frac{1}{2A}\begin{bmatrix} y_{23} & y_{31} & y_{12} & 0 & 0 & 0 \\ 0 & 0 & 0 & x_{32} & x_{13} & x_{21} \\ x_{32} & x_{13} & x_{21} & y_{23} & y_{31} & y_{12} \end{bmatrix} \qquad (41)$$

and

$$\mathbf{B}_h = \frac{3}{A}\begin{bmatrix} \zeta_{21}y_{30} & \zeta_{32}y_{10} & \zeta_{13}y_{20} & 0 & 0 & 0 \\ 0 & 0 & 0 & \zeta_{12}x_{30} & \zeta_{23}x_{10} & \zeta_{31}x_{20} \\ \zeta_{12}x_{30} & \zeta_{23}x_{10} & \zeta_{31}x_{20} & \zeta_{21}y_{30} & \zeta_{32}y_{10} & \zeta_{13}y_{20} \end{bmatrix} = \overline{\mathbf{B}}_h\mathbf{Z}, \qquad (42)$$

where

$$\overline{\mathbf{B}}_h = \frac{3}{A}\begin{bmatrix} y_{30} & y_{10} & y_2 & 0 & 0 & 0 \\ 0 & 0 & 0 & -x_{30} & -x_{10} & -x_{20} \\ -x_{30} & -x_{10} & -x_{20} & y_{30} & y_{10} & y_{20} \end{bmatrix}, \quad \mathbf{Z} = \begin{bmatrix} \zeta_{21} & 0 & 0 & 0 & 0 & 0 \\ 0 & \zeta_{32} & 0 & 0 & 0 & 0 \\ 0 & 0 & \zeta_{13} & 0 & 0 & 0 \\ 0 & 0 & 0 & \zeta_{21} & 0 & 0 \\ 0 & 0 & 0 & 0 & \zeta_{32} & 0 \\ 0 & 0 & 0 & 0 & 0 & \zeta_{13} \end{bmatrix}. \qquad (43)$$

6.3 The Generalized Higher Order Stiffness Matrix

The higher order stiffness matrix in terms of $\mathbf{q}_h$ is given by the second of (12), which for a plate of thickness h becomes

$$\mathbf{K}_{qh} = \int_A \mathbf{B}_h^T (h\mathbf{E})\,\mathbf{B}_h\,dA. \qquad (44)$$

For constant $h\mathbf{E}$ we can express (44) in closed form as

$$\underset{6\times6}{\mathbf{K}_{qh}} = A\,\underset{6\times6}{\overline{\mathbf{B}}_h^T}\,\underset{3\times3}{h\mathbf{E}}\,\underset{3\times6}{\overline{\mathbf{B}}_h} * \underset{6\times6}{\mathbf{J}}, \qquad (45)$$

where the asterisk denotes *entry-by-entry matrix product*, and $\mathbf{J}$ is a purely numeric matrix:

$$\mathbf{J} = \frac{1}{A}\int_A \begin{Bmatrix} \zeta_{21} \\ \zeta_{32} \\ \zeta_{13} \\ \zeta_{21} \\ \zeta_{32} \\ \zeta_{13} \end{Bmatrix} \begin{bmatrix} \zeta_{21} & \zeta_{32} & \zeta_{13} & \zeta_{21} & \zeta_{32} & \zeta_{13} \end{bmatrix} dA = \frac{1}{12}\begin{bmatrix} 2 & -1 & -1 & 2 & -1 & -1 \\ -1 & 2 & -1 & -1 & 2 & -1 \\ -1 & -1 & 2 & -1 & -1 & 2 \\ 2 & -1 & -1 & 2 & -1 & -1 \\ -1 & 2 & -1 & -1 & 2 & -1 \\ -1 & -1 & 2 & -1 & -1 & 2 \end{bmatrix}. \qquad (46)$$

The explicit expression for the upper triangle entries of K_{qh} is as follows:

$$K_{qh}[1,1] = 2k(E_{11}y_{30}^2 - 2E_{13}x_{30}y_{30} + E_{33}x_{30}^2)$$

$$K_{qh}[1,2] = k((E_{13}x_{10} - E_{11}y_{10})y_{30} + (E_{13}y_{10} - E_{33}x_{10})x_{30})$$

$$K_{qh}[1,3] = k((E_{13}x_{20} - E_{11}y_{20})y_{30} + (E_{13}y_{20} - E_{33}x_{20})x_{30})$$

$$K_{qh}[1,4] = 2k(E_{13}y_{30}^2 - (E_{33} + E_{12})x_{30}y_{30} + E_{23}x_{30}^2)$$

$$K_{qh}[1,5] = k((E_{12}x_{10} - E_{13}y_{10})y_{30} + (E_{33}y_{10} - E_{23}x_{10})x_{30})$$

$$K_{qh}[1,6] = k((E_{12}x_{20} - E_{13}y_{20})y_{30} + (E_{33}y_{20} - E_{23}x_{20})x_{30})$$

$$K_{qh}[2,2] = 2k(E_{11}y_{10}^2 - 2E_{13}x_{10}y_{10} + E_{33}x_{10}^2)$$

$$K_{qh}[2,3] = k((E_{13}x_{10} - E_{11}y_{10})y_{20} + (E_{13}y_{10} - E_{33}x_{10})x_{20})$$

$$K_{qh}[2,4] = k((E_{33}x_{10} - E_{13}y_{10})y_{30} + (E_{12}y_{10} - E_{23}x_{10})x_{30})$$

$$K_{qh}[2,5] = 2k(E_{13}y_{10}^2 - (E_{33} + E_{12})x_{10}y_{10} + E_{23}x_{10}^2)$$

$$K_{qh}[2,6] = k((E_{33}x_{10} - E_{13}y_{10})y_{20} + (E_{12}y_{10} - E_{23}x_{10})x_{20})$$

$$K_{qh}[3,3] = 2k(E_{11}y_{20}^2 - 2E_{13}x_{20}y_{20} + E_{33}x_{20}^2)$$

$$K_{qh}[3,4] = k((E_{33}x_{20} - E_{13}y_{20})y_{30} + (E_{12}y_{20} - E_{23}x_{20})x_{30})$$

$$K_{qh}[3,5] = k((E_{12}x_{10} - E_{13}y_{10})y_{20} + (E_{33}y_{10} - E_{23}x_{10})x_{20})$$

$$K_{qh}[3,6] = 2k(E_{13}y_{20}^2 - (E_{33} + E_{12})x_{20}y_{20} + E_{23}x_{20}^2)$$

$$K_{qh}[4,4] = 2k(E_{33}y_{30}^2 - 2E_{23}x_{30}y_{30} + E_{22}x_{30}^2)$$

$$K_{qh}[4,5] = k((E_{23}x_{10} - E_{33}y_{10})y_{30} + (E_{23}y_{10} - E_{22}x_{10})x_{30})$$

$$K_{qh}[4,6] = k((E_{23}x_{20} - E_{33}y_{20})y_{30} + (E_{23}y_{20} - E_{22}x_{20})x_{30})$$

$$K_{qh}[5,5] = 2k(E_{33}y_{10}^2 - 2E_{23}x_{10}y_{10} + E_{22}x_{10}^2)$$

$$K_{qh}[5,6] = k((E_{23}x_{10} - E_{33}y_{10})y_{20} + (E_{23}y_{10} - E_{22}x_{10})x_{20})$$

$$K_{qh}[6,6] = 2k(E_{33}y_{20}^2 - 2E_{23}x_{20}y_{20} + E_{22}x_{20}^2)$$

where $k = 3/(2A^2)$. Having formed K_{qh}, the first of (12) says that the higher order stiffness is $K_h = (1 - \gamma)H_h^T K_{qh}H_h$. Thus the 6×9 matrix H_h, which relates $q_h = H_h v$, remains to be determined.

6.4 Building H_h

We will build H_h as the product of five transformation matrices:

$$\underset{6\times9}{H_h} = \underset{6\times6}{H_{qm}} \; \underset{6\times6}{H_{ms}} \; \underset{6\times6}{H_{sr}} \; \underset{6\times3}{H_{r\theta}} \; \underset{3\times9}{H_{\theta v}}. \tag{47}$$

These five matrices link the following vectors:

$$q_h = H_{qm}m, \quad m = H_{ms}s, \quad s = H_{ms}r, \quad r = H_{r\theta}\tilde{\theta}, \quad \tilde{\theta} = H_{\theta v}v. \tag{48}$$

291

Vectors $\mathbf{q}_h$ and $\mathbf{v}$ are given by (38) and (24), respectively. The others are

$$
\mathbf{m} = \begin{Bmatrix} \tilde{u}_{x4} \\ \tilde{u}_{x5} \\ \tilde{u}_{x6} \\ \tilde{u}_{y4} \\ \tilde{u}_{y5} \\ \tilde{u}_{y6} \end{Bmatrix}, \qquad
\mathbf{s} = \begin{Bmatrix} \tilde{u}_{m4} \\ \tilde{u}_{m5} \\ \tilde{u}_{m6} \\ \tilde{u}_{t4} \\ \tilde{u}_{t5} \\ \tilde{u}_{t6} \end{Bmatrix}, \qquad
\mathbf{r} = \begin{Bmatrix} \tilde{u}_{m4} \\ \tilde{u}_{m5} \\ \tilde{u}_{m6} \\ \tilde{\theta}_1 \\ \tilde{\theta}_2 \\ \tilde{\theta}_3 \end{Bmatrix}, \qquad
\tilde{\theta} = \begin{Bmatrix} \tilde{\theta}_1 \\ \tilde{\theta}_2 \\ \tilde{\theta}_3 \end{Bmatrix}.
\tag{49}
$$

Here $\mathbf{m}$, $\mathbf{s}$ and $\mathbf{r}$ collects $x-y$ and $m-t$ midpoint degrees of freedom, respectively, of the hierarchical LST element discussed in Sections A.1-A.2 of the Appendix (recall that m and t denote median and normal-to-median directions). Vector $\tilde{\theta}$ collects the hierarchical corner rotations $\tilde{\theta}_i$ defined in Section A.3. We list below the expression of the matrices in (47), referring all derivations to the Appendix.

$$
\mathbf{H}_{qm} = \tfrac{1}{9} \begin{bmatrix}
-10 & 2 & 2 & 0 & 0 & 0 \\
2 & -10 & 2 & 0 & 0 & 0 \\
2 & 2 & -10 & 0 & 0 & 0 \\
0 & 0 & 0 & -10 & 2 & 2 \\
0 & 0 & 0 & 2 & -10 & 2 \\
0 & 0 & 0 & 2 & 2 & -10
\end{bmatrix}
\tag{50}
$$

$$
\mathbf{H}_{ms} = -\tfrac{3}{2} \begin{bmatrix}
x_{30}/a_{12} & 0 & 0 & -y_{30}/a_{12} & 0 & 0 \\
0 & x_{10}/a_{23} & 0 & 0 & -y_{10}/a_{23} & 0 \\
0 & 0 & x_{20}/a_{31} & 0 & 0 & -y_{20}/a_{31} \\
y_{30}/a_{12} & 0 & 0 & x_{30}/a_{12} & 0 & 0 \\
0 & y_{10}/a_{23} & 0 & 0 & x_{10}/a_{23} & 0 \\
0 & 0 & y_{20}/a_{31} & 0 & 0 & x_{20}/a_{31}
\end{bmatrix},
\tag{51}
$$

$$
\mathbf{H}_{sr} = \begin{bmatrix}
1 & 0 & 0 & 0 & 0 & 0 \\
0 & 1 & 0 & 0 & 0 & 0 \\
0 & 0 & 1 & 0 & 0 & 0 \\
\dfrac{S_3}{A} & \dfrac{a_{12}a_{23}}{A} & \dfrac{-a_{12}a_{31}}{A} & \tfrac{1}{2}a_{12} & \tfrac{1}{2}a_{12} & -\tfrac{1}{2}a_{12} \\
\dfrac{-a_{23}a_{12}}{A} & \dfrac{S_1}{A} & \dfrac{a_{23}a_{31}}{A} & -\tfrac{1}{2}a_{23} & \tfrac{1}{2}a_{23} & \tfrac{1}{2}a_{23} \\
\dfrac{a_{31}a_{12}}{A} & \dfrac{-a_{31}a_{23}}{A} & \dfrac{S_2}{A} & \tfrac{1}{2}a_{31} & -\tfrac{1}{2}a_{31} & \tfrac{1}{2}a_{31}
\end{bmatrix}
\tag{52}
$$

$$
\mathbf{H}_{r\theta} = \begin{bmatrix} -\dfrac{A\alpha_h}{4a_{12}} & \dfrac{A\alpha_h}{4a_{12}} & 0 \\[2mm] 0 & -\dfrac{A\alpha_h}{4a_{23}} & \dfrac{A\alpha_h}{4a_{23}} \\[2mm] \dfrac{A\alpha_h}{4a_{31}} & 0 & -\dfrac{A\alpha_h}{4a_{31}} \\[2mm] 1 & 0 & 0 \\ 0 & 1 & 0 \\ 0 & 0 & 1 \end{bmatrix}
\tag{53}
$$

Here the a's and s's are defined in (23), and α_h is a scalar parameter introduced in Section A.6 of the Appendix. Finally,

$$
\mathbf{H}_{\theta v} = \frac{1}{4A} \begin{bmatrix} x_{32} & y_{32} & 4A & x_{13} & y_{13} & 0 & x_{21} & y_{21} & 0 \\ x_{32} & y_{32} & 0 & x_{13} & y_{13} & 4A & x_{21} & y_{21} & 0 \\ x_{32} & y_{32} & 0 & x_{13} & y_{13} & 0 & x_{21} & y_{21} & 4A \end{bmatrix}.
\tag{54}
$$

6.5 Closed Form Evaluation

Multiplying symbolically the middle three matrices in (47) a surprisingly simple closed-form expression emerges for $\mathbf{H}_{m\theta} = \mathbf{H}_{ms}\mathbf{H}_{sr}\mathbf{H}_{r\theta}$. If we choose $\alpha_h = 5/4$, which as shown in Part III is optimal for pure bending, then

$$
\mathbf{H}_{m\theta} = \frac{3}{16}
\begin{bmatrix}
\dfrac{(-S_3 + \frac{3}{5}a_{12}^2)y_{30} + Ax_{30}}{\frac{2}{5}a_{12}^2} & \dfrac{(S_3 + \frac{3}{5}a_{12}^2)y_{30} - Ax_{30}}{\frac{2}{5}a_{12}^2} & y_{30} \\[4mm]
y_{10} & \dfrac{(-S_1 + \frac{3}{5}a_{23}^2)y_{10} + Ax_{10}}{\frac{2}{5}a_{23}^2} & \dfrac{(S_1 + \frac{3}{5}a_{23}^2)y_{10} - Ax_{10}}{\frac{2}{5}a_{23}^2} \\[4mm]
\dfrac{(S_2 + \frac{3}{5}a_{31}^2)y_{20} - Ax_{20}}{\frac{2}{5}a_{31}^2} & y_{20} & \dfrac{(S_2 - \frac{3}{5}a_{31}^2)y_{20} - Ax_{20}}{\frac{2}{5}a_{31}^2} \\[4mm]
\dfrac{(S_3 - \frac{3}{5}a_{12}^2)x_{30} + Ay_{30}}{\frac{2}{5}a_{12}^2} & \dfrac{(-S_3 - \frac{3}{5}a_{12}^2)x_{30} + Ay_{30}}{\frac{2}{5}a_{12}^2} & -x_{30} \\[4mm]
-x_{10} & \dfrac{(S_1 - \frac{3}{5}a_{23}^2)x_{10} + Ay_{10}}{\frac{2}{5}a_{23}^2} & \dfrac{(-S_1 - \frac{3}{5}a_{23}^2)x_{10} - Ay_{10}}{\frac{2}{5}a_{23}^2} \\[4mm]
\dfrac{(-S_2 - \frac{3}{5}a_{31}^2)x_{20} - Ay_{20}}{\frac{2}{5}a_{31}^2} & -x_{20} & \dfrac{(S_2 - \frac{3}{5}a_{31}^2)x_{20} + Ay_{20}}{\frac{2}{5}a_{31}^2}
\end{bmatrix}
\tag{55}
$$

With $\mathbf{H}_{m\theta}$ directly computable, the fastest evaluation of $\mathbf{K}_h$ is obtained as follows. First form $\mathbf{H}_{q\theta} = \mathbf{H}_{qm}\mathbf{H}_{m\theta}$, which can be done quickly because (50) is a block-diagonal numeric matrix. Next, obtain the higher order stiffness in terms of hierarchical rotations:

$$
\underset{3\times 3}{\mathbf{K}_{\theta h}} = \underset{3\times 6}{\mathbf{H}_{q\theta}^T} \; \underset{6\times 6}{\mathbf{K}_{qh}} \; \underset{6\times 3}{\mathbf{H}_{q\theta}}.
\tag{56}
$$

Finally, K_h is obtained from

$$K_h = (1 - \gamma)H_{\theta v}^T \, K_{\theta h} \, H_{\theta v}. \tag{57}$$
$$\quad {}_{9 \times 9} \qquad {}_{9 \times 3 \ 3 \times 3 \ 3 \times 9}$$

The congruential transformation (57) can be speeded up because of the special nature of $H_{\theta v}$, cf. (54), and the bulk of the numerical work is actually spent in (56).

6.6 Generic Stiffness Template and the IET

The expression (57) has significance that transcends this particular element. It is an *generic* expression for the higher-order stiffness of any satisfactory membrane triangle with this freedom configuration. The transformation matrix $H_{\theta v}$ is always given by (54). Only the generalized stiffness $K_{\theta h}$, which is a higher order stiffness in terms of the hierarchical corner rotations $\tilde{\theta}_i$, changes from element to element. Since this is a 3×3 symmetric matrix, it follows that the higher order stiffness of all elements of this type form a six parameter family.

Using (33) for K_b, it follows that the *generic template* for the total stiffness is

$$K = K_b + K_h = \frac{1}{A}L(\alpha_b) \, (hE) \, L(\alpha_b)^T + (1 - \gamma)H_{\theta v}^T K_{\theta h}H_{\theta v}. \tag{58}$$

with each component contributing 3 to the rank of K, and where the dependence of the force-lumping matrix L on α_b has been emphasized. It is easy to show that any element that befits this template passes the individual element test (IET) of Bergan and Nygård, and consequently no numerical verification to that effect is necessary. In this regard it is interesting that the 1988 Allman triangle befits (58), and consequently must pass the IET; further details are given in Section A.9 of the Appendix.

7. CONCLUDING REMARKS

We have presented the derivation of a plane stress triangle with drilling freedoms using the extended free formulation (EFF). The main advantage over the FF triangle derived in [1] is that an explicit form is obtained for the higher order stiffness. This simplifies the symbolic determination of optimal parameters by energy balance, as investigated in Section 2 of Part III. In addition the explicit derivation reveals an generic template form that all elements of this type must fit. Other element implementation details, such as consistent node force calculations, as well as performance of the EFF element with respect to other 9-dof triangles, are discussed in Part III.

References

[1]   P. G. Bergan and C. A. Felippa, A triangular membrane element with rotational degrees of freedom, *Computer Methods in Applied Mechanics & Engineering*, 50, 1985, pp. 25–69

[2]   B. M. Irons and S. Ahmad, *Techniques of Finite Elements*, Ellis Horwood, Chichester, England, 1980

[3]   D. J. Allman, A compatible triangular element including vertex rotations for plane elasticity analysis, *Computers & Structures*, 19, 1984, pp. 1–8

[4]   R. D. Cook, On the Allman triangle and a related quadrilateral element, *Computer & Structures*, 22, 1986, pp. 1065–1067

[5]   R. D. Cook, A plane hybrid element with rotational D.O.F. and adjustable stiffness, *International Journal of Numerical Methods in Engineering*, 24, 1987, pp. 1499–1508

[6]   P. G. Bergan and C. A. Felippa, Efficient implementation of a triangular membrane element with drilling freedoms, Finite Element Handbook series, ed. by T. J. R. Hughes and E. Hinton, Pineridge Press, 1986, pp. 139–152

[7]   D. J. Allman, A compatible triangular element including vertex rotations for plane elasticity analysis, *International Journal of Numerical Methods in Engineering*, 26, 1988, pp. 2645–2655

[8]   R. H. MacNeal and R. L. Harder, A refined four-noded membrane element with rotational degrees of freedom, *Computer & Structures*, 28, 1988, pp. 75–88

[9]   T. J. R. Hughes and F. Brezzi, On drilling degrees of freedom, *Computer Methods in Applied Mechanics & Engineering*, 72, 1989, pp. 105–121

[10]   A. Ibrahimbegovic (1990), A novel membrane finite element with an enhanced displacement interpolation, *Finite Elements in Analysis and Design*, 7, 167–179

[11]   P. G. Bergan and M. K. Nygård, Finite elements with increased freedom in choosing shape functions, *International Journal of Numerical Methods in Engineering*, 20, 1984, pp. 643–664

[12]   C. A. Felippa, Refined finite element analysis of linear and nonlinear two-dimensional structures, Ph. D. Dissertation, Department of Civil Engineering, University of California at Berkeley, Berkeley, CA, 1966

[13]   A. J. Carr, A refined finite element analysis of thin shell structures including dynamic loadings, Ph. D. Dissertation, Department of Civil Engineering, University of California at Berkeley, Berkeley, CA, 1968

[14]   P. G. Bergan, Plane stress analysis using the finite element method. Triangular element with 6 parameters at each node, Division of Structural Mechanics, The Norwegian Institute of Technology, Trondheim, Norway, 1967

[15]   J. L. Tocher and B. Hartz, Higher order finite element for plane stress, Proc. ASCE, *Journal of the Engineering Mechanics Division*, 93, EM4, pp. 149–174, 1967

[16]   C. A. Felippa and S. Alexander, Membrane triangles with corner drilling freedoms: III. Implementation and performance evaluation, in this report.

[17]   F. Frey, Shell finite elements with six degrees of freedom per node, in *Analytical and Computational Methods for Shells*, CAD Vol. 3, ed. by A. K. Noor, T. Belytschko and J. C. Simo, American Society of Mechanical Engineers, ASME, New York, 1989, pp. 291–316

[18]   M. K. Nygård, The free formulation for nonlinear finite elements with applications to shells, Dr. Ing. Thesis, Div. of Structural Mechanics, Norwegian Institute of Technology, Trondheim, Norway, 1986

[19]   P. G. Bergan and M. K. Nygård, Nonlinear shell analysis using free formulation finite elements, *Proc. Europe-US Symposium on Finite Element Methods for Nonlinear Problems*, held at Trondheim, Norway, August 1985, Springer-Verlag, Berlin, 1986

[20]   C. A. Felippa, Parametrized multifield variational principles in elasticity: I. Mixed functionals, *Communications in Applied Numerical Methods*, 5, 1989, pp. 69–78

[21]   C. A. Felippa, Parametrized multifield variational principles in elasticity: II. Hybrid functionals and the free formulation, *Communications in Applied Numerical Methods*, 5, 1989, pp. 79–88

[22]   C. A. Felippa and C. Militello, Developments in variational methods for high-performance plate and shell elements, in *Analytical and Computational Methods for Shells*, CAD Vol. 3, ed. by A. K. Noor, T. Belytschko and J. C. Simo, American Society of Mechanical Engineers, ASME, New York, 1989, pp. 191–216

[23]   C. A. Felippa and C. Militello, Variational formulation of high performance finite elements: parametrized variational principles, *Computers and Structures*, 36, 1990, pp. 1–11

[24]   C. A. Felippa, The extended free formulation of finite elements in linear elasticity, *Journal of Applied Mechanics*, 56, 1989, pp. 609–616

[25]   C. A. Felippa and P. G. Bergan, A triangular plate bending element based on an energy-orthogonal free formulation, *Computer Methods in Applied Mechanics & Engineering*, 61, 1987, pp. 129–160

[26]   C. A. Felippa and C. Militello, Membrane triangles with corner drilling freedoms: II. The ANDES element, in this report.

[27]   P. G. Bergan and L. Hanssen, A new approach for deriving 'good' finite elements, MAFELAP II Conference, Brunel University, 1975, in *The Mathematics of Finite Elements and Applications – Volume II*, ed. by J. R. Whiteman, Academic Press, London, 1976

[28]   P. G. Bergan, Finite elements based on energy orthogonal functions, *International Journal of Numerical Methods in Engineering*, 15, 1980, pp. 1141–1555

[29]   C. A. Felippa and R. W. Clough, The finite element method in solid mechanics, in *Numerical Solution of Field Problems in Continuum Physics*, ed. by G. Birkhoff and R. S. Varga, SIAM–AMS Proceedings II, American Mathematical Society, Providence, R.I., 1969, pp. 210–252

Appendix A. AUXILIARY DERIVATIONS

A.1 The LST Interpolation

Let $w = w(\zeta_1, \zeta_2, \zeta_3)$ denote any quantity being quadratically interpolated over the six-node linear strain triangle (LST), for example the displacement components. The node values of w are w_i, $i = 1, \ldots 6$. The hierarchical LST interpolation is [29]

$$w = [\, w_1 \quad w_2 \quad w_3 \quad \widetilde{w}_4 \quad \widetilde{w}_5 \quad \widetilde{w}_6\,] \begin{Bmatrix} \varphi_1 \\ \varphi_2 \\ \varphi_3 \\ \varphi_4 \\ \varphi_5 \\ \varphi_6 \end{Bmatrix} = \mathbf{w}^T \begin{Bmatrix} \zeta_1 \\ \zeta_2 \\ \zeta_3 \\ 4\zeta_1\zeta_2 \\ 4\zeta_2\zeta_3 \\ 4\zeta_3\zeta_1 \end{Bmatrix} = \mathbf{w}^T \varphi. \tag{59}$$

where the *hierarchical* nodal values $\widetilde{w}_4$, $\widetilde{w}_5$ and $\widetilde{w}_6$ are defined as the midpoint deviations from linearity

$$w_4 = \tfrac{1}{2}(w_1 + w_2) + \widetilde{w}_4, \qquad w_5 = \tfrac{1}{2}(w_2 + w_3) + \widetilde{w}_5, \qquad w_6 = \tfrac{1}{2}(w_3 + w_1) + \widetilde{w}_6. \tag{60}$$

If one sets $\widetilde{w}_4 = \widetilde{w}_5 = \widetilde{w}_6 = 0$, (60) collapses to the linear interpolation of the three-node constant strain triangle (CST), a property characteristic of hierarchical elements.

Two types of shape functions appear in (60). Following the free-formulation (FF) terminology, the three linear shape functions associated with the corner nodes, namely $\varphi_1 = \zeta_1$, $\varphi_2 = \zeta_2$, and $\varphi_3 = \zeta_3$, are called *basic* shape functions, because they provide the rigid-body and constant strain motions when w is identified with the displacement components u_x and u_y. The three quadratic shape functions associated with the midpoint nodes, namely $\varphi_4 = 4\zeta_1\zeta_2$, $\varphi_5 = 4\zeta_2\zeta_3$ and $\varphi_6 = 4\zeta_3\zeta_1$, are called *higher order* shape functions. The higher order functions are not energy orthogonal to the lower order ones according to the definitions given below. As we shall see, (60) is *not* suitable as a departure point for the internal displacement expansion of an EFF element, but it is useful as an intermediate step.

A.2 Generalized Interpolation

A generalization of the quadratic interpolation (60) is

$$w = \sum_{i=1}^{6} q_i \phi_i(\zeta_1, \zeta_2, \zeta_3) = [\, q_1 \quad q_2 \quad q_3 \quad q_4 \quad q_5 \quad q_6\,] \begin{Bmatrix} \phi_1 \\ \phi_2 \\ \phi_3 \\ \phi_4 \\ \phi_5 \\ \phi_6 \end{Bmatrix}, \tag{61}$$

in which the coefficients q_i are not necessarily node values but may be interpreted as generalized coordinates. The associated functions ϕ_i are called *generalized shape functions*. These functions no longer enjoy the nodal interpolation properties of the ordinary shape functions φ_i.

To construct EFF elements we shall keep the same three basic shape functions in (62):

$$\phi_1 = \varphi_1 = \zeta_1, \qquad \phi_2 = \varphi_2 = \zeta_2, \qquad \phi_3 = \varphi_3 = \zeta_3, \tag{62}$$

As for the higher order shape functions, the most general choice may be written

$$\begin{aligned}
\phi_4 &= \mu_1(\zeta_1^2 + \zeta_2^2) + \mu_2\zeta_3^2 + \mu_3\zeta_1\zeta_2 + \mu_4(\zeta_2\zeta_3 + \zeta_3\zeta_1) \\
\phi_5 &= \mu_1(\zeta_2^2 + \zeta_3^2) + \mu_2\zeta_1^2 + \mu_3\zeta_2\zeta_3 + \mu_4(\zeta_3\zeta_1 + \zeta_1\zeta_2) \\
\phi_6 &= \mu_1(\zeta_3^2 + \zeta_1^2) + \mu_2\zeta_2^2 + \mu_3\zeta_3\zeta_1 + \mu_4(\zeta_1\zeta_2 + \zeta_2\zeta_3)
\end{aligned} \tag{63}$$

where μ_1, μ_2, μ_3 and μ_4 are numerical coefficients, at least one of which must be nonzero. Because the functions may. be scaled by an arbitrary nonzero common factor, only three coefficients are in fact independent. The grouping of the terms in (64) is dictated by triangular symmetries. In subsequent developments we shall restrict the choice to *energy orthogonal functions* defined below. The general case is briefly commented upon in subsection A.8.

A.3 Energy Orthogonal Shape Functions

A higher order shape function ϕ_j ($j = 4, 5, 6$) is said to be *energy orthogonal* with respect to the basic shape functions ϕ_i ($i = 1, 2, 3$) if the area integral of any product of their triangle-coordinate derivatives is zero. [This definition applies strictly to the case in which the thickness and material properties are constant over the element. But these conditions hold in the limit of infinitesimally small elements, which is the same limit of interest for the patch test.] This condition can be expressed as

$$\int_A \frac{\partial \phi_i}{\partial \zeta_m} \frac{\partial \phi_j}{\partial \zeta_n} \, dA = 0, \qquad i, m, n = 1, 2, 3, \qquad j = 4, 5, 6. \tag{64}$$

But since all derivatives of ϕ_i are constant, (65) is equivalent to

$$\int_A \frac{\partial \phi_j}{\partial \zeta_n} \, dA = 0, \tag{65}$$

which expresses the fact that the *element mean value of the first derivatives of an energy orthogonal shape function must vanish*.

Applying this condition to (64) we find that the higher order shape functions are energy orthogonal if

$$2\mu_1 + \mu_3 + \mu_4 = 0, \qquad \mu_2 + \mu_4 = 0. \tag{66}$$

Given μ_1 and μ_2, which may not be simultaneously zero, these relations determine μ_3 and μ_4. Because (as noted above) only three coefficients in (64) are actually independent, it follows that the energy orthogonal subclass forms a one-parameter family. Note that (60), in which $\mu_3 = 4$, others zero, violates (67).

Two physically transparent sets of shape functions supplied by these relations are

$$\begin{Bmatrix} \phi_4 \\ \phi_5 \\ \phi_6 \end{Bmatrix} = \begin{Bmatrix} (\zeta_1 - \zeta_2)^2 \\ (\zeta_2 - \zeta_3)^2 \\ (\zeta_3 - \zeta_1)^2 \end{Bmatrix}, \tag{67}$$

$$\begin{Bmatrix} \phi_4 \\ \phi_5 \\ \phi_6 \end{Bmatrix} = \begin{Bmatrix} (\zeta_3 - \frac{1}{3})^2 \\ (\zeta_1 - \frac{1}{3})^2 \\ (\zeta_2 - \frac{1}{3})^2 \end{Bmatrix} = \frac{2}{9} \begin{Bmatrix} (-\zeta_1 - \zeta_2 + 2\zeta_3)^2 \\ (-\zeta_2 - \zeta_3 + 2\zeta_1)^2 \\ (-\zeta_3 - \zeta_1 + 2\zeta_2)^2 \end{Bmatrix}, \tag{68}$$

which correspond to taking $\mu_1 = 1$, $\mu_2 = 0$, and $\mu_1 = -2/9$, $\mu_2 = 8/9$, respectively. The first set vanishes on the triangle medians, whereas the second set vanishes on lines parallel to sides passing through the centroid. Any linear combination of these functions, such as

$$\phi_4 = c_1(\zeta_3 - \frac{1}{3})^2 + c_2(\zeta_1 - \zeta_2)^2 \tag{69}$$

is also energy orthogonal. Moreover, the sets (68) and (69) are not independent because they can be linked through the linear transformations

$$\begin{Bmatrix} (\zeta_1 - \frac{1}{3})^2 \\ (\zeta_2 - \frac{1}{3})^2 \\ (\zeta_3 - \frac{1}{3})^2 \end{Bmatrix} = \frac{2}{3} Q \begin{Bmatrix} (\zeta_1 - \zeta_2)^2 \\ (\zeta_2 - \zeta_3)^2 \\ (\zeta_3 - \zeta_1)^2 \end{Bmatrix}, \qquad \begin{Bmatrix} (\zeta_1 - \zeta_2)^2 \\ (\zeta_2 - \zeta_3)^2 \\ (\zeta_3 - \zeta_1)^2 \end{Bmatrix} = \frac{3}{2} Q^T \begin{Bmatrix} (\zeta_1 - \frac{1}{3})^2 \\ (\zeta_2 - \frac{1}{3})^2 \\ (\zeta_3 - \frac{1}{3})^2 \end{Bmatrix}, \tag{70}$$

where

$$Q = \tfrac{1}{3} \begin{bmatrix} -1 & 2 & 2 \\ 2 & -1 & 2 \\ 2 & 2 & -1 \end{bmatrix} \tag{71}$$

is an orthogonal matrix. Thus we confirm that all energy orthogonal sets can be related by a linear transformation, and all of them would produce the same higher order stiffness. Consequently the choice of basis for the higher order functions is merely a matter of convenience. For the element derived here we select (68) as this choice leads to a fairly simple generalized higher order stiffness matrix K_{qh}, derived in Section 4. Thus the generalized interpolation formula (62) becomes

$$w = [q_1 \quad q_2 \quad q_3 \quad q_4 \quad q_5 \quad q_6] \begin{Bmatrix} \zeta_1 \\ \zeta_2 \\ \zeta_3 \\ (\zeta_1 - \zeta_2)^2 \\ (\zeta_2 - \zeta_3)^2 \\ (\zeta_3 - \zeta_1)^2 \end{Bmatrix} = q^T \phi. \tag{72}$$

A.4 Freedom Transformations

We need to establish the transformations $q = T_{qw} w$, $w = T_{qw}^{-1} q$ that connect nodal values to generalized coordinates. Formulas (73) and (60) are related by equating their left hand sides because they both correspond to *complete* quadratic expansions referred to linearly independent bases:

$$w = w^T \varphi = q^T \phi = w^T T_{qw}^T \phi. \tag{73}$$

Thus $\varphi = T_{qw}^T \phi$. Evaluating this relation at the six nodes yields

$$\begin{bmatrix} 1 & 0 & 0 & \tfrac{1}{2} & 0 & \tfrac{1}{2} \\ 0 & 1 & 0 & \tfrac{1}{2} & \tfrac{1}{2} & 0 \\ 0 & 0 & 1 & 0 & \tfrac{1}{2} & \tfrac{1}{2} \\ 0 & 0 & 0 & 1 & 0 & 0 \\ 0 & 0 & 0 & 0 & 1 & 0 \\ 0 & 0 & 0 & 0 & 0 & 1 \end{bmatrix} = T_{qw}^T \begin{bmatrix} 1 & 0 & 0 & \tfrac{1}{2} & \tfrac{1}{2} & 0 \\ 0 & 1 & 0 & 0 & \tfrac{1}{2} & \tfrac{1}{2} \\ 0 & 0 & 1 & \tfrac{1}{2} & 0 & \tfrac{1}{2} \\ 1 & 1 & 0 & 0 & \tfrac{1}{4} & \tfrac{1}{4} \\ 0 & 1 & 1 & \tfrac{1}{4} & 0 & \tfrac{1}{4} \\ 1 & 0 & 1 & \tfrac{1}{4} & \tfrac{1}{4} & 0 \end{bmatrix} \tag{74}$$

Solving we get

$$T_{qw} = \begin{bmatrix} 1 & 0 & 0 & \tfrac{8}{9} & -\tfrac{4}{9} & \tfrac{8}{9} \\ 0 & 1 & 0 & \tfrac{8}{9} & \tfrac{8}{9} & -\tfrac{4}{9} \\ 0 & 0 & 1 & -\tfrac{4}{9} & \tfrac{8}{9} & \tfrac{8}{9} \\ 0 & 0 & 0 & -\tfrac{10}{9} & \tfrac{2}{9} & \tfrac{2}{9} \\ 0 & 0 & 0 & \tfrac{2}{9} & -\tfrac{10}{9} & \tfrac{2}{9} \\ 0 & 0 & 0 & \tfrac{2}{9} & \tfrac{2}{9} & -\tfrac{10}{9} \end{bmatrix} \qquad T_{qw}^{-1} = \begin{bmatrix} 1 & 0 & 0 & 1 & 0 & 1 \\ 0 & 1 & 0 & 1 & 1 & 0 \\ 0 & 0 & 1 & 0 & 1 & 1 \\ 0 & 0 & 0 & -1 & -\tfrac{1}{4} & -\tfrac{1}{4} \\ 0 & 0 & 0 & -\tfrac{1}{4} & -1 & -\tfrac{1}{4} \\ 0 & 0 & 0 & -\tfrac{1}{4} & -\tfrac{1}{4} & -1 \end{bmatrix} \tag{75}$$

Setting w to u_x and u_y in turn we can write

$$\begin{Bmatrix} q_x \\ q_y \end{Bmatrix} = \begin{bmatrix} T_{qw} & 0 \\ 0 & T_{qw} \end{bmatrix} \begin{Bmatrix} m_x \\ m_y \end{Bmatrix}. \tag{76}$$

From this 12×12 transformation we extract the 6×6 matrix H_{qm} given in (50).

A.5 Hierarchical Drilling Freedoms

We now study the "migration" of freedoms of the hierarchical LST into drilling and eliminable freedoms. The continuum-mechanics rotation about the z axis, positive counterclockwise, is defined by formula (27). For the hierarchical LST element we set w to u_x and u_y in turn and evaluate θ making use of (39) to get

$$\theta = \frac{1}{4A} \begin{bmatrix} u_{x1} & u_{x2} & u_{x3} & u_{y1} & u_{y2} & u_{y3} & \tilde{u}_{x4} & \tilde{u}_{x5} & \tilde{u}_{x6} & \tilde{u}_{y4} & \tilde{u}_{y5} & \tilde{u}_{y6} \end{bmatrix} \begin{Bmatrix} x_{23} \\ x_{31} \\ x_{12} \\ y_{23} \\ y_{31} \\ y_{12} \\ 4(\zeta_1 x_{31} + \zeta_2 x_{23}) \\ 4(\zeta_2 x_{12} + \zeta_3 x_{31}) \\ 4(\zeta_3 x_{23} + \zeta_1 x_{12}) \\ 4(\zeta_1 y_{31} + \zeta_2 y_{23}) \\ 4(\zeta_2 y_{12} + \zeta_3 y_{31}) \\ 4(\zeta_3 y_{23} + \zeta_1 y_{12}) \end{Bmatrix} \quad (77)$$

Note that θ varies linearly over the element. It follows that only *three* independent drilling freedoms may be defined, and the obvious locations are the corner points. Any additional drilling freedom (chosen, for example, at the centroid) would not be linearly independent. The three corner drilling rotations θ_1, θ_2 and θ_3 at the corners are related to the other freedoms by replacing the corner triangular coordinates in (78):

$$\begin{Bmatrix} \theta_1 \\ \theta_2 \\ \theta_3 \end{Bmatrix} = \frac{1}{4A} \begin{bmatrix} x_{23} & x_{31} & x_{12} & y_{23} & y_{31} & y_{12} & 4x_{31} & 0 & 4x_{12} & 4y_{31} & 0 & 4y_{12} \\ x_{23} & x_{31} & x_{12} & y_{23} & y_{31} & y_{12} & 4x_{23} & 4x_{12} & 0 & 4y_{23} & 4y_{12} & 0 \\ x_{23} & x_{31} & x_{12} & y_{23} & y_{31} & y_{12} & 0 & 4x_{31} & 4x_{23} & 0 & 4y_{31} & 4y_{23} \end{bmatrix} \begin{Bmatrix} u_{x1} \\ u_{x2} \\ u_{x3} \\ u_{y1} \\ u_{y2} \\ u_{y3} \\ \tilde{u}_{x4} \\ \tilde{u}_{x5} \\ \tilde{u}_{x6} \\ \tilde{u}_{y4} \\ \tilde{u}_{y5} \\ \tilde{u}_{y6} \end{Bmatrix} \quad (78)$$

Subsequent manipulations are facilitated by defining the *hierarchical rotations* $\tilde{\theta}_i = \theta_i - \theta_0$, $i = 1, 2, 3$, where θ_0 is the CST rotation, that is, the mean rotation obtained if one sets $\tilde{u}_{x4} = \tilde{u}_{x5} \ldots \tilde{u}_{y6} = 0$:

$$\theta_0 = \frac{1}{4A} \left(x_{23}u_{x1} + x_{31}u_{x2} + x_{12}u_{x3} + y_{23}u_{y1} + y_{31}u_{y2} + y_{12}u_{y3} \right) \quad (79)$$

Then (79) simplifies to a matrix relation that involves only the hierarchical midpoint displacements:

$$\tilde{\theta} = \begin{Bmatrix} \tilde{\theta}_1 \\ \tilde{\theta}_2 \\ \tilde{\theta}_3 \end{Bmatrix} = \frac{1}{A} \begin{bmatrix} x_{31} & 0 & x_{12} & y_{31} & 0 & y_{12} \\ x_{23} & x_{12} & 0 & y_{23} & y_{12} & 0 \\ 0 & x_{31} & x_{23} & 0 & y_{31} & y_{23} \end{bmatrix} \begin{Bmatrix} \tilde{u}_{x4} \\ \tilde{u}_{x5} \\ \tilde{u}_{x6} \\ \tilde{u}_{y4} \\ \tilde{u}_{y5} \\ \tilde{u}_{y6} \end{Bmatrix} = \mathbf{H}_{\theta m} \mathbf{m}. \quad (80)$$

For reasons explained in subsection A.6, we shall link $\widetilde{\theta}$ to vector s of (49) as $\widetilde{\theta} = \mathbf{H}_{\theta m}\mathbf{H}_{ms}$s. Matrix $\mathbf{H}_{ms}$, which is given in (51), can be constructed by inspection of Figure 2. Carrying out this multiplication and using the definitions in (23) we obtain

$$
\left\{\begin{array}{c}\widetilde{\theta}_1 \\ \widetilde{\theta}_2 \\ \widetilde{\theta}_3\end{array}\right\} = \left[\begin{array}{cccccc} -\dfrac{S_3 + a_{12}^2}{Aa_{12}} & 0 & -\dfrac{S_2 - a_{31}^2}{Aa_{31}} & a_{12}^{-1} & 0 & a_{31}^{-1} \\ -\dfrac{S_3 - a_{12}^2}{Aa_{12}} & -\dfrac{S_1 + a_{23}^2}{Aa_{23}} & 0 & a_{12}^{-1} & a_{23}^{-1} & 0 \\ 0 & -\dfrac{S_1 - a_{23}^2}{Aa_{23}} & -\dfrac{S_2 + a_{31}^2}{Aa_{31}} & 0 & a_{23}^{-1} & a_{31}^{-1} \end{array}\right] \left\{\begin{array}{c}\widetilde{u}_{m4} \\ \widetilde{u}_{m5} \\ \widetilde{u}_{m6} \\ \widetilde{u}_{t4} \\ \widetilde{u}_{t5} \\ \widetilde{u}_{t6}\end{array}\right\}. \tag{81}
$$

A.6 Choosing Eliminable Freedoms

The $12 - 9 = 3$ eliminable freedoms must be displacements because no more linearly independent drilling freedom choices remain. From symmetry and invariance considerations four possible choices emerge:

(1) The hierarchical midpoint freedoms directed along the side directions: u_{s4}, u_{s5}, u_{s6}.

(2) The hierarchical midpoint freedoms directed along the normal directions: u_{n4}, u_{n5}, u_{n6}.

(3) The hierarchical midpoint freedoms directed along the median directions: u_{m4}, u_{m5}, u_{m6}.

(4) The hierarchical midpoint freedoms directed along the normal-to-the-median directions: u_{t4}, u_{t5}, u_{t6}.

Choices (1) and (4) lead to transformation matrices that are singular for *any* triangle. Choice (2) leads to a transformation matrix that is singular for right-angled triangles. That leaves choice (3), which as shown below has a well conditioned inverse. The necessary relation relating $\widetilde{\theta}$ to s is available in (82). This is rendered square by augmenting it with the trivial relations $\widetilde{u}_{mi} = \widetilde{u}_{mi}$, $i = 4, 5, 6$:

$$
\left\{\begin{array}{c}\widetilde{u}_{m4} \\ \widetilde{u}_{m5} \\ \widetilde{u}_{m6} \\ \widetilde{\theta}_1 \\ \widetilde{\theta}_2 \\ \widetilde{\theta}_3\end{array}\right\} = \left[\begin{array}{cccccc} 1 & 0 & 0 & 0 & 0 & 0 \\ 0 & 1 & 0 & 0 & 0 & 0 \\ 0 & 0 & 1 & 0 & 0 & 0 \\ -\dfrac{S_3 + a_{12}^2}{Aa_{12}} & 0 & -\dfrac{S_2 - a_{31}^2}{Aa_{31}} & a_{12}^{-1} & 0 & a_{31}^{-1} \\ -\dfrac{S_3 - a_{12}^2}{Aa_{12}} & -\dfrac{S_1 + a_{23}^2}{Aa_{23}} & 0 & a_{12}^{-1} & a_{23}^{-1} & 0 \\ 0 & -\dfrac{S_1 - a_{23}^2}{Aa_{23}} & -\dfrac{S_2 + a_{31}^2}{Aa_{31}} & 0 & a_{23}^{-1} & a_{31}^{-1} \end{array}\right] \left\{\begin{array}{c}\widetilde{u}_{m4} \\ \widetilde{u}_{m5} \\ \widetilde{u}_{m6} \\ \widetilde{u}_{t4} \\ \widetilde{u}_{t5} \\ \widetilde{u}_{t6}\end{array}\right\} \tag{82}
$$

or $\mathbf{r} = \mathbf{H}_{rs}$s in the notation of (46). The determinant of $\mathbf{H}_{rs}$ is $a_{12}a_{23}a_{31}/2A^3$. Thus $\mathbf{H}_{rs}$ is nonsingular for any nondegenerate triangle. Symbolic inversion of this transformation provides matrix $\mathbf{H}_{sr}$ given in (52).

A.7 Elimination of Hierarchical Median Displacements by Collocation

We now proceed to eliminate $\widetilde{u}_{m4}$, $\widetilde{u}_{m5}$ and $\widetilde{u}_{m6}$ through kinematic constraints. To fix the ideas consider $\widetilde{u}_{m4}$. From the boundary expansion (29) on side 1-2 we can obtain the normal displacement d_n in terms of the freedoms on that side. The hierarchical value at 4 is

$$
\begin{aligned}
\widetilde{d}_{n4} &= d_{n4} - \tfrac{1}{2}(d_{n1} + d_{n2}) \\
&= \left[\psi_{n1}(\xi)d_{n1} + \psi_{n2}(\xi)d_{n2} + \alpha_h\left(\psi_{\theta1}(\xi)\theta_1 + \psi_{\theta2}(\xi)\theta_2\right)\right]_{\xi=0} - \tfrac{1}{2}(d_{n1} + d_{n2}) \\
&= \tfrac{1}{8}\alpha_h\ell_{12}(\theta_2 - \theta_1) = \tfrac{1}{8}\alpha_h\ell_{12}(\widetilde{\theta}_2 - \widetilde{\theta}_1).
\end{aligned} \tag{83}
$$

Here parameter α_b of (29) has been renamed α_h to emphasize the fact that we can vary both independently for the basic and higher order stiffness. Assuming the collocation

$$
\widetilde{u}_{m4} = \widetilde{u}_{n4} \cos(n_{12}, m_{12}) = \widetilde{d}_{n4}(b_{12}/\ell_{12}), \tag{84}
$$

where the b_{ij} are defined in (23), we find

$$\widetilde{u}_{m4} = \tfrac{1}{8}\alpha_h b_{12}(\widetilde{\theta}_2 - \widetilde{\theta}_1). \tag{85}$$

Repeating this procedure for the other two sides and collecting into one matrix equation we get

$$\left\{ \begin{array}{c} \widetilde{u}_{m4} \\ \widetilde{u}_{m5} \\ \widetilde{u}_{m6} \end{array} \right\} = \tfrac{1}{8}\alpha_h \left[\begin{array}{ccc} -b_{12} & b_{12} & 0 \\ 0 & -b_{23} & b_{23} \\ b_{31} & 0 & -b_{31} \end{array} \right] \left\{ \begin{array}{c} \widetilde{\theta}_1 \\ \widetilde{\theta}_2 \\ \widetilde{\theta}_3 \end{array} \right\}. \tag{86}$$

Augmenting this with the trivial equations $\widetilde{\theta}_i = \widetilde{\theta}_i$ ($i = 1, 2, 3$) as last three rows and replacing $b_{ij} = 2A/a_{ij}$ yields the transformation matrix $H_{r\theta}$ listed in (53). An energy balance analysis presented in Section 2 of Part III shows that the best value for α_h is

$$\alpha_h = 5/4, \tag{87}$$

a value that has been hardwired into (55).

A.8 What Happens for Non Energy-Orthogonal Functions?

The original FF does not depend on the energy orthogonality concept although the variational justification of Refs. [21–24] does. To assess the effect of that condition on this element, symbolic experiments (with Macsyma) were conducted with elements derived with the general assumption (62) for the higher order shape functions. The orthogonality condition (67) was replaced by

$$2\mu_1 + \mu_3 + \mu_4 = \delta_1, \qquad \mu_2 + \mu_4 = \delta_2, \tag{88}$$

where δ_1 and δ_2 may be regarded as deviations from energy orthogonality.

The EFF higher order stiffness depends on two parameters: γ and α_h, where γ defines the scaling of K_h as per Eq. (12). These parameters are selected to match pure-bending energies on regular mesh units, as described in Part III [16]. When the energy orthogonal sets are selected, the matching can be made so that a set (γ, α_h) works for *all* aspect ratios. With (89) it was found that such matching was possible only if

$$\delta_2 = \tfrac{1}{2}\delta_1. \tag{89}$$

One choice that verifies this condition is

$$\left\{ \begin{array}{c} \phi_4 \\ \phi_5 \\ \phi_6 \end{array} \right\} = \left\{ \begin{array}{c} (\zeta_1 - \zeta_2)^2 + \delta_2\,\phi_B \\ (\zeta_2 - \zeta_3)^2 + \delta_2\,\phi_B \\ (\zeta_3 - \zeta_1)^2 + \delta_2\,\phi_B \end{array} \right\}, \tag{90}$$

in which $\phi_B = \zeta_1\zeta_2 + \zeta_2\zeta_3 + \zeta_3\zeta_1$. This is not energy orthogonal if $\delta_2 \neq 0$. Closer examination, however, showed that the same higher order stiffness matrix K_h was produced for any value of δ_2; thus adding ϕ_B has no effect.

Any deviation from the condition (90) made matching impossible: only specific element aspect ratios could be energy balanced. Thus it appears that the main effect of departure from energy orthogonality is a degradation in element accuracy. Consequently the general assumption (62)–(64) was not pursued further.

8.1 Allman Triangles Fit the Generic Template

The rank-sufficient Allman triangle [7] was constructed with incompatible cubic shape functions. Numerically integrated versions of this element have been symbolically analyzed as prelude to the evaluation presented in Part III. Four triangle integration rules, labeled as follows, were considered:

$1c$ The 1-point centroidal integration rule.

$3m$ The 3-midpoint rule of quadratic accuracy.

$3i$ The 3-interior point rule, also of quadratic accuracy, with points at $\zeta_i = 2/3$, $\zeta_j = \zeta_k = 1/6$.

$7i$ The 7-interior point rule of cubic accuracy.

The resultant (total) stiffness matrices will be denoted by K^{A1c}, K^{A3m}, K^{A3i} and K^{A7}, respectively. All of them were found to fit the generic template (58) in the sense that

$$K^{A1c} = K_b(4/3)$$
$$K^{A3m} = K_b(1) + K_h^{3m} = K_b(1) + H_{\theta v}^T K_{qh}^{3m} H_{\theta v}$$
$$K^{A3i} = K_b(1) + K_h^{3i} = K_b(1) + H_{\theta v}^T K_{qh}^{3i} H_{\theta v} \tag{91}$$
$$K^{A7i} = K_b(1) + K_h^{7i} = K_b(1) + H_{\theta v}^T K_{qh}^{7i} H_{\theta v}$$

where the argument of K_b is the value of α_b obtained by setting constant stress states. The centroid-integrated stiffness K^{A1c} is of course rank deficient by 3. The 3-point-integrated Allman elements are effectively linear-strain, quadratic displacement triangles because such sampling "filters out" quadratic strain variations. The higher order stiffness of these 3-point integrated elements does not fit into the present EFF family except for specific geometries. For example, for the equilateral triangle, K_h^{3m} coincides with EFF's K_h if $1 - \gamma = 1/4$ and $\alpha_h = (32 \pm \sqrt{82})/24$, whereas K_h^{3i} is obtained if $1 - \gamma = 1/36$ with the same $\alpha_h = (32 \pm \sqrt{82})/24$. To achieve equivalence for more general geometries, however, it becomes necessary to generalize the present EFF formulation by allowing *three* α_h coefficients, one per side, with α_{hi} depending on the magnitude of the opposite angle.

The main practical value of the decomposition (92) is that it shows that the numerically integrated Allman elements pass the patch test without any numerical experiments. The equivalent EFF elements, however, have parameter values that do not agree with the optimal ones determined in Part III. As a consequence, the performance of all Allman triangles deteriorates for high aspect ratios.

303

MEMBRANE TRIANGLES WITH CORNER DRILLING FREEDOMS: II. THE ANDES ELEMENT

SUMMARY

This is the second article in a three-Part series on the construction of 3-node, 9-dof membrane elements with normal-to-its-plane rotational freedoms (the so-called drilling freedoms) using parametrized variational principles. In this Part, one such element is derived within the context of the Assumed Natural Deviatoric Strain (ANDES) formulation. The higher order strains are obtained by constructing three parallel-to-sides pure-bending modes from which natural strains are obtained at the corner points and interpolated over the element. To attain rank sufficiency, an additional higher order "torsional" mode, corresponding to equal hierarchical rotations at each corner with all other motions precluded, is incorporated. The resulting formulation has five free parameters. When these parameters are optimized against pure bending by energy balance methods, the resulting element is found to coalesce with the optimal EFF element derived in Part I. Numerical integration as a strain filtering device is found to play a key role in this achievement.

1. INTRODUCTION

In the first Part of this article series [1], a 9-dof triangular membrane element with three corner drilling freedoms was constructed within the framework of the extended free formulation (EFF). In the present work, we undertake the derivation of an element with the same freedom configuration, using the Assumed Natural Deviatoric Strain (ANDES) formulation.

ANDES represents a recent variant of the Assumed Natural Strain (ANS) formulation. The latter is in turn a relatively new development. A restricted form of the assumed strain method, not involving natural strains, was introduced in 1969 by Willam [2]. He constructed a 4-node plane stress element by assuming a constant shear strain independent of the direct strains, and using a strain-displacement mixed variational principle; the resulting element is identical to that derivable by selective one-point integration. A different approach advocated by Ashwell and coworkers [3] viewed "strain elements" as a way to obtain appropriate displacement fields by integration of assumed compatible strain fields. (In fact, this was the same technique used by Turner *et. al.* [4] for deriving the constant strain membrane triangle in their celebrated 1956 paper.)

These and other forms of assumed strain techniques were overshadowed in the 1970s by developments in reduced and selective integration methods for displacement models. The assumed strain approach in natural coordinates, inaugurated in a pioneer paper by MacNeal [5], has attracted increased attention since 1980. Among the main contributors we may cite Bathe and Dvorkin [6], Park and Stanley [8,9], Crisfield [7], Simo and Hughes [10], Huang and Hinton [11], and Jang and Pinsky [12]. The name "assumed natural strain" and the acronym ANS are due to Park and Stanley [9].

ANS applications have been focused on plates and shell elements because of the effectiveness of this formulation in producing elements with low distortion sensitivity, balanced stress/displacement accuracy, and which are easily extendible to geometrically nonlinear analysis. These advantages are somewhat counterbalanced by the fact that *a priori* satisfaction of the patch test is not guaranteed, even for flat elements, and *a posteriori* verifications to that effect are required.

The basic steps of the ANS formulation are summarized in Box 1. The narrative assumes that the element to be constructed has nodal displacement degrees of freedom collected in vector v (these are those nodal variables common with other elements, also called the *visible* degrees of freedom, or *connectors*), elastic modulus matrix E, and volume V. A generally incompatible strain field (that is, one not necessarily derivable from displacements), is built in natural coordinates, transformed into Cartesian coordinates where it is expressed as e $=$ Bv, and used to compute the stiffness matrix K by the standard formula $\int_V \mathbf{B}^T \mathbf{E} \mathbf{B} \, dV$. From the standpoint of connected elements, an ANS element looks exactly like a displacement model and can be easily implemented into a standard finite element code. Extensions to geometrically and materially nonlinear analysis are equally straightforward.

ANDES is a variant of ANS that exploits the fundamental decomposition of the stiffness equations described in Box 1 of Part I [1]:

$$\mathbf{K}\mathbf{v} = (\mathbf{K}_b + \alpha \mathbf{K}_h)\mathbf{v} = \mathbf{p}, \tag{1}$$

where $\alpha > 0$ is a scaling coefficient. Assumptions are made only on the "deviatoric" portion $\mathbf{e}_d$ of the element strains, namely the portion that integrates to zero over the element volume: $\int_V \mathbf{e}_d \, dV = 0$. Thus instead of $\mathbf{e} = \mathbf{B}\mathbf{v}$ we eventually get, by the procedure outlined in Box 2, $\mathbf{e}_d = \mathbf{B}_d \, \mathbf{v}$, and

$$\mathbf{K}_h = \alpha \int_V \mathbf{B}_d^T \mathbf{E} \mathbf{B}_d \, dV. \tag{2}$$

The basic stiffness matrix $\mathbf{K}_b$ is constructed by the same procedure described in Box 2 of Part I. The mean portion of the strains, namely $\bar{\mathbf{e}}$, is left to be determined variationally from the constant stress assumptions used to develop $\mathbf{K}_b$, and has no effect on the stiffness equations.

The main advantage of ANDES over ANS is that elements constructed with the former technique are guaranteed to pass the individual element test of Bergan and Hanssen [13] (a strong form of the patch test that demands pairwise cancellation of surface tractions among adjacent elements in a constant stress state). There are cases when an ANS element and the corresponding ANDES element with $\alpha = 1$ coalesce. The ANDES formulation retains an edge, however, in that the scaling coefficient remains available to improve the element performance. Furthermore, the availability of $\mathbf{K}_h$ helps in the construction of element level error estimators [14] for r and h mesh adaptation.

The variational justification of the ANDES formulation was developed by Felippa and Militello [15,16], to which the reader is referred for details. This justification built on previous work [17,18] on the variational foundations of the ANS formulation. The first ANDES elements constructed using this theory were 9-dof Kirchoff plate bending triangles presented in [19]. The technique has also been used to formulate C^0 plate bending elements [14].

The present paper describes the first application of ANDES to membrane elements with drilling degrees of freedom. The main objective is to illustrate another application of this relatively new technique and assess its advantages and shortcomings when compared to FF and EFF.

2. THE TRIANGULAR ELEMENT

The geometry and degree-of-freedom configuration of triangular element is identical to that developed in Part I, to which the reader is referred for notation, geometric and behavioral relationships.

2.1 Extracting the Higher Order Behavior

From the EFF development in the Appendix of Part I we learned that the most effective way to exhibit the higher order element behavior is to extract the hierarchical corner rotations $\tilde{\theta}_i$ from the total corner rotations θ_i:

$$\tilde{\theta}_i = \theta_i - \theta_0, \tag{16}$$

Box 1   Construction of K by the ANS Formulation

Step S.1.   Select locations in the element where "natural straingage" locations are to be chosen. For many ANS elements these gages are placed on *reference lines* (in 2D elements) or *reference planes* (in 3D elements), but this is not a general rule. By appropriate interpolation express the element natural strains ϵ in terms of the "straingage readings" g at those locations:

$$\epsilon = A_\epsilon\, g, \tag{3}$$

where ϵ is a strain field in natural coordinates that must include all constant strain states. (For structural elements the term "strain" is to be interpreted in a generalized sense.)

Step S.2.   Relate the Cartesian strains e to the natural strains:

$$e = T\epsilon = TA_\epsilon g = Ag \tag{4}$$

at each point in the element. (If $e \equiv \epsilon$, or if it is possible to work throughout in natural coordinates, this step is skipped.) The resulting Cartesian strain interpolation is

$$e = TA_\epsilon g = Ag. \tag{5}$$

If **T** is constant over the element, as in the case of the triangle studied here, the step during which interpolation is effected is irrelevant.

Step S.3.   Relate the natural straingage readings g to the visible degrees of freedom

$$g = Qv, \tag{6}$$

where **Q** is a straingage-to-node displacement transformation matrix. Techniques for doing this vary from element to element and it is difficult to state rules that apply to every situation. Often the problem is amenable to breakdown into subproblems; for example

$$g = Q_1 v_1 + Q_2 v_2 + \cdots \tag{7}$$

where $v_1, v_2, \ldots$ are conveniently selected subsets of v. Some of these components may be derivable from displacements while others are not.

307

Box 1   Construction of K by the ANS Formulation (Continued)

Step S.4.   For a three-dimensional element of volume V and elastic modulus matrix $\mathbf{E}$, the element stiffness matrix is given by

$$\mathbf{K} = \mathbf{Q}^T \mathbf{K}_a \mathbf{Q}, \qquad \text{with} \qquad \mathbf{K}_a = \int_V \mathbf{A}^T \mathbf{E} \mathbf{A} \, dV. \tag{8}$$

Should $\mathbf{B} = \mathbf{AQ}$ be readily available one may use the standard formula

$$\mathbf{K} = \int_V \mathbf{B}^T \mathbf{E} \mathbf{B} \, dV. \tag{9}$$

In general this stiffness matrix does not necessarily pass the individual element test of Bergan and Hanssen [13] (a strong form of the patch test that demands pairwise cancellation of node forces between adjacent elements in constant stress states). For this to happen, $\mathbf{K}$ must admit the decomposition

$$\mathbf{K} = \mathbf{K}_b + \mathbf{K}_h = \upsilon^{-1} \mathbf{L} \mathbf{E} \mathbf{L}^T + \mathbf{K}_h, \tag{10}$$

where $\upsilon = \int_V dV$ is the element volume measure, $\mathbf{L}$ is a force-lumping matrix derivable as discussed in Box 1 of Part I and $\mathbf{K}_h$ is orthogonal to the rigid body and constant strain test motions. In other words, the ANS element must coalesce with the ANDES formulation with $\alpha = 1$. The equivalence may be checked by requiring that

$$\overline{\mathbf{B}} = \overline{\mathbf{A}}\mathbf{Q} = \upsilon^{-1} \mathbf{L}^T, \tag{11}$$

where $\overline{\mathbf{A}}$ denotes the mean part of $\mathbf{A}$ (cf. Box 2). As of this writing, no general techniques for explicit construction of ANS fields that satisfy these conditions *a priori* are known.

If the patch test is not satisfied, one should switch to the ANDES formulation by replacing the basic stiffness constructed from constant strain, namely $\upsilon \overline{\mathbf{B}}^T \mathbf{E} \overline{\mathbf{B}}$, with one constructed from constant stress assumptions.

Box 2   Construction of K_h by the ANDES Formulation

Steps H.1 to *H.3*.   Identical to the first three steps *S.1* through *S.3* in Box 1.

Step H.4.   Split the Cartesian strain field into mean (volume-averaged) and deviatoric strains:

$$e = \bar{e} + e_d = (\bar{A} + A_d)\, g, \tag{12}$$

where $\bar{A} = v^{-1} \int_V TA_\epsilon\, dV$, and $e_d = A_d\, g$ has mean zero value over V. For elements of simple geometry this decomposition can often be done in advance, and e_d constructed directly. Furthermore, this step may also be carried out on the natural strains if T is constant, as is the case for the elements here.

Step H.5.   The higher-order stiffness matrix is given by

$$K_h = \alpha Q^T K_d Q, \quad \text{with} \quad K_d = \int_V A_d^T E A_d\, dV, \tag{13}$$

where $\alpha = j_{22} > 0$ is a scaling coefficient (see Box 1).

It is often convenient to combine the product of A and Q into a single strain-displacement matrix called (as usual) B, which splits into $\bar{B}$ and B_d:

$$e = AQv = (\bar{A} + A_d)Qv = (\bar{B} + B_d)v = B\, v, \tag{14}$$

in which case

$$K_h = \int_V B_d^T E B_d\, dV. \tag{15}$$

where $i = 1, 2, 3$ is the corner index and θ_0 is the rotation of the Constant Strain Triangle (CST):

$$\theta_0 = \frac{1}{4A} \left(x_{23}v_{x1} + x_{31}v_{x2} + x_{12}v_{x3} + y_{23}v_{y1} + y_{31}v_{y2} + y_{12}v_{y3} \right).$$ (17)

From (16) and (17) we readily perceive the fundamental transformation

$$\begin{Bmatrix} \widetilde{\theta}_1 \\ \widetilde{\theta}_2 \\ \widetilde{\theta}_3 \end{Bmatrix} = \frac{1}{4A} \begin{bmatrix} x_{32} & y_{32} & 4A & x_{13} & y_{13} & 0 & x_{21} & y_{21} & 0 \\ x_{32} & y_{32} & 0 & x_{13} & y_{13} & 4A & x_{21} & y_{21} & 0 \\ x_{32} & y_{32} & 0 & x_{13} & y_{13} & 0 & x_{21} & y_{21} & 4A \end{bmatrix} \begin{Bmatrix} v_{x1} \\ v_{y1} \\ \theta_1 \\ v_{x2} \\ v_{y2} \\ \theta_2 \\ v_{x3} \\ v_{y3} \\ \theta_3 \end{Bmatrix},$$ (18)

or

$$\widetilde{\theta} = \mathbf{H}_{\theta v} \mathbf{v}.$$ (19)

The unscaled higher order stiffness of this element fits the *generic template* introduced in Section 6.6 of Part I:

$$\mathbf{K}_h = \mathbf{H}_{\theta v}^T \mathbf{K}_{\theta h} \mathbf{H}_{\theta v}.$$ (20)

The main objective of all formulations investigated here, as well as those in Part I, is to construct the 3×3 matrix $\mathbf{K}_{\theta h}$, which represents the higher order stiffness in terms of the hierarchical rotations $\widetilde{\theta}$.

Guided by these considerations, we begin by decomposing the visible degree of freedom vector into basic (CST) and higher order, as follows:

$$\mathbf{v} = \mathbf{v}_b + \mathbf{v}_h = \mathbf{v}_b + \mathbf{P}\widetilde{\theta},$$ (21)

where

$$\mathbf{v}_b = \begin{Bmatrix} v_{x1} \\ v_{y2} \\ \theta_0 \\ v_{x2} \\ v_{y2} \\ \theta_0 \\ v_{x3} \\ v_{y3} \\ \theta_0 \end{Bmatrix}, \qquad \mathbf{v}_h = \begin{Bmatrix} 0 \\ 0 \\ \widetilde{\theta}_1 \\ 0 \\ 0 \\ \widetilde{\theta}_2 \\ 0 \\ 0 \\ \widetilde{\theta}_3 \end{Bmatrix} = \begin{bmatrix} 0 & 0 & 0 \\ 0 & 0 & 0 \\ 1 & 0 & 0 \\ 0 & 0 & 0 \\ 0 & 0 & 0 \\ 0 & 1 & 0 \\ 0 & 0 & 0 \\ 0 & 0 & 0 \\ 0 & 0 & 1 \end{bmatrix} \begin{Bmatrix} \widetilde{\theta}_1 \\ \widetilde{\theta}_2 \\ \widetilde{\theta}_3 \end{Bmatrix}.$$ (22)

To simplify the problem of building higher order strain fields, we further split the hierarchical rotations into mean and deviatoric:

$$\begin{Bmatrix} \widetilde{\theta}_1 \\ \widetilde{\theta}_2 \\ \widetilde{\theta}_3 \end{Bmatrix} = \begin{Bmatrix} \bar{\theta} \\ \bar{\theta} \\ \bar{\theta} \end{Bmatrix} + \begin{Bmatrix} \theta'_1 \\ \theta'_2 \\ \theta'_3 \end{Bmatrix}$$ (23)

310

where $\bar{\theta} = \frac{1}{3}(\tilde{\theta}_1 + \tilde{\theta}_2 + \tilde{\theta}_3)$ and $\theta'_i = \tilde{\theta}_i - \bar{\theta}$. Consequently $\theta'_1 + \theta'_2 + \theta'_3 = 0$. In matrix form

$$\tilde{\theta} = \bar{\theta} + \theta', \tag{24}$$

which in terms of the nodal displacement vector becomes

$$\mathbf{v} = \mathbf{v}_b + \mathbf{P}(\bar{\theta} + \theta'), \tag{25}$$

where $\mathbf{P}$ is the 9×3 matrix shown above. The deviatoric corner rotations define the linear deviatoric-rotation field:

$$\theta' = \theta'_1 \zeta_1 + \theta'_2 \zeta_2 + \theta'_3 \zeta_3, \tag{26}$$

which integrates to zero over the element. For future use we note the matrix relation

$$\begin{Bmatrix} \theta'_1 \\ \theta'_2 \\ \theta'_3 \\ \bar{\theta} \end{Bmatrix} = \frac{1}{3} \begin{bmatrix} 2 & -1 & -1 \\ -1 & 2 & -1 \\ -1 & -1 & 2 \\ 1 & 1 & 1 \end{bmatrix} \begin{Bmatrix} \tilde{\theta}_1 \\ \tilde{\theta}_2 \\ \tilde{\theta}_3 \end{Bmatrix} = \left\{ \begin{bmatrix} 1 & 0 & 0 \\ 0 & 1 & 0 \\ 0 & 0 & 1 \\ \frac{1}{3} & \frac{1}{3} & \frac{1}{3} \end{bmatrix} - \frac{1}{3} \begin{bmatrix} 1 & 1 & 1 \\ 1 & 1 & 1 \\ 1 & 1 & 1 \\ 0 & 0 & 0 \end{bmatrix} \right\} \begin{Bmatrix} \tilde{\theta}_1 \\ \tilde{\theta}_2 \\ \tilde{\theta}_3 \end{Bmatrix} \tag{27}$$

or

$$\begin{Bmatrix} \theta' \\ \bar{\theta} \end{Bmatrix} = (\mathbf{J}' - \bar{\mathbf{J}}) \tilde{\theta}. \tag{28}$$

The hierarchical rotation decomposition is associated with a similar decomposition of the higher order strains:

$$\mathbf{e}_d = \mathbf{e}_b + \mathbf{e}_t, \tag{29}$$

where subscripts b and t identify "pure bending" and "torsional" strain fields, respectively. The former is generated by the deviatoric rotations θ' whereas the latter is generated by the mean hierarchical rotation $\bar{\theta}$. We now proceed to examine these two components in turn.

2.2 The Pure-Bending Field

This field is produced by pure inplane-bending modes associated with the deviatoric corner rotations $\theta'_i, i = 1, 2, 3$. One way to visualize the nature of these modes is to think of a tiny triangle superposed on a thin plane beam bent to constant curvature in its plane. Place the triangle centroid at neutral axis height. Then rotate the triangle so that its 3 sides align in turn with the bending direction.

From this visualization it follows that the *reference lines* mentioned in Box 1 are the triangle sides. The *straingage locations* are chosen at the triangle corners. The *natural strains* are the three direct strains parallel to the triangle sides, traversed in the counterclockwise sense. These strains are collected in the vector

$$\epsilon_b = \{ \epsilon_{b21} \quad \epsilon_{b32} \quad \epsilon_{b13} \}^T. \tag{30}$$

The natural strain ϵ_{jk} at corner i will be written $\epsilon_{jk|i}$, the bar being used for reading convenience. Vector ϵ_b at corner i is denoted by ϵ_{bi}. Our objective is to construct the 3×3 matrices $\mathbf{Q}_{bi}$ that relate natural straingage readings to the deviatoric rotations:

$$\epsilon_{b1} = \mathbf{Q}_{b1} \theta', \qquad \epsilon_{b2} = \mathbf{Q}_{b2} \theta', \qquad \epsilon_{b3} = \mathbf{Q}_{b3} \theta', \tag{31}$$

311

Once these are known the natural bending strains can be easily obtained by linear interpolation over the triangle: $\epsilon_b = (Q_{b1}\zeta 1 + Q_{b2}\zeta_2 + Q_{b3}\zeta_3)\theta' = Q_b\,\theta'$.

Consider the natural strain $\epsilon_{b21}(P)$ at an arbitrary point P of the triangle. Denote by $d_{21|P}$ the signed distance from the centroid to P measured along the internal normal to side 21. In particular, for the corners we have

$$d_{21|3} = \frac{4A}{3\ell_{21}}, \qquad d_{21|1} = d_{21|2} = -\tfrac{1}{2}d_{21|3} = -\frac{2A}{3\ell_{12}}. \tag{32}$$

We shall assume that $\epsilon_{b21|P}$ depends only on $d_{21|P}$ divided by the side length ℓ_{21}, which introduces a distance scaling. These dimensionless ratios will be called $\chi_{21|P} = d_{21|P}/\ell_{21}$, which specialized to the corners become

$$\chi_{21|3} = \frac{4A}{3\ell_{21}^2}, \qquad \chi_{21|1} = \chi_{21|2} = -\frac{2A}{3\ell_{21}^2}. \tag{33}$$

Formulas for corners 2 and 3 are obtained by cyclic permutation. According to the assumption just stated, the natural straingage readings $\epsilon_{b21|i}$ at corner i depend only on $\chi_{21|i}$, multiplied by as yet unknown weighting factors. This can be written in matrix form as follows:

$$
\epsilon_{b1} = \begin{Bmatrix} \epsilon_{b21|1} \\ \epsilon_{b32|1} \\ \epsilon_{b13|1} \end{Bmatrix} = \begin{bmatrix} \rho_1\chi_{21|1} & -\rho_2\chi_{21|1} & \rho_4\chi_{21|1} \\ \rho_5\chi_{32|1} & \rho_3\chi_{32|1} & -\rho_3\chi_{32|1} \\ -\rho_1\chi_{13|1} & \rho_4\chi_{13|1} & \rho_2\chi_{13|1} \end{bmatrix} \begin{Bmatrix} \theta'_1 \\ \theta'_2 \\ \theta'_3 \end{Bmatrix} = Q_{b1}\theta',
$$

$$
\epsilon_{b2} = \begin{Bmatrix} \epsilon_{b21|2} \\ \epsilon_{b32|2} \\ \epsilon_{b13|2} \end{Bmatrix} = \begin{bmatrix} \rho_2\chi_{21|2} & -\rho_1\chi_{21|2} & \rho_4\chi_{21|2} \\ \rho_4\chi_{32|2} & \rho_1\chi_{32|2} & -\rho_2\chi_{32|2} \\ -\rho_3\chi_{13|2} & \rho_5\chi_{13|2} & \rho_3\chi_{13|2} \end{bmatrix} \begin{Bmatrix} \theta'_1 \\ \theta'_2 \\ \theta'_3 \end{Bmatrix} = Q_{b2}\theta', \tag{34}
$$

$$
\epsilon_{b3} = \begin{Bmatrix} \epsilon_{b21|3} \\ \epsilon_{b32|3} \\ \epsilon_{b13|3} \end{Bmatrix} = \begin{bmatrix} \rho_3\chi_{21|3} & -\rho_3\chi_{21|3} & \rho_5\chi_{21|3} \\ \rho_4\chi_{32|3} & \rho_2\chi_{32|3} & -\rho_1\chi_{32|3} \\ -\rho_2\chi_{13|3} & \rho_4\chi_{13|3} & \rho_1\chi_{13|3} \end{bmatrix} \begin{Bmatrix} \theta'_1 \\ \theta'_2 \\ \theta'_3 \end{Bmatrix} = Q_{b3}\theta',
$$

where ρ_1 through ρ_5 are dimensionless weight factors to be determined on the basis of energy balancing for rectangular mesh units, as discussed in Section 3. The distribution and sign of these factors is made on the basis of triangular symmetries.

The strain field is energy orthogonal if

$$\rho_1 + \rho_2 = 2\rho_3, \qquad \rho_4 + \rho_5 = 0, \tag{35}$$

but these conditions will not be assumed *a priori*. The optimal element described in Section 3.2 will be found, however, to satisfy (35).

The natural strains can be related to Cartesian strains by the transformation

$$
\epsilon = \begin{Bmatrix} \epsilon_{12} \\ \epsilon_{23} \\ \epsilon_{31} \end{Bmatrix} = \begin{bmatrix} c_{21}^2 & s_{21}^2 & s_{21}c_{21} \\ c_{32}^2 & s_{32}^2 & s_{32}c_{32} \\ c_{13}^2 & s_{13}^2 & s_{13}c_{13} \end{bmatrix} \begin{Bmatrix} e_{xx} \\ e_{yy} \\ 2e_{xy} \end{Bmatrix} = T^{-1}e. \tag{36}
$$

312

where $c_{21} = x_{21}/\ell_{21}, s_{21} = y_{21}/\ell_{21}, c_{32} = x_{32}/\ell_{32}, s_{32} = y_{32}/\ell_{32}, c_{13} = x_{13}/\ell_{13}$ and $s_{13} = y_{13}/\ell_{13}$. The inverse of this relation is

$$\begin{Bmatrix} e_{xx} \\ e_{yy} \\ 2e_{xy} \end{Bmatrix} = \frac{1}{4A^2} \begin{bmatrix} y_{23}y_{13}\ell_{21}^2 & y_{31}y_{21}\ell_{32}^2 & y_{12}y_{32}\ell_{13}^2 \\ x_{23}x_{13}\ell_{21}^2 & x_{31}x_{21}\ell_{32}^2 & x_{12}x_{32}\ell_{13}^2 \\ (y_{23}x_{31} + x_{32}y_{13})\ell_{21}^2 & (y_{31}x_{12} + x_{13}y_{21})\ell_{32}^2 & (y_{12}x_{23} + x_{21}y_{32})\ell_{13}^2 \end{bmatrix} \begin{Bmatrix} \epsilon_{12} \\ \epsilon_{23} \\ \epsilon_{31} \end{Bmatrix}$$

(37)

or, in compact matrix notation, $\mathbf{e} = \mathbf{T}\boldsymbol{\epsilon}$. Note that $\mathbf{T}$ is constant over the triangle. Combining with (30) we get the Cartesian corner strains as $\mathbf{e}_{bi} = \mathbf{B}_{bi}\boldsymbol{\theta}' = \mathbf{T}\mathbf{Q}_{bi}\boldsymbol{\theta}'$, $i = 1, 2, 3$. The Cartesian strains are obtained by linearly interpolating over the element:

$$\mathbf{e}_b = (\mathbf{B}_{b1}\zeta_1 + \mathbf{B}_{b2}\zeta_2 + \mathbf{B}_{b3}\zeta_3)\boldsymbol{\theta}' = \mathbf{B}_b\boldsymbol{\theta}'. \tag{38}$$

2.3 The Torsional Field

The higher order stiffness produced by the pure bending fields alone is rank deficient (2 instead of 3) because of the deviatoric constraint $\sum \theta_i' = 0$. To complete the construction of a rank-sufficient higher order stiffness we need to build a strain field associated with the degree of freedom setting $\theta_i = \bar{\theta}$, others zero. This may be viewed as forcing each corner of the triangle to rotate by the same amount while the corner displacements are precluded. A displacement-based solution to this problem is provided by the cubic field of the QST triangle constructed by Felippa [21] and developed by Carr [22] as membrane component for refined analysis of thin shells. The QST expansion is

$$u_x = \begin{Bmatrix} v_{x1} \\ v_{x,x|1} \\ v_{x,y|1} \\ v_{x2} \\ v_{x,x|2} \\ v_{x,y|2} \\ v_{x3} \\ v_{x,x|3} \\ v_{x,y|3} \\ v_{x0} \end{Bmatrix}^T \begin{Bmatrix} \zeta_1^2(3 - 2\zeta_1) + 2\zeta_1\zeta_2\zeta_3 \\ \zeta_1^2(y_{12}\zeta_2 - y_{31}\zeta_3) + (x_{13} - x_{21})\zeta_1\zeta_2\zeta_3 \\ \zeta_1^2(x_{21}\zeta_2 - x_{13}\zeta_3) + (y_{31} - y_{12})\zeta_1\zeta_2\zeta_3 \\ \zeta_2^2(3 - 2\zeta_2) + 2\zeta_1\zeta_2\zeta_3 \\ \zeta_2^2(y_{23}\zeta_3 - y_{12}\zeta_1) + (x_{21} - x_{32})\zeta_1\zeta_2\zeta_3 \\ \zeta_2^2(x_{32}\zeta_3 - x_{21}\zeta_1) + (y_{12} - y_{23})\zeta_1\zeta_2\zeta_3 \\ \zeta_3^2(3 - 2\zeta_3) + 2\zeta_1\zeta_2\zeta_3 \\ \zeta_3^2(y_{31}\zeta_1 - y_{23}\zeta_2) + (x_{32} - x_{13})\zeta_1\zeta_2\zeta_3 \\ \zeta_3^2(x_{13}\zeta_1 - x_{32}\zeta_2) + (y_{23} - y_{31})\zeta_1\zeta_2\zeta_3 \\ 27\zeta_1\zeta_2\zeta_3 \end{Bmatrix} \tag{39}$$

where $v_{x,x|i}$ and $v_{x,y|i}$ denote $\partial u_x/\partial x$ and $\partial u_x/\partial y$, respectively, evaluated at corner i. A similar interpolation holds for the y displacement component u_y. The torsional mode with unit rotations $\theta_i = \bar{\theta} = 1$ is imposed by setting the QST nodal displacements to

$$v_{xi} = v_{yi} = v_{x,x|j} = v_{y,y|j} = 0, \quad v_{x,y|j} = -\bar{\theta}, \quad v_{y,x|j} = \bar{\theta}, \quad i = 0, 1, 2, 3, \quad j = 1, 2, 3.$$

(40)

Differentiating (39) with respect to x and y and setting the freedoms to (40), we obtain the torsional

313

strain field

$$e_{txx} = -\frac{1}{A}\Big[\zeta_1 y_{23}(y_{31}\zeta_3 - y_{12}\zeta_2) + \zeta_2 y_{31}(y_{12}\zeta_1 - y_{23}\zeta_3) + \zeta_3 y_{12}(y_{23}\zeta_2 - y_{31}\zeta_1)\Big]\bar{\theta},$$

$$e_{tyy} = \frac{1}{A}\Big[\zeta_1 x_{32}(x_{21}\zeta_2 - x_{13}\zeta_3) + \zeta_2 x_{13}(x_{32}\zeta_3 - x_{21}\zeta_1) + \zeta_3 x_{21}(x_{13}\zeta_1 - x_{32}\zeta_2)\Big]\bar{\theta},$$

$$2e_{txy} = -\frac{1}{A}\Big[\zeta_1 x_{32}(y_{31}\zeta_3 - y_{12}\zeta_2) - \zeta_1 y_{23}(x_{21}\zeta_2 - x_{13}\zeta_3)$$

$$+ \zeta_2 x_{13}(y_{12}\zeta_1 - y_{23}\zeta_3) - \zeta_2 y_{31}(x_{32}\zeta_3 - x_{21}\zeta_1)$$

$$+ \zeta_3 x_{21}(y_{23}\zeta_2 - y_{31}\zeta_1) - \zeta_3 y_{12}(x_{13}\zeta_1 - x_{32}\zeta_2)\Big]\bar{\theta},$$

$$(41)$$

where A is the triangle area. In matrix form

$$\mathbf{e}_t = \left\{ \begin{array}{c} e_{txx} \\ e_{tyy} \\ 2e_{txy} \end{array} \right\} = \mathbf{B}_t\, \bar{\theta}. \tag{42}$$

This strain field is compatible, varies quadratically, and vanishes at the corners and centroid. Integrating over the triangle and using the fact that $x_{12} + x_{23} + x_{31} = 0$ and $y_{12} + y_{23} + y_{31} = 0$ it may be verified that all strain components are energy orthogonal.

The field (41) appears unduly complicated. Conversion to natural strains through the transformation (36) reveals, however, its intrinsic simplicity:

$$\epsilon_t = \left\{ \begin{array}{c} \epsilon_{t21} \\ \epsilon_{t32} \\ \epsilon_{t13} \end{array} \right\} = \mathbf{T}^{-1}\mathbf{e}_t = \tfrac{3}{2} \left[\begin{array}{cc} \chi_{21|1} & \zeta_{21}\zeta_3 \\ \chi_{32|2} & \zeta_{32}\zeta_1 \\ \chi_{13|3} & \zeta_{13}\zeta_2 \end{array} \right] \bar{\theta}, \tag{43}$$

where $\zeta_{21} = \zeta_2 - \zeta_1$, $\zeta_{32} = \zeta_3 - \zeta_2$ and $\zeta_{13} = \zeta_1 - \zeta_3$. For future use, it is of interest to consider a *midpoint-filtered* version of (43), obtained by evaluating it at the three triangle midpoints 4, 5, 6 and then interpolating linearly over the triangle:

$$\epsilon_t^m = \left\{ \begin{array}{c} \epsilon_{t21}^m \\ \epsilon_{t32}^m \\ \epsilon_{t13}^m \end{array} \right\} = 3 \left[\begin{array}{cc} \chi_{21|1} & \zeta_{21} \\ \chi_{32|2} & \zeta_{32} \\ \chi_{13|3} & \zeta_{13} \end{array} \right] \bar{\theta}. \tag{44}$$

To facilitate combination with the bending field, it is convenient to define the "spread" matrix form of (44) in which each column receives one third of the strain:

$$\epsilon_t^m = \left\{ \begin{array}{c} \epsilon_{t21}^m \\ \epsilon_{t32}^m \\ \epsilon_{t13}^m \end{array} \right\} = \left[\begin{array}{ccc} \chi_{21|1}\zeta_{21} & \chi_{21|1}\zeta_{21} & \chi_{21|1}\zeta_{21} \\ \chi_{32|2}\zeta_{32} & \chi_{32|2}\zeta_{32} & \chi_{32|2}\zeta_{32} \\ \chi_{13|3}\zeta_{13} & \chi_{13|3}\zeta_{13} & \chi_{13|3}\zeta_{13} \end{array} \right] \left\{ \begin{array}{c} \bar{\theta} \\ \bar{\theta} \\ \bar{\theta} \end{array} \right\} = \mathbf{Q}_t^m \left\{ \begin{array}{c} \bar{\theta} \\ \bar{\theta} \\ \bar{\theta} \end{array} \right\} \tag{45}$$

3. THE STIFFNESS MATRIX

Having constructed the higher order strain fields, the computation of the higher-order stiffness can proceed according to the general rules laid out in Box 2. The bending and torsional strain fields are combined as

$$e_d = B_b\theta' + B_t\bar{\theta} = (B_bJ' - B_t\bar{J})\,\tilde{\theta} = B_d\tilde{\theta}, \qquad (46)$$

where J' and $\bar{J}$ are the numerical matrices in (28). We shall evaluate the higher order stiffness in terms of $\tilde{\theta}$, namely

$$K_{\theta h} = \int_A B_d^T (hE)B_d\, dA \qquad (47)$$

where h is the plate thickness, by numerical quadrature. The 9×9 higher order stiffness K_h then follows from the congruential transformation (19). At this point, however, we still have the undetermined ρ_i coefficients present in B_d.

3.1 The Optimal Element

For reasons that will be immediately apparent, we are particularly interested in *three point quadrature rules* defined parametrically by

$$\int_A F(\zeta_1, \zeta_2, \zeta_3)\, dA \approx \frac{A}{3}\Big[F(\xi, \eta, \eta) + F(\eta, \xi, \eta) + F(\eta, \eta, \xi) \Big] \qquad (48)$$

where $0 \le \xi \le 1$ and $\eta = \frac{1}{2}(1 - \xi)$. In practice the two most interesting rules of this type are $\xi = 2/3$ (the interior-three-point rule) and $\xi = 0$ (the midpoint rule), both of which exhibit quadratic accuracy. But in the present context it is instructive to leave ξ free, excluding only the cases $\xi = 1$ (corners) and $\xi = 1/3$ (centroid). A symbolic analysis with Macsyma, described fully in Section 2 of Part III [20], shows that the choice

$$\rho_1 = 0, \quad \rho_2 = 1 - \xi, \quad \rho_3 = \tfrac{1}{2}(1 - \xi), \quad \rho_4 = \rho_5 = 0, \qquad (49)$$

has the following properties:

1. It achieves pure-bending energy balance for rectangular mesh units of *arbitrary* aspect ratio, a test discussed in detail in Section 2 of Part III.

2. Let $K_{\theta h}(\xi)$ be the stiffness obtained with the integration rule (48) and the choice (49) for the ρ coefficients. Then the scaled stiffness

$$K_{\theta h} = \frac{2}{8(\xi - 1)^2(\xi - \frac{1}{3})^2}K_{\theta h}(\xi), \qquad (50)$$

is independent of ξ, and coincides with that of the optimal EFF element derived in Part I [1].

For practical calculations, it is convenient to use the midpoint rule $\xi = 0$ in which case $K_{\theta h} = \frac{9}{4}K_{\theta h}(0)$ for $\rho_2 = 1$, $\rho_3 = \frac{1}{2}$, others zero. If these are replaced in (34), the matrices Q_{bi} reduce to the simple form

$$\mathbf{Q}_{b1} = \begin{bmatrix} 0 & -\chi_{21|1} & 0 \\ 0 & \frac{1}{2}\chi_{32|1} & -\frac{1}{2}\chi_{32|1} \\ 0 & 0 & \chi_{13|1} \end{bmatrix}, \quad \mathbf{Q}_{b2} = \begin{bmatrix} \chi_{21|2} & 0 & 0 \\ 0 & 0 & -\chi_{32|2} \\ -\frac{1}{2}\chi_{13|2} & 0 & \frac{1}{2}\chi_{13|2} \end{bmatrix}, \quad \mathbf{Q}_{b3} = \begin{bmatrix} \frac{1}{2}\chi_{21|3} & -\frac{1}{2}\chi_{21|3} & 0 \\ 0 & \chi_{32|3} & 0 \\ -\chi_{13|3} & 0 & 0 \end{bmatrix}. \quad (51)$$

The seven-interior-point quadrature rule was also tried, but then it was found impossible to construct an energy-balanced element. Because this rule accounts for quadratic strain variations in the torsional mode, the foregoing negative result suggests that linear strain variations are required to attain an optimal element.

3.2 The Combined Natural Strain Field

Having chosen the optimal ρ coefficients and the midpoint integration rule, it is possible to obtain the complete higher-order natural strain field. This is done by combining the bending matrices (51) with the filtered torsional strain expression (45):

$$\epsilon_d = (\mathbf{Q}_b \mathbf{J}' - \mathbf{Q}_t^m \tilde{\mathbf{J}})\,\tilde{\theta} = \mathbf{Q}_d \tilde{\theta} = (\mathbf{Q}_{d1}\zeta_1 + \mathbf{Q}_{d2}\zeta_2 + \mathbf{Q}_{d3}\zeta_3)\tilde{\theta}, \quad (52)$$

where

$$\mathbf{Q}_{d1} = \begin{bmatrix} -\chi_{21|1} & -2\chi_{21|1} & -\chi_{21|1} \\ 0 & \frac{1}{2}\chi_{32|1} & -\frac{1}{2}\chi_{32|1} \\ \chi_{13|1} & \chi_{13|1} & 2\chi_{13|1} \end{bmatrix}, \quad \mathbf{Q}_{d2} = \begin{bmatrix} 2\chi_{21|2} & \chi_{21|2} & \chi_{21|2} \\ -\chi_{32|2} & -\chi_{32|2} & -2\chi_{32|2} \\ -\frac{1}{2}\chi_{13|2} & 0 & \frac{1}{2}\chi_{13|2} \end{bmatrix},$$

$$\mathbf{Q}_{d3} = \begin{bmatrix} \frac{1}{2}\chi_{21|3} & -\frac{1}{2}\chi_{21|3} & 0 \\ \chi_{32|3} & 2\chi_{32|3} & \chi_{32|3} \\ -2\chi_{13|3} & -\chi_{13|3} & -\chi_{13|3} \end{bmatrix}. \quad (53)$$

Evaluation at the midpoints gives

$$\mathbf{Q}_{d4} = \begin{bmatrix} \frac{1}{2}\chi_{21|4} & -\frac{1}{2}\chi_{21|4} & 0 \\ \chi_{32|4} & 2\chi_{32|4} & \chi_{32|4} \\ -2\chi_{13|4} & -\chi_{13|4} & -\chi_{13|4} \end{bmatrix}, \quad \mathbf{Q}_{d5} = \begin{bmatrix} -\chi_{21|5} & -2\chi_{21|5} & -\chi_{21|5} \\ 0 & \frac{1}{2}\chi_{32|5} & -\frac{1}{2}\chi_{32|5} \\ \chi_{13|5} & \chi_{13|5} & 2\chi_{13|5} \end{bmatrix},$$

$$\mathbf{Q}_{d6} = \begin{bmatrix} 2\chi_{21|6} & \chi_{21|6} & \chi_{21|6} \\ -\chi_{32|6} & -\chi_{32|6} & -2\chi_{32|6} \\ -\frac{1}{2}\chi_{13|6} & 0 & \frac{1}{2}\chi_{13|6} \end{bmatrix}. \quad (54)$$

where $\chi_{ji|4} = \frac{1}{2}(\chi_{ji|1} + \chi_{ji|2})$, etc. Note that the structure of $\mathbf{Q}_{d4}$, $\mathbf{Q}_{d5}$, $\mathbf{Q}_{d6}$ mimics that of $\mathbf{Q}_{d3}$, $\mathbf{Q}_{d1}$, and $\mathbf{Q}_{d2}$, respectively, the only change being the evaluation point.

3.3 Fast Computation of $\mathbf{K}_h$

With the explicit strain expressions of Section 3.2 we are now in a position to try for the fastest computation of $\mathbf{K}_h$. For this we proceed as follows. First evaluate

$$\mathbf{E}_n = \mathbf{T}^T \mathbf{E} \mathbf{T}, \quad (55)$$

which may be interpreted as a stress-strain matrix in natural coordinates. Then apply the midpoint rule, which for uniform thickness h yields

$$\mathbf{K}_{\theta h} = \frac{9}{4}\frac{Ah}{3}(\mathbf{Q}_{d4}^T\mathbf{E}_n\mathbf{Q}_{d4} + \mathbf{Q}_{d5}^T\mathbf{E}_n\mathbf{Q}_{d5} + \mathbf{Q}_{d6}^T\mathbf{E}_n\mathbf{Q}_{d6}) \tag{56}$$

Finally, transform to physical coordinates via (20), in which advantage should be taken of the special form (18) of $\mathbf{H}_{\theta v}$. These are essentially the same computational steps described in Appendix 2 of [19] for the 'AQR' ANDES plate bending triangle.

4. CONCLUDING REMARKS

We have presented the derivation of a plane stress triangle with drilling freedoms using the assumed natural deviatoric strain (ANDES) formulation. It is somewhat surprising that the optimal choice in the energy-balance sense described in Section 2 of Part III [20] coalesces with the optimal EFF element. This result suggest that this may in fact be the best available triangular element with the present freedom configuration.

Numerical integration is seen to play a crucial role in achieving an optimal element. The key effect is the function of the 3-point rule as a *strain filtering device* for the torsional mode. Note that strain filtering was not needed for the EFF derivation in Part I, which dealt throughout with quadratic displacements and linear strains.

Despite the coalescence, the ANDES derivation displays a different flavor than EFF. The formulation offers greater flexibility in that one is not restricted to compatible strain fields, allowing element developers to bypass detailed kinematic analysis. By way of contrast, the present element was formulated in two months whereas the derivation of the final EFF form took over one year. The difference may become more appreciable as one proceeds to shells and solid elements.

On the other hand, FF and EFF do provide explicitly the internal displacement field. This knowledge is useful in the calculation of consistent node force vectors — a topic further treated in Sections 3–4 of Part III — consistent mass matrices, and geometric stiffness matrices. In cases where the same element is available from both assumed-strain and assumed-displacement formulations (the present element as well as DKT being examples), one would prefer the latter for tasks that demand knowledge of internal displacements.

Acknowledgements

References

[1] K. Alvin, H. M. de la Fuente, B. Haugen and C. A. Felippa, Membrane triangles with corner drilling freedoms: I. The EFF element, in this report.

[2] K. J. Willam, Finite element analysis of cellular structures, Ph. D. Dissertation, Dept. of Civil Engineering, University of California, Berkeley CA, 1969

[3] D. G. Ashwell, Strain elements, with applications to arches, rings and cylindrical shells, in *Finite Elements for Thin Shells and Curved Members*, ed. by D. G. Ashwell and R. H. Gallagher, Wiley-Interscience, London, 1976

[4] M. J. Turner, R. W. Clough, H. C. Martin, and L. J. Topp, Stiffness and deflection analysis of complex structures, *Journal of Aeronautical Sciences*, 23, 1956, pp. 805–824

[5] R. H. MacNeal, Derivation of element stiffness matrices by assumed strain distribution, *Nuclear Engrgr. Design*, 70, 1978, pp. 3–12

[6] K. J. Bathe and E. N. Dvorkin, A four-node plate bending element based on Mindlin/Reissner plate theory and a mixed interpolation, *Int. J. Numer. Meth. Engrg.*, 21, 1985, pp. 367–383

[7] M. A. Crisfield, A four-noded thin plate element using shear constraints — a modified version of Lyons' element, *Computer Methods in Applied Mechanics & Engineering*, 38, 1983, pp. 93–120

[8] K. C. Park and G. M. Stanley, A curved C^0 shell element based on assumed natural-coordinate strains, *Journal of Applied Mechanics*, 53, 1986, pp. 278–290

[9] K. C. Park, An improved strain interpolation for curved C^0 elements, *Int. J. Numer. Meth. Engrg.*, 22, 1986, pp. 281–288

[10] J. C. Simo and T. J. R. Hughes, On the variational foundations of assumed strain methods, *Journal of Applied Mechanics*, 53, 1986, pp. 51–54

[11] H. C. Huang and E. Hinton, A new nine node degenerated shell element with enhanced membrane and shear interpolation, *Int. J. Numer. Meth. Engrg.*, 22, 1986, pp. 73–92

[12] J. Jang and P. M. Pinsky, An assumed covariant strain based 9-node shell element, *Int. J. Numer. Meth. Engrg.*, 24, 1987, pp. 2389–2411

318

[13]   P. G. Bergan and L. Hanssen, A new approach for deriving 'good' finite elements, MAFELAP II Conference, Brunel University, 1975, in *The Mathematics of Finite Elements and Applications — Volume II*, ed. by J. R. Whiteman, Academic Press, London, 1976

[14]   C. Militello, Application of Parametrized variational principles to the finite element method, *Ph. D. Dissertation*, Department of Aerospace Engineering Sciences, University of Colorado, Boulder, CO, 1991

[15]   C. A. Felippa and C. Militello, Developments in variational methods for high-performance plate and shell elements, in *Analytical and Computational Methods for Shells*, CAD Vol. 3, ed. by A. K. Noor, T. Belytschko and J. C. Simo, American Society of Mechanical Engineers, ASME, New York, 1989, pp. 191–216

[16]   C. A. Felippa and C. Militello, Variational formulation of high performance finite elements: parametrized variational principles, *Computers and Structures*, 36, 1990, pp. 1–11

[17]   C. Militello and C. A. Felippa, A variational justification of the assumed natural strain formulation of finite elements: I. Variational principles, *Computers and Structures*, 34, 1990, pp. 431–438

[18]   C. Militello and C. A. Felippa, A variational justification of the assumed natural strain formulation of finite elements: II. The four node C^0 plate element, *Computers and Structures*, 34, 1990, pp. 439–444

[19]   C. Militello and C. A. Felippa, The first ANDES elements: 9-DOF Kirchhoff plate bending triangles, *Computer Methods in Applied Mechanics and Engineering*, 93, 1991, pp. 217–246

[20]   C. A. Felippa and S. Alexander, Membrane triangles with corner drilling freedoms: III. Implementation and performance evaluation, in this report.

[21]   C. A. Felippa, Refined finite element analysis of linear and nonlinear two-dimensional structures, Ph. D. Dissertation, Department of Civil Engineering, University of California at Berkeley, Berkeley, CA, 1966

[22]   A. J. Carr, A refined finite element analysis of thin shell structures including dynamic loadings, Ph. D. Dissertation, Department of Civil Engineering, University of California at Berkeley, Berkeley, CA, 1968

MEMBRANE TRIANGLES WITH CORNER DRILLING FREEDOMS: III. IMPLEMENTATION AND PERFORMANCE EVALUATION

SUMMARY

This paper completes a three-Part series on the formulation of 3-node, 9-dof membrane triangles with corner drilling freedoms based on parametrized variational principles. The first four sections cover element implementation details including determination of optimal parameters and treatment of distributed loads. Then three elements of this type, labeled ALL, FF and EFF-ANDES, are tested on standard plane stress problems. ALL represents numerically integrated versions of Allman's 1988 triangle; FF is based on the free formulation triangle presented by Bergan and Felippa in 1985; and EFF-ANDES represent two different formulations of the optimal triangle derived in Parts I and II. The numerical studies indicate that the ALL, FF and EFF-ANDES elements are comparable in accuracy for elements of unitary aspect ratios. The ALL elements are found to stiffen rapidly in inplane bending for high aspect ratios, whereas the FF and EFF elements maintain accuracy. The EFF and ANDES implementations have an edge in formation speed over the FF.

1. INTRODUCTION

This paper is the last in an article series [1,2] that deals with the formulation and evaluation of high-performance triangular membrane elements with corner drilling freedoms. Those elements were derived using two recently developed techniques: the Extended Free Formulation or EFF [3] and the Assumed Natural Deviatoric Strain or ANDES [4, 5].

Part III has two main objectives:

1. To complete the theoretical derivations of Parts I and II with formulation and implementation details. These include the determination of optimal parameters by energy-balance methods, and the conversion of distributed applied loads to node forces. A third topic: accurate recovery of strains and stresses, is deferred because the study of superconvergent stress points (Barlow points) is still in progress.

2. To carry out a comparative evaluation of triangular elements of this type derived with three different construction methods: Allman's, FF and EFF-ANDES. The comparison involve accuracy for known test problems, accuracy degradation for high element aspect ratios, and computer formation times.

Table 1 summarizes notational conventions for the elements considered in following sections.

2. PARAMETER DETERMINATION

The EFF and ANDES triangles derived in Parts I and II, respectively, initially carry along a set of numerical parameters, most of which affect the higher order stiffness:

$$K^{EFF} = K_b(\alpha_b) + (1 - \gamma)K_h^u(\alpha_h), \tag{1}$$

$$K^{ANDES} = K_b(\alpha_b) + \alpha K_h^u(\rho_1, \rho_2, \rho_3, \rho_4, \rho_5). \tag{2}$$

where K_h^u is the unscaled higher order stiffness. Parameter α_b must be the same for all elements in an assembly, for otherwise the patch test would be violated. All other parameters may, in principle, vary from element to element without affecting convergence.

Equations (1)-(2) display a total of 3 and 7 parameters for the EFF and ANDES elements, respectively. The presence of these parameters is both a nuisance and an opportunity. In production-level programs one should *never* leave such parameters to be defined by users, as that would demand specialized knowledge. On the other hand, they provide the opportunity to improve the element performance in some respects, a process that may define "optimal values" for at least some of them. Such values may then be either hardwired in the element subroutine, or in the element-calling programs.

In the most favorable case the best value of a parameter is *element independent*; if so it can be set once and for all. Example are the "magic values" $\alpha_b = 3/2$, $\alpha_h = 5/4$ for (1). Next best is dependence on material properties but not on geometry; such parameters may be left as subroutine

Table 1 Element Notational Conventions

Identifier	Description
ALL-3i	1988 Allman triangle [6] numerically integrated by the 3-interior-point rule with sample points at $\left(\frac{2}{3}, \frac{1}{6}, \frac{1}{6}\right)$, $\left(\frac{1}{6}, \frac{2}{3}, \frac{1}{6}\right)$, $\left(\frac{1}{6}, \frac{1}{6}, \frac{2}{3}\right)$.
ALL-3m	*Ibid.*, numerically integrated by the 3-midpoint rule.
ALL-7i	*Ibid.*, numerically integrated by the 7-internal-point rule.
CST	Constant Strain Triangle; same as EFF(0,0,0).
EFF($\alpha_b, \alpha_h, \beta$)	EFF triangle constructed in Part I, with free parameters.
EFF	EFF triangle with optimal parameters (6), except that $\beta = \max(\frac{1}{2}(1 - 4\nu^2), 0.01)$ to maintain rank.
FF(β)	FF element constructed in [7] with $\alpha_b = \frac{3}{2}$ but with $\beta = 1 - \gamma$ as free parameter.
FF	FF element with $\beta = \frac{1}{2}$.
AND($\alpha_b, \alpha, \rho_1, \ldots \rho_5$)-7$i$	ANDES triangle constructed in Part II, with free parameters, numerically integrated by the 7-interior-point rule.
AND($\alpha_b, \alpha, \rho_1, \ldots \rho_5$)-3$\xi$	As above but numerically integrated by the parametrized 3-point rule with sample points at $\left(\xi, \frac{1}{2}(1 - \xi), \frac{1}{2}(1 - \xi)\right)$, $\left(\frac{1}{2}(1 - \xi), \xi, \frac{1}{2}(1 - \xi)\right)$, $\left(\frac{1}{2}(1 - \xi), \frac{1}{2}(1 - \xi), \xi\right)$ for $0 \le \xi < 1$, but excluding $\xi = \frac{1}{3}$.
AND	As above, upon substitution of the optimal parameters (7). Coalesces with EFF.
EFFAND	Designates indistinctly the optimal EFF or ANDES triangles.

arguments to be set by calling routines that may examine constitutive properties. A typical example is the higher order stiffness scaling factors $\beta = 1 - \gamma$ for EFF and α for ANDES. Least favorable is when the best value depends on element geometry; if so some compromises may be called for.

2.1 The Bending Test

For the present elements, parameters will be determined by an energy balance method on rectangular mesh units under simple but nonuniform motions. (This method resembles a linear patch test whose satisfaction is sought on an energy sense.) A modification of the test described by Bergan and Felippa [7] for the FF element is used. More specifically, we require exact energy response to pure bending in the configuration shown in Figure 1. The material is isotropic with elastic modulus E, Poisson's
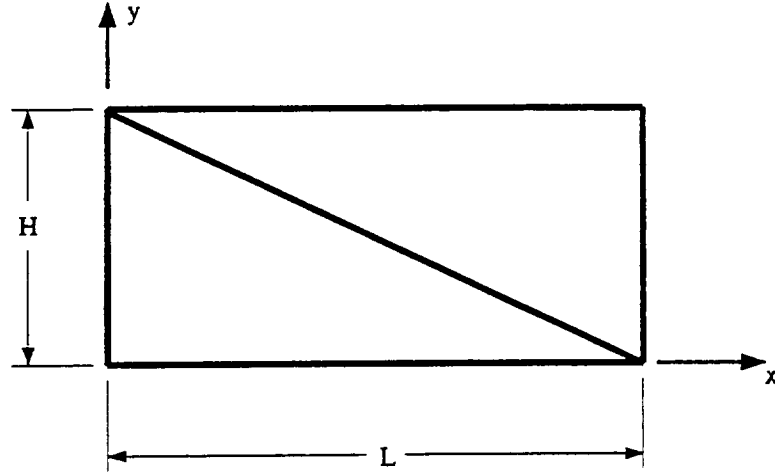
Figure 1. Mesh unit used for optimal parameter determination.

ratio ν, and uniform thickness h. Each mesh unit is assembled with two triangles; because of the symmetry the results would be identical if four half-thickness overlaid triangles (with no internal nodes) were used.

The $0 \le x \le L, 0 \le y \le H$ mesh unit is subjected to the pure-bending displacement field

$$u_x = -\kappa xy, \qquad u_y = \tfrac{1}{2}\kappa(x^2 + \nu y^2), \qquad \theta = \kappa x, \tag{3}$$

where $\kappa = M/(EI)$, with $I = \tfrac{1}{12}hH^3$, is the bending curvature. This produces an *equilibrium* plane stress state $\sigma_{xx} = E\kappa y$, others zero. The exact strain energy stored in the elastic body that occupies the mesh unit domain is

$$U_{ex} = \frac{1}{3}Eh\kappa^2 LH^3 = \frac{1}{3}Eh\kappa^2 L^2 r^3, \tag{4}$$

where $r = H/L$ or $r^{-1} = L/H$ are used as aspect ratio measures in the sequel.

Let $\mathbf{v}$ be the nodal displacement vector obtained by evaluating (3) at the nodes. The strain energy taken up by the finite element assembly is

$$U_{FE} = \tfrac{1}{2}\mathbf{v}^T\mathbf{K}\mathbf{v}, \tag{5}$$

where $\mathbf{K}$ is the total stiffness of the assembly. If the triangle stiffnesses contain parameters, these are taken to be the same for both. The strain energy ratio $\eta = U_{FE}/U_{ex}$ obtained through Macsyma is listed in Table 2 for several elements. The identification conventions of Table 1 are followed. All data pertain to isotropic elements; for the ANDES element of Part II only the case $\nu = 0$ is shown to prevent the equations from overflowing the page. Table 3 complements Table 2 by giving numeric values for specific values of parameters, Poisson's ratio ν and aspect ratio r.

It should be noted that if $\nu = 0$, the test of Figure 1 could be further simplified by moving the (x, y) axes to the center of the rectangle. Because of symmetry only one triangle would then need

323

to be considered. But this simplified test, which was in fact the one used in [7], does not properly account for the y-contraction effect if $v \neq 0$ because the displacement field (3) applied to the nodes would not be distinguishable from a y rigid-body motion.

2.2 Nice Solutions for EFF and ANDES

The energy-balancing condition $\eta = 1$ leads to algebraic Riccati equations in the free parameters. The resulting system is linear in β and α, quadratic in parameters such as α_b, α_h and the ρ_i, and quartic or higher in the aspect ratio r. A solution of these equations is called "nice" if it yields *real* values for the parameters that are *independent* of r. Being aspect-ratio independent, these solutions are of significant practical value. They are sought by equating coefficients of powers of r to 0 or 1.

The parametrized EFF element has the surprisingly simple nice solution

$$\alpha_b = \tfrac{3}{2}, \qquad \alpha_h = \tfrac{5}{4}, \qquad \beta = 1 - \gamma = \tfrac{1}{2}(1 - 4v^2), \tag{6}$$

The values for α_b and α_h emerge as *double roots* of quadratic equations while β is the root of a linear equation; thus (6) is the only such solution.

For the ANDES element the situation is more complicated. All nice solutions of the Riccati equations of the 7-point integrated element are imaginary. For the 3-point-integrated element with ξ-parametrized sample points (cf. Table 1), the value $\alpha_b = 3/2$ is exceptional in the sense that the nice solution

$$\alpha_b = \tfrac{3}{2}, \quad \rho_1 = \rho_4 = \rho_5 = 0, \quad \rho_1 = 2\rho_2 = 1 - \xi, \quad \alpha = \frac{2}{8(\xi - 1)^2(\xi - \tfrac{1}{3})^2}, \tag{7}$$

is unique (it appears as a double root of a quadratic). This can be generalized to arbitrary v by multiplying α by $(1 - 4v^2)$. If $\alpha_b < 3/2$, many other solution families exist that satisfy $\rho_4 = \rho_5 = 0$, $\rho_1 = \rho_2 - 1 + \xi$; for example, if $v = \xi = 0$, $\alpha_b = 0$, $\rho_3 = \tfrac{1}{2}\rho_2 = (5 \pm \sqrt{15})/4$, $\alpha = 9/(-16 \mp \sqrt{15})$. But since all these solutions lead to the same $\mathbf{K}$, nothing new emerges. On setting the values (7), the resulting element coalesces with the optimal EFF.

2.3 The FF Triangle

For the FF element of [7] an "almost nice" solution is possible. If $\alpha_b = \tfrac{3}{2}$, the condition $\eta = 1$ yields the "balancing β" as

$$\beta = 1 - \gamma = \frac{3}{8} \frac{(1 - 4v^2)(r^8 + 6r^6 + 11r^4 + 6r^2 + 1)}{r^8 + 3r^6 + 8r^4 + 5r^2 + 1 + v(3r^6 + 3r^4 + r^2)}. \tag{8}$$

This expression differs somewhat from the numerical results presented in [7] because the energy balance test done in that paper was on a different mesh unit that did not account for lateral contraction.

Equation (8) has the disadvantage of depending on the aspect ratio r; thus securing the correct energy balance for bending along x does not imply such balance for bending about y unless $r = 1$ (square mesh unit). Nonetheless for a given v the dependence is mild; for example if $v = 0$, β

Table 2. Energy Ratios for Mesh Unit of Figure 1
under Pure Bending — Isotropic Material

Element	Energy ratio $\eta = U_{FE}/U_{ex}$	Nice solutions of $\eta = 1$
ALL-3m	$\left[72 - 48\nu^2 + (5 - 9\nu)r^{-2} + 2r^{-4}\right]/[64(1 - \nu^2)]$	None
ALL-3i	$\left[1880 - 1296\nu^2 + (79 - 91\nu)r^{-2} + 6r^{-4}\right]/[1728(1 - \nu^2)]$	None
ALL-7i	$\left[264 - 180\nu^2 + (15 - 19\nu)r^{-2} + 2r^{-4}\right]/[240(1 - \nu^2)]$	None
CST	$\left[6(2 - \nu^2) + 3(1 - \nu)r^{-2}\right]/[8(1 - \nu^2)]$	None
EFF $(\alpha_b, \alpha_h, \beta)$	$\begin{aligned}\big[&(16\alpha_h^2 - 52\alpha_h + 43)\beta + 2\alpha_b^2 - 12\alpha_b + 36 - 18\nu^2 \\ &+ \big((\alpha_h^2(16\nu + 32) - \alpha_h(80 + 64\nu) + 50 + 55\nu)\beta \\ &+ (1 - \nu)(4\alpha_b^2 - 12\alpha_b - 9)\big)r^{-2} \\ &+ (48\alpha_h^2 - 120\alpha_h + 75)\beta r^{-4}\big]/[24(1 - \nu^2)]\end{aligned}$	$\alpha_b = \tfrac{3}{2},\ \alpha_h = \tfrac{5}{4},$ $\beta = 1 - \gamma = \tfrac{1}{2}(1 - 4\nu^2)$
FF(β)	$\begin{aligned}\big[&(45 - 36\nu^2 + 8\beta)r^8 + (270 - 216\nu^2 + (24\nu + 24)\beta)r^6 \\ &+ (495 - 396\nu^2 + (24\nu + 64)\beta)r^4 \\ &+ (270 - 216\nu^2 + (8\nu + 40)\beta)r^2 + 45 - 36\nu^2 + 8\beta\big] \\ &/\big[48(1 - \nu^2)(r^8 + 6r^6 + 11r^4 + 6r^2 + 1)\big]\end{aligned}$	None (but see Section 2.3)
AND$(\alpha_b, \alpha,$ $\rho_1 \ldots \rho_5)$-7i $(\nu = 0)$	$\begin{aligned}\Big[&\Big(\big((60\rho_5 - 60\rho_4 + 480\rho_3 - 120\rho_2 - 120\rho_1)\rho_5 \\ &+ (45\rho_4 - 240\rho_3 + 180\rho_2 + 180\rho_1)\rho_4 \\ &+ (960\rho_3 - 480\rho_2 - 480\rho_1)\rho_3 + (195\rho_2 + 330\rho_1 + 12)\rho_2 \\ &+ 195\rho_1^2 - 12\rho_1 + 4\big)\alpha + 360\alpha_b^2 - 2160\alpha_b + 3240\Big) \\ &+ \Big(\big((300\rho_5 - 240\rho_4 - 720\rho_3 + 480\rho_2 + 600\rho_1 - 48)\rho_5 \\ &+ (210\rho_4 + 1080\rho_3 - 480\rho_2 - 420\rho_1 - 24)\rho_4 \\ &+ (1440\rho_3 - 1320\rho_2 - 1080\rho_1 - 48)\rho_3 \\ &+ 330\rho_2^2 + 600\rho_1\rho_2 + 390\rho_1^2 - 24\rho_1 + 8\big)\alpha \\ &+ 720\alpha_b^2 - 2160\alpha_b + 1620\Big)r^{-2} \\ &+ \Big(\big(540\rho_5^2 - 540\rho_4\rho_5 + 405\rho_4^2 + 15\rho_2^2 \\ &- 30\rho_1\rho_2 - 12\rho_2 + 15\rho_1^2 + 12\rho_1 + 4\big)\alpha\Big)r^{-4}\Big]/1080\end{aligned}$	None

325

Table 2. Energy Ratios (Continued)

Element	Energy ratio $\eta = U_{FE}/U_{ex}$	Nice solutions of $\eta = 1$
AND(α_b, α, $\rho_1 \ldots \rho_5$) -3ξ ($\nu = 0$)	$\Big\{ \big[[(9\xi^4 - (18\rho_2 - 18\rho_1 + 24)\xi^3 + (12\rho_5^2$ $+ \rho_3(96\rho_5 + 48\rho_4) + \rho_1(24\rho_5 + 12\rho_4 + 96\rho_3 + 6\rho_2$ $- 30) + \rho_2(24\rho_5 + 12\rho_4 + 96\rho_3 + 30) + 12\rho_4\rho_5$ $+ 3\rho_4^2 + 192\rho_3^2 + 21\rho_2^2 + 21\rho_1^2 + 22)\xi^2$ $+ (\rho_1(-16\rho_5 - 8\rho_4 - 64\rho_3 - 4\rho_2 + 14)$ $+ \rho_2(-16\rho_5 - 8\rho_4 - 64\rho_3 - 14) + \rho_3(-64\rho_5 - 32\rho_4)$ $- 8\rho_5^2 - 8\rho_4\rho_5 - 2\rho_4^2 - 128\rho_3^2 - 14\rho_2^2$ $- 14\rho_1^2 - 8)\xi + 4\rho_5^2 + \rho_3(32\rho_5 - 16\rho_4)$ $- 4\rho_4\rho_5 + \rho_1(-8\rho_5 + 12\rho_4 - 32\rho_3 + 22\rho_2 - 2)$ $+ \rho_2(-8\rho_5 + 12\rho_4 - 32\rho_3 + 2) + 3\rho_4^2 + 64\rho_3^2$ $+ 13\rho_2^2 + 13\rho_1^2 + 1)\alpha + 24\alpha_b^2 - 144\alpha_b + 216 \big]$ $+ \big[(18\xi^4 + (72\rho_5 + 36\rho_4 + 72\rho_3 + 36\rho_1 - 48)\xi^3$ $+ (72\rho_5^2 + \rho_3(144\rho_5 + 72\rho_4 - 120) + \rho_1(72\rho_5$ $+ 36\rho_4 + 120\rho_3 - 24\rho_2 - 60) + \rho_4(72\rho_5 - 60)$ $- 120\rho_5 + 18\rho_4^2 + 96\rho_3^2 - 24\rho_2\rho_3 + 6\rho_2^2$ $+ 42\rho_1^2 + 44)\xi^2 + (56\rho_5 - 48\rho_5^2 + \rho_1(-48\rho_5$ $- 24\rho_4 - 80\rho_3 + 16\rho_2 + 28) + \rho_4(28 - 48\rho_5)$ $+ \rho_3(-96\rho_5 - 48\rho_4 + 56) - 12\rho_4^2 - 64\rho_3^2$ $+ 16\rho_2\rho_3 - 4\rho_2^2 - 28\rho_1^2 - 16)\xi + 20\rho_5^2$ $+ \rho_1(40\rho_5 - 28\rho_4 - 72\rho_3 + 40\rho_2 - 4) + \rho_2(32\rho_5$ $- 32\rho_4 - 88\rho_3) - 8\rho_5 + \rho_4(-16\rho_5 - 4)$ $+ \rho_3(-48\rho_5 + 72\rho_4 - 8) + 14\rho_4^2 + 96\rho_3^2 + 22\rho_2^2$ $+ 26\rho_1^2 + 2)\alpha + 48\alpha_b^2 - 144\alpha_b + 108 \big] r^{-2}$ $+ \big[9\xi^4 + (18\rho_2 - 18\rho_1 - 24)\xi^3 + (108\rho_5^2$ $+ 108\rho_4\rho_5 + 27\rho_4^2 + 9\rho_2^2 - 30\rho_2$ $+ \rho_1(30 - 18\rho_2) + 9\rho_1^2 + 22)\xi^2 + (14\rho_2$ $- 72\rho_5^2 - 72\rho_4\rho_5 - 18\rho_4^2 - 6\rho_2^2 + \rho_1(12\rho_2 - 14)$ $- 6\rho_1^2 - 8)\xi + 36\rho_5^2 - 36\rho_4\rho_5 + 27\rho_4^2$ $+ \rho_2^2 - 2\rho_2 + \rho_1(2 - 2\rho_2) + \rho_1^2 + 1)\alpha \big] r^{-4} \Big\}/72$	$\alpha_b = \frac{3}{2},$ $\rho_1 = \rho_4 = \rho_5 = 0,$ $\rho_2 = 2\rho_3 = 1 - \xi,$ $\alpha = \dfrac{2}{8(\xi - 1)^2(\xi - \frac{1}{3})^2}$

Table 3   Energy Ratio η for Specific Elements, ν and r

ν	$1/r$	ALL-3m	ALL-3i	ALL-7i	CST	EFFAND	FF
0	1/4	1.130	1.091	1.104	1.523	1.000	1.009
	1/2	1.146	1.100	1.116	1.594	1.000	0.997
	1	1.234	1.137	1.171	1.875	1.000	0.998
	2	1.938	1.326	1.483	3.000	1.000	1.009
	4	10.375	2.708	4.233	7.500	1.000	1.016
	8	134.125	18.236	39.233	25.500	1.000	1.020
	16	2069.125	240.347	563.233	97.500	1.000	1.021
1/4	1/4	1.153	1.113	1.126	1.569	1.000	1.030
	1/2	1.164	1.119	1.135	1.625	1.000	1.020
	1	1.229	1.149	1.178	1.850	1.000	1.020
	2	1.867	1.309	1.448	2.750	1.000	1.029
	4	10.417	2.614	4.128	6.350	1.000	1.035
	8	140.617	18.503	40.448	20.750	1.000	1.038
	16	2197.417	252.725	595.328	78.350	1.000	1.039
1/2	1/4	1.251	1.202	1.219	1.766	1.000	1.103
	1/2	1.255	1.207	1.225	1.812	1.000	1.095
	1	1.302	1.231	1.258	2.000	1.000	1.096
	2	1.958	1.378	1.517	2.750	1.000	1.103
	4	12.083	2.799	4.550	5.750	1.000	1.108
	8	172.583	21.818	48.683	17.750	1.000	1.110
	16	2734.583	311.225	737.217	65.750	1.000	1.111

varies from 0.375 to 0.547 and so the "compromise" value of 1/2 was recommended in [7] for general use. This is confirmed by Table 3, in which one can see that the deviation of $\eta(\nu, r)$ from 1 for FF($\frac{1}{2}$) never exceeds 12%.

2.4 Orthotropic Material

All previous results can be extended to an orthotropic material characterized by the strain-stress relation

$$\begin{Bmatrix} \epsilon_{xx} \\ \epsilon_{yy} \\ \gamma_{xy} \end{Bmatrix} = \begin{bmatrix} \frac{1}{E_1} & \frac{\nu_{12}}{E_1} & 0 \\ \frac{\nu_{21}}{E_2} & \frac{1}{E_2} & 0 \\ 0 & 0 & G \end{bmatrix} \begin{Bmatrix} \sigma_{xx} \\ \sigma_{yy} \\ \sigma_{xy} \end{Bmatrix},$$

implying that the principal orthotropy axes are directed along the bending directions. The displacement equilibrium solution (5) has to be suitable modified. All previous nice solutions were found to apply if ν^2 is replaced by $\nu_{12}\nu_{21}$. The case of general anisotropic material has not been investigated, as for such materials the construction of a pure-bending equilibrium solution is difficult.

3. BODY LOAD LUMPING

The conversion of distributed loads to node forces (a process herein called *load lumping*) in high-performance elements displays several points of interest. Discrepancies arise with respect to the well ordered world of conforming elements. These can only be explained satisfactorily through the underlying variational principles. To focus subsequent discussions it is convenient to distinguish between interior or body loads, and boundary loads.

If body loads $\mathbf{b}^T = \{b_x \; b_y\}$ *per unit volume* are given within a two-dimensional FF or EFF element, the variational formulation says that the consistent node force vector $\mathbf{p}$ is given by the usual formula

$$\mathbf{p} = \int_A \mathbf{N}_u^T \, h\mathbf{b} \, dA, \tag{9}$$

where h is the element thickness and $\mathbf{N}_u$ is a 2×9 matrix of shape functions that gives the internal displacements $\mathbf{u}$ in terms of the visible degrees of freedom:

$$\mathbf{u} = \left\{ \begin{array}{c} u_x \\ u_y \end{array} \right\} = \mathbf{N}_u \mathbf{v}. \tag{10}$$

In the FF and EFF, the shape functions $\mathbf{N}_u$ are not usually known directly but result from transformations on modal functions initially constructed in terms of generalized coordinates (cf. Part I).

But if the element is of ANS or ANDES type the internal displacements $\mathbf{u}$ are not necessarily known, because the assumed strains may not be integrable. A heuristic solution is to use the $\mathbf{p}$ vector of an FF, EFF, or conforming element with the same $\mathbf{v}$. This expedient device has been used *sotto voce* in stress-assumed hybrid elements for over two decades.

Although the subject is not treated here, it should be noted that a similar obstacle arises when computing the consistent mass matrix and geometric stiffness matrices of assumed strain elements. These two calculations require knowledge of the internal displacements and their gradients, respectively.

4. BOUNDARY LOAD LUMPING

Suppose boundary loads $\mathbf{t}$ ("surface tractions" in continuum mechanics terminology) are specified *per unit length* and *thickness* on the boundary S of a two-dimensional FF, EFF, or ANDES element. The variational formulation presented in [8] asserts that, under certain assumptions examined further in Section 4.3,

$$\mathbf{p} = \int_S \mathbf{N}_d^T \, h\mathbf{t} \, dS. \tag{11}$$

where $\mathbf{N}_d$ are the shape functions for the *boundary* displacement field. In general $\mathbf{u}$ and $\mathbf{d}$ do not match on S, so (11) is not necessarily the same as $\int_S \mathbf{N}_u^T \, h\mathbf{t} \, dS$. The following difficulties may arise.

1. $\mathbf{N}_d$ may depend on free parameters, for example the rotational factor α in equation (29) of Part I. The optimal value of these parameters may be different for the basic and higher order
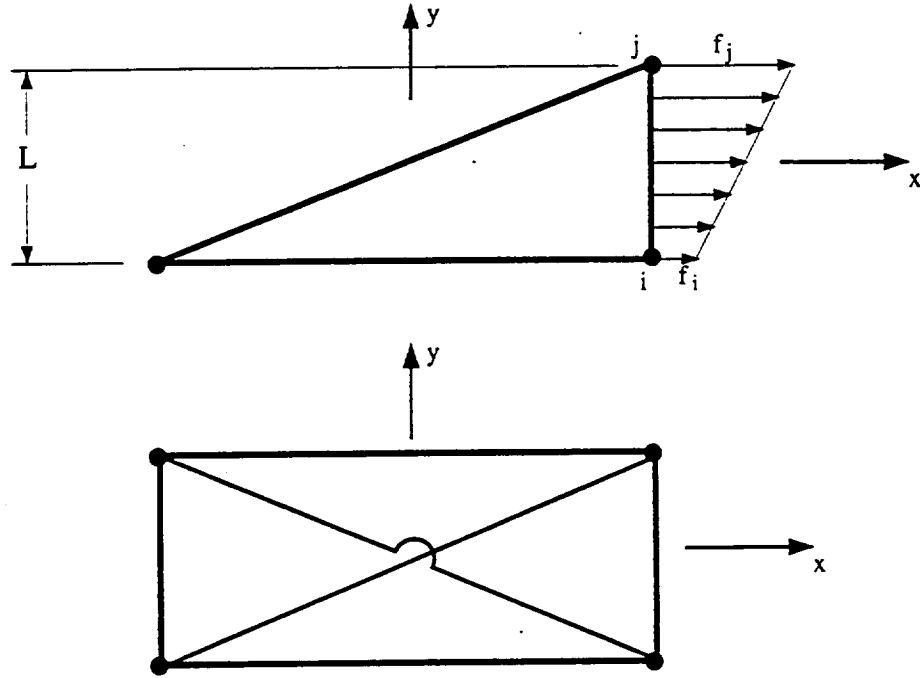
Figure 2. Triangle side subjected to normal linearly-varying load f

parts; for example in the optimal EFF element, $\alpha_b = 3/2$ but $\alpha_h = 5/4$. Which value should be used for $\mathbf{p}$?

2. The assumptions that lead to (11) may not be applicable, and if so the *internal displacement* $\mathbf{u}$ evaluated on the boundary, rather than $\mathbf{d}$, appears for portions of $\mathbf{t}$.

These difficulties are best assessed through a detailed example relevant to the present application. A side of length L of a right-angled EFF triangle of constant thickness h is subjected to a normal distributed load f (per unit of length and h) that varies linearly from f_i at node i to f_j at node j. The x and y angles are placed as shown in Figure 2. We shall see that nodes forces p_x, p_y and p_θ at nodes i and j depend on f_i and f_j through formulas that can be placed in the generic form

$$p_{xi} = \tfrac{1}{2}\big(\psi_t f_i + (1 - \psi_t) f_j\big)hL, \qquad p_{yi} = 0, \qquad p_{\theta i} = \tfrac{1}{8}\omega\big(\psi_r f_i + (1 - \psi_r) f_j\big)hL^2,$$
$$p_{xj} = \tfrac{1}{2}\big((1 - \psi_t) f_i + \psi_t f_j\big)hL, \qquad p_{yj} = 0, \qquad p_{\theta j} = -\tfrac{1}{8}\omega\big((1 - \psi_r) f_i + \psi_r f_j\big)hL^2. \tag{12}$$

Here ψ_t, ψ_r and ω are numerical coefficients (subscripts t and r stand for translation and rotation, respectively.) A simple calculation shows that translational equilibrium is always satisfied by (12), but that rotational equilibrium for $f_i \neq f_j$ requires $12\psi_t - 6\omega\psi_r = 8 - 3\omega$. Table 4 collects results from several methods outlined below.

4.1 Boundary Shape Functions

Table 4 Load Lumping Formulas for Case of Figure 2

Identifier label	Method description	Coefficients of (12)			Rotational equilibrium?
		ψ_t	ψ_r	ω	
$\mathrm{HCI}(\alpha_f)$	Eq. (11) with Hermite cubic interpolation shape functions	$\frac{7}{10}$	$\frac{3}{5}$	$\frac{2}{3}\alpha_f$	Only if $\alpha_f = 1$ unless $f_i = f_j$
LI	Eq. (11) with linear interpolation shape functions	$\frac{2}{3}$	any	0	Yes
EBZ	Energy balance, $\nu = 0$	$\frac{37}{48}$	$\frac{17}{24}$	1	Yes
EBH	Energy balance, $\nu = \frac{1}{2}$	$\frac{5}{6}$	$\frac{5}{6}$	1	Yes
EBQ	$\nu = \frac{1}{4}$ interpolating EBZ and EBH	$\frac{77}{96}$	$\frac{37}{48}$	1	Yes

The simplest load lumping technique consists of using (11) with N_d from the boundary interpolation for the basic stiffness. This is exact if the boundary loads are uniform, and in any case reasonable from the standpoint of convergence.

Using the cubic Hermite interpolation — equation (19) of Part I — with rotation shape functions multiplied by α_f yields the coefficients listed under label 'HCI(α_f)' in Table 4. A similar calculation using linear interpolation yields the coefficients listed under label 'LI'. This is effectively the CST load lumping, for which the fixed-end nodal moments p_θ vanish.

4.2 Energy Balance

A different procedure uses energy balance (EB) concepts similar to those exploited in Section 2. Embed the triangle into the four-triangle rectangular mesh unit illustrated in Figure 2(b). A stress field that equilibrates the boundary loads is

$$\sigma_{xx} = (1 - \zeta)f_i + \zeta f_j, \quad \sigma_{yy} = \sigma_{xy} = 0, \tag{13}$$

where $\zeta = \frac{1}{2} + x/L$ is a side isoparametric coordinate. The associated strain field is easily integrable if h is constant and the material is isotropic. Taking symmetric boundary conditions about the mesh unit midcenter one gets the displacement field

$$u_x = c_m x - c_b xy, \quad u_y = -c_m \nu y + \frac{1}{2}(x^2 + \nu y^2), \quad \theta = c_b x, \tag{14}$$

in which $c_m = \frac{1}{2}(f_j + f_i)/E$ and $c_b = (f_j - f_i)/(EL)$. Evaluate this at the nodes of the mesh assembly to form the 12×1 displacement vector $\mathbf{v}$. Evaluate the 12×12 EFF stiffness $\mathbf{K}$ of the assembly using the optimal parameters (6). From the energy condition $\frac{1}{2}\mathbf{v}^T\mathbf{K}\mathbf{v} - \mathbf{v}^T\mathbf{p} = \min$ the force vector is taken to be $\mathbf{p} = \mathbf{K}\mathbf{v}$ from which the forces on nodes i and j can be extracted. For Poisson's ratios $\nu = 0$ and $\nu = \frac{1}{2}$ this method gives a formula that befits (12), with the coefficients listed under labels 'EBZ' and 'EBH', respectively, in Table 4.

330

4.3 Locality Lost

What happens if $\nu \neq 0$ and $\nu \neq \frac{1}{2}$? Then the expressions given by the EB method bring in the triangle dimension normal to side $i-j$, and forces appears on the third corner! This is contrary to intuition, but the variational principle in [8] explains this mystery. The original boundary traction energy term is $\int_S h\mathbf{tu}\,dS$ rather than $\int h\mathbf{td}\,dS$. The key assumption in the reduction to the latter is that $\mathbf{t}$ be in the range of $\sigma_n^u = \mathbf{n}^T(\mathbf{EDu})$, namely the normal projection of the internal stresses generated by the internal displacement field $\mathbf{u}$.

Now the internal displacement field (14) is in the range of the applied load f, but is not exactly representable by EFF elements if $\nu \neq 0$. Thus σ_n^u can match any constant f exactly through the basic modes, but a linearly varying f only approximately through the higher order modes. (The case $\nu = \frac{1}{2}$ is a fluke in that the higher order stiffness vanishes on setting the optimal $\beta = \frac{1}{2}(1-4\nu^2) = 0$ and only the basic stiffness survives.) As a result the boundary term $\int_S h\mathbf{tu}\,dS$ emerges on part of the linear variation of f. This destroys locality because $\mathbf{u}$ along an element side does not necessarily depend only on freedoms located on that side.

For the numerical experiments in Section 6 the case $\nu = \frac{1}{4}$, labeled 'EBQ' in Table 4, is handled by linear interpolation of the coefficients for EBZ and EBH, a device that maintains locality despite being variationally inconsistent.

4.4 Rotational Disequilibrium

A comparative analysis of HCI, EBZ and EBH leads to the following conflict. For *uniform* load $(f_i = f_j = f)$ the three expressions coincide if $\alpha_f = \frac{3}{2}$ for HCI, giving

$$p_{xi} = p_{xj} = \tfrac{1}{2}fL \quad \text{(as expected)}, \qquad p_{\theta i} = -p_{\theta j} = \tfrac{1}{8}fL^2. \tag{15}$$

By running uniform stretch problems, reported in Section 6, it is readily verified that these "fixed-end moments" are the correct ones. But for a varying force $(f_i \neq f_j)$ HCI *violates* rotational equilibrium unless $\alpha_f = 1$. This violation does not affect ultimate convergence as the mesh size is refined, but may worsen coarse-mesh results.

Thus both techniques for computing node forces are found to have limitations. Use of (11) maintains locality but may lead to inaccurate or out-of-equilibrium formulas. The energy balance technique is accurate and upholds equilibrium, but brings in material properties and may lose locality.

4.5 Practical Recommendations

In production programs the force computation module may not be aware of "interior details" such as the element type and material properties. Then it appears best to take a compromise value for the coefficients. For example: $\psi_t = 3/4 = 0.75$, $\psi_r = 2/3$ and $\omega = 1$, a set that satisfies rotational equilibrium. The difference between two equilibrium force systems is a self-equilibrated force system. By Saint-Venant's principle its effect should be felt only within a few element layers. Thus for fine meshes the choice for load lumping should make little difference. But the effect
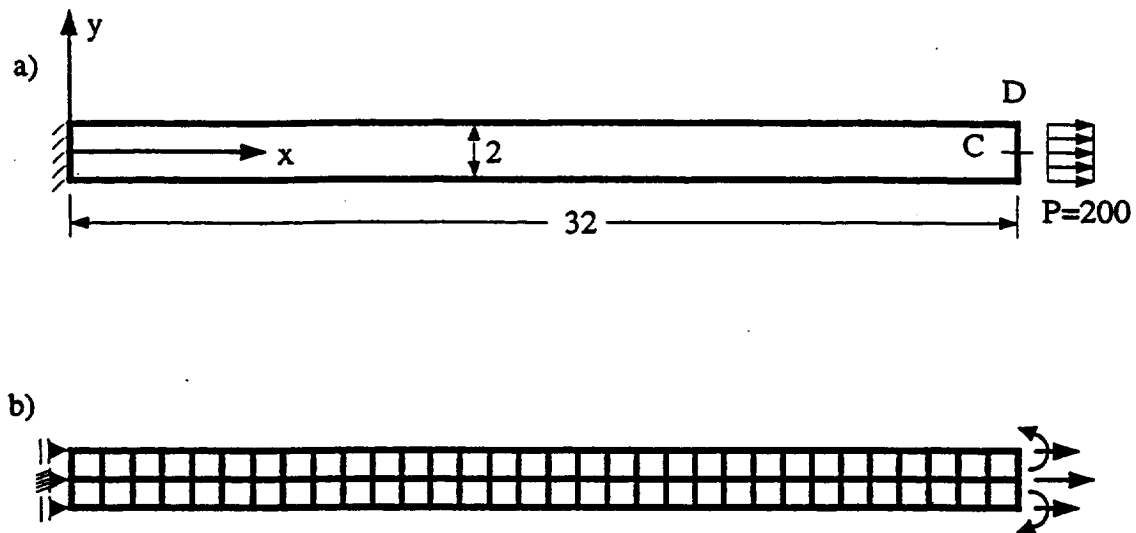
Figure 3. Slender beam under axial loading: $E = 32$, ν varies, $h = 1$;
root contraction allowed for $\nu \neq 0$; four-overlaid-triangle
mesh units used; a 32×2 mesh is shown in (b).

can be important for coarse meshes, or when accurate local stresses are desired. The numerical experiments of Section 6 corroborate this observation.

For distributed forces *tangential* to element sides no such difficulties arise because the only possible tangential displacement interpolation is linear. Consequently the node force lumping of the constant strain triangle (CST) can be used.

5. ACCURATE RECOVERY OF STRAINS AND STRESSES

One of the goals of high-performance elements is to achieve comparable accuracy in stresses and displacements at any location. Two steps are necessary to attain that objective:

1. Identify superconvergent points (also called Barlow points) at which higher order stresses (or stress components) are most accurate.

2. Devise interpolation-extrapolation procedures for "transporting" that accuracy to other locations of interest; for example the corner points.

For the EFFAND and FF membrane elements these steps are being investigated and will be the subject of a future communication.

6. EXAMPLE 1: UNIFORMLY STRETCHED BEAM

The first numerical example, illustrated in Figure 3, is a cantilever beam of rectangular cross section and length/height ratio 16:1. The beam is under constant uniaxial stress $\sigma_{xx} = 100$. Consequently

Table 5 Results for Beam Under Uniaxial Loading

Element	Load Lumping	Quantity	Poisson's ratio		
			$\nu = 0$	$\nu = 1/4$	$\nu = 1/2$
EFFAND	EB or HCI ($\frac{3}{2}$)	v_{xD}	100.00	100.00	100.00
EFFAND	EB or HCI ($\frac{3}{2}$)	v_{xC}	100.00	100.00	100.00
EFFAND	EB or HCI ($\frac{3}{2}$)	Max σ_{xx} error	0%	0%	0%
EFFAND	HCI (1)	v_{xD}	101.12	101.32	103.92
EFFAND	HCI (1)	v_{xC}	99.74	99.73	99.63
EFFAND	HCI (1)	Max σ_{xx} error	22%	29%	71%
EFFAND	LI	v_{xD}	103.35	103.94	111.75
EFFAND	LI	v_{xC}	99.23	99.19	98.88
EFFAND	LI	Max σ_{xx} error	61%	87%	211%
CST	LI	v_{xD}	100.00	100.00	100.00
CST	LI	v_{xC}	100.00	100.00	100.00
CST	LI	Max σ_{xx} error	0%	0%	0%

the beam functions as a bar throughout its length as long as root contraction for $\nu \neq 0$ is permitted; it is also important to set the drilling rotation to zero at the root. A regular 32×2 mesh of square elements, each square being fabricated by four half-thickness overlaid triangles, is used. The elastic modulus $E = 32$ is chosen so that the exact end deflection is always 100.
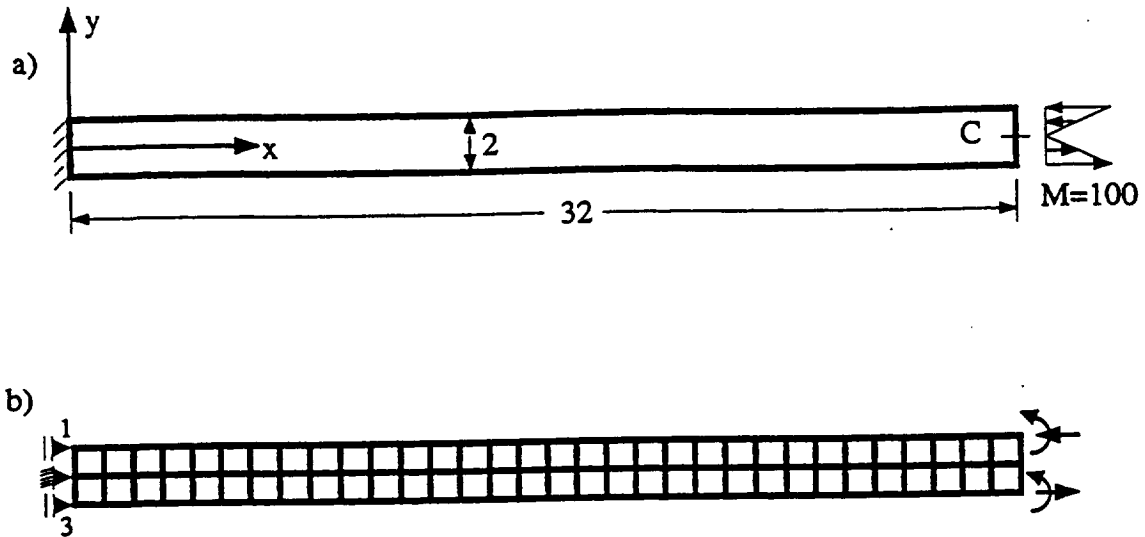
Figure 4. Slender cantilever beam under end moment: $E = 768$, v varies, $h = 1$; root contraction for $v \neq 0$ allowed; four-overlaid-triangle mesh units; a 32 × 2 mesh is shown in (b).

Of course this problem should be solved exactly by any membrane element with any mesh. The purpose of the example is to illustrate potential difficulties with the treatment of the applied distributed loads $f \equiv \sigma_x = 100$ at $x = 32$. All energy balance (EB) load lumping methods listed in Table 4, as well as HCI(3/2), yield fixed-end moments $\pm fH^2/8 = \pm 125$ at the top/bottom nodes of the end section, whereas HCI(1) yields $\pm fH^2/12 = \pm 83.33$. On the other hand, the linear interpolation method (LI) gives zero end moments. All these load lumpings satisfy equilibrium.

Displacement results as well as maximum stress errors for EFFAND and CST elements are shown in Table 5. For EFFAND all load lumpings giving (15) yield the exact solution as expected. For Poisson's ratios $v = 0$ and $\frac{1}{4}$ the end displacement error induced by LI is of the order of 3%, which is not unreasonable. But maximum stress errors at near-end locations reach levels of 60 to 90%. Errors disappear rapidly as one moves from the end, as it may be expected from Saint-Venant's principle, and are imperceptible for $x < 28$. For many applications, however, those stress error levels would be intolerable.

Results for HCI(1) fall 1/3 of the way between those of EB and LI. Errors for $v = 1/2$ are about three times higher, these being exacerbated by the use of a very low $\beta = 0.01$.

Obviously the CST has no problems with LI load lumping or root drilling rotation settings, and would be the cheapest and safest element for this problem. This observation underscores a general rule well known to practitioners of finite element methods: *Any refinement device — here, the inclusion of drilling freedoms — increases the potential for element misuse.*

334

Table 6 Tip Deflections (exact=100) for Beam under End Moment

Element	ν	Load Lumping	Mesh: x-subdivisions × y-subdivisions				
			32 × 2	16 × 2	8 × 2	4 × 2	2 × 2
ALL-3i	0	EBZ	87.99	75.47	37.01	5.51	0.42
ALL-3m	0	EBZ	81.02	51.62	9.64	0.74	0.04
ALL-7i	0	EBZ	85.43	67.44	23.65	2.55	0.17
CST	0	LI	53.33	33.33	13.33	3.92	1.02
EFFAND	0	EBZ	100.00	100.00	100.00	100.00	100.00
FF	0	EBZ	100.25	99.15	98.38	98.08	97.98
ALL-3i	1/4	EBQ	87.08	76.48	38.32	5.42	0.39
ALL-3m	1/4	EBQ	81.36	53.57	9.59	0.70	0.03
ALL-7i	1/4	EBQ	84.92	69.09	24.25	2.47	0.16
CST	1/4	LI	54.05	36.36	15.75	4.82	1.28
EFFAND	1/4	EBQ	99.99	99.99	99.99	99.96	100.07
FF	1/4	EBQ	98.36	97.17	96.58	96.34	96.27
ALL-3i	1/2	EBH	81.26	72.61	35.76	4.58	0.31
ALL-3m	1/2	EBH	76.80	51.06	8.26	0.56	0.02
ALL-7i	1/2	EBH	79.48	65.95	21.98	2.04	0.17
CST	1/2	LI	50.00	36.36	17.39	5.63	1.52
EFFAND	1/2	EBH	99.98	99.98	99.98	99.98	99.97
FF	1/2	EBH	91.27	90.66	90.22	90.06	90.01
EFFAND	0	HCI($\frac{3}{2}$)	97.51		97.50		97.50
EFFAND	0	HCI(1)	100.00		100.01		100.00
EFFAND	0	LI	99.98		100.01		100.01
EFFAND	0	EBZ	100.00		100.00		100.00
EFFAND	0	EBQ	99.99		100.00		100.00
EFFAND	0	EBH	99.97		99.99		100.00
EFFAND	1/2	HCI($\frac{3}{2}$)	98.68		97.67		97.51
EFFAND	1/2	HCI(1)	101.36		100.19		100.00
EFFAND	1/2	LI	101.66		100.20		99.99
EFFAND	1/2	EBZ	101.75		100.09		99.99
EFFAND	1/2	EBQ	100.31		100.04		100.00
EFFAND	1/2	EBH	99.98		99.98		99.97

7. EXAMPLE 2: CANTILEVER UNDER END MOMENT

We take up again the slender cantilever beam of Example 1, but now subjected to an end moment $M = 100$. The problem is illustrated in Figure 4. The modulus of elasticity is adjusted to $E = 768$ so that the exact tip deflection $\delta_{tip} = ML/(2EI)$ is 100. Regular meshes ranging from 32 × 2 to 2 × 2 are used, each rectangle mesh unit being composed of four half-thickness overlaid triangles. The element aspect ratios vary from 1:1 through 16:1.

Table 6 reports computed tip deflections (y displacement at C). It displays the effect of four variables: element type, element aspect ratio, load lumping, and Poisson's ratio. The first two are

the most important. The element types are identified following Table 1.

The root clamping condition was imposed by setting

$$v_{x1} = v_{x2} = v_{x3} = 0, \quad v_{y2} = 0, \quad \theta_{x1} = \theta_{x2} = \theta_{x3} = 0, \tag{16}$$

where 1, 2, 3 are the root nodes, numbered from the top. It is essential to leave v_{y1} and v_{y3} unrestrained for $v \neq 0$. This allows for the Poisson's contraction at the root and makes the exact solution merge with the displacement solution (3) over the entire beam.

The first 18 lines of Table 6 compare elements for aspect ratios varying from 1:1 to 16:1 as columns, and Poisson's ratios of 0, 0.25 and 0.50. The EB load lumping formula appropriate to v is used for all elements, except for CST, for which the LI lumping — which is consistent for that element — is used. The last 12 lines compare the effect of different load lumping formulas on EFFAND.

Because two elements through the height are used, the discretizations are nothing more that repetitions of the test mesh unit of Figure 1 along the length. Consequently the computed deflections should be $100/\eta(v, r)$. This provides a valuable numerical confirmation of the Macsyma results of Tables 2–3. Discrepancies from $100/\eta$ for elements other than EFFAND and CST are due to the use of EB load lumpings which were not rederived for each element.

Because $\eta(v, r) \equiv 1$ for EFFAND, that triangle should maintains full accuracy for all v and r. The slight discrepancy from 100.00% for $v = 0.25$ is caused by EBQ not being in exact energy balance, as explained in Section 4.3. The slight discrepancy for $v = 0.5$ is due to the use of $\beta = 1 - \gamma = 0.01$ rather than 0 to keep correct rank.

The FF element with fixed $1 - \gamma = 0.5$ maintains good to excellent accuracy. The Allman triangles perform well for unit aspect ratios, but rapidly become overstiff for aspect ratios over 2:1, and are inferior to the CST for aspect ratios exceeding 8:1. Of the three numerically integrated versions $3i$ is consistently superior, followed by $7i$.

The last 12 lines in Table 6 show that the EFFAND accuracy for low Poisson's ratio is not affected by the choice of load lumping formula as long as equilibrium is maintained. In fact the results for $v = 0.25$ are virtually identical to $v = 0$, and are not shown here. The effect becomes more significant, however, as v approaches $1/2$. For $v = 0$ the only visible difference from the exact solution are the results for HCI(3/2), which violates rotational equilibrium by about 3%.

8. EXAMPLE 3: CANTILEVER UNDER END SHEAR

The shear-loaded cantilever beam defined in Figure 5 has been selected as a test problem for plane stress elements by many investigators since originally proposed in [9]. A full root-clamping condition is implemented by constraining both displacement components to zero at nodes located on the $x = 0$ section. Drilling rotations must not be constrained at the root because the term $\partial u_y/\partial x$ in the continuum-mechanics definition is nonzero there. The applied shear load varies parabolically over the end section and is consistently lumped at the nodes.
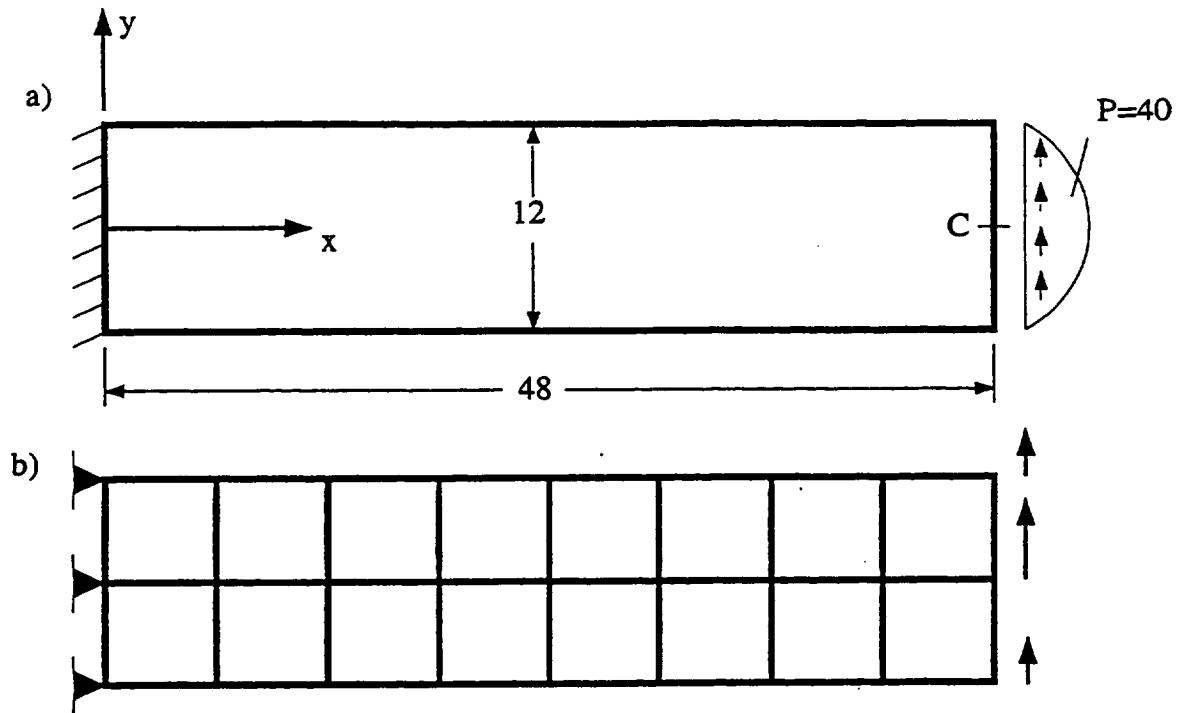
Figure 5. Cantilever under end shear: $E = 30000$, $v = 1/4$, $h = 1$; root
contraction not allowed; four-overlaid-triangle mesh units;
a 8×2 mesh is shown in (b).

The main comparison value is the tip deflection $\delta_C = v_{yC}$ at the center of the end-loaded cross section. One perplexing question concerns the analytical value of δ_C. An approximate solution derived from 2-D elasticity (based on a polynomial Airy stress function) gives $\delta_{el} = 0.34133 + 0.00145 = 0.35583$, where the first term comes from the bending deflection $PL^3/3EI$, $I = H^3/12$, and the second from a quadratic shear field. The shear term coefficient in the second term results from assuming a warping-allowed root-clamping condition that is more "relaxed" than the fully-clamped condition prescribed on the FE model. Consequently in [9] it was argued that δ_{el} should be an upper bound, which was verified by the conforming FE models tested at that time.

The finest grid results in [7] gave, however, $\delta_C \approx 0.35587$, which exceeds that "bound" in the fifth place. The finest EFFAND mesh ran here — 128×32 — gave a still larger value: 0.35601. The apparent explanation for this paradox is that if $v \neq 0$, a mild singularity in σ_{yy} and τ_{xy}, induced by the restraint $u_y|_{x=0} = 0$, develops at the corners of the root section. This singularity "clouds" convergence of digits 4-5. (In retrospect it would have been better to allow for lateral contraction effects as in Example 2 to avoid this singularity.) The percentage results in Tables 3-5 of [7] therefore contain errors in the 4th place.

Tables 4 gives computed deflections for rectangular mesh units with aspect ratios of 1:1, 2:1 and 4:1, respectively. Mesh units consist of four half-thickness overlaid triangles. For reporting purposes the load was scaled by $100/0.35601$ so that the "theoretical solution" becomes 100.00.

Table 7　Tip Deflections (exact = 100) for Beam under End Shear

Element	Mesh: x-subdivisions × y-subdivisions				
	8 × 2	16 × 4	32 × 8	64 × 16	128 × 32
ALL-3i	96.41	98.59	99.59	99.91	99.99
ALL-3m	82.70	94.78	98.57	99.62	99.91
ALL-7i	89.43	96.88	99.16	99.79	99.96
CST	55.09	82.59	94.90	98.65	99.66
EFFAND	101.68	100.30	100.03	100.00	100.00
FF	99.15	99.71	99.87	99.96	99.99
	4 × 2	8 × 4	16 × 8	32 × 16	64 × 32
ALL-3i	82.27	93.22	97.86	99.38	99.83
ALL-3m	54.23	81.84	94.52	98.50	99.61
ALL-7i	70.71	89.63	96.93	99.15	99.77
CST	37.85	69.86	90.04	97.25	99.28
EFFAND	96.68	98.44	99.37	99.78	99.93
FF	94.27	97.85	99.23	99.74	99.92
	2 × 2	4 × 4	8 × 8	16 × 16	32 × 32
ALL-3i	42.53	72.66	90.72	97.32	99.27
ALL-3m	12.39	31.81	63.68	87.24	96.41
ALL-7i	26.16	56.93	83.54	95.14	98.69
CST	17.83	43.84	75.01	92.13	97.86
EFFAND	92.24	96.99	98.70	99.48	99.81
FF	89.26	96.37	98.66	99.50	99.83

The data in Table 7 generally follows the patterns of the previous example; the main difference being the lack of drastically small percentages because element aspect ratios only go up to 4:1. Of the three Allman triangle versions again ALL-3i outperformed the others. The results for FF and the optimal EFF-ANDES triangles are very similar, without the latter displaying the clear advantages of Example 2. The data for FF and CST changes slightly from that of Tables 3-5 of [7] on two accounts: four-triangle, rather than two-triangle, macroelements are used to eliminate y-directionality, and the normalizing "theoretical" solution changes by +0.00014 as explained above.

9. EXAMPLE 4: COOK'S PROBLEM

Table 8 gives results computed for the plane stress problem defined in Figure 6. This problem was proposed by Cook [10] as a test case for nonrectangular quadrilateral elements. There is no known analytical solution but the EFFAND results for the 64 × 64 mesh may be used for comparison purposes. The last 6 lines in Table 8 pertain to quadrilateral elements. Results for HL, HG and Q4 are taken from [10] whereas those for Q6 and QM6 are taken from [11]. Results for the free-formulation quadrilateral FFQ are taken from Nygård's thesis [12]. Further data on other elements is provided in [13].
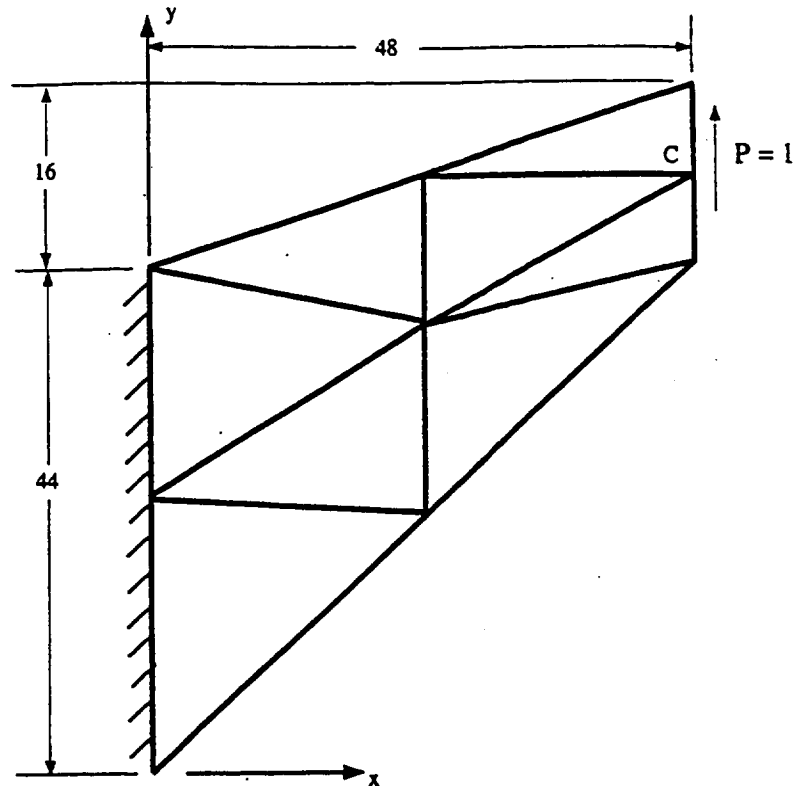
Figure 6. Wing-like plane stress structure (Cook's problem):
$E = 1$, $v = 1/3$, $h = 1$; root contraction not allowed;
two-triangle mesh units; a 2 × 2 mesh is shown.

For triangle tests, quadrilaterals were assembled with two triangles in the shortest-diagonal-cut layout illustrated in Figure 6 for a 2 × 2 mesh. Cutting the quadrilaterals the other way or using four-overlaid-triangle macroelements yields stiffer results.

The performance of the drilling-freedom triangles was similar, with ALL-3i giving the best results, especially for coarse meshes. It should be noted that accuracy of the FF, EFF and ANDES triangles for this problem is dominated by the basic stiffness response. Consequently the deflection values provided by the FF and EFFAND elements, which share the same basic stiffness, are virtually identical.

10. ELEMENT FORMATION TIMES

Table 9 gives a breakdown of formation times of the stiffness matrix for an individual triangle. Times are on milliseconds measured on a Sun 4/260; all floating-point computations being carried out in double precision (DP). T_b and T_h denotes times spent in forming the basic and higher order stiffness matrices, respectively. All elements use the same basic stiffness routine written in 1984. For elements labeled ANDES-1991, EFF-1991 and FF-1986, the subroutines listed in the Appendix, compiled with f77 for Sun-OS level 4.1.1, were used. The element labeled FF-1984 shows the

Table 8 Results for Cook's Problem

| Element | Vertical deflection at C for subdivision |
	2 × 2	4 × 4	8 × 8	16 × 16	32 × 32	64 × 64
ALL-3i	21.61	23.00	23.66	23.88	23.94	
ALL-3m	16.61	21.05	23.02	23.69	23.87	
ALL-7i	19.01	21.83	23.43	23.81	23.91	
CST	11.99	18.28	22.02	23.41		
EFFAND	20.56	22.45	23.43	23.80	23.91	23.95
FF	20.36	22.42	23.41	23.79	23.91	
FFQ	21.66	23.11	23.79	23.88	23.94	
HL	18.17	22.03		23.81		
HG	22.32	23.23		23.91		
Q4	11.85	18.30		23.43		
Q6	22.94	23.48				
QM6	21.05	23.02				

timing for the first FF element implementation reported in [7], and illustrates the progress since made in reducing the higher order stiffness formation time. The CST is formed by the basic stiffness subroutine when called with $\alpha_b = 0$, in which case all computations dealing with rotational freedoms are skipped. No data is given for the ALL elements because their shape function subroutines are far from optimized, and as a result their formation times are between 5 to 10 times — depending on the integration rule — those of ANDES and EFF.

Table 9 DP Element Formation Times on Sun 4/260 in msec

Implementation	T_b	T_h	$T_b + T_h$	K_h code bytes
ANDES-1991	1.34	1.55	2.89	4739
EFF-1991	1.34	1.90	3.24	6698
FF-1986	1.34	2.07	3.41	4507
FF-1984	1.34	6.71	8.05	8173
CST	0.77	0.00	0.77	

From this data it can be concluded that the ANDES implementation has a slight edge over that of the EFF, which is turn is somewhat faster than the FF-1986 implementation. The last column of Table 9 gives the length in nonblank characters of the K_h subroutine, excluding comments. As can be seen the FF-1986 implementation is the most compact one, closely followed by ANDES.

340

11. CONCLUDING REMARKS

The present study confirms the beneficial effect of adding drilling degrees of freedom to 3-node plane stress triangles when in-plane bending performance is to be enhanced. Successful elements of this type can be constructed using methods that lead to element families. Two such families have been compared here: numerically integrated versions of the Allman triangle, and the FF, EFF and ANDES triangles based on parametrized variational principles.

The numerical studies indicate that the performance of most of the 9-dof triangles is comparable for meshes containing elements of unit aspect ratio, or in problems where in-plane bending actions are secondary. (It can be argued, however, whether drilling freedoms are cost-effective under such conditions.) As regards the three tested versions of the Allman triangle, the one integrated with the 3-interior-point rule consistently outperformed the other two. For meshes containing elements of high aspect ratio under dominant in-plane bending action, the FF, EFF and ANDES elements with optimal parameters clearly outperformed the others.
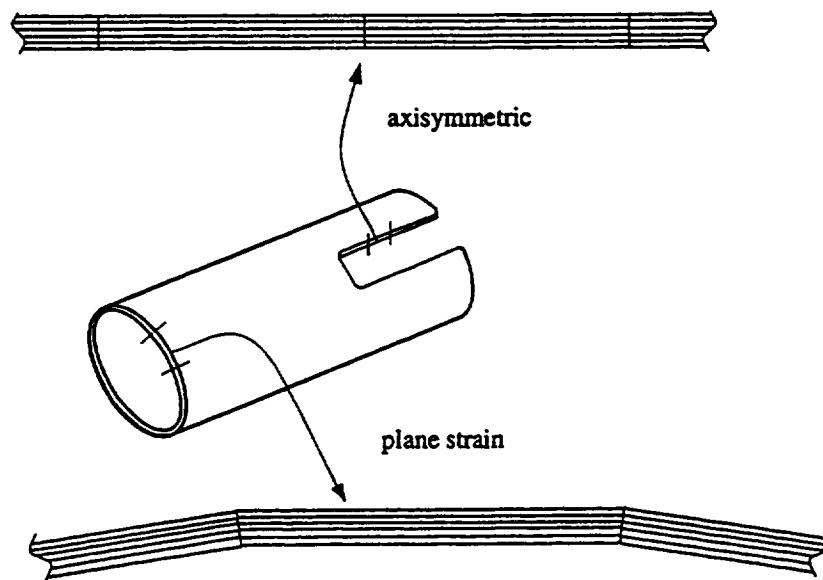
Figure 7. Elongated mesh units in thin-tube wall modeling.

Meshes with highly elongated triangles are quite common in many slender structures such as composite tubes and aerospace vehicle skins. Triangles with aspect ratios of 20:1 or even 50:1 are not uncommon (see Figure 7). To handle such problems it would be advantageous to extend the present EFF and ANDES elements to plane strain and axisymmetric conditions.

Despite substantial variation in implementation "flavors", the performance differences among the optimal FF, EFF and ANDES elements are relatively slight. Any of them would make a

fine choice for a general-purpose program whether as a stand-alone two-dimensional element, or as the membrane component of flat shell elements. The ANDES formulation appears to have a substantial edge in simplicity that would be valuable in extending the rotational-freedom concept to three-dimensional elements. This is counterbalanced, however, by the advantages accruing from the knowledge of internal displacements in FF and EFF elements in the applications discussed in Sections 3–4.

Acknowledgements

References

[1]   K. Alvin, H. M. de la Fuente, B. Haugen and C. A. Felippa, Membrane triangles with corner drilling freedoms: I. The EFF element, in this report.

[2]   C. A. Felippa and C. Militello, Membrane triangles with corner drilling freedoms: II. The ANDES element, in this report.

[3]   C. A. Felippa, The extended free formulation of finite elements in linear elasticity, *Journal of Applied Mechanics*, 56, 1989, pp. 609–616

[4]   C. A. Felippa and C. Militello, Developments in variational methods for high-performance plate and shell elements, in *Analytical and Computational Methods for Shells*, CAD Vol. 3, ed. by A. K. Noor, T. Belytschko and J. C. Simo, American Society of Mechanical Engineers, ASME, New York, 1989, pp. 191–216

[5]   C. A. Felippa and C. Militello, Variational formulation of high performance finite elements: parametrized variational principles, *Computers and Structures*, 36, 1990, pp. 1–11

[6]   D. J. Allman, A compatible triangular element including vertex rotations for plane elasticity analysis, *International Journal of Numerical Methods in Engineering*, 26, 1988, pp. 2645–2655

[7]   P. G. Bergan and C. A. Felippa, A triangular membrane element with rotational degrees of freedom, *Computer Methods in Applied Mechanics & Engineering*, 50, 1985, pp. 25–69

[8]   C. A. Felippa, Parametrized multifield variational principles in elasticity: II. Hybrid functionals and the free formulation, *Communications in Applied Numerical Methods*, 5, 1989, pp. 79–88

[9]   C. A. Felippa, Refined finite element analysis of linear and nonlinear two-dimensional structures, Ph. D. Dissertation, Department of Civil Engineering, University of California at Berkeley, Berkeley, CA, 1966

[10]   R. D. Cook, Improved two-dimensional finite element, *Journal of the Structural Division*, ASCE, 100, ST6, pp. 1851–1863, 1974

[11]   R. L. Taylor, P. J. Beresford and E. L. Wilson, A non-conforming element for stress analysis, *International Journal for Numerical Methods in Engineering*, 10, pp. 1211–1219, 1976

[12]   M. K. Nygård, The free formulation for nonlinear finite elements with applications to shells, Dr. Ing. Thesis, Div. of Structural Mechanics, Norwegian Institute of Technology, Trondheim, Norway, 1986

[13]   R. D. Cook, Ways to improve the bending response of finite elements, *International Journal for Numerical Methods in Engineering*, 11, pp. 1029–1039, 1977

[14]   P. G. Bergan and C. A. Felippa, Efficient implementation of a triangular membrane element with drilling freedoms, Finite Element Handbook series, ed. by T. J. R. Hughes and E. Hinton, Pineridge Press, 1986, pp. 139–152

Appendix A. COMPUTER PROGRAMS

This Appendix provides listings of the Fortran subroutines that implement several of the elements tested in the present study. A brief description of the subroutines is given below. A detailed description of calling sequences is presented in the comments at the beginning of the code.

SM4M. This is a *driver* subroutine for computing the *total* stiffness matrix of membrane elements with 3 degrees of freedom per node, one being a drilling freedom. It is normally called to form the stiffness matrix of a quadrilateral composed of either two triangles, or four "overlaid" triangles of half thickness. It can also form a single triangle.

SM3MB. This forms the 9×9 basic stiffness matrix K_b used by all high-performance elements. Coefficient α_b has been left as a free parameter to facilitate certain studies as well as to permit the formation of the CST, which is obtained if $\alpha_b = 0$.

SM3MHFF. Forms the higher order stiffness of the 1985 Bergan-Felippa triangle using a fast implementation that is a slight modification of that presented in [14]. The scaling factor $\beta = 1 - \gamma$ is left as a parameter although $\beta = 0.5$ is recommended.

SM3MHEFF. Forms the higher order stiffness of the optimal EFF triangle described in Part I. It has $\alpha_h = 5/4$ hardwired, but the scaling factor β is left as a subroutine parameter.

SM3MHANDES. Forms the higher order stiffness of the optimal ANDES element described in Part II. The optimal ρ factors (7) are hardwired for the midpoint rule $\xi = 0$.

The numerically integrated Allman elements are formed by subroutine SM3MALL. This is not listed here because its shape function implementation is far from optimized and as a result the element formation is slow.

Some general comments on these subroutines follow.

Initialization. None of the subroutines clears the stiffness array internally. They simply add the stiffness matrix entries to the incoming array. The calling program is supposed to take care of initialization. In conjunction with the locator array LS discussed below, this decision is intended to simplify macroelement formation.

Stiffness Locator. All subroutines utilize a location pointer array LS to direct stiffness entries into the stiffness array SM. This has two practical uses:

(a) The ordering of degrees of freedom can be easily changed, as illustrated in the examples given under the USAGE section of SM4M and SM3MB. Note, however, that the sequential ordering LS = 1, 2, 3, ... has different interpretation in the driver SM4M and triangle subroutines as regards the position of drilling freedoms.

(b) The formation of macroelements is facilitated. This is already illustrated by the method used by SM4M to merge triangles by simply setting up their stiffness locator arrays appropriately. Another important application, not illustrated here, is the formation of shell elements in which the plane stress stiffness becomes the membrane component.

```
C=DECK SM4M
C=PURPOSE Driver to form material membrane stiffness of quad assembly
C=AUTHOR C. A. Felippa, June 1984
C=VERSION July 1991
C=EQUIPMENT Machine independent
C=KEYWORDS finite element
C=KEYWORDS material stiffness matrix membrane plane stress drilling
C=BLOCK ABSTRACT
C
C       SM4M is a driver that forms the material stiffness matrix of a
C       membrane quadrilateral formed by 2 or 4 triangles (optionally a
C       single triangle).  Three nodal dof (2 translations, 1 drilling
C       rotation) are assumed.  Several element formulations may be used.
C
C=END ABSTRACT
C=BLOCK USAGE
C
C       The calling sequence is
C
C        CALL SM4M (TYPE, OPT, X, Y, DM, ALPHAB, GAMMA,
C                   IAT, LS, SM, M, STATUS)
C
C       The inputs are:
C
C       TYPE(1:3) Element type argument (upper case assumed):
C                 ALL   Allman's element
C                 AND   ANDES-1991 element
C                 CST   CST, drilling freedoms are ignored
C                 EFF   EFF-1991 element
C                 FF    FF-1984 element, fast reformulation of 1986
C
C       TYPE(4:5) For ALL elements specifies integration rule:
C                 1C    1-interior point (centroid)
C                 3I    3-interior-point rule
C                 3M    3-midpoint rule
C                 7I    7-interior-point rule
C
C       OPT       Options character (upper case assumed):
C                 B     Form basic stiffness only (FF/EFF)
C                 H     Form higher order stiffness only (FF/EFF)
C                 If neither of these, form total stiffness.
C
C       X         (4 x 1) array of x coordinates of quad nodes.
C                 (only first 3 used if IAT=0).
C
C       Y         (4 x 1) array of y coordinates of quad nodes.
C                 (only first 3 used if IAT=0).
C
C       DM        (3 x 3) membrane force-to-strain constitutive matrix.
C                 Assumed to be already thickness-integrated.
```

345

```
C
C     ALPHAB    Rotational lumping factor for basic stiffness
C               Applies to AND/FF/EFF elements only.
C
C     GAMMA     (1-GAMMA) is H.O. stiffness scale factor (AND/EFF/FF)
C
C                    1 o+++++++o 4          1 o+++++++o 4
C                      +  +      +            +       + +
C                      +  IAT=1  +            +  IAT=2  +
C                      +      +  +            +  +       +
C                    2 o+++++++++++o 3      2 o+++++++++++o 3
C
C     IAT       Identifier of assembly type (cf. sketch above):
C                 0   Single triangle.
C                 1   2 triangles: 123 and 341 (diagonal 1-3)
C                 2   2 triangles: 124 and 234 (diagonal 2-4)
C                 3   4 half-thick overlaid triangles: 123,341,124,234
C
C     LS        (12 x 1) array of stiffness location pointers.
C               For the standard freedom ordering
C                 ux1,uy1,theta2, ux2,  ...  uy4,theta4
C               set LS = 1,2,3,4,5,6,7,8,9,10,11,12.  To get
C                 ux1,uy1,ux2,uy2, ... uy4,theta1, ... theta4
C               set LS = 1,2,9,3,4,10,5,6,11,6,7,12, and so on.
C               Other settings are useful when this element is to be
C               inserted in a shell element as membrane component.
C
C     SM        Incoming stiffness array.  NOT CLEARED by SM4M.
C
C     M         First dimension of SM in calling program.
C
C     The outputs are:
C
C     SM        Output stiffness array with bending stiffness
C               coefficients added in.  The (i,j)-th entry of the
C               (12 x 12) element membrane stiffness is added
C               to SM(K,L) where K=LS(I) and L=LS(J).
C
C     STATUS    Status character variable.  Blank if no error
C               detected; else returns appropriate message.
C .
C=END USAGE
C=BLOCK FORTRAN
      subroutine    SM4M
     $   (type, opt, x, y, dm, alphab, gamma, iat, ls, sm, m, status)
C
C                 A R G U M E N T S
C
      character     type*(*), opt, status*(*)
      double precision  x(3),y(3),dm(3,3), alphab,gamma
      integer       iat, m, ls(*)
      double precision  sm(m,m)
C
```

```
C                     T Y P E   &   D I M E N S I O N
C
      double precision   xt(3), yt(3), f, fb, fh
      integer            i, j, ias, n, p
      integer            ntrigs(0:3), tnodes(3,4, 0:3), lst(9)
      integer            nt(3)
C
C                     D A T A
C
      data               ntrigs /1,2,2,4/
      data               tnodes /1,2,3, 9*0,
     $                           1,2,3, 3,4,1, 6*0,
     $                           1,2,4, 2,3,4, 6*0,
     $                           1,2,3, 3,4,1, 1,2,4, 2,3,4/
C
C                     L O G I C
C
      status =     ' '
      ias =      max(0,min(iat,3))
      f  =       1.D0/(1+ias/3)
      fb =       f
      fh =       f*(1.D0-gamma)
      if (opt .eq. 'B')             fh = 0.0
      if (opt .eq. 'H')             fb = 0.0
C
      do 3000  j = 1,ntrigs(ias)
        do 2500   i = 1,3
          n =      tnodes(i,j,ias)
          nt(i) =  n
          xt(i) =  x(n)
          yt(i) =  y(n)
          lst(2*i-1) =   ls(3*n-2)
          lst(2*i  ) =   ls(3*n-1)
          lst( i+6) =    ls(3*n  )
 2500     continue
C
        if (type(1:3) .eq. 'ALL')           then
          p =      ichar(type(4:4))-ichar('0')
          if (type(5:5) .eq. 'M')           p = -3
          call   SM3MALL  (xt,yt, dm, p, f, lst,sm,m, status)
        else if (type(1:3) .eq. 'CST')      then
          call   SM3MB (xt,yt, dm, 0.0D0, fb, lst,sm,m, status)
        else if (type(1:3) .eq. 'AND' .or.
     $           type(1:3) .eq. 'EFF' .or.
     $           type(1:2) .eq. 'FF')     then
          call   SM3MB (xt,yt, dm, alphab,fb, lst,sm,m, status)
          if (type(1:3) .eq. 'AND')     then
            call   SM3MHANDES (xt,yt, dm, fh, lst,sm,m, status)
          else if (type(1:3) .eq. 'EFF')     then
            call   SM3MHEFF (xt,yt, dm, fh, lst,sm,m, status)
          else if (type(1:2) .eq. 'FF')     then
            call   SM3MHFF (xt,yt, dm, fh, lst,sm,m, status)
          end if
```

347

```
          else
             status =    'SM4M: Illegal TYPE argument'
          end if
          if (status(1:1) .ne. ' ')      return
 3000     continue
       return
       end
C=END FORTRAN
```

C=DECK SM3MB
C=PURPOSE Form basic membrane stiffness of 9-dof triangle
C=AUTHOR C. A. Felippa, June 1984
C=VERSION June 1984
C=EQUIPMENT Machine independent
C=KEYWORDS finite element membrane plane stress
C=KEYWORDS basic material stiffness matrix
·C=BLOCK ABSTRACT
C
C   SM3MB forms the basic stiffness matrix of a 9-dof plane
C   stress triangle (see CMAME, vol 50, pp 25-69).
C   It can generate the CST as special case.
C
C=END ABSTRACT
C=BLOCK USAGE
C
C   The calling sequence is
C
C   CALL   SM3MB (X, Y, DM, ALPHAB, F, LS, SM, M, STATUS)
C
C   The inputs are:
C
C   X   (3 x 1) array of x coordinates of triangle nodes.
C   Y   (3 x 1) array of y coordinates of triangle nodes.
C   DM   (3 x 3) matrix relating in-plane forces to strains.
C   ALPHAB   Rotational lumping factor; if zero form CST.
C   F   Factor by which stiffness entries will be multiplied.
C   LS   (9 x 1) array of stiffness location pointers.
C   For the conventional dof arrangement
C   vx1,vy1,theta1,vx2,vy2,theta2,vx3,vy3,theta3
C   set LS = 1,2,4,5,7,8,3,6,9. The arrangement
C   vx1,vy1,vx2,vy2,vx3,vy3,theta1,theta2,theta3
C   is obtained if LS = 1,2,3,4,5,6,7,8,9.
C   SM   Incoming material stiffness array.
C   M   First dimension of SM in calling program.
C
C   The outputs are:
C
C   SM   Output stiffness array with basic stiffness
C   coefficients added in. The (i,j)-th entry of the
C   basic element stiffness is added to SM(K,L),
C   where K=LS(I) and L=LS(J).
C   STATUS   Status character variable. Blank if no error
C   detected.

348

```
C
C=END USAGE
C=BLOCK FORTRAN
      subroutine    SM3MB
     $              (x, y, dm, alphab, f, ls, sm, m, status)
C
C                   T Y P E   &   D I M E N S I O N
C
      character*(*)  status
      integer        m, ls(9)
      double precision   x(3),y(3), dm(3,3), alphab,f, sm(m,m)
      double precision   area2, c, lt(9,3)
      double precision   e11, e12, e13, e22, e23, e33
      double precision   x21, x32, x13, y21, y32, y13
      double precision   x12, x23, x31, y12, y23, y31
      double precision   s1, s2, s3
      integer        i, j, k, l, n
C
C                   L O G I C
C
      status =    ' '
      if (f .eq. 0.0)        return
      x21 =        x(2) - x(1)
      x12 =       -x21
      x32 =        x(3) - x(2)
      x23 =       -x32
      x13 =        x(1) - x(3)
      x31 =       -x13
      y21 =        y(2) - y(1)
      y12 =       -y21
      y32 =        y(3) - y(2)
      y23 =       -y32
      y13 =        y(1) - y(3)
      y31 =       -y13
      area2 =    y21*x13 - x21*y13
      if (area2 .le. 0.0)      then
        status = 'SM3MB: Negative area'
        if (area2 .eq. 0.0)    status = 'SM3MB: Zero area'
        return
      end if
      lt(1,1) =    y23
      lt(2,1) =    0.0
      lt(3,1) =    y31
      lt(4,1) =    0.0
      lt(5,1) =    y12
      lt(6,1) =    0.0
      lt(1,2) =    0.0
      lt(2,2) =    x32
      lt(3,2) =    0.0
      lt(4,2) =    x13
      lt(5,2) =    0.0
      lt(6,2) =    x21
      lt(1,3) =    x32
```

```
        lt(2,3) =   y23
        lt(3,3) =   x13
        lt(4,3) =   y31
        lt(5,3) =   x21
        lt(6,3) =   y12
        n =         6
        if (alphab .ne. 0.0)         then
          lt(7,1) =  y23*(y13-y21)*alphab/6.
          lt(7,2) =  x32*(x31-x12)*alphab/6.
          lt(7,3) =  (x31*y13-x12*y21)*alphab/3.
          lt(8,1) =  y31*(y21-y32)*alphab/6.
          lt(8,2) =  x13*(x12-x23)*alphab/6.
          lt(8,3) =  (x12*y21-x23*y32)*alphab/3.
          lt(9,1) =  y12*(y32-y13)*alphab/6.
          lt(9,2) =  x21*(x23-x31)*alphab/6.
          lt(9,3) =  (x23*y32-x31*y13)*alphab/3.
          n =         9
        end if
C
        c =         0.5D0*f/area2
        e11 =       c * dm(1,1)
        e22 =       c * dm(2,2)
        e33 =       c * dm(3,3)
        e12 =       c * dm(1,2)
        e13 =       c * dm(1,3)
        e23 =       c * dm(2,3)
        do 3000  j = 1,n
          l =         ls(j)
          s1 =        e11*lt(j,1) + e12*lt(j,2) + e13*lt(j,3)
          s2 =        e12*lt(j,1) + e22*lt(j,2) + e23*lt(j,3)
          s3 =        e13*lt(j,1) + e23*lt(j,2) + e33*lt(j,3)
          do 2500  i = 1,j
            k =         ls(i)
            sm(k,l) =  sm(k,l) + (s1*lt(i,1) + s2*lt(i,2) + s3*lt(i,3))
            sm(l,k) =  sm(k,l)
 2500     continue
 3000   continue
        return
        end
C=END FORTRAN
```

C
C   SM3MANDES forms the higher order element stiffness matrix
C   of a 9-dof membrane triangle based on the ANDES formulation.

```
C           Implementation moderately optimized for speed.
C
C=END ABSTRACT
C=BLOCK USAGE
C
C           The calling sequence is
C
C               CALL SM3MHANDES (X, Y, DM, F, LS, SM, M, STATUS)
C
C           The inputs are:
C
C           X           (3 x 1) array of x coordinates of triangle nodes
C           Y           (3 x 1) array of y coordinates of triangle nodes
C           DM          (3 x 3) matrix constitutive matrix already
C                           integrated through the thickness
C           F           Factor by which all stiffness entries will be multiplied.
C           SM          Incoming material stiffness array.
C           LS          (9 x 1) array of stiffness location pointers
C                           (see examples in SM3MB)
C           M           First dimension of SM in calling program.
C
C           The outputs are:
C
C           SM          Output stiffness array with higher order stiffness
C                       coefficients added in.
C                       The (i,j)-th entry of the basic element stiffness is added
C                       to SM(K,L), where K=LS(I) and L=LS(J).
C           STATUS      Status character variable.  Blank if no error
C                       detected.
C
C=END USAGE
C=BLOCK FORTRAN
        subroutine    SM3MHANDES
      $               (x, y, dm, f, ls, sm, m, status)
C
C                     A R G U M E N T S
C
        integer            ls(9), m
        double precision   x(3),y(3), dm(3,3), f, sm(m,m)
        character          status*(*)
C
C                     T Y P E   &   D I M E N S I O N
C
        double precision   x12, x21, x23, x32, x31, x13
        double precision   y12, y21, y23, y32, y31, y13
        double precision   l21,l32,l13
        double precision   chi213,chi321,chi132
        double precision   area, area2, area43
        double precision   c(3,3), e(3,3), et(3), d(3), qm(3,3,3)
        double precision   t(3,3), tfac, kth(3,3)
        double precision   s(3), xyij(6), sum, w(3), wfac
        integer            i, j, k, l
C
```

```
C                    L O G I C
C
      status =    ' '
      if (f .eq. 0.0)          return
      x12 =       x(1) - x(2)
      x21 =       -x12
      x23 =       x(2) - x(3)
      x32 =       -x23
      x31 =       x(3) - x(1)
      x13 =       -x31
      y12 =       y(1) - y(2)
      y21 =       -y12
      y23 =       y(2) - y(3)
      y32 =       -y23
      y31 =       y(3) - y(1)
      y13 =       -y31
      area2 =     x21*y31-x31*y21
      if (area2 .le. 0.0)      then
        status = 'SM3MHANDES: Negative area'
        if (area2 .eq. 0.0)    status = 'SM3MHANDES: Zero area'
        return
      end if
      area =      0.5D0*area2
      l21 =       sqrt(x21**2+y21**2)
      l32 =       sqrt(x32**2+y32**2)
      l13 =       sqrt(x13**2+y13**2)
      tfac =      0.25D0/area**2
      t(1,1) =    tfac*y23*y13*l21**2
      t(1,2) =    tfac*y31*y21*l32**2
      t(1,3) =    tfac*y12*y32*l13**2
      t(2,1) =    tfac*x23*x13*l21**2
      t(2,2) =    tfac*x31*x21*l32**2
      t(2,3) =    tfac*x12*x32*l13**2
      t(3,1) =    tfac*(y23*x31+x32*y13)*l21**2
      t(3,2) =    tfac*(y31*x12+x13*y21)*l32**2
      t(3,3) =    tfac*(y12*x23+x21*y32)*l13**2
      wfac =      0.75D0*f*area
      e(1,1) =    wfac*dm(1,1)
      e(1,2) =    wfac*dm(1,2)
      e(1,3) =    wfac*dm(1,3)
      e(2,1) =    wfac*dm(2,1)
      e(2,2) =    wfac*dm(2,2)
      e(2,3) =    wfac*dm(2,3)
      e(3,1) =    wfac*dm(3,1)
      e(3,2) =    wfac*dm(3,2)
      e(3,3) =    wfac*dm(3,3)
      do 1600  j = 1,3
        do 1400  i = 1,3
          et(i) =  e(i,1)*t(1,j)+e(i,2)*t(2,j)+e(i,3)*t(3,j)
1400      continue
        do 1500  i = 1,3
          c(i,j) = t(1,i)*et(1)+t(2,i)*et(2)+t(3,i)*et(3)
1500      continue
```

```
1600    continue
      area43 =      (2.D0/3.D0)*area2
      chi213 =      area43/l21**2
      chi321 =      area43/l32**2
      chi132 =      area43/l13**2
      qm(1,1,1) =  -0.25*chi213
      qm(1,2,1) =  -qm(1,1,1)
      qm(1,3,1) =   0.0
      qm(2,1,1) =   0.25*chi321
      qm(2,2,1) =   0.50*chi321
      qm(2,3,1) =   qm(2,1,1)
      qm(3,1,1) =  -0.50*chi132
      qm(3,2,1) =  -0.25*chi132
      qm(3,3,1) =   qm(3,2,1)
      qm(1,1,2) =  -0.25*chi213
      qm(1,2,2) =  -0.50*chi213
      qm(1,3,2) =   qm(1,1,2)
      qm(2,1,2) =   0.0
      qm(2,2,2) =  -0.25*chi321
      qm(2,3,2) =  -qm(2,2,2)
      qm(3,1,2) =   0.25*chi132
      qm(3,2,2) =   qm(3,1,2)
      qm(3,3,2) =   0.50*chi132
      qm(1,1,3) =   0.50*chi213
      qm(1,2,3) =   0.25*chi213
      qm(1,3,3) =   qm(1,2,3)
      qm(2,1,3) =  -0.25*chi321
      qm(2,2,3) =   qm(2,1,3)
      qm(2,3,3) =  -0.50*chi321
      qm(3,1,3) =   0.25*chi132
      qm(3,2,3) =   0.0
      qm(3,3,3) =  -qm(3,1,3)
      kth(1,1) =   0.0
      kth(1,2) =   0.0
      kth(1,3) =   0.0
      kth(2,2) =   0.0
      kth(2,3) =   0.0
      kth(3,3) =   0.0
      do 2800  k = 1,3
        do 2600  j = 1,3
          d(1) = c(1,1)*qm(1,j,k)+c(1,2)*qm(2,j,k)+c(1,3)*qm(3,j,k)
          d(2) = c(2,1)*qm(1,j,k)+c(2,2)*qm(2,j,k)+c(2,3)*qm(3,j,k)
          d(3) = c(3,1)*qm(1,j,k)+c(3,2)*qm(2,j,k)+c(3,3)*qm(3,j,k)
          do 2500  i = 1,j
            kth(i,j) = kth(i,j) +
     $                 qm(1,i,k)*d(1)+qm(2,i,k)*d(2)+qm(3,i,k)*d(3)
            kth(j,i) = kth(i,j)
2500        continue
2600      continue
2800    continue
      s(1) =   kth(1,1) + kth(1,2) + kth(1,3)
      s(2) =   kth(2,1) + kth(2,2) + kth(2,3)
      s(3) =   kth(3,1) + kth(3,2) + kth(3,3)
```

353

```
      xyij(1) =  0.25*x32/area
      xyij(2) =  0.25*y32/area
      xyij(3) =  0.25*x13/area
      xyij(4) =  0.25*y13/area
      xyij(5) =  0.25*x21/area
      xyij(6) =  0.25*y21/area
      do 4000  j = 1,9
        l =     ls(j)
        do 3600  i = 1,3
          if (j .le. 6)      then
            w(i) =  s(i)*xyij(j)
          else
            w(i) =  kth(i,j-6)
          end if
3600      continue
        sum =    w(1) + w(2) + w(3)
        do 3700  i = 1,j
          k =        ls(i)
          if (i .le. 6)      then
            sm(k,l) =  sm(k,l) + sum*xyij(i)
          else
            sm(k,l) =  sm(k,l) + w(i-6)
          end if
          sm(l,k) =  sm(k,l)
3700      continue
4000    continue
      return
      end
C=END FORTRAN
```

C=DECK SM3MHEFF
C=PURPOSE Form high-order material stiffness of 9-dof EFF triangle
C=AUTHOR C. A. Felippa
C=VERSION June 1991
C=EQUIPMENT Machine independent
C=KEYWORDS finite element
C=KEYWORDS material stiffness matrix
C=KEYWORDS triangle membrane high-order extended free formulation
C=BLOCK ABSTRACT
C
C   SM3MEFF forms the higher order stiffness matrix of a 9-dof
C   membrane triangle based on the extended free formulation.
C   This implementation has alphah=5/4 hardwired, and is
C   optimized for maximum formation speed.
C
C=END ABSTRACT
C=BLOCK USAGE
C
C   The calling sequence is
C
C   CALL   SM3MHEFF (X, Y, DM, F, LS, SM, M, STATUS)
C
C   The inputs are:

```
C
C          X            (3 x 1) array of x coordinates of triangle nodes
C          Y            (3 x 1) array of y coordinates of triangle nodes
C          DM           (3 x 3) matrix constitutive matrix already
C                       integrated through the thickness
C          F            Factor by which all stiffness entries will be multiplied.
C                       It is beta or 0.5*beta
C          SM           Incoming material stiffness array.
C          LS           (9 x 1) array of stiffness location pointers
C                       (see examples in SM3MB).
C                       three rotational DOF will appear at the end.
C          M            First dimension of SM in calling program.
C
C     The outputs are:
C
C          SM           Output stiffness array with higher order stiffness
C                       coefficients added in.
C                       The (i,j)-th entry of the basic element stiffness is added
C                       to SM(K,L), where K=LS(I) and L=LS(J).
C                       (Drilling freedoms are internally 7,8,9)
C
C
C          STATUS       Status character variable.  Blank if no error
C                       detected.
C
C=END USAGE
C=BLOCK FORTRAN
       subroutine     SM3MHEFF
      $               (x, y, dm, f, ls, sm, m, status)
C
C                      A R G U M E N T S
C
       integer            ls(9), m
       double precision   x(3),y(3), dm(3,3), f, sm(m,m)
       character*(*)      status
C
C                      T Y P E   &   D I M E N S I O N
C
       double precision   x0,y0, x10,x20,x30, y10,y20,y30
       double precision   x12, x21, x23, x32, x31, x13
       double precision   y12, y21, y23, y32, y31, y13
       double precision   aa12,aa23,aa31,ss12,ss23,ss31,ss1,ss2,ss3
       double precision   caa12,caa23,caa31, sum
       double precision   ca,cax10,cax20,cax30,cay10,cay20,cay30
       double precision   area, area2, kfac
       double precision   kqh(6,6),hmt(6,3),hqt(6,3),kth(3,3)
       double precision   s(3),w(6),xyij(3)
       double precision   e11,e22,e33,e12,e13,e23
       integer            i,j,k,l
C
C                      L O G I C
C
       status =    ' '
       if (f .eq. 0.0)          return
```

```
x12 =       x(1) - x(2)
x21 =       -x12
x23 =       x(2) - x(3)
x32 =       -x23
x31 =       x(3) - x(1)
x13 =       -x31
y12 =       y(1) - y(2)
y21 =       -y12
y23 =       y(2) - y(3)
y32 =       -y23
y31 =       y(3) - y(1)
y13 =       -y31
area2 =     x21*y31-x31*y21
if (area2 .le. 0.0)        then
  status = 'SM3MBEFF: Negative area'
  if (area2 .eq. 0.0)    status = 'SM3MBEFF: Zero area'
  return
end if
area  =     0.5D0*area2
x0 =        (x(1)+x(2)+x(3))/3.
y0 =        (y(1)+y(2)+y(3))/3.
x10 =       x(1) - x0
x20 =       x(2) - x0
x30 =       x(3) - x0
y10 =       y(1) - y0
y20 =       y(2) - y0
y30 =       y(3) - y0
aa12 =      2.25D0*(x30**2+y30**2)
aa23 =      2.25D0*(x10**2+y10**2)
aa31 =      2.25D0*(x20**2+y20**2)
caa12 =     15.D0/(32.*aa12)
caa23 =     15.D0/(32.*aa23)
caa31 =     15.D0/(32.*aa31)
ss12 =      x12**2+y12**2
ss23 =      x23**2+y23**2
ss31 =      x31**2+y31**2
ss1 =       0.25D0*(ss12-ss31)
ss2 =       0.25D0*(ss23-ss12)
ss3 =       0.25D0*(ss31-ss23)
cay10 =     0.1875D0*y10
cay20 =     0.1875D0*y20
cay30 =     0.1875D0*y30
cax10 =     0.1875D0*x10
cax20 =     0.1875D0*x20
cax30 =     0.1875D0*x30
hmt(1,1) = caa12*((-ss3+0.6D0*aa12)*y30+area*x30)
hmt(1,2) =  3.*cay30 - hmt(1,1)
hmt(1,3) = cay30
hmt(2,1) = cay10
hmt(2,2) = caa23*((-ss1+0.6D0*aa23)*y10+area*x10)
hmt(2,3) =  3.*cay10 - hmt(2,2)
hmt(3,1) = caa31*((ss2+0.6D0*aa31)*y20-area*x20)
hmt(3,2) = cay20
```

```fortran
      hmt(3,3) =  3.*cay20 - hmt(3,1)
      hmt(4,1) = caa12*((ss3-0.6D0*aa12)*x30+area*y30)
      hmt(4,2) = -3.*cax30 - hmt(4,1)
      hmt(4,3) = -cax30
      hmt(5,1) = -cax10
      hmt(5,2) = caa23*((ss1-0.6D0*aa23)*x10+area*y10)
      hmt(5,3) = -3.*cax10 - hmt(5,2)
      hmt(6,1) = caa31*((-ss2-0.6D0*aa31)*x20-area*y20)
      hmt(6,2) = -cax20
      hmt(6,3) = -3.*cax20 - hmt(6,1)
      do 2000  j = 1,3
        sum =      (2.D0/9.)*(hmt(1,j)+hmt(2,j)+hmt(3,j))
        hqt(1,j) =  sum - (4.D0/3.)*hmt(1,j)
        hqt(2,j) =  sum - (4.D0/3.)*hmt(2,j)
        hqt(3,j) =  sum - (4.D0/3.)*hmt(3,j)
        sum =      (2.D0/9.)*(hmt(4,j)+hmt(5,j)+hmt(6,j))
        hqt(4,j) =  sum - (4.D0/3.)*hmt(4,j)
        hqt(5,j) =  sum - (4.D0/3.)*hmt(5,j)
        hqt(6,j) =  sum - (4.D0/3.)*hmt(6,j)
 2000   continue
      kfac =      1.5D0*f/area2
      e11 =       kfac * dm(1,1)
      e22 =       kfac * dm(2,2)
      e33 =       kfac * dm(3,3)
      e12 =       kfac * dm(1,2)
      e13 =       kfac * dm(1,3)
      e23 =       kfac * dm(2,3)
      kqh(1,1) = 2*(e11*y30**2-2*e13*x30*y30+e33*x30**2)
      kqh(1,2) = ((e13*x10-e11*y10)*y30+(e13*y10-e33*x10)*x30)
      kqh(1,3) = ((e13*x20-e11*y20)*y30+(e13*y20-e33*x20)*x30)
      kqh(1,4) = 2*(e13*y30**2-(e33+e12)*x30*y30+e23*x30**2)
      kqh(1,5) = ((e12*x10-e13*y10)*y30+(e33*y10-e23*x10)*x30)
      kqh(1,6) = ((e12*x20-e13*y20)*y30+(e33*y20-e23*x20)*x30)
      kqh(2,1) = kqh(1,2)
      kqh(2,2) = 2*(e11*y10**2-2*e13*x10*y10+e33*x10**2)
      kqh(2,3) = ((e13*x10-e11*y10)*y20+(e13*y10-e33*x10)*x20)
      kqh(2,4) = ((e33*x10-e13*y10)*y30+(e12*y10-e23*x10)*x30)
      kqh(2,5) = 2*(e13*y10**2-(e33+e12)*x10*y10+e23*x10**2)
      kqh(2,6) = ((e33*x10-e13*y10)*y20+(e12*y10-e23*x10)*x20)
      kqh(3,1) = kqh(1,3)
      kqh(3,2) = kqh(2,3)
      kqh(3,3) = 2*(e11*y20**2-2*e13*x20*y20+e33*x20**2)
      kqh(3,4) = ((e33*x20-e13*y20)*y30+(e12*y20-e23*x20)*x30)
      kqh(3,5) = ((e12*x10-e13*y10)*y20+(e33*y10-e23*x10)*x20)
      kqh(3,6) = 2*(e13*y20**2-(e33+e12)*x20*y20+e23*x20**2)
      kqh(4,1) = kqh(1,4)
      kqh(4,2) = kqh(2,4)
      kqh(4,3) = kqh(3,4)
      kqh(4,4) = 2*(e33*y30**2-2*e23*x30*y30+e22*x30**2)
      kqh(4,5) = ((e23*x10-e33*y10)*y30+(e23*y10-e22*x10)*x30)
      kqh(4,6) = ((e23*x20-e33*y20)*y30+(e23*y20-e22*x20)*x30)
      kqh(5,1) = kqh(1,5)
      kqh(5,2) = kqh(2,5)
```

```
        kqh(5,3) = kqh(3,5)
        kqh(5,4) = kqh(4,5)
        kqh(5,5) = 2*(e33*y10**2-2*e23*x10*y10+e22*x10**2)
        kqh(5,6) = ((e23*x10-e33*y10)*y20+(e23*y10-e22*x10)*x20)
        kqh(6,1) = kqh(1,6)
        kqh(6,2) = kqh(2,6)
        kqh(6,3) = kqh(3,6)
        kqh(6,4) = kqh(4,6)
        kqh(6,5) = kqh(5,6)
        kqh(6,6) = 2*(e33*y20**2-2*e23*x20*y20+e22*x20**2)
        kth(1,1) =   0.0
        kth(1,2) =   0.0
        kth(2,2) =   0.0
        kth(1,3) =   0.0
        kth(2,3) =   0.0
        kth(3,3) =   0.0
        do 3500  j = 1,3
          do 3200  i = 1,6
            w(i) =    kqh(i,1)*hqt(1,j) + kqh(i,2)*hqt(2,j)
     $              + kqh(i,3)*hqt(3,j) + kqh(i,4)*hqt(4,j)
     $              + kqh(i,5)*hqt(5,j) + kqh(i,6)*hqt(6,j)
3200      continue
          do 3300  i = 1,j
            kth(i,j) = kth(i,j) + hqt(1,i)*w(1) + hqt(2,i)*w(2)
     $                          + hqt(3,i)*w(3) + hqt(4,i)*w(4)
     $                          + hqt(5,i)*w(5) + hqt(6,i)*w(6)
          kth(j,i) = kth(i,j)
3300      continue
3500    continue
        s(1) =    kth(1,1) + kth(1,2) + kth(1,3)
        s(2) =    kth(2,1) + kth(2,2) + kth(2,3)
        s(3) =    kth(3,1) + kth(3,2) + kth(3,3)
        ca =         0.25D0/area
        xyij(1) =  ca*x32
        xyij(2) =  ca*y32
        xyij(3) =  ca*x13
        xyij(4) =  ca*y13
        xyij(5) =  ca*x21
        xyij(6) =  ca*y21
        do 4000  j = 1,9
          l =    ls(j)
          do 3600  i = 1,3
            if (j .le. 6) then
              w(i) =  s(i)*xyij(j)
            else
              w(i) =  kth(i,j-6)
            end if
3600      continue
        sum =    w(1) + w(2) + w(3)
        do 3700  i = 1,j
          k =       ls(i)
          if (i .le. 6) then
            sm(k,l) =  sm(k,l) + sum*xyij(i)
```

```
              else
                 sm(k,l)  =   sm(k,l) + w(i-6)
              end if
              sm(l,k)  =   sm(k,l)
 3700         continue
 4000     continue
       return
       end
C=END FORTRAN
```

```
C=DECK SM3MHFF
C=PURPOSE Form HO material stiffness of 9-dof membrane FF-1984 triangle
C=AUTHOR C. A. Felippa, June 1984
C=VERSION September 1986
C=EQUIPMENT Machine independent
C=KEYWORDS finite element
C=KEYWORDS material stiffness matrix
C=KEYWORDS triangle membrane high-order free formulation FF 1984
C=BLOCK ABSTRACT
C
C     SM3MH forms the high order stiffness matrix of the Bergan-
C     Felippa membrane triangle (CMAME, vol 50, pp 25-69).  A faster
C     reformulation (Finite Element Handbook Series, Pineridge
C     Press, pp 139-152) of the original implementation is used.
C
C=END ABSTRACT
C=BLOCK USAGE
C
C     The calling sequence is
C
C        CALL      SM3MHFF (X, Y, DM, F, LS, SM, M, STATUS)
C
C     The inputs are:
C
C     X          (3 x 1) array of x coordinates of triangle nodes
C     Y          (3 x 1) array of y coordinates of triangle nodes
C     DM         (3 x 3) matrix relating membrane  forces to strains
C     F          Factor by which stiffness entries will be multiplied.
C     LS         (9 x 1) array of stiffness location pointers
C                (see SM3MB for examples)
C     SM         Incoming material stiffness array.
C     M          First dimension of SM in calling program.
C
C     The outputs are:
C
C     SM         Output stiffness array with higher order stiffness
C                coefficients added in.  The (i,j)-th entry of the
C                (9 by 9) H.O. membrane stiffness is added to
C                SM(K,L), where K=LS(I) and L=LS(J).
C                (Drilling freedoms are 7,8,9 internally).
C     STATUS     Status character variable.  Blank if no error
C                detected.
C
```

```
C=END USAGE
C=BLOCK FORTRAN
      subroutine    SM3MHFF
     $              (x, y, dm, f, ls, sm, m, status)
C
C                   A R G U M E N T S
C
      character*(*)  status
      integer        ls(9), m
      double precision  x(3), y(3), dm(3,3), f, sm(m,m)
C
C                   L O C A L   V A R I A B L E S
C
      double precision      xc(3), yc(3), dxc(3), dyc(3), hh(3,9)
      double precision      sqh(3,3), qx(3,3), qy(3,3), r(3,3)
      double precision      area, area2, lambda, cj, sj, csj
      double precision      e11, e12, e13, e22, e23, e33, jxx, jxy, jyy
      double precision      det, gamma, ggg, mu, mux, muy, mumu, tau
      double precision      sum, s1, s2, s3, s4, s5, s6, x0, y0
      integer        i, j, k, l
C
C                   L O G I C
C
      status =      ' '
      area2 =       (y(2)-y(1))*(x(1)-x(3)) - (x(2)-x(1))*(y(1)-y(3))
      if (area2 .le. 0.0)      then
        status = 'SM3MHFF: Negative area'
        if (area2 .eq. 0.0)    status = 'SM3MHFF: Zero area'
        return
      end if
      if (f .eq. 0.0)          return
      x0 =          (x(1)+x(2)+x(3))/3.0
      y0 =          (y(1)+y(2)+y(3))/3.0
      area =        0.5*area2
      lambda =      1.0/sqrt(area)
      xc(1) =       lambda * (x(1)-x0)
      xc(2) =       lambda * (x(2)-x0)
      xc(3) =       lambda * (x(3)-x0)
      yc(1) =       lambda * (y(1)-y0)
      yc(2) =       lambda * (y(2)-y0)
      yc(3) =       lambda * (y(3)-y0)
      dxc(1) =      xc(3) - xc(2)
      dxc(2) =      xc(1) - xc(3)
      dxc(3) =      xc(2) - xc(1)
      dyc(1) =      yc(3) - yc(2)
      dyc(2) =      yc(1) - yc(3)
      dyc(3) =      yc(2) - yc(1)
      e11 =         dm(1,1) * f
      e22 =         dm(2,2) * f
      e33 =         dm(3,3) * f
      e12 =         dm(1,2) * f
      e13 =         dm(1,3) * f
      e23 =         dm(2,3) * f
```

```fortran
      jxx =      -2.*(xc(1)*xc(2)+xc(2)*xc(3)+xc(3)*xc(1))/3.0
      jxy =       (xc(1)*yc(1)+xc(2)*yc(2)+xc(3)*yc(3))/3.0
      jyy =      -2.*(yc(1)*yc(2)+yc(2)*yc(3)+yc(3)*yc(1))/3.0
C
      do 2500  j = 1,3
         mux =      -3.0*xc(j)/2.0
         muy =      -3.0*yc(j)/2.0
         mumu =     mux**2 + muy**2
         mu =       sqrt(mumu)
         gamma =    2.0/mu
         tau =      0.25D0*(dxc(j)**2+dyc(j)**2-gamma**2)
         ggg =      (mumu-3.0*tau)*gamma*lambda/24.
         cj =        mux/mu
         sj =        muy/mu
         r(1,j) =   -lambda * (cj*xc(1)+sj*yc(1)) + ggg
         r(2,j) =   -lambda * (cj*xc(2)+sj*yc(2)) + ggg
         r(3,j) =   -lambda * (cj*xc(3)+sj*yc(3)) + ggg
         csj =       cj*sj
         qx(j,1) =  -0.5*csj*cj
         qx(j,2) =  -0.5*sj**3
         qx(j,3) =  -csj*sj
         qy(j,1) =   0.5*cj**3
         qy(j,2) =   0.5*csj*sj
         qy(j,3) =   csj*cj
         s1 =       e11*qx(j,1) + e12*qx(j,2) + e13*qx(j,3)
         s2 =       e12*qx(j,1) + e22*qx(j,2) + e23*qx(j,3)
         s3 =       e13*qx(j,1) + e23*qx(j,2) + e33*qx(j,3)
         s4 =       e11*qy(j,1) + e12*qy(j,2) + e13*qy(j,3)
         s5 =       e12*qy(j,1) + e22*qy(j,2) + e23*qy(j,3)
         s6 =       e13*qy(j,1) + e23*qy(j,2) + e33*qy(j,3)
         do 2400  i = 1,j
           sqh(i,j) = jxx * (qx(i,1)*s1+qx(i,2)*s2+qx(i,3)*s3)
     $            + jxy * (qx(i,1)*s4+qx(i,2)*s5+qx(i,3)*s6
     $                    +qy(i,1)*s1+qy(i,2)*s2+qy(i,3)*s3)
     $            + jyy * (qy(i,1)*s4+qy(i,2)*s5+qy(i,3)*s6)
2400     continue
2500  continue
C
      hh(1,7) =      r(2,2)*r(3,3) - r(2,3)*r(3,2)
      hh(2,8) =      r(3,3)*r(1,1) - r(3,1)*r(1,3)
      hh(3,9) =      r(1,1)*r(2,2) - r(1,2)*r(2,1)
      hh(1,9) =      r(1,2)*r(2,3) - r(1,3)*r(2,2)
      hh(3,7) =      r(2,1)*r(3,2) - r(3,1)*r(2,2)
      hh(2,7) =      r(2,3)*r(3,1) - r(2,1)*r(3,3)
      hh(1,8) =      r(3,2)*r(1,3) - r(1,2)*r(3,3)
      hh(3,8) =      r(3,1)*r(1,2) - r(3,2)*r(1,1)
      hh(2,9) =      r(1,3)*r(2,1) - r(2,3)*r(1,1)
      det =      r(1,1)*hh(1,7) + r(1,2)*hh(2,7) + r(1,3)*hh(3,7)
      do 2700  i = 1,3
         hh(i,7) =   -hh(i,7)/det
         hh(i,8) =   -hh(i,8)/det
         hh(i,9) =   -hh(i,9)/det
         sum =       -0.25D0*lambda*(hh(i,7)+hh(i,8)+hh(i,9))
```

```
        do 2600  j = 1,3
          hh(i,2*j-1) =  -sum*dxc(j)
          hh(i,2*j  ) =  -sum*dyc(j)
2600      continue
2700    continue
C
      do 4000  j = 1,9
        l =        ls(j)
        s1 =    sqh(1,1)*hh(1,j) + sqh(1,2)*hh(2,j) + sqh(1,3)*hh(3,j)
        s2 =    sqh(1,2)*hh(1,j) + sqh(2,2)*hh(2,j) + sqh(2,3)*hh(3,j)
        s3 =    sqh(1,3)*hh(1,j) + sqh(2,3)*hh(2,j) + sqh(3,3)*hh(3,j)
        do 3500  i = 1,j
          k =        ls(i)
          sm(k,l) =  sm(k,l) + (s1*hh(1,i) + s2*hh(2,i) + s3*hh(3,i))
          sm(l,k) =  sm(k,l)
3500      continue
4000    continue
      return
      end
C=END FORTRAN
```

PARAMETRIZED VARIATIONAL PRINCIPLES
FOR MICROPOLAR ELASTICITY

ABSTRACT

A parametrized six-field variational principle for micropolar compressible linear elasticity is presented. The primary variables are symmetric and skew stresses, symmetric and skew strains, micropolar rotations, and displacements. The governing functional is characterized by six free parameters. The connection between this formulation and the functionals with relaxed stress symmetry and independent rotations fields proposed by Reissner and Hughes-Brezzi for classical (non-polar) linear elasticity is examined. It is shown that the Hughes-Brezzi functionals are special cases of the parametrized functional but that the Reissner functionals are not. The former may be interpreted as a regularization (consistent stabilization) of the Reissner functionals that places them within the framework of micropolar elasticity. An eight-field parametrized principle that accounts for couple stresses is briefly described in the Appendix.

1. GOVERNING EQUATIONS

Consider a compressible linear micropolar body under static loading that occupies the volume V. The body is bounded by the surface S, with outward external normal n_i. The surface is decomposed into $S : S_d \cup S_t$. Displacements are prescribed on S_d while surface tractions are prescribed on S_t. Rectangular Cartesian coordinates will be used throughout.

The four unknown volume fields are the displacement vector u_i, the infinitesimal strain tensor γ_{ij}, the stress tensor τ_{ij}, and the (antisymmetric) microrotation tensor θ_{ij}. The stress and strain tensors are not symmetric. The symmetric and antisymmetric parts of the stress tensor are σ_{ij} and s_{ij}, respectively. The symmetric and antisymmetric parts of the strain tensor are e_{ij} and ϕ_{ij}, respectively. The antisymmetric tensor of infinitesimal rotations (also called macrorotations) is ω_{ij}.

The problem data include: the body force field b_i per unit of volume in V, body couples c_i per unit of volume in V, prescribed displacements $\hat{d}_i$ on S_d, and prescribed surface tractions $\hat{t}_i$ on S_t.

The governing field equations for an *isotropic* micropolar continuum without couple stresses are written below following Novacki (1970), with some notational changes. In the following equations, δ_{ij} is the Kronecker delta, ϵ_{ijk} denotes the permutator symbol ($\epsilon_{ijk} = +1$ or -1 if i, j, k are distinct and form a positive or negative permutation, respectively, of 1, 2, 3; else $\epsilon_{ijk} = 0$), λ and μ are the Lamé coefficients, and κ is a micropolar modulus that relates the antisymmetric tensors ϕ_{ij} and s_{ij}. In addition, a comma denotes partial derivative with respect to the space coordinate whose index follows.

Strain-displacement and rotation-displacement equations in V:

$$
\begin{aligned}
\gamma_{ij} &= u_{j,i} - \theta_{ij} = e_{ij} + \omega_{ij} - \theta_{ij} = e_{ij} + \phi_{ij}, \\
\omega_{ij} &= \tfrac{1}{2}(u_{j,i} - u_{i,j}), \\
e_{ij} &= \tfrac{1}{2}(\gamma_{ij} + \gamma_{ji}) = \tfrac{1}{2}(u_{j,i} + u_{i,j}), \\
\phi_{ij} &= \tfrac{1}{2}(\gamma_{ij} - \gamma_{ji}) = \tfrac{1}{2}(u_{j,i} - u_{i,j}) - \theta_{ij} = \omega_{ij} - \theta_{ij}.
\end{aligned}
\tag{1}
$$

Constitutive equations in V:

$$
\begin{aligned}
\tau_{ij} &= (\mu + \kappa)\gamma_{ij} + (\mu - \kappa)\gamma_{ji} + \lambda\delta_{ij}\gamma_{kk} = \sigma_{ij} + s_{ij}, \\
\sigma_{ij} &= \tfrac{1}{2}(\tau_{ij} + \tau_{ji}) = 2\mu e_{ij} + \lambda\delta_{ij}e_{kk}, \\
s_{ij} &= \tfrac{1}{2}(\tau_{ij} - \tau_{ji}) = 2\kappa \phi_{ij}.
\end{aligned}
\tag{2}
$$

Equilibrium equations in V:

$$
\begin{aligned}
\tau_{ji,j} + b_i &= \sigma_{ji,j} + s_{ji,j} + b_i = 0, \\
\epsilon_{ijk}\tau_{jk} + c_i &= 0.
\end{aligned}
\tag{3}
$$

Stress boundary conditions on S_t:

$$
\tau_{ij}n_j = \hat{t}_i.
\tag{4}
$$

Displacement boundary conditions on S_d:

$$u_i = \hat{d}_i. \tag{5}$$

The foregoing equations apply if the presence of couple stresses m_{ij} is neglected. The variational treatment is extended to that case in the Appendix.

For completeness, and to facilitate correlation with other references, equations (1)–(5) are restated below in direct (index-free) tensor notation:

$$
\begin{aligned}
&\underline{\gamma} = \nabla u - \underline{\theta} = \underline{e} + \underline{\omega} - \underline{\theta} = \underline{e} + \underline{\phi}, \\
&\underline{\omega} = \tfrac{1}{2}(\nabla - \nabla^T)u = \text{skew } (\nabla u), \\
&\underline{e} = \tfrac{1}{2}(\nabla + \nabla^T)u = \text{symm } (\nabla u) = \text{symm } \underline{\gamma}, \\
&\underline{\phi} = \underline{\omega} - \underline{\theta} = \tfrac{1}{2}(\nabla - \nabla^T)u - \underline{\theta} = \text{skew } (\nabla u - \underline{\theta}) = \text{skew } \underline{\gamma}, \\
&\underline{\tau} = (\mu + \kappa)\underline{\gamma} + (\mu - \kappa)\underline{\gamma}^T + \lambda \underline{I} \text{ trace } \underline{\gamma} = \underline{\sigma} + \underline{s}, \\
&\underline{\sigma} = \text{symm } \underline{\tau} = 2\mu \underline{e} + \lambda \underline{I} \text{ trace } \underline{\gamma}, \\
&\underline{s} = \text{skew } \underline{\tau} = 2\kappa \underline{\phi}, \\
&\text{div } \underline{\tau} + b = \text{div } (\underline{\sigma} + \underline{s}) + b = 0, \\
&2\,\text{axial } \underline{\tau} + c = 0,
\end{aligned}
\quad\Bigg\} \quad \text{in } V \tag{6}
$$

$$\tau_n = \hat{t} \quad \text{on } S_t,$$

$$u = \hat{d} \quad \text{on } S_d.$$

Here an underlined bold symbol denotes a second order or higher tensor. This convention is used to distinguish tensors from their vector/matrix representations introduced in Section 2.1. No such distinction is needed for vectors such as **u**.

2. NOTATION

2.1 Matrix Notation

To facilitate the construction and manipulation of variational matrix expressions, stresses and strains will be arranged as column vectors constructed from the respective tensors. The arrangement rules vary according to the symmetry properties and are best illustrated by specifics.

For symmetric stress and strain tensors:

$$\underline{\sigma} = \begin{bmatrix} \sigma_{11} & \sigma_{12} & \sigma_{13} \\ \sigma_{12} & \sigma_{22} & \sigma_{23} \\ \sigma_{13} & \sigma_{23} & \sigma_{33} \end{bmatrix} \equiv \sigma = \begin{Bmatrix} \sigma_{11} \\ \sigma_{22} \\ \sigma_{33} \\ \sigma_{23} \\ \sigma_{31} \\ \sigma_{12} \end{Bmatrix}, \qquad \underline{e} = \begin{bmatrix} e_{11} & e_{12} & e_{13} \\ e_{12} & e_{22} & e_{23} \\ e_{13} & e_{23} & e_{33} \end{bmatrix} \equiv e = \begin{Bmatrix} e_{11} \\ e_{22} \\ e_{33} \\ 2e_{23} \\ 2e_{31} \\ 2e_{12} \end{Bmatrix}, \quad (7)$$

where $\sigma_{31} = \sigma_{13}$ and $e_{31} = e_{13}$. The factor of 2 in e maintains equivalence of stress-strain inner products; cf. (12) below.

For antisymmetric (skew) stress and strain tensors:

$$\underline{s} = \begin{bmatrix} 0 & s_{12} & s_{13} \\ -s_{12} & 0 & s_{23} \\ -s_{13} & -s_{23} & 0 \end{bmatrix} \equiv s = \begin{Bmatrix} s_{23} \\ s_{31} \\ s_{12} \end{Bmatrix}, \qquad \underline{\phi} = \begin{bmatrix} 0 & \phi_{12} & \phi_{13} \\ -\phi_{12} & 0 & \phi_{23} \\ -\phi_{13} & -\phi_{23} & 0 \end{bmatrix} \equiv \phi = \begin{Bmatrix} 2\phi_{23} \\ 2\phi_{31} \\ 2\phi_{12} \end{Bmatrix}$$
$$(8)$$

$$\underline{\theta} = \begin{bmatrix} 0 & \theta_{12} & \theta_{13} \\ -\theta_{12} & 0 & \theta_{23} \\ -\theta_{13} & -\theta_{23} & 0 \end{bmatrix} \equiv \theta = \begin{Bmatrix} 2\theta_{23} \\ 2\theta_{31} \\ 2\theta_{12} \end{Bmatrix}, \qquad \underline{\omega} = \begin{bmatrix} 0 & \omega_{12} & \omega_{13} \\ -\omega_{12} & 0 & \omega_{23} \\ -\omega_{13} & -\omega_{23} & 0 \end{bmatrix} \equiv \omega = \begin{Bmatrix} 2\omega_{23} \\ 2\omega_{31} \\ 2\omega_{12} \end{Bmatrix}$$
$$(9)$$

where $s_{31} = -s_{13}$ and $\phi_{31} = -\phi_{13}$. The factor of 2 applies only to kinematic skew (rotational) tensors, and again maintains inner product equivalence; cf. (12) below.

For general (unsymmetric) stress and strain tensors:

$$\underline{\tau} = \begin{bmatrix} \tau_{11} & \tau_{12} & \tau_{13} \\ \tau_{21} & \tau_{22} & \tau_{23} \\ \tau_{31} & \tau_{32} & \tau_{33} \end{bmatrix} \equiv \tau = \begin{Bmatrix} \tau_{11} \\ \tau_{22} \\ \tau_{33} \\ \tau_{23} \\ \tau_{31} \\ \tau_{12} \\ \tau_{32} \\ \tau_{13} \\ \tau_{21} \end{Bmatrix}, \qquad \underline{\gamma} = \begin{bmatrix} \gamma_{11} & \gamma_{12} & \gamma_{13} \\ \gamma_{21} & \gamma_{22} & \gamma_{23} \\ \gamma_{31} & \gamma_{32} & \gamma_{33} \end{bmatrix} \equiv \gamma = \begin{Bmatrix} \gamma_{11} \\ \gamma_{22} \\ \gamma_{33} \\ \gamma_{23} \\ \gamma_{31} \\ \gamma_{12} \\ \gamma_{32} \\ \gamma_{13} \\ \gamma_{21} \end{Bmatrix}. \quad (10)$$

With these conventions operations between tensors of equal type can be easily translated to matrix form. For example, the inner products

$$\underline{\sigma} : \underline{e} = \sigma_{ij} e_{ij} = \sigma^T e, \qquad \underline{s} : \underline{\phi} = s_{ij} \phi_{ij} = s^T \phi. \tag{11}$$

Problems arise, however, in combining different types. For example, $\tau = \sigma + s$ is an inconsistent matrix operation because vectors σ and s have different dimensions. This difficulty can be circumvented by introducing "uncompressed" versions, in which components of symmetric and skew

366

tensors are arranged as general tensors:

$$
{}^{*}\sigma = \left\{\begin{array}{c} \sigma_{11} \\ \sigma_{22} \\ \sigma_{33} \\ \sigma_{23} \\ \sigma_{31} \\ \sigma_{12} \\ \sigma_{23} \\ \sigma_{31} \\ \sigma_{12} \end{array}\right\}, \quad
{}^{*}s = \left\{\begin{array}{c} 0 \\ 0 \\ 0 \\ s_{23} \\ s_{31} \\ s_{12} \\ -s_{23} \\ -s_{31} \\ -s_{12} \end{array}\right\}, \quad
{}^{*}e = \left\{\begin{array}{c} e_{11} \\ e_{22} \\ e_{33} \\ e_{23} \\ e_{31} \\ e_{12} \\ e_{23} \\ e_{31} \\ e_{12} \end{array}\right\}, \quad
{}^{*}\phi = \left\{\begin{array}{c} 0 \\ 0 \\ 0 \\ \phi_{23} \\ \phi_{31} \\ \phi_{12} \\ -\phi_{23} \\ -\phi_{31} \\ -\phi_{12} \end{array}\right\}. \tag{12}
$$

Furthermore, $\tau = {}^{*}\tau$ and $\gamma = {}^{*}\gamma$, thus no distinction is needed there. This convention will let us consistently expand expressions such as the inner product of total stresses and strains:

$$
\tau_{ij}\gamma_{ij} = \tau^{T}\gamma = ({}^{*}\sigma + {}^{*}s)^{T} ({}^{*}e + {}^{*}\phi) = \sigma^{T}e + s^{T}\phi. \tag{13}
$$

2.2 Matrix Form of Governing Equations

Using the matrix notation of Section 2.1, field equations (1)–(3) may be represented as follows. Strain-displacement equations:

$$
\gamma = {}^{*}e + {}^{*}\phi, \qquad e = Du, \qquad \phi = \omega - \theta = Ru - \theta. \tag{14}
$$

Constitutive equations:

$$
\tau = {}^{*}\sigma + {}^{*}s, \qquad \sigma = Ee, \qquad s = G\phi. \tag{15}
$$

Equilibrium equations:

$$
D^{T}\sigma + R^{T}s + b = 0, \qquad 2s + c = 0. \tag{16}
$$

In the above equations,

$$
D = \begin{bmatrix} \partial/\partial x_1 & 0 & 0 \\ 0 & \partial/\partial x_2 & 0 \\ 0 & 0 & \partial/\partial x_3 \\ \partial/\partial x_2 & \partial/\partial x_1 & 0 \\ 0 & \partial/\partial x_3 & \partial/\partial x_2 \\ \partial/\partial x_3 & 0 & \partial/\partial x_1 \end{bmatrix}, \quad
R = \begin{bmatrix} -\partial/\partial x_2 & \partial/\partial x_1 & 0 \\ 0 & -\partial/\partial x_3 & \partial/\partial x_2 \\ \partial/\partial x_3 & 0 & -\partial/\partial x_1 \end{bmatrix} \tag{17}
$$

are the symmetric gradient and curl operators, respectively, in matrix form, and

$$
E = \begin{bmatrix} \lambda+2\mu & \mu & \mu & 0 & 0 & 0 \\ \mu & \lambda+2\mu & \mu & 0 & 0 & 0 \\ \mu & \mu & \lambda+2\mu & 0 & 0 & 0 \\ 0 & 0 & 0 & \mu & 0 & 0 \\ 0 & 0 & 0 & 0 & \mu & 0 \\ 0 & 0 & 0 & 0 & 0 & \mu \end{bmatrix}, \quad
G = \kappa \begin{bmatrix} 1 & 0 & 0 \\ 0 & 1 & 0 \\ 0 & 0 & 1 \end{bmatrix} \tag{18}
$$

In the sequel E and G are not restricted to these isotropic forms but can be *arbitrary nonsingular* symmetric matrices. This allows anisotropy in the constitutive equations, subjected however to the restriction that the pairs (σ, e) and (s, γ) remain constitutively uncoupled.

For future use, introduce the constitutive matrix C that relates τ to γ:

$$\tau = C\gamma, \qquad C = \begin{bmatrix} E & 0 \\ 0 & G \end{bmatrix}. \tag{19}$$

2.3 Reduction to Classical Elasticity

Micropolar elasticity reduces to classical linear elasticity if the couple body force c vanishes. If so the second equilibrium equation $2s + c = 0$ shows that $s = 0$, and $\tau = \sigma + s = \sigma$ is symmetric. Under the assumption that G is nonsingular, the second constitutive equation in (16) gives $\phi = G^{-1}s = 0$, and $\gamma = e + \phi = e$ is symmetric. Furthermore, $\theta = \omega$, that is, microrotations and continuum-mechanics rotations coalesce.

2.4 Field Dependency

For the investigation of variational methods in Sections 3 and 4, the field-dependency notational conventions used by Felippa (1989a,b,c,1991) and Felippa and Militello (1989,1990) are followed. An *independently varied* field will be identified by a superposed tilde, for example $\tilde{u}$. A dependent field is identified by writing the independent field symbol as superscript. For example, if the displacements are independently varied, the derived symmetric strain and stress fields are

$$e^u = D\tilde{u}, \qquad \sigma^u = Ee^u = ED\tilde{u}. \tag{20}$$

Using this convention, tildeless symbols such as u, e and σ are reserved for the *exact* or for *generic* fields. If a symbol derives from two independently varied fields, both fields appear as superscripts: for example $\phi^{u\theta} = R\tilde{u} - \tilde{\theta}$.

2.5 Integral Abbreviations

Volume and surface integrals may be abbreviated by placing domain-subscripted parentheses and square brackets, respectively, around the integrand. For example:

$$(f)_V \overset{\text{def}}{=} \int_V f \, dV, \qquad [f]_S \overset{\text{def}}{=} \int_S f \, dS, \qquad [f]_{S_d} \overset{\text{def}}{=} \int_{S_d} f \, dS, \qquad [f]_{S_t} \overset{\text{def}}{=} \int_{S_t} f \, dS. \tag{21}$$

If f and g are vector functions, and p and q tensor functions, their inner product over V is denoted in the usual manner

$$(f, g)_V \overset{\text{def}}{=} \int_V f_i g_i \, dV = \int_V f^T g \, dV, \qquad (p, q)_V \overset{\text{def}}{=} \int_V p_{ij} q_{ij} \, dV = \int_V p^T q \, dV, \tag{22}$$

and similarly for surface integrals, in which case square brackets are used.

3. GENERALIZED STRAIN ENERGY FOR CLASSICAL ELASTICITY

The method used to construct parametrized micropolar variational principles in Section 4 represents a generalization of the corresponding principles of classical linear hyperelasticity, which are summarized in this section. These principles have the general form

$$\Pi = U - P. \tag{23}$$

Here U is the generalized strain energy, which characterizes the stored energy of deformation, and P is the forcing potential, which characterizes all other contributions. The conventional form of P is

$$P^c = (\mathbf{b}, \bar{\mathbf{u}})_V + [\bar{\mathbf{u}} - \hat{\mathbf{d}}, \bar{\sigma}_n]_{S_d} + [\hat{\mathbf{t}}, \bar{\mathbf{u}}]_{S_t}. \tag{24}$$

where $\sigma_n = \sigma^T \mathbf{n}$, $\mathbf{n}$ being the unit external normal on S. The other two forms of P, called P^d and P^t for displacement-generalized and traction-generalized, respectively, are studied by Felippa (1989a,b,c). These (mesh-dependent) forms are of interest in hybrid finite element discretizations. As the forcing potential is not affected by parametrization, attention will be focused on U.

For a *compressible* material, the generalized strain energy introduced in Felippa and Militello (1989,1990) has the following structure:

$$U = \tfrac{1}{2} j_{11}(\bar{\sigma}, \mathbf{e}^\sigma)_V + j_{12}(\bar{\sigma}, \bar{\mathbf{e}})_V + j_{13}(\bar{\sigma}, \mathbf{e}^u)_V + \tfrac{1}{2} j_{22}(\sigma^e, \bar{\mathbf{e}})_V + j_{23}(\sigma^e, \mathbf{e}^u)_V + \tfrac{1}{2} j_{33}(\sigma^u, \mathbf{e}^u)_V, \tag{25}$$

where j_{11} through j_{33} are numerical coefficients. The three independent fields are stresses $\bar{\sigma}$, strains $\bar{\mathbf{e}}$ and displacements $\bar{\mathbf{u}}$. Following the matrix notational conventions stated in Section 2.4, the derived fields that appear in (25) are

$$\sigma^e = \mathbf{E}\bar{\mathbf{e}}, \quad \sigma^u = \mathbf{ED}\bar{\mathbf{u}}, \quad \mathbf{e}^\sigma = \mathbf{E}^{-1}\bar{\sigma}, \quad \mathbf{e}^u = \mathbf{D}\bar{\mathbf{u}}. \tag{26}$$

As an example, the U of Hu-Washizu's functional is obtained by setting $j_{12} = -1$, $j_{13} = 1$, $j_{22} = 1$, all others being zero:

$$U_H(\bar{\sigma}, \bar{\mathbf{e}}, \bar{\mathbf{u}}) = \tfrac{1}{2}(\sigma^e, \bar{\mathbf{e}})_V + \tfrac{1}{2}(\bar{\sigma}, \mathbf{e}^u - \bar{\mathbf{e}})_V + \tfrac{1}{2}(\sigma^u - \sigma^e, \mathbf{e}^\sigma)_V = \tfrac{1}{2}(\sigma^e, \bar{\mathbf{e}})_V + (\bar{\sigma}, \mathbf{e}^u - \bar{\mathbf{e}})_V. \tag{27}$$

Equation (25) can be rewritten in matrix form as

$$U = \tfrac{1}{2} \int_V \begin{Bmatrix} \bar{\sigma} \\ \sigma^e \\ \sigma^u \end{Bmatrix}^T \begin{bmatrix} j_{11}\mathbf{I} & j_{12}\mathbf{I} & j_{13}\mathbf{I} \\ & j_{22}\mathbf{I} & j_{23}\mathbf{I} \\ symm & & j_{33}\mathbf{I} \end{bmatrix} \begin{Bmatrix} \mathbf{e}^\sigma \\ \bar{\mathbf{e}} \\ \mathbf{e}^u \end{Bmatrix} dV. \tag{28}$$

where $\mathbf{I}$ denotes the 6×6 identity matrix. The functional-generating symmetric matrix

$$\mathbf{J} = \begin{bmatrix} j_{11} & j_{12} & j_{13} \\ j_{12} & j_{22} & j_{23} \\ j_{13} & j_{23} & j_{33} \end{bmatrix} \tag{29}$$

369

is seen to fully characterize (25) and consequently, once the forcing potential P is selected, the functional (23). (To justify the symmetry of $\mathbf{J}$ note, for example, that $j_{13}(\tilde{\sigma}, \mathbf{e}^u)_V = \frac{1}{2}j_{13}(\tilde{\sigma}, \mathbf{e}^u)_V + \frac{1}{2}j_{13}(\mathbf{e}^\sigma, \sigma^u)_V$, etc.)

On replacing (26) into (28), U may be expressed in terms of the three independent fields as

$$U = \frac{1}{2} \int_V \begin{Bmatrix} \tilde{\sigma} \\ \tilde{\mathbf{e}} \\ \tilde{\mathbf{u}} \end{Bmatrix}^T \begin{bmatrix} j_{11}\mathbf{E}^{-1} & j_{12}\mathbf{I} & j_{13}\mathbf{D} \\ j_{12}\mathbf{I} & j_{22}\mathbf{E} & j_{23}\mathbf{ED} \\ j_{13}\mathbf{D}^T & j_{23}\mathbf{D}^T\mathbf{E} & j_{33}\mathbf{D}^T\mathbf{ED} \end{bmatrix} \begin{Bmatrix} \tilde{\sigma} \\ \tilde{\mathbf{e}} \\ \tilde{\mathbf{u}} \end{Bmatrix} dV, \tag{30}$$

Using (30) the first variation of U may be presented as

$$\delta U = (\Delta\mathbf{e}, \delta\tilde{\sigma})_V + (\Delta\sigma, \delta\tilde{\mathbf{e}})_V - (\mathrm{div}\,\sigma', \delta\tilde{\mathbf{u}})_V + [\sigma'_n, \delta\tilde{\mathbf{u}}]_S, \tag{31}$$

where

$$\Delta\mathbf{e} = j_{11}\mathbf{e}^\sigma + j_{12}\tilde{\mathbf{e}} + j_{13}\mathbf{e}^u, \quad \Delta\sigma = j_{12}\tilde{\sigma} + j_{22}\sigma^e + j_{23}\sigma^u, \quad \sigma' = j_{13}\tilde{\sigma} + j_{23}\sigma^e + j_{33}\sigma^u. \tag{32}$$

The last term in (32) combines with contributions from the forcing potential variation. For example, if P is the conventional forcing potential (24), the complete variation of $\Pi^c = U - P^c$ is

$$\delta\Pi^c = (\Delta\mathbf{e}, \delta\tilde{\sigma})_V + (\Delta\sigma, \delta\tilde{\mathbf{e}})_V - (\mathrm{div}\,\sigma' + \mathbf{b}, \delta\tilde{\mathbf{u}})_V + [\sigma'_n - \hat{\mathbf{t}}, \delta\tilde{\mathbf{u}}]_{S_t} - [\tilde{\mathbf{u}} - \hat{\mathbf{d}}, \delta\tilde{\sigma}_n]_{S_d}. \tag{33}$$

Using P^d or P^t does not change the volume terms. Consequently the Euler equations associated with the volume terms of the first variation

$$\Delta\mathbf{e} = \mathbf{0}, \quad \Delta\sigma = \mathbf{0}, \quad \mathrm{div}\,\sigma' + \mathbf{b} = \mathbf{0}, \tag{34}$$

are independent of the forcing potential. For consistency of the Euler equations with the field equations of classical elasticity one must have $\Delta\mathbf{e} = \mathbf{0}$, $\Delta\sigma = \mathbf{0}$ and $\sigma' = \sigma$ if the assumed stress and strain fields reduce to the exact ones. Therefore

$$j_{11} + j_{12} + j_{13} = 0, \quad j_{12} + j_{22} + j_{23} = 0, \quad j_{13} + j_{23} + j_{33} = 1. \tag{35}$$

Because of these constraints, the maximum number of independent parameters that define the entries of matrix $\mathbf{J}$ is three. The specialization of these functionals to conventional and parametrized forms is discussed by Felippa and Militello (1989,1990).

Insofar as $\mathbf{E}^{-1}$ appears in (30), this development is valid only for compressible elasticity. Extensions of this variational principle to cover incompressibility are discussed by Felippa (1992).

4. GENERALIZED STRAIN ENERGY FOR MICROPOLAR ELASTICITY

For a micropolar elastic material without couple stresses the variational principle is structurally similar to (23):

$$\Pi_m = U_m - P_m, \tag{36}$$

where U_m now also depends on $\tilde{s}$, $\tilde{\phi}$ and $\tilde{\theta}$, and P_m may be P_m^c, P_m^d or P_m^t. The following generalization of U to U_m is postulated:

$$U_m = \frac{1}{2} \int_V \begin{Bmatrix} \tilde{\sigma} \\ \sigma^\epsilon \\ \sigma^\mu \\ \tilde{s} \\ s^\phi \\ s^{\mu\theta} \end{Bmatrix}^T \begin{bmatrix} j_{11}I_6 & j_{12}I_6 & j_{13}I_6 & 0 & 0 & 0 \\ j_{12}I_6 & j_{22}I_6 & j_{23}I_6 & 0 & 0 & 0 \\ j_{13}I_6 & j_{23}I_6 & j_{33}I_6 & 0 & 0 & 0 \\ 0 & 0 & 0 & j_{44}I_3 & j_{45}I_3 & j_{46}I_3 \\ 0 & 0 & 0 & j_{45}I_3 & j_{55}I_3 & j_{56}I_3 \\ 0 & 0 & 0 & j_{46}I_3 & j_{56}I_3 & j_{66}I_3 \end{bmatrix} \begin{Bmatrix} e^\sigma \\ \tilde{e} \\ e^\mu \\ \phi^s \\ \tilde{\phi} \\ \phi^{\mu\theta} \end{Bmatrix} dV, \tag{37}$$

where I_6 and I_3 denote the identity matrices of order 6 and 3, respectively, and the new derived fields are

$$\phi^s = G^{-1}\tilde{s}, \quad s^\phi = G\tilde{\phi}, \quad \phi^{\mu\theta} = R\tilde{u} - \tilde{\theta}, \quad s^{\mu\theta} = G\phi^{\mu\theta} = G(R\tilde{u} - \tilde{\theta}). \tag{38}$$

The block structure of the kernel matrix in (37) results from the inner product orthogonality (14) of symmetric and antisymmetric tensors. The symmetry of the j coefficients is an assumption that remains to be verified.

On substituting (38) and (26) into (37), U_m is expressed in terms of the six independently varied fields $\tilde{\sigma}$, $\tilde{e}$, $\tilde{u}$, $\tilde{s}$, $\tilde{\phi}$ and $\tilde{\theta}$:

$$U_m = \frac{1}{2} \int_V \begin{Bmatrix} \tilde{\sigma} \\ \tilde{e} \\ \tilde{u} \\ \tilde{s} \\ \tilde{\phi} \\ \tilde{\theta} \end{Bmatrix}^T \begin{bmatrix} j_{11}E^{-1} & j_{12}I_6 & j_{13}D & 0 & 0 & 0 \\ j_{12}I_6 & j_{22}E & j_{23}ED & 0 & 0 & 0 \\ j_{13}D^T & j_{23}D^TE & j_{33}D^TED & j_{46}R^T & j_{56}R^TG & -j_{66}R^TG \\ & & +j_{66}R^TGR & & & \\ 0 & 0 & j_{46}R & j_{44}G^{-1} & j_{45}I_3 & -j_{46}I_3 \\ 0 & 0 & j_{56}GR & j_{45}I_3 & j_{55}G & -j_{56}G \\ 0 & 0 & -j_{66}GR & -j_{46}I_3 & -j_{56}G & j_{66}G \end{bmatrix} \begin{Bmatrix} \tilde{\sigma} \\ \tilde{e} \\ \tilde{u} \\ \tilde{s} \\ \tilde{\phi} \\ \tilde{\theta} \end{Bmatrix} dV. \tag{39}$$

The kernel matrix in the above quadratic form must be symmetric, a condition that verifies the symmetry assumptions in (37). As for the forcing potential, the conventional form changes to

$$P_m^c = (b, \tilde{u})_V + \tfrac{1}{2}(c, \tilde{\theta})_V + [\tilde{u} - \hat{d}, \tau_n]_{S_d} + [\hat{t}, \tilde{u}]_{S_t} = P^c + \tfrac{1}{2}(c, \theta)_V + [\tilde{u} - \hat{d}, s_n]_{S_d}. \tag{40}$$

Similarly, the generalized forcing potentials P_m^d and P_m^t are obtained by augmenting P^d and P^t, respectively, with $\tfrac{1}{2}(c, \tilde{\theta})_V + [\tilde{u} - \hat{d}, s]S_d$. [The $\frac{1}{2}$ in the c term arises from the presence of factor 2 in the definition (9) of the microrotation vector θ.]

The first variation of U_m is

$$\delta U_m = \left(\Delta e, \delta\tilde{\sigma}\right)_V + \left(\Delta\sigma, \delta\tilde{e}\right)_V - \left(\mathbf{D}^T\sigma' + \mathbf{R}^T s', \delta\tilde{u}\right)_V \\ + \left(\Delta\phi, \delta\tilde{s}\right)_V + \left(\Delta s, \delta\tilde{\phi}\right)_V - \left(s', \delta\tilde{\theta}\right)_V + [\sigma_n' + s_n', \delta\tilde{u}_n]_S. \tag{41}$$

where Δe, $\Delta\sigma$ and σ are the same as in (32), and

$$\Delta\phi = j_{44}\phi^s + j_{45}\tilde{\phi} + j_{46}\phi^{u\theta}, \quad \Delta s = j_{45}\tilde{s} + j_{55}s^\phi + j_{56}s^{u\theta}, \quad s' = j_{46}\tilde{s} + j_{56}s^\phi + j_{66}s^{u\theta}. \tag{42}$$

Note that $(\mathbf{D}^T\sigma' + \mathbf{R}^T s') = \operatorname{div}\sigma' + \operatorname{div}s' = \operatorname{div}\tau'$, where $\tau' = {}^*\sigma' + {}^*s'$. The first variation of $\Pi_m = U_m - P_m^c$ is

$$\delta\Pi_m = \left(\Delta e, \delta\tilde{\sigma}\right)_V + \left(\Delta\sigma, \delta\tilde{e}\right)_V - \left(\operatorname{div}\tau' + \mathbf{b}, \delta\tilde{u}\right)_V + \left(\Delta\phi, \delta\tilde{s}\right)_V \\ + \left(\Delta s, \delta\tilde{\phi}\right)_V - \tfrac{1}{2}\left(2s' + \mathbf{c}, \delta\tilde{\theta}\right)_V + [\tau_n' - \hat{\mathbf{t}}, \delta\tilde{u}]_{S_t} - [\tilde{u} - \hat{\mathbf{d}}, \delta\tilde{\tau}_n]_{S_d}. \tag{43}$$

Following the same argument as in Section 3, it is found that consistency with the field equations requires, in addition to (35), that

$$j_{44} + j_{45} + j_{46} = 0, \qquad j_{45} + j_{55} + j_{56} = 0, \qquad j_{46} + j_{56} + j_{66} = 1. \tag{44}$$

It follows that the parametrized functional of micropolar elasticity

$$\Pi_m = U_m(\tilde{\sigma}, \tilde{e}, \tilde{u}, \tilde{s}, \tilde{\phi}, \tilde{\theta}) - P_m, \tag{45}$$

depends on $12 - 6 = 6$ free parameters through U_m. Specific instances of (45) are characterized by the functional-generating symmetric matrix

$$\mathbf{J}_m = \begin{bmatrix} j_{11} & j_{12} & j_{13} & 0 & 0 & 0 \\ j_{12} & j_{22} & j_{23} & 0 & 0 & 0 \\ j_{13} & j_{23} & j_{33} & 0 & 0 & 0 \\ 0 & 0 & 0 & j_{44} & j_{45} & j_{46} \\ 0 & 0 & 0 & j_{45} & j_{55} & j_{56} \\ 0 & 0 & 0 & j_{46} & j_{56} & j_{66} \end{bmatrix}, \tag{46}$$

subjected to the six constraints (35) and (44). The nonzero 3×3 blocks in $\mathbf{J}_m$ characterize weightings for symmetric and antisymmetric fields, respectively, and one is free to "mix or match." For example,

$$\mathbf{J}_m = \begin{bmatrix} 0 & -1 & 1 & 0 & 0 & 0 \\ -1 & 1 & 0 & 0 & 0 & 0 \\ 1 & 0 & 0 & 0 & 0 & 0 \\ 0 & 0 & 0 & 0 & -1 & 1 \\ 0 & 0 & 0 & -1 & 1 & 0 \\ 0 & 0 & 0 & 1 & 0 & 0 \end{bmatrix}, \tag{47}$$

represents the choice of the Hu-Washizu principle for both symmetric and antisymmetric fields.

The variational principles of Reissner (1965) and Hughes and Brezzi (1989) will be now examined in light of the preceding developments.

5. NON-POLAR FUNCTIONALS WITH INDEPENDENT ROTATIONS

5.1 The Reissner Functionals

Reissner (1965) proposed a functional of Hellinger-Reissner type for classical (non-polar) elasticity ($c = 0$) in which u, τ and θ are to be treated as independent fields. In this functional the stress symmetry condition $s = 0$ appears as a weak condition with θ playing the rôle of multiplier. In the present notation the functional, herein called $\Pi_{R1} = U_{R1} - P_R^c$, can be written as

$$U_{R1} = -\tfrac{1}{2}(\bar{\sigma}, \mathbf{E}^{-1}\bar{\sigma})_V + (\bar{\tau}, \nabla\bar{u} - \bar{\theta})_V, \qquad P_R^c = P^c + \left[\bar{u} - \hat{d}, \bar{s}_n\right]_{S_d}, \tag{48}$$

where ∇u is the gradient of the displacement vector. Expanding inner products, noting that $\tau^T (\nabla u - \theta) = \tau^T \gamma^{\mu,\phi} = (^*\sigma + ^*s)^T (^*e^u + ^*\phi^{u,\phi})$, and making use of (13) yields

$$
\begin{aligned}
U_{R1} &= -\tfrac{1}{2}(\bar{\sigma}, e^{\sigma})_V + (\bar{\sigma}, e^u)_V + (\bar{s}, \phi^{u\theta})_V \\
&= -\tfrac{1}{2}(\bar{\sigma}, e^{\sigma})_V + \tfrac{1}{2}(\bar{\sigma}, e^u)_V + \tfrac{1}{2}(\bar{\sigma}^u, \bar{e})_V + \tfrac{1}{2}(\bar{s}, \phi^{u\theta})_V + \tfrac{1}{2}(s^{u\theta}, \tilde{\phi})_V.
\end{aligned}
\tag{49}
$$

This corresponds to taking

$$
\mathbf{J}_m = \begin{bmatrix}
-1 & 0 & 1 & 0 & 0 & 0 \\
0 & 0 & 0 & 0 & 0 & 0 \\
1 & 0 & 0 & 0 & 0 & 0 \\
0 & 0 & 0 & 0 & 0 & 1 \\
0 & 0 & 0 & 0 & 0 & 0 \\
0 & 0 & 0 & 1 & 0 & 0
\end{bmatrix}.
\tag{50}
$$

It can be seen that the first consistency condition in (44), namely $j_{44} + j_{45} + j_{46} = 0$, is violated. Consequently Π_{R1} is not a valid functional for micropolar elasticity. Inspection of (50) reveals that conditions (44) can be met by simply changing j_{44} to -1, and that is precisely the regularization of Hughes-Brezzi described in Section 5.2.

Reissner also proposed a second functional $\Pi_{R2} = U_{R2} - P_R^c$ of Hu-Washizu type, in which

$$
\begin{aligned}
U_{R2} &= \tfrac{1}{2}(\bar{e}, \mathbf{E}\bar{e})_V + (\bar{\sigma}, e^u - \bar{\gamma})_V + (\bar{s}, \phi^{u\theta} - \tilde{\phi})_V \\
&= \tfrac{1}{2}(\sigma^e, \bar{e}) + \tfrac{1}{2}(\bar{\sigma}, e^u - \bar{e})_V + \tfrac{1}{2}(\sigma^u - \sigma^e, e^{\sigma})_V + \tfrac{1}{2}(\bar{s}, \phi^{u\theta} - \tilde{\phi})_V + \tfrac{1}{2}(s^{u\theta} - \bar{s}^\phi, \phi^s)_V
\end{aligned}
\tag{51}
$$

which corresponds to the $\mathbf{J}_m$ of (47) except that $j_{55} = 0$. Now the second consistency equation in (44) is violated. Thus this second functional is also inconsistent with micropolar elasticity, but may be corrected by changing j_{55} to 1.

5.2 The Hughes-Brezzi Functionals

Hughes and Brezzi (1989) investigated the possible application of the Reissner functionals to construct finite elements with "drilling" degrees of freedom for classical elasticity. Their analysis shows that the first Reissner functional would lead to *unstable* discrete approximations. The physical

cause of this instability is that deviations from stress symmetry do not produce strain energy. To circumvent that difficulty, they proposed stabilizing U_{R1} by adding a penalty-like term of the form

$$-\frac{1}{2\bar{\kappa}}(\bar{s}, \bar{s})_V,$$ (52)

where $\bar{\kappa} > 0$ is a pseudo-modulus with dimensions of stress (in their paper this modulus is called γ, a symbol used here for total strain). Although $\bar{\kappa}$ plays the same role as κ in the micropolar theory, for the intended application it is a *fictitious* quantity to be chosen by numerical experiments. The term (52) can be encompassed in the present framework by choosing $\mathbf{G} = \bar{\kappa}\mathbf{I}_3$, which allows that term to be written as $-\frac{1}{2}(\bar{s}, \phi^s)_V$. Adding this to U_{R1} yields the first Hughes-Brezzi functional:

$$
\begin{aligned}
U_{HB1} &= -\tfrac{1}{2}(\bar{\tau}, \mathbf{C}^{-1}\bar{\tau})_V + (\bar{\tau}, \nabla\bar{\mathbf{u}} - \bar{\theta})_V \\
&= -\tfrac{1}{2}(\bar{\sigma}, \mathbf{e}^\sigma)_V - \tfrac{1}{2}(\bar{s}, \phi^s)_V + \tfrac{1}{2}(\bar{\sigma}, \mathbf{e}^u)_V + \tfrac{1}{2}(\sigma^u, \bar{\mathbf{e}})_V + \tfrac{1}{2}(\bar{s}, \phi^{u\theta})_V + \tfrac{1}{2}(s^{u\theta}, \bar{\phi})_V.
\end{aligned}
$$ (53)

This befits the form (37) with the generating matrix

$$
\mathbf{J}_m = \begin{bmatrix}
-1 & 0 & 1 & 0 & 0 & 0 \\
0 & 0 & 0 & 0 & 0 & 0 \\
1 & 0 & 0 & 0 & 0 & 0 \\
0 & 0 & 0 & -1 & 0 & 1 \\
0 & 0 & 0 & 0 & 0 & 0 \\
0 & 0 & 0 & 1 & 0 & 0
\end{bmatrix},
$$ (54)

whose coefficients satisfy (35) and (44). Thus the stabilization procedure has also the effect of rendering the functional consistent with micropolar elasticity.

For the second Reissner functional, the stabilization term added to U_{R2} is $\frac{1}{2}(s^\phi, \bar{\phi})_V$, which effectively transforms the first term in (51) from $(\bar{\mathbf{e}}, \mathbf{E}\bar{\mathbf{e}})_V$ to $(\bar{\gamma}, \mathbf{C}\bar{\gamma})_V$. The resulting $\mathbf{J}_m$ is (47).

An obvious generalization of this "repeating block" rule is

$$
\mathbf{J}_m = \begin{bmatrix}
j_{11} & j_{12} & j_{13} & 0 & 0 & 0 \\
j_{12} & j_{22} & j_{23} & 0 & 0 & 0 \\
j_{13} & j_{23} & j_{33} & 0 & 0 & 0 \\
0 & 0 & 0 & j_{11} & j_{12} & j_{13} \\
0 & 0 & 0 & j_{12} & j_{22} & j_{23} \\
0 & 0 & 0 & j_{13} & j_{23} & j_{33}
\end{bmatrix},
$$ (55)

with the coefficients satisfying (35). This three-parameter family permits symmetric and antisymmetric stress and strain fields to be *merged* into total stresses and strains. The resulting functionals $\Pi(\bar{\tau}, \bar{\gamma}, \bar{\mathbf{u}}, \bar{\theta})$ may be viewed as having at most four independent fields. Note, however, that this choice is but a special case of (46).

5.3 A Two Field Functional

The simplest generating matrix with the block structure (55) is

$$
\mathbf{J}_m = \begin{bmatrix}
0 & 0 & 0 & 0 & 0 & 0 \\
0 & 0 & 0 & 0 & 0 & 0 \\
0 & 0 & 1 & 0 & 0 & 0 \\
0 & 0 & 0 & 0 & 0 & 0 \\
0 & 0 & 0 & 0 & 0 & 0 \\
0 & 0 & 0 & 0 & 0 & 1
\end{bmatrix},
\tag{56}
$$

The resulting two-field functional is $\Pi_A = U_A - P^c$, with

$$
U_A(\bar{\mathbf{u}}, \tilde{\theta}) = \tfrac{1}{2}(\tilde{\sigma}^u, \mathbf{e}^u)_V + \tfrac{1}{2}(s^{u\theta}, \phi^{u\theta})_V.
\tag{57}
$$

This may be viewed as a generalization of the minimum potential energy functional, to which it reduces if the second term is dropped. It can be obtained from a more general functional for elastoplasticity proposed by Atluri (1980), who recommends taking $\bar{\kappa} = 4\mu$ in $s^{u\theta} = \bar{\kappa}\phi^{u\theta}$. Hughes and Brezzi (1989) also investigated the functional (57) but made no recommendation on $\bar{\kappa}$.

6. CONCLUSIONS

The functional $\Pi_m = U_m - P_m$ extends the parametrized functional $\Pi = U - P$ of classical linear hyperelasticity to include three more independently varied antisymmetric fields: skew stresses, skew strains, and microrotations. This extension is made here in the context of micropolar elasticity without couple stresses.

Another application of these functionals is the construction of finite element interpolations for classical linear elasticity in which the rotational field θ is varied independently from the displacements. The objective is to relax stress symmetry into a weak condition. It is in this context that the functionals of Hughes-Brezzi have been proposed. A membrane element with drilling freedoms based on these functionals has recently been constructed by Ibrahimbegovic (1990). The present study indicates that the Hughes-Brezzi functionals fit the framework of micropolar elasticity if fictitious modulus $\bar{\kappa}$ is identified with the micropolar modulus κ.

The Hughes-Brezzi functionals can be readily generalized into a three-parameter family defined by (55), in which the same weighting is applied to symmetric and antisymmetric fields. However this is just a subspace of the six-parameter functional (45) characterized by the $\mathbf{J}_m$ matrix (46), which allows such weights to be separately chosen.

ACKNOWLEDGEMENTS

REFERENCES

Askar, A. (1985). *Lattice Dynamical Foundations of Continuum Theories*, World Scientific Pub. Co., Singapore.

Atluri, S. N. (1980). On some new general and complementary energy theorems for the rate problems in finite strain, classical elastoplasticity, *J. Struct. Mech.*, 8, 61–92.

Berglund, K. (1977). Special micromodels for micropolar continua, in *Continuum Models of Discrete Systems*, University of Waterloo Press, 703–718.

Felippa, C. A.(1989a). Parametrized multifield variational principles in elasticity: I. Mixed functionals, *Communications in Applied Numerical Methods*, 5, 79–88.

Felippa, C. A. (1989b). Parametrized multifield variational principles in elasticity: II. Hybrid functionals and the free formulation, *Communications in Applied Numerical Methods*, 5, 89–98.

Felippa, C. A. (1989c). The extended free formulation of finite elements in linear elasticity, *Journal of Applied Mechanics*, 56, 609–616.

Felippa, C. A. (1992). Parametrized variational principles encompassing compressible and incompressible elasticity, *International Journal of Solids and Structures*, 29, 57–68.

Felippa, C. A. and Militello, C. (1989). Developments in variational methods for high-performance plate and shell elements, in *Analytical and Computational Methods for Shells*, CAD Vol. 3, ed. by A. K. Noor, T. Belytschko and J. C. Simo, American Society of Mechanical Engineers, ASME, New York, 191–216.

Felippa, C. A. and Militello, C. (1990). The variational formulation of high-performance finite elements: parametrized variational principles, *Computers & Structures*, 36, 1–11.

Hughes, T. J. R. and Brezzi, F. (1989). On drilling degrees of freedom, *Computer Methods for Applied Mechanics and Engineering*, 72, 105–121.

Ibrahimbegovic, A. (1990), A novel membrane finite element with an enhanced displacement interpolation, *Finite Elements in Analysis and Design*, 7, 167–179.

Novacki, W. (1970). *Theory of Micropolar Elasticity*, Springer-Verlag, Berlin.

Reissner, E. (1965). A note on variational theorems of elasticity, *International Journal of Solids and Structures*, 1, 93–95.

Appendix. Parametrized Functional for a Micropolar Medium with Couple Stresses

In this Appendix the preceding variational formulation is extended to account for the presence of couple stresses m_{ij}. Two changes in the field equations occur. The angular-momentum equilibrium equation gains a divergence term:

$$m_{ji,j} + \epsilon_{ijk}\tau_{jk} + c_i = 0, \tag{58}$$

The constitutive equations must be augmented by a relation between the couple stresses and microrotation vector derivatives, which for the isotropic case is

$$m_{ij} = \pi_1\delta_{ij}\theta_{k,k} + \pi_2\theta_{i,j} + \pi_3\theta_{j,i}. \tag{59}$$

Here π_1, π_2 and π_3 are constitutive coefficients with dimension of force, and for compactness we have used the microrotational vector components $\theta_1 = 2\theta_{23}$, $\theta_2 = 2\theta_{31}$ and $\theta_3 = 2\theta_{12}$ in accordance to the convention of Eq. (9). The gradients of θ_i will be denoted by $\chi_{ji} = \theta_{i,j}$, which may be interpreted as "curvatures."

In addition, the boundary conditions (4)–(5) are augmented with

$$m_{ji}n_j = m_{ni} = \widehat{w} \text{ on } S_w, \qquad \theta_i = \hat{\theta}_i \text{ on } S_\theta, \tag{60}$$

where $S : S_w \cup S_\theta$.

Next, define the vectors and matrices

$$\mathbf{m} = \{ m_{11} \quad m_{22} \quad m_{33} \quad m_{23} \quad m_{31} \quad m_{12} \quad m_{32} \quad m_{13} \quad m_{21} \}^T,$$

$$\chi = \{ \chi_{11} \quad \chi_{22} \quad \chi_{33} \quad \chi_{23} \quad \chi_{31} \quad \chi_{12} \quad \chi_{32} \quad \chi_{13} \quad \chi_{21} \}^T,$$

$$\mathbf{H} = \begin{bmatrix} \pi_4 & \pi_1 & \pi_1 & 0 & 0 & 0 & 0 & 0 & 0 \\ \pi_1 & \pi_4 & \pi_1 & 0 & 0 & 0 & 0 & 0 & 0 \\ \pi_1 & \pi_1 & \pi_4 & 0 & 0 & 0 & 0 & 0 & 0 \\ 0 & 0 & 0 & \pi_2 & 0 & 0 & \pi_3 & 0 & 0 \\ 0 & 0 & 0 & 0 & \pi_2 & 0 & 0 & \pi_3 & 0 \\ 0 & 0 & 0 & 0 & 0 & \pi_2 & 0 & 0 & \pi_3 \\ 0 & 0 & 0 & \pi_3 & 0 & 0 & \pi_2 & 0 & 0 \\ 0 & 0 & 0 & 0 & \pi_3 & 0 & 0 & \pi_2 & 0 \\ 0 & 0 & 0 & 0 & 0 & \pi_3 & 0 & 0 & \pi_2 \end{bmatrix}, \quad \mathbf{Q} = \begin{bmatrix} \partial/\partial x_1 & 0 & 0 \\ 0 & \partial/\partial x_2 & 0 \\ 0 & 0 & \partial/\partial x_3 \\ 0 & 0 & \partial/\partial x_2 \\ \partial/\partial x_3 & 0 & 0 \\ 0 & \partial/\partial x_1 & 0 \\ 0 & \partial/\partial x_3 & 0 \\ 0 & 0 & \partial/\partial x_1 \\ \partial/\partial x_2 & 0 & 0 \end{bmatrix}, \tag{61}$$

in which $\pi_4 = \pi_1 + \pi_2 + \pi_3$. Matrix $\mathbf{H}$ can be generalized to account for anisotropy without difficulty. Little is known experimentally about couple stress constitutive behavior, however, even in the isotropic case.

With the foregoing definitions, the matrix field equations that include the effect of the couple stresses are

$$\chi = \mathbf{Q}\theta, \qquad \mathbf{m} = \mathbf{H}\chi, \qquad \mathbf{Q}^T\mathbf{m} + 2\mathbf{s} + \mathbf{c} = 0. \tag{62}$$

The first two are appended to the kinematic relations (14) and constitutive equations (15), respectively, whereas the latter replaces the second of (16).

A parametrized variational principle that accounts for couple stresses is easily obtained by including two independently varied fields: couple stresses $\widetilde{m}$ and curvatures $\tilde{\chi}$. Functionals U_m and P_m^c are augmented with couple stress terms

$$U_{mcs} = U_m + U_{cs}, \qquad P_{mcs}^c = P_m^c + P_{cs}^c, \tag{63}$$

377

where

$$U_{cs} = \frac{1}{2} \int_V \begin{Bmatrix} \widetilde{\mathbf{m}} \\ \mathbf{m}^\chi \\ \mathbf{m}^\theta \end{Bmatrix}^T \begin{bmatrix} j_{77}\mathbf{I}_9 & j_{78}\mathbf{I}_9 & j_{79}\mathbf{I}_9 \\ & j_{88}\mathbf{I}_9 & j_{89}\mathbf{I}_9 \\ symm & & j_{99}\mathbf{I}_9 \end{bmatrix} \begin{Bmatrix} \chi^m \\ \widetilde{\chi} \\ \chi^\theta \end{Bmatrix} dV, \tag{64}$$

$$P_{cs}^c = \left[\widehat{\mathbf{w}}, \bar{\theta}\right]_{S_w} + \left[\theta - \hat{\theta}, \widetilde{\mathbf{m}}_n\right]_{S_\theta}. \tag{65}$$

The derived fields in (64) are $\mathbf{m}^\chi = \mathbf{H}\widetilde{\chi}$, $\chi^m = \mathbf{H}^{-1}\mathbf{m}$, $\chi^\theta = \mathbf{Q}\,\theta$, and $\mathbf{m}^\theta = \mathbf{H}\mathbf{Q}\,\theta$; also $\mathbf{I}_9$ denotes the 9×9 identity matrix.

The first variation of $\Pi_{mcs} = U_{mcs} + P_{mcs}^c$ is

$$\begin{aligned} \delta\Pi_{mcs} = &\left(\Delta\mathbf{e}, \delta\bar{\sigma}\right)_V + \left(\Delta\sigma, \delta\bar{\mathbf{e}}\right)_V - \left(\mathbf{R}^T\tau' + \mathbf{b}, \delta\bar{\mathbf{u}}\right)_V + \left(\Delta\phi, \delta\bar{\mathbf{s}}\right)_V \\ &+ \left(\Delta\mathbf{s}, \delta\bar{\phi}\right)_V - \frac{1}{2}\left(\mathbf{Q}^T\mathbf{m}' + 2\mathbf{s}' + \mathbf{c}, \delta\bar{\theta}\right)_V + \left[\tau_n' - \hat{\mathbf{t}}, \delta\bar{\mathbf{u}}\right]_{S_t} \\ &- \left[\bar{\mathbf{u}} - \hat{\mathbf{d}}, \delta\bar{\tau}_n\right]_{S_d} + \left[\mathbf{m}_n' - \widehat{\mathbf{w}}, \delta\bar{\mathbf{u}}\right]_{S_m} - \left[\bar{\theta} - \hat{\theta}, \delta\widetilde{\mathbf{m}}_n\right]_{S_\theta}. \end{aligned} \tag{66}$$

where $\mathbf{m}' = j_{79}\widetilde{\mathbf{m}} + j_{89}\mathbf{m}^\chi + j_{99}\mathbf{m}^\theta$. The consistency conditions are (36), (45), and

$$j_{77} + j_{78} + j_{79} = 0, \qquad j_{78} + j_{88} + j_{89} = 0, \qquad j_{79} + j_{89} + j_{99} = 1. \tag{67}$$

It is seen that extending the variational principle (45) to accommodate couple stresses brings three additional free parameters, for a total of nine. This may be reduced to three free parameters, however, by extending the rule (55) with another 3×3 repeating block. Note that if one chooses $j_{99} = 1$, others zero, $U_{cs} = \frac{1}{2}\left(\bar{\theta}^T\mathbf{Q}^T\mathbf{H}\mathbf{Q}\bar{\theta}\right)_V$, and no additional independent fields over those in (45) appear.

The couple-stress theory of elasticity attracted theoretical attention in the 1960s but it is rarely used in practice, particularly in static situations. For modeling micropolar and oriented media the simpler equations of Section 1 are more common. This is especially true in homogenization of filamentary composite materials, where the body couple $\mathbf{c}$ and the micropolar modulus κ can be estimated from component-level non-polar data complemented by statistical and periodicity arguments; see for example Berglund (1977).

Although couple stress models can be generated in the continuum limit of regular and defective-lattice theories — see for example Askar (1985) — the difficulties in characterizing and measuring moduli such as π_1, π_2 and π_3 are significant, and the theory has to be regarded as experimentally inconclusive. Furthermore the additional boundary conditions (60) are not easily interpreted physically. Consequently the main development of the paper focuses on the zero-couple-stress case. This has the additional advantage that the reduction to the classical non-polar case is easily accomplished.

REPORT DOCUMENTATION PAGE

Public reporting burden for this collection of information is estimated to average 1 hour per response, including the time for reviewing instructions, searching existing data sources, gathering and maintaining the data needed, and completing and reviewing the collection of information. Send comments regarding this burden estimate or any other aspect of this collection of information, including suggestions for reducing this burden, to Washington Headquarters Services, Directorate for Information Operations and Reports, 1215 Jefferson Davis Highway, Suite 1204, Arlington, VA 22202-4302, and to the Office of Management and Budget, Paperwork Reduction Project (0704-0188), Washington, DC 20503.

1. AGENCY USE ONLY (Leave blank)	2. REPORT DATE January 1996	3. REPORT TYPE AND DATES COVERED Final Contractor Report

4. TITLE AND SUBTITLE

Coupled Structural, Thermal, Phase-Change and Electromagnetic Analysis for Superconductors, Volume I

5. FUNDING NUMBERS

WU–505–10–11
G–NAG3–934

6. AUTHOR(S)

C.A. Felippa, C. Farhat, K.C. Park, C. Militello, and J.J. Schuler

7. PERFORMING ORGANIZATION NAME(S) AND ADDRESS(ES)

College of Engineering
University of Colorado
Campus Box 429
Boulder, Colorado 80309

8. PERFORMING ORGANIZATION REPORT NUMBER

E–8471

9. SPONSORING/MONITORING AGENCY NAME(S) AND ADDRESS(ES)

National Aeronautics and Space Administration
Lewis Research Center
Cleveland, Ohio 44135–3191

10. SPONSORING/MONITORING AGENCY REPORT NUMBER

NASA CR–194457
CU–CSSC–93–06–I

11. SUPPLEMENTARY NOTES

Project Manager, Christos C. Chamis, Structures Division, NASA Lewis Research Center, organization code 5200, (216) 433–3252.

12a. DISTRIBUTION/AVAILABILITY STATEMENT

Unclassified - Unlimited
Subject Category 39

This publication is available from the NASA Center for Aerospace Information, (301) 621–0390.

12b. DISTRIBUTION CODE

13. ABSTRACT (Maximum 200 words)

Described are the theoretical development and computer implementation of reliable and efficient methods for the analysis of coupled mechanical problems that involve the interaction of mechanical, thermal, phase-change and electromagnetic subproblems. The focus application has been the modeling of superconductivity and associated quantum-state phase-change phenomena. In support of this objective the work has addressed the following issues: (1) development of variational principles for finite elements, (2) finite element modeling of the electromagnetic problem, (3) coupling of thermal and mechanical effects, and (4) computer implementation and solution of the superconductivity transition problem. The main accomplishments have been: (1) the development of the theory of parametrized and gauged variational principles, (2) the application of those principled to the construction of electromagnetic, thermal and mechanical finite elements, and (3) the coupling of electromagnetic finite elements with thermal and superconducting effects, and (4) the first detailed finite element simulations of bulk superconductors, in particular the Meissner effect and the nature of the normal conducting boundary layer. The theoretical development is described in two volumes. Volume I describes mostly formulations for specific problems. Volume II describes generalization of those formulations.

14. SUBJECT TERMS

Superconductivity; Coupled descriptions; Phase change; Mechanical; Thermal electromagnetic; Finite elements; Computer codes; Solution methods

15. NUMBER OF PAGES
383

16. PRICE CODE
A17

17. SECURITY CLASSIFICATION OF REPORT	18. SECURITY CLASSIFICATION OF THIS PAGE	19. SECURITY CLASSIFICATION OF ABSTRACT	20. LIMITATION OF ABSTRACT
Unclassified	Unclassified	Unclassified	

National Aeronautics and
Space Administration

Lewis Research Center
21000 Brookpark Rd.
Cleveland, OH 44135-3191